GEOLOGICAL SURVEY OF CANADA

OPEN FILE 2009

SELECTED LOREX CONTRIBUTIONS

LOREX 79

Limited facsimile edition of publications

resulting from the 1979 Lomonosov Ridge Experiment

with a Summary of Scientific Results

Edited by J.R. Weber

1989

TABLE OF CONTENTS

INTRODUCTION

Ever since Heezen and Ewing (1961) proposed that the seismic belt bisecting the Eurasia Basin of the Arctic Ocean (Fig. 1) signifies the continuation of the Mid-Atlantic Ridge, earth scientists have speculated that the Lomonosov Ridge might be a rafted fragment split off the Eurasian continental shelf at the time of the opening of the Eurasia Basin in the Early Tertiary. However, because of the scarcity of geophysical and geological data the continental nature of the Lomonosov Ridge had never been unambiguously demonstrated prior to the LOREX expedition.

In 1966 the late Morris Innes, Chief of the Gravity Division of the Dominion Observatory, asked me to study the feasibility of establishing a line of gravity stations from Alert to the North Pole (Fig. 2). This request led to the deployment of two small-scale expeditions to the vicinity of the North Pole in 1967 and in 1969. They were logistically supported by the Polar Continental Shelf Project (PCSP). The primary objective was to establish a line of gravity stations from Alert to the North Pole and to ascertain the crustal nature of the Lomonosov Ridge from gravity observations and plumbline deflection measurements. The need for accurate positioning resulted in the development of new techniques for obtaining celestial and satellite fixes from a moving platform in the immediate polar region and included for the first time the use of an acoustic bottom reference system for determining the fine structure of the ice drift relative to the ocean floor.

It was originally intended to continue the systematic study of the Lomonosov Ridge at two-year intervals as an on-going project of PCSP and the Earth Physics Branch (the former Dominion Observatory, now part of the Geological Survey of Canada) which would include other geophysical parameters, such as seismic, geomagnetic and heatflow measurements. But because of financial and manpower commitments to the AIDJEX project, which lasted from 1971 to 1976 (Untersteiner, 1979), plans for the North Pole series were postponed. By 1976, however, when manpower and resources became available for other Arctic Basin studies, the cost of logistic operations in the Arctic had approximately quadrupled, making it impossible to support a continuation of the North Pole series within the regular budget of PCSP and the Earth Physics Branch (EPB) alone. It was therefore decided that a one-time concerted departmental effort be made to study all those aspects of geophysics and marine geology for which we had the expertise and which could be carried out from a drifting ice station over a relatively short period of time. The scientific program was to be planned and coordinated by EPB and the logistic support provided by PCSP. Jack Sweeney and I subsequently prepared a detailed logistic and scientific plan for a multidisciplinary expedition to the Lomonosov Ridge in the spring of 1978 (Weber and Sweeney, 1977). We were given a free hand, the only constraint being that the cost was to come from regular annual PCSP and EMR branch budgets; no special funds would be made available. This was a very exciting proposition. We code-named the expedition LOREX, for Lomonosov Ridge Experiment, and set about planning the operation with enthusiasm. For a number of reasons, the expedition date was postponed to 1979. The help provided by Frank Hunt and Fred Alt from PCSP, in planning the logistics and putting together the field equipment, was invaluable.

Invitations were sent to the arctic geoscience community to participate on a cost-sharing basis, and in due course researchers from other Canadian government agencies and Canadian and U.S. universities joined the expedition. These additions were mainly in the fields of physical and chemical oceanography and navigation.

We chose the vicinity of the North Pole as our area of operation because there the ridge is narrow and the speed and direction of the Transpolar Drift Current is such that the ice stations had the best chance of drifting across the entire ridge from the Makarov to the Fram basin during the short, three-months time window available for the operation. However, to airlift the large quantity of supplies and equipment (230 metric tons as it turned out) over 1000 km from the nearest air strip and land it on sea ice posed an enormous logistic problem. Although we looked at every possible option, there were no civilian aircraft available in Canada capable of carrying out the airlift alone. The problem was solved by Canadian Armed Forces Hercules aircraft delivering 175 tons of fuel, explosives, buildings and machinery to the LOREX site by the "Low Altitude Parachute Extraction System" (Lapes), using Thule, Greenland as staging point, while Wardair's Dash-7 STOL aircraft

moved the remaining 55 tons plus personnel from Alert to the site. The Dash-7 also carried out the evacuation at the end of the operation.

The site for the LOREX main camp was occupied on March 21, 1979. The scientific program lasted from April 1 to May 29, and on June 10 the evacuation was completed. The most significant scientific results are summarized below.

Although LOREX was intended as a one-time departmental effort, the expedition was so successful that immediately on termination plans were made for another, similar, multidisciplinary expedition to the Alpha Ridge. This new expedition, benefiting from the LOREX experience and results, took place in the spring of 1983 and was codenamed CESAR 83 for Canadian Expedition to Study the Alpha Ridge.

As an aid to the reader, two bathymetric overview maps of the Arctic Ocean, one of the Amerasia Basin (Fig. 1), and the other of the Eurasia Basin (Fig. 2), have been included. They contain most of the geographical names used in this volume. The nomenclature is that most commonly used in Canada and Europe and differs in some cases from that used on Perry et al.'s (1986) *Bathymetry of the Arctic Ocean* map. For a comparison between the different nomenclatures see Johnson et al.(1989). These two maps were compiled for the volume *Climatology, Oceanography and Geology of the Arctic Seas* edited by Herman (Weber, 1989).

All publications emanating from LOREX have been collected, and published refereed articles have been assigned a LOREX Contribution Number. They consist of twenty-eight refereed articles, twenty abstracts and three internal reports and are listed in the Appendix.

At a workshop meeting on *Future Arctic Ocean Science* held at the Earth Physics Branch on November 12 and 13, 1985 (Weber et al., 1986), it was recommended that a facsimile edition of the LOREX Contributions, and subsequently also of the CESAR Contributions, be produced as limited editions for distribution to LOREX and CESAR participants and libraries. The Geological Survey of Canada has undertaken to produce by photocopy 500 bound copies of each set. The first of these is the present volume, entitled **Selected LOREX Contributions.**

SUMMARY OF LOREX RESULTS

Seafloor Morphology and Crustal Structure

Results from LOREX **bathymetry** show that the Lomonosov Ridge near the North Pole consists of several slightly tilted en echelon fault blocks with tops facing the Makarov Basin. The Makarov-facing slope with a gradient of up to 250 m/km is much steeper than the Fram-facing slope with a gradient not exceeding 100 m/km. The shallowest depth recorded was 956 m. Comparison of the LOREX bathymetric map with other maps revealed that the Lomonosov Ridge is accurately positioned on the 1954 Soviet map but is located from 15 to 25 km too far south on the latest U.S. and Canadian charts.

Gravity observations indicate (1) that the density structure of the ridge is typical of a relatively low density continental crust, (2) that the Marvin Spur consists of rocks of comparable density to that of the Lomonosov Ridge, that (3) the Makarov Basin sediments are pierced by high density seamounts of possibly volcanic origin (the Marvin Seamounts), and, (4) that the depth to Moho is 13 km in the Makarov Basin and 11 km in the adjoining Fram Basin.

For the first time portable digital recording seismographs were used on the Arctic Ocean. Results of reversed **seismic refraction** profiles show that the Lomonosov Ridge near the North Pole has a crustal depth of 27 km, and a p-wave velocity structure similar to that found in the outer Kara and Barents continental shelves. The root of the Lomonosov Ridge appears asymmetric in cross section and significant structural changes occur in the upper crustal structure along strike.

Seismic reflection air gun profiles and the records of the intermediate depth seismic reflection experiment reveal that (1) both Makarov and Fram Basins are floored by horizontal layers of well

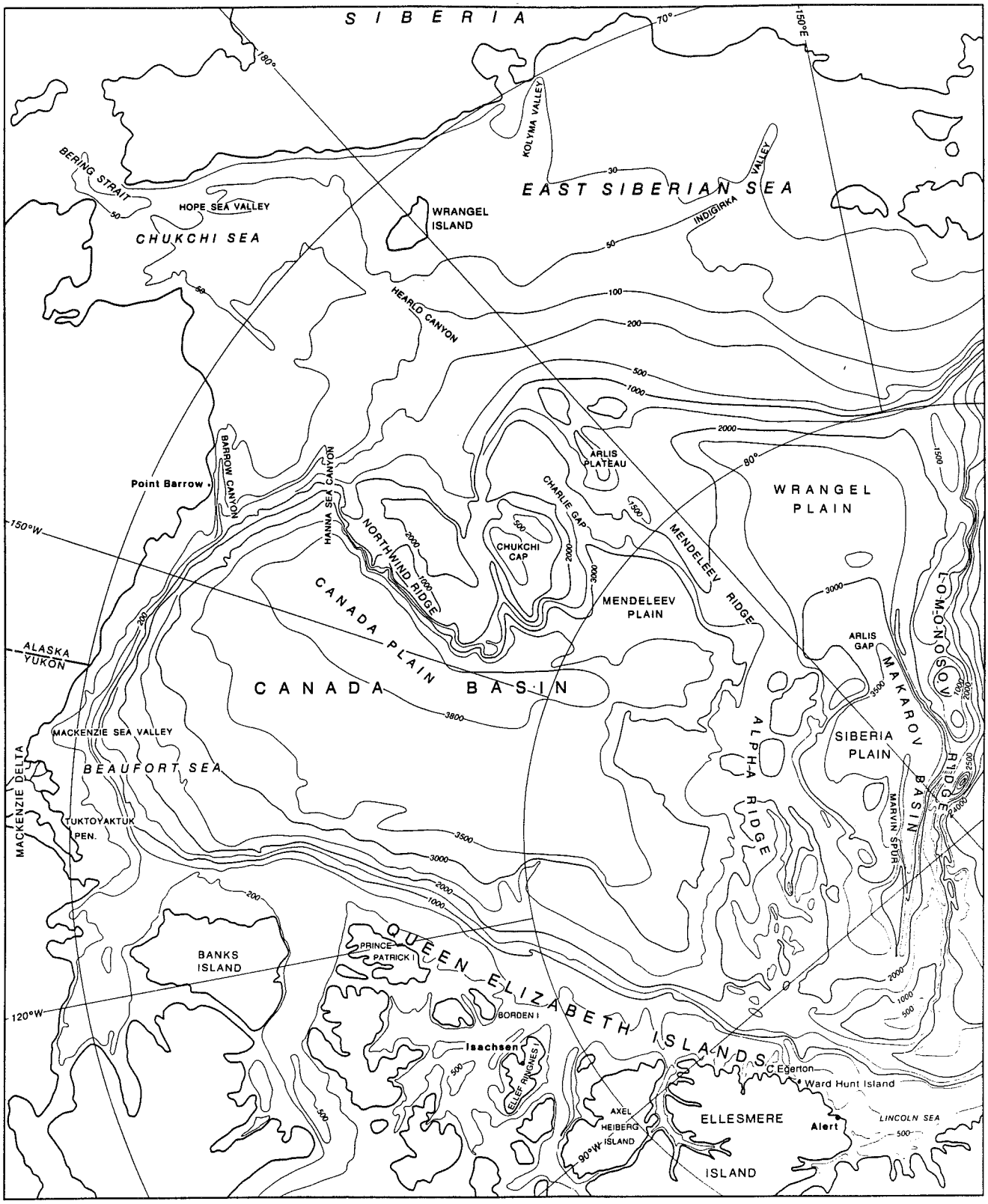

Figure 1. Bathymetric map of the Amerasia Basin. Except for some modifications of the contouring over the Alpha Ridge, based on CESAR data, the contours agree with those of Perry et al. (1986).

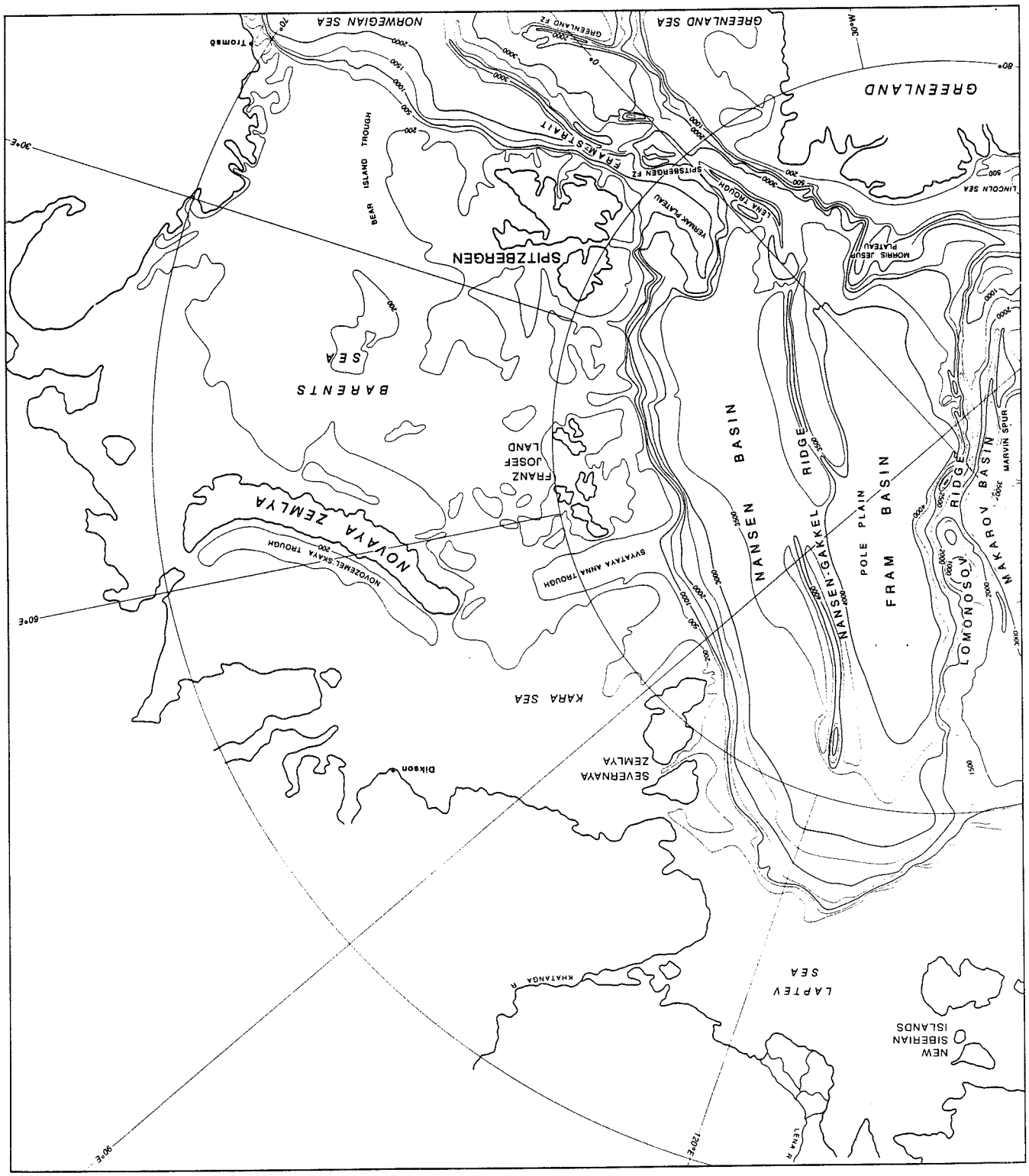

Figure 2. Bathymetric map of the Eurasia Basin. The contouring of the Nansen-Gakkel Ridge has been modified and differs from Perry et al. (1986).

stratified, unconsolidated sediments, at least 2 km thick, which abut unconformably against the ridge flanks, (2) the Makarov Basin contains a well-defined subhorizontal reflector at about 1 km below the seabed, (3) the horizontally stratified sediments in the Makarov Basin also abut against the Marvin Seamounts indicating that these structures originated before the onset of sedimentation, (4) on the Lomonosov Ridge sediments are absent from the Makarov-facing flank while the crest and Fram-facing flank are covered with a thin veneer (<100 m) of stratified, unconsolidated to semiconsolidated sediments that lie conformably on the underlying bedrock topography and appear to be slowly eroding by current scour, and (5) lithologic stratifications are present within the interior of the Lomonosov Ridge.

Sediment cores recovered from the ridge crest and Makarov flank consist of glacial-marine sediments and reworked components. The sediments have been organized into twelve stratigraphic units, Alpha to Mu, and have been designated the Makarov Basin Formation. The age of these sediments and their origin - whether they are primarily of glacial-marine origin, or whether they represent reworked material derived from the ridge itself - remains inconclusive. Based on radiometric dating of fossils in the uppermost strata, a sedimentation rate of just over 1 mm/1000 a has been suggested for the Lomonosov-Makarov sediments.

A series of low-level (300 m) **aeromagnetic** lines were flown along approximately 500 km of the Lomonosov Ridge and orthogonally to it by the Geological Survey of Canada in the years 1979 and 1980. A zone of distinctive anomalies in excess of 1000 nT strikes parallel to the crest of the ridge in the vicinity of the North Pole. An analysis of the anomalies indicates that the causative bodies have magnetizations similar to those normally associated with basic rocks such as oceanic basalt. The causative bodies also appear to extend to depth of the order of 30 km. It is inferred that they probably consist of a swarm of fairly narrow dykes that intrude the sedimentary rocks of the Lomonosov Ridge as a result of dilation of the crust caused by sea-floor spreading in the Arctic Ocean. These narrow dykes could produce a single composite linear magnetic anomaly, but would be difficult to detect seismically and would not have sufficient volume to affect the average density of the ridge.

Two-layer interpretations of the **magnetotelluric** (MT) data recorded at three ice stations which drifted across the Lomonosov Ridge and adjacent basins suggest the presence of one kilometer of highly conductive sediments in the basins. There is no indication of these sediments on the ridge; thus the MT data confirm the seismic reflection results along the same traverse. Soviet MT data on the Lomonosov Ridge closer to the Siberian shelf indicate several kilometers of conductive sediments; hence the surficial nature of the ridge must vary considerably along its length. Linear inversions of the magnetotelluric data, using Oldenburg's method, suggest the presence of well-resolved zones of high conductivity at depth greater than 120-150 km beneath the Lomonosov Ridge and at least 70-80 km beneath the Fram Basin; these zones may be related to the region of maximum partial melt in the asthenosphere. Thus the lithosphere seems to be thicker beneath the ridge than beneath Fram Basin. The data also suggest that there is an intermediate conducting layer, similar to that found beneath many continental areas, at a depth of 20 to 50 km beneath the ridge.

A new light-weight digital recording thermal gradiometer was used to measure **heat flow**. Values are highest in the Fram Basin (75-85 mWm), intermediate in the Makarov Basin (60-70 mWm) and slightly lower on the Lomonosov Ridge (60-65 mWm). These values are consistent with the ridge being composed of sedimentary rocks, and with a moderately thick layer of slowly accreting sediments in the basins.

The **deflection of the vertical** across the Lomonosov Ridge, determined from astro and satellite doppler navigation, ranged in magnitude from 5 to 15 arc seconds and confirmed the existence of a deep, relatively low density root.

Navigation, Pack Ice Motion and Water Masses

Postprocessing of **satellite doppler navigation** data from the three LOREX stations produced mean three-hour station positions to an accuracy of ±24 m horizontally and ±0.45 m vertically.

Ellipsoidal height variations were in excess of 5 m. Calculated mean station velocities over a 60 day period ranged from 0 to 1240 m/h with an average velocity of 225 m/h.

The **astro navigation** program, carried out at all three LOREX camps, produced 87 line of position (LOP) fixes. Of these, 42 fixes with a mean position accuracy of ±1.1 arc seconds (±33 m) were correlated with the satellite doppler positions.

Strain rate and total strain based on relative changes in the station positions indicate major changes in the pattern of **ice pack deformation** as the stations drifted across the Lomonosov Ridge. Total strain reflects mainly plastic deformation taking place in episodic events while changes in strain rate also show diurnal oscillations.

Results from the **physical oceanography** program include (1) the observation that the deep water of the central Arctic Ocean consists of an upper, less saline deep water layer, originating from the Greenland or Norwegian Sea, and, below 1500 m, of a lower deep water layer which had its salinity augmented within the Arctic Ocean, (2) the confirmation of significantly higher salinity in the deep water of the Makarov Basin, and of the isolation of bottom waters by the Lomonosov Ridge, which suggests deep water production in the Amerasia Basin, (3) the observation, on May 1, 1979, that while the LOREX satellite station *Iceman* was drifting in a northerly direction in the vicinity of 89°20'N, 160°E, it appeared to have drifted across an oceanic front into a significantly different water mass, resulting, over the next five days, in a salinity decrease from 30°/oo to below 29°/oo and a temperature increase of 0.2 C of the surface water which coincided with a 3 m increase of the ellipsoidal height of the sea level, and, (4) records from moored current meters that indicate slow bottom currents in the abyss, while on the Lomonosov Ridge pulsating bottom currents, strong enough to cause erosion, flow diagonally across the crest into the Makarov Basin.

Significant results from the **chemical oceanography** program include (1) the observation that artificial radionuclide tracers believed to have come from the Irish Sea had appeared within a short period of time at mid-depth near the North Pole, (2) the confirmation of the presence of a strongly advective structure in the central Arctic Ocean, and (3) the postulation that shelf processes play a dominant role in the carbonate chemistry of surface and near surface waters.

SELECTED LOREX CONTRIBUTIONS

Following are photocopies of twenty-four of the twenty-eight LOREX Contributions and one extended abstract. Four M.Sc. theses, Lowings' (# 7), Morris' (# 17) and Quek's (# 19 and 20) with over 700 pages of text were not included.

EOS

TRANSACTIONS, AMERICAN GEOPHYSICAL UNION
VOLUME 60 NUMBER 42 OCTOBER 16, 1979

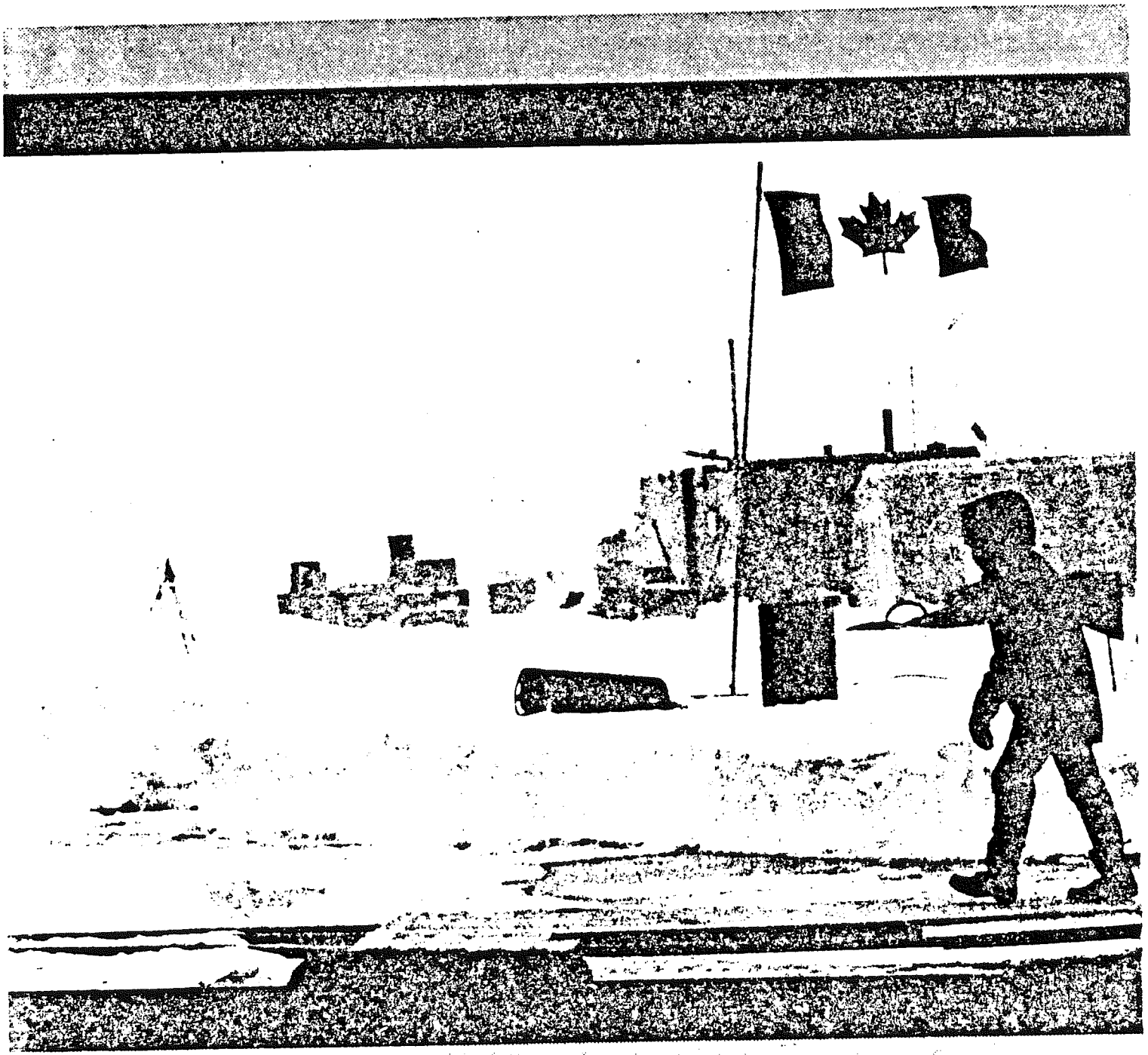

Cover. Main Camp as it appeared on May 1 after the ice broke and the marine geology buildings were separated from the rest of the camp by a lead of open water. (Photo by J. R. Weber from a 35-mm color slide.)

The Lomonosov Ridge Experiment: 'Lorex 79'[1]

J. R. Weber

Department of Energy, Mines and Resources
Ottawa, Canada

Introduction

In the spring of 1979 the Department of Energy, Mines and Resources (EMR) undertook a large-scale, multidisciplinary project to study the nature and origin of the Lomonosov Ridge. The scientific program was planned and coordinated by the Earth Physics Branch, and the logistic support was provided by the Polar Continental Shelf Project. Scientists from other branches of EMR, from the Department of Fisheries and Oceans (DFO), and from a number of universities in Canada and the U.S.A. took part in the project code named Lorex 79.

The Lomonosov Ridge is an aseismic submarine mountain range that bisects the Arctic Ocean into the Amerasia and Eurasia Basins (Figure 1). It rises sharply to a height of some 3 km above the adjacent abyssal plains, the Makarov Basin to the west, and the Fram Basin to the east. It is close to 200 km wide where it approaches the North American and Eurasian continental shelves but narrows to 25 km at its midpoint near the North Pole. Its relatively flat top, the steepness of its flanks, and results from previous geophysical measurements indicate that it may be a sedimentary structure of continental origin rather than a structure of oceanic origin [*Sweeney et al.*, 1978]. In this context it has been suggested on several occasions that it is a rafted fragment split off the Eurasian continental shelf at the time of the opening of the North Atlantic and the Eurasia Basin in Early Tertiary times. However, since the available geophysical, geological, and bathymetric data are relatively sparse and often of doubtful quality (because of the enormously difficult operating conditions), the continental nature of the Lomonosov Ridge has never been unambiguously demonstrated.

In 1967, and again in 1969, the Earth Physics Branch (then the Dominion Observatory) of EMR carried out two expeditions with the Polar Continental Shelf Project to the vicinity of the North Pole. The prime objective of these surveys was to establish a line of gravity stations from Alert on Ellesmere Island to the Pole and to obtain as many gravity observations as possible in the vicinity of the Pole and across the Lomonosov Ridge. The need for accurate positioning for these observations resulted in the development of new techniques for obtaining astro and satellite fixes from a moving platform in the immediate polar region and included, for the first time, the use of an acoustic bottom reference system for determining the fine structure of the ice drift in relation to the ocean floor. The gravity observations obtained during these two expeditions provided a basis for compiling a preliminary structural model of the Lomonosov Ridge [*Lillestrand and Weber*, 1974].

From these preliminary surveys grew a plan to conduct a concentrated survey of the ridge by making use of the existing talent and expertise in Arctic geophysics within the department. The fields of study were to consist of bathymetry; gravity; plumb line deflection measurements; subbottom profiling; shallow (air gun), intermediate (reflection), and deep crustal (refraction) seismic; coring and dredging; bottom photography; heat flow measurements; and geomagnetic and magnetotelluric soundings. The range of studies was later enlarged by including teams, from McGill and Dalhousie universities and from the University of Washington, that added physical and chemical oceanography to the program.

The Planning Stage

The basic plan was to establish a main camp and two satellite camps on the drifting pack ice upstream of the ridge and let the transpolar current transport the stations across it. The time period for the operation was defined by a 3-month window, starting when daylight conditions in the polar region were adequate for landing on the ice and ending well before the onset of the melt season. On this basis we estimated that March 14 was the earliest possible date on which the search could begin and that the evacuation should be completed not later than June 15. Taking into account the time required for the search and for the airlift and possible delays caused by weather and other unforeseen circumstances, the scientific program was planned to last for 60 days (April 1 to May 30).

From the scientific point of view, the most desirable location is where the ridge is narrowest and the chances are best for drifting across the entire structure from the Makarov to the Fram Basin. By studying the

Fig. 1. Arctic sea floor nomenclature. Bathymetric contours at 0.5, 1, 2, 3, and 4 km. Also shown are the locations of the expedition's staging points Alert, Thule, and Resolute, as well as the positions of Lorex Base and Fram 1 at the end of April.

[1]Contribution 815 of the Earth Physics Branch

Eos, vol. 60, no. 42, pages 715-721

paths of stations that have drifted across the ridge in the past, we concluded that in the polar region, in springtime, the ice drifts, on the average, at a speed of 5 km/d in a grid direction of 210°, and the optimum location for the deployment of the camps would be in the vicinity of 88°N and 155°E, just over 1000 km from Alert.

However to airlift the staggering quantity of supplies and materials that are required for an operation of the size of Lorex, over such a long distance, posed an enormous logistic problem. The total weight of the Lorex camps amounted to nearly 230 metric tons and consisted of buildings, tents, and lumber (13 tons), general camping equipment (including power plants), snowmobiles and a loader (12 tons), food supplies (5 tons), scientific equipment (41 tons), explosives (11 tons), and 720 drums of fuel (147 tons) for fixed-wing and helicopter operations and for heat and power. The major airlift of fuel and other bulk freight could not realistically be carried out over such a great distance by readily available aircraft such as DC 3's and Twin Otters. Even for the newly developed DeHavilland Dash-7 STOL aircraft the distance proved to be too long. The Lockheed C-130 Hercules was the only aircraft available to conduct the airlift quickly and economically, but it required a runway of 1500 m in length. We believed it was unlikely we could find such a runway in the proposed deployment area without spending an inappropriately long time searching, because the pack ice moves comparatively quickly in the transpolar current and tends to break up in the vicinity of the Lomonosov Ridge (V. Venediktov, personal communication, 1972).

In the end we decided that Lorex could only be staged by enlisting the assistance of military aircraft to paradrop the bulk supplies and by using the Dash-7 to move the balance of the freight. Under this scheme the Canadian Forces Hercules aircraft would deliver the 175 tons of fuel, explosives, buildings and lumber, and the loader to the Lorex site by the Low Altitude Parachute Extraction System (Lapes) method, using Thule, Greenland, as staging point, and the Dash-7 would move the remaining 55 tons plus the personnel from Alert to the site. The Dash-7 would also carry out the evacuation at the end of the operation.

The Execution

On March 8, 1979, the advance party arrived in Alert to take care of the cargo arriving from Resolute Bay by commercial freighter aircraft and to start the search for a suitable Lorex site, using two DeHavilland Twin Otter aircraft. On March 20, after a number of delays because of weather and aircraft problems, a manned midway fuel cache equipped with a beacon was established between Alert and the target area. The eventual Lorex site was found the next day, at 88°38'N, 172°W. It consisted of a thick, multiyear ice floe adjacent to a large area of 2-m-thick first-year ice large enough to accommodate the Dash-7 and the Lapes deliveries at the same time. The airlift began on March 23 with the Dash-7 flights from Alert followed on March 25 with the start of the Lapes deliveries from Thule. On April 1 the build-up of the Main Camp was completed, and on April 2 and 3 the airlift of the two satellite camps, Snowsnake and Iceman, was completed. On May 29 the Dash-7 returned for the evacuation and on June 10 the last piece of equipment was off the ice.

The Scientific Program

Navigation

All three stations were equipped with Transit Satellite receivers. Positions were computed on-line at Lorex Base, whereas the raw satellite data from Snowsnake and Iceman recorded on magnetic tape cassettes were collected every few days and processed at the main camp on an HP2100 computer. Accepting only passes with standard deviations of less than 50 m, a daily average of 30 passes for Lorex Base and 20 passes each for the satellite camps was obtained. During the whole period of operation, positions, rate and direction of drift were provided in near real time to the scientists. Generally the accuracy of the drift path positions is estimated to have a standard deviation of ± 25m. For specific time periods, coinciding with plumb line deflection measurements, the system was capable of providing positioning accuracies of up to ± 10 m.

The drift path of the three stations determined from the satellite receivers is shown in Figure 2 along with the drift paths of the 1967 and 1969 Dominion Observatory Polar Expeditions. Specially marked are the positions of Lorex Base and the two satellite camps on April 14, when all systems were first operational, and on May 27, before the satellite camps were dismantled. The relative translation and rotation of the whole ice field is indicated by the change of configuration of the three stations between the two dates and shows that it moved surprisingly uniformly. The satellite camps were located some 60 km from Lorex Base and about 100 km from one another.

In addition to the satellite receivers, the three stations were also equipped with Trisponder remote stations and a radar ranging system with directional antennae, which allowed ranging to the helicopter, which in turn was equipped with a Trisponder master station and an omni-undirectional antenna. This system was used mainly for precise positioning of the helicopter for bathymetric and gravity traverses.

Both helicopter and Twin Otter were equipped with VLF navigation, which has a position accuracy of around ± 1 km.

Plumb Line Deflection Measurements

By means of a Wild T-4 theodolite, a series (each series lasting from 8 to 12 hours depending on the drift rate of daylight) of star observations was taken at Lorex Base between March 31 and April 13, and again on May 2 and 3, and at Iceman from April 15 to 29. The standard deviation of a single star fix is estimated at better than ±60 m, while the drift path position for a good series is expected to have a standard deviation of about ±15 m. These astro observations, in conjunction with the satellite fixes, will allow the determination of the plumb line deflection along the drift path. These measurements complement gravity measurements and provide additional constraints on the density structure of the ridge.

Bathymetry

In conjunction with the gravity survey, some 250 bathymetric stations were established by helicopter traverse, using the seismic reflection method. In addition, continuous depth profiles were obtained from echo

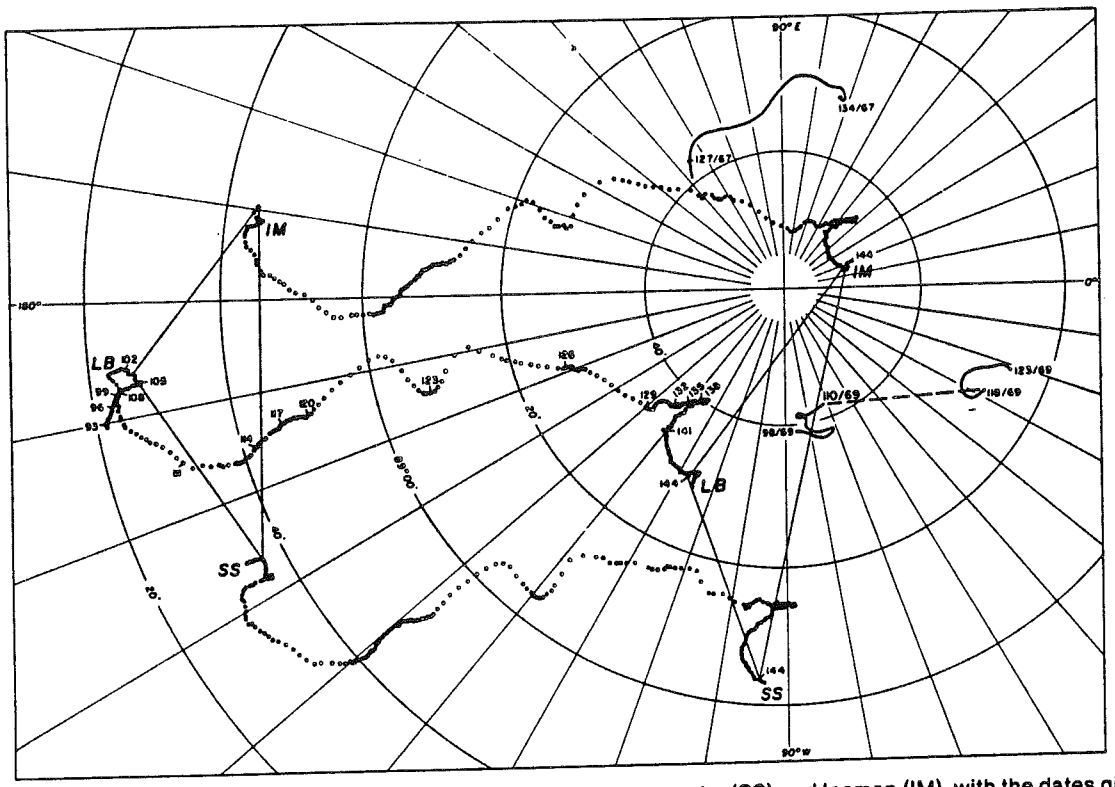

Fig. 2. Drift path of Lorex Base (LB) and the two satellite camps, Snowsnake (SS) and Iceman (IM), with the dates given in Julian days. The triangles drawn between the three camps on day 93 and again on day 144 illustrates the rotation and relative translation that has taken place between the stations during the 41-day period. Also shown are the drift paths of the 1967 and 1969 Dominion Observatory Polar Expeditions.

sounders installed at the two satellite camps and from the sub-bottom profiler at Lorex Base. Figure 3 shows a preliminary bathymetric contour map based on the Lorex and the 1967 and 1969 data. The shallowest depth recorded was 956 m. Comparison with the latest bathymetric map of the Arctic Ocean [*Sobczak and Sweeney*, 1978] shows that, in this area, the crest of the ridge is located about 25 km further south than had previously been assumed.

Gravity

Some 260 gravity stations were established by traversing in a helicopter. In addition, gravity data were collected along each of the three drift paths by a recording gravity meter at each camp. Survey coverage extends 80 km into the flanking basins on either side of the Lomonosov Ridge and about 100 km along the ridge crest. Preliminary results show that free air anomalies over the crest of the ridge range between 65 and 120 mGal (1 mGal = 10^{-5} ms^{-2}), but are generally between 70 and 95 mGal (equivalent to about 400 m of bathymetric relief). Based on the location of the 70 mGal contours, the width of the crest appears to change from 8 to 22 to 35 km in two well-defined steps along the Fram Basin flank. The gravity gradient leading to the crest along the Makarov flank (90 mGal in 10 km) is about twice that along the Fram flank (50 mGal in 10 km).

Profiles into the Makarov Basin show two subordinate ridges, both parallel to the Lomonosov Ridge. The larger ridge (1-km relief, +20 mGal amplitude) 80 km away is colinear with the Marvin Seamounts, but no evidence for a seamount was found in the survey area. A second ridge, 40 km further out, appears largely buried (relief uncertain, +10 mGal amplitude).

Generally, the gravity pattern along each Fram Basin profile is similar: from the Lomonosov Ridge high it falls sharply to a minimum (0 to −35 mGal) about 40 km into the basin and becomes somewhat more positive further out. The minimum is less pronounced than expected and may indicate that the ridge does not have a very large low density root.

Sub-bottom Profiling and Shallow Seismic

Between April 8 and May 26, 1060 hours of 3 kHz bathymetric sub-bottom profiling and 880 hours of continuous, high resolution, air gun reflection profiling records were collected at Lorex Base. The sub-bottom system consisted of an eight transducer array and transceiver coupled to a graphic recorder. The shallow seismic equipment included one 10 cubic inch air gun and a single active hydrophone. Analog signal processing involved time variable gain amplification and pass-band filtering. Output was displayed on a second graphic recorder and recorded on magnetic tape (unprocessed signal only).

Maximum penetration for the two systems was 100 ms and 1.2 s (two-way travel time), respectively, corresponding roughly to unconsolidated sediment thickness of 75 m and 1100 m. In general the results show that thick sequences of well-stratified, undisturbed sediments found in both the Makarov and Fram basins pinch out on the flanks of the Lomonosov Ridge. The morphology of the ridge itself is highly variable and,

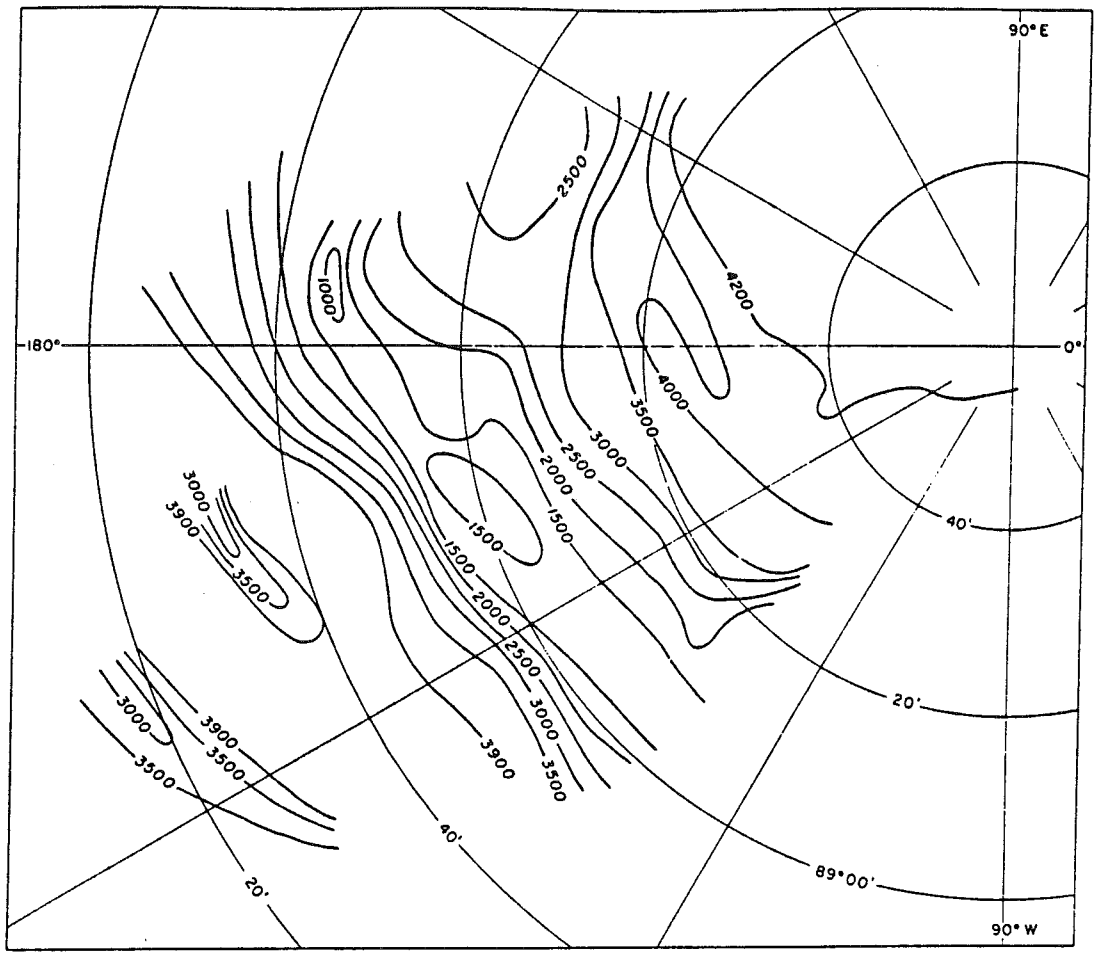

Fig. 3. Preliminary bathymetric contour map based on some 250 seismic reflection soundings obtained on gravity traverses.

along the drift path of the main camp, shows three prominent crests at 1391 m, 1956 m, and 1575 m below sea level, suggesting that the ridge may consist of fault blocks on echelon. Sediment cover is minimal on the south flank, and relatively thin stratified sediments are found on the north flanks.

Intermediate Reflection Seismic

A digitally recorded cross-shaped seismometer array with four 540-m legs consisting of a total of 24 seismometer stations spaced at 90-m intervals was in operation at Lorex Base from April 5 to May 12. Explosive charges were shot about five times a day, depending on the drift rate. In the 38 days of operation, 205 high-quality seismic reflection records were obtained along main camp track. Reflections from sedimentary layers ranging from ocean floor to basement will permit the determination of seismic velocities, thicknesses, and dips of these layers. The depth to the Mohorovicic discontinuity may be determined from 95 of the records.

Deep Crustal Seismic Refraction

A reversed refraction profile, normal to the Lomonosov Ridge, was recorded using programmable digital cassette systems. Recorder spacings were about 10 km, with shot to recorder distances of up to 200 km. Explosive charges of up to 800 kg were detonated at a depth of 100 m beneath the ice and produced good signal-to-noise ratios. A second reversed profile, lying along the ridge, was obtained with recorder spacings of approximately 6 km and shot to recorder distances of up to 150 km. A preliminary interpretation indicates that the crust-mantle interface may be at a depth of about 20 km, intermediate between typically continental and oceanic results.

Heat Flow Measurements

Between April 5 and May 13, a total of 42 gradiometer observations were made in the sea bottom sediments; 22 in the Makarov Basin, 10 on the Lomonosov Ridge and 10 in the Fram Basin, including one at the Fram 1 site. A new lightweight, digital-recording, Bullard-style thermal gradiometer, with 7 thermistor

sensors spaced at 40-cm intervals, commonly gave sediment penetrations of 3 m by using 45 kg of lead weight in water depths to 4200 m. Using a needle probe, over 300 conductivity measurements were completed on 21 cores. Bottom water temperatures and water temperature profiles were collected both over the ridge and the two adjacent basins. Several preliminary measurements were made with a portable gamma ray spectrometer to determine if varying proportions of U, Th and K could be detected in the recovered cores.

Tentative results from the Makarov Basin indicate a heat flow of about 60 mWm^{-2}, with temperature gradients in the sediments ranging from 59 to 69 mKm^{-1}. A series of heat flow measurements on the flanks of a possible extension of the Marvin Spur revealed no thermal expression of the feature. Preliminary heat flow results over the ridge and basins are similar to the results reported previously by *Lachenbruch and Marshall* [1966] and *Lubimova et al.* [1976]. Observations of bottom water temperatures and gradients in the Makarov Basin showed no detectable gradient over the bottom 40 m of the water column and spatial variations of less than 6×10^{-3} K about a mean of -0.3°C.

Geomagnetic Experiments

Recording proton precession vertical gradiometers were installed at the two satellite camps, Iceman and Snowsnake. Each station contained two proton precession magnetometers (PPM), one suspended through the ice at a depth of 140 m and the other on the surface. The vertical gradient obtained from the difference of the total force measurements responds to spatially varying fields or magnetic anomalies along the drift path but is insensitive to time variations in the field. At Snowsnake, good data appear to have been obtained during most of the 6-week recording period. At Iceman the suspended magnetometer failed to provide a good signal, and reliable data were obtained only from the magnetometer installed on the surface.

Electrical conductivity measurements were made by using magnetotelluric (MT) recording stations installed at Lorex Base and at the two satellite camps. In addition 3-component-recording fluxgate magnetometers were installed 100 km south of Base over the Makarov Basin and 50 km to the south over the flank of the ridge. The MT stations were operated for about 6 weeks and the magnetic variation stations for 4 weeks. Good data appear to have been obtained at most of these stations, though the MT station at Lorex Base had to be moved after about 3 weeks because of severe ice movements. A fourth MT system, which sampled at 5-second intervals, recorded data for brief intervals at the two satellite camps and was operated at Lorex Base as it passed over the ridge.

Seabed Investigations

A total of 42 Benthos gravity cores (including two from the Fram 1 site), varying in length from 0.2 m to 1.7 m, were collected. In addition, 10 Shipek grab samples were recovered and 4 dredge stations occupied.

Sediments of the Makarov basin included dense brown, slightly sandy to sandy lutites and stiff, layered, grey-brown lutites. These two units could possibly represent interbedded pelagic turbidite sequences. Sediments of the Fram basin are predominantly firm lutites. Layering in these sediments is well defined by marked and abrupt changes in color from light browns to grey browns. Sediment samples from the ridge have a higher proportion of sand-sized material, primarily quartz with minor dark minerals, lithic fragments, worm tubes, foraminifera tests, and shell fragments. A 30 cm^3 botryoidal-shaped manganese nodule was recovered in a dredge sample on the south flank of the ridge.

Approximately 1100 black and white and color photographs of the sea floor were collected from 14 stations using an Arctic deep sea camera system developed at the Bedford Institute. The unit was deployed through the ice and suspended 2.5 m above the seabed. The camera/flash units were triggered on a 10- to 60-second interval, depending on the ice drift rate. Initial examination of the results revealed the presence of biogenic tracks and trails and manganese-coated pebbles and cobbles on a soft clay seafloor.

Physical Oceanography

At Lorex Base a total of 31 continuous sound velocity profiles (to a depth of 2000 m) and 11 continuous bathythermograph profiles (to a depth of 1830 m) were collected using the new, Sippican Corporation, extended depth expendable sound velocity probes (XSV) and conventional bathythermograph probes (XBT). These probes were interfaced with a signal processor and strip chart recorder. Preliminary results indicate subtle differences in the sound velocity and thermal (hence salinity) regimes in the two basins. The velocity data will be used for the precise conversion of travel times to depths to obtain an accurate bathymetric profile of the ridge.

At Iceman, current speed and direction, water temperature, and conductivity were measured daily to depths of 1400 m and 400 m, respectively, using an Aanderaa current meter. In addition an Aanderaa current meter fixed at a depth of 5 m sampled velocity every 10 minutes throughout the experiment and an Inter-Ocean current meter recorded time series at a depth of 50 m. Boundary layer phenomena were studied using a Kaijo-Denki ultrasonic current meter positioned 50 cm below the ice. It recorded current velocity only when that velocity exceeded 5 cm/s; about 20 good quality records of 30 minutes each were obtained.

On April 5 and 6, two pair of recording current meters were moored at a depth of 1440 m near the crest of the ridge and at a depth of 3565 m on the north flank of the ridge. The instruments were floated 25 m and 200 m above the bottom and sampled water temperature and current speed and direction at 10-minute intervals. On May 27 and June 2 the current meters were recovered by divers using a transponding acoustic release system to bring the instruments to the surface. All four instruments recorded satisfactorily throughout the mooring period.

Chemical Oceanography

At satellite camp Snowsnake, detailed measurements were made of salinity, temperature, and nutrients from the surface to depths of 3000 m, using water-sampling bottles and reversing thermometers. These measurements showed the presence of a number of distinct water masses, including water originating in the North Pacific and Atlantic. Differences were apparent in the properties of water samples taken from depths greater than 1500 m on the two sides of the Lomonosov Ridge.

Water samples were stored for subsequent measurement of the stable oxygen isotope ratio O_{18}/O_{16}, which should provide an additional aid to the identification of the various water types.

In order to estimate rates of mixing of surface and deeper water layers, a number of two hundred-liter samples were collected from depths of up to 3000 m and processed at the station to isolate dissolved inorganic carbon for measurement of carbon-14. Also, for dating studies, samples were taken for determination of tritium, which enters the surface waters of the oceans from the atmosphere. Two ice cores were taken with the aim of looking at changes in the tritium content of surface waters over a time period of a few years.

Large volumes of surface water (up to 4000 l) were processed to permit measurement of the radioactive nuclides Cs-137,Cs-134, Pu-239 and Pu-240, which are introduced to the ocean as atmospheric fallout from nuclear weapons testing and now, in increasing quantities, from nuclear fuel-reprocessing plants.

As part of a study of the carbonate system in arctic waters, alkalinity and pH measurements were made. These data will permit the flux of carbon dioxide between the Arctic Ocean surface and atmosphere to be estimated.

Water samples were collected and stored for the measurement of a number of trace metals: cadmium, copper, nickel, and zinc. Data on the distribution of these elements will assist the study of their behavior in the marine environment.

Biological Investigations

At Lorex Base, fourteen plankton tows were recovered from 300 m. Initial observations indicate planktonic life to be more prolific in the Makarov than in the Fram Basin.

Acoustic Experiment

Fram 1, an American-sponsored drifting ice station with international participation was operating 250 km off the northeast coast of Greenland, concurrently with Lorex. It carried out oceanographic and geophysical studies in the vicinity of the Nansen-Gakkel Ridge. An acoustic experiment was carried out between Lorex and Fram 1 with the objective of studying low-frequency acoustic wave propagation and of measuring ambient noise levels between the two sites. For this purpose, explosive charges were set off at the Lorex satellite camp Iceman and at Fram 1 and recorded at these sites over a 20-day period starting April 20. The shots consisted of two 0.9-kg and two 25-kg charges daily at each site. The Lorex intermediate and deep seismic shots were also recorded.

Diving Activities

Nineteen manned dives were made with a total underwater time of 9 hours, which included observation and filming of geophysical equipment, the study of the ice and water column, and investigation of 'ice chandeliers.' One dive was carried out by His Excellency The Right Honourable Edward Schryer, Governor General of Canada.

Acknowledgments

The following individuals and agencies were responsible for the principal research and support activities.

Satellite Navigation: D. Wells, Atlantic Oceanographic Laboratory, Bedford Institute of Oceanography, DFO; J. Popelar, Earth Physics Branch, EMR, and Geodetic Survey of Canada, EMR.

Astro Navigation: Geodetic Survey of Canada, EMR, and G. W. Johnson, University of Minnesota.

Bathymetry: J. R. Weber, Earth Physics Branch, EMR.

Gravity: J. F. Sweeney, Earth Physics Branch, EMR.

Sub-bottom Profiling, Seabed Investigations, Sonar Velocity, and Bathythermograph Profiling, Biological Investigations: S. Blasco and C. F. M. Lewis, Geological Survey of Canada, Atlantic Geoscience Centre, EMR, Bedford Institute of Oceanography, DFO.

Intermediate Seismic: A. Overton, Geological Survey of Canada, EMR.

Deep Seismic: A. Mair, Earth Physics Branch, EMR.

Heat Flow: A. Judge, Earth Physics Branch, EMR.

Geomagnetic Studies: E. R. Niblett, Earth Physics Branch, EMR.

Physical Oceanography: (Camp Iceman) E. R. Pounder, McGill University.

Bottom Current Measurements: K. Aagaard, University of Washington.

Chemical Oceanography: R. Moore, Dalhousie University.

Acoustic Experiment: H. Kutschale, Lamont-Doherty Geological Observatory.

Diving Activities: J. MacInnis, under contract with National Geographic Society.

Chief Scientist: J. R. Weber, Earth Physics Branch.

Operations Manager: F. P. Hunt, Polar Continental Shelf Project.

Camp Manager: A. Alt, Polar Continental Shelf Project.

Finally, on behalf of all the Lorex participants, I would like to acknowledge the support and enthusiasm for the project by the management of the Earth Physics Branch and the Polar Continental Shelf Project. The logistic assistance and personal involvement of the 435th Squadron of the Canadian Armed Forces and the personnel of the Canadian Forces Base Alert is also gratefully acknowledged.

References

Lachenbruch, A. H., and B. V. Marshall, Heat flow through the Arctic Ocean floor, the Canada Basin-Alpha Rise boundary, *J. Geophys. Res., 71*, 1223-1248, 1966.

Lillestrand, R. L., and J. R. Weber, Plumbline deflection near the North Pole, *J. Geophys. Res., 79*, 3347-3352, 1974.

Lubimova, E. A., V. N. Nikitina, and G. A. Tomara, Thermal fields of the inland and marginal seas of the USSR, (in Russian), in *Geological and Geophysical Studies and the Results of Heat Flow Determinations*, pp. 43-52, Nauka, Moscow, 1976.

Sobczak, L. W., and J. F. Sweeney, Bathymetry of the Arctic Ocean, in *Arctic Geophysical Review*, vol. 45, edited by J. F. Sweeney, pp. 7-14, Earth Physics Branch, Department of Energy, Mines and Resources, Ottawa, Canada, 1978.

Sweeney, J. F., E. Irving, and J. W. Geuer, Evolution of the Arctic Basin, in *Arctic Geophysical Review*, vol. 45, edited by J. F. Sweeney, pp. 91-100, Earth Physics Branch, Department of Energy, Mines and Resources, Ottawa, Canada, 1978.

J. R. (Hans) Weber was born in Switzerland and obtained his electrical engineering degree from the Swiss Institute of Technology (ETH). He came to Canada in 1953 to join the Arctic Institute of North America's Baffin Island expedition to the Penny Ice Cap which fired his lifelong enthusiasm for the Arctic. An exchange fellowship to the University of Alberta led to a Ph.D. degree in physics. During the IGY he carried out glacier studies in Ellesmere Island. After joining the Dominion Observatory, (now the Earth Physics Branch of the Department of Energy, Mines, and Resources) in 1960, Weber carried out gravity surveys at sea, over the Arctic Islands and Arctic Ocean and led two geophysical expeditions to the North Pole. He contributed to the development of techniques for measuring glacier thicknesses and for precise navigation in the polar region. As a principal investigator during the Aidjex (Arctic Dynamics Joint Experiment) project in the Beaufort Sea he developed instrumentation for measuring ocean tilt and wind-induced tilt changes of sea ice. Weber is a fellow of the Arctic Institute of North America and a member of the AGU and CGU.

Geolog, v. 9, p. 58-64, 1980

NORTH POLE GEOLOGY UNDER THE SEA ICE AT LOREX 79

C.F.M. Lewis

During April and May 1979, the Department of Energy, Mines and Resources (E.M.R.) conducted a major polar expedition to investigate the nature and origin of the Lomonosov Ridge near the North Pole. This ridge, equivalent in relief and size to a major mountain range, rises almost 3,000 m above the floor of the Arctic Ocean and extends about 1,700 km between northern Canada and U.S.S.R.

Mike Lewis

According to some theorists, the ridge is an ancient sliver of the Eurasian continent that was shifted to its present position by rifting and sea floor spreading processes within the last 60 million years. Others suggest the ridge stands as mute and relict evidence of former upheavals and buckling of the oceanic crust possibly with outpourings of volcanic rocks. Clearly the formation of such an extensive feature has played a major role in the evolution of the Arctic Ocean basin, and a proper understanding of the timing and mechanics of its emplacement is bound to improve our understanding of the continental margins surrounding the Arctic Ocean including the rocks and resources of Arctic Canada.

The ocean sediments may provide a record of the influence of this major ridge on deep sea sedimentation processes. This seabed record could lead also to insights about ancient oceanographic conditions and the history of ice cover on the Arctic Ocean.

The overall scientific program called LOREX 79 was conceived and developed by the Earth Physics Branch (E.P.B.) of E.M.R., with Hans Weber taking the lead role in planning and in serving as the expedition's chief scientist. The Polar Continental Shelf Project also of E.M.R. supported the program magnificently with transport, food, shelter, fuel and Arctic expertise. The Canadian Armed Forces ultimately mobilized a squadron of Hercules aircraft to deliver fuel and shelter materials onto the sea ice using their impressive low altitude parachute extraction system to eject freight just above 'ground' level.

At an early stage in the planning, and following our initial experience with marine geology in the Arctic Ocean at AIDJEX in 1975, the Geological Survey of Canada (G.S.C.) was invited to take responsibility for the investigation of the surficial characteristics of the Lomonosov Ridge. Brian Bornhold carried out much of the preliminary planning and Steve Blasco took charge of the actual field project. We all managed to participate on the ice, ably

assisted by Fred Jodrey, Robbie Burns, Ray Jubb and Bob Murphy. Our success in the midst of Arctic rigours, equipment breakdowns, and low levels of manpower owes much to Steve Blasco's dynamic leadership and the thorough support we received in preparing for this venture at G.S.C.'s Atlantic Geoscience Centre based in the Bedford Institute of Oceanography (B.I.O.), Dartmouth.

The marine geology investigation operated round the clock as a five-point program: (1) coring and sampling of bottom sediments, (2) photography of the ocean floor with deep sea cameras (provided by Bedford Institute of Oceanography's Photographic Unit), (3) echo sounding to measure the depth of water and to record the layering in near surface sediments up to 75 m below the seabed, (4) seismic reflection profiling to determine the stratigraphy and structure of the unconsolidated sediments up to 1,100 m beneath the seabed, and (5) sound velocity measurement in the water column to calibrate depths to the seabed inferred by acoustic ranging in (3) and (4) above. With this program, we were in a position to describe the seabed morphology and to analyze the stratigraphy and structure of the surficial sediments that mantle the ridge and adjacent ocean basins. The cores and bottom photographs will enable us to document the composition and age of the sediments and to infer the history and nature of sedimentary processes within the Lomonosov Ridge environment.

Our light-weight hydraulic winch used for deep sea coring and photography also carried instruments to the bottom for the heat flow program of Earth Physics Branch and for underwater photography by the National Geographic Society (N.G.S.). The echo sounding and seismic reflection profiling equipment were adapted from geophysical survey systems that are used conventionally aboard marine research vessels. Special timing equipment was designed to adjust the triggering rate of these sounding systems to the slow and variable speeds of the drifting ice cover. Other specialized techniques were implemented to protect the equipment from severe cold, to "tune" the systems for deep water work, and to reduce the interfering effect of ice noises on the reflected sea bottom signals.

The geological activities complemented, and were coordinated with, the studies of several other programs covering the geophysics of the ridge, oceanography of the water column, and the navigation and position fixing of scientific observations. The Earth Physics Branch and its associates assessed the geophysics of the ridge by investigating its physical properties.

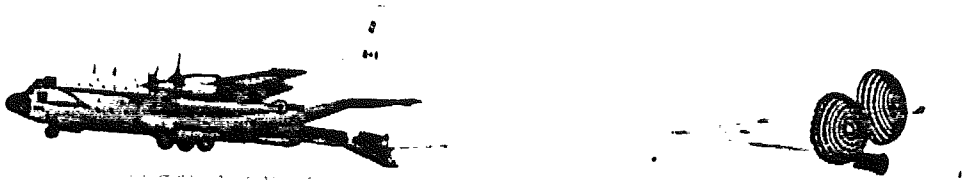

A Canadian Armed Forces Hercules aircraft delivers about 15 tons of building materials on articulated sled pallets in early April. About 200 tons of supplies were ferried and delivered to the LOREX site by this LAPES (Low Altitude Parachute Extraction) system. (B.I.O. photograph)

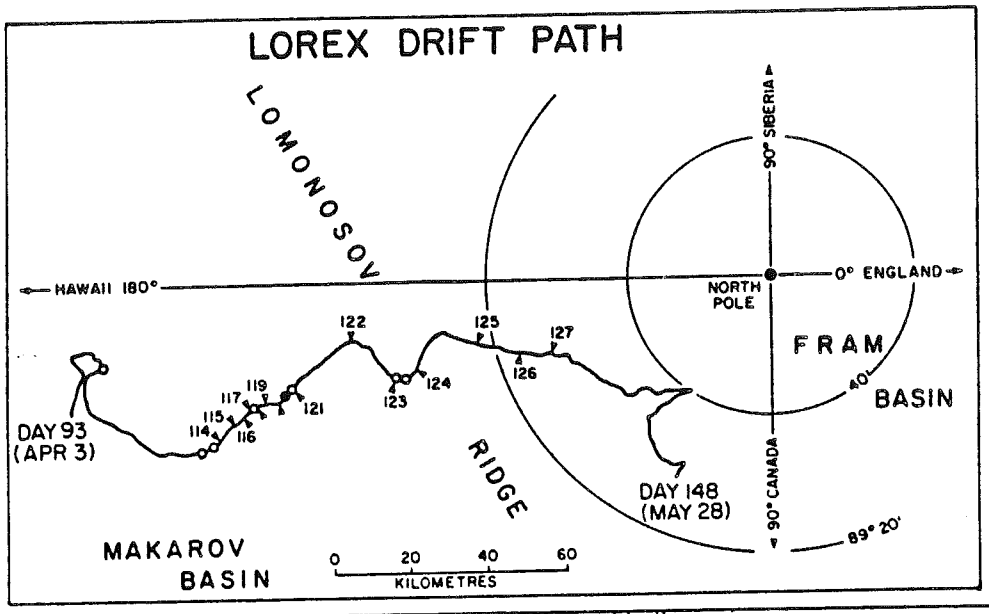

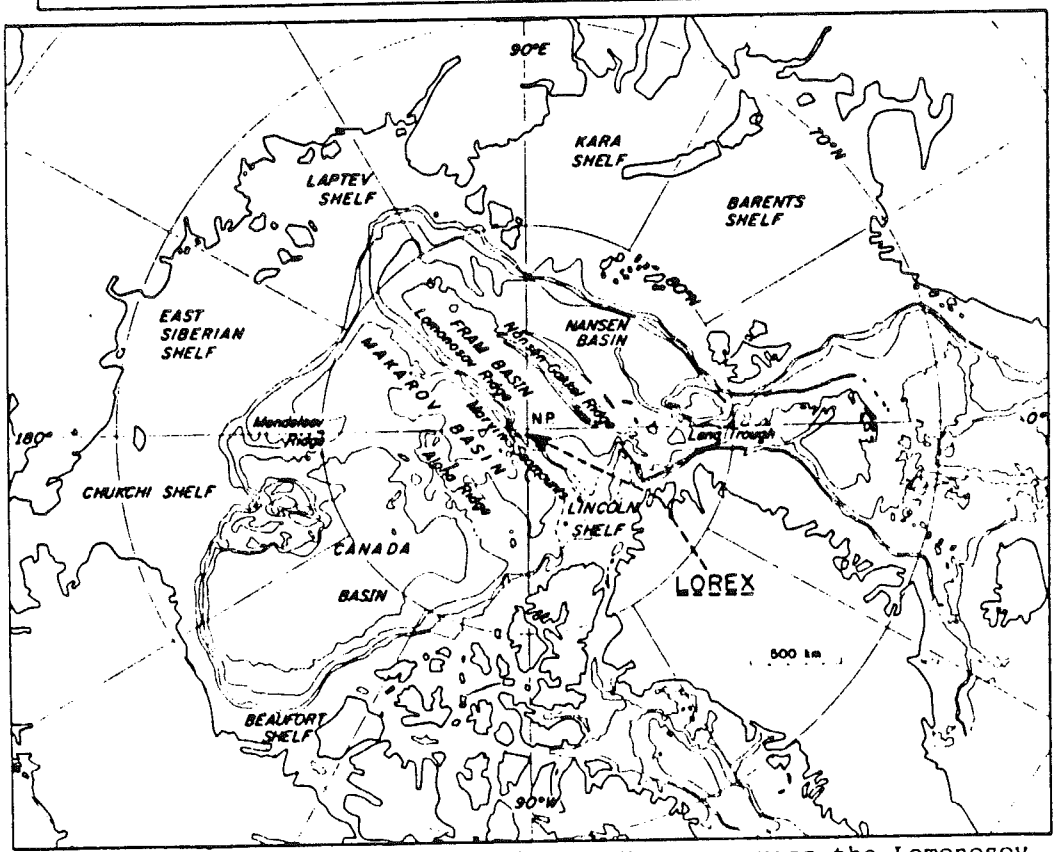

The detailed drift path of the main LOREX camp across the Lomonosov Ridge near the North Pole, April 3 to May 28, 1979, is shown above a regional map of physiographic features in the Arctic Ocean. Two satellite camps about 60 km distant drifted on parallel routes above and below the path shown for the main camp. The satellite camps supported much of the oceanography while marine geology and heat flow studies were concentrated at the main camp. Gravity, seismology and magnetic studies for the most part were conducted regionally using air support. Regional map courtesy of Jack Sweeney, Earth Physics Branch, E.M.R.

By using refraction seismology techniques, Alex Mair, Gutz Buchbinder, Dave Forsyth and Don Anderson measured variations in the seismic wave velocity of the Ridge rocks and the mantle below. Gravity and bathymetry surveys, conducted by Hans Weber and Jack Sweeney with Dave Halliday and Nicholas Courtier, revealed regional variations in the shape of the ridge and in the density contrast of its rocks. By measuring magnetic fields conventionally and by observing a time series in magnetic gradients just below the ice, Ron Niblet, Ron Kurtz, Adrian Camfield, Richard Coles and Malcolm Drury hope to detect the presence of naturally induced electrical currents in the earth and ocean and to infer variations in the electrical and magnetic properties of rocks in the ridge vicinity. From measurements of the flow of geothermal heat at the ocean floor Alan Judge and Vic Allen will compare the thermal conductivity of ridge rocks with those beneath the adjacent ocean basins. Peter Hood and Tony Overton with Robbie Burns from G.S.C., implemented respectively, aeromagnetic and intermediate-depth seismic reflection studies to provide additional information on the distribution of magnetic properties, seismic wave velocities and rock structure in the Lomonosov Ridge area.

With receivers, computers and teletype machines nursed by Dave Wells, Fred Muise and Sid Spencer from the Bedford Institute of Oceanography, satellite signals were tracked and processed to fix the position of the drifting ice camp within 100 m about every hour for the whole two-month period. These positions were "fine-tuned" by Dave Wells (B.I.O.) and Joe Popelar (E.P.B.) as the primary reference for locating all scientific observations. Also by comparing the satellite transit positions with those determined by star observations using a levelled telescope, Gerry Johnson (University of Minnesota), Bob Lillestrand (Control Data Corp.), with Brian Hennessey and Larry Mousseau (Geodetic Survey of Canada) feel that it may be possible to measure deflections of the vertical, and thereby infer the gravitational attraction of nearby dense rocks in the ridge or adjacent ocean basin.

Investigations of the water column complemented the geophysical and geological studies and took advantage of the logistic resources of the LOREX program. Chemical oceanographers Robert Moore and Malcolm Lowings from Dalhousie University analyzed water samples to determine their composition and age. Ocean currents were measured in the upper 1,500 m of the water column by Paddy Stalinski and Paul Peltola from McGill University and physical oceanographers Knut Aagaard with Clark Darnall and Steve Harding from the University of Washington moored current meters within 200 m of the bottom to survey water movements over the crest and past the base of the ridge. Experimental measurements on the long distance propagation of sound in the ocean were conducted by Barry Allen of Lamont-Doherty Geological Observatory between LOREX and FRAM 1,700 km distant (84°30'N, 6°50'W).

FRAM 1 was a multidisciplinary, international scientific camp sponsored by the U.S. Office of Naval Research. As presently planned the FRAM projects will continue to at least 1982 as a series of annual Arctic Ocean expeditions with the disciplines and locations changing from year to year. FRAM 1, in 1979, operated concurrently with LOREX within 40 to 120 km of the active Nansen sea floor spreading ridge. Among the participants was a Canadian team from the Atlantic Geoscience Centre staffed by Ruth Jackson (G.S.C.), Dave Heffler (G.S.C.), Ian Reid (Dalhousie University) and Don Locke (G.S.C.) who measured sediment thickness and ocean crustal structure using reflection and refraction seismics. A.G.C. plans to continue these investigations in the Arctic Ocean at future FRAM sites.

Except for the aeromagnetics, all LOREX studies depended on the sea ice for support and transport. Living quarters for 30 people were established on strong ice, several years old, in three locations about 60 km apart once the six-month polar night waned in late

Some LOREX personnel on the ice April 22, 1979 (Photograph courtesy of National Geographic Society - Kristof). Front row from left to right: Dave Wells, (B.I.O.), Tony Overton (G.S.C.), Sam Raymond (N.G.S.), Alan Judge (E.P.B.), Brian Bornhold (G.S.C.), Norm Fenerty (B.I.O.), Fred Jodrey (G.S.C.). Second row from left to right: Robbie Burns (G.S.C.), Ernie Tymrick (P.C.S.P. Air Support), Wayne Oryschack (P.C.S.P. Air Support), Joe McInnis (N.G.S.), Al Giddins (ABC TV), Gilbert Grosvenor (N.G.S.), J.R. (Hans) Weber, LOREX Chief Scientist holding Peary's flag, Name not recorded (Press Support), Stephen Nourse (P.C.S.P Air Support), Vic Allen (E.P.B.), Steve Blasco (G.S.C.). Back row from left to right: Dave Halliday (E.P.B.), Name not recorded (Press Air Support), Russ Bomberry (P.C.S.P. Air Support), Frank Benoit (P.C.S.P. Chef), Fred Muise (B.I.O.), Joe Jenko (Press Air Support), Peter Hill (P.C.S.P. Air Support), Name not recorded (Press Support), George Benoit (P.C.S.P.). The LOREX activities attracted considerable attention from the Press. Additional organizations that sent reporters besides those already mentioned included CBC-TV, Weekend News Supplement of The Canadian, Québec Science, Canadian Press and the Edmonton Journal.

Figs. 1-10, Members of LOREX team. (1) Fred Alt (P.C.S.P.) LOREX Camp Manager; (2) Fred Jodrey (G.S.C./A.G.C., Dartmouth) holed up while talking to Robbie Burns (G.S.C., Ottawa); (3) Alex Mair (E.P.B.), Seismology Chief; (4) Dave Forsyth (E.P.B.), seismologist, in one of his busier moments; (5) Jack Sweeney (E.P.B.); (6) Steve Blasco (G.S.C./A.G.C., Dartmouth); (7) Barry Allen (Lamont-Doherty) left, with Paddy Stalinski and Paul Peltola of McGill University; (8) Joe Popelar (E.P.B.); (9) Santa Claus disguised as Roger Belanger (B.I.O., Dartmouth); (10) Chief Scientist Hans Weber (E.P.B.), second from left, convinces his management their money is well spent, Ken Whitham (E.P.B. Director-General) on left with George Hobson (P.C.S.P. Director) on right and John Keys (E.M.R. Adm. for Science and Technology).

March. The expedition depended entirely upon the rather important assumption that the average movement of ice in the Transpolar Drift Stream would carry the scientific party and their instruments across the Lomonosov Ridge in two months or less. Because of wind and current stress on its upper and lower surfaces, the Arctic ice canopy is nearly always in motion. Fortunately, in this assumption and in most other aspects of the experiment, we were successful.

By the end of the first month, the main LOREX camp was drifting onto the flanks of the ridge, at times with speeds up to 1 km/hour but usually about 1 km/day. And by the end of the second month, we had run down the quarry completely, passing within 37 km of the North Pole on May 17. We were euphoric. We, as marine geologists, had captured 40 short cores, 10 grab samples, 4 dredge hauls, 1,100 bottom photographs, 1,080 hours of echo sounding, 42 profiles of temperature and/or sound velocity, 14 plankton tows and 880 hours of airgun reflection profiling, all nicely distributed across the Lomonosov Ridge and into the adjacent Makarov and Fram ocean basins at 3,900 and 4,200 m depth respectively. Except for the seismology team who were constrained by adverse flying conditions and the magnetists who lost instruments to "hungry" pressure ridges everyone else had done as well or better. With all this in hand, we began talking up an assult on the Alpha Ridge in the older western Arctic Ocean in the early 1980's! Even the prospect of shepherding home tons of freight scarcely dimmed the exhilarating sense of accomplishment at mastering the challenge of this unique Canadian polar expedition. LOREX 79 had come a long way in advancing the sophistication and scope of Arctic investigations since the Polar Continental Shelf Project initiated marine geology studies in the Canadian Arctic Archipelago two decades ago.

Paddy Doyle (P.C.S.P. Air Support), winner of LOREX track and field event, enjoys his prize. (B.I.O. photograph).

Our preliminary geological results which appear in G.S.C.'s Current Research, G.S.C. Paper 79-1C, suggest the Lomonosov Ridge is indeed a sliver from the old Eurasian block but not all participants agree. The first major exposure of all the LOREX results will occur next May 22-27 in Toronto at the joint scientific meetings of the Canadian and American Geophysical Unions. Then, as new facts and ideas unfold, we shall perceive to what extent the theories of Arctic Ocean evolution are confirmed or modified and in which directions future research should go.

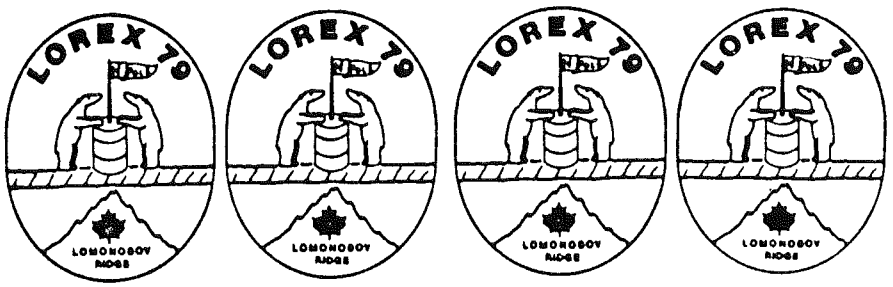

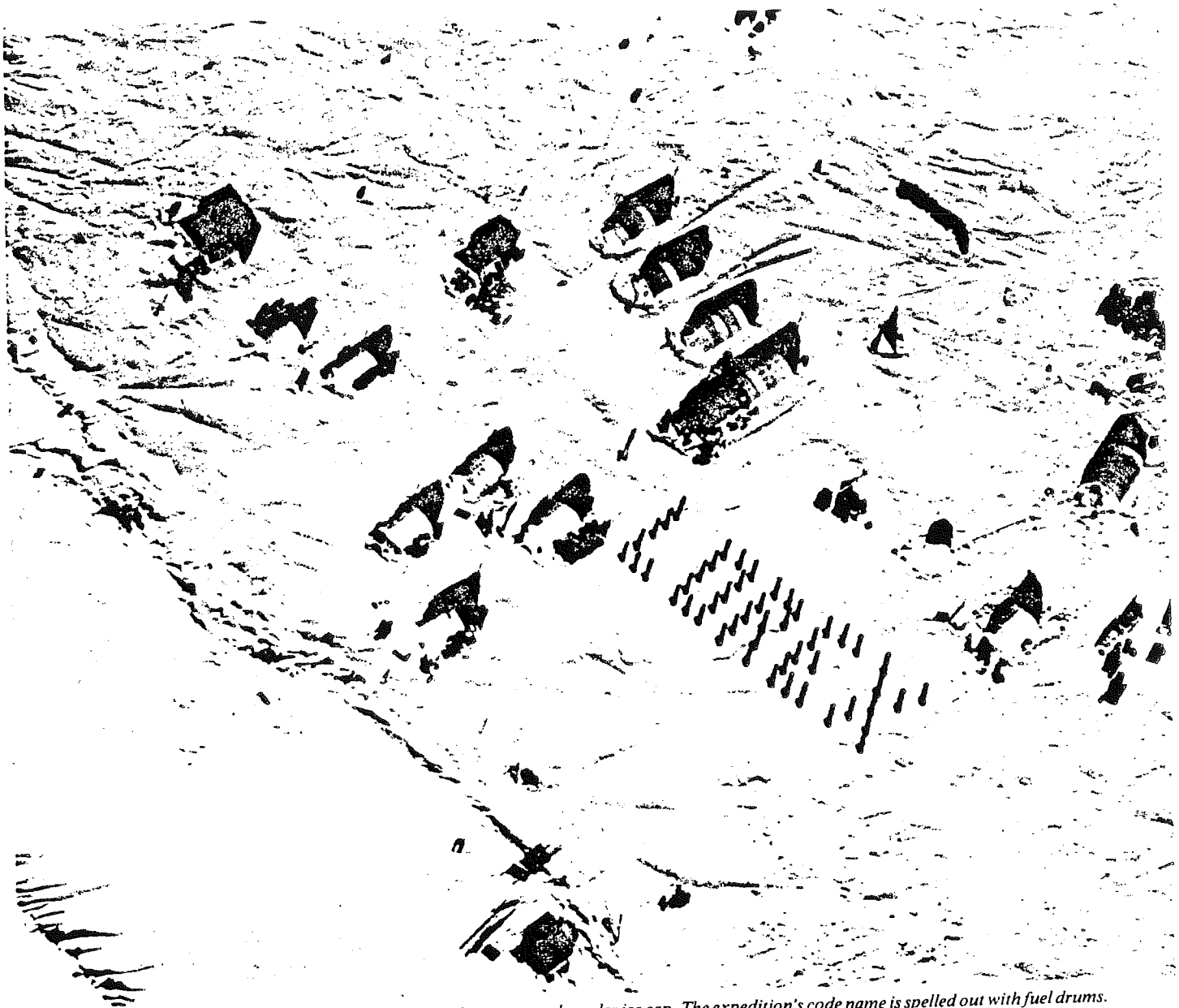

For two months scientists lived and worked at this camp on the polar ice cap. The expedition's code name is spelled out with fuel drums.

1—Lorex Expedition

Joe MacInnis explores the Arctic depths

Canadian Geographic, v. 100, no. 6, p. 18-26, 1980

Joseph B. MacInnis

Over my head, the ice pressed down into the ocean with a furious invisible force. Flat and hummocked, it stretched like an ominous hurricane cloud all the way to Russia. From within the comfort of my diving suit I looked up at the thin wash of sunlight trying to squeeze through the iron-hard roof. The dominant colours were navy blue and purple, a massive twilight stitched together by pale streaks where the ice was beginning to crack.

I was swimming alone in the sub-zero waters below ice-station *Lorex*, a small scientific community drifting towards the North Pole. *Lorex*, a two-month expedition, had been established in March of 1979 by the Canadian government to learn more about the unknown earth beneath the central Arctic Ocean and its relation to the Canadian Arctic.

I finned over toward a rectangular tray hanging in the darkness like a balloon's gondola. Repetitive low-

Dr. MacInnis, a Fellow of this Society and a member of the Order of Canada, is the internationally known diving doctor, author, lecturer, and film-maker. A world authority on medical aspects of diving and working at great ocean depths, he has developed a lively interest in maritime history, oceanography and the underwater world. Last summer he located the wreck of HMS BREADALBANE, *sunk 127 years ago in the Arctic. The purposes and work of the Lorex expedition, with which he deals here, are explained in the article which follows, written by Dr. J.R. Weber.*

pitched bleeps emitted from eight black boxes within, echoing from the seafloor some three miles below. Over the two-month period these recorded echoes would provide a profile of the ocean floor and would delineate the shape of a rugged submarine mountain chain.

In a faded pearl light beyond the gondola hung a silver cylindrical air gun. Silent now, it sent out a periodic ear-shattering blast that travelled beneath the ocean floor and back, reflecting geological secrets of past millennia.

I swam slowly over to the cold corona of light surrounding a small shaft cut through the ice. As I watched, a vertical cylindrical metal frame issued from the light and stopped below the hole. Then, with the precision of a satellite, the frame pivoted slowly and came to rest in a horizontal position, exposing a camera and strobe light. After a few seconds it started down, lowered by a thin cable into the towering walls of blackness. I watched it grow smaller and disappear, beginning an hour-long journey to the bottom of the sea.

I swam over to the hard white edge of the shaft and looked up. Six feet above me, framed by iridescent ice and folds of clear water, were five scientists and technicians of ice-station *Lorex*.

Although ice is the most obvious feature of the Arctic Ocean, these men had not come here to study it. Their main interest lay some 13,000 ft. below in the sunless abyss. The 16 *Lorex* projects, supported by 34 tons of scientific instrumentation, were aimed at learning more about the solid earth beneath the sea.

Isolated by cold, darkness and distance, the Arctic is the world's least known ocean. In ancient times people living in Europe believed that the far north was the end of the world, Ultima Thule, a giant precipice suspended in darkness. In the Middle Ages people imagined that the top of the world held a huge continent crossed by four giant rivers. They were almost right; there is a land mass here, but it is submerged beneath freezing miles of water and ice.

The floor of the Arctic Ocean is dominated by a huge triangular basin. This central basin, almost twice the size of Alaska, has an average depth of 12,000 ft. Running across its width for almost 1,100 miles is a massive rib of rock, a towering spine of the Earth called the Lomonosov Ridge, named for an 18th Century Russian scientist and poet, equally little known to North Americans. Understanding the nature and origin of this feature was the key to solving the geologic history of the Arctic, and the expedition was dubbed the Lomonosov Ridge Experiment, shortened to Lorex.

I plunged my eyes deep into the gloomy waters and tried to see the ridge. Neither just mountain range nor just escarpment, but a bit of both, it runs from the northern tip of Canada's Ellesmere Island, almost under the Pole, to Russia's New Siberian Islands. The ridge is the major feature of the Arctic Basin and divides it into the Amerasia and Eurasia Basins. Unlike any other part of the ocean floor, this unique topographical feature seems to evoke those ancient biblical words: "Let there be a firmament in the midst of the waters, and let it divide the waters from the waters."

The Lomonosov Ridge was discovered by the Russians in 1948. Working from a series of ice stations, they found a steep wall of rock and mud rising almost 10,000 ft. above the sea bed. Almost as long as the distance between Ottawa and Halifax, or Saskatoon and Vancouver, its flat, plateau-like top is, in some places, less than 20 miles across.

Twenty-six men in rotating teams would camp for two months on the restless plate of ice floating over my head. Working for 18 hours a day they would send and receive thousands of signals to and from the sea floor. Dozens of instruments and cameras would allow them to study the shape and structure of the seafloor and ridge. Every few hours they would monitor a satellite to plot their exact position of drift. Their constant hope was that the unpredictable currents would carry them over the ridge at least once before the camp broke up into its final white pieces — and they

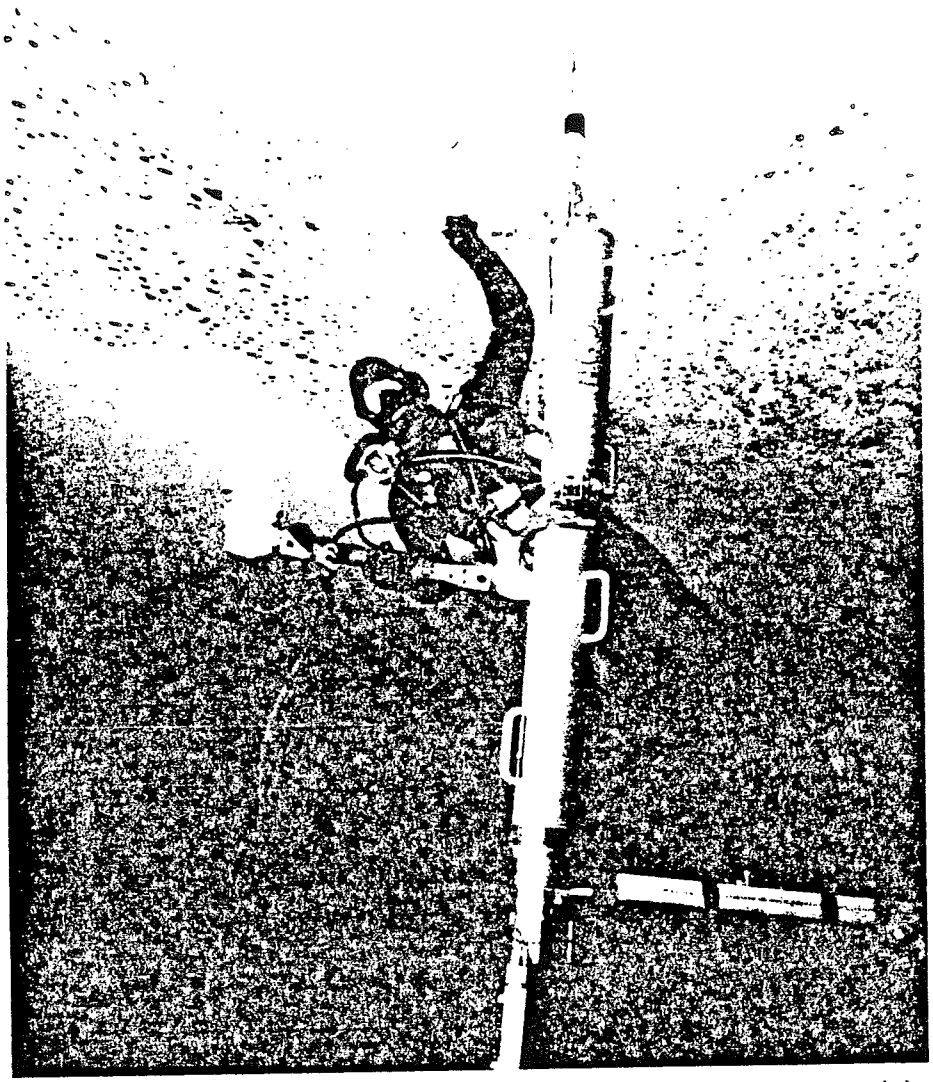

Swimming underneath the pack ice supporting the Lorex camp, Joe MacInnis helps guide an underwater camera through the ice hole as it is being winched to the surface.

did this.

I swam back toward the dive hole. In the clear polar water it was difficult to believe that the ice above me was drifting two miles a day towards the ridge. There was no sensation of movement only a quiet crystal stillness. Just before surfacing I looked up. The thin jagged crack that ran below the dive tent seemed wider... or did it?

After the dive I walked across the ice to "downtown" *Lorex* to chat with Dr. J.R. Weber, the chief scientist. From the window of his small bunk house and office I could see a dozen white tents and red, tunnel-shaped dwellings. They were clustered around a snow-trampled square and two of them contained diesel generators, the electric pulse of the camp. In the centre of the square someone had placed a small salute to the 24 hours of Arctic daylight — a sundial.

"One of the most important factors in studying the seafloor from the polar drifting station," Dr. Weber told me, "is knowing precisely where you are. We've been working on this problem since my first North Pole expedition in 1967. It meant developing new techniques for obtaining star and satellite fixes."

In a low wooden structure only a few feet away across the frozen snow, two men stood next to a computer that monitored some 20 Transit satellite passes each day. By measuring the rate of change of a satellite's position they were able to plot the erratic path of *Lorex* as it drifted closer to the Pole.

"To give us a more detailed view of the Ridge, we've set up two auxiliary camps 25 miles from here," Dr. Weber continued. "In addition, these camps allow us to triangulate our position when we are using the helicopter for scientific work."

Dr. Weber used the helicopter almost every day. He flew out ahead of the main camp, landed on the ice, and surveyed the earth far below him. His "eyes" were two instruments resting on the ice that measured subtle changes in the earth's gravity and topography. Detailed analyses of the data would tell Weber much about the shape of the ridge and whether it was composed of volcanic or sedimentary rock.

It was from a helicopter that you began to appreciate the diminutive size of *Lorex*. As you lifted away from the buildings the vastness of the ice took over. The horizon filled with bleached and broken floes, and as the helicopter gained altitude, the camp was swiftly lost in the whiteness.

One day I flew over to *Iceman*, the smaller of the two auxiliary camps. As we approached from the air I could see the ominous shadow where the pack ice had recently split open. One morning five men had awakened to see black water not far from the door of their sleeping tent. Their generator was on the other side of the crack,

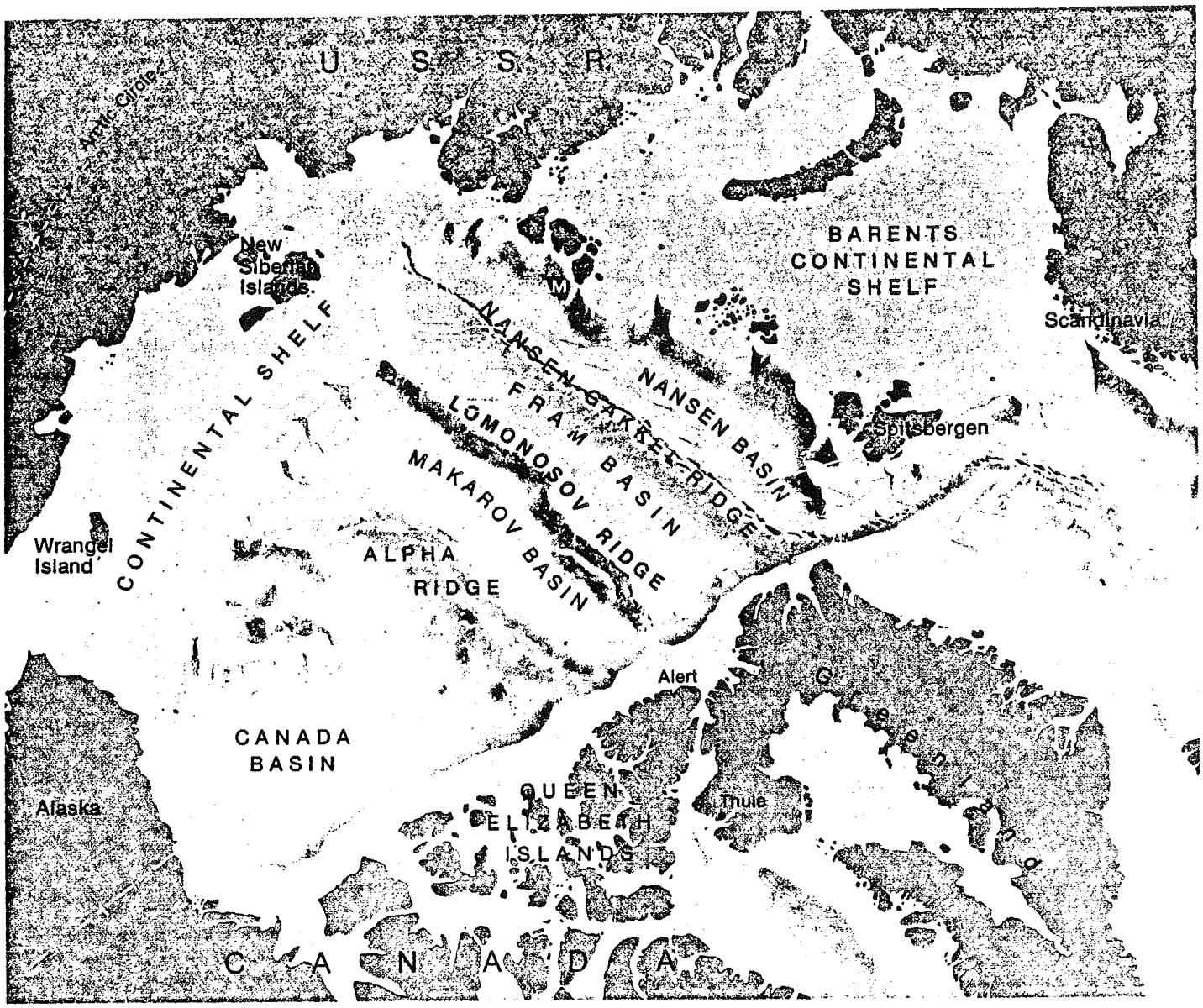

The Lomonosov Ridge is a steep-sided rise which bisects the Arctic Ocean. The Nansen and Fram basins together are referred to as the Eurasia basin; the Canada and Makarov basins form the Amerasia basin. The Transpolar Current, which carried the FRAM *and the* SEDOV *across the top of the world, is indicated by blue arrows.*

slowly drifting away with the retreating floe. It was retrieved by helicopter. As we landed I could see its blue diesel breath puffing into the sky.

At the far end of the *Lorex* main camp was a red tunnel tent with a hand-lettered sign posted over the door: *Lorex Slum and Polar Bar.* As you stepped out of the sting of the polar wind and into the warmth of the tent you were greeted by the jovial laughter of Steve Blasco, a marine geologist. Blasco, who looks like Santa Claus with a dark beard, was a man obviously in love with his work. Nothing delighted him more than showing a visitor through the cluttered interior of his tent, explaining the complexity of his computers, sensing equipment, and data displays.

Blasco has a non-stop sense of humour. If you arrived late at night he would offer you smoked oysters and Cointreau while gleefully describing "the frightening hardships of Arctic research."

Every 60 seconds, Blasco's tent floor trembled with a sledge hammer thump. Looking down through a small ice hole at the rear of the tent you could see a profusion of bubbles. They came from the submerged air gun — the same gun I had seen earlier on my dive. Like the pop produced by a collapsing paper bag, a sound wave was generated by the sudden release of high pressure air in the water.

"One day the gun jammed open," Blasco told me, "and the air roared out at 2,500 pounds per square inch. The Arctic Ocean surged up the hole into the tent under our beds and out the door. For a minute I thought we'd sprung a leak."

I looked closely at the intricate trac-

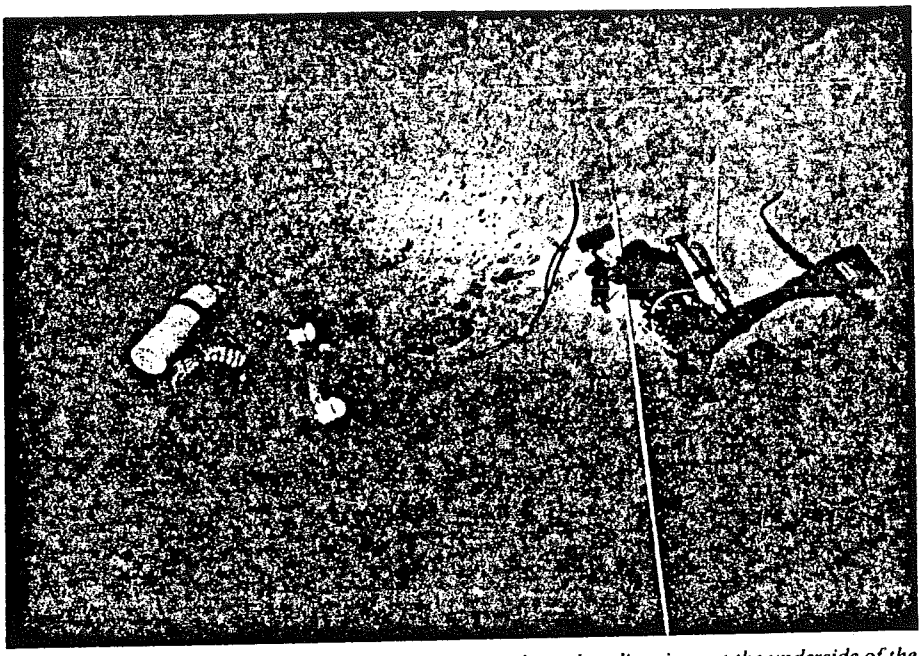

Using powerful lamps, Dr. MacInnis (L) and another diver inspect the underside of the ice, which blocks virtually all sunlight.

ings of the ocean floor being recorded on two of Blasco's instruments. "Marine geology is a little like looking at the cross-section of a cake," he said. "The bleeps coming from the gondola, as you call it, reflect off the seafloor and tell us about the shape of the cake and the thickness of the icing. The Lomonosov Ridge is a steep-sided rugged mountain chain with only a thin veneer of soft sediments on its crest in this area. The air gun has a much more powerful output and reflection, and tells us about the cake itself. The ridge is composed of gigantic blocks of rocks crushed together by some herculean effort of nature."

Blasco steered me gently over to a thin cylindrical core of mud stretched out on the table. One of his assistants, Brian Bornhold, was carefully splitting it down the centre.

"To determine what kind of icing we have, we collect samples of the seafloor by dropping heavily weighted steel or plastic barrels into the bottom, and by retrieving the sediment plug from each barrel. We also take hundreds of photos of the seafloor. It's like fitting the pieces of a giant puzzle together. Each piece complements the other."

A few days later I walked a quarter of a mile from the main camp with Tony Overton. I watched as this gentle geophysicist, fingers working against the cold, prepared the fuse and lowered a 40-pound dynamite charge through the ice into the sea some 100 ft. down. We waited in the clock-tick of a silent white world. The explosion thudded up against the ice floe like shock waves from an earthquake.

"This is what is called an intermediate seismic," Tony said, "a look at the deeper layers of the cake. To study the sediments thousands of feet below the seabed, we need a higher energy source. But the really big explosions, some of them 1,500-pounders, are being fired off by Alex Mair. They have been detected by instruments as far away as Greenland."

One day I dove beneath the ice with photographer Al Giddings to film the irregular white keel of a pressure ridge. We dropped through the six-foot dive hole and swam cautiously "south" for about 150 ft. Hard above our eyelids were the beginnings of hundreds of square miles of ice, so we swam hesitantly, concerned about leaving the open security of the dive hole.

Slowly at first my 2,000-watt movie lights picked up distant shivers of white. These faint wildfire reflections were the sawtooth folds and crags of the pressure ridge. Gliding through the lucent salt-deep I could almost feel the forces that had formed this ridge and thousands like it across the Arctic. Here was the submerged evidence of two giant floes which had crashed together with sounds of cannons, creating the brute beauty of fractured blocks driven deep into the water.

I looked ahead at the tangled whiteness that ran out to the limits of my vision. Carefully, with Al at my elbow, I swam into an opening between two piano-sized blocks. Around the corner was a quivering ice-water corridor that led into the heart of the ridge. I stopped. Here, shaped in ivory, were the slanted forces of nature, delicately balanced.

The shattered ice and its internal

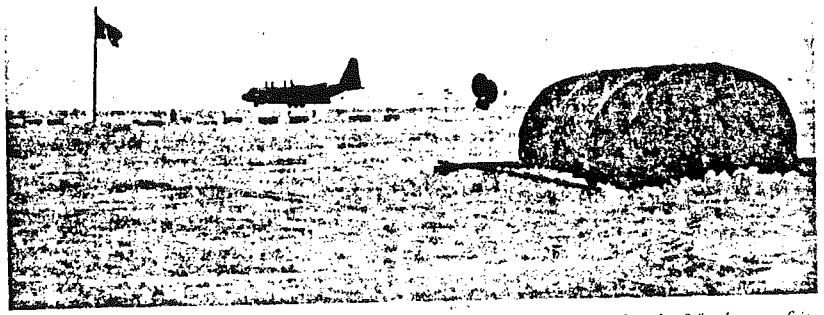

Parachutes burst out of a low-flying Hercules transport to pull a load of fuel out of its cargo hold. About 200 tons of equipment and supplies, including 772 drums of diesel fuel, were airlifted to the Lorex camp using low altitude drops; this aircraft is too large to land on the ice.

It takes a strong sense of humour to cope with living on drifting ice for two months. Hence the sign on Steve Blasco's tent, which was the headquarters for Lorex's marine geology experiments. Here Blasco tended his complex array of instruments and data recorders, served liqueurs to midnight guests, and slept when he could. In this photo he and Mike Lewis, also of the Bedford Institute of Oceanography, are moving equipment after a crack opened underneath the tent and it had to be moved to firmer ice.

architecture were a symbol of how little we know about the deep Arctic Ocean. Although the ice lies on the surface, few humans have explored its inner chambers. Here was another dominion, similar to and yet different from the old earth far below. One was bathed in sunlight, the other in perpetual darkness. Each was in motion, although moving to different rhythms. Both were mostly solid, although not forever.

On the way back to the dive hole I looked closely at a thin crack that hung like a blue lightning bolt in a purple sky. This time I was certain. The crack was wider.

Several hundred yards away from the warmth of the dive tent was a box-like structure of raw plywood. From the outside, only two small windows and a black stove-pipe distinguished it from a large packing crate. But the structure was well insulated and a small stove could raise its interior temperature to 150°F. *Lorex* boasted that rarest of all Arctic structures — a sauna.

The sauna was built by Lief Lundgaard, the camp's resident ice expert, who moved around as silently as a snowfall. To look into his bearded face and bemused eyes was to be reminded of his countryman, Fridtjof Nansen, the first scientist to explore the high Arctic systematically. As a scientist and writer, Nansen was perhaps the most outstanding figure in the distinguished line of Arctic explorers from Frobisher to Admiral Byrd.

Unlike those of us living comfortably at *Lorex*, Nansen did his work the hard way. In 1893 he and 12 companions sailed their small ship, the *Fram*, into the ice north of the New Siberian Islands. Drifting for 35 months over thousands of miles, they gathered enough information to form the first scientific image of the Arctic Ocean. Among other things they discovered that it had a deep central basin. In June of 1896 the *Fram* emerged triumphantly from the ice north of Spitsbergen.

Since Nansen's time this cold and distant ocean had been studied at intervals by small groups of men flying over it in aircraft and drifting across it in ice camps. In 1937, the Russians built their first North Pole station, Severnyj Polyus I, at 89°25′ North. Since then they have established over 25 scientific stations in the North Pole area. Since the 1950s, Canadian and American scientists have been busy

taking the oceanographic pulse of the Arctic. During *Lorex*, the United States conducted a parallel series of experiments at ice-station *Fram*, about 100 miles north of Greenland.

Lundgaard's daily challenge was to make life as comfortable as possible for the *Lorex* scientists, and to reassure them about the stability of the ice underfoot. He and camp manager Fred Alt seemed to be everywhere, solving problems and organizing the hundreds of details that kept the camp running. Both men had been on the ice in early March to receive the first shipments of food, scientific equipment and diesel fuel. In his spare time, Lief built the sauna.

At 40°F below, a sauna is a heart-pounding experience. One evening I went inside and stayed until the sweat dripped off my forehead. When I opened the door to come out there was a crash of sunlight and my vision went misty. I looked down to see my body smoking in a cloud of steam and the hair on my arms turning frost-white, as if suddenly aged.

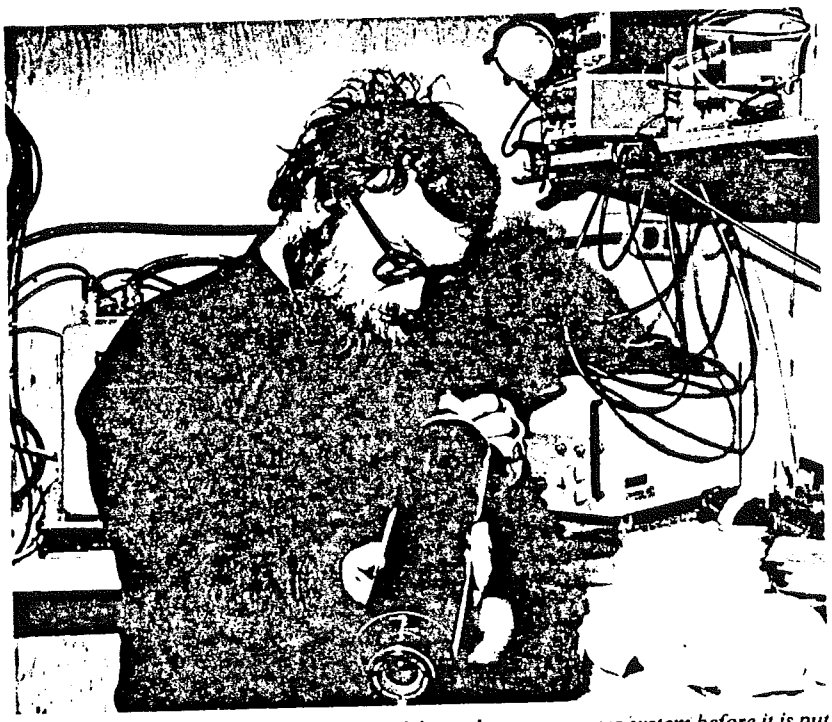

Above: Steve Blasco does a final check of the underwater camera system before it is put into its stainless steel casing and lowered to the ocean floor. Below: first close-up photos of the crest of the Lomonosov Ridge show coarse gravel sediments, about 90 million years old.

Within seconds the vapour diminished and I felt a stab of discomfort in my feet. It was necessary to keep moving to prevent them freezing to the ice. Someone had planted a striped pole next to the sauna and like everyone else in camp, I couldn't resist climbing up an incline of ice blocks to have my picture taken standing next to "the North Pole."

Even today, 71 years after it was discovered, the North Pole occupies a special place in our imaginations. We are intrigued by its frozen remoteness and fascinated by the men who made its history. They were tough, vain and single-minded individuals who plodded hundreds of miles across an unpredictable, unstable terrain. Each of them burned with the ambition to be first. Only one was.

About May 17th, after some five weeks of drifting, the main *Lorex* camp passed within 22 miles of the Pole. A few days earlier, with every scientist hunched over his recording equipment, the camp drifted over the crest of the Lomonosov Ridge. Within a distance of 22 miles the seafloor suddenly reared up from a 12,000 to a 4,000-foot depth, revealing a bumpy anvil-like plateau. Five days later, the scientists were looking down the other side, a more gradually inclined slope which resembles the foothills of the Rockies.

No one was more pleased with *Lorex's* wobbling path than Alan Judge, a geophysicist studying the dissipation of the Earth's internal heat through the upper layers of the sediments. I watched him as he prepared his thermal probe, a thin aluminum tube, packed with electronics and topped by heavy weights. In a place of such intense cold, it seemed unlikely there would be any heat under all those miles of dark water. However, the delicate instrument Judge held in his hand was sensitive to changes as slight as a thousandth of a degree.

"A series of readings across the seafloor," he told me, "can tell us if the Earth's crust below us is made up of oceanic or continental rocks. This in turn will help us determine the origin

and nature of the ridge. Did it form by breaking away from the Eurasian Continental Shelf . . . was it created by volcanic process . . . or does it have its origins in the collision of two tectonic plates?" Much as drifting floes collide to form pressure ridges of deformed ice, the surface of the Earth consists of continental and ocean plates floating on a mobile interior and, over millions of years, these plates collide to form mountain chains and ridges.

To understand the effect of a major feature such as the Lomonosov Ridge on ocean circulation, studies must be made of the miles of water that surround it. Three of the *Lorex* scientists spent hundreds of hours lowering instruments to measure the physical and chemical highlights of the depths. Each recording of temperature, salinity or of nutrients helped to resolve such questions as the origin, age and distribution of the water masses within the Arctic Ocean.

One of the most elaborate *Lorex* projects was carried out by Knut Aagaard who wanted to measure the deep ocean currents swirling aroûnd the ridge. In early April he flew out in a small aircraft, cut through the ice and released four current measuring devices. Two were placed on the crest of the ridge and two were dropped at its base. For almost two months these meters measured and stored information about the direction and speed of the hidden waters.

Finding and recovering the meters meant searching for their weak signal transmissions across miles of faceless ice. When Aagaard's small aircraft brought him within range he transmitted a command signal to release the buoyant metering devices from their heavily weighted moorings now trapped under the ice. Aagaard could home in on their transmitter. A hole was cut and divers worked through the blackness to haul each precious package back to the surface.

The reward of the search was a 52-day record of the invisible Niagaras that flowed around the ridge. As expected, the currents were stronger near the crest than at the base. They moved up and down as well as along the slope, sometimes as fast as four inches per second, and seemed to vary in speed on a time-scale of three or four days.

Gus Buchbinder from the Earth Physics Branch of EM&R wires a 50-lb. charge of dynamite to be used in a seismic study of the nature of the Earth's crust under the Lomonosov Ridge. Up to 2,000 lbs. of dynamite were exploded underwater for some experiments.

"It is a noisy ocean," Aagaard told me later, "a gusty ocean, something like the atmosphere, but on a much longer time-scale."

As Aagaard talked I realized that he shares with his fellow marine scientists a special quality of projection. Without actually going there he can transpose himself into the deep sea. His mental picture of his work is so intense that his words seemed to come, not from the surface, but somewhere just above the seafloor.

To drift for weeks across the Arctic Ocean is to wonder about the life that inhabits the waters. One afternoon a young ring seal swam up into the dive hole and peered at the strange two-

Members of the Lorex expedition worked long hours under often difficult conditions but a certain amount of tomfoolery was essential to morale. This unofficial post office in a tent was set up to receive the mail that arrived once a week from the south. Santa Claus delivered it around the camp during one of his visits to the ice station from the North Pole.

legged creatures taking his picture. He was probably looking for his lunch of polar cod, small fish about three inches long, that were attracted by our lights. Polar cod are the only fish near the centre of the Arctic Ocean.

Life does not survive easily in these bitter waters. The ice cover reduces the sun's penetration and the annual production of plankton is low compared to other oceans.

The food chains, physiology and behaviour of marine life in the High Arctic are still a mystery. We do know that certain shallow water species are found deeper at lower latitudes. But it is almost certain that many animals and plants, particularly those living in the dark corners of the major cordillera and troughs, remain to be discovered.

An effective way of searching the deep sea-floor is with lowered cameras. The *Lorex* team had two such systems both designed to work in the icy depths. During 20 lowerings over 2,500 photographs were taken, several of which showed clusters of small red shrimp paddling through the deep. These photos also record several generations of tracks and trails left by bottom-feeding creatures yet to be identified.

On one of my last dives beneath the polar pack, we slipped through the dive hole and finned over to a cluster of ice crystals hanging from the flat ceiling. It was one of several we had found, each made up of hundreds of paper-thin sheets of clear ice held together like a gathering of diamonds.

These "chandeliers," as we called them, were formed as fresh-water from the ice above dripped into the sub-zero ocean. In their sparkling interiors we saw the pale bodies of amphipods, tiny crustaceans which seemed to be hiding from bigger teeth. The sheets of ice were so fragile that if we brushed our neoprene gloves through the water next to them they shattered like broken glass.

The chandeliers were a symbol of the camp above us. In time they would break up and disappear into the sea. A hint of things to come occurred on April 27th when the ice floe which supported *Lorex* began to fracture. Within hours several cracks split the runway and an opening as wide as a street appeared beneath the dive tent. Steve Blasco was forced to move his equipment to a new location for his final month of work. On June 10th, with the expedition successfully completed, the *Lorex* camp was abandoned to the elements.

How far we had come in the 71 years since Peary! In those days of sextants and sledges, the struggle was to get to the Pole. Today, when our scientific interest ranges from satellites to the seafloor, the challenge is to gather knowledge as effectively as possible.

What emerged from the two-month *Lorex* expedition was a significant contribution to Arctic geoscience and oceanography by a small group of Canadian scientists. Although many aspects of the data have yet to be resolved, it appears that millions of years ago the Lomonosov Ridge did break away from the Eurasian land mass and that today it is inching its way towards Alaska.

Seventy years from now scientists, wearing a highly sophisticated version of today's armoured diving suits, will be able to descend to the ridge, walk along its crest, and gather first-hand information. Like human curiosity, marine science is a quest that never ends. As in the *Lorex* expedition, each fragment gathered contributes to the whole, a deepsea portrait, not entirely complete, but stunning in its beauty and complexity. □

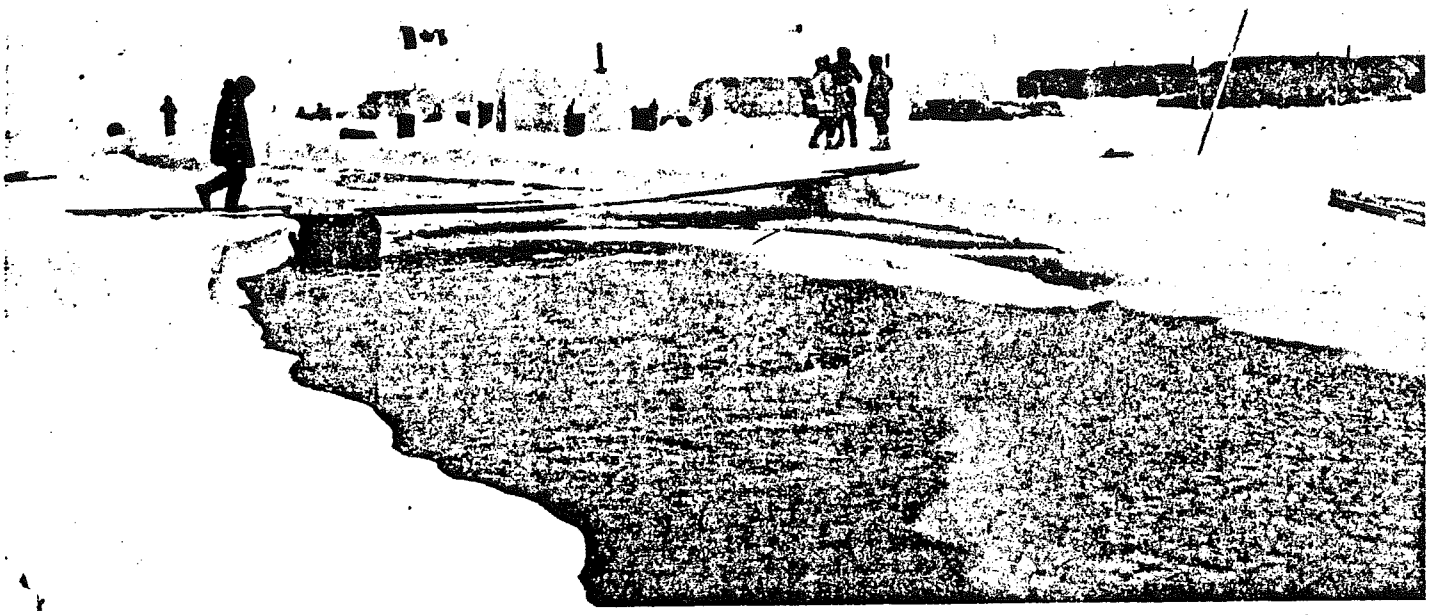

One of the many problems to contend with when you live on the polar ice cap is fissures in the ice. Midway through the Lorex expedition, a crack split the camp in two. Anyone who slipped off this bridge would have fallen into bone-chilling water, 12,000 ft. deep.

2—Lorex Expedition

Our scientists learn more about the Arctic

Canadian Geographic, v. 100, no. 6, p. 27-31, 19890

J.R. Weber

For a long time the Russians knew much more than Canadians about the Canadian sector of the Arctic Ocean.

The government of Canada has been trying in recent years to redress this imbalance of oceanographic knowledge by sending scientific expeditions north to learn everything they can about the Arctic.

The most ambitious and most recent expedition, between mid-March and mid-June, 1979, was named *Lorex* — for "Lomonosov Ridge experiment" — because it concentrated on the higher of two submarine ridges discovered on the ocean floor by Soviet hydrographers. (Lomonosov, incidentally, was an 18th Century Russian scientist, grammarian and poet.)

Rising some 8,000 to 10,000 ft. from the ocean floor, the Lomonosov Ridge extends from Ellesmere Island, high in the Canadian Arctic, past the North Pole and beyond to the New Siberian Islands, a distance of 1,100 miles. It splits the entire Arctic Ocean into the Eurasia and Amerasia basins.

As chief scientist for the expedition, I led a team varying in numbers from 30 to 36 people which occupied three camps or stations on drifting pack ice for 60 days. Drifting is a big part of the story; the pack ice is constantly being driven by winds and currents, sometimes moving at speeds close to a mile an hour.

The expedition had only 60 days for its scientific work within the three-month timetable because two weeks were needed to set up the camps and two more weeks to evacuate them.

Overall timing was dictated by two basic facts; with the polar night due to end when the sun rises March 21, it becomes light enough by March 15 to land an aircraft; and about June 15 the ice can be expected to begin melting.

Planning sustained by good luck did enable the main *Lorex* camp to drift across the entire width of the ridge, from the Amerasia to the Eurasia basin, within the more restrictive span of 60 days. One of the two satellite camps drifted within eight miles of the North Pole.

Since the historic three-year drift of Nansen's ship *Fram*, between 1893 and 1896, over the top of the world from the New Siberian Islands to Spitsbergen, there have been a number of other exciting adventures associated with drifting across the Arctic, once thought of as ice or earth or both.

Dr. Weber is a geophysicist with the Earth Physics Branch of EM&R in Ottawa. His Arctic experience dates back to 1953 when he came to Canada from Switzerland to join an expedition to Baffin Island to study the Penny Ice Cap. He has pioneered new methods of navigating in the Arctic and of studying glaciers and polar sea ice.

Dr. Weber (L) greeted Governor-General Edward Schreyer when he visited the Lorex camp on May 17, 1979. By coincidence, this was the day the camp drifted closest to the North Pole. Later, the Governor-General was taken on a dive underneath the ice by Dr. Joe MacInnis.

From the Middle Ages down to the 1890s geographers believed that the North Pole was surrounded by land or by an archipelago of islands. That concept lost credibility after the voyage of the *Fram*. It was found that, along the entire track of the *Fram*, the ocean was more than 10,000 ft. deep. This misled many to believe that the whole Arctic was a single oceanic deep.

Since World War II, the Russians have shown us that, far from being a flat abyssal plain, the Arctic basin has a very complicated structure of depressions, ridges and other elevations. Its seafloor geology is at least as diversified as that of the Atlantic and Pacific and doubtless will yield more surprises before its geological mapping is completed.

The notion after 1896 that the Arctic was one oceanic deep seemed to be confirmed by more depth soundings in the late 1930s. These soundings were made by the Soviet ice station *North Pole 1*, which drifted from the North Pole in 1937 to the east Greenland coast in 1939, and by the Soviet ice-breaker *Sedov* (previously a Newfoundland sealing ship) which drifted from 1937 to 1940 on a track similar to that of the *Fram*. A Soviet airborne expedition also made deep soundings in the Amerasia Basin in 1941.

Systematic exploration of the entire Arctic was begun by the Soviets in 1948, using aircraft to land on ice. This program was expanded in 1950 with the use of the "North Pole" series of drifting stations, and continues to this day. By 1959 they had taken more than 20,000 depth soundings of the ocean floor, as well as having done much to record water temperatures and salinity, and to collect sediment and rock samples.

Americans did not join in scientific Arctic exploration until 1951 when they mounted Operation Ski Jump, an airborne hydrographic, oceanographic and geophysical reconnaissance survey of part of the Amerasia Basin north of Alaska. This lasted two springs, and was followed in 1952 by year-round occupation of drifting ice islands.

One such island, *Fletcher's Ice Island T-3*, was occupied on and off from 1952 to 1974. Now drifting between Wrangel Island and the New Siberian Islands, it is expected to be swept into the North Atlantic by the Transpolar Current by 1983. This prediction suggests our confidence in new scientific knowledge.

The remarkably long life of ice islands contrasts with the shorter span of ice floes. Floes consist of frozen sea water, average 10 ft. thick, and can break up at any time. Ice islands are fragments from the Ellesmere Island ice shelf, and consist of fresh water ice which can be 100 ft. thick and may extend over areas of many square miles; so long as they stay in the Arctic Ocean they have a life expectancy of decades.

The Russian Severnyj Polyus (North Pole) stations are well equipped with oceanographic and geophysical laboratories, also with both rotary and fixed wing aircraft; they remain occupied from one to several years —

until they drift into the Atlantic Ocean via the Greenland Current or, for some other reason, lose their usefulness.

Until 1954 the USSR had kept secret their advances in deepsea measurements and their program of systematically mapping the Arctic seafloor. Deepsea measurements have become another science, called bathymetry. The Russians have shown they are good at it. In 1955 they published a bathymetric map of the whole Arctic Ocean, which caused a sensation for Arctic specialists on this continent. It showed for the first time the major seafloor features, including the extent of the continental shelves surrounding the ocean and the Lomonosov Ridge.

North Americans simply hadn't realized the magnitude and scope of Russian circumpolar surveying. Canadians did not know the extent of our continental shelf in the Arctic.

When the first Conference on the Seas took place at Geneva in 1958, participating countries decided that their mineral rights in the seas should extend to the edge of their continental shelves. Canadian delegates were embarrassed when the Russians produced the only existing bathymetric map which showed the extent of our Arctic shelf. And was that map correct?

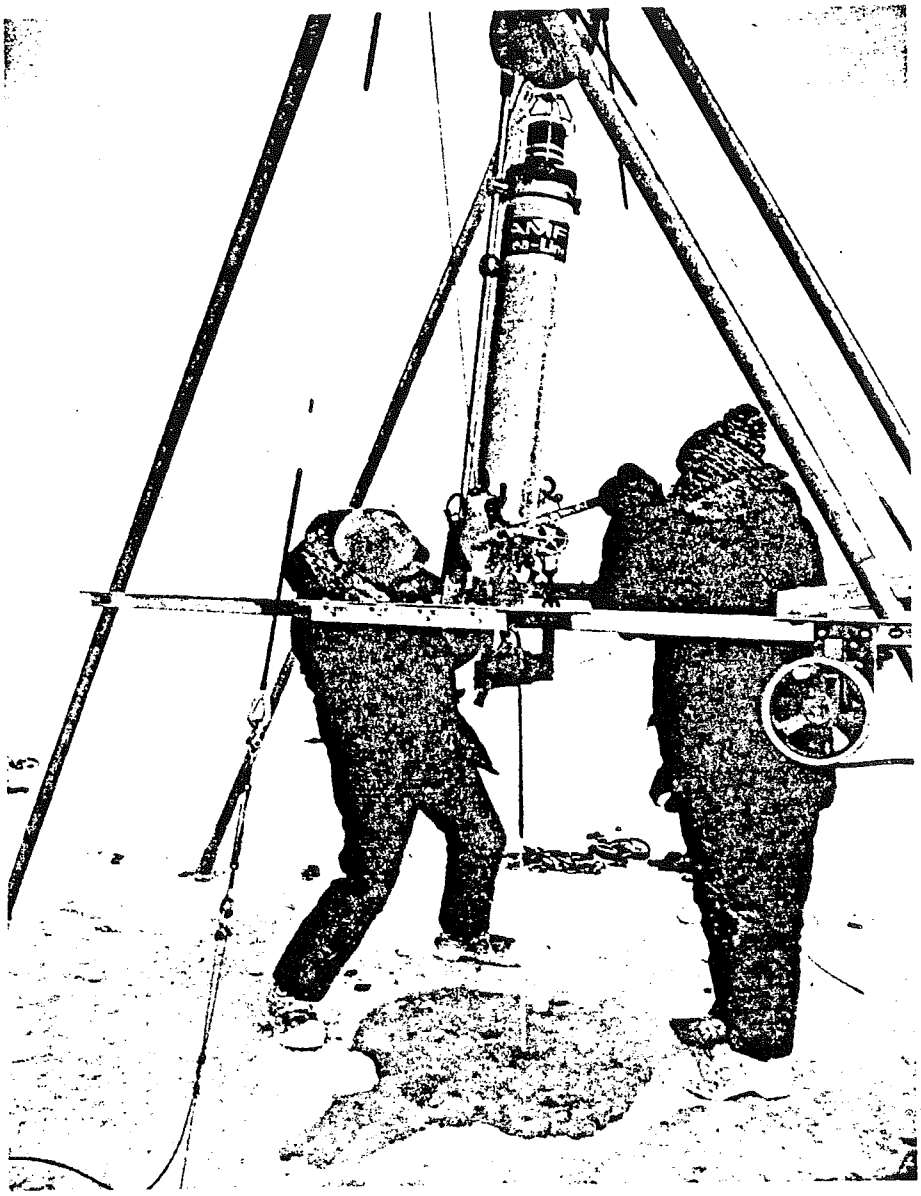

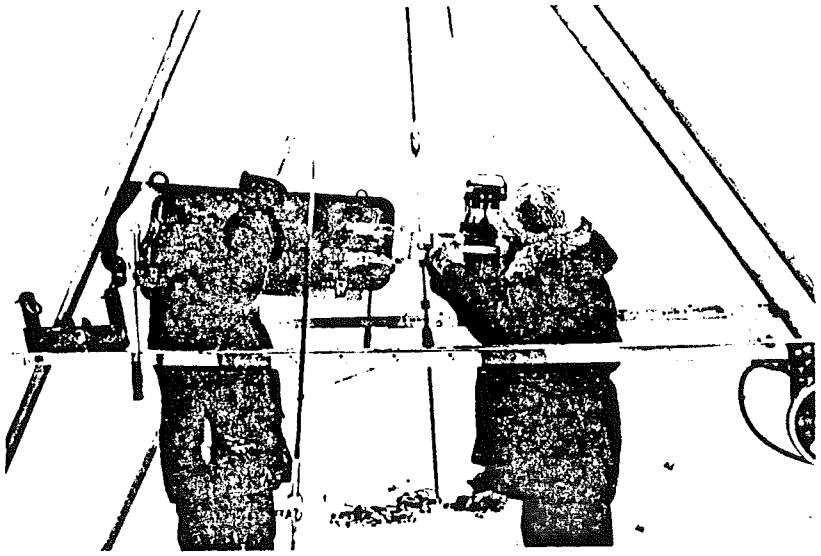

These oceanographers are standing on polar ice directly above the Lomonosov Ridge. Working in intense cold, they are struggling to lower instruments to the crest of the ridge to record the underwater currents there. Knut Aagaard (R, above) and Clark Darnall (L, above), both of the University of Washington, recovered the instruments two months later. Data stored on magnetic tape showed that pulsating currents of North Atlantic water from the direction of Spitsbergen sweep over the ridge into the Amerasia basin, slowly eroding the ridge. The yellow cylinder (above) is a transmitter-receiver called a transponder. It was activated by an acoustic signal to release an anchor, allowing the instruments to float back to the surface. Left: the current meter is the black cylinder with a rotary impeller on top; the red rectangular plate is a current vane, which records the direction of the flow.

Above: the long cold task of drilling and chopping an ice hole in order to lower scientific instruments into the sea. It took one or two days to cut each hole through ice varying in thickness between 8 to 20 ft. Above, R: Fred Jodrey, an oceanographer from the Bedford Institute, chips through the last few inches to make a clean cut. A safety line is around his waist. Below: Dr. Weber (centre) visits Snowsnake, one of the auxiliary camps. To his left are Ross Bomberry, a Canadian pilot, and Sam Raymond, president of Benthos Corp., an American manufacturer of oceanographic equipment.

Consequently Canada created its Polar Continental Shelf Project, within the federal Dept. of Energy, Mines & Resources (which then had a different name), to co-ordinate surveys of the waters over the Arctic shelf. Thus, it was in 1959 that Canadian scientists finally joined their Russian and American counterparts in exploring the Arctic Ocean — although, until 1967, their activities were confined to the shelf and the adjacent abyssal plain off the Queen Elizabeth Islands.

Then called the Dominion Observatory, the Earth Physics Branch of the Dept. of EM&R carried out geophysical expeditions to the North Pole area in 1967 and 1969. Results in 1969 indicated the Lomonosov Ridge may be a sedimentary structure of continental rather than oceanic origin. It has a steep flank and a relatively flat top; no earthquakes originate here and there are no signs of volcanic activity, past or present.

Geophysicists have suggested that the ridge was once part of the Barents continental shelf, north of European Russia, and was rafted to its present position by seafloor spreading which began some 40 to 70 million years ago, perhaps about the time that the North Atlantic opened up due to the spreading apart of continental land masses. However, the possible continental origin of the Lomonosov Ridge has not been established; clearly, understanding of the mechanics of the ridge's formation will help us to unravel structural history of the Arctic Ocean and — ultimately — may help scientists to locate natural resources such as hydrocarbons and other minerals.

Just what did we do on the *Lorex* enterprise? Very simply, we were gathering data and making observations. For the lay reader, it will suffice to mention the principal fields of study. These included: bathymetry, gravity and plumbline deflection measurements, the latter involving some 50 star observations daily in the daytime; seismic soundings; sampling bottom sediments and rocks; bottom photography; heat flow measurements; geomagnetic experiments; physical and chemical oceanography; and biological investigations.

Nineteen manned dives with a total underwater time of nine hours were made; and more than 1,000 photos of the seafloor were taken with a deepsea camera developed for Arctic use by the Bedford Institute of Oceanog-

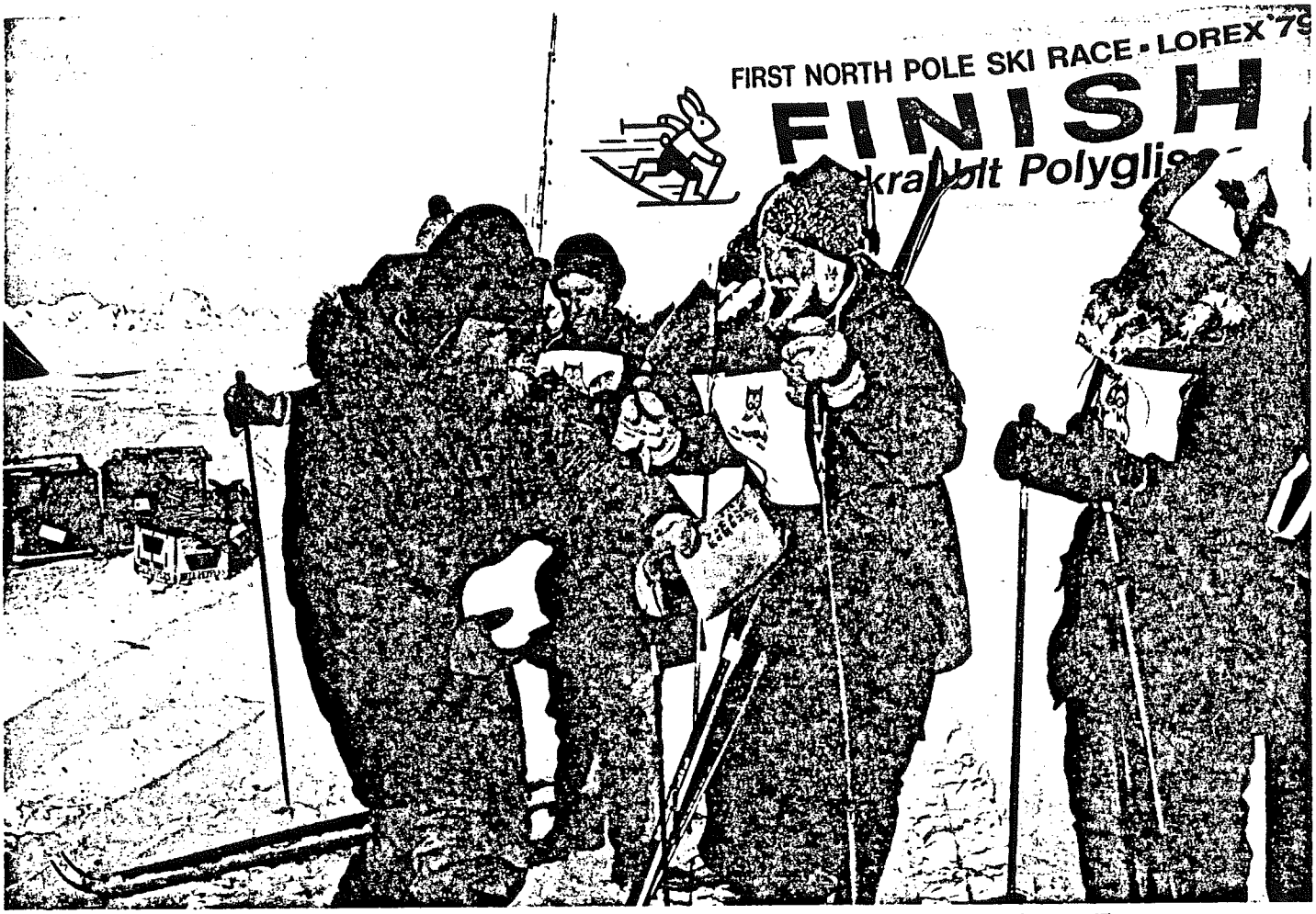

To break the monotony and to give everyone a bit of exercise, Dr. Weber organized a 2½-mile cross-country ski race. (The course was originally longer, but a crack in the ice cut across a loop in the trail.) Dubbed the first North Pole ski race, it actually took place near the Pole. Dr. Weber (centre) placed third and was awarded a polar bear sculpted from ice.

raphy at Dartmouth, N.S.

Airlifting the supplies and equipment for *Lorex* posed a major logistical problem because this meant flying 250 tons over a great distance. An armed forces squadron based in Edmonton flew 16 missions with Hercules aircraft from Thule, Greenland, to parachute the bulk of fuel and supplies down to the main camp. Personnel, and the rest of the equipment and supplies, were taken from Alert in 19 flights to the *Lorex* sites, using Dash-7 STOL aircraft.

Surveys over the ice were carried out by helicopter, while a Twin Otter provided transportation between the camps and to Alert. Radio navigational aids made it possible for these aircraft to fix their geographical positions at all times within about one kilometre.

Lorex and *Fram I*, an American drifting ice station doing oceanographic and geophysical studies, cooperated in an acoustic experiment.

Extensive bathymetric soundings and measurements, along with data from the two previous Canadian North Pole expeditions, made it possible to compile a contour map of the ocean floor. The shallowest and deepest depths recorded were 3,133 ft. over the ridge crest and 14,137 ft. in the Fram Basin.

When we consider that the early Russian hydrographers worked under relatively primitive conditions, it is remarkable that they could pinpoint the location of the Lomonosov Ridge in the polar area much more accurately than contemporary mapmakers using more sophisticated tools. While the 1955 Russian map could not delineate details precisely, the main features of the ridge were correctly located and clearly defined. The pioneer work of the Russians undoubtedly reflected their thoroughness and perseverance.

The Russians and Americans continue their long-range Arctic studies; and now Canada has a well-developed and much more active presence in its Arctic sector. Science promises to do more and to mean more in the circumpolar regions, with major implications in terms of geopolitics and economics, oceanography and geography — involving, indeed, the earth sciences as a whole.

As research and resource development unfold, the Arctic part of the world will become increasingly interesting and meaningful to Canada, and to our neighbours. □

Geos, v. 9, no. 3, p. 2-7, 1980

Exploring the Arctic Seafloor

Pack ice provides the platform for LOREX, a drifting research station which traverses the Arctic Basin over its longest mountain range

LOREX leader J.R. (Hans)Weber, born in Switzerland, obtained degrees in electrical engineering from the Swiss Institute of Technology and Physics from the University of Alberta. He came to Canada in 1953 to join the Arctic Institute of North America's Baffin Island expedition to the Penny Ice Cap, and during the International Geophysical Year carried out glacier studies in Ellesmere Island. After joining the Dominion Observatory, now EMR's Earth Physics Branch, in 1960, Weber carried out gravity surveys at sea, over the Arctic Islands and Arctic Ocean, and led two geophysical expeditions to the North Pole. He helped develop techniques to measure glacier thickness and for precise navigation in the polar region, and he invented instruments for measuring ocean tilt and wind-induced tilt changes of sea ice.

By J.R. Weber

A map of the floor of the Arctic Ocean looks like a free-form ashtray, shallow as oceans go, seldom as deep as 5000 m. It is crossed by three more or less parallel submarine mountain ranges, like ridges to hold a giant cigar. The central, and longest, ridge, the Lomonosov Ridge, passes close to the geographical north pole. It is 1800 km long and rises 3000 m above the floor of the Arctic Ocean. It bisects the ocean basin, between the Canadian and Siberian continental shelves, and separates the Amerasia and Eurasia basins (Fig. 1).

This great ridge has been the subject of speculation since it was discovered during the winter of 1948-49 by Russian scientists who named it Lomonosov after the 18th century Russian scientist-poet-grammarian.

Some geophysicists theorize that the Lomonosov Ridge was once part of the Barents continental shelf and was rafted to its present position by the process of seafloor spreading. This would have happened 40 to 70 million years ago, possibly at the same time that the North Atlantic opened up. Others suggest that the ridge was formed by other processes.

This speculation is not only academic. Understanding the mechanics of the formation of the ridge will help unravel the tectonic history of the Arctic Ocean. Ultimately, it should help scientists locate areas rich with natural resources like hydrocarbons and other minerals.

A major, multidisciplinary, polar expedition to investigate the nature and origin of the Lomonosov Ridge was conducted by EMR in the spring of 1979. The expedition was codenamed LOREX 79, for the Lomonosov Ridge Experiment 1979.

The plan was to establish three stations on the pack ice upstream of the Lomonosov Ridge and let the Transpolar Current, the same current that carried the explorer Fridtjof Nansen's *Fram* across the Arctic Ocean from 1893 to 1896, transport them across the ridge. The hope was that at least one of these stations would drift across its entire width. The timing was critical, as was the initial location of the camps.

The expedition had only a three-month window of work time. The polar night ends when the sun appears above the horizon on March 21, and daylight conditions become sufficiently bright to land aircraft from March 15. The ice begins to melt June 15, and the platform of our camp could crack and begin to disintegrate after that date. We estimated two weeks at each end of the period for the establishment and the evacuation of the camps. This left April and May for the scientific program.

The optimum location for the camps was 100 km from the North Pole and 900 km from Alert, where the ridge is narrow and the chances of drift right across it highest.

These careful calculations, plus some good luck, paid off. The main camp drifted 160 km, across the entire width of the ridge from the Amerasia to the Eurasia basin over the 60-day period of scientific work. One of the satellite camps drifted to within 12 km of the geographical North Pole.

Airlifting, over such a long distance, the staggering quantity of 250 tons of supplies and equipment required for an operation the size of LOREX was an enormous logistics problem. It was solved with the assistance of the Canadian Armed Forces 435 Squadron of the Tactical Airlift School, Edmonton, which paradropped the bulk of fuel and supplies at the LOREX site. Their Lockheed C-130 Hercules aircraft flew 16 missions from Thule, Greenland for the job. The balance of equipment, supplies and personnel was flown out of Alert in 19 flights using the newly developed De Havilland Dash-7 STOL aircraft. At the end of the operation in June the same Dash-7 carried out the evacuation of all personnel and equipment to Alert.

The population of the LOREX camps varied from 30 to 36. Surveys over the ice were by helicopter, and transport between the camps and to Alert by Twin Otter aircraft. Radio navigational aids gave the aircraft their geographical position at all times to an accuracy of about 1 km.

Geoscience studies were conducted at the main camp, while oceanographic studies were carried out at the satellite camps. Satellite camp Iceman was the site for physical oceanography including salinity, temperature, depth and current measurements, and acoustics, or sound propagation studies. Satellite camp Snowsnake housed the chemical oceanographers, responsible for nutrients and trace element sampling and carbonate chemistry.

Concurrently with LOREX the multidisciplinary expedition FRAM 1, described by Robin Falconer in the following article, was operating some 600 km away in the vicinity of the Nansen-Gakkel Ridge. From planning to execution, the two expeditions kept in close touch. This resulted in excellent logistics and scientific cooperation and culminated in a one-day special session at the joint meeting of the Canadian and American Geophysical Unions in Toronto in May 1980. The session was entirely devoted to the LOREX and FRAM 1 scientific results.

The preliminary results of the LOREX geoscience studies, which follow, received their first public exposure at this joint scientific meeting.

Bathymetry

Over 250 individual depth soundings and gravity measurements and some 600 km of echo soundings and gravity recordings were obtained. A 100 m contour map (Fig. 2) of the ocean floor was compiled from these results and from the data collected from the two previous North Pole expeditions. The shallowest and deepest depths recorded were 956 m over the ridge crest and 4306 m in the Fram Basin, respectively. The average slope of the Makarov flank from near the base to near the crest of the ridge is as steep as 14°, whereas the corresponding slope of the Fram flank does not exceed 6°. The Fram Basin is more than 300 m deeper than the Makarov Basin. Comparison of this contour map with the General Bathymetric Chart of the Oceans (GEBCO, 5th edition, 1979) shows the ridge crest between 18 and 34 km further south than on the GEBCO map.

Figure 2 shows the drift tracks of the LOREX main camp and the two satellite camps, Iceman and Snowsnake, as well as those of the 1967 and 1969 expeditions.

Satellite Transit Navigation

All three stations were equipped with Transit Satellite receivers. Positions were computed on-line at the main station, whereas the raw satellite data from Snowsnake and Iceman were collected every few days and processed at the main camp on a HP 2100 computer. By computing the positions from satellite passes simultaneously for all three stations it was possible to determine the horizontal positions of the station to better than 50 m (Fig. 2) and the geoidal heights to better than 50 cm.

Plumbline deflection measurements

Star observations were made with a Wild T-4 theodolite at the main camp and at Iceman. The plumbline deflections were computed from the difference between the astronomically determined drift path

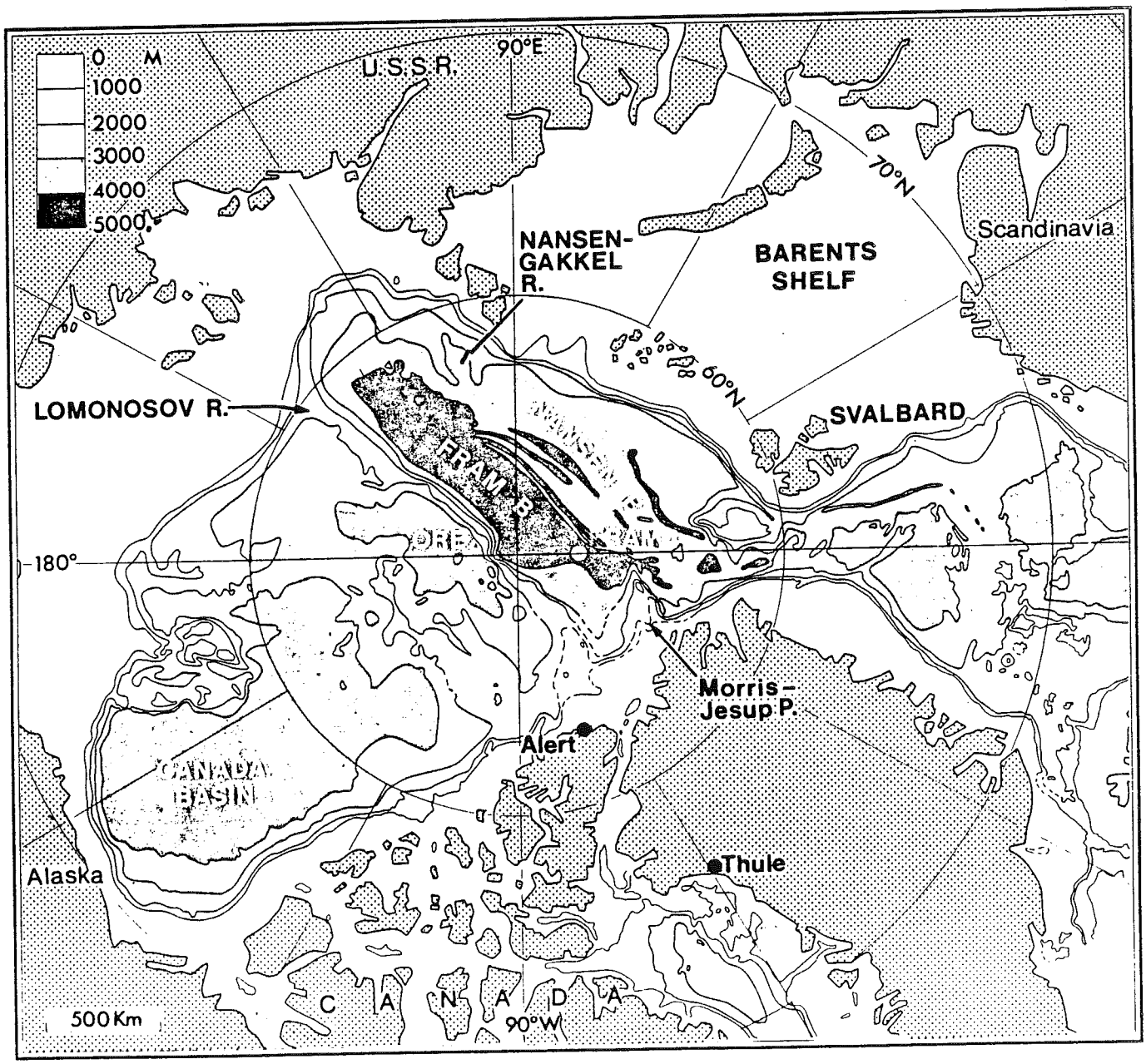

Figure 1. *Arctic Ocean seafloor features* — *Eléments naturels du fond sous-marin de l'Arctique*

and the transit satellite drift path. The deflections ranged in magnitude from 30 to 60 microradians, and pointed towards the ridge crest for stations located over the ridge, and away from the ridge crest for stations located over the ocean basins. These measurements complement gravity measurements and tell us more about the density structure of the ridge.

Marine Geology

A high resolution, shallow seismic reflection profiler, consisting of a 10-cubic inch compressed air gun, was located at the main camp. Its powerful sound waves mapped the top 1200 m of the ocean floor, showing the ridge to consist of fault blocks whose tops are covered with a thin layer, less than 75 m, of unconsolidated sediments (Fig. 3). Since these stratified sediments lie conformably upon (parallel to) the irregular fault block tops, they appear to have been deposited before the faulting process started. Sea floor photographs show that these sediments are presently being eroded by the current (Fig. 4).

Strong pulsating water currents with velocities in excess of 12 cm per second (cm/s) sweep across the ridge crest; this has been confirmed by the data obtained from self-recording current meters moored to the ocean floor near the ridge crest and recovered 50 days later. The shallow seismic measurements further reveal a total absence of unconsolidated

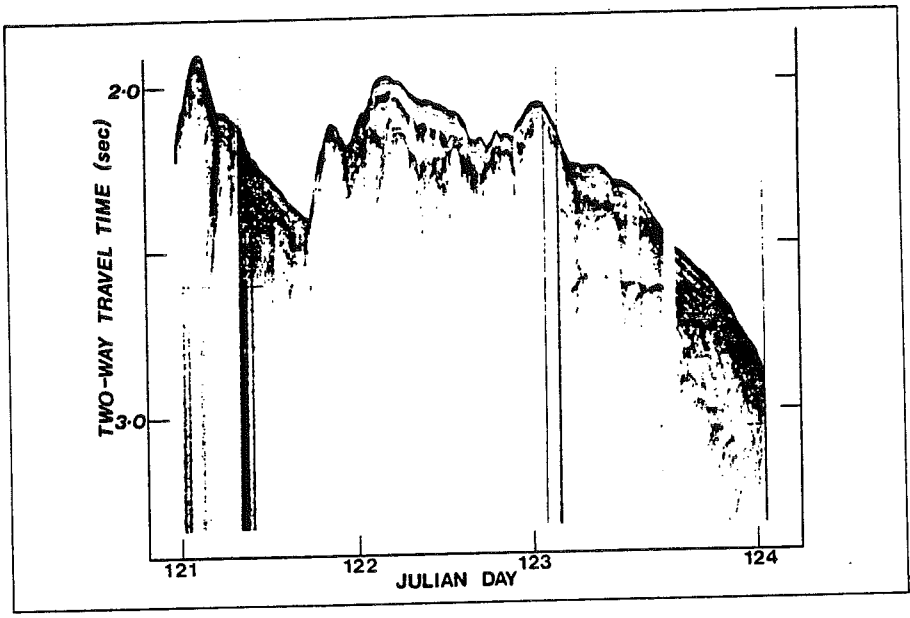

3a

Figure 2. *Bathymetry of the ocean floor recorded on LOREX 79 as it crossed the Lomonosov Ridge. The dots on the LOREX drift tracks, spaced at three-hour intervals, show the variable speed of the drift, ranging from zero to 1100 m/hr, at which the ice drifted over the 60-day period. The numbers indicate Julian days*

Bathymétrie du fond océanique enregistrée au cours de LOREX 79 au moment où le camp dérivait au-dessus de la dorsale de Lomonossov. Les points sur le tracé de dérivation de LOREX, mesurés à des intervalles de trois heures, indiquent la vitesse variable de dérivation de la banquise, qui s'inscrit dans une fourchette de 0 à 1100 m/h, au cours des 60 jours qu'a durés l'expédition. Les chiffres renvoient aux jours du calendrier

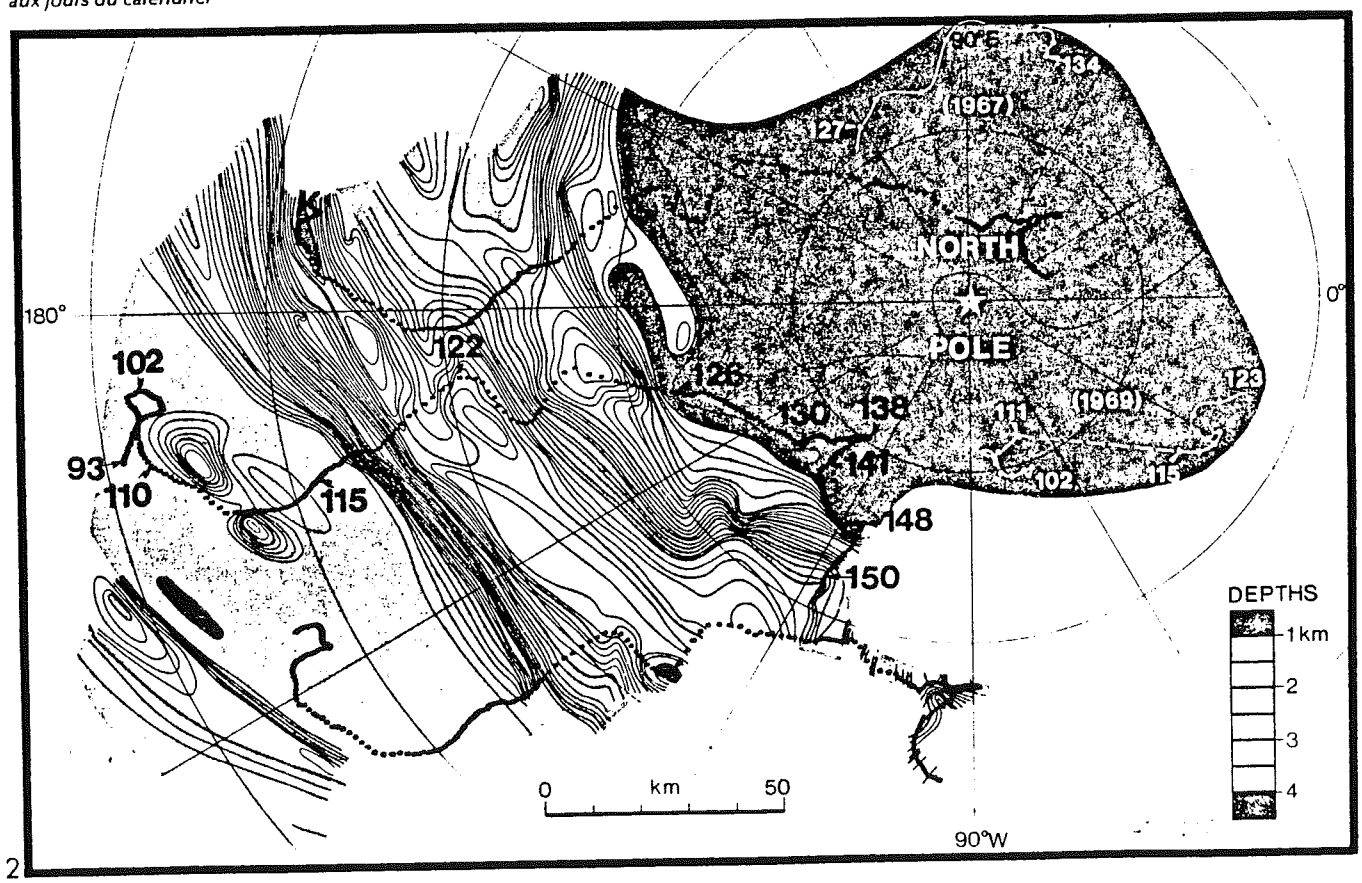

2

sediments on the Makarov flank, and more than 1100 m of well stratified flat-lying unconsolidated sediments, that infill the Makarov and Fram basins and abut unconformably against the ridge flank.

Forty-two sediment cores, up to 1.7 m long, were recovered from the two basin floors and from the ridge. In light of our knowledge that the sedimentation rate in the Arctic Ocean basins is about 1 mm per 1000 years, the sediments collected will provide insight about oceanographic conditions and the history of the ice cover during the last 1-1/2 million years. A preliminary analysis of a core from the ridge crest shows spores and microfossils as old as 350 million years. One of the microfossils, the Dinoflagellate Luxadinium Propatulum, originally inhabited water depth of about 200 m and became extinct about 80 million years ago.

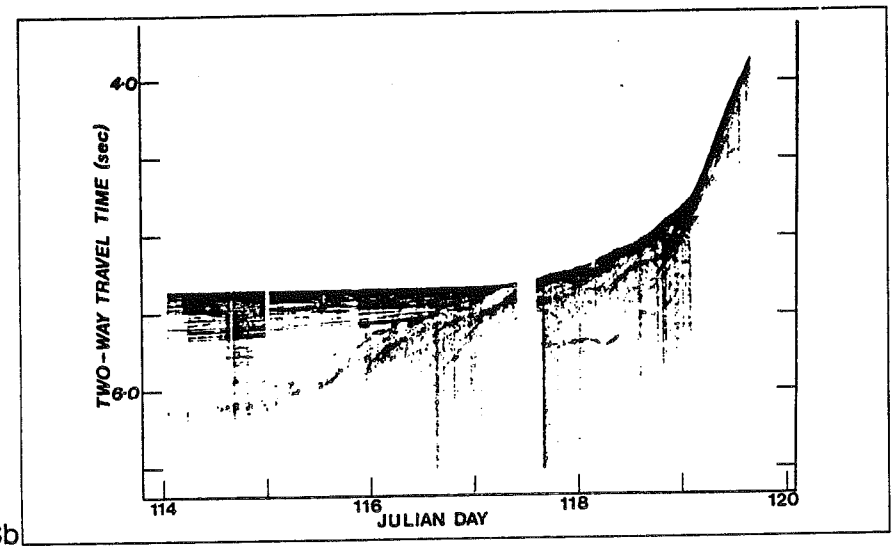

3b

Figure 3. *Shallow seismic profiles, a. top of Lomonosov Ridge. b. edge of Makarov Basin*

Profils sismiques peu profonds, a) au sommet de la dorsale de Lomonossov et b) à la pointe du bassin de Makarov

S.M. Blasco, AGC, GSC, BIO/CGA, CGC, IOB

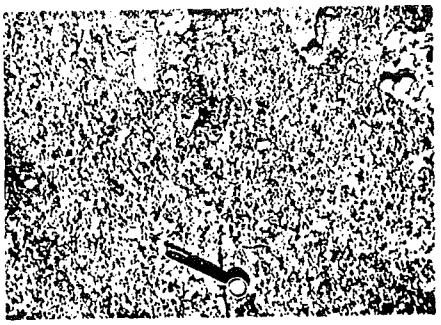

4

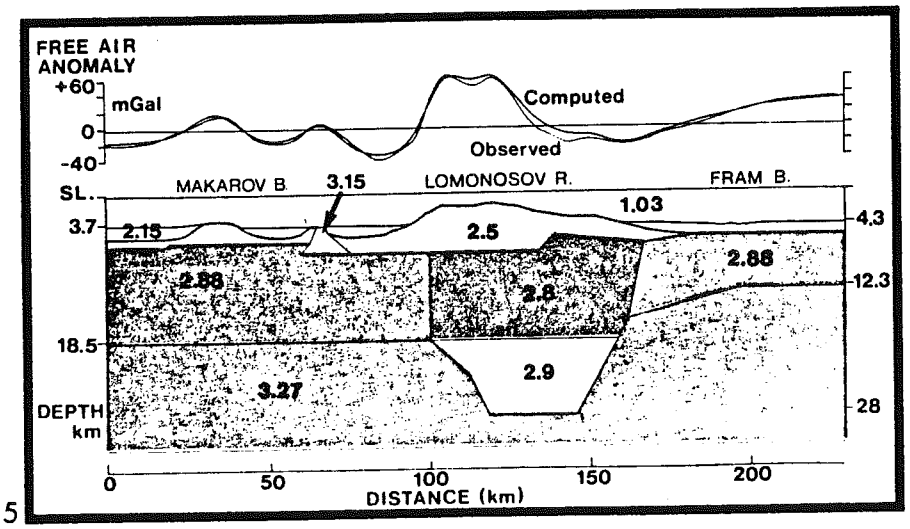

5

The results of the sub-bottom profiling and of the core analysis strongly support the hypothesis that the ridge was part of a continental shelf less than 100 million years ago.

Intermediate reflection seismic

Intermediate seismic reflection profiling was conducted at the main camp. A cross-shaped geophone array picked up the echo of explosives detonated at its centre. Preliminary results confirm a layer of approximately 1 km thick horizontally stratified sediments under-lying both ocean basins adjacent to the ridge flank. Both the rock below the unconsolidated basin sediments, and the core of the ridge adjacent to the flanks, also reveal a complex structure of reflecting layers. These reflections may arise from faulted sedimentary or sill or dyke structures that extend at depth, some distance beyond the ridge flanks into the adjacent ocean basins. Further analysis of the intermediate reflection seismic data should reveal the nature of the geological structure to a depth of at least 10 km.

Deep crustal refraction seismic

Deep crustal seismic results were obtained on two partially reversed refraction profiles along and across the ridge. The Makarov and Fram Basins are modelled with a 1 km thick sedimentary layer underlain by a material with a velocity of about 4.7 km per second (km/s) and a thickness of 3 to 4 km. The uppermost 6 to 7 km of the ridge core has a similar velocity and may be the same material, conceivably a vesicular oceanic basalt. Material with velocities in this range are, however, common elements of continental crust. Immediately beneath this layer on the ridge a thick layer of 6.6 km/s material is evident. The lack of any evidence for material of intermediate density, with velocities in the 5.5 to 6.3 km/s range, is anomalous if we assume conti-

Figure 4. *Seafloor photograph, taken in 1830 m of water, showing current erosion and associated coarse gravel pavement, and an outcrop of older semiconsolidated sediments in the bottom left. The compass vane is aligned in the direction of current flow towards the bottom right.*

Photo du fond océanique, prise à une profondeur de 1830 mètres, montrant l'érosion par le courant et le dallage de gravier grossier associé, ainsi qu'un affleurement de sédiments plus anciens, semi-consolidés, en bas, à gauche. L'aiguille de la boussole est alignée dans la direction du courant vers le bas, à droite

N.E. Fenerty, BIO/IOB

Figure 5. *Gravity crustal model of the area crossed by LOREX 79: Makarov Basin, Lomonosov Ridge, and Fram Basin*

Modèle gravimétrique de la croûte dans la région traversée par LOREX 79: bassin de Makarov, dorsale de Lomonossov et bassin de Fram

nental-type crust. However this sequence of materials is quite typical for oceanic crust.

The crust-mantle boundary, as indicated by a sharp break from material with velocity of 6.6 km/s to 8.3 km/s, with a good upper-mantle reflection break, indicates crustal depths of 12.5 km for the Makarov Basin, 16 km for the Fram Basin and 28 km for the Lomonosov Ridge.

The implications of these preliminary results are (1) that while a thin veneer of continental sediments may be present, the core of Lomonosov Ridge, in the area of the survey, is composed of an oceanic sequence of rocks and (2) that the Makarov and Fram Basins were formed at different times.

Gravity

The free-air gravity anomaly (difference between observed and theoretical gravity at sea level) is characterized by a positive linear anomaly of between 60 and 85 milligal (mgal) centered over the ridge crest. This is flanked by two negative anomaly troughs of up to -50 mgal centered approximately along the 3900 isobaths on either side of the ridge. Further away from the ridge the free-air anomaly field is generally positive (~25 mgal) over the Fram abyssal plain and negative (~-20mgal) over the Makarov abyssal plain.

We have constructed a preliminary, very generalized, two-dimensional crustal model from bathymetry, and shallow, intermediate and deep seismic information available. This model explains the observed free-air anomaly in terms of density contrasts within the crust (Fig. 5).

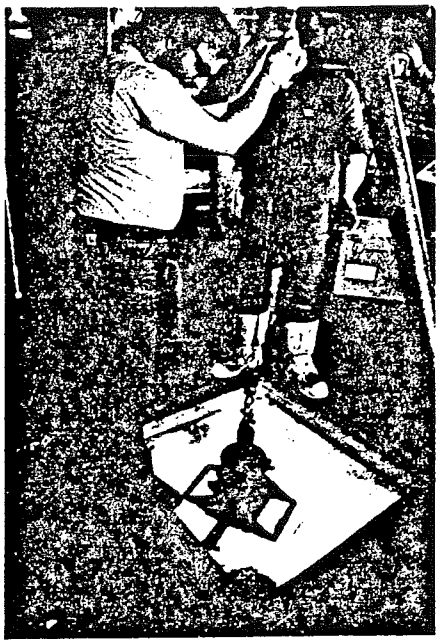

Stephen Blasco, Geological Survey of Canada, lowers a grab sampler through a hole in the ice platform

M. Stephen Blasco, de la Commission géologique du Canada, descend un carottier dans un trou foré dans la banquise

It shows the Lomonosov Ridge to have a root 28 km deep, imbedded in a higher density oceanic crust. The gravity high centered over the crest reflects the ridge bathymetry, caused by displacement of water by higher density rock. Since there is no seismic evidence for low density troughs deep enough to explain the gravity lows, the negative troughs on either side of the ridge must be caused by the density contrast between the root and the surrounding higher density crustal and mantle rock. The fact that the gravity anomalies are higher and the water depth greater in the Fram Basin implies that it has thinner crust (12.3 km) than the Makarov Basin (18.5 km).

Two implications follow from this preliminary gravity model: (1) the lower density of the root compared with the crust of the adjacent basin may indicate that the Lomonosov Ridge is a continental fragment, and (2) the thicker crust of the Makarov Basin may indicate it was formed before the Fram Basin.

Magnetic Studies

Magnetovariational and magnetotelluric fields were recorded at the three stations. The two main conclusions reached from these studies are, (1) the crust and upper mantle beneath the ridge are electrically similar to those beneath the adjacent basins, and (2) there is up to one kilometer of highly conductive sediments in the basins and almost none on the ridge.

Results from an aeromagnetic survey flown along and across some 500 km of the Lomonosov Ridge at a height of 300 m show a zone of anomalies of over 1000 nanoteslas, centered on the southern flank, parallel to the ridge crest. We conclude that the Lomonosov Ridge is composed of igneous rather than sedimentary rocks, or at least that it has had a considerable amount of associated igneous activity during its recent geological past.

Heat Flow

A total of 42 heat flow measurements were made by penetrating the sea bottom sediments with a 3 m long gradiometer probe. The probe was left in the ground for a minimum of 20 minutes while seven heat sensors, spaced equidistant along the probe, recorded the temperature gradient. In addition, over 300 thermal conductivity measurements were made with a hypodermic needle probe on 21 cores retrieved by the marine geologists. The resulting calculated heat flux from the interior of the earth is highest in the Fram Basin. This is consistent with an age of 40 million years for the margin of a basin containing an active spreading centre. The head flows measured on the Lomonosov Ridge are slightly higher than those in the Makarov Basin. If we assume a crustal thickness of 28 km for the ridge, the observed values correspond to a low heat production, as would be generated by a composition of sediments underlain by a basement of gneisses or granodiorites. This reasoning is consistent with the theory of a continental fragment originating from the Barents Continental Shelf.

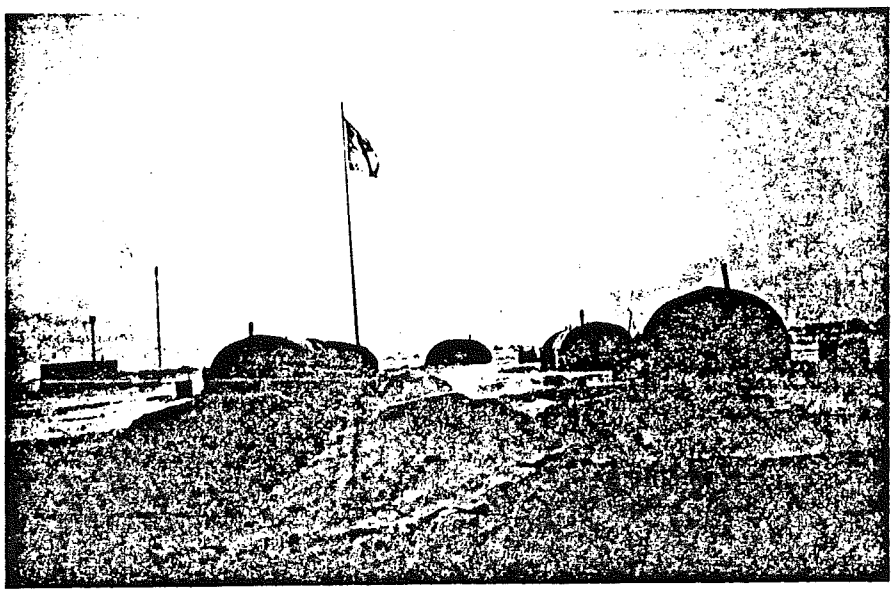

The main LOREX camp in high winds and drifting snow at beginning of May 1979

Le camp principal LOREX, au milieu des vents violents et des rafales de neige, au début de mai 1979

Conclusions

Preliminary marine geological results support the theory that the Lomonosov Ridge was once part of the Barents Continental Shelf. Gravity and geothermal studies indicate that most of the ridge and its root is of continental origin, and deep crustal refraction seismic and magnetic studies imply that the ridge core may be composed of oceanic rocks. Preliminary refraction seismic interpretation seems to indicate that the crust of the Makarov Basin is thinner than that of the Fram Basin. On the other hand, gravity interpretation shows the reverse to be true. This discrepancy has not yet been resolved.

The next step in unravelling the geological history of the ridge is to synthesize the separate studies. In particular, analysis of the intermediate reflection seismic results from below the unconsolidated sediments, and their correlation with the deep refraction seismic data, promises to go a long way in unlocking the secret of Lomonosov's origin. □

Acknowledgements

The scientific program was conceived and developed by EMR's Earth Physics Branch, which had conducted two geophysical expeditions to the vicinity of the North Pole in 1967 and 1969. The logistic support of the expedition was provided by the Polar Continental Shelf Project of EMR.

The following individuals and agencies were responsible for the principal geoscience research and support activities:

Satellite Navigation: David Wells, Dept. of Fisheries and Oceans, and Joe Popelar, Earth Physics Branch (EPB), EMR

Astro Navigation: Geodetic Survey of Canada, EMR and G.W. Johnson, U. of Minnesota

Bathymetry and Gravity: J.R. Weber and J.F. Sweeney, EPB, EMR

Marine Geology: S.M. Blasco and C.F.M. Lewis, Atlantic Geoscience Centre, Geological Survey of Canada (GSC), EMR

Reflection Seismic: Tony Overton, GSC

Refraction Seismic: J.A. Mair, EPB

Geomagnetic Studies: E.R. Niblett and Adrian Camfield, EPB

Aeromagnetic Survey: Peter Hood, GSC

Heat Flow: Alan Judge, EPB

Chief Scientist: J.R. Weber, EPB

Operations Manager: Frank Hunt, Polar Continental Shelf Project (PCSP), EMR

Camp Manager: Fred Alt, PCSP

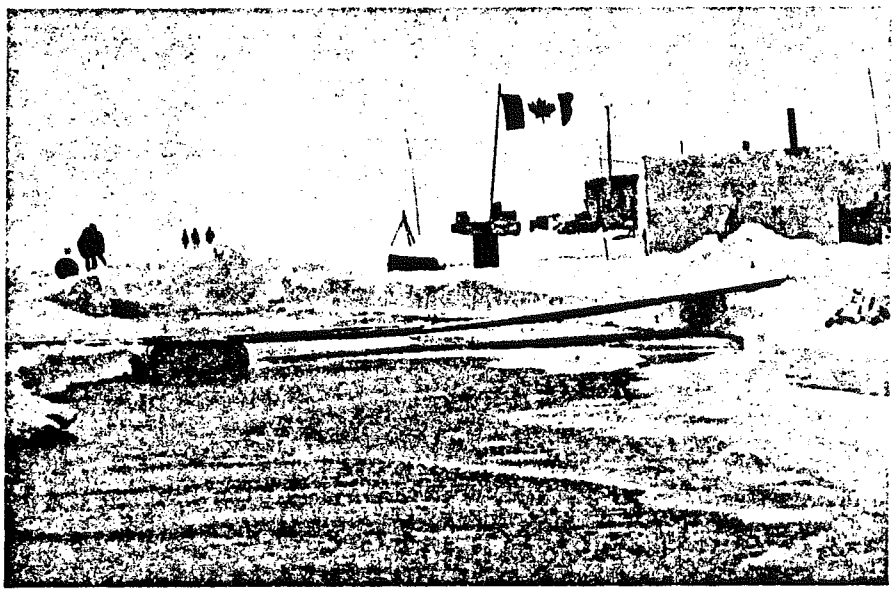

A huge crack split the LOREX camp, May 1, 1979. The ice refroze in few days
Une fissure énorme a coupé le camp LOREX en deux, le 1er mai 1979. La glace a gelé à nouveau quelques jours plus tard

The main camp at end of April 1979 with LOREX spelled out in oil drums
Le camp principal à la fin d'avril 1979 avec le mot LOREX écrit à l'aide de bidons d'huile

Tectonophysics, 89 (1982) 217–237
Elsevier Scientific Publishing Company, Amsterdam – Printed in The Netherlands

CONTINENTAL RIDGES IN THE ARCTIC OCEAN: LOREX CONSTRAINTS *

J.F. SWEENEY [1,**], J.R. WEBER [1] and S.M. BLASCO [2]

[1] *Earth Physics Branch, Department of Energy, Mines and Resources, Ottawa, Ont., K1A OY3 (Canada)*
[2] *Atlantic Geoscience Centre, Bedford Institute of Oceanography, Dartmouth, N.S., B2Y 4A2 (Canada)*

(Final version received March 10, 1982)

ABSTRACT

Sweeney, J.F., Weber, J.R. and Blasco, S.M., 1982. Continental ridges in the Arctic Ocean: LOREX constraints. In: G.L. Johnson and J.F. Sweeney (Editors), Structure of the Arctic. *Tectonophysics*, 89: 217–237.

Recent multidisciplinary geophysical measurements over the Lomonosov Ridge close to the North Pole support the widely held belief that it was formerly part of Eurasia. The known lithologies, ages, P-wave velocity structure and thickness of the crust along the outer Barents and Kara continental shelves are similar to permitted or measured values of these parameters newly acquired over the Lomonosov Ridge. Seismic, gravity and magnetic data in particular show that the ridge basement is most likely formed of early Mesozoic or older sedimentary or low-grade metasedimentary rocks over a crystalline core that is intermediate to basic in composition. Short-wavelength magnetic anomaly highs along the upper ridge flanks and crest may denote the presence of shallow igneous rocks. Because of the uncertain component of ice-rafted material, seafloor sediments recovered from the ridge by shallow sampling techniques cannot be clearly related to ridge basement lithology without further detailed analysis. The ridge is cut at the surface and at depth by normal faults that appear related to the development of the Makarov Basin. This and other data are consistent with the idea that the Makarov Basin was formed by continental stretching rather than simple seafloor spreading. Hence the flanking Alpha and Lomonosov ridges may originally have been part of the same continental block. It is suggested that in Late Cretaceous time this block was sheared from Eurasia along a trans-Arctic left-lateral offset that may have been associated with the opening of Baffin Bay. The continental block was later separated from Eurasia when the North Altantic rift extended into the Arctic region in the Early Tertiary. The data suggest that the Makarov Basin did not form before the onset of rifting in the Artic.

---

* Contribution from the Earth Physics Branch No. 964, LOREX contribution No. 9.
** Present address: Pacific Geoscience Centre, P.O. Box 6000, Sidney, B.C., V8L 4B2 (Canada)

0040-1951/82/0000–0000/$02.75

INTRODUCTION

It is generally believed that the Arctic Ocean basin developed in at least two distinct stages. Consensus regarding the evolution of the Eurasia Basin has been long-standing (Fig. 1). The age and mode of origin of the Canada and Makarov basins, however, remains uncertain. The Lomonosov Ridge divides the area of agreement from the area of ambiguity.

Since the early 1960's when Heezen and Ewing (1961) and Wilson (1963)

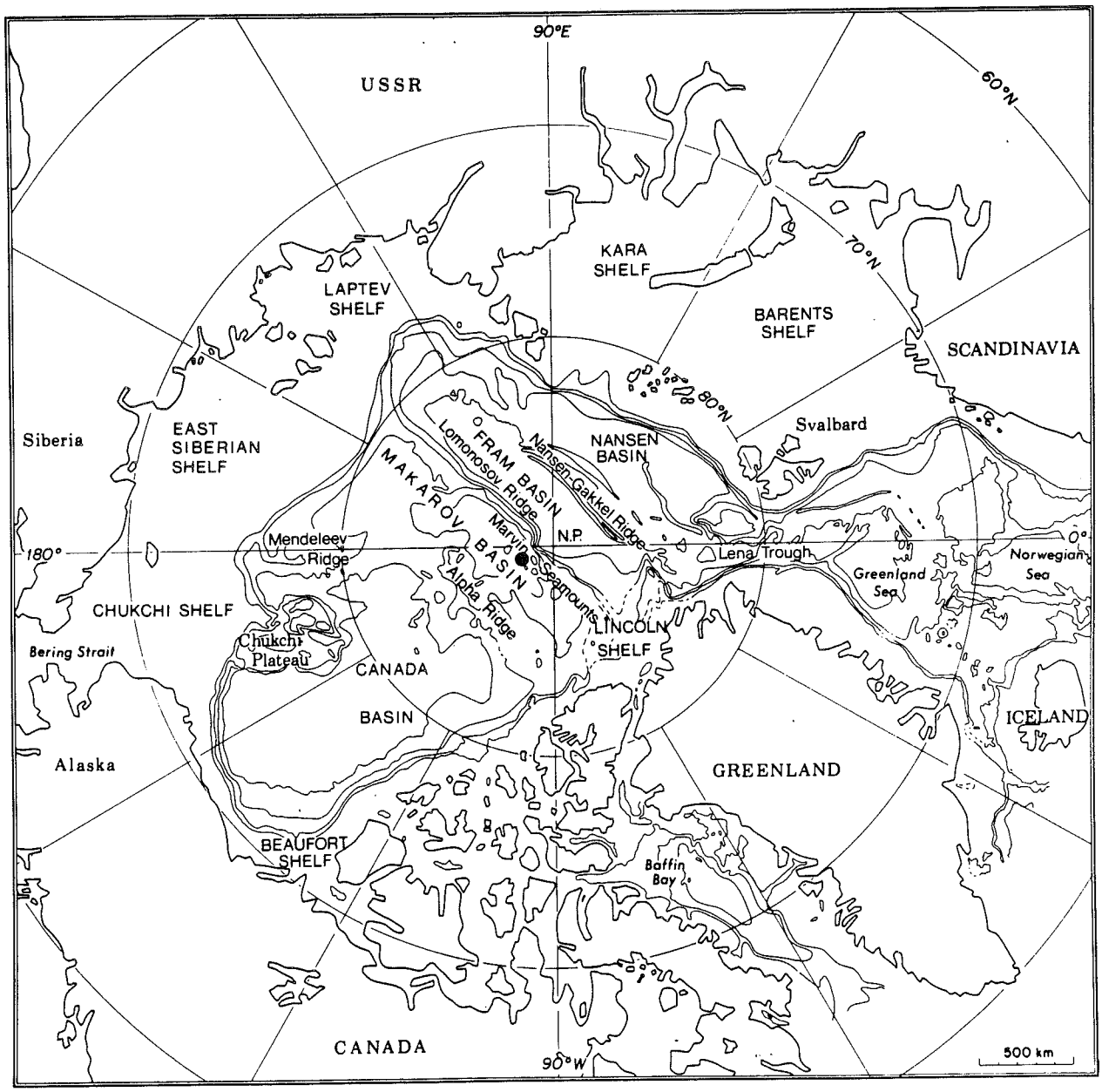

Fig. 1. Arctic seafloor nomenclature and gross bathymetry. Fram and Nansen basins together are called 'Eurasia Basin'. Dot indicates initial position of LOREX camps. Contour interval is 1 km. Also shown is 500 m contour.

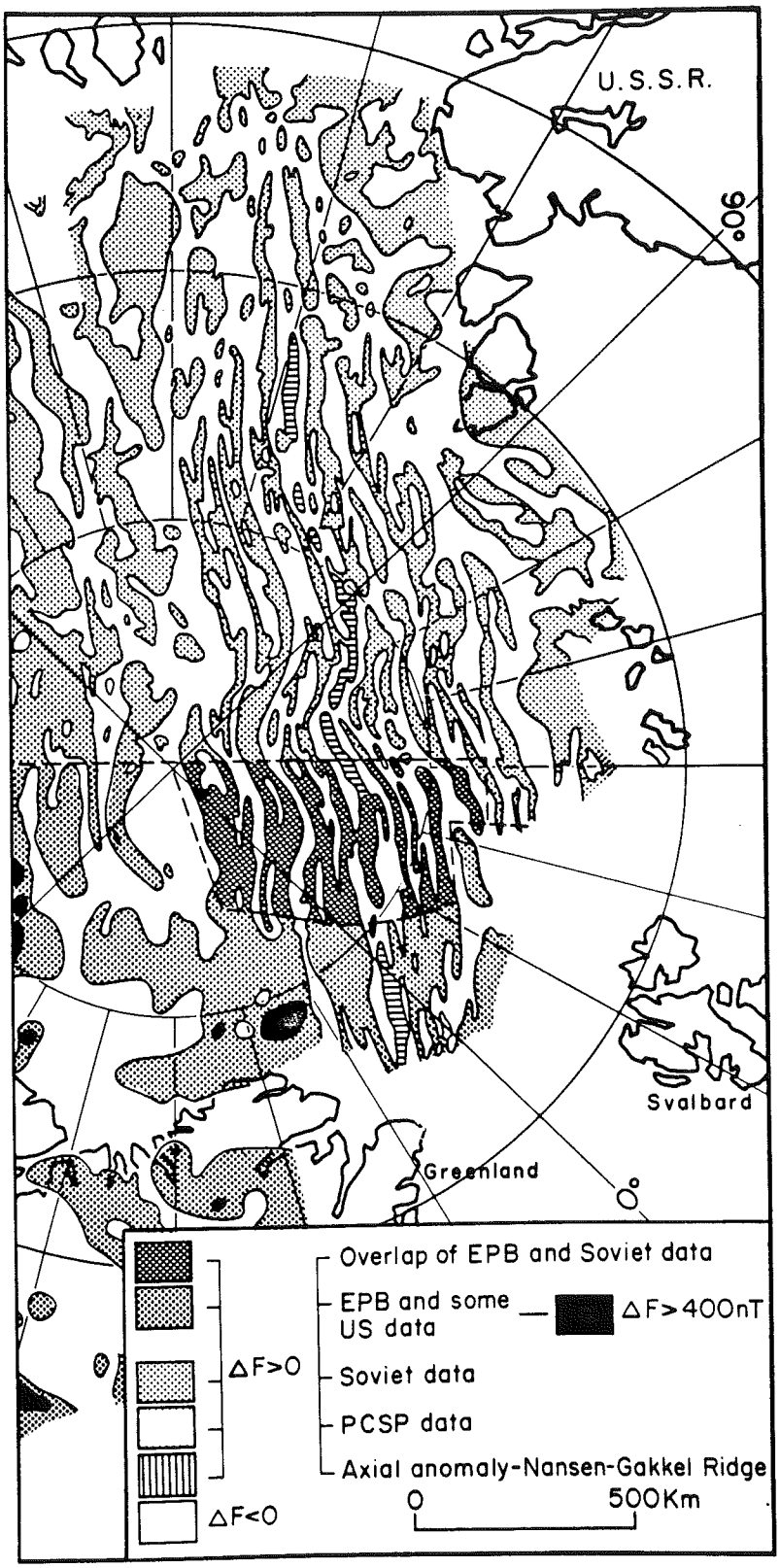

Fig. 2. Schematic map of the anomalous magnetic field in the Eurasia Basin (modified from Coles et al., 1978).

recognized that the Eurasia Basin is the extension of the North Atlantic seafloor into the Arctic, it has been commonly assumed that the Lomonosov Ridge was originally part of the outermost Barents and Kara continental shelves and that it was split off and transported to its present position in the Arctic Ocean by seafloor accretion centred along the Nansen–Gakkel Ridge. In other words, the Lomonosov Ridge should be a sliver of continental material.

There are two major reasons for believing this. The first is the overall morphology and geophysical character of the ridge. It is relatively narrow and quite linear with few lateral irregularities (Fig. 1). The flanks are steep and the crest appears relatively flat and smooth. These characteristics suggested to Dietz and Shumway (1961) that the Lomonosov Ridge may be a fault block rather than a volcanically constructed or an otherwise thermally generated feature. Reconnaissance gravity, magnetic (Ostenso,1962; Karasik et al., 1971; Coles et al., 1978), heat flow (Judge and Jessop, 1978), magnetotelluric (DeLaurier, 1978) and plumbline deflection (Lillestrand and Weber, 1974) data from the ridge show that it can be composed of continental-type material, although interpretation of individual parameters has generally been unconstrained by other measurements.

The second and more compelling argument for its continental nature is the presence within the Eurasia Basin of a magnetic anomaly pattern that is approximately symmetric about the Nansen–Gakkel Ridge (Fig. 2). Heat flow patterns and present seismicity along the ridge plus its seismic continuity with the mid-Atlantic Ridge to the south indicate that the Nansen–Gakkel Ridge is an accreting margin and the Eurasia Basin a product of activity along this axis over the last 50–70 Ma (e.g., Pitman and Talwani, 1972; Vogt et al., 1979). That is, prior to the inception of the Eurasia Basin, the Lomonosov Ridge was adjacent to or part of the polar continental margin of western Eurasia.

With this background in mind, the Lomonosov Ridge Experiment (LOREX), carried out during the spring of 1979, was designed to collect data bearing on ridge structure and composition and, from this, to discover what processes allowed such an apparently long narrow fragment to break off so cleanly from its parent continental margin. Several of the marine geological and geophysical returns from this experiment are presented here and, from them, the nature and mode of origin of the Lomonosov Ridge are assessed. Details as to logistics, instrumentation and methods of data collection can be found in Weber (1979), Blasco et al. (1979), Coles (1980), Aagaard (1981) and Mair and Forsyth (1982).

THE LOREX DATABASE

It was decided that a multidisciplinary corridor of data collected completely across the ridge offered the best chance to achieve the stated scientific goals. Two factors dictated the location of the initial camp sites. The first is the transpolar current that carries the pack ice obliquely across the ridge toward Greenland. The

second is the time between first light in mid-March and the start of the melt season in early June. This 2.5 month window plus the average drift rate for pack ice in this region of about 5 km/day (Weber and Sweeney, 1977) required that the camps be positioned upstream of the most narrow part of the ridge. That is, in the Makarov Basin close to the North Pole (Fig. 1).

From this starting point the camps drifted successfully across the ridge (Fig. 3a, b). Bathymetry and gravity measurements were recorded continuously at each camp and about 250 spot readings were made on helicopter traverses along lines normal to the ridge. Near bottom currents were measured in the crestal region (Pounder, 1980; Aagaard, 1981). High resolution shallow seismic reflection profiling and intermediate depth reflection profiling of the sediment column and basement were conducted along the drift path of the Main Camp (Fig. 3a; Blasco et al., 1979; Overton, 1980). In addition, two pseudo-reversed crustal refraction profiles, one normal (Fig. 3b) and one parallel to the trend of the ridge, were carried out at predetermined sites over the feature (Mair and Forsyth, 1982). Aeromagnetic data were collected at low altitude (300 m) along and across the Lomonosov Ridge from the LOREX camps to the Lincoln Shelf (Hood and Bower, 1980). Magnetic total field measurements were also taken along the drift paths of the LOREX satellite camps (Coles, 1980) and magnetic induction and magnetotelluric data were collected at all three ice camps (Camfield et al., 1980).

Morphology and seabed geology

Ridge morphology derived from these data confirm earlier reconnaissance descriptions. The Lomonosov Ridge rises sharply from the abyssal depths of the Fram (4200 m) and Makarov (3900 m) basins and crests at 950–1500 m below sea-level in the region studied (Weber, 1979; Fig. 3b). Average slopes on the Makarov flank are steeper, up to 14°, than those on the Fram flank, less than 7° (Weber, 1980). Near surface samples of the seabed were obtained by gravity coring, grab sampling and dredging along the drift track of the Main Camp (Fig. 3a). Overall, sediments recovered from abyssal depths are much finer grained than those retrieved from the ridge itself. Makarov Basin sediments, however, contain far more silt-rich interbeds than Fram Basin sediments which are composed mainly of firm clay layers (Blasco et al., 1979). Sediments recovered from the Lomonosov Ridge contain almost no recognizable turbidites and have a large sand-sized fraction, dominantly quartz with minor feldspar. Dredge samples from the ridge included fingernail-sized pieces of recrystalized dolomitized chalk, a manganese nodule and a fragment of biotite schist. Bottom photographs show a coarse gravel pavement over much of the crest and Makarov flank of the ridge. Three types of micro-fossil populations have been recognized within the top few centimeters of a core recovered from the Fram flank of the ridge in 1721 m of water (site B25 in Fig. 3b): Late Cenozoic pollen, mid-Cretaceous dinoflagellates and Upper Devonian spore fragments that have been

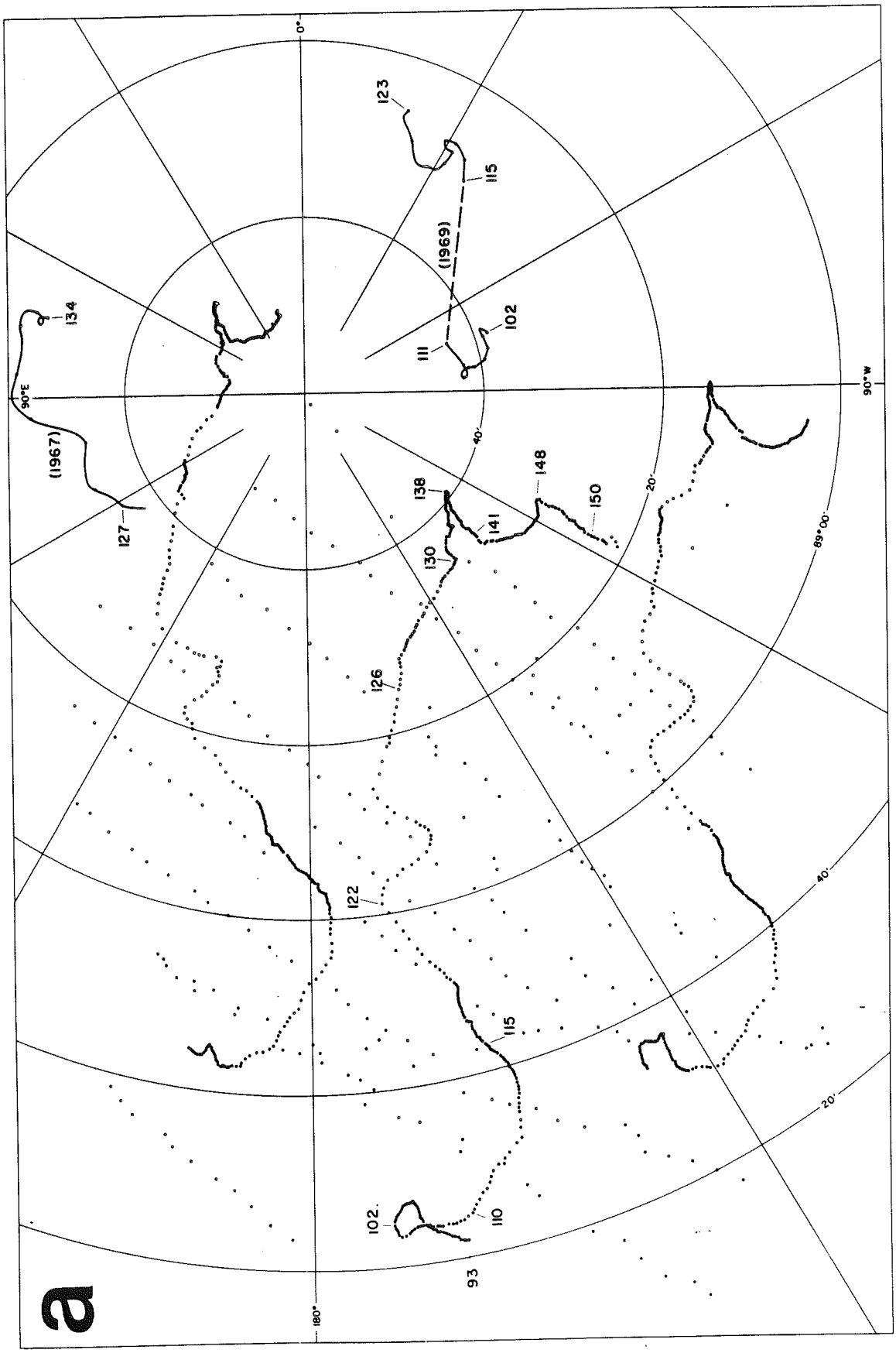

Fig. 3a. Drift tracks of LOREX camps. Main camp (geophysics and marine geology) and two satellite camps (physical and chemical oceanography) set up initially in isosceles triangle as an aid to aircraft navigation. Helicopter traverse spot landings indicated. Dates given in Julian days. Also shown are drift paths of 1967 and 1969 Dominion Observatory Polar Expeditions.

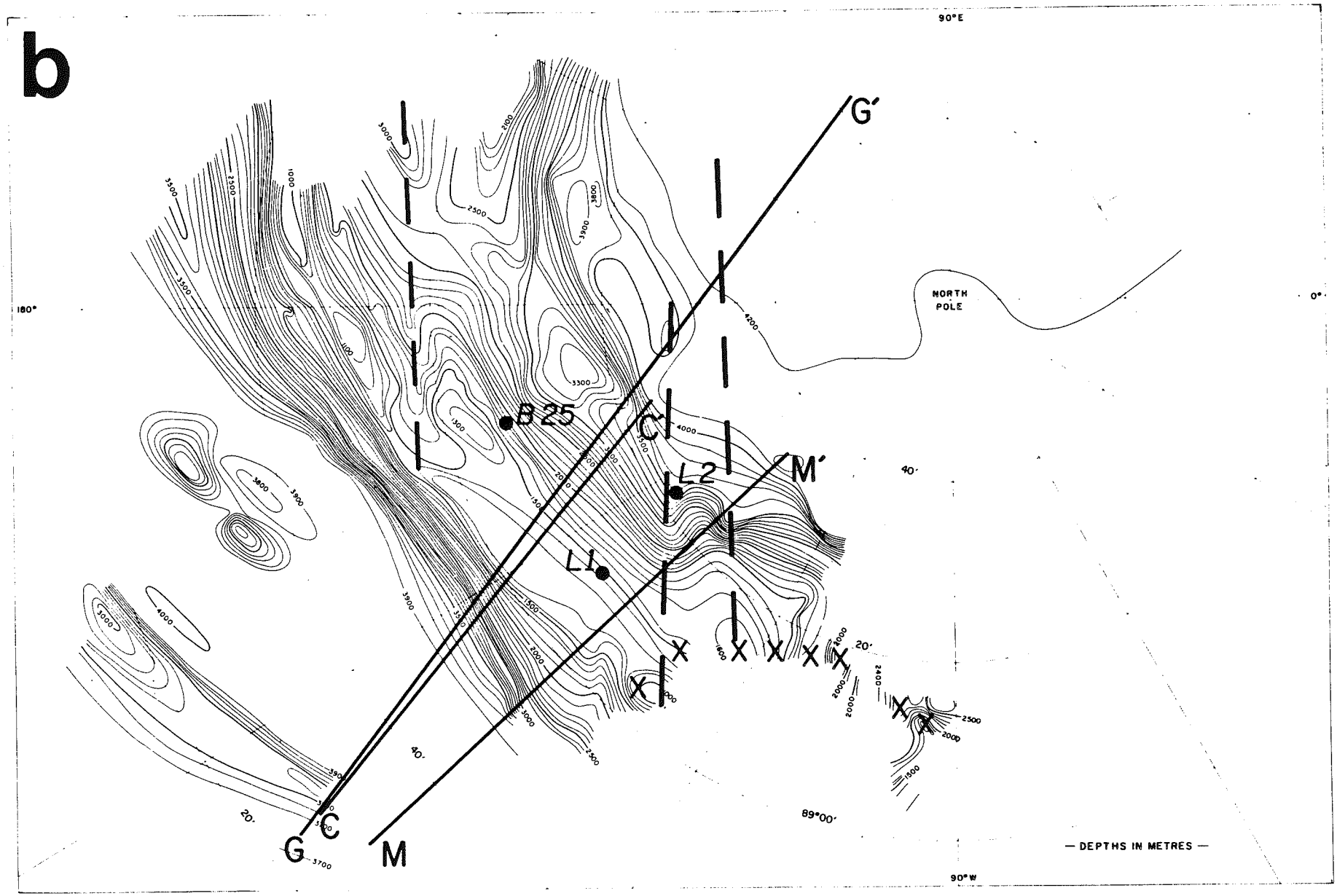

Fig. 3b. LOREX bathymetry. Contour interval 100 m. Profile location of crustal seismic ($C-C'$), magnetic ($M-M'$) and gravity ($G-G'$) models are given. Current meter mooring sites ($L1$, $L2$) are indicated and core B25 retrieval site is marked. Short-wavelength magnetic anomaly highs indicated by $\times$. Dashed lines indicate possible seafloor lineaments.

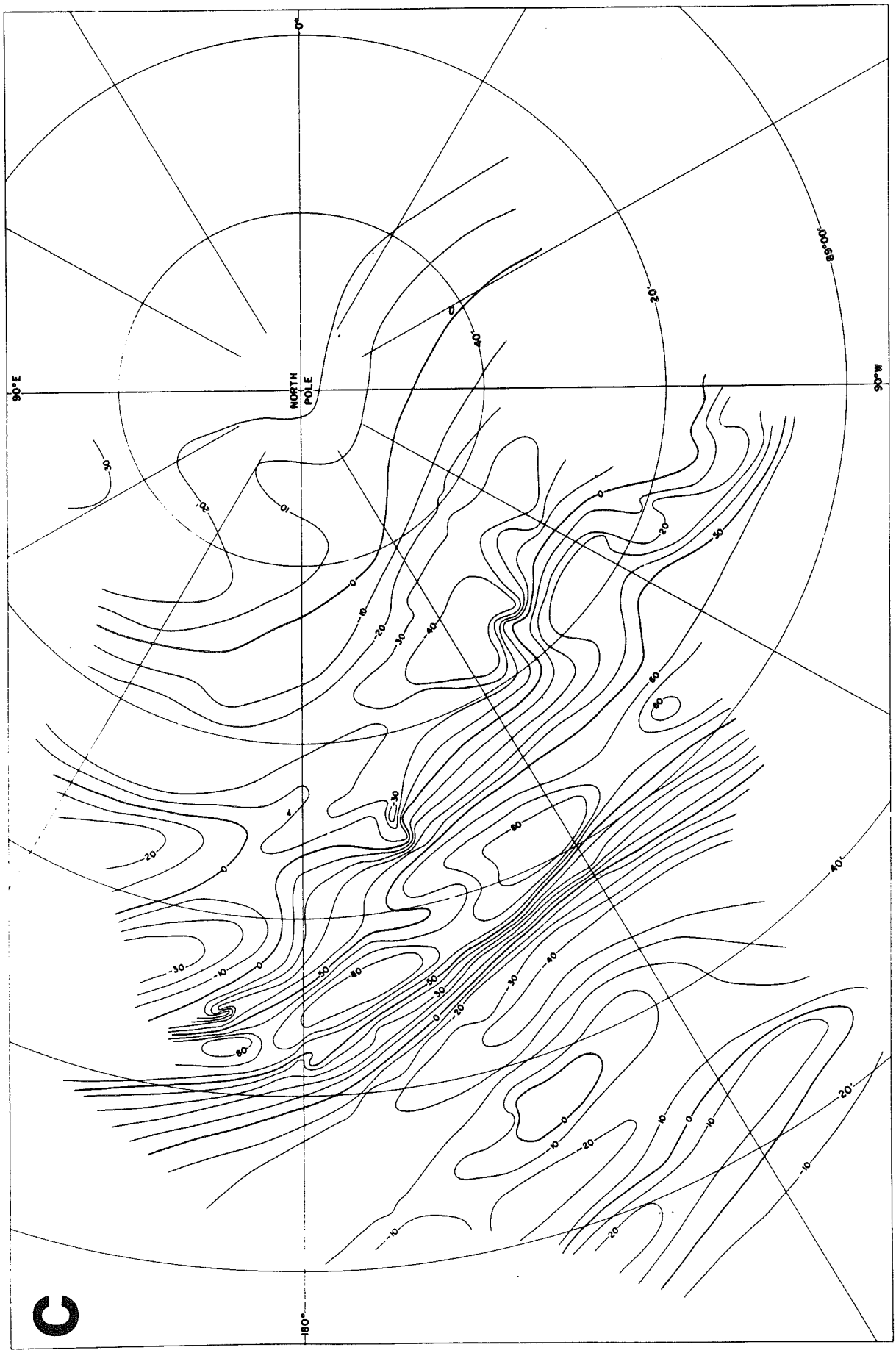

Fig. 3c. LOREX free-air gravity. Contour interval 10 mGal.

reworked several times (Blasco et al., 1979). The dinoflagellates and spores have undergone significant thermal alteration.

At the top of the Fram flank (Fig. 3b), near-bottom current speeds in excess of 12 cm/s have been measured (Aagaard, 1981). The currents are pulsed and appear to flow to the east-southeast (toward Greenland) diagonally across the ridge into the Makarov Basin. The indicated current pattern plus seawater temperature profiles suggest that close to the North Pole cold water from the Eurasia Basin is spilling over the top of the Lomonosov Ridge and then sinking adiabatically into Makarov Basin thereby producing a downslope current along the Makarov flank (Aagaard, 1980, 1981; Pounder, 1980).

Seismic structure

As reported elsewhere (Blasco et al., 1979; Weber, 1980), shallow seismic returns indicate that less than 40 m of stratified conformable, unconsolidated sediment overlies the Fram flank of the ridge while the Makarov flank appears to be sediment-free. The crest appears to be made up of several slightly tilted enechelon fault blocks with (sediment-free) scarps facing the Makarov Basin and tops conformably overlain by about 75 m of stratified unconsolidated sediments (Fig. 4). The sediments are truncated by the faults which extend into the underlying basement rocks. In the Fram and Makarov basins sediments are stratified, flat-lying and at least 1100 m thick close to the ridge. These unconsolidated deposits unconformably abut the ridge flanks and show little evidence of internal deformation (Blasco et al., 1979).

Basement beneath the Makarov Basin exhibits significant relief on the shallow seismic records and it outcrops at about 20 km and also between 50 and 60 km from

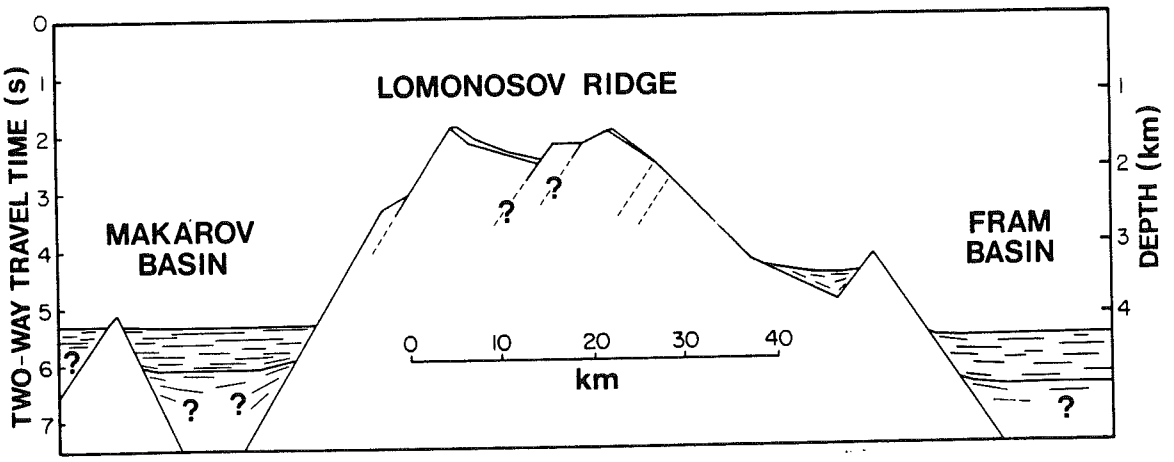

Fig. 4. Generalized shallow seismic structure (line drawing from original data in Blasco et al., 1979; Weber, 1980). Fault traces penetrate near-surface basement and are dashed where weakly established in the seismic records.

the ridge (Fig. 3b). The arch-like appearance of the outermost bathymetric feature results from contouring of widely spaced data. Much less regular topography, a series of seamounts for example, may be present.

Structures within Lomonosov Ridge basement rocks are not apparent in preliminary analysis of records from the intermediate reflection experiment (Overton, 1980). This may indicate a preponderance of high angle structures or perhaps a highly contorted and discontinuous structural pattern or, less likely, a lack of significant structure within the ridge core. More detailed interpretation of these records is presently underway (A. Overton, pers. commun., 1981).

Details of the LOREX crustal refraction experiment are reported elsewhere in this issue (Mair and Forsyth, 1982). Results are described briefly here for a profile extending across the Lomonosov Ridge into the adjacent deep basins (J.A. Mair and D.A. Forsyth, pers. commun., 1980, 1981; Fig. 5a).

Close to the ridge the Fram Basin crust is thicker by 3–4 km overall than the crust of the Makarov Basin, chiefly because of differences in the extent of the 6.6 km/s layer. Each basin contains about 1 km of unconsolidated sediments (2.7 km/s) that overlie a few kilometers of 4.7 km/s basement (Layer 2?) with the remainder of the crust formed by rocks with P-wave velocities of at least 6.6 km/s (Layer 3?). The crust beneath the crest of the ridge is made up entirely of the same two basement velocity units. The 4.7 km/s layer, up to 6 km thick, forms the topographic portion of the feature while the 6.6 km/s unit extends to a depth of about 27 km. The mass of the crustal root is skewed toward the Makarov Basin and, although a fault trace is

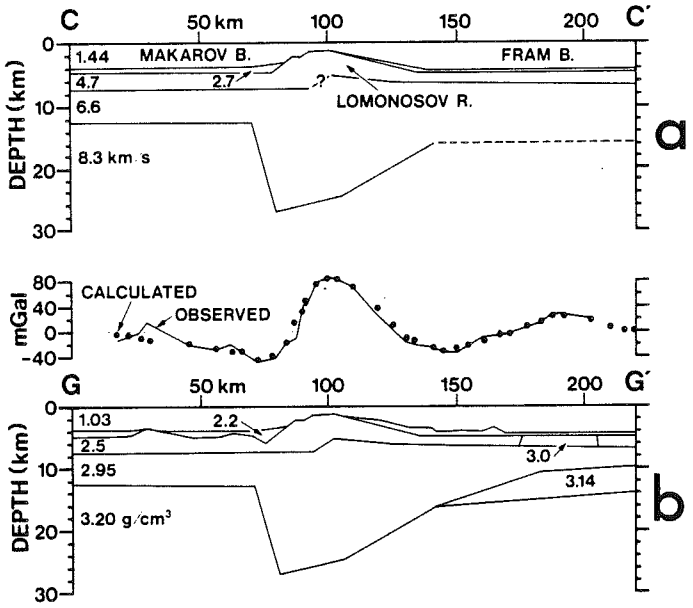

Fig. 5a. P-wave velocity crustal model (from Mair and Forsyth, 1982). Moho dashed beneath Fram Basin to indicate diminished resolution of refraction data beyond base of ridge flank. Velocities in km/s. Profile location given in Fig. 3b.

b. Two-dimensional free-air gravity model based on P-wave velocity horizons in (a). Densities in g/cm^3. Profile location given in Fig. 3b.

not evident on the records, the boundary between the two crustal layers appears to be offset below the ridge crest with the downthrown block toward the Makarov Basin. More detailed aspects of crustal structure and composition, such as the existence of enechelon fault blocks within ridge basement or differences in rock type between the ridge and the deep basins, cannot be resolved with the refraction data.

Magnetic and conductivity structure

Previous high-level reconnaissance surveys show the ridge to be associated with an irregular magnetic anomaly pattern of low relief save for local highs along its crest and Makarov flank close to the North Pole (e.g., Coles et al., 1978). The low-level Hood and Bower (1980) aeromagnetic returns support this regional picture and, in addition, show a spatial correlation in Makarov Basin between positive magnetic anomalies and basement relief as determined from LOREX bathymetric, gravity and shallow seismic work (Figs. 3b, c and 4). A zone of linear magnetic highs in excess of 1000 nT lies parallel to the ridge crest along the Makarov flank just south of the LOREX traverse.

Coles (1980) showed that a strongly positive magnetic anomaly of up to 400 nT is present over the ridge along the LOREX drift path. A preliminary magnetic crustal model constrained to be below the mid-crustal P-wave velocity horizon (Fig. 5a) shows that a tabular region of highly susceptible rocks (0.06 SI) at depths between 7 and 17 km can account for the observed anomaly data (Fig. 6). This tabular zone extends, at depth, well into the Makarov Basin. The base of the model is loosely constrained and could be extended to include the crustal root beneath the ridge with appropriate lowering of the rock susceptibility. A shallower model top, however, appreciably degrades the fit to the observed field (R.L. Coles, pers. commun., 1981).

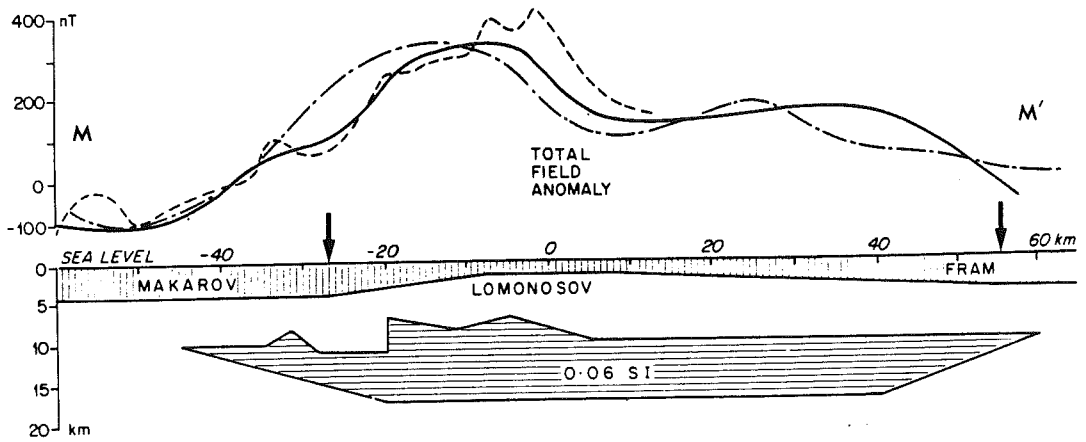

Fig. 6. Proposed magnetic source within the crust below the Lomonosov Ridge (modified from Coles, 1980). The model total field (solid line) is compared with LOREX data (dashed line) and 1970 airborne measurements (dot-dash line). Arrows indicate base of ridge. Profile location given in Fig. 3b.

Shallower magnetic sources within the ridge are indicated by the presence of small short-wavelength positive anomalies that coincide, in two instances, with local topographic maxima on the Fram flank near the crestal region (Fig. 3b; Coles, 1980).

Camfield et al. (1980) have reduced the time varying component of the geomagnetic and geoelectric fields to transfer functions and apparent resistivities and two points become evident. First, the ridge does not have a conducting core; induced electrical currents flow parallel to the ridge in the adjacent deep seas rather than within the ridge. Second, spatial changes in magnetotelluric apparent resistivities appear to correlate with the depth of the highly conducting seawater. A simple two-layer two-dimensional model of the ridge involving seawater and the underlying rock was constructed from LOREX bathymetric data. The modeled electrical response agrees reasonably well with measured variations except in the Fram Basin adjacent to the base of the ridge where the model response falls off more rapidly than the observations. It has not proved possible to decrease this mismatch by adding model inhomogeneities of reasonable conductivity beneath the Fram Basin. The large observed response over the basin may arise from the three-dimensional form of the ridge on the Fram side (Figs. 1 and 3b) or from problems of incomplete separation of variation fields from internal and external currents. (P.A. Camfield, R.D. Kurtz, pers. commun., 1981, 1982).

Electrical conductivity anomalies are typically attributed to variations in rock temperature, to changes in rock porosity or to the concentration and continuity of conducting minerals within the earth. Heat flow from 21 measurements along the Main Camp drift path show a rather undistorted pattern over the region of interest: 60–70 mWm^{-2} in Makarov Basin, 60–65 mWm^{-2} on the ridge flanks and crest, 75–85 mWm^{-2} in Fram Basin (A.S. Judge, pers. commun., 1981). That is, the present thermal regime appears to have a rather deep-seated subcrustal source. Electrical inhomogeneity beneath the Fram Basin, if any, may therefore be unrelated to temperature variations within the earth.

Gravity

The free-air gravity anomaly field is dominated by a prominent high, between 60 and 90 mGal, that extends along the crest of the Lomonosov Ridge (Fig. 3c). This anomaly is flanked by similarly trending lows, generally between −20 and −50 mGal, centred just beyond the ridge flanks in each basin. Secondary highs in Makarov Basin coincide with bathymetric and basement relief (Fig. 3b). As with bathymetric representation of these features, ellipticity of gravity anomaly contours results from the spacing of the collected data (Fig. 3a).

A crustal density model (Fig. 5b) was constructed with density blocks defined by P-wave velocity horizons derived from the refraction and shallow-reflection studies (e.g., Fig. 5a). In the absence of firm control of Moho depth in Fram Basin far from

the ridge, the crust–mantle boundary was inclined very slightly to reflect its documented shallowing (Jackson and Reid, 1980) toward the Nansen–Gakkel Ridge. No attempt was made to account for the small positive gravity anomalies associated with basement relief in the Makarov Basin (see Weber, 1980). The mantle, the unconsolidated sediment layer and seawater were assigned fixed density values. Remaining block densities were adjusted until a good fit between the calculated and observed gravity fields was achieved.

This simple approach worked well except in the Fram Basin where calculated free-air values were consistently much less than the observed anomaly. The position of this discrepancy close to the base of the ridge coincides with the zone where electromagnetic observations cannot be fitted with a two dimensional model. It appears that crust beneath the Fram Basin either is thinner than the seismic refraction model suggests (Weber, 1980) or is more dense close to the ridge than crust below the Makarov Basin. Pursuing the latter option, reduced rock porosity yields increased rock density and, because geostatic pressures rapidly eliminate pore space as depth of burial increases, significant reductions in pore volume are possible mainly within rocks of the upper crust. Accordingly, a zone representing reduced porosity was added to the Fram Basin gravity model in Layer 2 (Fig. 5b).

A density of 3.0 g/cm^3 was considered a reasonable maximum for unporous Layer 2 material and significantly higher densities were tried but, despite greatly improved fits, the calculated gravity anomaly remained well below the observed field in all cases. To adjust this, an additional block (density = 3.14 g/cm^3) was added to the gravity model within the lower crust. The existence of either of these blocks is not supported by other LOREX data sets, although a similar deep zone (Layer 3b) is known elsewhere in the Arctic in oceanic crust of the Canada Basin (Mair and Lyons, 1981). The crustal refraction experiment could not detect such a layer beneath the Fram Basin (Fig. 5a).

SYNTHESIS

Geophysical parameters provide gross compositional properties of rocks within the core of the feature. Ridge structure is indicated mainly by the reflection and refraction results and, to some extent, by aero- and surface magnetic field data. The average age of rocks that make up the Lomonosov Ridge cannot be well bracketed but some tentative comparisons can be made.

Composition

Near-bottom seawater velocity patterns suggest that, in the study area, pulsed competent currents are presently scouring much of the crest and Makarov flank of the Lomonosov Ridge (Aagaard, 1981). The flow may pick up finer material from the upper parts of the ridge and carry it down along the Makarov flank into the

abyss where it is deposited. This current behaviour can explain much of what is observed in bottom photographs and recovered bottom sediments. First is the finer-grained nature of abyssal sediments relative to those of the ridge crest and flanks. Second, the silt-rich interbeds in Makarov Basin may be turbidites produced by scouring episodes related to variations in the velocity of currents descending from the adjacent ridge.

The fraction of recovered or photographed crestal material derived from local sources is unclear. The detritus is abundant, widespread and similar in texture and composition along the drift track. Slumping or scouring of ridge material may be a significant component of this clastic deposit but the present crestal seabed also is probably armoured with ice-rafted debris from which the finer fraction has been removed by near-bottom currents. Support for this contention is the similarity in composition between recovered material from the ridge and ice-rafted debris recovered elsewhere from Arctic seafloor sediments of Alpha Ridge and in Canada Basin (Clark et al., 1980). Ice-rafted material together with atmospheric dust may account for as much as 80% of the sediment deposited in the Arctic Basin over the last 5 Ma (Mullen et al., 1972).

Near the Lomonosov Ridge, deposition by currents appears to have strongly affected the pattern of sediment accumulation within the Makarov Basin for many millions of years. The unconformable contact between basement rocks and the overlying undeformed horizontally stratified material indicates that major sedimentation not only postdates development of the ridge but also is not the result of pelagic processes (Blasco et al., 1979; Fig. 4).

Local igneous bodies along or close to the ridge crest may be indicated by the distribution of short-wavelength positive magnetic anomalies (Hood and Bower, 1980; Coles, 1980; Fig. 3b). The large amplitude magnetic high along the Makarov flank, for example, could be evidence of a major dike or a series of closely spaced dikes that parallel the trend of the ridge. Sources within the upper crust may contribute little, however, to the long-wavelength magnetic high associated with the ridge. The high magnetic susceptibility needed to generate an acceptable crustal model indicates that much of the lower crust beneath the ridge and nearby Makarov Basin may be composed of intermediate to basic rocks. A deeper model base with correspondingly reduced rock susceptibilities does not appreciably alter this contention. Gravity and refraction crustal models yield a density and minimum P-wave velocity for the lower crust of 2.95 g/cm^3 and 6.6 km/s, respectively. Both are reasonable values for the suggested range of rock types.

If the upper crust beneath the ridge is relatively nonmagnetic, then its modeled average density and minimum P-wave velocity of 2.50 g/cm^3 and 4.7 km/s respectively indicate that, overall, it is composed neither of highly magnetic rocks such as FeTi-rich basalts, nor of lithologies with high P-wave velocities including igneous intrusives and high grade metamorphic rocks, nor of dense rocks including dolomites and crystalline rocks with low porosity. Rock types that satisfy the geophysical

constraints fall mainly into the sedimentary or low-grade metasedimentary categories but porous crystalline rocks such as vesicular basalt are not excluded. As indicated, rock fragments recovered from the Lomonosov Ridge can not be reliably related to its basement lithology.

Structure

Normal faulting, both at the surface and deep within the crust below the ridge crest, is indicated by the combined seismic data (Figs. 4 and 5a). Downthrown blocks lie to the south toward the Makarov Basin in all cases. Fault strike and the existence of lateral offsets cannot be determined with assurance, nor can the large apparent offset at depth be physically connected to the set of smaller enechelon displacements close to the surface. If the ridge is a series of imbricated fault blocks, then it is reasonable to suppose because of its linear character that offsets within the ridge trend more or less parallel to its strike. Structural trends may be complicated, however, by the 45° change in orientation of the ridge axis adjacent to the LOREX corridor (Sobczak, 1977; Fig. 1). Subparallel with this direction, three regional lineaments at about 90°W are tentatively identified based on alignment of valleys, embayments, arches and peaks in seafloor morphology (Fig. 3b). These proposed features partially transect the ridge but do not appear to continue into the Makarov Basin. Closer to the Laptev Shelf, the ridge may be cut by highly oblique major faults proposed on the basis of patterns in aeromagnetic data (Karasik et al., 1971). Along the ridge further toward North America, intense magnetic anomalies over the Makarov flank are aligned with the ridge axis (Hood and Bower, 1980). In other words, the structural character of the ridge appears variable and may be quite complex.

Linear magnetic anomalies in the Makarov Basin appear to be aligned with the Lomonosov Ridge (Taylor et al., 1981). As indicated earlier, several LOREX data sets show that, near the ridge, the magnetic anomalies coincide with basement relief and do not represent reversals. The Makarov Basin may not have been formed by simple seafloor spreading. Further evidence for this may be the unrealistically young age of 18 Ma estimated for the basin crust by Taylor et al. (1981) using an empirical seafloor age versus depth relation (Sclater et al., 1971). Such a recent history of accretion is precluded by the absence of significant heat flow anomalies (Judge and Jessop, 1978) and the lack of a topographic spreading ridge remnant within the Makarov Basin. Although Taylor et al. questioned its applicability to small ocean basins, the Sclater et al. relation may fail in basins not produced by a spreading ridge. Instead, Makarov Basin may represent a zone of thinned or stretched continental crust in which a combination of fault blocks and igneous features form the basement surface. The magnetic crustal model allows the possibility that continental-type rocks may be present below part of the basin (Fig. 6; Coles, 1980). The

extent and distribution of basement structure within the Makarov Basin would be revealed by additional shallow seismic and gravity profiling.

Age

The time of origin of the Lomonosov Ridge places a minimum age on the rocks that comprise it. Given its presumed origin, if the ridge is composed of shelf-type clastic sedimentary rocks, then a crude estimate of their age is provided by the average density and P-wave velocity determined for the upper crust below the feature (see Fig. 5). Comparison of these values with both rock density and P-wave velocity versus age data from Birch (1942) indicates that ridge basement may be made up of early Mesozoic or older clastic rocks. This age assignment, such as it is, is necessarily tentative and it applies only to the given rock types. Thick Paleozoic and Mesozoic successions are present in archipelagos along the outer Barents and Kara shelves (Harland, 1973a, b) and such rocks may form much of the margin that faces the Eurasia Basin. This is in keeping with the above density–velocity age estimates.

PERSPECTIVES

What is known now about the Lomonosov Ridge that wasn't known before LOREX? The structural information has been most definitive and it shows that the ridge has undergone a period of tensional faulting. The time of faulting is not clear but it postdates an interval of undisturbed sedimentation along what is now the ridge crest. The significance of the structures is equally ambiguous but the southerly direction of downfaulting indicates that the offsets may be related to the development of the Makarov Basin. This suggestion is preliminary given our ignorance of the timing of events and the uncertain extent of the structures in question. Local causes, such as faulting associated with the nearby zone of changing ridge orientation, are by no means precluded.

This leaves open the question of ridge origin. Leaving the uncertainties aside, the compositional and age constraints provided by LOREX data favor a crustal block containing early Mesozoic or older clastic sedimentary or low-grade metasedimentary rocks in its upper part and intermediate to basic crystalline rocks in its lower part. A relatively deep crustal root and the absence of a high P-wave velocity (7.3–7.6 km/s) basal layer is considered to be typical of submarine plateaus with continental as opposed to oceanic affinities (Carlson et al., 1980). The P-wave velocity structure measured along the outer Barents and Kara shelves is similar to that determined for the Lomonosov Ridge (Eldholm and Talwani, 1977; Beliayevsky et al., 1968; Mair and Forsyth, 1982). The thick Paleozoic and Mesozoic sediments of these outer shelves are among the rock types permitted for the upper crust below the ridge. In short, it is likely that the ridge was once part of the Eurasian polar shelf as Wilson (1963) suggested.

The compositional constraints taken by themselves, however, allow that the Lomonosov Ridge crust could be a pile of vesicular basalts overlying a core of basic rocks and therefore oceanic in nature. It is the morphology of the ridge and the correspondence between the measured properties of its crust and those of the outer polar shelves of western Eurasia that make this possibility less likely, especially when one considers that, before the Eurasia Basin existed, the Lomonosov Ridge was juxtaposed with the Barents and Kara shelves.

How the ridge became separate is less clear. If the faults within the ridge are not related to the opening of the Eurasia Basin, then the separating event may not have involved rifting. Yet the accretionary origin of the Eurasia Basin requires large scale movement of the ridge normal to the line of separation. One major difference between present and early events in the Arctic Basin is the location of the pole of rotation between the Eurasia and North American plates. Prior to the opening of the Eurasia Basin significant separation between the two plates took place in Late Cretaceous and possibly earlier time about a pole in northern Greenland (Fig. 7; Pitman and Talwani, 1972). Separation continues today about a pole in Siberia. Close to this pole, focal mechanism solutions indicate that left-lateral shearing is taking place along the modern plate boundary zone (Chapman and Solomon, 1976).

If the present plate dynamics can be applied to the past, then similar displacements may have occurred between the impinging plates close to their former pole of rotation in northern Greenland (Fig. 7). That is, during Cretaceous time before the Eurasia Basin existed, the terrain about to become the Lomonosov Ridge sheared from Eurasia and was displaced left-laterally along a newly formed plate boundary that may have been delineated by earlier events: an episode of shearing between eastern North America and western Europe in the Triassic (Roy, 1972) and the Jurassic welding of a continental block to Eurasia along a zone to the east of the Cherskiy foldbelt (Fujita and Newberry, 1982; Fig. 7). Shearing between the ridge and Eurasia continued until the outset of the Tertiary when the rotation pivot began its move into Siberia (Pitman and Talwani, 1972) thereby allowing the North Atlantic rift to extend into the Arctic region. Seafloor accretion began along what is now the Nansen–Gakkel Ridge and the Lomonosov Ridge was separated from Eurasia as the spreading proceeded (Wilson, 1963).

The route of the proposed shear around Greenland is conjectural (Fig. 7). To the east of Greenland, initial rifting to open the North Atlantic was accompanied by right-lateral transform movements (Eldholm and Talwani, 1977), in apparent contradiction to the sense of offset indicated by the present scenario. The zone between Greenland and Ellesmere Island, on the other hand, has long been thought to represent a major left-lateral offset (e.g., Wilson, 1963) that was created in Late Cretaceous or Early Tertiary time by the opening of Baffin Bay. The shearing of the Lomonosov Ridge from Eurasia and the origin of Baffin Bay may therefore be genetically linked. This suggestion, which implies that Baffin Bay was initiated prior to the opening of the Eurasia Basin, is tentative because the available constraints are

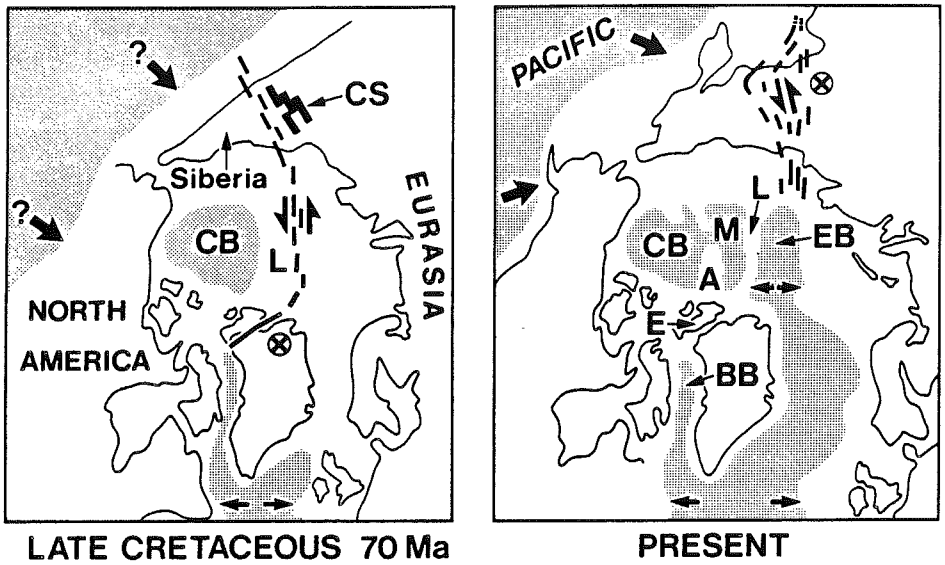

Fig. 7. Cartoon of proposed Cretaceous to present history of Lomonosov Ridge (*L*). Plate boundary zones are dashed. Late Cretaceous pole of rotation for opening of North Atlantic from Pitman and Talwani (1972). Present pole position and plate boundary zone from Chapman and Solomon (1976). *A* = Alpha Ridge, *BB* = Baffin Bay, *CB* = Canada Basin, *CS* = Cherskiy foldbelt, *E* = Ellesmere Island, *EB* = Eurasia Basin, *M* = Makarov Basin.

not clear about the age relationship between the two basins (Srivastava, 1978; Jackson et al., 1979; Vogt et al., 1979) and estimates of the amount of left-lateral displacement along the Greenland–Ellesmere zone vary widely (Christie et al., 1981).

As proposed, this two stage history of ridge movements relative to Eurasia is a consequence of the transition from a compressional to a tensional tectonic regime in Arctic regions produced by the migration of the pole of opening for the North Atlantic to the opposite side of the Arctic at the end of Mesozoic time (Sweeney et al., 1978). As a product of crustal extension, the Makarov flank of the Lomonosov Ridge may thereby have been created distinctly after the shearing stage of ridge movements associated with compression in the Arctic. This implies the non-existence of the Makarov Basin when the ridge sheared from Eurasia and it suggests that the initial Lomonosov block may have included what is now the Alpha Ridge, considered by several workers beginning with King et al. (1966) to be a continental fragment. The Makarov Basin may have been produced by stretching and collapse of continental crust when the newly formed Lomonosov block was split in two by processes as yet undefined. Basement rocks of these two major Arctic submarine ridges may therefore have a common origin and the continental sliver initially sheared from Eurasia may have been much broader than the present Lomonosov Ridge.

This scheme explains how a relatively slender linear fragment can be split from a continent and be carried large distances away, but additional information is needed

on several fronts to more critically evaluate the story. Better constraints are needed on the mode of origin of the Makarov Basin, on the nature of the crust below the Alpha Ridge, on the character of the junction between the submarine ridges and the bordering continents and on the connections, if any, between the genesis of Baffin Bay and the development of the Arctic Basin. These problems remain central targets for future Arctic seafloor basement geophysical studies.

ACKNOWLEDGEMENTS

Dave Halliday reduced the gravity data and helped collect it. Suzanne Juneau generated computer models of crustal density structure. The first author (JFS) benefited from critiques and discussions with J.A. Mair and D.A. Forsyth regarding crustal P-wave velocity models, with P.A. Camfield, R.L. Coles, J.M. DeLaurier and R.D. Kurtz regarding electrical and magnetic crustal structure and with B.D. Bornhold and D.L. Clark regarding glacial-marine sedimentation. C.J. Yorath and M.R. Dence suggested several improvements to a preliminary version of the manuscript. Tactical and logistic support for LOREX was provided by the Polar Continental Shelf Project, the Canadian Forces Base at Alert and the 435th Squadron of the Canadian Armed Forces.

REFERENCES

Aagaard, K., 1980. Moored current measurements over the Lomonosov Ridge. EOS, Trans. Am. Geophys. Union, 61: 279.

Aagaard, K., 1981. On the deep circulation in the Arctic Ocean. Deep-Sea Res., 28A: 251–268.

Beliayevsky, N.A., Borisov, A.A., Volvovsky, I.S. and Schukin, Yu.K., 1968. Transcontinental crustal sections of the U.S.S.R. and adjacent areas. Can. J. Earth Sci., 5: 1067–1078.

Birch, F. (Editor), 1942. Handbook of Physical Constants. Geol. Soc. Am., Spec. Pap., 36, 325 pp.

Blasco, S.M., Bornhold, B.D. and Lewis, C.F.M., 1979. Preliminary results of surficial geology and geomorphology studies of the Lomonosov Ridge, central Arctic Basin. Geol. Surv. Can., Pap. 79-1C: 73–83.

Blasco, S.M., Lewis, C.F.M. and Bornhold, B.D., 1980. Surficial geology and geomorphology of the Lomonosov Ridge. EOS, Trans. Am. Geophys. Union, 61: 276.

Camfield, P.A., Kurtz, R.D., Drury, M.J. and Niblett, E.R., 1980. Magnetovariational and magnetotelluric studies over the Lomonosov Ridge and the Makarov and Fram Basins of the Arctic Ocean: Operation LOREX. EOS, Trans. Am. Geophys. Union, 61: 277.

Carlson, R.L., Christensen, N.I. and Moore, R.P., 1980. Anomalous crustal structures in ocean basins: Continental fragments and oceanic plateaus. Earth Planet. Sci. Lett., 51: 171–180.

Chapman, M.E. and Solomon, S.C., 1976. North American-Eurasian plate boundary in northeast Asia. J. Geophys. Res., 81: 921–930.

Christie, R.L., Dawes, P.R., Frisch, T., Higgins, A.K., Hurst, J.M., Kerr, J.W. and Peel, J.S., 1981. Geological evidence against major displacement in the Nares Strait. Nature, 291: 478–480.

Churkin, M. Jr., 1972. Western boundary of the North American Continental plate in Asia. Geol. Soc. Am. Bull., 83: 1027–1036.

Clark, D.L., Whitman, R.R., Morgan, K.A. and Mackey, S.D., 1980. Stratigraphy and glacial-marine sediments of the Amerasian Basin, central Arctic Ocean. Geol. Soc. Am., Spec. Pap., 181: 57 pp.

Coles, R.L., 1980. The LOREX magnetic gradient and total field experiment, 1979. Geomagn. Lab. Rep., Earth Phys. Br., Ottawa, 12 pp. (unpublished).

Coles, R.L., Hannaford, W. and Haines, G.V., 1978. Magnetic anomalies and the evolution of the Arctic. In: J.F. Sweeney (Editor), Arctic Geophysical Review. Publ. Earth Phys. Branch, 45: 51–66.

Delaurier, J.M., 1978. Arctic Ocean sediment thicknesses and upper mantle temperatures from magneto-telluric soundings. In: J.F. Sweeney (Editor), Arctic Geophysical Review. Publ. Earth Phys. Branch, 45: 35–50.

Dietz, R.S. and Shumway, G., 1961. Arctic Basin geomorphology. Geol. Soc. Am. Bull., 72: 1319–1330.

Eldholm, O. and Talwani, M., 1977. Sediment distribution and structural framework of the Barents Sea. Geol. Soc. Am. Bull., 88: 1015–1029.

Fujita, K. and Newberry, J.T., 1982. Tectonic evolution of northeastern Siberia and adjacent regions. In: G.L. Johnson and J.F. Sweeney (Editors), Structure of the Arctic. Tectonophysics, 89: 337–357.

Harland, W.B., 1973a. Mesozoic geology of Svalbard. In: M.G. Pitcher (Editor), Arctic Geology. Am. Assoc. Pet. Geol., Mem., 19: 135–148.

Harland, W.B., 1973b. Tectonic evolution of the Barents Shelf and related plates. In: M.G. Pitcher (Editor), Arctic Geology. Am. Assoc. Pet. Geol., Mem., 19: 599–608.

Heezen, B.C. and Ewing, M., 1961. The Mid-Oceanic Ridge and its extension through the Arctic Basin. In: G.O. Raasch (Editor), Geology of the Arctic. Univ. Toronto Press, Toronto, Ont., pp. 622–642.

Hood, P. and Bower, M., 1980. Aeromagnetic reconnaissance: LOREX project. EOS, Trans. Am. Geophys. Union, 61: 277.

Jackson, H.R. and Reid, I., 1980. Crustal refraction and seismic reflection results from FRAM 1. EOS, Trans. Am. Geophys. Union, 61: 276.

Jackson, H.R., Keen, C.E. and Falconer, R.K.H., 1979. New geophysical evidence for sea-floor spreading in central Baffin Bay. Can. J. Earth Sci., 16, 2122–2135.

Judge, A.S. and Jessop, A.M., 1978. Heat flow north of 60°N. In: J.F. Sweeney (Editor), Arctic Geophysical Review. Publ. Earth Phys. Branch, 45: 25–33.

Karasik, A.M., Gurevich, N.I., Masolov, V.N. and Shchelovanov, V.G., 1971. Some features of deep structure and origin of Lomonosov Ridge according to aeromagnetic data. Geofiz. Met. Razv. Arktike, Leningrad, 1971: 9–19 (in Russian).

King, E.R., Zietz, I. and Alldredge, L.R., 1966. Magnetic data on the structure of the central Arctic region. Geol. Soc. Am. Bull., 77: 619–646.

Lillestrand, R.L. and Weber, J.R., 1974. Plumbline deflection near the North Pole. J. Geophys. Res., 79: 3347–3352.

Mair, J.A., 1980. Structures of the Arctic Ocean. EOS, Trans. Am. Geophys. Union, 61: 276.

Mair, J.A. and Forsyth, D.A., 1982. Crustal structures of the Canada Basin near Alaska, the Lomonosov Ridge and adjoining basins near the North Pole. In: G.L. Johnson and J.F. Sweeney (Editors), Structure of the Arctic. Tectonophysics, 89: 239–253.

Mair, J.A. and Lyons, J.A., 1981. Crustal structure and velocity anisotropy beneath the Beaufort Sea. Can. J. Earth Sci., 18: 724–741.

Mullen, R.E., Darby, D.A. and Clark, D.L., 1972. Significance of atmospheric dust and ice rafting for Arctic Ocean sediment. Geol. Soc. Am. Bull., 83: 205–212.

Ostenso, N.A., 1962. Geophysical investigations of the Arctic Ocean basin. Geophys. and Polar Res. Center Res. Rep. 4, Univ. Wisconsin, Madison, 124 pp.

Overton, A., 1980. Intermediate reflection profiles. EOS, Trans. Am. Geophys. Union, 61: 276.

Pitman, W.C. III and Talwani, M., 1972. Sea-floor spreading in the North Atlantic. Geol. Soc. Am. Bull., 83: 619–646.

Pounder, E.R., 1980. Physical oceanography in the central Arctic. EOS, Trans. Am. Geophys. Union, 61: 278.

Roy, J.L. 1972. A pattern of rupture of the eastern North America-western Europe paleoblock. Earth Planet. Sci. Lett., 14: 103–114.

Sclater, J.G., Anderson, R.N., Bell. H. and Lee M., 1971. Elevation of ridges and evolution of the central eastern Pacific. J. Geophys. Res., 76: 7889–7915.

Sobczak, L.W., 1977. Bathymetry of the Arctic Ocean north of 85°N latitude. Tectonophysics, 42: T27–T33.

Srivastava, S.P., 1978. Evolution of the Labrador Sea and its bearing on the early evolution of the North Atlantic. Geophys. J.R. Astron. Soc., 52: 313–357.

Sweeney, J.F., Irving, E. and Geuer, J.W., 1978. Evolution of the Arctic Basin. In: J.F. Sweeney (Editor), Arctic Geophysical Review. Publ. Earth Phys. Branch, 45: 91–100.

Taylor, P.T., Kovacs, L.C., Vogt, P.R. and Johnson, G.L., 1981. Detailed aeromagnetic investigation of the Arctic Basin, 2. J. Geophys. Res., 86: 6323–6333.

Vogt, P.R., Taylor, P.T., Kovacs, L.C. and Johnson, G.L., 1979. Detailed aeromagnetic investigation of the Arctic Basin. J. Geophys. Res., 84: 1071–1089.

Weber, J.R., 1979. The Lomonosov Ridge experiment: 'LOREX 79'. EOS, Trans. Am. Geophys. Union, 60: 715–721.

Weber, J.R., 1980. Exploring the Arctic seafloor. GEOS, Dep. Energy Min. Resour., Ottawa, Summer 1980, pp. 2–7.

Weber, J.R. and Sweeney, J.F., 1977. The Lomonosov Ridge experiment. Dep. Energy, Min. Resour., Ottawa, 47 pp. (unpublished).

Wilson, J.T., 1963. Hypothesis of the Earth's behaviour. Nature, 198: 925–929.

Tectonophysics, 89 (1982) 239–253
Elsevier Scientific Publishing Company, Amsterdam – Printed in The Netherlands

CRUSTAL STRUCTURES OF THE CANADA BASIN NEAR ALASKA, THE LOMONOSOV RIDGE AND ADJOINING BASINS NEAR THE NORTH POLE *

J.A. MAIR and D.A. FORSYTH

Hudson's Bay Oil and Gas Company Ltd., Calgary, Alta. (Canada)
Earth Physics Branch, Department of Energy, Mines and Resources, Ottawa, Ont. (Canada)

(Final version received December 22, 1981)

ABSTRACT

Mair, J.A. and Forsyth, D.A., 1982. Crustal structures of the Canada Basin near Alaska, the Lomonosov Ridge and adjoining basins near the North Pole. In: G.L. Johnson and J.F. Sweeney (Editors), Structure of the Arctic. *Tectonophysics*, 89: 239–253.

Seismic refraction surveys conducted in 1976 and 1979 over the broken ice surface of the Arctic Ocean, reveal distinctly different crustal structures for the Fram, Makarov and Canada basins. The Canada Basin, characterized by a 2–4 km thick sedimentary layer and a distinct oceanic layer 3B of 7.5 km/s velocity has the thickest crust and is undoubtedly the oldest of the three. The crust of the Makarov Basin has a thin sedimentary layer of less than 1 km and is about 9 km in total thickness. The Fram Basin has a similarly thin sedimentary layer but is 3–4 km thicker than the Makarov as it approaches the Lomonosov Ridge near the North Pole. The ridge itself is cored by material with a velocity of 6.6 km/s and may be a metagabbro similar to oceanic layer 3A. This ridge root material extends to a depth of about 27 km, where a change occurs to upper-mantle material with a velocity of 8.3 km/s. The core is overlain by up to 6 km of material with a velocity of about 4.7 km/s which could be oceanic layer 2A basalts or continental crystalline rocks with some sedimentary material.

The Fram Basin probably began to open contemporaneously with the North Atlantic about 70 m.y. ago, by spreading along the Nansen–Gakkel Ridge. Although not yet dated, the Makarov Basin is probably no older than the initiation of the Fram Basin and may be much younger. The Alpha Ridge may once have been part of the Lomonosov Ridge, splitting off to form the Makarov Basin between 70 and 25 m.y. ago, and possibly contributing to the Eurekan Orogeny of 25 m.y. ago, evident on Ellesmere Island. In contrast, the likely age of the Canada Basin lies in the 125–190 m.y. range and may have been formed by the counter-clockwise rotation of Alaska and the Northwind Ridge away from the Canadian Arctic Islands. The Lomonosov Ridge emerges from this scenario as a block resulting from a strike-slip shear zone on the European continental shelf, related to the opening of the Canada basin (180-120 my) and then becomes an entity broken from this shelf by the opening of the Eurasia Basin (70–0 m.y.).

---

* Contribution of Earth Physics Branch No. 992, LOREX Contribution No. 10.

0040/1951/82/0000–0000/$02.75

INTRODUCTION

The tectonic history of the Arctic Basin remains relatively obscure due in part to the logistical difficulties of exploration in this remote and inhospitable area of the world. The data base from which we may hope to unravel this history is slowly improving but concensus even as to general concepts of the tectonics has not been reached. Sweeney et al. (1978) give a review of published geophysical studies current to 1978 for this area and discuss some of these concepts.

The main physiographic features of the Arctic Basin and the surrounding 'continental' structures are sketched in Fig. 1. In 1976 a seismic refraction survey was conducted in the Beaufort Sea of the Canada Basin (Mair and Lyons, 1981) and in 1979 a similar survey was conducted near the North Pole across a narrow flexure of the Lomonosov Ridge into the adjoining Makarov and Fram basins. The crustal structures of these features, as interpreted from the refraction data, provide a valuable constraint on models of the evolution of the Arctic Basin. We compare the crustal structures obtained from our surveys with models of features obtained elsewhere, to place them within a continental–taphrogenic–oceanic context and then propose an evolutionary scenario that might explain these features.

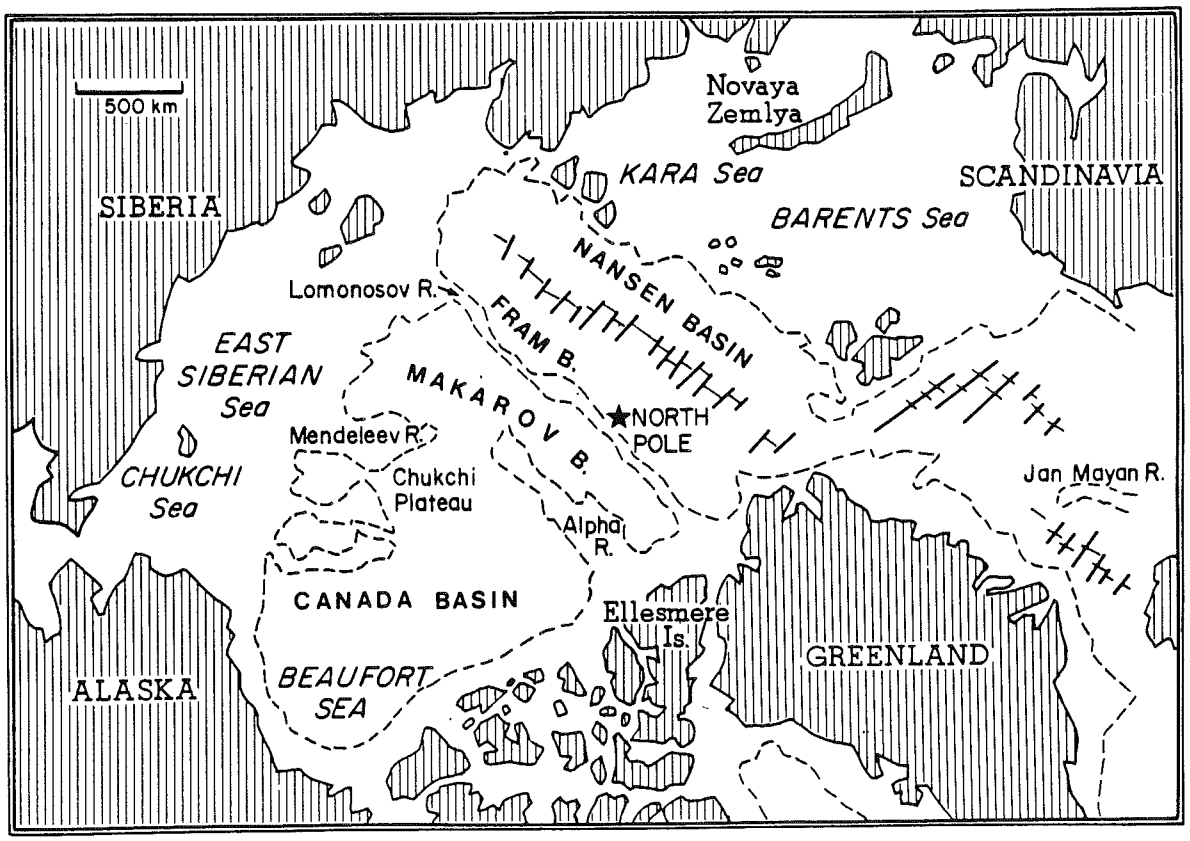

Fig. 1. Principal physiographic features of the Arctic seas and margins.

Figure 2 indicates the location of the refraction profiles obtained during the AIDJEX (Arctic Ice Dynamics Joint Experiment) project in 1976. The interpreted crustal profile from the deep water of the Canada Basin towards the continental rise of Alaska (*C–A*) has been joined in Fig. 3 to a multi-fold CDP reflection profile

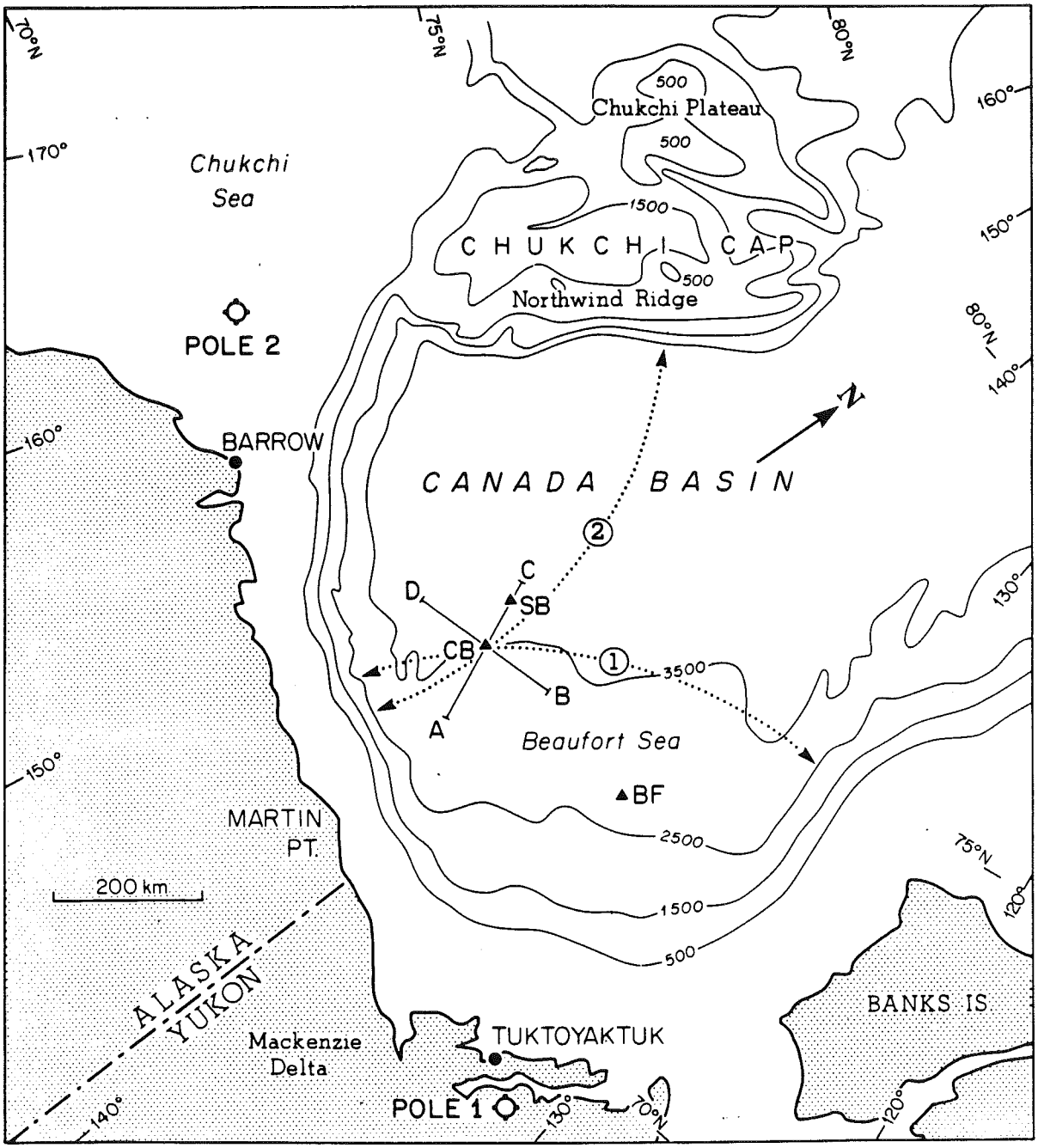

Fig. 2. Refraction profiles from operation AIDJEX in the Beaufort Sea. *A*, *B*, *C* and *D* are shotpoints while remote camps are labelled *SB*, *CB* and *BF*. Bathymetry is in meters (From Mair and Lyons, 1981).

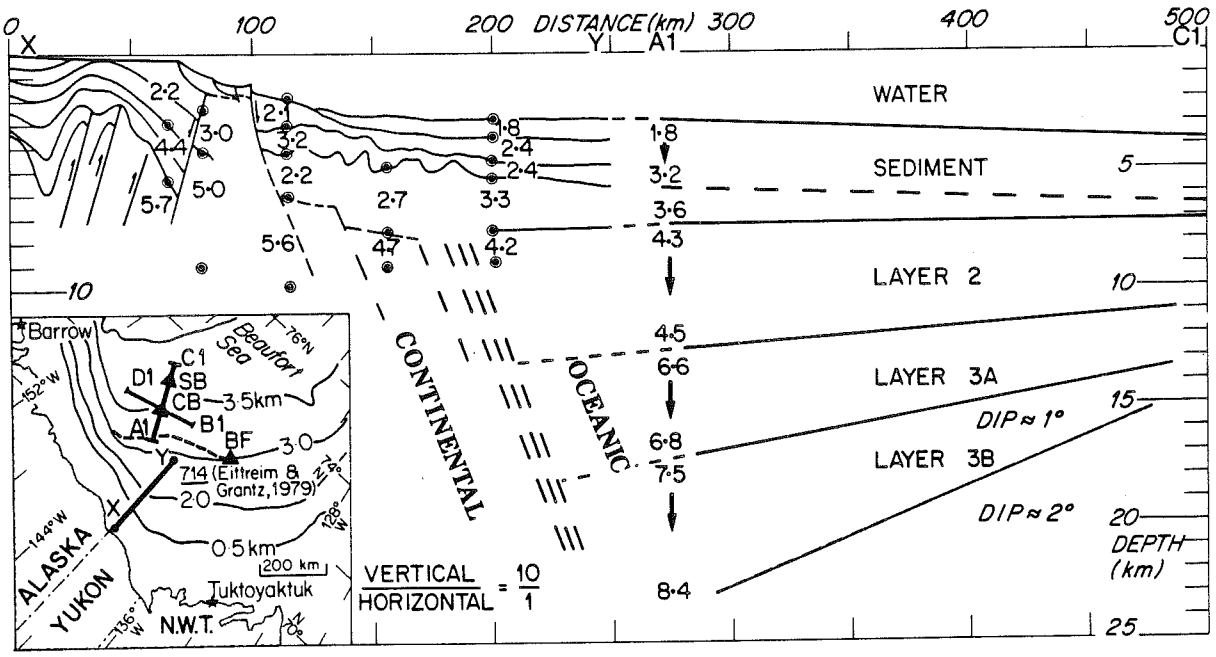

Fig. 3. North American continental–oceanic transition compiled from Mair and Lyons (1981) and Eittreim and Grantz (1979).

(X–Y) from Eittreim and Grantz (1979), (Mair and Lyons, 1981). The velocity and depth of the sediments are in good agreement where these profiles join. Near the continental edge of Alaska, the deep structure was not revealed by the CDP work and the continental–oceanic crustal contact as indicated in Fig. 3 is speculative. The deeper basin structure is considered to be typically oceanic beneath a 3–5 km thick blanket of sediment. In addition, the velocity anisotropy of the upper mantle determined by Mair and Lyons (1981) suggests that the Northwind Ridge rotated to its present position about pole *2* (Fig. 2) in the Chukchi Sea.

LOMONOSOV RIDGE–FRAM AND MAKAROV BASINS

Figure 4 indicates the location of the refraction profiles collected during the LOREX (Lomonosov Ridge Experiment) project in 1979 and the bathymetry of this part of the Arctic Basin. Preliminary interpretation of two pseudo-reversed strike profiles are shown in Fig. 5. Beneath a poorly resolved upper crust of perhaps 6 km thickness lies a layer with a thickness exceeding 20 km and a well sampled compressional velocity of 6.5–6.6 km/s. Beneath this layer a relatively sharp transition zone grades into a velocity typical of upper mantle material. The velocity gradient within this transition zone was derived with the aid of synthetic sections to produce the secondary events evident in the 60–100 km distance range in Fig. 5. A final interpretation will be published when more details of the upper crust become available from the intermediate range seismic work conducted by others during the

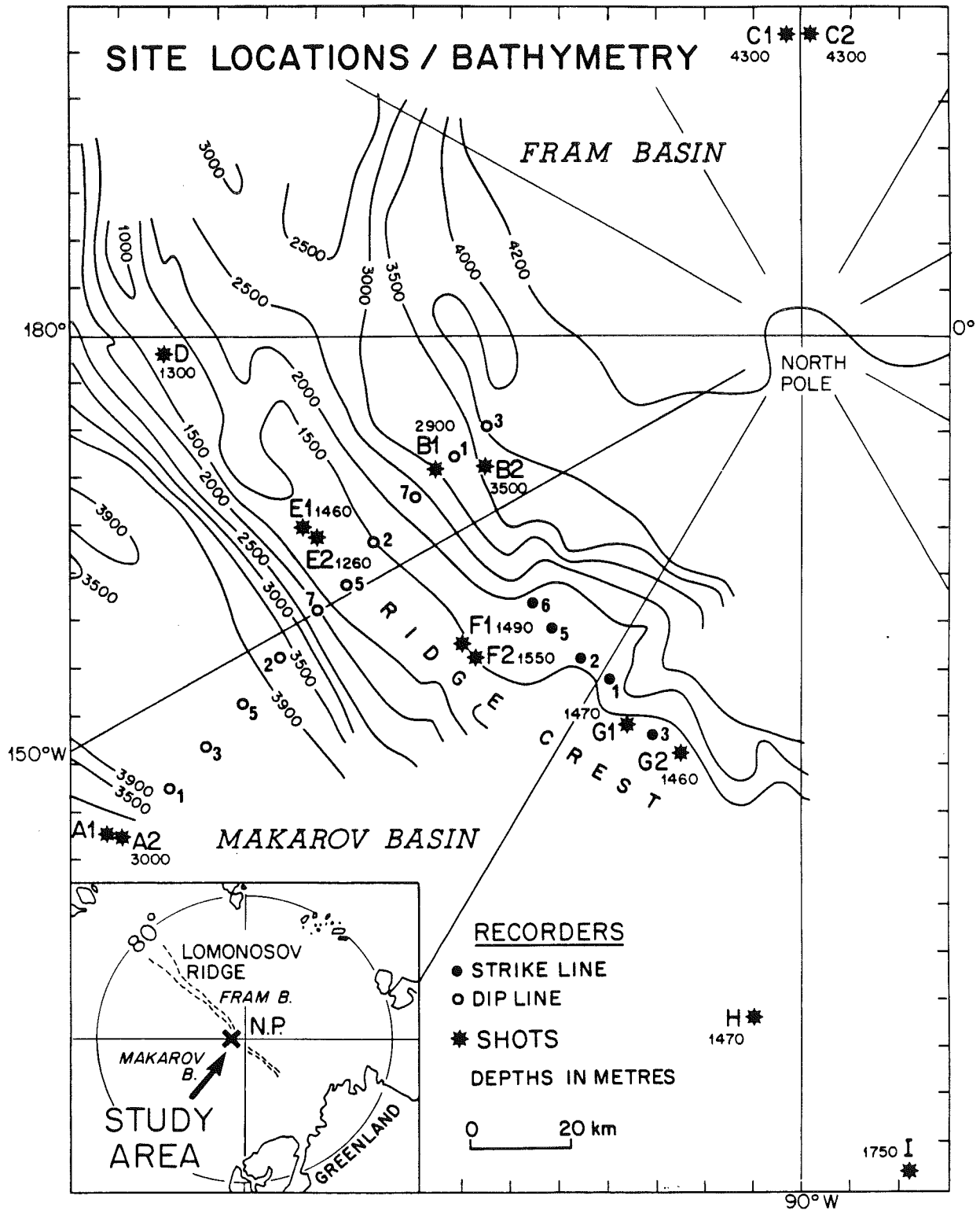

Fig. 4. Shotpoints (stars), recording stations (dots and circles) and bathymetry for the area of project LOREX.

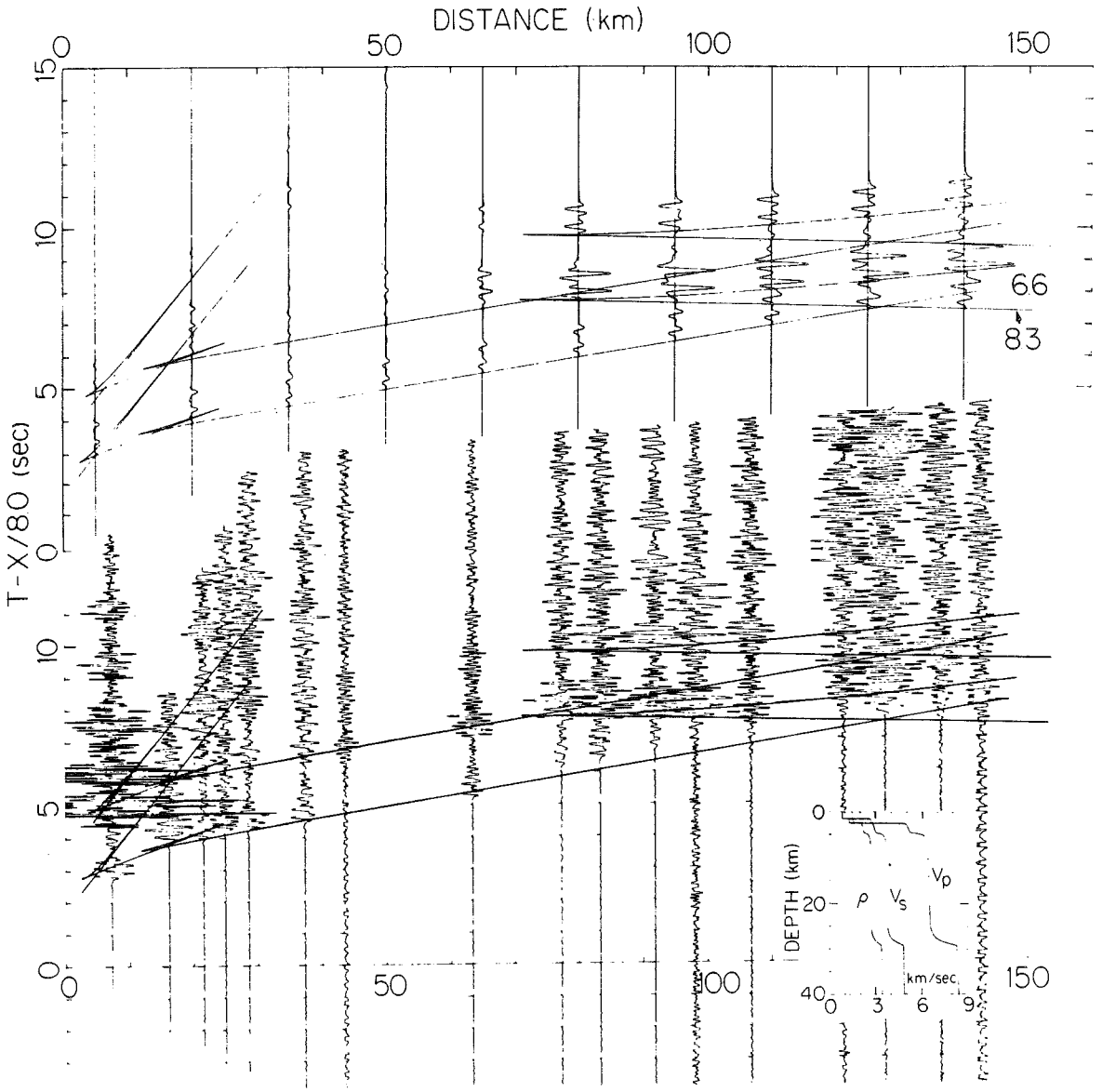

Fig. 5. Comparison of synthetic crustal response with data along east to west strike profile (*I-6* in Fig. 4), Lomonosov Ridge. Inset shows P- and S-wave velocity crustal models.

LOREX project; however, the general form of the deeper crustal structure of the Lomonosov Ridge will not differ greatly from that indicated here.

A preliminary interpretation of several dip profiles is shown in Figs. 6, 7 and 8. The 9 km thickness of the oceanic crust near the Lomonosov Ridge on the Makarov Basin side is believed to be well resolved by first arrival refracted events and the high amplitude secondaries that are consistent with a double bounce post-critical reflection from the upper–mantle as shown in Fig. 6. The thickness of the oceanic crust near the ridge on the Fram side is probably thicker than shown with a dip component of perhaps 2°, giving a rapid thinning of this crust as it approaches the

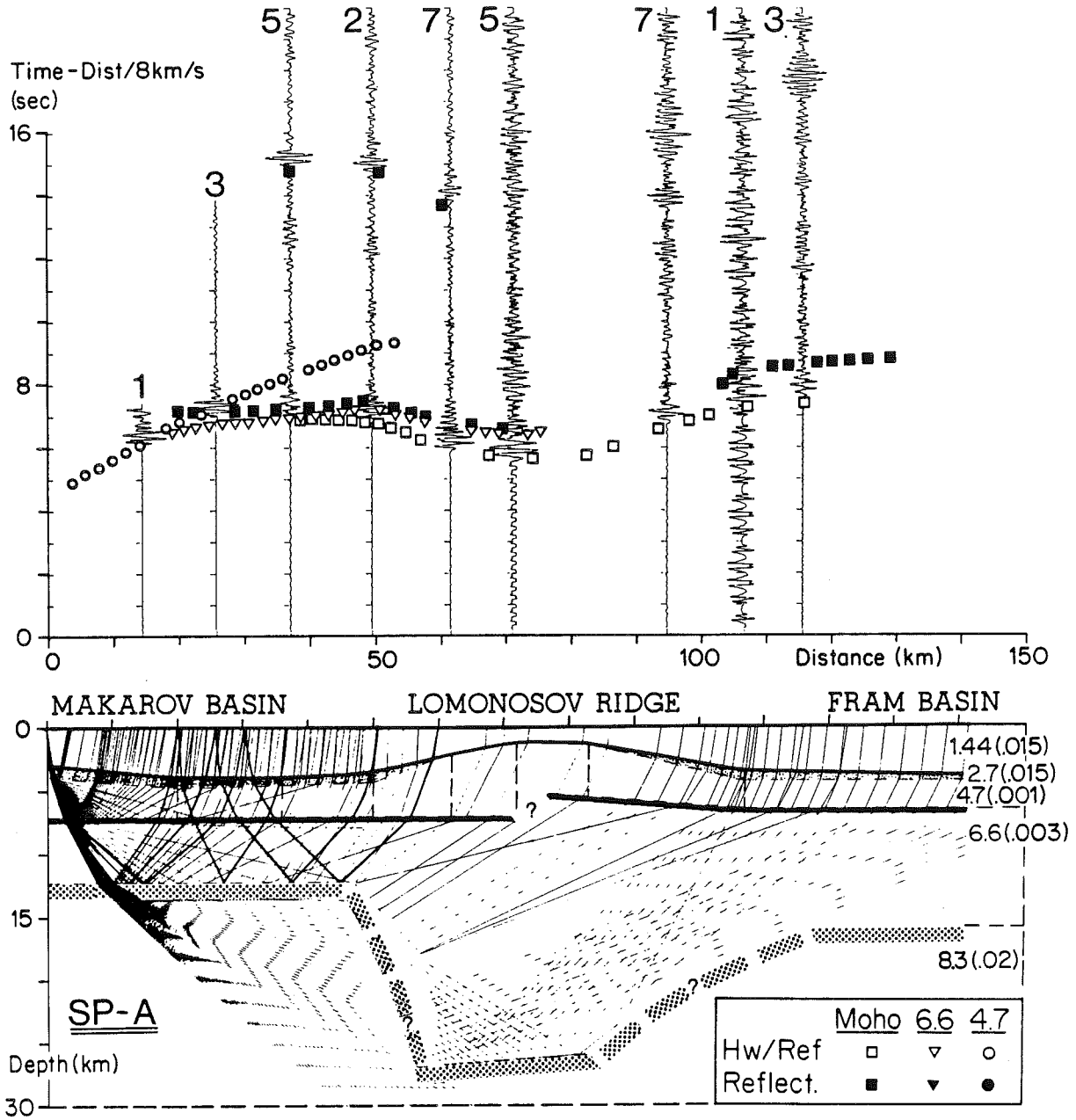

Fig. 6. Refraction profile from the Makarov (A_1, A_2 in Fig. 4) to the Fram Basin.

active spreading center separating the Fram and Nansen basins. The root structure beneath the Lomonosov Ridge might then be even more asymmetric than illustrated.

SYSTEMATICS OF CRUSTAL TYPES

Berckhemer et al. (1975) attempted to relate crustal models, interpreted from refraction data gathered on the Ethiopian Shield and the Afar region, within a

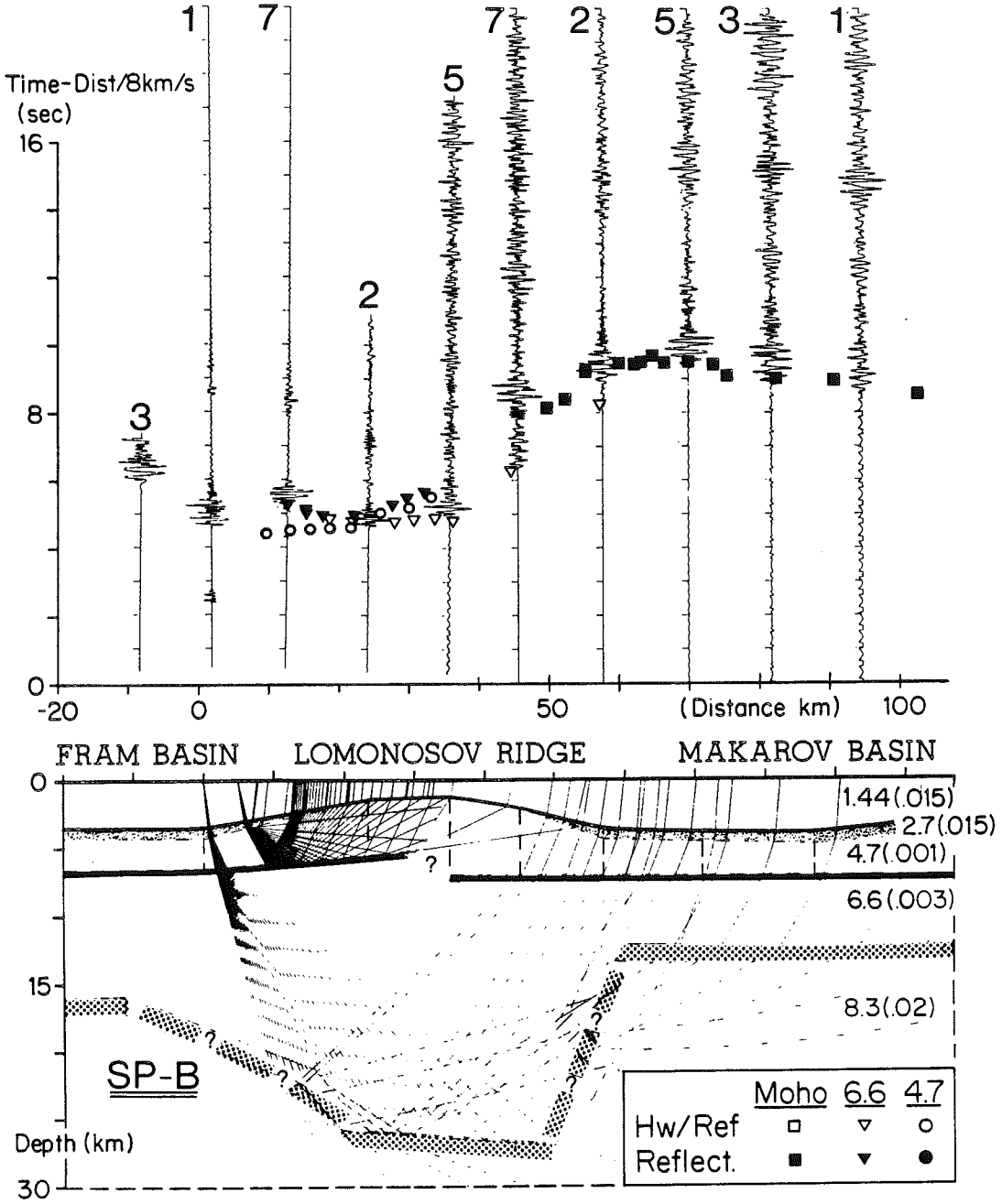

Fig. 7. Refraction profile from the Fram (B_1, B_2 in Fig. 4) to the Makarov Basin.

general scheme of continental–taphrogenic–oceanic crustal structures. Their result is reproduced in Fig. 9. The distinguishing features evident in this figure are the thinning of acidic rocks (velocities near 6 km/s) from thicknesses of 10–20 km in ancient continental shields to zero within oceanic crust, and the overall thinning of total crustal thickness within this sequence.

Figure 10a indicates that a similar schematic can be obtained for Arctic continental features grading into the oceanic crust of the Canada Basin. The two 6.3 km/s

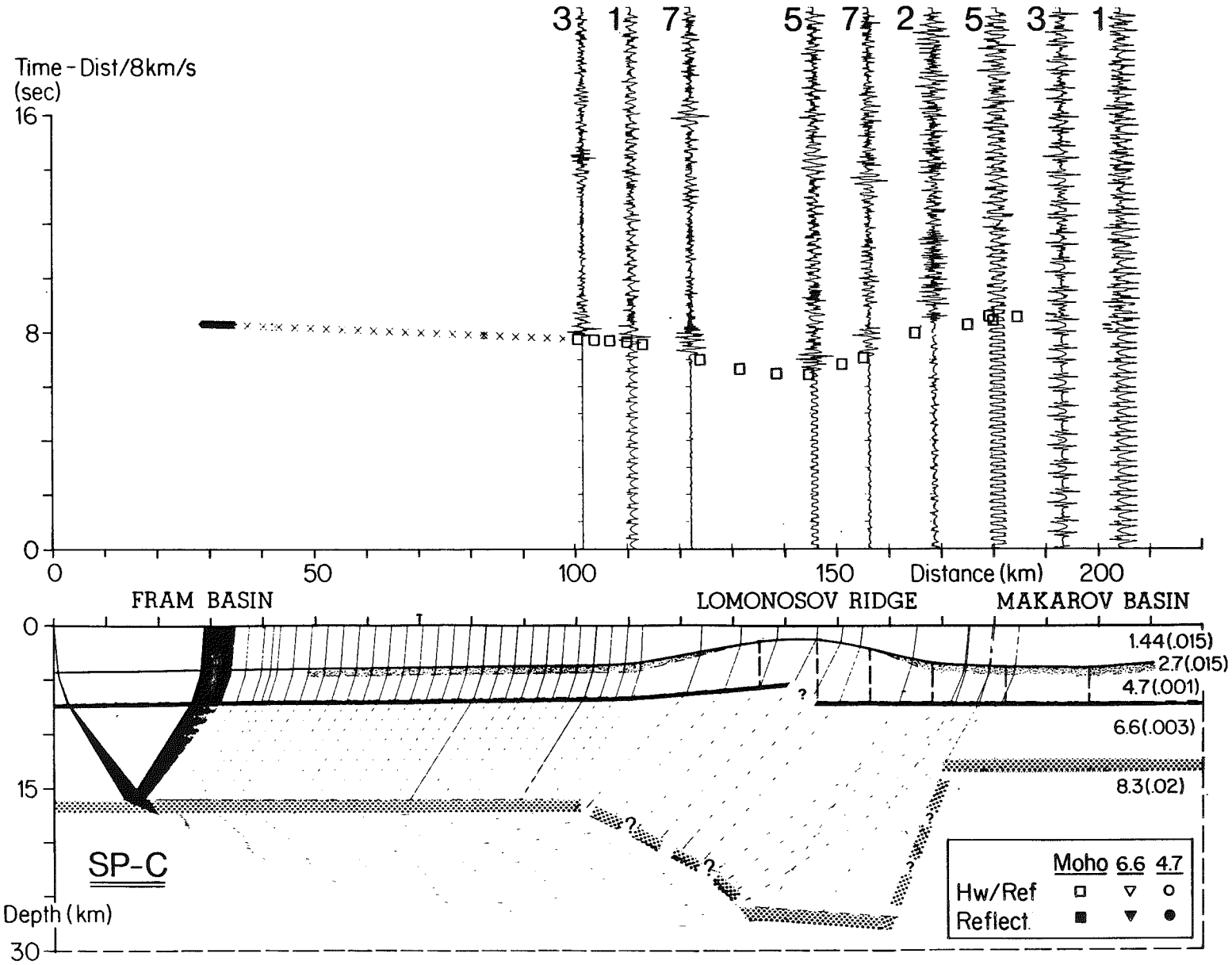

Fig. 8. Longer range refraction profile from the Fram (C_1, C_2 in Fig. 4) to the Makarov Basin corroborating the structure derived from Fig. 7. Note that crustal structure beneath Fram Basin not well constrained between shot point *C* and station *3*.

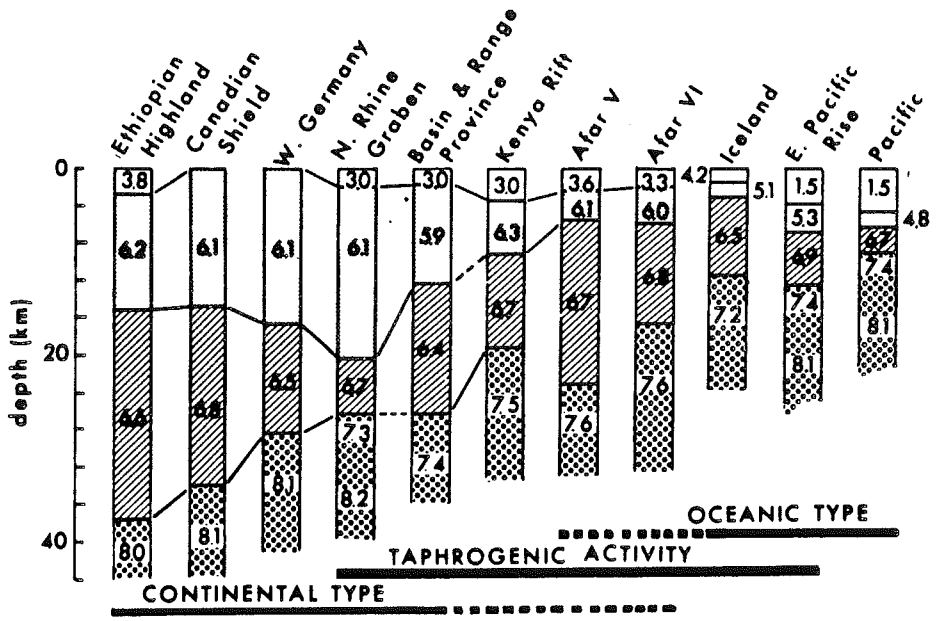

Fig. 9. Comparison of crustal structures from Berckhemer et al. (1975).

sections shown for the Sverdrup Basin are meant to indicate that limestone, encountered by deep drilling in this area and known to have this velocity, may overlie granitic rocks of similar velocity. The Sverdrup Basin is a taphrogenic

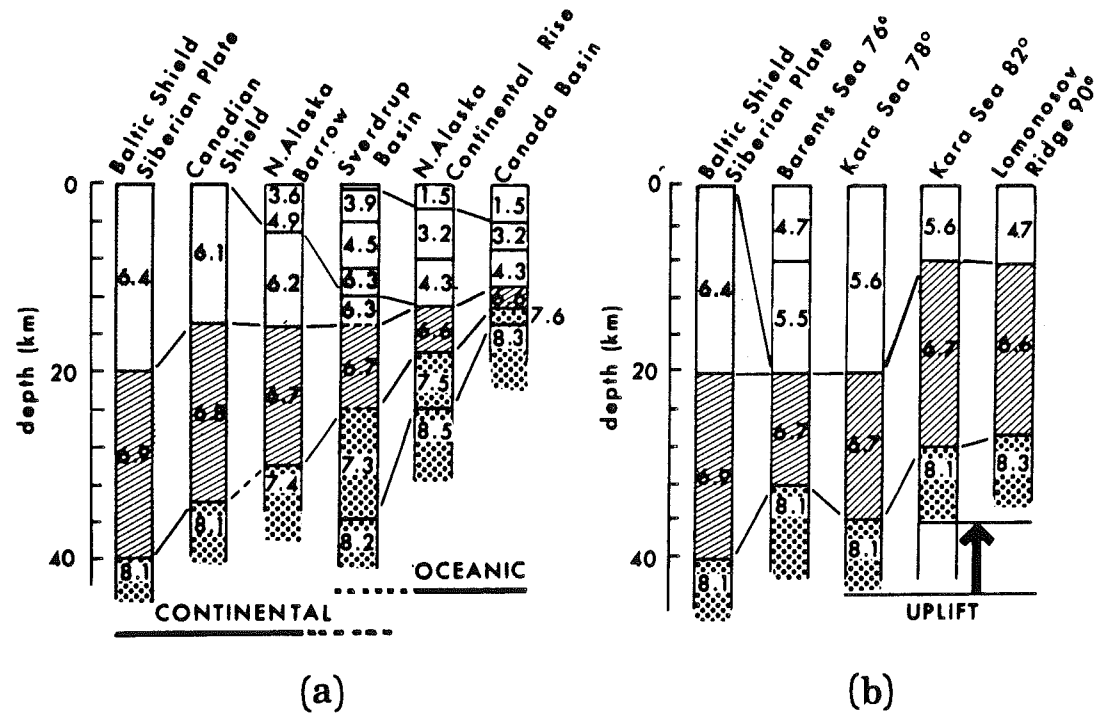

Fig. 10. Comparison of crustal structures grading into the Canada Basin with structures from the Lomonosov Ridge and the Baltic Shield. (From Sweeney et al., 1981; Mair and Lyons, 1981.) Indicated uplift discussed in text.

structure (Forsyth et al., 1979). Figure 10b indicates that the structures beneath the now shallow Barents and Kara Seas and the Lomonosov Ridge do not follow Berckhemer's classification, appearing to be neither related to ancient continental shields nor modern ocean basins, i.e., while the crusts are thick enough to be considered continental they do not exhibit velocities typical of the acidic rocks. The Barents and Kara Sea 78° sections may then represent an intermediate or 'old shelf' type of crustal structure characterized by a thick (>20 km) sedimentary section (P-wave velocities near 5.5 km/s) deposited on an older oceanic crust. Figure 11 places these areas in a schematic of oceanic crustal types arranged in a supposed order of increasing age. Oceanic crust beneath the Alaska Rise is estimated to be Upper Jurassic to Lower Cretaceous in age (150–120 m.y.) (Eittreim and Grantz, 1979; Mair and Lyons, 1981). No older oceanic basin structures within the Arctic have been reported to the authors' knowledge. It is suggested that the structures below the Barents and Kara seas are the result of a very thick sedimentary section deposited upon an ancient oceanic crust that predates the Jurassic.

The resemblance between the structure below the Kara Sea at 82°N and that of the Lomonosov Ridge at 90° in Fig. 11 is striking granted that upper crustal velocity control is poor. Closing of the Fram and Nansen basins would place these structures together and their similarity provides support for the suggestion (see for example, Wilson, 1963) that the Lomonosov Ridge is a fragment rifted from the Baltic Shelf. Eldholm and Talwani (1977) indicate that some areas of the Barents Sea have subsided less than others (e.g. The Svalbard Platform). They suggest that areas with relatively thin sediments result from a combination of reduced subsidence rates and greater erosional effects when above sea level. These effects along with the rifting process may account for the indicated uplift of the sections shown in Figs. 10b and

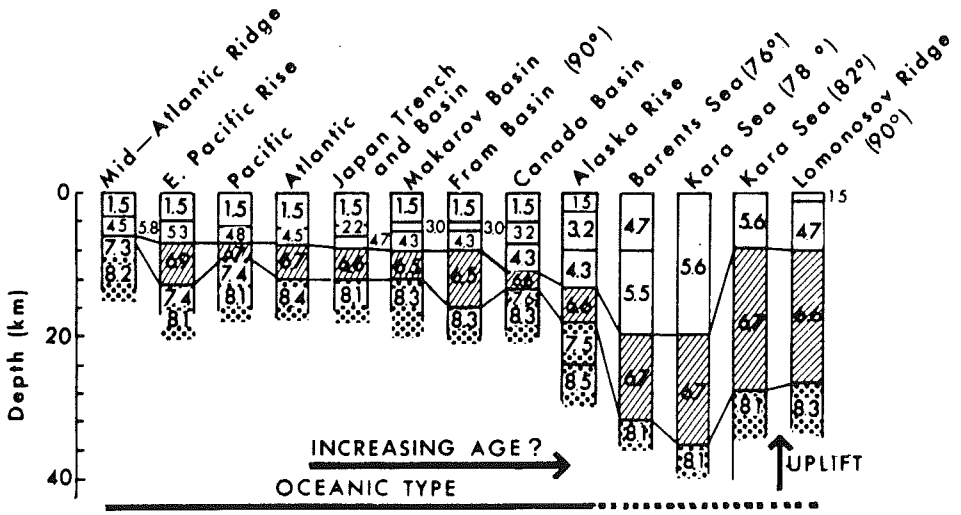

Fig. 11. Present oceanic structures. Uplift discussed in text.

11 and their thickened root material relative to the shelf areas nearer the Baltic Shield. If the more northerly crustal sections were once similar in structure to the Barents and Kara seas further inland then subsequent relative uplifts along the outer shelf may have created a high standing region from which a 10–12 km section of sediments has been eroded. The upper crust of the Lomonosov Ridge in the LOREX area may therefore prove to be a highly metamorphosed and ancient sedimentary section mixed with oceanic basalts.

DISCUSSION

While the foregoing has included some conjectural comment that seemed pertinent as the areas were discussed, the following attempts a more global description of Arctic tectonics.

A cartoon of how the Arctic may have appeared 150 m.y. ago is shown in Fig. 12-III with the (now) northern parts of Alaska and Chukhotsk pressed against northern Canada. Prior to this time northern Canada and the Baltic shield may have faced an ancestral Pacific Ocean and parts of Alaska and Chukhotsk had not as yet accreted to these cratons. The figure shows three zones of weakness (ancient sutures?), the Caledonian, Ural and Franklinian fold belts. The Pacific edge of the Arctic–Chukhotsk block was subject to subduction of an ancestral oceanic plate resulting in the separation of the block from the continent along the existing zones of weakness, possibly by back-arc spreading (Uyeda, 1981). Some 10,000 km of the ancestral Pacific plate, now no longer in existence, have been subducted beneath continental margins to the north. Back-arc spreading continued until Chukhotsk docked against the Kolyma Block of Siberia at perhaps 120 m.y. and formed a juvenile Canada Basin, isolated from the Atlantic and Pacific systems and surrounded by continental structures as depicted in Fig. 12-II.

During late Jurassic–early Cretaceous time the Barents and Kara shelves included the Lomonosov Ridge bordering the deeper Canada Basin. The Lomonosov Ridge structure, possibly mountainous during the rifting/shearing stage associated with the opening of the Canada Basin, may have shed large quantities of sediment into the surrounding shallow seas and into the deep Canada Basin.

Subduction of the Pacific Plate continued, bringing in allochthonous terranes to the southern margins of Alaska and Chukhotsk and renewing back-arc spreading behind the Aleutian, Kurile and Japan Island arcs. Figure 12-I shows these features as they appear at present and indicates that the scale of present day back-arc features is not greatly different than that supposed for the creation of the Canada Basin. The scale differences that do exist could be accommodated with greater spreading rates (approximately 10 cm/yr) of the ancestral Pacific plates.

The Nansen and Fram basins reveal their age through magnetic striping with initial spreading beginning about 70 m.y. and continuing at present as part of the North Atlantic system. Renewed rifting again uplifted the outer Barents and Kara

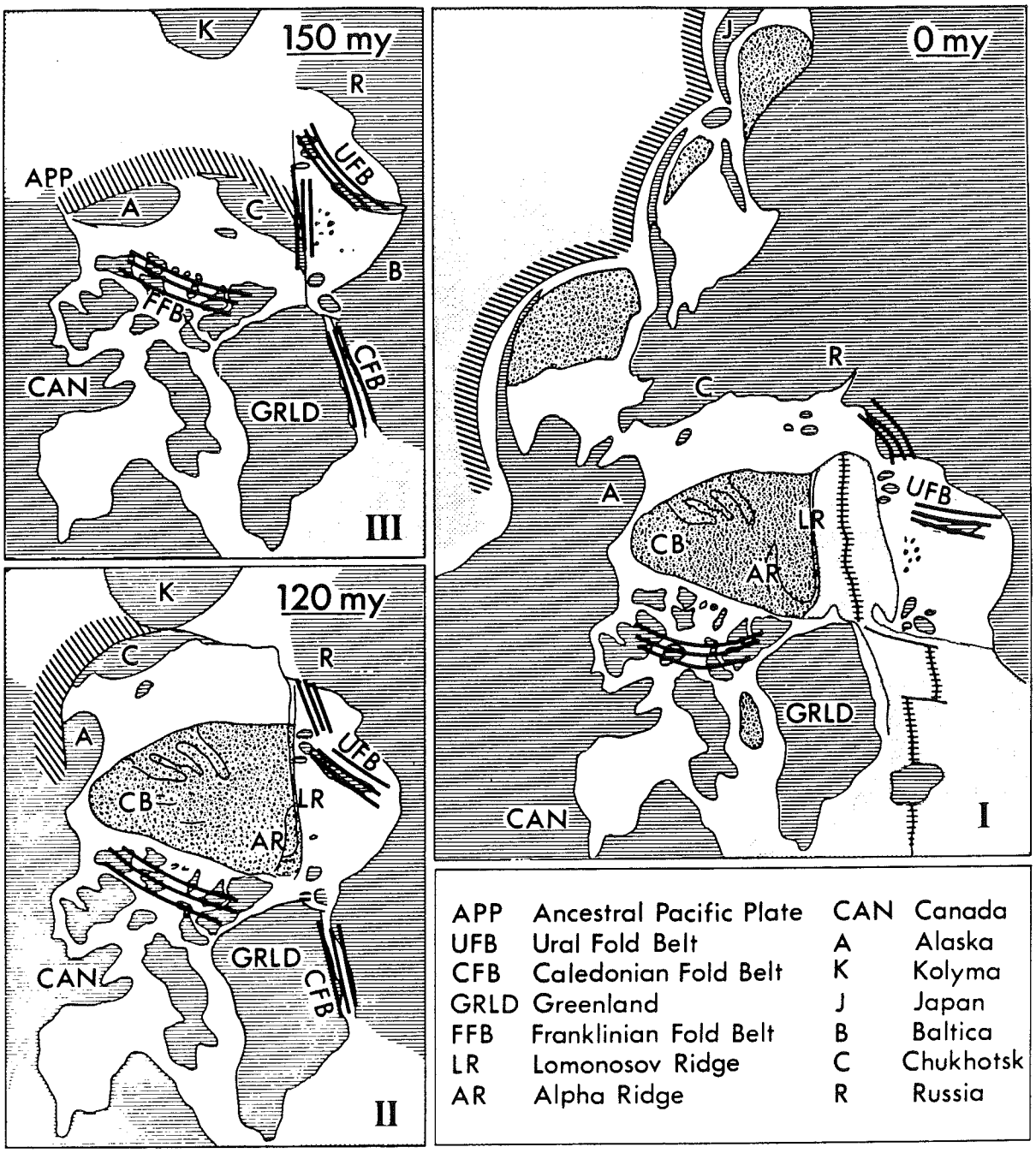

Fig. 12. Cartoon of the development of the Arctic region from 150 m.y. to present.

shelves and split off the Lomonosov Ridge from the Kara Sea structure at 82°. Great quantities of sediment may have been eroded from these mountainous structures and deposited within the Kara Sea and the Canada Basin. While the appropriate share of this sediment load may be accounted for within the present-day shallow Kara and Barents seas there is no obvious repository for the remaining share within the Makarov Basin, which in the LOREX area exhibits only a thin sedimentary cover.

We suggests that at this time of rifting and uplift the Alpha and Lomonosov Ridges were together, the Alpha Ridge receiving this sedimentary load; then during a later rifting episode the Alpha Ridge separated from the Lomonosov Ridge to create the Makarov Basin. That the initiation of the Makarov Basin would thus be more recent than the age of initiation of the Fram Basin is perhaps consistent with the Makarov Basin's thinner oceanic crust relative to that of the Fram where they approach the Lomonosov Ridge.

The true nature of the Alpha Ridge we leave unto CESAR (Canadian Expedition to Study the Alpha Ridge), a multidisciplinary study proposed for the spring of 1983.

CONCLUSIONS

(1) The Kara Sea at 82°N and the Lomonosov Ridge near the North Pole exhibit similar crustal configurations and, though separated now by the modern Nansen and Fram Basins, may once have been part of the same crustal block.

(2) This crustal block does not exhibit detectable thicknesses of acidic/granitic rocks and may therefore be of taphrogenic or oceanic origin.

(3) In the Kara Sea at 78°N the block may be 40 km in total crustal thickness, some 20 km of which may be of sedimentary origin. In the Kara Sea at 82°N, the total crust has thinned by about 8 km, exhibiting thickened root material and sediments that may be less than 8 km thick.

(4) Uplift of the northern edge of the Kara Sea and the Lomonosov Ridge by perhaps 10–12 km may thus have occurred in times past creating a mountain range, founded on an ancient oceanic crust, that joined Greenland to Siberia.

(5) The timing of these uplift stages should be revealed in the depositional sequences of the Kara and Barents sea areas. Two of these stages should correspond to uplifts caused by rifting during the opening of the Canada Basin and more recently by the opening of the Fram and Nansen basins.

ACKNOWLEDGEMENTS

We would like to sincerely thank A. Green, J. Sweeney and M. Berry for constructive reviews of the manuscript.

REFERENCES

Berckhemer, H., Baier, B., Bartelsen, H., Behle, A., Burkhardt, H., Bebrande, H., Makris, J., Miller, H. and Vees, R., 1975. Deep seismic soundings in the Afar region and on the highland of Ethiopia. In: R. Pilger and A. Rosler (Editors), Afar Depression of Ethiopia. Schweizerbart, Stuttgart—Inter-Union Commission on Geodyn. Sci. Rep., 14: 89–107.

Eittreim, S. and Grantz, A., 1979. CDP seismic sections of the western Beaufort continental margin. In: C.E. Keen (Editor), Crustal Properties across Passive Margins. Tectonophysics, 59: 251–262.

Eldholm, O. and Talwani, M., 1977. Sediment distribution and structural framework of the Barents Sea. Geol. Soc. Am. Bull., 88: 1015–1029.

Forsyth, D.A., Mair, J.A. and Fraser, I., 1979. Crustal structure of the central Sverdrup Basin. Can. J. Earth Sci., 16: 1581–1598.

Mair, J.A. and Lyons, J.A., 1981. Crustal structure and velocity anisotropy beneath the Beaufort Sea. Can. J. Earth Sci., 18: 724–741.

Sweeney, J.F., Coles, R.L., DeLaurier, J.M., Forsyth, D.A., Irving, E., Judge, A.S., Sobczak, L.W. and Wetmiller, R.J., 1978. Arctic geophysical review—a summary. In: J.F. Sweeney (Editor), Arctic Geophysical Review. Publ. Earth Phys. Br., Ottawa, 45: 101–108.

Uyeda, S., 1981. Subduction zones and back-arc basins—a review. Geol. Rundsch., 70: 552–569.

Wilson, J.T., 1963. Hypothesis of the Earth's behavior. Nature, 198: 925–929.

A SEISMIC REFLECTION PROFILE ACROSS THE LOMONOSOV RIDGE, CENTRAL ARCTIC OCEAN

A. Overton, Geological Survey of Canada, Ottawa, Ontario

(Excerpt from Society of Exploration Geophysicists, Technical Program Abstracts and Bibliographies, 52nd Annual Meeting, 1982, Dallas, p. 87-89, with more detailed figures.)

Introduction

From March to June of 1979, the Department of Energy, Mines and Resources (Canada) coordinated a multidisciplinary geophysical and oceanographic expedition code-named LOREX to investigate the nature and origin of the Lomonosov Ridge near the north geographical pole (Weber, 1979). As part of this experiment, seismic reflection profiling was conducted from the ice station along its drift path across the ridge. More than 200 good quality reflection records were obtained along a 185 km drift path which crossed the ridge from the Amerasia Basin to the Eurasia Basin.

Instrumentation and Method

A 48 station cross array was used with 91.4 m station spacing measured from the centre of the array. The size of the array was limited by zones of weakness on the ice sheet. Several hours of strong winds in excess of 45 km/hour opened cracks and leads around the campsite. The seismic array was fortuitously positioned to minimise problems from ice breakup. The arms of the array were oriented at approximately 45 degrees to the axis of the Lomonosov Ridge. Times of solar alignment with the arms of the array were noted periodically to check this orientation throughout the course of the experiment. Each station consisted of a nine 14 Hz seismometer pattern aligned with the arms of the array and seismometer spacing of 11.4 m. Dynamite charges ranging from 0.9 to 18.1 kg were detonated in the centre of the cross array at a depth of 90 m. These shots were digitally recorded on a Sereel model 338A seismograph system and digital tape recorder.

Results

Use of the cross array permitted the computation of true dips and the positions of steeply dipping reflected events. The limited size of the array, however, did not permit reliable computation of sedimentary velocities. Sedimentary thicknesses in this discussion are computed using an assumed nominal velocity of 2 km/sec. Thus, 2 sec of reflection time are taken to represent 2 km of sedimentary thickness. Water depths were computed using an average velocity of 1.483 km/sec (Blasco et al, 1979). Water depth measurements range from 3950 m on the Amerasia side of the ridge and 4200 m on the Eurasia side to 1480 m at the ridge crest. Dip calculations on the ridge structure average 10.3 degrees on the Amerasia flank and 6.5 degrees on the Eurasia flank, showing the asymmetrical cross-section. Of 205 shots recorded, 79 of the lighter shots (0.9 to 2.3 kg) were computer plotted in sectional form. The unprocessed records are shown to contain the usual normal moveout curvature, the ghost and bubble pulse interference. A comparison section with these effects removed shows a marked improvement in structural resolution. The processing was accomplished with an Apple microcomputer system. Two point recursive algorithms were most effective in ghost and bubble pulse removal.

The two subarrays of the cross-spread were processed as separate sections and show the geologic structures underlying the drift path. Records were plotted side by side without regard for variations in spacing, but are related to their actual positions as shown in Fig. 1(a-c). Similar dips on the two subarrays illustrate the consistent orientation of 45 degrees with the ridge axis. One anomalous reversal is seen at location 111 on the Amerasia flank. Dip

structures are not migrated. The seismic reflection profile shows the ridge to be an asymmetric, block faulted structure rising 2700 m above flat lying sediments at depths exceeding 4000 m in the adjacent basins. The ridge surface has an irregular morphology having slopes exceeding 7 degrees on the Eurasia side. Reflections showing lithologic stratification within the ridge core are somewhat obscured by strong scattered events from the irregular morphology of the ridge surface; however, some layering on the tops of the fault blocks is evident. Events from within the core suggest that the ridge was formed by overthrusting toward the Eurasia Basin. Sediments on the Amerasia side appear as a graben approximately 2 km thick with well defined stratification showing basin like thickening toward the centre. A pronounced reflection from a synclinal structure at a depth of about 1 km below the sea floor suggests a marked change in depositional environment. The sediments of the graben abut unconformably against the ridge on one side and against a buried ridge whose highest peaks barely penetrated the sea floor under the drift path on the south side. This structure may be part of the Marvin Spur which bathymetric charts show projecting from the Lomonosov Ridge and developing into a series of seamounts (Sobczak and Sweeney, 1978). Sediments on the Eurasia side show more pronounced stratification with total thicknesses exceeding 2 km. An unconformity separates an upper flat-lying sequence of about 1 km thickness from a lower homoclinal sequence which thickens in excess of 1 km away from the ridge. Some sedimentary structures are controlled by the coarse features of the underlying ridge surface.

References

Blasco, S.M., Bornhold, B.D., and Lewis, C.F.M., 1979. Preliminary results of surficial geology and geomorphology studies of the Lomonosov Ridge, Central Arctic Basin, in Current research, Part C, Geological Survey of Canada, paper 79-1C, p. 78-83.

Sobczak, L.W., and Sweeney, J.F., 1978. Bathymetry of the Arctic Ocean, in Arctic geophysical review, J.F. Sweeney, ed., Pub. Earth Physics Branchy, v. 45, p.7-14.

Weber, J.R., 1979. The Lomonosov Ridge experiment: "Lorex 79", Trans. AGU, v. 60, p. 715-721.

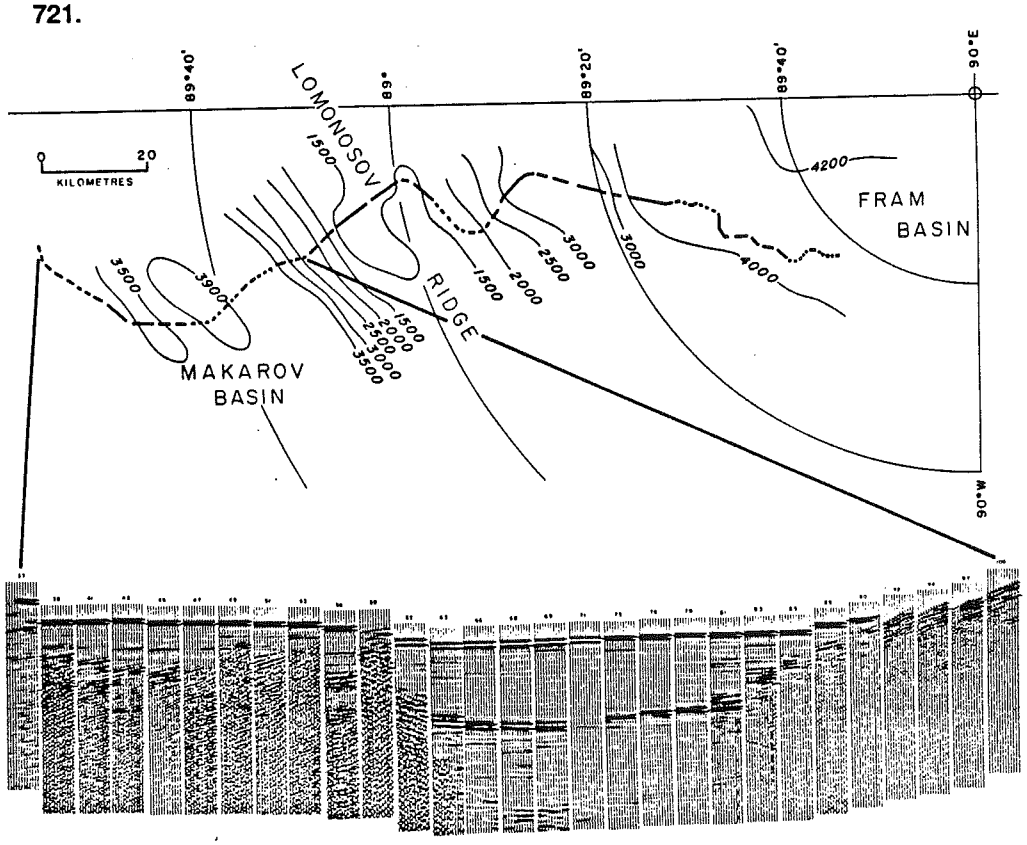

(a)

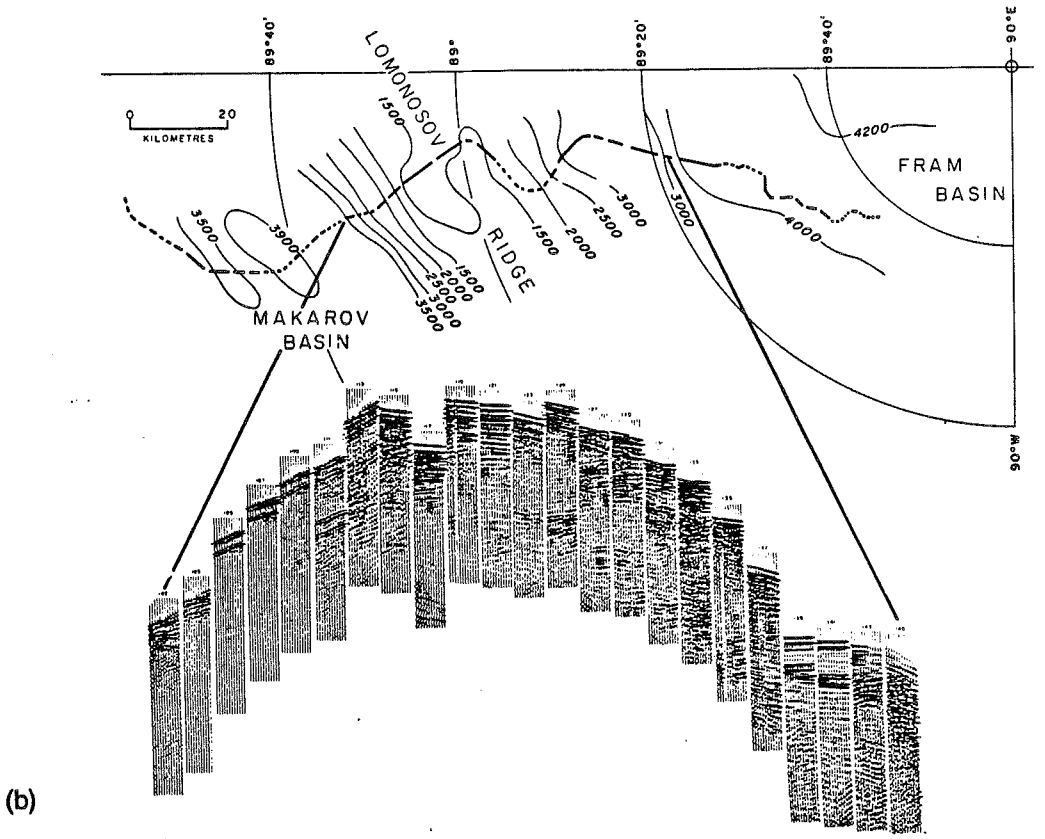

(b)

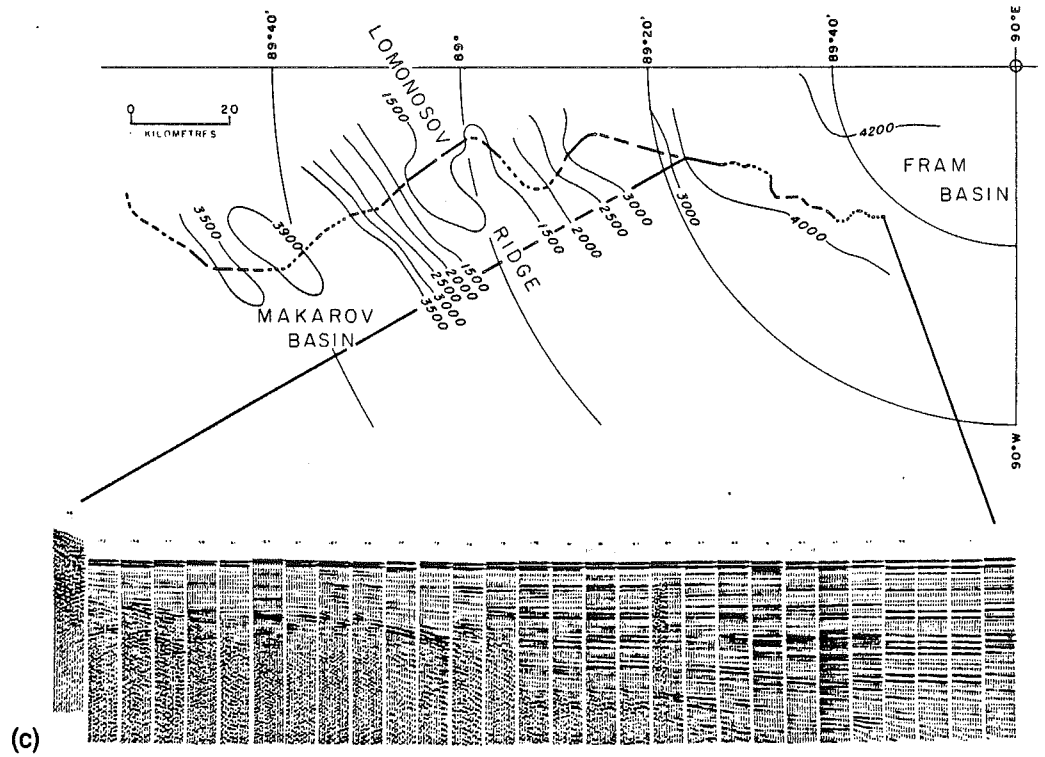

(c)

Fig. 1. Seismic reflection profile along LOREX drift path: (a) across Makarov Basin to Lomonosov Ridge; (b) across Lomonosov Ridge; (c) into Fram Basin.

ARCTIC
VOL. 36, NO. 2 (JUNE 1983) P. 121-142

Maps of the Arctic Basin Sea Floor: A History of Bathymetry and its Interpretation

J.R. WEBER[1]

Contribution of the Earth Physics Branch No. 1045; LOREX Contribution No. 13

ABSTRACT. The history of oceanographic exploration of the Arctic Ocean basin from the beginning of this century to the present is summarized. Soviet, U.S. and Canadian contributions after World War II are described in some detail including sounding methods and navigational techniques. The major bathymetric charts of the Arctic Ocean basin from 1954 on are discussed. Comparison of the LOREX bathymetric map with other maps reveals that the Lomonosov Ridge is accurately positioned on early Soviet maps but is grossly in error on later U.S. and Canadian maps. It is shown that map makers relied too much on early U.S. submarine data (the only such data that were declassified) and that the latest General Bathymetric Map of the Oceans (GEBCO) is therefore suspect of being inaccurate in areas where publicly available sounding data are scant.

Key words: Arctic Ocean basin, bathymetry, Lomonosov Ridge, LOREX

RÉSUMÉ. Un résumé de l'historique de l'exploration du bassin océanique arctique depuis le début du siècle est présenté. Les contributions soviétiques, américaines et canadiennes depuis la deuxième guerre mondiale sont décrites avec quelques détails incluant des méthodes de sondage et des techniques de navigation. Les cartes bathymétriques principales du bassin océanique émises depuis 1954 sont discutées. La comparaison de la carte bathymétrique établie par LOREX avec d'autres cartes montre que l'emplacement de la dorsale de Lomonosov est exact sur les premières cartes établies par les Soviétiques, alors qu'il est erroné sur les cartes américaines et canadiennes plus récentes. Il est démontré que les cartographes se sont trop fiés sur les premières données sous-marines américaines (les seules données accessibles au public) et que, par conséquent, les données de la dernière édition de la carte bathymétrique générale des océans (GEBCO) peuvent être inexactes dans les régions où les résultats de sondages accessibles au public sont peu abondants.

Mots clés: bassin océanique arctique, mesures bathymétrique, la dorsale de Lomonosov, LOREX

Traduit par P. Morel, département de l'energie, mines et ressources.

РЕЗЮМЕ. В работе подводится итог истории океанографических исследований бассейна Северного Ледовитого океана с начала столетия до настоящего времени. Подробно описываются вклады советских, американских и канадских ученых после Второй Мировой войны, включая описания методов эхолотных исследований и навигационной техники. Обсуждаются основные батиметрические карты бассейна Северного Ледовитого океана, составленные с 1954 года. Сравнение батиметрической карты LOREX с другими картами показало, что хребет Ломоносова точно указан на первых советских картах, но на более поздних американских и канадских картах допущены крупные ошибки. Указывается, что составители карт слишком полагались на первые данные Соединенных Штатов, полученные в результате исследований на подводных лодках, /только эти данные были рассекречены/ и что последняя "Общая батиметрическая карта океанов" (GEBCO) поэтому не может быть точной в районах, где отсутствует достаточное количество рассекреченных данных исследований рельефа морского дна.

Translation Bureau, Multilingual Services Division, Secretary of State Canada.

INTRODUCTION

For almost sixty years after the *Fram* drifted across the polar sea it was believed that the Arctic Ocean abyssal plain consisted of one deep basin. The highly successful Soviet airborne expedition to the Pole of Relative Inaccessibility in 1941 neither proved nor disproved the one-basin concept, but it did show that airplanes provided a practical and relatively inexpensive means of systematically exploring the Arctic Ocean basin. After World War II the Soviets initiated two programs of data collection in the Arctic Ocean: the High Latitude Airborne Expedition, which takes place every spring and was designated NORTH-series, and the more permanent NORTH POLE-series which is maintained for two to several years. Both programs are still in operation today. In 1948 Soviet scientists found the Lomonosov Ridge but kept the discovery secret until 1954. In the early 1950s the United States started a program of airborne expeditions and occupations of ice islands; from 1957 on these were complemented by submarine expeditions. Although the last ice island occupied by the U.S. was abandoned in 1974, springtime airborne operations are still being carried out. In 1958 the Canadian Government created the Polar Continental Shelf Project (PCSP), an imaginative and very effective organization with a broad mandate to coordinate and support field activities in the Canadian High Arctic, which catapulted Canada to the forefront of polar research. Long-range planning permitted the systematic bathymetric and gravity mapping of the Canadian Arctic continental shelf. PCSP supported two small-scale airborne expeditions to the North Pole in 1967 and 1969, the forerunners of the much larger multidisciplinary Lomonosov Ridge Experiment in 1979 (LOREX 79).

The first modern map that shows the ocean divided into two basins was published by the Soviets in 1954. With the exception of the chart compiled by the Canadian Defence Research Board in 1956 the early maps were all small-scale and appeared in scientific journals. Individual soundings were not

[1]Department of Energy, Mines and Resources, Earth Physics Branch, Gravity, Geothermics and Geodynamics Division, 1 Observatory Crescent, Ottawa, Ontario, Canada K1A 0Y3

printed and the contouring reflected, to some extent, the compiler's personal bias in favour of a particular theory of evolution of the ocean floor. By 1967 all the major physiological features had been discovered, and the first official chart was compiled by the Canadian Hydrographic Service in preparation for the first General Bathymetric Chart of the Oceans (GEBCO) published the following year. During the next decade a British, a U.S. and a second Canadian chart were produced, followed, in 1979, by the second GEBCO chart. The Soviets never produced any charts that were available to the public.

The major sea-floor features of the Arctic Ocean and place names mentioned in the text are shown in Figure 1. The names are those generally used today by Canadian geoscientists and correspond largely to the Beal *et al.* (1966) and Treshnikov *et al.* (1966) scheme of nomenclature which appears to be the only scheme in which most of the terms have been approved by the U.S. Board of Geographic Names and the International Hydrographic Bureau (Sweeney and Haines, 1978). Listed below are the names of submarine features used on U.S. maps that differ from the nomenclature used in this text.

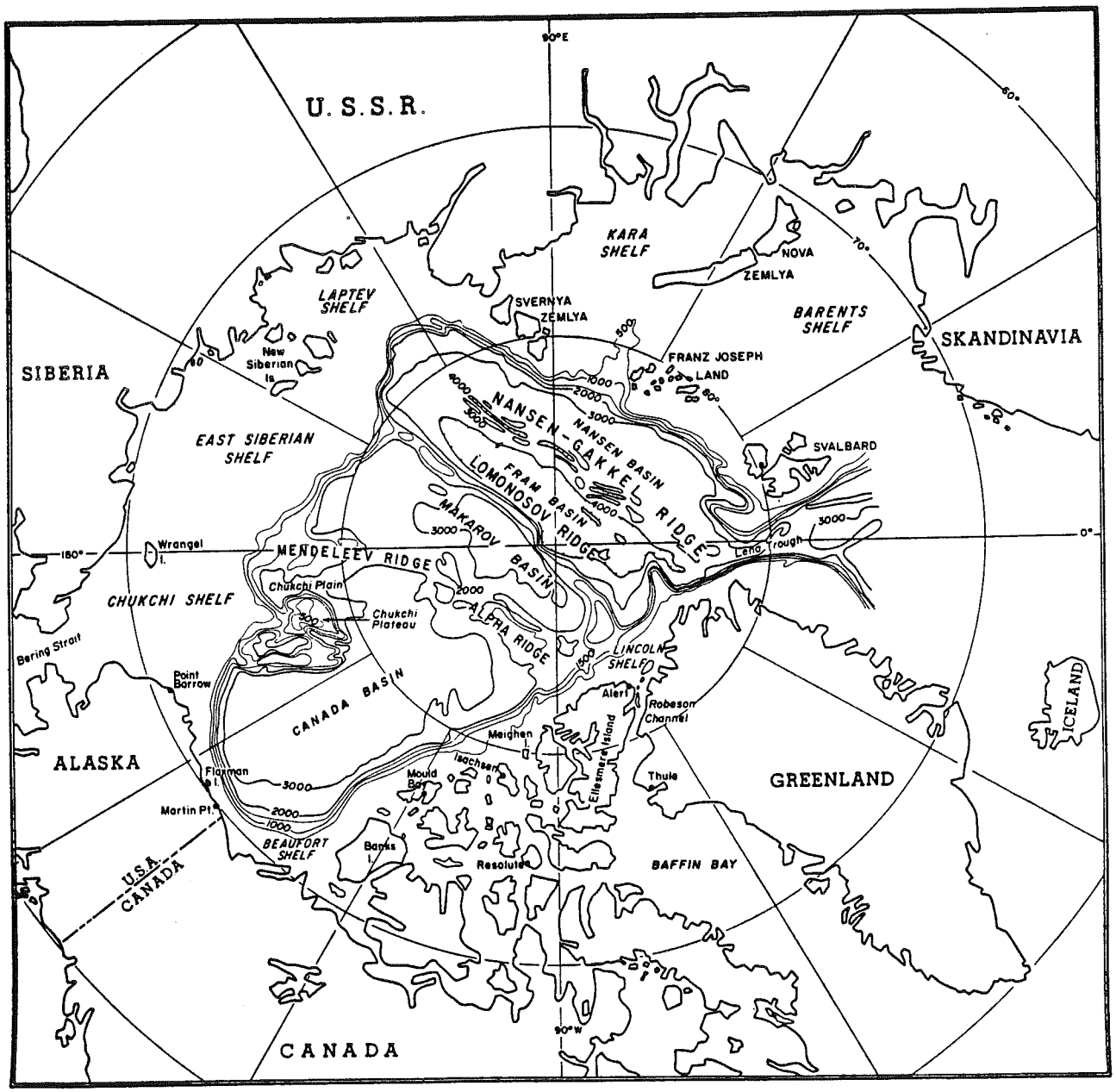

FIG. 1. Overview map of Arctic Ocean with names used in text. Nomenclature of sea floor features is that commonly used on Canadian maps and scientific papers.

Canadian nomenclature	*U.S. nomenclature*
Nansen-Gakkel Ridge	Arctic Mid Ocean Ridge Mid Arctic Ridge Nansen Ridge
Mendeleev Ridge	Mendeleyev Ridge
Fram Basin	Amundsen Basin
Makarov Basin	Fletcher Abyssal Plain
Nansen Basin	Barents Abyssal Plain

The methodology of early Soviet hydrographic surveys, a description of Soviet aircraft types mentioned in the text, and a list of acronyms have been included in the Appendices.

EARLY HYDROGRAPHIC EXPLORATIONS

From the Middle Ages until the end of the nineteenth century geographers believed that the North Pole was surrounded by land or by an archipelago of islands. This concept lost credibility after Nansen's ship *Fram* drifted with the arctic pack ice from the New Siberian Islands to Svalbard between 1893 and 1896 (Nansen, 1897). It was found that the ocean along the entire length of *Fram*'s drift path was more than 3000 m deep. This led many geographers to believe that the whole Arctic Ocean basin was a single oceanic deep, although, based on analysis of tidal data alone, Harris (1904) postulated that it was divided by a barrier or ridge into two basins with different periods of oscillation.

During the first decade of the twentieth century Bob Bartlett, supporting Peary's attempts on the North Pole, made a number of soundings off the northern coast of Ellesmere Island that outlined the general shape of part of its continental shelf.

One of the goals of the government-sponsored Canadian Arctic Expedition 1913-1918 under the command of Vilhjalmur Stefansson was to chart the waters of the Beaufort Sea north of Mackenzie Delta and Banks Island. Stefansson's ship, the *Karluk*, became beset in the pack ice near Flaxman Island, Alaska. For five months the *Karluk* drifted west until she was crushed near Wrangel Island on 10 January 1914; during that time the expedition's oceanographer, James Murray, indefatigably took soundings, dredged bottom sediments and collected biological and water samples (McKinlay, 1976). The soundings were recorded in the ship's log, but the samples sank with the *Karluk* and Murray's notes were lost with him when he attempted to reach the Siberian mainland on foot (McKinlay, pers. comm. 1980). Had the samples survived, the difference between Amerasian and Eurasian waters would have been discovered, and the existence of a dividing ridge predicted, some 30 years earlier.

In the spring of the same year Stefansson, with Storkerson and another companion, sledged over the ice of the Beaufort Sea from Martin Point, Alaska, beyond the continental shelf, to Norway Island near the west coast of Banks Island. He took soundings every 40 to 50 miles but unfortunately was limited to a maximum depth of 1386 m by the length of his sounding wire (Stefansson, 1921).

On 15 March 1918, starting from Flaxman Island, Storkerson sledged 280 km out into the Beaufort Sea where he established a station on the sea ice. From 8 April to 9 October he drifted with the pack ice between latitudes 72°45′ and 74°N and longitudes 145° to 150°W, taking numerous soundings (map compiled by Geodetic Survey of Canada, in Stefansson, 1921), keeping meteorological records and taking celestial positions. Storkerson had planned to occupy the station for a year, but he fell ill with asthma and was forced to return prematurely to Flaxman Island which he reached on 8 November. During the whole drifting period the party of 5 men and 17 dogs lived entirely "off the land", eating exclusively seal and bear meat and cooking and heating with seal blubber and bear fat. Storkerson had no doubt that they could survive on the ice indefinitely by hunting. There is every indication that their ice floe was, in fact, a tabular iceberg of the type which is now called an ice island. Storkerson mentions (Stefansson, 1921:699) that their floe could best be described as a large island, seven miles wide by at least 15 miles long and, judging from the freeboard near their camps, 50-60 feet thick. It moved at a different speed from the surrounding field of smaller floes, and apparently it never broke up during the entire six months they lived on it. He also comments on the appearance of the "land" which reminded him of certain stretches of prairie. Storkerson's was the prototype scientific drifting station, antedating the Russian explorer Papanin's North Pole drift by 19 years.

With Stefansson's expeditions the first phase of Canada's exploration of the Polar Sea came to an end. Robert Borden, prime minister of Canada during the First World War, was a staunch supporter of Stefansson. On his retirement in 1920 he was succeeded by Arthur Meighen who the following year was defeated by the Liberals under Mackenzie King. The King government had little interest in Canada's Arctic, and nearly forty years slipped away before the exploration of Canada's arctic coastal waters was seriously resumed.

In 1927 Sir Hubert Wilkins, flying from Alaska, landed his aircraft on the ice some 1300 km north of Bering Strait. By setting off an explosive charge and using a stop watch to measure the time it took for the echo to return from the ocean floor, he obtained a depth of 5440 m (Wilkins, 1928). This sounding later turned out to be erroneous (he may have heard a multiple echo), but for the next twenty years it was much quoted in support of the opinion of a single deep Arctic Ocean basin. The opinion was seemingly confirmed by 38 depth soundings made in 1937 between the North Pole and the East Greenland coast, along the nine-month drift path of the Soviet research station now known as North Pole 1 (Papanin, 1946). Further support came from the Soviet icebreaker *Sedov*, which made 46 soundings while drifting in the Eurasia Basin, following *Fram*'s path, between 1937 and 1940 (Armstrong, 1958).

Somewhat earlier Vilhjalmur Stefansson (1921) had introduced the concept of the "Pole of Relative Inaccessibility", i.e., the point in the Arctic which would be most difficult for an explorer to reach. Soviet pilots engaged in ice reconnaissance along the Northern Sea Route suggested an airborne expedition to the area of the Pole of Relative Inaccessibility. During April 1941 personnel from the Soviet All-Union Arctic Institute (VAI), in three successive flights in a ski-equipped four-engine N-169 aircraft based at Wrangel Island, estab-

lished three stations in the regions of the Wrangel and Mendeleev abyssal plains between latitudes 78° and 81°N and between longitudes 175°E and 170°W. They stayed four to five days at each station, taking soundings, measuring temperature and salinity, sampling the water colum and the seabed, and taking meteorological, gravitational and magnetic observations. To take soundings the Soviets used a motor-driven wire winch, an improvement over the hand-operated winches used on the *Fram, Sedov* and North Pole 1 expeditions. Their depth measurements of 2427 m, 1856 m and 3370 m showed large variations but neither confirmed nor disproved the depth determined by Wilkins (Treshnikov, 1966).

The Soviet airborne expeditions were highly successful. They demonstrated the advantages of using aircraft over letting a ship freeze into the ice or occupying an ice station for a long period of time. Aircraft provided choice of location, simplified the logistics and, in some cases, decreased the cost. The importance of choice of location for bathymetric surveys will be discussed later. Reliance on aircraft was a turning point in arctic exploration for which the Soviets deserve every credit.

HYDROGRAPHIC SURVEYS AFTER WORLD WAR II THE SOVIET CONTRIBUTION

The NORTH-Series Expeditions

The war interrupted arctic scientific explorations, but in 1948 VAI started a program of systematic exploration of the whole of the Arctic Ocean which they called "High-Latitude Air Expeditions" (HLAE). Several aircraft were used to land parties at a series of points on the floating ice on the Arctic Ocean during a period of approximately six weeks in spring. Lightweight, portable equipment was developed specially for the job. The routine of making oceanographic, magnetic, gravimetric (using a pendulum gravimeter) and meteorological observations was carefully worked out so that only a few hours were required at each stopping place. There are no detailed accounts of the early HLAE, but many landings were made (Armstrong, 1958).

During the 1948, 1949 and 1950 HLAE, groups of scientists were landed to carry out short-term observations, each lasting from a few hours to a few days, at 87 points distributed over the Arctic Ocean (Somov, 1955). Discoveries included the basic features of relief of the ocean floor and information on the scale and limits of the distribution of the Atlantic water layer. The surveys revealed that, far from being a flat abyssal plain, the Arctic Basin has a very complicated structure with both depressions and submarine ridges and elevations. The most significant discovery was made on 17 April 1948, at 86°26' N, 145°E, where a relatively shallow depth of 1290 m was recorded. Further soundings at smaller intervals, the same year and again the following year, revealed the outline of a massive submarine mountain range, rising 3000 m above the sea floor and extending 1800 km from Ellesmere Island to the New Siberian Islands. It was named after M.V. Lomonosov, the eighteenth-century Russian scientist, grammarian and poet.

The HLAE took place every year from 1948 to the present, with the possible exception of the seasons 1951-1953. The aircraft landing sites from 1937 to 1957 are illustrated in Figure 2 (Laktionov and Shamont'ev, 1957).

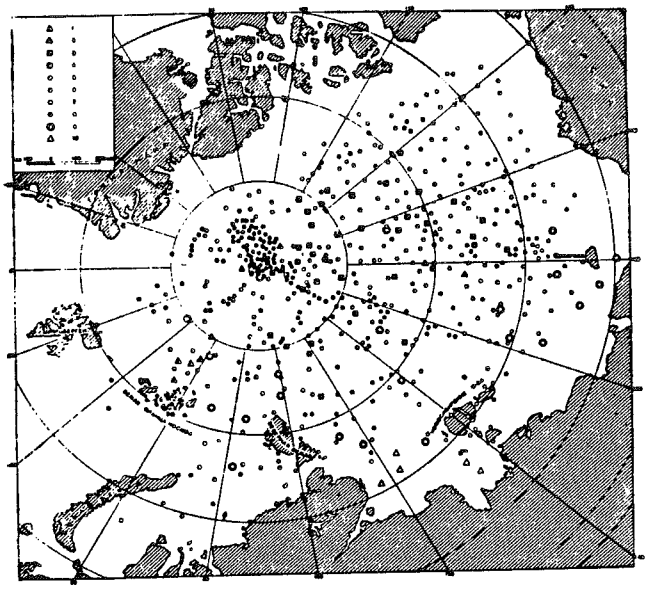

FIG. 2. Landing sites of Soviet aircraft on ice: (1) - 1937; (2) - 1941; (3) - 1948; (4) - 1949; (5) - 1950; (6) - 1954; (7) - 1955; (8) - 1956; (9) - 1957. On water: (10) - 1950.

These annual springtime High-Latitude Air Expeditions were renamed NORTH-series. Since the late 1950s the scope of these operations has increased tremendously, although few details are known outside the Soviet Union. On 29 April 1967, enroute to Ice Island T-3, one of the aircraft from the Arctic Research Laboratory at Point Barrow landed at the Soviet station NORTH-67. Brewer (1967) reported that the station consisted of 70 Jamesway-type buildings and that the operation involved some 300 people, 100 of whom were pilots. A 1500-m runway allowed aircraft of the Hercules C-130 type to land. The station was serviced by an average of six flights a day from the mainland, which required the presence of an air traffic controller. At the time of their two-hour visit, nine Polish-built Antonov AN-2s, one LI-2, one Ilyushin IL-14, and one helicopter were parked on the ice, and a second helicopter was flying. The scientific studies being carried out included gravity, seismology, oceanography and meteorology.

The NORTH POLE-Series of Drifting Stations

In April 1950 a 16-man party and 60 tons of equipment and supplies were landed some 1200 km north of Bering Strait, where a camp was established on a large floe of multi-year ice. Although the camp was meant to be evacuated in October, the work of collecting scientific data was so successful that the occupation of the station was extended to April 1951. To enable the station to be re-supplied for the winter, a 900-m runway was built on the old ice in the fall; the surface was smoothed by

chopping away hummocks and flooding depressions with sea water. Scientific studies included meteorology, physical and chemical oceanography, microbiology, collection of bottom sediments, magnetic and gravity observations, and study of the properties of sea ice. Using a motor-driven winch with a 7-strand steel cable 5000 m long and 1.2 mm diameter, and a 10-kg sounding lead, the scientists took 285 soundings (Somov, 1955).

This was the first time a scientific drifting ice station had operated all year round. The occupants had little experience in coping with the intense cold of the polar night and with the flood of meltwater on the floe during the summer. They lived in double-walled tents, black on the outside with a white inner lining, which were enclosed in the winter in an igloo-like shell of snow blocks and which were difficult to heat and ventilate adequately. In the summer the tents soaked up the meltwater like wicks. Three times the camp had to be moved by sled dogs and a jeep, because of ice breakup. That they managed to keep up an uninterrupted full-fledged scientific program is a tribute to Russian ingenuity and perseverance. Some of the scientific results, including the 285 depth soundings (but not gravity observations, which appear to be a highly classified subject) were released as a Soviet contribution to the International Geophysical Year (Somov, 1955).

This operation, under the leadership of M.M. Somov from VAI, was the beginning of the NORTH POLE-series of drifting stations, and was later designated NP2 (Papanin's drifting station from 1937-1938 was renamed NP1).

In 1954, NP3 and NP4 were established under the leadership of Treshnikov (later director of the Arctic and Antarctic Research Institute in Leningrad), Tolstikov, Gordienko and Dralkin. They were followed by NP5 (1955), NP6 (1956), NP7 (1957), NP8 (1959), and NP9 (1960). The experiences gained from NP2 enabled the researchers to equip these stations much more comfortably and efficiently. Besides meteorological, oceanographic and geophysical laboratories, their inventory included a bulldozer for preparing runways and pulling loads, and a piano for entertainment. Fixed-wing and rotary-wing aircraft were permanently stationed at the camp (Gordienko and Laktionov, 1960; Treshnikov, 1960).

The Soviets did not confine their survey activities to international waters. There is evidence that during the early 1950s they extended their soundings to the inter-island channels of the Canadian Queen Elizabeth Islands.

To date 25 stations have been established. They remain occupied from one to several years until they either "exit" via the Greenland Current into the Atlantic or otherwise lose their usefulness. Currently (December 1982) NP25 is located over the Alpha-Mendeleev Ridge at 170°W.

THE AMERICAN CONTRIBUTION

Airborne Expeditions and Drifting Ice Islands

It was not until April 1951 that U.S. scientists joined in the exploration of the Arctic Ocean by mounting two airborne expeditions to the Beaufort Sea. Supported by the U.S. Air Force Cambridge Research Centre and using a C-47 aircraft, they established six stations north of Martin Point, Alaska, between latitudes 73° and 76° N. The observations consisted of seismic soundings, gravity measurements and determination of the ice drift (Crary *et al.*, 1952). Concurrently, sponsored by the U.S. Office of Naval Research (ONR), Project Skijump was inaugurated. Twelve landings on the ice north of Point Barrow were made by a Navy R-4D aircraft. Salinity, temperature and depth (STD) measurements were made at three sites using winch and Nansen bottles. The following year, refuelling the R-4D on the ice from a Navy P-2V aircraft, scientists established five more hydrographic stations and reached 82°22'N. The operation ended prematurely when the port landing gear of the R-4D collapsed and the aircraft had to be abandoned. The observations showed that water temperature and salinity values differed significantly from those obtained by Nansen on the *Fram*, and that a large anticyclonic (clockwise) gyral exists north of Alaska. From these observations Worthington (1953:550-551) concluded that "there is a submarine ridge, running roughly from Ellesmere to the New Siberian Islands, which separates the deepest water of the Beaufort Sea from the remainder of the basin", and that "the sill depth of the ridge should not exceed 2300 m." Ironically, the Americans were unaware of the Soviet NORTH and NORTH POLE-series operations and did not know that the existence of the Lomonosov Ridge had in fact been confirmed five years earlier.

The brief-landing type of airborne survey was replaced in 1952 by year-round occupation of drifting ice islands. Unlike ice floes, which consist of frozen sea water, are on the average 3 m thick, and can break up at any time, ice islands originate mainly from the Ellesmere Island Ice Shelf, consist of freshwater ice up to 60 m thick, may extend over an area of many square kilometres, and have, as long as they remain in the Arctic Ocean, a life expectancy of decades. The best known of these ice islands, Fletcher's Ice Island T-3, has been occupied at intervals from 1952 to 1974 (Hunkins, 1977); it is presently (December 1982) located over the Nansen-Gakkel Ridge and is expected to be swept into the North Atlantic by the Transpolar Current within the next year. Other drifting ice islands that were occupied were Alpha (1957/58), Charlie (1959), and Arlis II (1961-1965). T-3 and Alpha served as U.S. stations during the International Geophysical Year.

Throughout its occupation, Alpha drifted over a ridge which was parallel to the Lomonosov Ridge. Although identified as a general feature on the 1954 Soviet chart, it was mapped in comparative detail for the first time from Station Alpha, from which it derives its name. Research on these ice islands embraced a broad range of oceanographic, geophysical, atmospheric and glaciological studies (Hunkins, 1960a, b, c, d; Hunkins *et al.*, 1962).

In 1960 the Americans resumed their airborne reconnaissance surveys under the sponsorship of ONR and the Geophysical and Polar Research Centre of the University of Wisconsin. Using Cessna 180 aircraft based along the north Alaskan coast and on drifting stations, they landed on the ice

of the Beaufort Sea, Chukchi Shelf, and Canada Basin to take depth soundings and gravity measurements. This program continued every spring until 1969, by which time over 800 stations had been established (Wold, 1973).

Submarine Expeditions

Since 1957 the U.S. Navy has operated nuclear submarines in the Arctic Ocean. Echograms from the ocean floor obtained from the USS *Nautilus* (1957, 1958), *Skate* (1958, 1959, 1962), *Sargo* (1960) and *Seadragon* (1960, 1962) have been analyzed by Beal (1969). Figure 3 shows the cruise tracks of the four submarines. The accuracy of the depth profiles obtained from the echograms depends on knowing: 1) the submarine's position and motion (which includes speed and change of speed, depth and change of depth); 2) thickness of the ice; and 3) velocity of sound in sea water. Positioning of the submarines was obtained by dead reckoning, by the Ships Inertial Navigation System (SINS), and by celestial fixes whenever possible. The accuracy of SINS on submarines is classified, but an inference can be made from Beal's (1969:24) remark that "if a volcano is misplaced ten miles on a map of the ocean floor, this itself is not apt to lead to serious mistakes in interpretation of geological history". Echograms are annotated with submarine speeds and keel depths, but these data remain classified. The ships' echo sounders were calibrated at constant speed of sound of 1463 $m \cdot s^{-1}$. No attempt has been made to correct for the variation of velocity with depth, so that basins appear approximately 100 m too shallow and the Lomonosov Ridge crest approximately 50 m too deep.

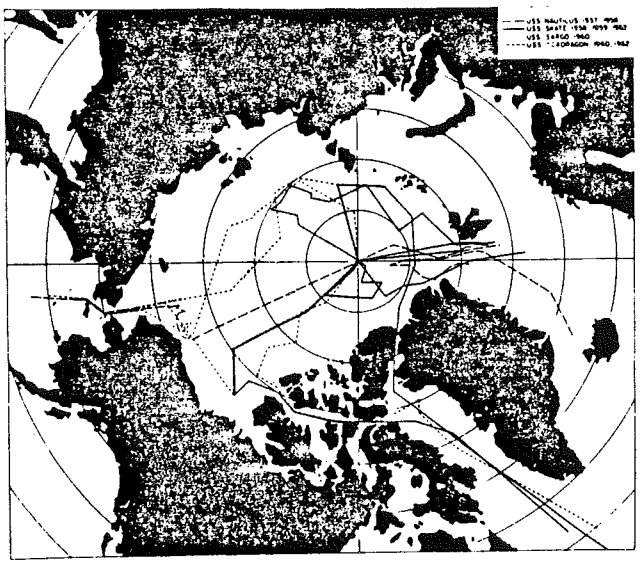

FIG. 3. U.S. nuclear submarine tracks in the Arctic Ocean 1958-1962. (Figure taken from *Polar Research*, 1970:51).

Beal prepared the depth profiles along the submarine tracks by digitizing the echograms once every 20 minutes. In his thesis the profiles are drawn at a horizontal scale of 1:5 000 000 and a vertical scale of 1:100 000. The geographical locations of the submarine tracks are drawn at a scale of about 1:33 000 000. The echograms and Beal's work sheets are classified, as are all post-1962 U.S. submarine depth data.

In 1975 and 1976 the British nuclear submarine *Sovereign* made a number of cruises into the Arctic Ocean. Although not an American contribution, it is mentioned in this context because some of its non-classified bathymetric data have been used in the compilation of the 1979 GEBCO map (Sobczak, pers. comm. 1980).

Surveys across the Alaskan Polar Continental Shelf

In 1951 the icebreaker USS *Burton Island* and in 1957 the icebreakers USS *Staten Island* and USCGC *Northwind* carried out continuous echo soundings across the continental slope into the Beaufort Sea north of Point Barrow (Fisher *et al.*, 1958).

In the course of conducting seismic reflection surveys across the continental shelf into the Beaufort Sea, bathymetric data were acquired by the U.S. Geological Survey between 1972 and 1978, and by the Geophysical Corporation of Alaska in 1973 (Greenberg *et al.*, 1981).

Based on all the data available, including Canadian soundings east of longitude 141°W, Greenberg *et al.* (1981) published a bathymetric map of the continental shelf, slope, and rise of the Beaufort Sea north of Alaska at a scale of 1:5 000 000.

The East Arctic Operations

In 1979 ONR initiated the East Arctic Operations, a continuing program of exploration of the Eurasia Basin. The initial operations, the FRAM expeditions, were conducted each spring from 1979 to 1982. Up to 20 people were airlifted from station Nord in Greenland onto camps on the ice pack to undertake 10-12 weeks of bathymetric, physical and chemical oceanographic, marine geophysical, atmospheric, biological and underwater acoustic studies. The expedition staff were from U.S., Canadian, Norwegian, and Danish universities and institutions. Financial support was provided by ONR, the National Science Foundation and Polar Continental Shelf Project.

In the spring of 1981 soundings were also taken in the western part of the Eurasia Basin by a temperature-salinity mapping program code-named EUBEX for Eurasia Basin Experiment. Flying in tandem in two Twin Otter aircraft, and landing on the ice at approximately 50-km intervals, scientists from the University of Washington carried out STD measurements.

The FRAM series expeditions have been superseded by the MIZEX-series (Marginal Ice Zone Experiment). Studies in physical oceanography along the southern edge of the permanent ice cover are scheduled to take place every spring beginning in 1983.

THE CANADIAN CONTRIBUTION

Geological Survey of Canada

Canadian investigations of the Arctic Ocean basin resumed,

after a lapse of 37 years, with a series of airborne magnetometer and scintillometer surveys by the Geological Survey of Canada. In spring 1955 a party led by L.W. Morley, using a Canso long-range amphibious aircraft, made a number of flights to measure the total magnetic field and gamma field background throughout the Canadian Arctic Archipelago and adjacent ocean (Gregory *et al.*, 1961). Two of the flights extended over the ocean some 200 km beyond the Sverdrup Islands. Over much of the offshore area, the magnetic and radiometric readings were found to be relatively uniform, but at the northwest end of one of the flights, at the limit of aircraft range, there was an unmistakable change in magnetic character. This was clear evidence of a dramatic change in bedrock topography or offshore geology in the area hitherto known only from Stefansson's soundings. That same year, a large party from the Geological Survey, known as Operation Franklin (Fortier *et al.*, 1963) was engaged in studying the geology of the archipelago, and E.F. Roots, who was responsible for structural and geomorphological interpretation on that operation, attempted to reconcile the magnetic results with the evolving knowledge of the geology of the area. He became convinced of the scientific value and operational feasibility of a concerted and systematic investigation of the geology, geophysics, oceanography and bathymetry of the area, and began to seek support for a continuing study. The continental shelf area, unknown except for that single offshore magnetic "teaser", was the logical place to begin.

The Polar Continental Shelf Project

In 1958 the International Conference on the Law of the Sea was held in Geneva. One of the resolutions adopted by the conference was that mineral and other resources underlying continental shelves should be considered to be the property of the country claiming the coastline adjacent to the shelf. As a signatory to this resolution, Canada found herself, in effect, claiming ownership to resources beneath a continental shelf that had never been delineated, and whose outline was inferred mainly from Soviet maps. In order to remedy this situation, early in 1958 the Canadian Cabinet approved a proposal to organize a project to "conduct surveys and scientific research in the continental shelf area of Arctic Canada". The organization was to be known as the Polar Continental Shelf Project (PCSP), and it was to come under the jurisdiction of the Department of Mines and Technical Surveys (now Energy, Mines and Resources) (Roots, 1968).

The project was authorized by Cabinet Directive on 5 April 1958, and was designed to conduct general mapping, oceanographic, hydrographic, geological, geophysical, geographical and related studies, to be undertaken on the Arctic Ocean continental shelf, on the islands of the Archipelago, and in the channels. It was to act as a logistic instrument for all divisions of the department in conducting research in the arctic regions of Canada. It was to supply logistic support and facilities to other agencies conducting research in the area. No fixed date was contemplated for the completion of the project. Its first director was Dr. E.F. Roots. He was succeeded in 1972 by Mr. George D. Hobson, who still holds the position.

The initial field headquarters was established in 1959 at Isachsen on Ellef Ringnes Island, where a permanent weather station was maintained. Experiments were carried out on the electromagnetic propagation characteristics of the area, with a view to designing and installing an electronic survey and positioning system to cover the major area of investigation. The initial program was supported by one Beaver and one Otter aircraft, both ski-wheel-equipped, which in the first year made nearly 500 landings on unprepared strips on both land and ice.

The full-scale research and survey program got underway in 1960. In the first year work was concentrated on the continental shelf to the northwest of Meighen, Ellef Ringnes and Borden islands in one area approximately 300 km long and extending some 400 km to sea. A low-frequency Decca Lambda hyperbolic position-fixing system was erected, with the master station on Ellef Ringnes Island and the slave stations on Meighen Island and Borden Island, to give immediate determination of positions to an accuracy of 200-800 m within an area 300 × 500 km (Sobczak and Weber, 1970).

Studies undertaken during the first year's operation included hydrographic soundings, STD measurements and water sampling at standard depths, current and tidal measurements, grab sampling and coring, gravity, seismic and magnetic measurements, and geological investigations of the sea floor sediments.

The results of the initial year indicated that increased air support and more suitable ground equipment were required to increase efficiency of data collection. This was accomplished in later years by the addition of helicopters, both small and large, replacement of the Beaver by more ski-wheel-equipped Otter aircraft, the addition of a twin-engine Beechcraft and other multi-engine specialized survey aircraft, and the acquisition of more suitable vehicles for travelling over snow, ice and frozen ground. The first year's work demonstrated that with a well-planned program and proper equipment it was feasible to conduct research under arctic conditions with reasonable comfort and considerable success.

The PCSP's basic plan of study has been maintained, although the scope of investigations has expanded year by year since 1959. At first, the project depended on the Isachsen Weather Station for accommodation and some facilities. In 1964 the main headquarters of the project was moved southwest to Mould Bay on Prince Patrick Island and six years later it was moved further southwest to Tuktoyaktuk on the Mackenzie River Delta.

In addition to the main camps, temporary camps are established in the Arctic Archipelago or on the ocean, as required. One such camp was established at Alert, Ellesmere Island, in 1967 and served as a base camp for a hydrographic and gravity survey in Robeson Channel and Lincoln Sea. On this particular survey a portable Decca Hi-Fix navigational system was used for positioning.

The purpose of the program has been to investigate, as thoroughly as possible, each area covered by the Decca Lambda electronic positioning system before moving the Decca

transmitter stations to new positions. The plan has been to leap-frog the stations progressively to the southwest; by 1975 the most westerly slave station was located on Herschel Island near the Yukon-Alaska border. In 1976 the Decca chain was moved to Amundsen Gulf where it has been deployed in inter-island surveys. In the fall of 1982 it was moved to the Ellesmere Island coast in order to fill in, in 1983, most of the gap left on the continental shelf between Meighen Island and Lincoln Sea.

The initial bathymetric survey was carried out with the use of a wire line, and with regular marine echo sounders either mounted on snowmobiles travelling on the ice, or carried in aircraft and operated through open leads or through holes drilled through the sea ice at landing places. From the beginning, one of the priorities was the development of an echo-sounding system with a transducer that allowed soundings to be made through the ice, thus eliminating the need for drilling a hole or searching for open leads. Such equipment, incorporating transducers sufficiently powerful and directional to sound reliably to depths of 2000 m, has been in use with both analog and digital output since 1961. Equipment and techniques were also developed to obtain echo soundings through open leads and cracks, from both helicopters and air-cushion vehicles (hovercraft) towing echo-sounding equipment while in flight. Extensive areas in critical straits and near the coastline have been surveyed by these methods, which give continuous sounding profiles rather than spot readings. Bathymetric surveys on the ice, between the islands, and on the continental shelf to a depth of 360 m (200 fathoms) are carried out at a 6-km (or less) grid interval. On the continental shelf between the 360 m and 1000 m isobaths, the grid interval is 10 km. These operations resulted in bathymetric mapping at a scale of 1:500 000 and regular hydrographic surveys at scales of 1:100 000 and 1:50 000. The cost per square kilometer of such surveys is now comparable with that of ship-borne surveys.

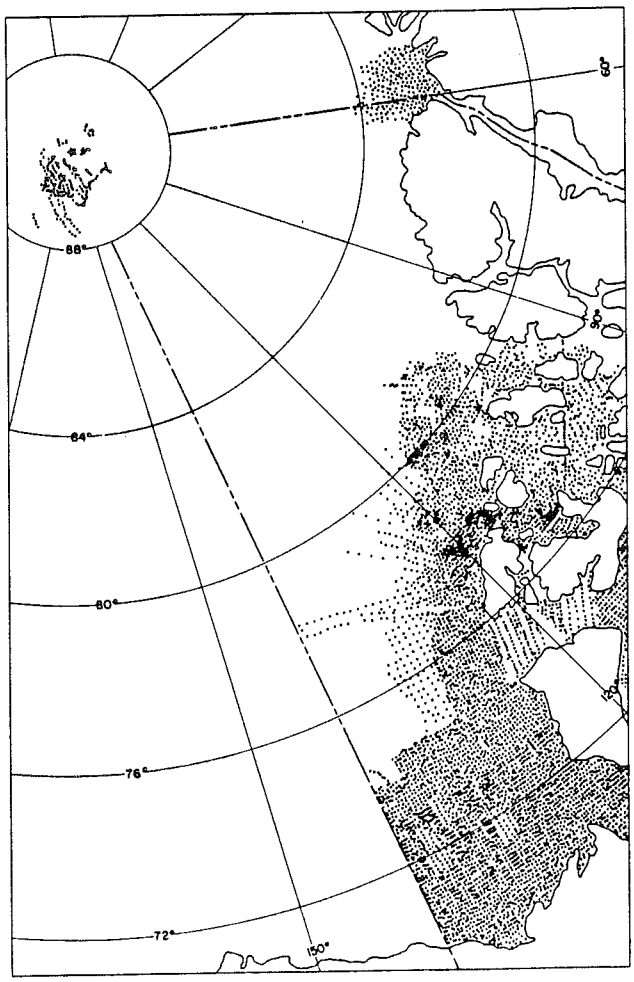

FIG. 4. Plot of Canadian bathymetric and gravity stations established on the Arctic Ocean and adjoining inter-island waters as of 1980.

Since 1961 the Gravity Division of the Earth Physics Branch and the Canadian Hydrographic Service have been undertaking joint bathymetric and gravity surveys as part of the PCSP activities. Usually two observers travel together in a helicopter, a hydrographer to operate the sounding equipment and a gravimetrist to read the gravimeter. By this method up to 26 stations can be established during a single 4-hr helicopter traverse. Figure 4 shows the locations of the gravity and bathymetric stations that have been established to date on the Arctic Ocean and adjoining inter-island waters. The bar chart in Figure 5 depicts the number of stations that were established on the polar continental shelf and beyond from 1960 to 1976. The count includes all stations on the ocean side of the Arctic Islands, the mainland coasts from Meighen Island to 141°W, and Lincoln Sea to 60°W; it excludes all inter-island surveys and the polar stations north of 85°.

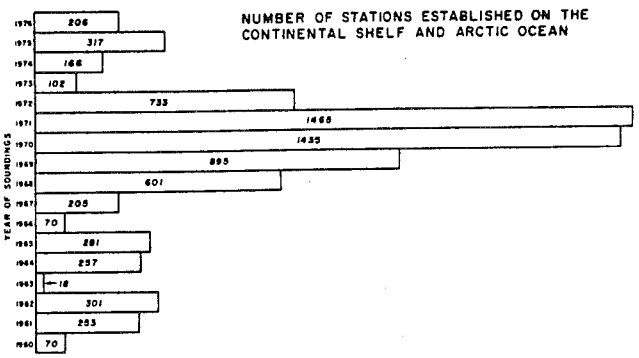

FIG. 5. Number of bathymetric and gravity stations established over the polar continental shelf, 1960-1976.

Polar Expeditions

The First Canadian North Pole Expedition. In 1967 the Dominion Observatory (now the Earth Physics Branch of the Department of Energy, Mines and Resources [EMR]) in cooperation with PCSP carried out a geophysical expedition to the vicinity of the North Pole. The main objectives of the expedition were to: 1) establish a line of gravity stations from

Alert to the North Pole, and obtain as many gravity observations as possible in the vicinity of the Pole and across the Lomonosov Ridge; 2) determine the deflection of the vertical at the North Pole (Lillestrand and Weber, 1974); and 3) develop and test new techniques for precise navigation in the polar region.

In the days before satellite receivers became commercially available and before very low frequency radio navigation aids, such as the Omega system, became operational in the polar region, the only means of positioning was by celestial observations. However, because of the unknown drift rate and direction of the ice, and because of atmospheric refraction, the accuracy of position fixes obtained from conventional sun observations could not be determiend to better than a few kilometres. This was unacceptable for the type of geodetic measurements that were planned. The problem of precise navigation in the polar area during the polar day was solved using a technique developed for this purpose by Lillestrand *et al.* (1967) from Control Data Corporation in Minneapolis. It involved continuous viewing of a number of celestial targets and solving by computer for ice drift and atmospheric refraction. Since minicomputers sufficiently rugged for field operations in the arctic winter environment were not yet available, zenith angles of the sun and of stars observed with a Kern DKM-3 theodolite, and atmospheric pressure and temperature, were relayed by amateur radio operators in Alert and Ottawa to Control Data Corporation in Minneapolis where the data were processed on a computer. The computed positions, the rate and direction of the ice drift at the time of the last observation, and a prediction on the probable ice movement during the next few hours were then relayed back to the ice station via the radio communications link. The purpose of this procedure was to position the observers within a few hundred metres upstream of the geographic North Pole and let them

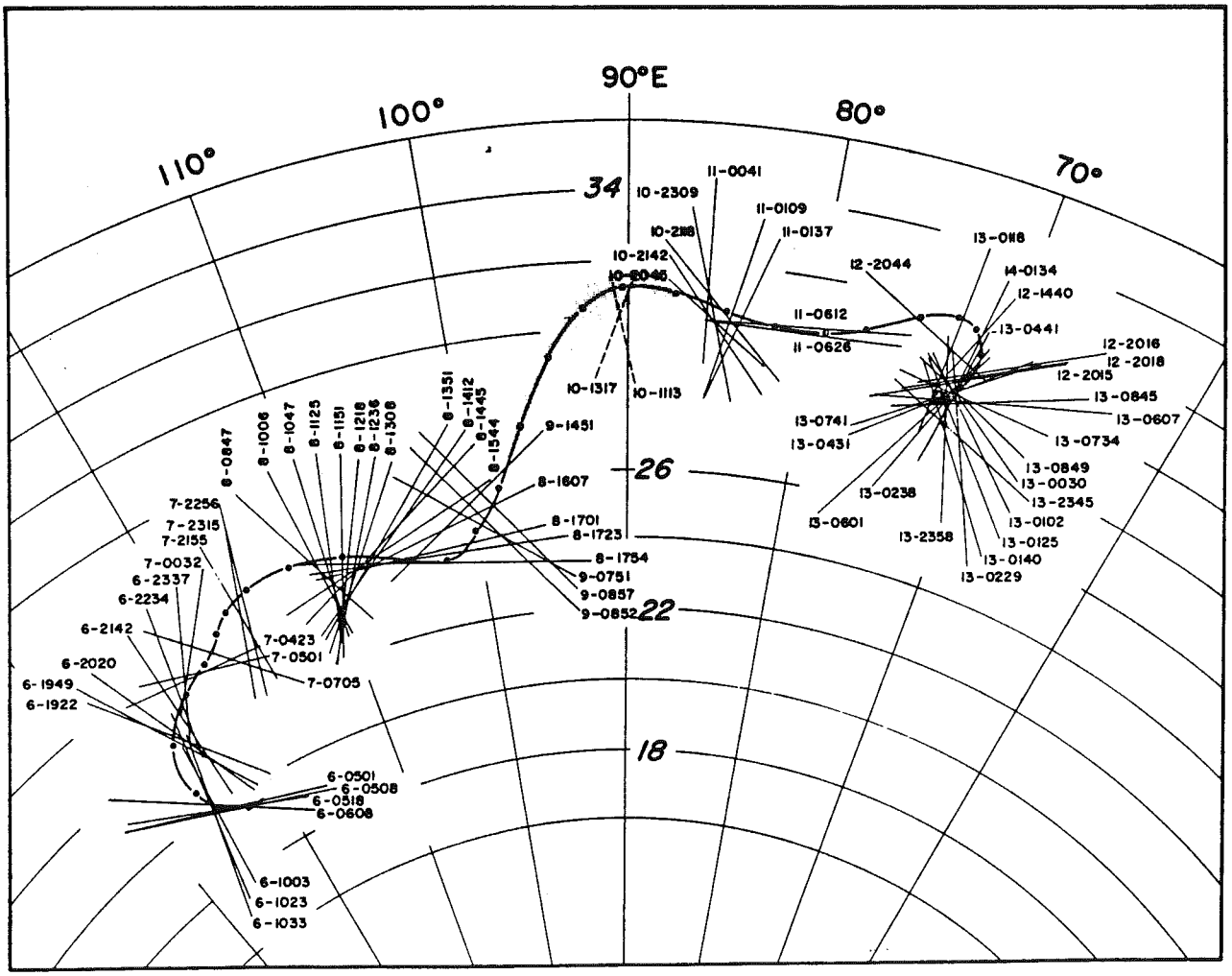

FIG 6 Drift track of the 1967 Canadian North Pole station with lines of positions determined from sun observations. Time intervals between dots on the track are six hours. Numbers beside position lines represent day of May 1967, and universal time at which the sun was observed. Numbers along 90°E meridian represent co-latitude in minutes.

drift across the Pole while carrying out plumb line deflection and gravity measurements. As it turned out, because of difficulties with the two single-engine Otter aircraft sent out to assist the scientists and, eventually, evacuate the camp, 900 km from base, the full program was not carried out.

Viewing of stars in daylight requires an up-to-date star catalogue especially generated for the particular geographical area and time period. Figure 6 shows the lines of positions of celestial targets, mostly of the sun, starting on 6 May at 1003 h GMT, minutes after the Bristol Freighter aircraft had landed on the ice with the seven expedition members, until 14 May at 0134, just before the camp personnel were evacuated to Alert. The solid line represents the computed drift path with a dot every six hours. Except for a 28-hour period of overcast weather (shaded area in Fig. 6), the sun was visible most of the time, but because of the presence of crystal fog in the air the stars were visible only occasionally. During the first six days the drift speed ranged from 300 to 700 $m \cdot h^{-1}$. It is estimated that the drift path positions are accurate to ± 200 m when only the sun is used as a target and to ± 50 m when the targets also include stars and planets. Figure 6 illustrates the ambiguity of determining the drift path by conventional survey methods during periods of rapid drift, without modern computing aids on hand. Consider, for instance, the time period from 0847 to 1754 on 8 May during which 16 sun observations were taken. The only way an observer on the ice, equipped with theodolite, watch, paper, pencil and ruler, can determine his position is from successive position line intersections. The positions thus obtained are scattered several kilometres about the actual drift path positions.

Although the gravity survey from Alert to the Pole and across the Lomonosov Ridge, and the plumb line deflection experiment, had to be abandoned, the knowledge acquired about navigation in the polar area proved invaluable in planning the 1969 and LOREX 79 polar expeditions.

The Second Canadian North Pole Expedition. Two years later the expedition returned to the north polar area and occupied an ice floe from 12 April to 3 May 1969. Their equipment included a Magnavox transit satellite receiver (the first commercial satellite receiver to operate in Canada; its raw data were recorded on punch paper tape and processed in Ottawa after the expedition returned), a Kern DKM-3 and a Wild T-2 theodolite, and an acoustic bottom reference system. In addition, the Twin Otter aircraft used for spot gravity measurements and depth soundings had an experimental Omega receiver on board (the forerunner of the Global Navigational System, a very low frequency, world-wide navigational aid). Because of clearer weather and lower sun angle in April the stars were much more visible than in 1967. Except for a period

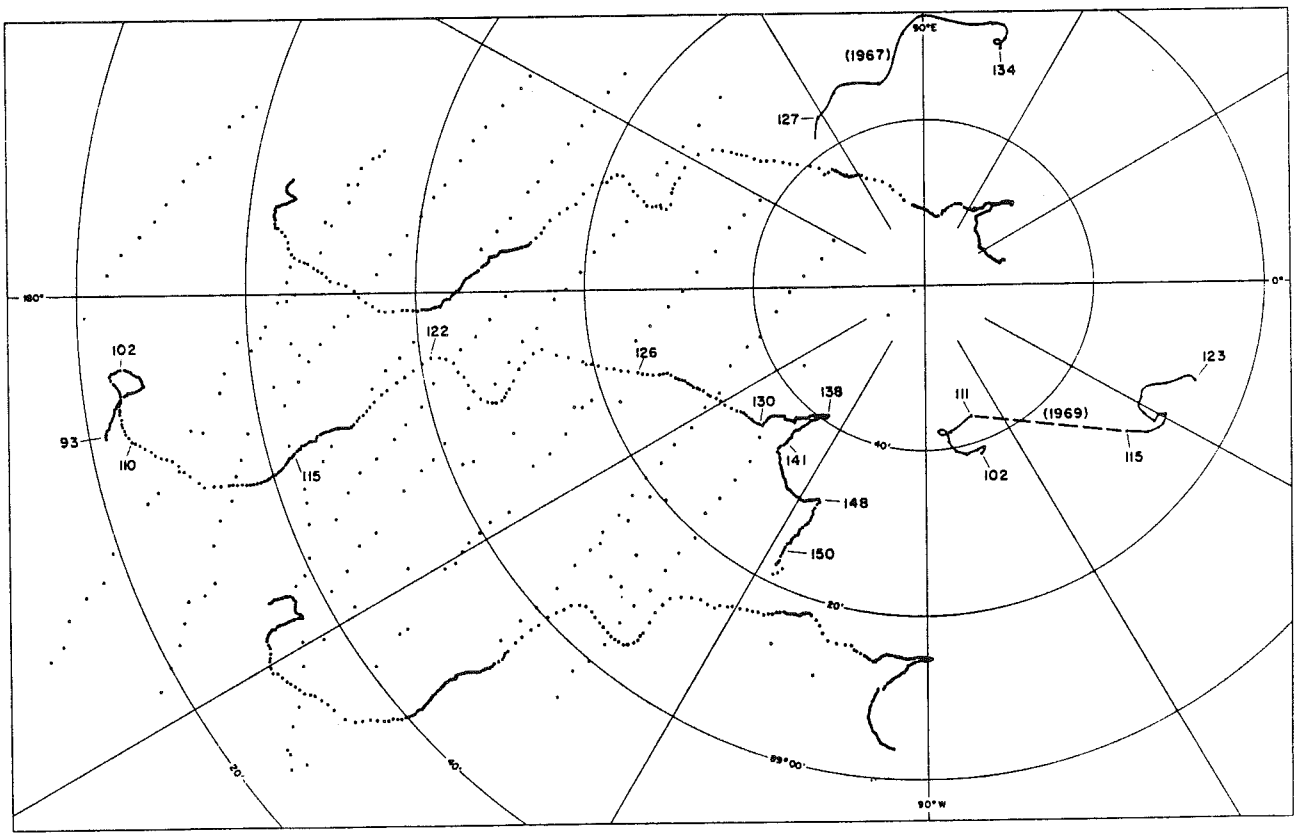

FIG. 7. Drift tracks of the 1967 and 1969 expeditions and of the three LOREX 79 camps. Numbers represent Julian days. Also shown are locations of spot soundings and gravity observations.

of four days, when a storm blew the ice station 40 km to the southeast while the satellite receiver was shut down, star and satellite position fixes were obtained continuously. By ranging once a minute from an acoustic transducer at the camp to two transponders on the sea bottom, the scientists obtained measurements of the fine structure of the ice drift relative to the ocean floor. By superimposing the acoustically-determined drift path on the path determined astronomically and by satellite receiver, they obtained the plumbline deflection along the drift path, and track positions, to an accuracy of better than ±40 m (Lillestrand and Weber, 1974).

Spot gravity and depth measurements between Alert and the Pole and across the Lomonosov Ridge were carried out using Twin Otter aircraft. Positions were obtained from sun observations of at least two hours using the T-2 theodolite with a Roelofs prism. Precise positions were later determined by computer, taking drift and atmospheric refraction into account, and are estimated to have on the average an accuracy of ±500 m. The drift paths of the 1967 and 1969 expedition are shown in Figure 7. The dots on the tracks, spaced at one-day intervals, illustrate the speed at which the stations drifted; the numbers refer to Julian days.

The LOREX 79 Expedition. In spring 1979 EMR undertook a large-scale, multidisciplinary project to study the nature and origin of the Lomonosov Ridge. The scientific program was planned and coordinated by the Earth Physics Branch, and logistic support was provided by the PCSP. Scientists from other branches of EMR, from the Department of Fisheries and Oceans and from a number of universities in Canada and the U.S.A. took part in the project which was code-named LOREX 79 (Weber, 1979, 1980; MacInnes and Weber, 1980).

Positioning of the LOREX 79 main camp, and the two satellite camps ~60 km from the main camp, was based on satellite Doppler observations of the Navy Navigation Satellite System. Real-time navigation fixes were computed from the on-line satellite receiver at the main camp approximately every hour (Wells and Grant, 1977). The two satellite camp receivers recorded raw data on cassettes which were collected every few days and flown to the main camp for off-line processing. In this way, ice camp positions were continuously updated with precisions of about ±250 m, which provided reference for the aircraft Global Navigational System (GNS) and useful information on ice speed and direction during the expedition. This represented a considerable improvement over the 1969 expedition when ice velocity information became available only months later, after the data had been processed in Ottawa.

A new software package has been developed for geodetic positioning of slowly moving platforms from satellite Doppler tracking (Popelar *et al.*, 1983). The three-dimensional data reduction model uses consecutive satellite passes for a sequential adjustment of the station coordinates and evaluation of mean linear velocities over pre-determined time intervals. The LOREX satellite Doppler data set has been reprocessed, using the new software and post-fitted precise satellite orbits providing mean station positions for 3-hr intervals with a horizontal precision of ±24 m and a vertical uncertainty of ±0.4 m. Drift velocities of up to 1200 $m \cdot h^{-1}$ were recorded.

During the month of April star observations were also taken using a Wild T-4 theodolite. The astronomical positions yielded about the same accuracy as the Transit Satellite fixes and were used to determine the plumbline deflections.

The drift paths of the LOREX 79 main and satellite camps, as they drifted across the Lomonosov Ridge with the Transpolar Current, are illustrated in Figure 7 as dots spaced at 3-hr intervals. The numbers 93 to 150 along the main camp drift track represent Julian days.

Some 270 spot soundings were carried out by helicopter and Twin Otter aircraft equipped with a GNS. Although no accuracy tests of the GNS seem to have been conducted in the polar region, we estimate from repeated comparisons with the main camp positions that the accuracy achieved on this operation is of the order of ±1000 m.

All soundings of the earlier expeditions, as well as all spot soundings on the LOREX 79 helicopter traverses, were taken by the seismic method using two geophones placed on the ice and dynamite charges ranging from 0.1 to 0.5 kg. Explosives were either drilled into the ice or, when feasible, detonated in the water. Spots for underwater detonation were chosen based on either the presence of cracks and/or open leads or the presence of thin ice that could be quickly pierced with an ice chisel or drilled with a hand auger. Soundings along the 1967 and 1969 drift paths were obtained at least twice a day. Depths at the LOREX 79 satellite camps were recorded on 3.5 kHz echo sounders, and at the main camp soundings were obtained from the 3 kHz sub-bottom profiler and from a 164-cm^3 shallow seismic air gun. Figure 7 shows the locations of most of the spot soundings that were established by helicopter and fixed-wing aircraft, as well as the drift tracks along which depth soundings were recorded.

Based on all the depth soundings that were taken on the three polar expeditions (over 300 spot soundings and 650 line kilometres of continuous echo and shallow seismic soundings), a 100-m contour map of the sea floor of the area around the North Pole was compiled. The map (Fig. 8) was prepared at a scale of 1:250 000 and extends from the Makarov Basin across the Lomonosov Ridge to the North Pole in the Fram Basin. The shallowest and deepest depths recorded were 955 m on the Lomonosov Ridge, and 4309 m in the Fram Basin, respectively.

JOINT CONTRIBUTIONS

The Arctic Ice Dynamics Joint Experiment

In 1970 the Arctic Ice Dynamics Joint Experiment (AIDJEX) was established for the purpose of studying the large-scale interaction between hydrosphere and atmosphere in the Arctic Ocean. This highly successful multidisciplinary, multi-agency project included U.S. and Canadian scientists and was supported by the National Science Foundation and PCSP. Pilot studies in spring 1970, 1971 and 1972 were followed in 1975

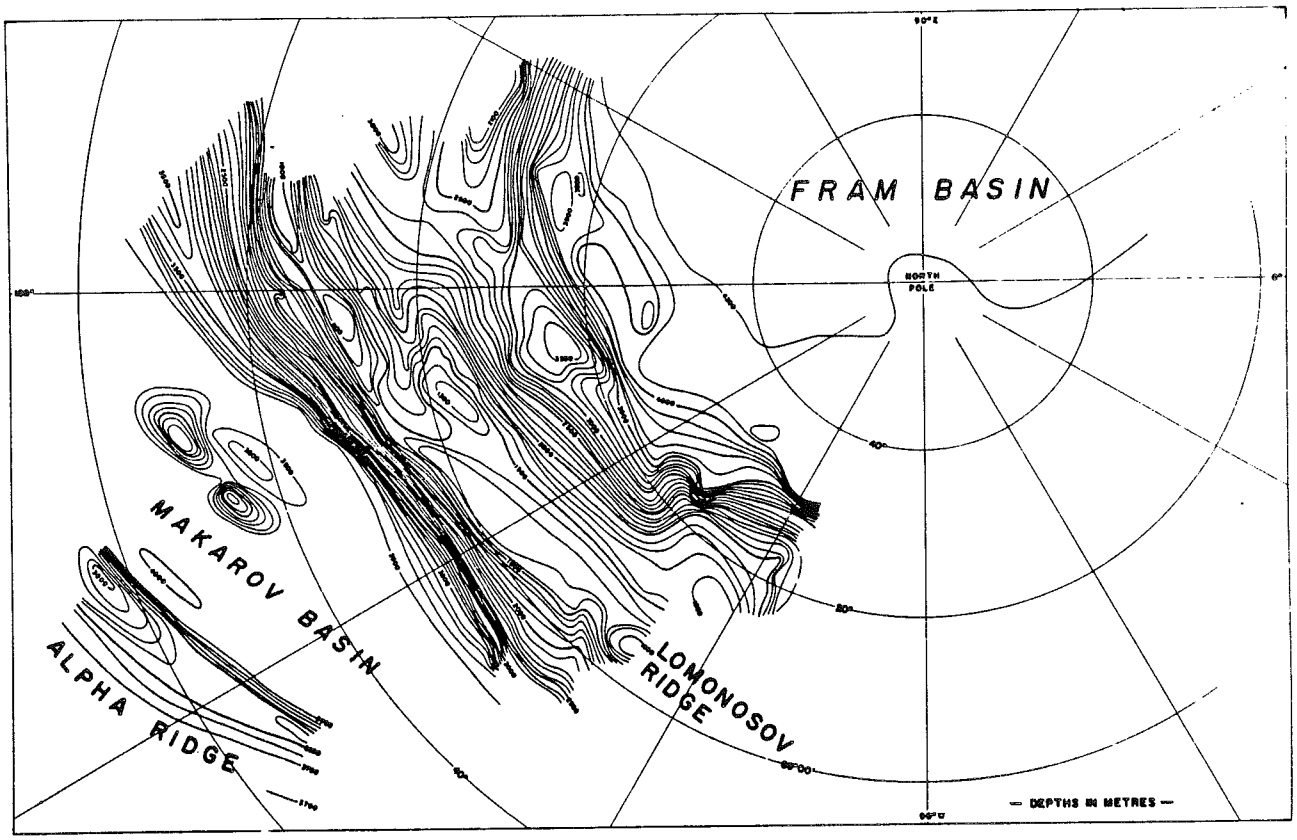

FIG. 8. LOREX 79 bathymetric map. Contour interval 100 m.

by the main experiment, during which four manned stations drifted for 15 months in the Beaufort Sea. This was the largest scientific operation of its kind ever to be undertaken in the Arctic Ocean. Continuous depth and gravity measurements and a seismic refraction survey were carried out by the Earth Physics Branch during the main experiment; these results added to the bathymetric and morphological knowledge of the Canada Basin.

THE MAPS AND CHARTS OF THE ARCTIC OCEAN BASIN

The 1954 Soviet Map

By 1954 the Soviets had established over 2000 soundings resulting in the compilation of a map of the arctic sea floor (Fig. 9) which, for the first time, revealed the existence of the Lomonosov Ridge (Burkhanov, 1956). Ya. Ya. Gakkel was the best known of the Russian hydrographers of that period and much of the credit for compiling the map goes to him. He had compiled a map showing part of the Lomonosov Ridge in 1949 but it was kept secret at the time. In recognition of Gakkel's contribution, the Arctic mid-oceanic ridge in the Eurasia Basin was named after him. Others who contributed significantly were Ostreikin, Tolstikov, Gordienko, Somov, Burkhanov and Treshnikov (Lloyd, pers. comm. 1980). Understandably, the map caused a sensation among arctic experts outside the Soviet Union, who until 1954 had been unaware of the scope and magnitude of Soviet exploration.

The DRB Chart

In 1956 the Defence Research Board of Canada (DRB) compiled a map of its own (Fig. 10). I have tried unsuccessfully to track down how and by whom the map was compiled; Surveys and Mapping Branch of Energy, Mines and Resources Canada, where the map was prepared, has no records (Falconer, pers. comm. 1981). It appears to have been compiled by using the Soviet map as a base and adding U.S. airborne and T-3 data, and by re-contouring Somov's NP2 soundings. Here, for the first time, the Alpha-Mendeleev Ridge is outlined as separating the Makarov Basin from the Canada Basin. For many years the DRB map remained the best bathymetric chart of the Arctic available to the public outside the Soviet Union. It is rumoured that the U.S. Navy used it to navigate the *Nautilus* to the North Pole in 1957.

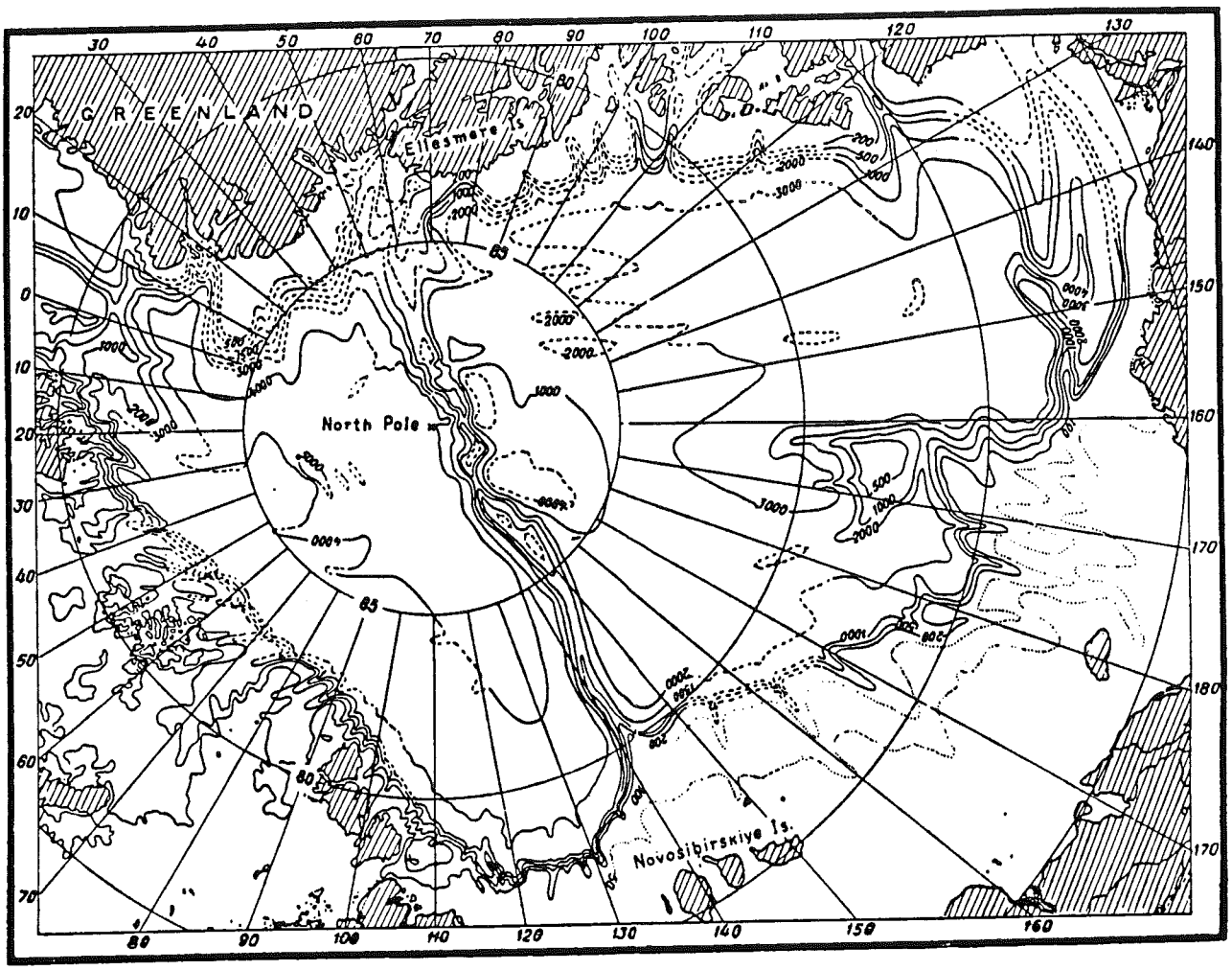

FIG. 9. 1954 Soviet bathymetric map of the Arctic Ocean.

The 1960 Soviet Map

By 1960, 900 deep-water oceanographic STD (salinity, temperature, depth) stations, 100 24-hr oceanographic stations, 300 hydrobiological stations and over 20 000 soundings had been established. These data resulted in the publication of a second Russian map (Fig. 11; Gordienko, 1960), which utilized data to 1 March 1959. Although generalized because of its small scale and because depth soundings are highly classified in the Soviet Union, it clearly delineates the Canada Basin, the Alpha-Mendeleev Ridge and the Makarov Basin, but the Nansen-Gakkel Ridge is not yet clearly defined. No Russian maps have since been published that show significantly more detail.

Heezen and Ewing

In Nansen Strait, between Spitzbergen and Greenland, the Norwegian Sea narrows to about 300 km from shelf to shelf. In 1912 Nansen postulated that a shallow east-west submarine ridge connects the two shelves, effectively separating the Arctic from the North Atlantic water. The existence of Nansen's Sill, as this hypothetical ridge became known, remained unchallenged until 1958 after the Russians had conducted a detailed bathymetric survey from three icebreakers. It was found that the ridge did not exist but rather that the relatively shallow strait was bisected by a narrow north-south trough over 4000 m deep (Laktionov, 1959), now known as Lena Trough (compare, e.g., Figs. 10 and 13). It has long been known (Linden, 1959) that the mid-oceanic seismic belt continues through the Arctic Ocean and that earthquake epicentres follow a line from Jan Mayen Island through Nansen Strait across the Eurasia Basin to the Laptev Sea. Heezen and Ewing (1961) speculated that this seismic belt signifies the continuation of the Mid-Atlantic Ridge and that the Lena Trough is a rift feature of the ridge. They re-examined the *Fram* and *Sedov* water depths and re-evaluated the Soviet data; i.e. by superimposing the Soviet

drift tracks and landing sites of the High Latitude Air Expeditions (Fig. 2) over the bathymetric charts (Figs. 9 and 11) they re-established the locations and values of Soviet soundings. Based on these data they revised the chart of the Eurasia Basin (Fig. 12), which shows the mid-oceanic ridge extending from the Lena Trough to the Laptev Shelf and bisecting the Eurasia Basin roughly halfway between the edge of the Barents Continental Shelf and the Lomonosov Ridge. It should be noted that, at this stage, the Nansen-Gakkel Ridge, as the Arctic mid-oceanic ridge later was named, was only a hypothesis of Heezen and Ewing's, the existence of which was not contradicted by known or inferred soundings. The bathymetric data were far too scarce and too scattered to delineate the ridge to more than a purely schematic representation. Although the Soviets had far more data available than did Heezen and Ewing, they apparently did not see the ridge because they were not looking for it, believing, at that time, that the Arctic Ocean was formed by subsidence of continental platforms (Saks *et al.*, 1955; Hakkel, 1958). Heezen and Ewing saw it because, as adherents of the then-emerging theory of plate tectonics, they were expecting it. The existence of the Nansen-Gakkel Ridge was not unequivocally confirmed until 1969 with the publication by Beal of the U.S. submarine bathymetry. Virtually no new unclassified depth data from the Eurasia Basin have become available until the last two years when detailed soundings were made near the Atlantic end of the ridge during the FRAM I and FRAM II expeditions. This leaves most of the Nansen-Gakkel Ridge still poorly mapped.

Ostenso's Bathymetric Map

In 1961 N. Ostenso compiled a new map of the Arctic Ocean sea floor based on all available unclassified material (Ostenso, 1962, 1963). The map (Fig. 13) is contoured at 200, (500), 1000, 2000, 3000, (3800), 4000 and 5000 m and as published is plotted at a scale of about 1:18 000 000. The data were weighted according to their indicated degree of control. Necessary interpretation and interpolations were made conser-

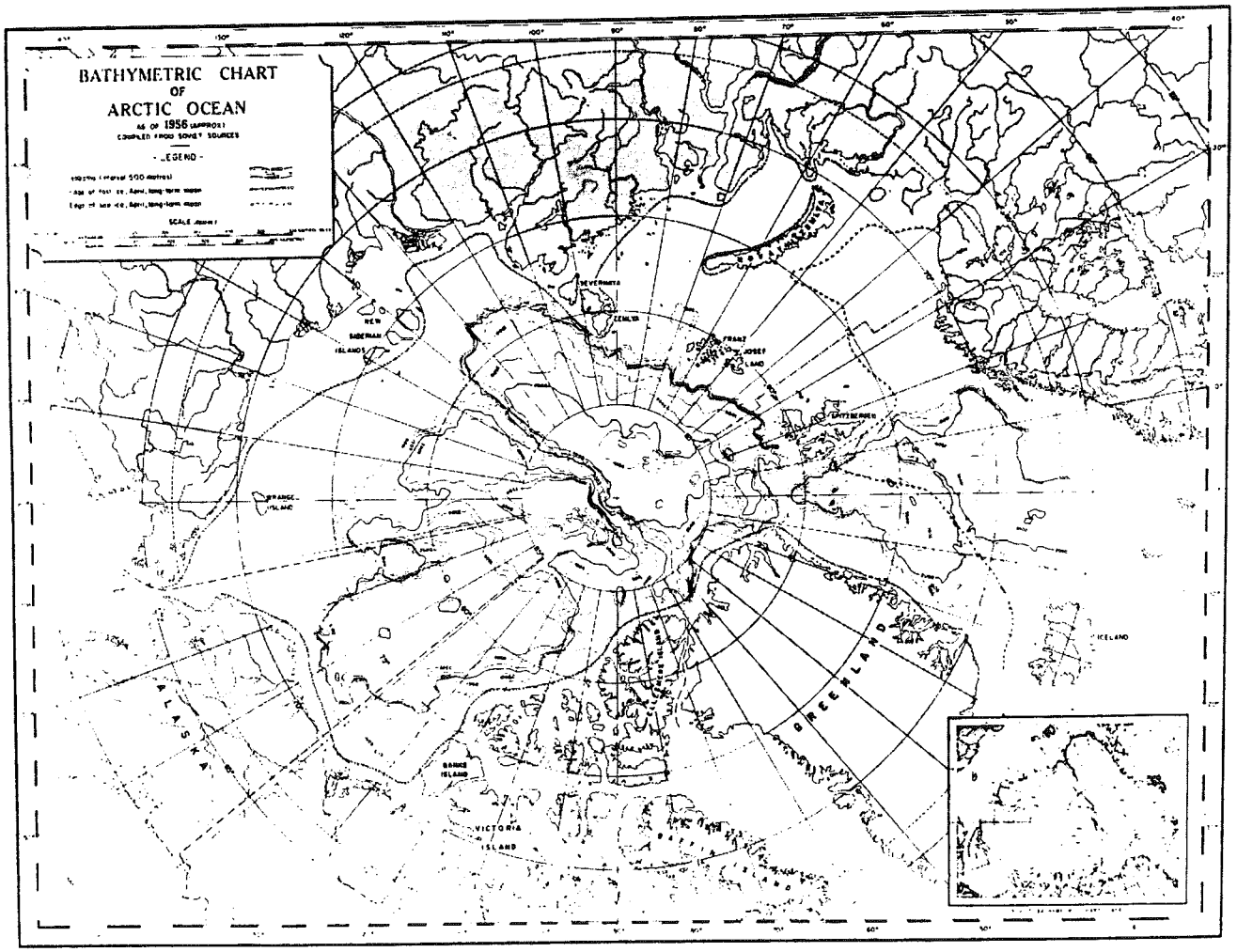

FIG. 10. 1956 Defence Research Board bathymetric chart of the Arctic Ocean.

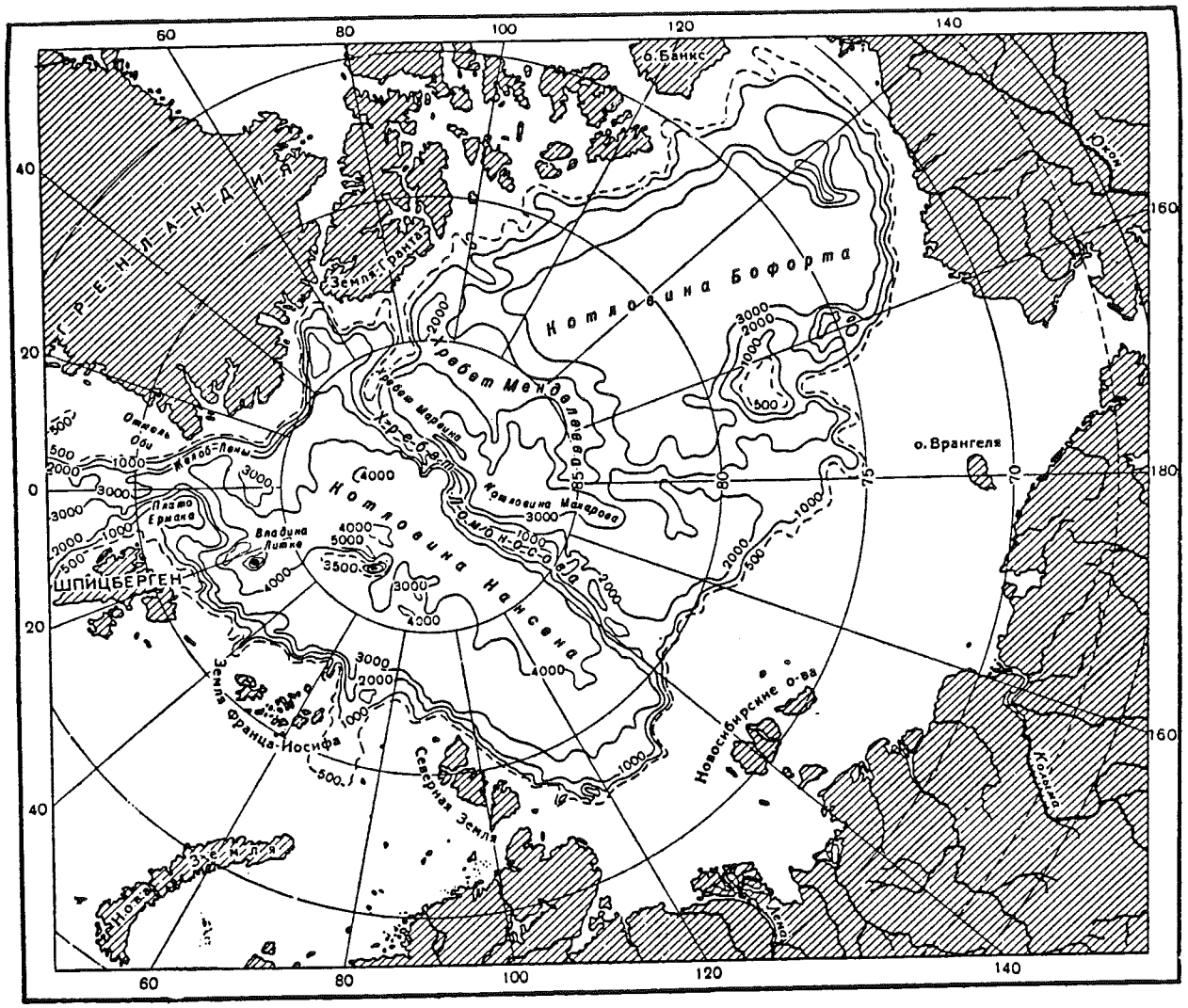

FIG. 11. 1959 Soviet bathymetric map of the Arctic Ocean.

vatively and detailed flexures of isobaths were made only when sufficient and reliable data warranted. This is apparent for the Eurasia Basin when compared with Heezen and Ewing's contouring.

Except for the Lena Trough region, the contours in the central part of the Arctic, in the region north of 80°, do not differ significantly from those on the DRB chart (Fig. 10).

Canadian Bathymetric Chart of 1967

In 1967 the Canadian Hydrographic Service published two charts of the Arctic Ocean north of 72° from longitude 0° to 90°W (map sheet 896) and from 90°W to 180° (map sheet 897). The map was compiled by De Leeuw (1967) from some 12 000 soundings of which about 6000 were from inside the Canadian Archipelago and Greenland inter-channel waters. Beyond the 200 m isobath the chart is contoured at 500-m intervals; the scale is 1:2 000 000. The bathymetry is colour-coded with six colour ranges and land masses are left blank. Except for the continental shelf of the Queen Elizabeth Islands, which had been charted by PCSP, and the Chukchi Rise, Alpha Ridge and Canada Basin, where the University of Wisconsin had been carrying out sounding operations, the chart does not differ significantly from Ostenso's.

The GEBCO Map of 1968

The Canadian Bathymetric Chart of 1967 served as the basis for the General Bathymetric Chart of the Oceans (GEBCO), 3rd edition, sheets CI and CII, which were published in Paris in 1968 by the Institute Géographique National at a scale of 1:3 100 000. The land topography is contoured at 1000-m in-

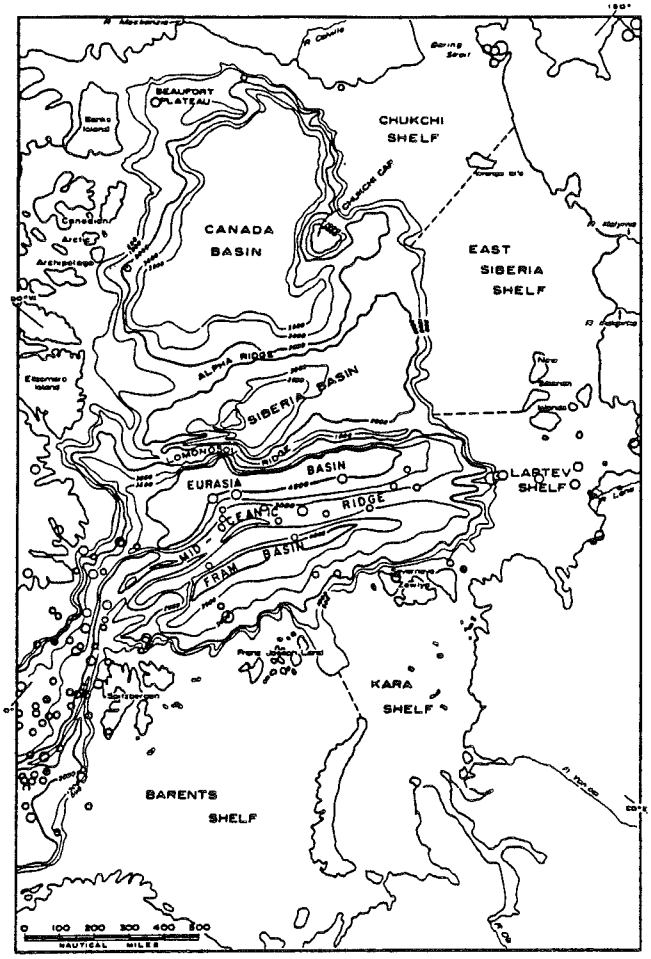

FIG. 12. Heezen and Ewing's 1961 bathymetry of the Arctic Ocean. Circles represent earthquake epicentres.

tervals and colour-coded. Other than the scale, and the fact that the GEBCO bathymetry shows more soundings, it is identical to Canadian Charts 896 and 897.

The British Admiralty North Polar Chart

In 1969 The United Kingdom Hydrographic Department published the North Polar Chart, Admiralty Chart No. 4006. It was compiled by Ritchie (1969) at an approximate scale of 1:7 500 000. Beyond the 100-fathom isobath the depth is contoured at 500-fathom intervals. The chart does not present any new information, and the contouring of the western half of the Arctic north of 72° is essentially an interpolation, in the old depth units, of the Canadian Hydrographic Charts 896 and 897. The balance of the Admiralty chart does not differ significantly from Ostenso's chart.

Heezen and Tharp's Map of the Arctic Region

In 1975 the American Geographical Society published "Map of the Arctic Region", sheet 14 of "The World Series". This is the most ambitious topographic-bathymetric map of the Arctic ever to have been produced. The coloured map, scale 1:5 000 000, measures approximately 120 × 150 cm; 18 colour steps cover an elevation range from a depth of 8000 m in the Aleutian Trench to a height of over 5000 m in the St. Elias Range. It was compiled by Bruce C. Heezen and Marie Tharp of the Lamont-Doherty Geological Observatory, based on all available unclassified soundings and on extensive use of Beal's (1969) submarine depth profiles. Topographic elevations are contoured at 1000-m intervals whereas the bathymetric contour intervals range from 500 m over steep slopes and over the Nansen-Gakkel Ridge to as little as 10 m over the abyssal plains. The ocean floor is depicted in great detail everywhere, without regard to how much or how little data are available. A portion of Heezen and Tharp's map with some of the isobaths removed is illustrated in Figure 14 (from Sobczak, 1977); the original has 100-m intervals over the abyssal plains and 200-m intervals over the Lomonosov Ridge. The Nansen-Gakkel Ridge is shown with numerous transform faults and flat-topped rectangular structures, illustrating the compilers' view on what the bottom topogaphy of an active spreading ridge might look like; however, the scant sounding data available for this region provide no evidence for such features (Sobczak, 1977). In their detailed aeromagnetic investigation of the Arctic Basin, Vogt *et al.* (1979:1087) comment on the transform faults on Heezen and Tharp's chart: "Contrary to the representation on the map the magnetic lineations are relatively continuous and execute smooth bends. The anomaly pattern suggests transform faults at only a few spots. Elsewhere, sharp offsets attributable to transform faults would have to be of small enough displacements (10 km or less) to escape resolution". Using newer, classified submarine data and re-evaluating the old, they also found that the central rift valley position of the Nansen-Gakkel Ridge may be up to 50 km displaced from that shown on the Heezen-Tharp chart.

Sobczak's Arctic Bathymetry

In 1978 the Earth Physics Branch of EMR published as part of Arctic Geophysical Review (Sweeney, 1978) a new map of the Arctic Ocean Basin. It was compiled by Sobczak and Sweeney (1978) at a scale of 1:7 500 000 and is, beyond the 200-m isobath, contoured at 500-m intervals. Although nearly 250 000 digitized soundings were used, the distribution is very uneven. For example, not a single sounding is available from the Laptev Shelf side of the Eurasia Basin south of 85°. The data used by Sobczak, and earlier by Heezen and Tharp, originate from the same sources, yet the interpretation is quite different. As an example, Sobczak's contouring north of 85° is depicted in Figure 15 (from Sobczak, 1979) with all the sounding data superimposed; dots represent soundings taken from the ice surface, straight lines indicate the location of the submarine traverses along which Beal (1969) determined water depths. The drawing illustrates the paucity of sounding data over the Nansen-Gakkel Ridge. Sobczak replaced Heezen and Tharp's elaborate diagrammatic representation of the Nansen-

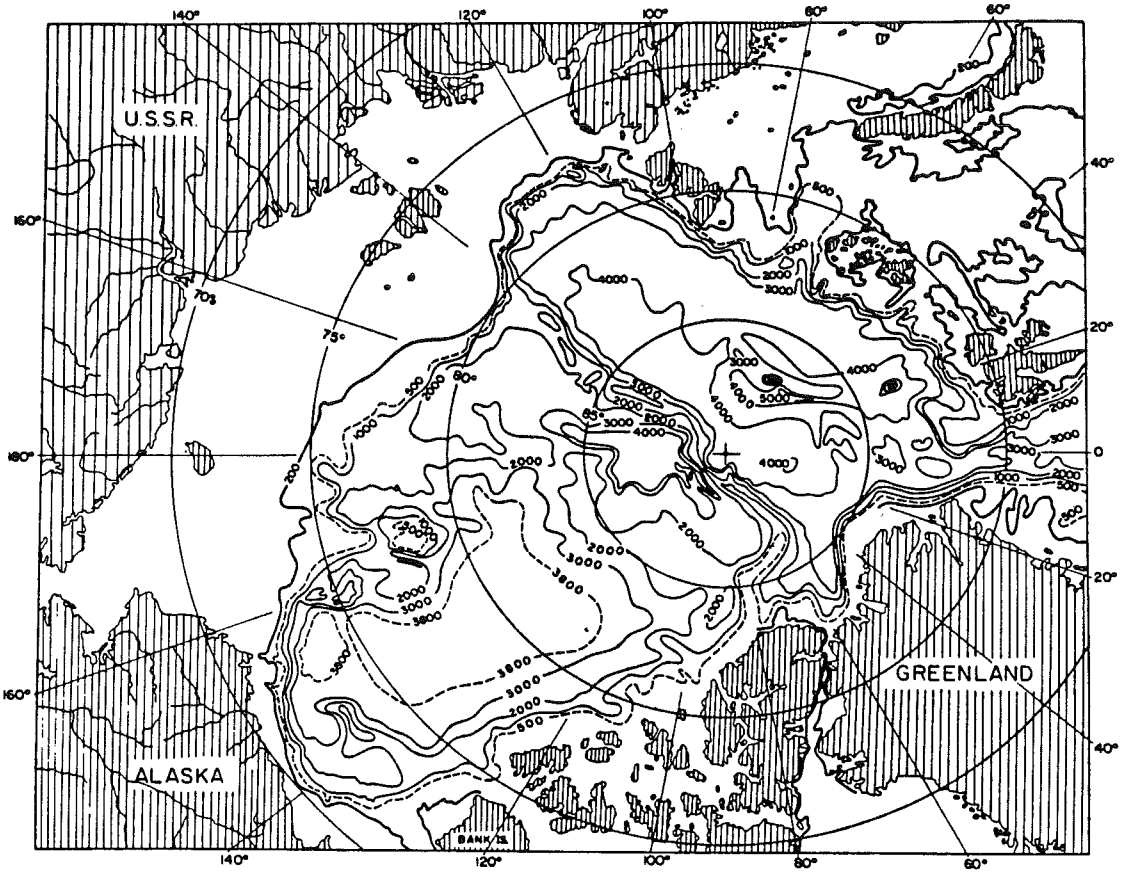

FIG. 13. Ostenso's 1962 bathymetry of the Arctic Ocean.

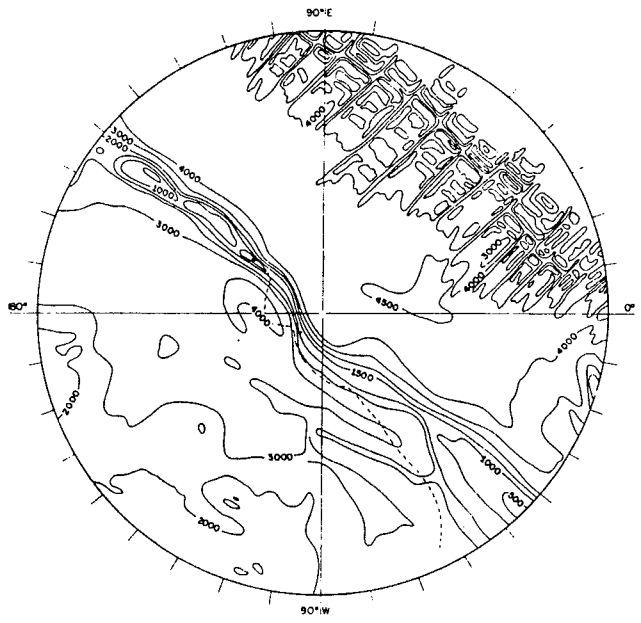

FIG. 14. 500-m contours of Heezen and Tharp's 1965 bathymetric chart north of 85°, superimposed on LOREX profiles (heavy line).

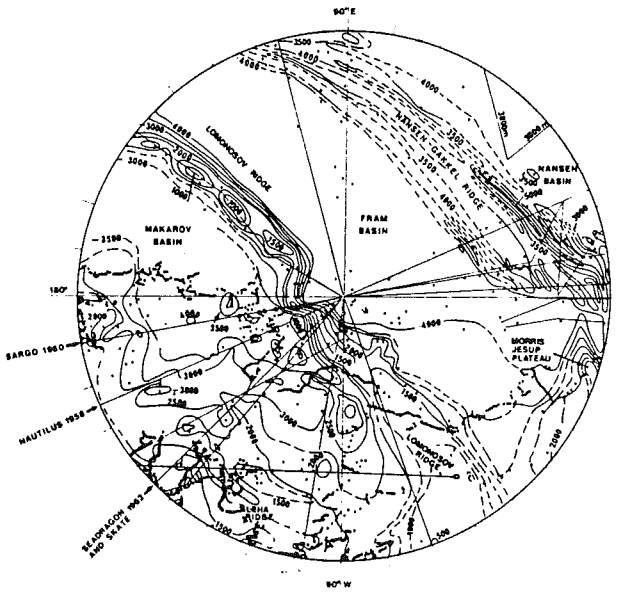

FIG. 15. Sobczak's bathymetry north of 85° including meridional tracks of the U.S. submarines *Seadragon* and *Skate* (1962), *Nautilus* (1958) and *Sargo* (1960).

Gakkel Ridge (Fig. 14) with a much simpler model consisting of a series of narrow, parallel ridges somewhat similar in character to Heezen and Ewing's (1961) original concept (Fig. 12). Where the contouring is necessarily speculative, the isobaths are represented by broken lines; this contrasts with Heezen and Tharp's map in which the reader cannot distinguish between fact and speculation.

The GEBCO Map of 1979

In 1979 the Canadian Hydrographic Service published Chart No. 517 of the General Bathymetric Chart of the Oceans under the authority of the International Hydrographic Commission. It encompasses the arctic regions north of 64° and is printed at a scale of 1:6 000 000. The topographic and bathymetric colour scheme is the same as for Heezen and Tharp's chart. The contour intervals range from 1000 m to 100 m depending on the sounding density. Unlike Heezen and Tharp's chart, however, the location of surface ship, submarine, and drifting station tracks, as well as individual soundings, are plotted, and areas with high density soundings, such as over the Canadian polar continental shelf, are delineated. This allows the user to gauge the reliability of the chart for any particular area. Contouring is conservative, and in the Arctic Ocean is generally the same as Sobczak's 1978 chart (but with greater contour density) since Sobczak was a principal compiler. Nevertheless, some of the speculative diagrammatic contouring of Heezen and Tharp, suggestive of transform faulting, has been retained — over Sobczak's objections (Sobczak, 1979; Monohan, 1979).

Residual Magnetic Anomaly Chart of the Arctic Ocean Region

In 1982 the Naval Research Laboratory and the Naval Ocean Research and Development Activity published a residual anomaly chart of the Arctic Ocean at a scale of 1:6 000 000. Printed over the coloured bathymetric chart are aeromagnetic profiles along the flight tracks with positive anomalies in red and negative anomalies in green. Printed in black on the back of the chart, for viewing on a light table, are earthquake epicentres and magnetic lineations. Although it is a specialized geophysical map it is mentioned here because the contours of the bathymetric base map are those of the GEBCO chart, except for the Lomonosov Ridge near the North Pole where the contours were corrected based on the LOREX bathymetry (Weber, 1979).

COMPARISONS AND CONCLUSIONS

Comparison of the LOREX 79 bathymetric map with the 1979 GEBCO chart, and with the 1975 Heezen and Tharp chart, reveals large discrepancies. The superimposition of the contours of the two charts on the LOREX 79 map is illustrated in Figures 16 and 17. The crest of the Lomonosov Ridge is offset by as much as 34 km on the GEBCO chart and by as much as 77 km on the Heezen and Tharp map.

Out of curiosity I made the same comparison with the 1954 Soviet map (taken from the DRB chart, Fig. 10). Surprisingly, this 25-year-old map agreed much better with the LOREX 79 survey (Fig. 18) than do the recent maps. For most of its length the location of the ridge crest lies within the positioning accuracy of the LOREX 79 survey. This at first seem unexpected since the Soviet surveys were carried out in the "horse and buggy" days of wire winches and sun positioning, long before sophisticated radio and satellite navigational aids became available and many years before nuclear-powered submarines began to cruise under the arctic pack ice.

Why is it that the old Soviet map is so much more accurate than our contemporary maps? The answer is suggested in Figure 15. In the LOREX 79 survey area, i.e. between 130°W and 160°E, there are only five soundings on the Lomonosov Ridge. The compilers relied heavily on Beal's (1969) submarine data from the *Seadragon* and *Skate* (1962), from the *Nautilus* (1958), and from the *Sargo* (1960), the meridional tracks of which are indicated in Figure 15. When the sub-

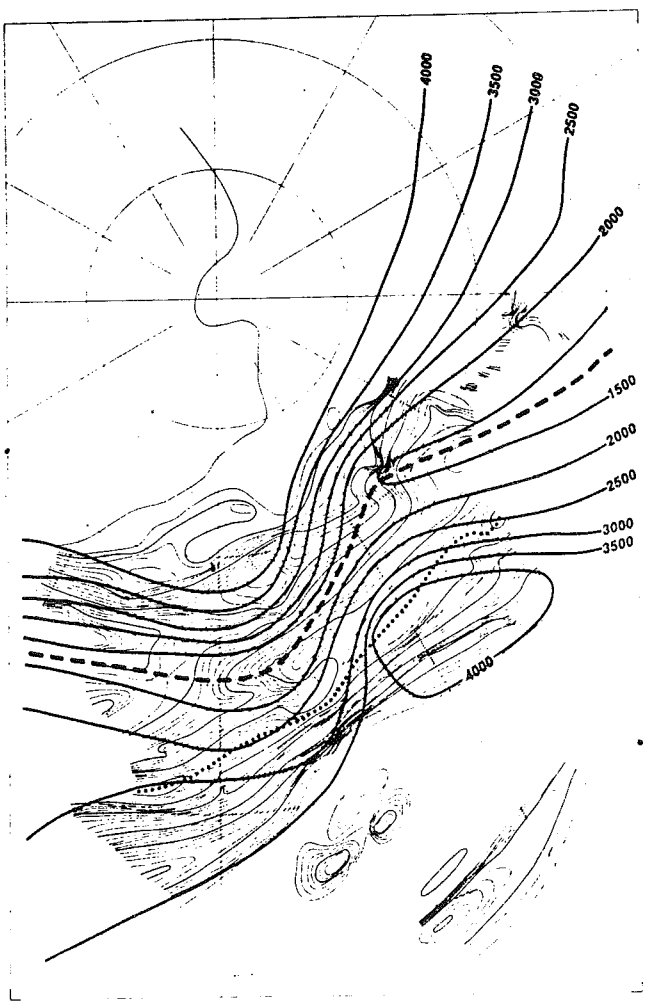

FIG. 16. LOREX 79 bathymetric map with Lomonosov Ridge crest (dotted line). Superimposed are the 500-m contour lines and ridge crest (broken line) of 1979 GEBCO chart.

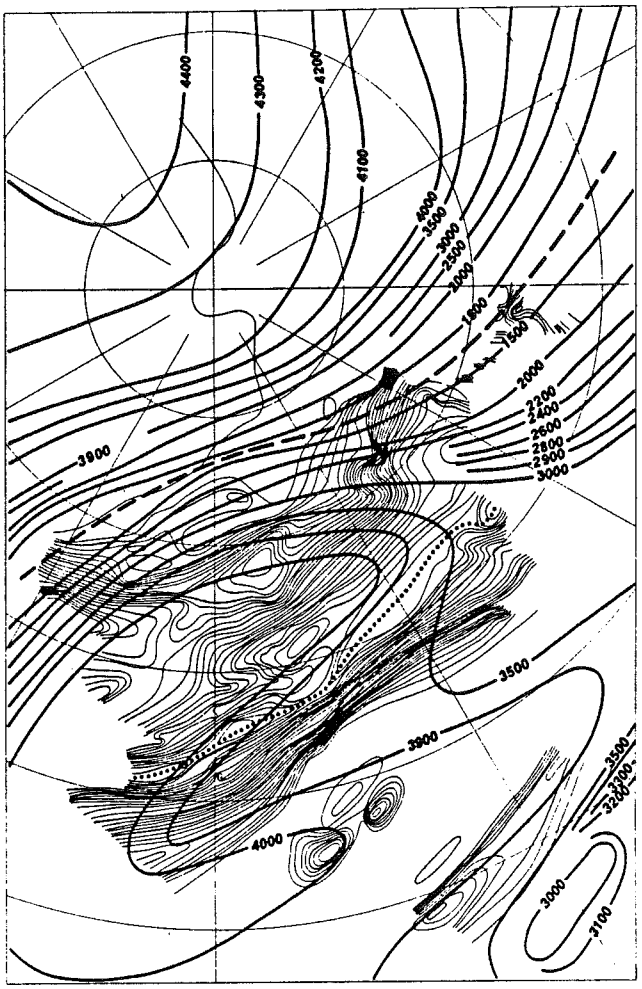

FIG. 17. LOREX 79 bathymetric map with Lomonosov Ridge crest (dotted line). Superimposed are the 500-m contour lines and ridge crest (broken line) of the 1975 Heezen and Tharp chart.

marine echogram profiles from Beal's thesis along these tracks are plotted against the LOREX 79 profiles (Fig. 19), it becomes obvious that the ship's inertial navigation system (SINS) was very inaccurate. Not only are three out of four profiles offset by as much as 40 km, but also, in the case of *Nautilus*, the ship's absolute speed must have been greater than assumed, giving the ridge the appearance of being narrower than it is. The depression in excess of 4000 m between meridians 130° and 160°W on the GEBCO map was a result of relying on the *Skate* and *Nautilus* tracks; the *Seadragon* track was ignored.

There is no reason to believe that the SINS of the submarine was more accurate elsewhere, and since many of the "blank" areas of the Arctic Ocean have been filled in, first by Heezen and Tharp and later by Sobczak, using Beal's submarine data, the bathymetry in these areas is suspect. It is the author's opinion that in areas where soundings are scarce, Ostenso's map and the DRB chart based on early Soviet data are still the most reliable maps to which the public has access.

There is no doubt that, with increasingly more sophisticated navigational aids, the U.S. and Soviet submarine fleets have gathered a wealth of accurate and detailed bathymetric data. However, as long as the two navies keep all of their bathymetric data secret, we shall continue to sound the Arctic Ocean slowly and expensively from the surface, duplicating the work that has already done from below.

ACKNOWLEDGEMENTS

I wish to thank Dr. Ned Ostenso, Mr. George Hobson, Dr. Fred Roots and Dr. Keith Arnold for reviewing and offering comments on the draft of this manuscript.

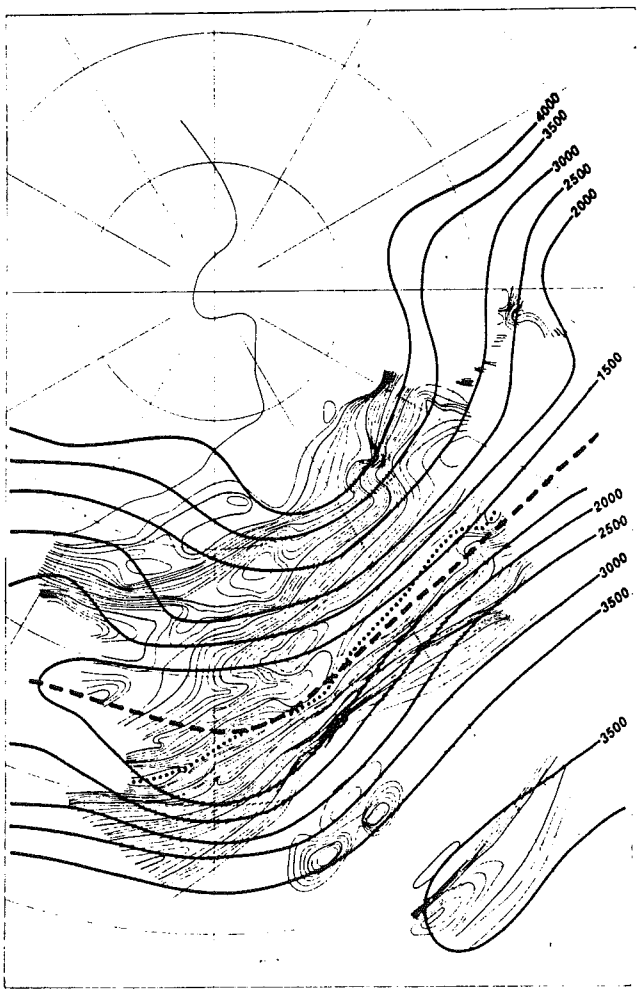

FIG. 18 LOREX 79 bathymetric map with Lomonosov Ridge crest (dotted line). Superimposed are the 500-m contour lines of the 1954 Soviet map.

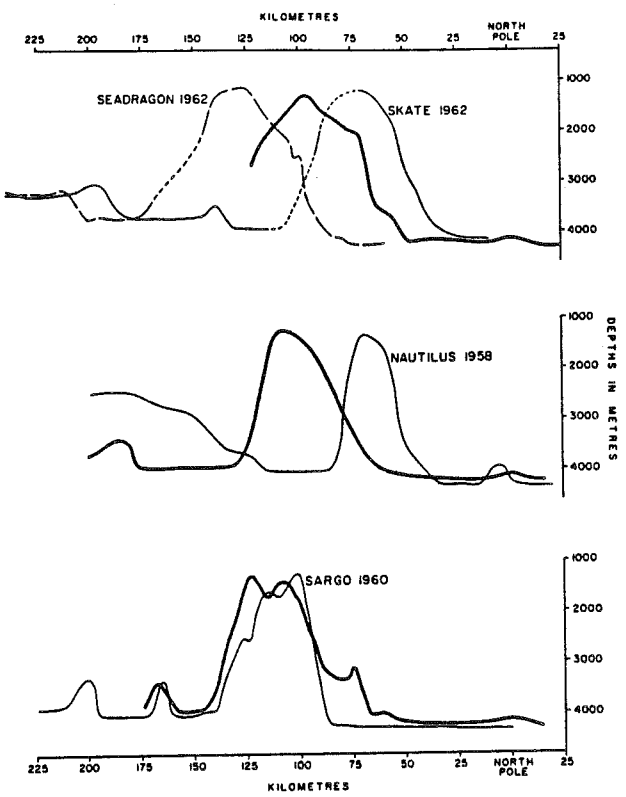

FIG. 19. Depth profiles of the submarine tracks of the *Seadragon* and *Skate* (1962), *Nautilus* (1958) and *Sargo* (1960) (cf. Fig. 15) superimposed on LOREX profiles (heavy line).

APPENDIX A

Methodology of the Early Soviet Hydrographic Surveys

Concurrently with the North Pole (NP) Series operation, the High Latitude Air Expeditions (HLAE) continued. Fuel and supplies were hauled to the NP stations and to the temporary HLAE base stations by Ilyushin IL-12 and Tupelov TU-4 aircraft (Laktionov and Shamont'ev, 1957). Two or three Antanov AN-2 aircraft stationed at the base camps were used for travel to the mainland. On the HLAE, scientists and technicians were divided into three groups: 1) a stationary unit that carried out continuous observations at the temporary base camp; 2) a hydrographic mobile unit; and 3) a geophysical mobile unit. Using LI-2 aircraft and flying in tandem, the mobile units typically established two or three stations at 150-200 km intervals before returning to base for refuelling. The hydrographic unit comprised a pilot and two hydrographers, and carried 600 kg of equipment consisting of:

Sled with gasoline engine driven winch, and 6000 m 1.2-mm diameter cable	150 kg
Bathythermographs and reversing thermometers	60 kg
Gravity corer	60 kg
Current meters	30 kg
Tent	40 kg
Manual ice auger, pick, shovel, ice net	40 kg
Explosives	50 kg
Containers for water samples	50 kg
Miscellaneous	120 kg

After selecting the ice floe and landing, the procedure for establishing a hydrographic station was as follows: measure ice thickness and blast hydro hole with explosives; unload equipment from aircraft; set up winch near hydro hole, erect tent over winch and hole, and heat tent with gasoline torches; measure depth and take gravity core; measure water temperature at standard depths and collect water samples. Astronomical station positioning, meteorological observations and snow and ice measurements were carried out at the same time by geophysicists from the second aircraft.

Observations sometimes included current measurements and at other times were limited to depth soundings and sediment sampling. Water samples were frozen and taken to the base station, and sediment samples were shipped to Leningrad for analysis. It took a maximum of 30 minutes to blast and clean out a hydro hole. A complete hydrographic station took six to eight hours, a sounding alone took three hours.

We know little of the equipment and duties of the geophysical units other than that the members of the units took astronomical and meteorological observations. Presumably they measured the force of gravity using a pendulum-type gravimeter, and observed the earth's magnetic field.

The pilots navigated by dead reckoning, by the sun and by making use of the powerful mainland- and ice-based radio beacons. Positioning of the mobile station must have been by sun and moon observation only, since viewing of stars in daylight requires a star catalogue for the particular area and time period, an impossible requirement in the pre-computer age. Depending on length of time the aircraft remained on the ground, rate of ice drift, latitude and sun angle, a position accuracy ranging between a few hundred metres and a few kilometres could be expected.

As of 1957 (Laktionov and Shamont'ev, 1957) depth was still measured by wire sounding, even at the NP stations, though experiments with echo sounders were in progress. It is surprising that the Russians were not using marine-type echo sounders, which had been in use for many years, and that they did not measure the depth at the mobile stations by the seismic method, since explosives were used for blasting the hydro holes.

The magnitude of the operations is illustrated by the fact that nearly 150 000 kg of cargo were airlifted to supply and maintain NP3 and NP4, and further that during 1954 a total distance of over one million kilometres was flown over the Arctic Ocean by all Soviet aircraft involved in these operations (Burkhanov, 1956). By way of comparison, some 230 000 kg of fuel, supplies and equipment were airlifted to the LOREX 79 camps and approximately 250 000 km were logged by all LOREX aircraft (Weber, 1979; Weber *et al.*, 1981).

The Soviet Aircraft Types

The *Ilyushin IL-12* is a twin-engine passenger and cargo aircraft with a range of 2000 km at a payload of 3000 kg. On fuel hauls to the ice station it was equipped as a tanker. The *IL-14* is a later, modified version of the *IL-12*. The *Tupelov TU-4* is a copy of the Boeing B-29 "Superfortress". The Soviet version of this four-engine aircraft was modified and widely used as civilian passenger and cargo aircraft. It has a range of 4000 km with accommodation for 72 passengers.

The *Antonov AN-2* is a large single-engine (1000 HP) biplane with STOL characteristics. Cruising at 200 km/h with a payload of 1240 kg, it has a range of 900 km. The minimum speed (40° flaps) is 64 km/h. Production started in 1950 and continued for some 20 years. It has been widely used in agriculture and surveying and as a cargo and passenger aircraft serving small settlements.

The *LI-2* is a Russian-built version of the twin-engine Douglas DC-3 aircraft.

APPENDIX B

List of Acronyms

AIDJEX	Arctic Ice Dynamics Joint Experiment (US, Canada)
DRB	Defence Research Board (Canada)
EMR	Department of Energy, Mines and Resources (Canada)
EUBEX	Eurasia Basin Experiment (US)
GEBCO	General Bathymetric Charts of the Oceans
GNS	Global Navigation System
HLAE	High Latitude Air Expeditions (USSR)
LOREX	Lomonosov Ridge Experiment (Canada)
MIZEX	Marginal Ice Zone Experiment (US)
ONR	Office of Naval Research (US)
PCSP	Polar Continental Shelf Project (Canada)
SINS	Ship's Inertial Navigation System
STD	Salinity, Temperature and Depth
VAI	Soviet All-Union Arctic Institute. After 1958 the Arctic and Antarctic Research Institute (USSR)

REFERENCES

ARMSTRONG, T. 1958. The Russians in the Arctic. Aspects of Soviet exploration and exploitation of the Far North, 1937-57. London: Methuen. 182 p.

BEAL, M.A. 1969. Bathymetry and structure of the Arctic Ocean. Ph.D. thesis, Oregon State University. 205 p.

_____, EDVALSON, K., HUNKINS, K., MOLLOY, A. and OSTENSO, N. 1966. The floor of the Arctic Ocean: geographical names. Arctic 19:215-219.

BREWER, M.C. 1967. The Soviet Drifting Station, NORTH-67. Arctic 20:263-266.

BURKHANOV, V. 1956. New Soviet Discoveries in the Arctic. Moscow: Foreign Languages Publishing House. 60 p.

CRARY, A.P., COTELL, R.D. and OLIVER, J. 1952. Geophysical Studies in the Beaufort Sea, 1951. Transactions AGU 33(2):211-216.

DE LEEUW, M.M. 1967. New Canadian bathymetric chart of the western Arctic Ocean, north of 72°. Deep-Sea Research 14:489-504.

FISHER, R.L., CARSOLA, A.J. and SHUMWAY, G. 1958. Deep-Sea bathymetry north of Point Barrow. Deep-Sea Research 5:1-6.

FORTIER, Y.O., BLACKADAR, R.G., GLENISTER, B.F., GREINER, H.R., McLAREN, D.J., McMILLAN, N.J., MORRIS, A.W., ROOTS, E.F., SOUTHER, J.G., THORSTEINSSON, R. and TOZER, E.T. 1963. Geology of the North-Central Part of the Arctic Archipelago, Northwest Territories (Operation Franklin). Geological Survey of Canada Memoir 320. 671 p. + maps.

GORDIENKO, P.A. and LAKTIONOV, A.F. 1960. Principal results of the latest oceanographic research in the Arctic Basin. Izvestiya Akademiya Nauk SSSR, Geographical Series 5:22-33. (Translated from the Russian by E.R. Hope. Defence Research Board translation T350R. Feb. 1961.)

GREENBERG, J., HART, P.E. and GRANTZ, A. 1981. Bathymetric map of the continental shelf, slope and rise of the Beaufort Sea north of Alaska. Miscellaneous Investigations Series, U.S. Geological Survey. 5 p. + map.

GREGORY, A.F., BOWER, M.E. and MORLEY, L.W. 1961. Geological interpretation of aerial magnetic and radiometric profiles, Arctic Archipelago, Northwest Territories. Geological Survey of Canada Bulletin 73:148.

HAKKEL', Ya. Ya. 1958. Signs of recent submarine activity in the Lomonosov Range. Priroda 4:87-90. (Translated from the Russian by E.R. Hope. Defence Research Board translation T296R. June 1958. 5 p.)

HARRIS, R.A. 1904. Some indication of land in the vicinity of the North Pole. National Geographic Magazine 15:255-261.

HEEZEN, B.C. and EWING, M. 1961. The Mid-Oceanic Ridge and its extension through the Arctic Basin. In: Raasch, G.O. (ed.). Geology of the Arctic. Proceedings, 1st International Symposium on Arctic Geology, 11-13 January 1960. 622-642.

HUNKINS, K. 1960a. Seismic studies of the Arctic Ocean floor. Air Force Cambridge Research Laboratory, AF 19 (604)-2030. 15 p.

_____. 1960b. Geophysical and oceanographic research in the Arctic Ocean. Lamont-Doherty Geological Observatory, Columbia University. Final Report AF 19 (604)-2030, ASTIA 253807.

_____. 1960c. Results of depth soundings taken from drifting station Charlie in the Arctic Ocean. Lamont-Doherty Geological Observatory, Columbia University.

_____. 1960d. Results of depth soundings taken at drifting station Bravo (T-3) in the Arctic Ocean. Lamont-Doherty Geological Observatory, Columbia University.

_____. 1977. Geophysical data summary for Fletcher's Ice Island (T-3) May 62 - Oct. 74. U.S. Office of Naval Research Technical Report No. CU-1-77. 219 p.

_____, HERRON, T., KUTCHALE, H. and PETER, G. 1962. Geophysical studies of the Chukchi Cap, Arctic Ocean. Journal of Geophysical Research 67:235-248.

LAKTIONOV, A.F. 1959. Bottom Topography of the Greenland Sea in the region of Nansen's Sill. Priroda 10:95-97. (Translated from the Russian by E.R. Hope. Defence Research Board translation T333R. Nov. 1959. 5 p.)

_____ and SHAMONT'EV, V.A. 1957. The use of aviation in oceanographic investigations in the Arctic. Problemy Arktiki 2:19-31. (Translated from the Russian by R.M. Holden. American Meteorological Society translation T-R-235. 17 p.)

LILLESTRAND, R.L., GROSCH, C.B. and VANELLI, B.D. 1967. Interim technical report on astronavigation during Dominion Observatory polar research project. Technical Report R.D. 1023. Minneapolis, MN: Control Data Corp.

LILLESTRAND, R.L. and WEBER, J.R. 1974. Plumbline deflection near the North Pole. Journal of Geophysical Research 79:3347-3352.

LINDEN, N.A. 1959. Seismic chart of the Arctic 1959 seismological and glaciological researches during the IGY. No. 2. Moscow: Academy of Sciences.

MacINNIS, J.B. and WEBER, J.R. 1980. LOREX Expedition. Canadian Geographic 100(6):18-31.

McKINLAY, W.L. 1976. Karluk, the Great Untold Story of Arctic Exploration. London: Weidenfeld & Nicholson. xiv + 170 p.

MONOHAN, D. 1979. Bathymetry of the Arctic Ocean north of 85° latitude - Discussion. Tectonophysics 60:293-297.

NANSEN, F. 1897. Farthest North. Westminster: Archibald Constable & Co. Vol. 1:510 p. Vol. 2:671 p.

NATIONAL ACADEMY OF SCIENCES. 1970. Polar Research: a survey. Washington, D.C.: Committee on Polar Research. NAS. 204 p.

OSTENSO, N.A. 1962. Geophysical Investigations of the Arctic Ocean Basin. University of Wisconsin, Research Report No. 4. 124 p.

_____. 1963. Physiography of the Arctic Ocean Basin. In: Proceedings, 13th Alaskan Science Conference. Alaska Division, American Association for the Advancement of Science. 92-114.

PAPANIN, I. 1946. Life on an Icefloe. Translated from the Russian by Fanny Smitham. London: Hutchinson & Co. 240 p.

POPELAR, J. and KOUBA, J. 1983 (in press). Satellite Doppler determination of differential sea ice motion in the vicinity of the North Pole. Marine Geodesy Journal 7.

RITCHIE, G.S. 1969. North Polar Chart, No. 4006. Taunton, U.K.: Hydrographer of the Navy.

ROOTS, E.F. 1968. Canadian Polar Continental Shelf Project, 1966. Polar Record 14:192-194.

SAKS, V.N., BELOV, N.A. and LAPINA, N.N. 1955. Our present concepts of the geology of the central Arctic. Priroda 7:13-22. (Translated from the Russian by E.R. Hope. Defence Research Board translation T196R. Oct. 1955. 19 p.)

SOBCZAK, L.W. 1977. Bathymetry of the Arctic Ocean north of 85° latitude. Tectonophysics 42:T-27 - T-33.

_____. 1979. Bathymetry of the Arctic Ocean north of 85° latitude - Reply. Tectonophysics 60:297-302.

_____ and SWEENEY, J.F. 1978. Bathymetry of the Arctic Ocean. In: Sweeney, J.F. (ed.). Arctic Geophysical Review. Publications of the Earth Physics Branch 45(4):7-14.

SOBCZAK, L.W. and WEBER, J.R. 1970. Gravity measurements over the Queen Elizabeth Islands and Polar Continental Margin. Gravity Map Series. Dominion Observatory Nos. 115-116. 14 p. with maps.

SOMOV, M.M. 1955. Observational data of the scientific research drifting station of 1950-1951. Leningrad: Moroskoy Transport. Vol. I, Sec. 4. (Translated by D. Kraus. American Meteorological Society, Boston. ASTIA Document No. AD 117135. 59 p.)

STEFANSSON, V. 1921. The Friendly Arctic. New York: Macmillan. 784 p.

SWEENEY, J.F. and HAINES, G.V. 1978. Arctic Geophysical Review - An Introduction. In: Sweeney, J.F. (ed.). Arctic Geophysical Review. Publications of the Earth Physics Branch 45(4):1-6.

TRESHNIKOV, A.F. 1960. The Arctic discloses its secrets. Priroda 2:25-32. (Translated from the Russian by E.R. Hope. Defence Research Board translation T357 R. Aug. 1961. 12 p.)

_____. 1966. At the Poles of the Earth. Moscow: Sovetskaya Rossiya Publishing House. (Translated from the Russian. Secretary of State Translation Bureau No. 123842. 30 p.)

_____, BALAKSHIN, L.L., BELOV, N.A., DEMENITSKAYA, R.M., DIBNER, V.D., KARASIK, A.M., SHPAIKHER, A.D. and SHURGAEVA, N.D. 1966. Geophysical names of the main relief sections of the seafloor in the Arctic Basin: Problemy Arktiki i Antarktiki 27:1-25.

VOGT, P.R., TAYLOR, P.T., KOVACS, L.C. and JOHNSON, G.L. 1979. Detailed aeromagnetic investigation of the Arctic Basin. Journal of Geophysical Research 84:1071-1089.

WEBER, J.R. 1979. The Lomonosov Ridge Experiment: "LOREX 79". EOS 60(42):715-721.

_____. 1980. Exploring the Arctic seafloor. Ottawa: Department of Energy, Mines and Resources. GEOS 9(3):2-7.

_____, SWEENEY, J.F. and JUDGE, A. 1981. CESAR 83, Canadian Expedition to Study the Alpha Ridge. Ottawa: Earth Physics Branch, Energy, Mines and Resources. Internal Report. 69 p.

WELLS, D.E. and GRANT, S.T. 1977. Reliable navigation through system integration. In: Proceedings, 16th Canadian Hydrographic Conference, Burlington, Ontario.

WILKINS, G.H. 1928. Flying the Arctic. New York: G.P. Putman's Sons. 336 p.

WOLD, R.J. 1973. Gravity surveys of the Arctic Ocean Basin. Final Report, Jan. 1973. University of Wisconsin, Department of Geological Sciences. 222 p.

WORTHINGTON, L.V. 1953. Oceanographic results of Project Skijump I and Skijump II in the Polar Sea, 1951-1952. Transactions AGU 34(4):543-551.

JOURNAL OF GEOPHYSICAL RESEARCH, VOL. 89, NO. B1, PAGES 473-481, JANUARY 10, 1984

CRUSTAL STRUCTURE OF THE LOMONOSOV RIDGE AND THE FRAM AND MAKAROV BASINS NEAR THE NORTH POLE

D. A. Forsyth

Division of Seismology and Geomagnetism, Energy, Mines and Resources, Canada, Earth Physics Branch

J. A. Mair

Dome Petroleum Ltd.

Abstract. Reversed refraction surveys were conducted along and across the Lomonosov Ridge as part of the 1979 Lomonosov Ridge Experiment. Interpretation of the strike profiles indicates a 5-km-thick upper crustal layer with a velocity of 4.7 km/s overlying a 15- to 20-km-thick layer of 6.6 km/s material. An upper mantle velocity of 8.3 km/s is indicated by a few P_n arrivals. High-amplitude reflection events recorded from this boundary can be successfully modeled by a transition zone of rapidly changing velocity over a depth interval of 5 km. Ray trace modeling of the dip profiles suggests a root structure extending to about 28-km depth flanked by crust thinning to a depth near 13 km beneath the Makarov Basin and a more gradual thinning to near 16 km beneath the Fram Basin. The similarity between the crust of the Lomonosov Ridge and that beneath the Barents and Kara seas supports the suggestion that the ridge is a slice rifted from the Baltic Shelf.

Introduction

The Lomonosov Ridge forms a nearly linear feature, approximately 1800 km in length, joining the continental rise near Ellesmere Island to that of northern Russia near the New Siberian Islands. The ridge narrows from 200 to 300 km near the continents to about 25 km (2000 m contour) near the north pole, where it exhibits a dextral displacement of about 70 km (Figure 1). It rises steeply to about 3 km above its adjacent abyssal plains with a relatively flat summit region. The discovery of the ridge in 1948 [Gakkel', 1954; Ostrekin, 1954] led many scientists to abandon their previous view that the Arctic Basin was oceanic in origin and to adopt the idea that the arctic waters were underlain by fold structures tying together age-equivalent regions of Eurasia, North America, and Greenland. This vew was then changed as the ridge's central position within the Arctic Basin and some indications of volcanism [Gakkel', 1958] were considered to be evidence of it being related to the structural series of mid-oceanic ridges [Leontiev, 1963]. The ridge is, however, aseismic in nature and lacks the morphological characteristics of a mid-oceanic ridge, denying its genesis as a spreading center [Herron et al., 1974]. The discovery of the seismically active Nansen-Gakkel Ridge and its demonstrated continuity with the Atlantic Ocean ridge system [Demenitskaya et al., 1964] has led to the more generally accepted view that the Lomonosov Ridge may be a fragment split from the continental shelf beneath the Barents and Kara seas of northern Europe.

Paper number 3B1632.
0148-0227/84/003B-1632$05.00

A review of deep crustal seismic studies conducted in the Arctic [Forsyth, 1978] shows several velocity-depth profiles of the continental-to-oceanic transition but no published data revealing the deep structure of the Lomonosov Ridge near the north pole. Shallow seismic refraction studies conducted on the Eurasian part of the ridge, as far north as latitude 85° [Demenitskaya and Kiselev, 1968], indicate a layered sedimentary sequence thinning from about 8 km near the shelf to about 3 km at 85°N. These sediments are underlain by a layer with a velocity of about 6.4 km/s.

During a 3-week period in May 1979, a crustal-scale seismic refraction survey was conducted in an area of the Lomonosov Ridge very near to the north pole. Figure 1 shows the site locations and the bathymetry of the Fram and Makarov basins adjoining the ridge. Typical shot sizes ranged from 50 to 200 kg of 60% Geogel (CIL trademark) at sites A, B, E, F, and G and from 220 to 500 kg at sites D, H, and I. Shots were detonated electrically after suspending at a depth of about 100 m beneath the ice that varied little from 3 m in thickness. Significant variations to greater than 6 m occurred locally beneath pressure ridges; however, these ridges were avoided in siting shots and receivers. Digital cassette-recording seismographs with automatic gain ranging were used to record the composited output of a 16-element array of vertical seismometers. The field equipment and techniques are the same as those described by Mair and Lyons [1981] for the Arctic Ice Dynamics Joint Experiment (AIDJEX) operation and will not be repeated here.

Data and Interpretation

The survey was originally planned as two conventional, reversed refraction profiles; however, operational constraints forced continual modification of the plan. The resulting survey attempted to map the structure of the ridge by means of two profiles, a dip profile across the ridge and a strike profile conducted along what was considered to be the ridge crest (Figure 1). While the dip profile ran reasonably normal to the ridge, navigation problems resulted in a less successful alignment

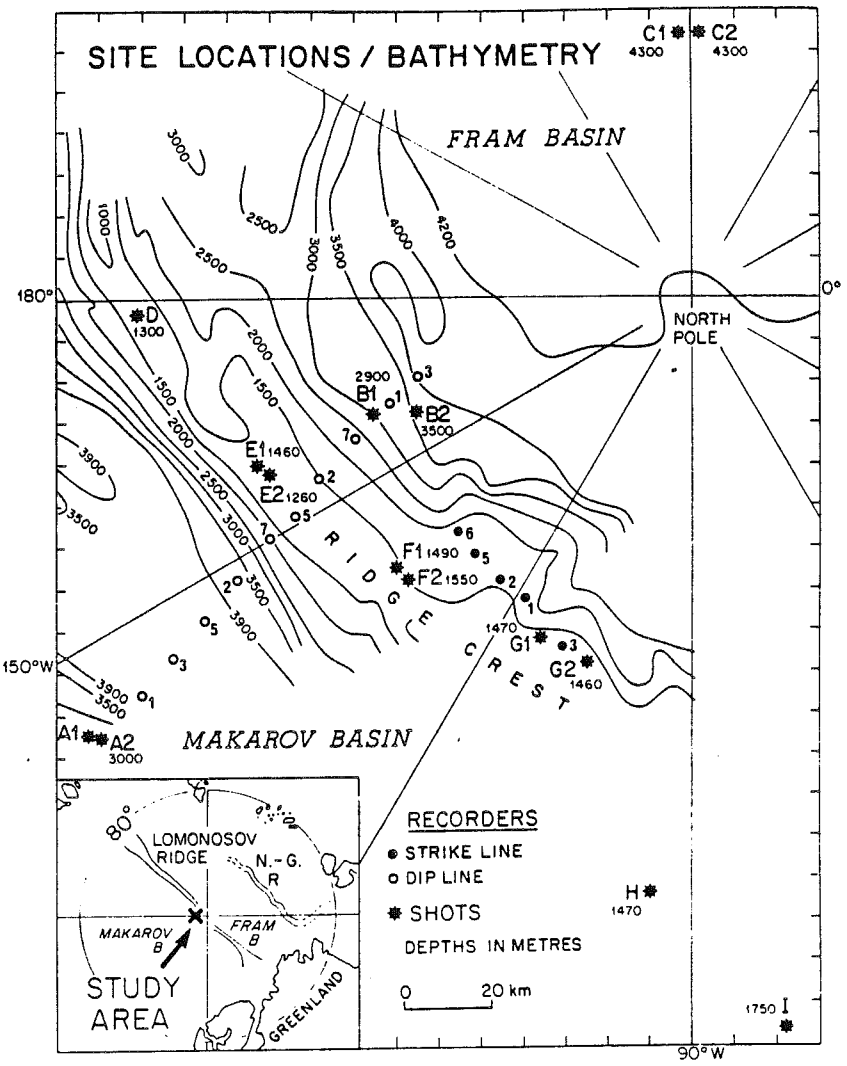

Fig. 1. Locations of shot points (stars) and receiving station (circles, dots) on a bathymetric map of the Lomonosov Ridge. N.-G. indicates Nansen-Gakkel spreading ridge.

of stations along the ridge crest. Water wave travel times detected at the recording stations and at the base camp monitor were used to effect minor corrections in arriving at the final estimates of the recording positions. An average horizontal water velocity of 1.46 km/s [Mair and Lyons, 1981] was assumed. The shot point to recorder distances are probably accurate to better than 500 m. The resulting survey arrangement is shown in Figure 1.

A preliminary look at the strike line data indicated a similar energy pattern between the pseudo-reversed profiles. In contrast, the dip line data were obviously more complex, the expected result of major variation in water depth and crustal structure. Thus it was decided to interpret the dip survey using ray trace modeling [Whittal and Clowes, 1979] to distinguish lateral structure and to check the proposed on strike model by computing synthetic seismograms [Chapman, 1978].

All record sections are presented with a time reduction of distance divided by 8.0 km/s. Data sections have been filtered using a zero phase bandpass filter of 4-12 Hz with cosine weighting to provide zero amplitudes at 2 and 24 Hz.

Strike Profiles

Shots detonated beneath the ice at points marked G_1, G_2, H, and I and recorded at sites 3, 1, 2, 5, and 6 (Figure 1) were used to construct profile 4 (Figure 2). The marginally reversed profile 5 was obtained using the same recording sites and shots from D, E_1, E_2, F_1, and F_2 (Figure 3). The data show clear first breaks from throughout the crust with the most distant breaks suggesting the crossover to upper mantle near 130 km. Coherent zones of secondary energy are evident, particularly on profile 4 (Figure 2) from shot point 1 to the west.

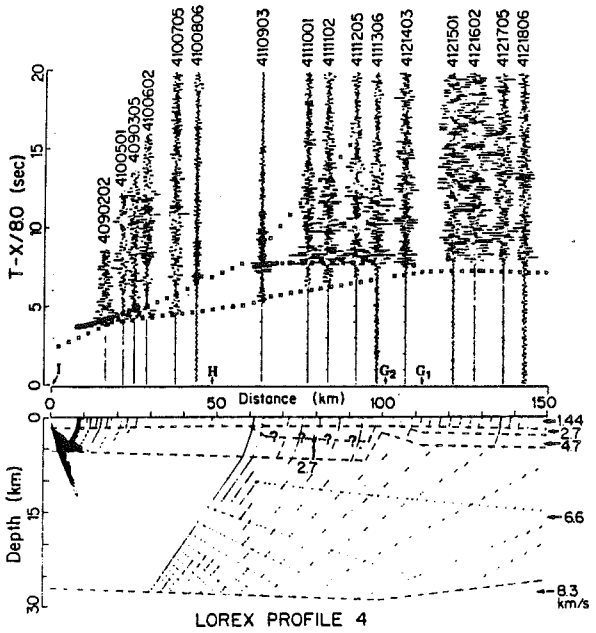

Fig. 2. Composite strike profile 4 from the east (shot point I) to the west. Crosses are refracted arrivals; circles are reflected events. Seismogram code: 409=G_1, 410=G_2, 411=H, 412=I; last number refers to site in Figure 1.

The strike profiles are approximations to "true amplitude" sections in that variations in shot energy have been accounted for by using factors proportional to the square root of the charge weight and attenuation with respect to distance by a factor proportional to the square of the shot point-to-station distances. The result appears to be reasonable in that no dramatic variations in amplitude correlate with shot number along the record sections.

As noted previously, the strike profiles appeared to have similar reversed times and lacked the rather dramatic trace-to-trace travel time variations noted on the dip profiles. The exception to this generalization involved records obtained from receiver site 3 and records generated from the neighboring shot points G_1 and G_2 where travel time anomalies of approximately 0.5 s (early) were evident. Bathymetric control was excellent and could not provide an explanation so that a plug of near-surface high-velocity material (or removal of sedimentary cover) was interpreted in this area. The ray trace model for the region of shot points G_1, G_2, and station 3 is incorporated into a more generalized model derived from combining all observations along the ridge into the sections shown in Figures 2 and 3.

There is little control on the velocity or thickness of the ocean bottom sediments. First arrivals at the closest stations to shot points G_1 and G_2 indicate a velocity of 2.0 km/s, while the nearest arrivals from shot points F_1 and F_2 suggest a velocity near 3.5 km/s. Mair and Lyons [1981] used a survey velocity of 1.8 km/s with a gradient of 0.5 km/s/km in modelling the brine-saturated sediments of the Canada Basin. Since Overton's [1982] data show sediment along and adjacent to the ridge flanks, a thin layer with an average velocity of 2.7 km/s has been incorporated in the ocean basin areas of our dip profiles and over the Fram Basin slope of the ridge on one strike profile.

Similarly, the 4.7 km/s velocity material is not well sampled in the data set. The arrivals at stations closest to shot points A and B indicate a velocity of about 4.5 km/s, while the strike profiles show a reasonably shallow change to 6.6 km/s. The velocity of 4.7 km/s was arrived at through the process of adjusting the travel time curves, including reflected branches, to fit the same model in a reversed sense along and across strike. Jackson et al. [1982] also determined a mean upper crustal velocity of 4.7 km/s for the Fram I area near the Arctic Mid-Ocean Ridge.

In the composite profile 5 (Figure 3) the significant features are the Moho transition at about 25 km and the thinning upper crustal layer beneath shot points G_1 and G_2. Profile 5 lies along the northern side of the Lomonosov Ridge (Figure 1), and the interpreted model is therefore applicable to the transition region into the Fram Basin. Comparison with the dip profile interpretation which follows indicates good agreement both in terms of the Moho depth of about 25 km and the intermediate (4.7/6.6) discontinuity between 5 and 7 km on the Fram side of the ridge. Note that the earlier arrival times at position 3 or from shots G_1 and G_2 are compatible with removal of the

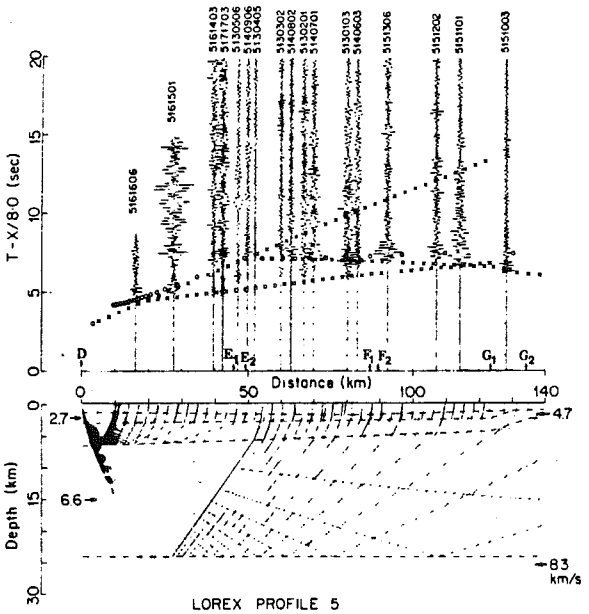

Fig. 3. Composite strike profile 5 from the west (shot point D) to the east. Crosses are refracted arrivals; circles are reflected events. Seismogram code: 513=E_2, 514=E_1, 515=D, 516=F_2, 517=F_1; last number refers to site in Figure 1.

sedimentary, 2.7 km/s material. Further, in the area of this shallowing "basement" the semi-reversed observations also suggest a thinning of the total crustal section to near 25 km between shot points D and G. The position of this anomaly lying between the bathymetric ravines on either side of shot points G_1 and G_2 (Figure 1) suggests that the ravines are structurally controlled and may be represented at depth by fractures striking obliquely to the Ridge.

The partly reversed strike profile 4 (Figure 2) appears to have most of its sampling paths beneath the main ridge but does not cross the dip lines. However, again there is generally good agreement with the dip data in that the intermediate discontinuity is at about 5 km and the Moho rises from near 30 km in the east toward the 25-km depth indicated for the area of the dip lines.

The basin of 2.7 km/s material outlined in question marks (Figure 2) has been modeled to account for the delay of first arrivals in the 60-100 km distance range. However, since most of these records are from the shot point H, there is a good possibility the delay may, in fact, be due to sediments beneath the shot point rather than structure beneath the receivers. We have no good data on the upper crust beneath shot points H and I, although water depths indicate that they are located on or near the ridge crest.

The lower crustal layer is well sampled in this study, and the strike lines in particular show good reversed evidence for a velocity of 6.6 km/s. The suggested upper mantle velocity of 8.3 km/s is not extensively sampled; however, the similarity in the Moho depths in a reversed sense along strike and the agreement in depths between dip and strike line models in the areas of intersection support the 8.3 km/s value. Jackson et al. [1982] found evidence for the 8.3 km/s upper mantle velocity in the Fram 1 area.

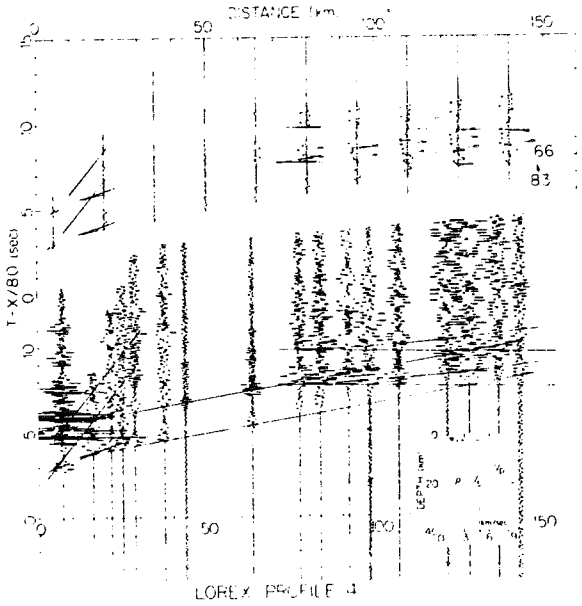

Fig. 4. Comparison of strike profile 4 with a synthetic section modeling mainly the lower crust/upper mantle response with the first multiple. The large-amplitude event on the first trace includes a water wave which has been removed for clarity on subsequent traces.

Synthetic Section

The synthetic traces were generated using the program described by Chapman [1978]. In his development, a WKBJ approximation to generalized ray theory was used. A synthetic shot pulse similar to a subcritical water-wave reflected pulse from the strike line data (Figure 4 at 7 km) is used as an estimate of the source wavelet for the synthetic section. Because there is little control on the velocity or near-surface structural variations, our synthetic calculations are directed at modeling the lower crust and crust-mantle response.

Profile 4 was chosen to model the response of the lower crust and crust-mantle (Moho) transition as it includes more seismograms than profile 5. Since the amplitude response is of most interest here, a time correction of 0.5 s was applied to data from shots from G_1, G_2, and station 3 to simplify profile 4. The result shows a well-defined 6.6 km/s arrival, a strong Moho reflection, and an upper mantle refracted event emergent at about 110 km (Figure 4).

The initial models with abrupt velocity discontinuities had to be modified with velocity gradients to limit the amplitude of reflections from the transition zone to 6.6 km/s material and from the Moho. The amplitude of the first arrival at 6.6 km/s is controlled by the nature of the 4.7-6.6 km/s transition and the velocity gradient in the 6.6 km/s material. A positive gradient of 0.003 s^{-1} has produced a reasonable fit to the observations shown in Figure 4. However, because of the trade-off mentioned above and the approximation to true amplitudes through application of recording system and shot factors for the original sections, the gradient of 0.003 s^{-1} within the 6.6 km/s layer is not necessarily signficiant.

The large-amplitude arrivals following the first Moho-reflected phase by about 2.2 s are suitably modeled in the synthetic section by the first mutliple, that is, the energy reflected from the ocean bottom and serving as a second source upon reflection from the sea (ice) surface.

A notable feature of seismograms recorded at station 3 is the higher frequency content of the reflected coda from the upper mantle. On profile 4 this is apparent on the seismograms at 62 and 108 km. Although these seismograms are from different shots, the reflected coda at about 8 s reduced time contains higher frequencies but lower amplitudes than adjacent traces. The first-arrival crustal phase at station 3 (8 km on Figure 4) appears normal relative to adjacent traces. A similar higher-frequency content in the mantle arrival response is notable on the reverse profile 5 (Figure 4) in seismograms at about 81, 83, and 130 km. This difference in attentuation for the region beneath shot points G_1, G_2, and station 3 is in general agreement with the suggestion of significantly less sedimentary (attenuating) material and a shallower "basement".

Dip Profiles

Dip profiles across the Lomonosov Ridge were constructed of seismograms obtained from shot points A_1, A_2, B_1, B_2, C_1, and C_2 recorded at the stations represented by open circles in Figure 1. For the dip profiles the amplitudes of individual seismograms are normalized so that the maximum amplitude within each seismogram is constant across the section. The signal-to-noise ratio is generally good, although several traces suffer from instrument noise.

Profile A (from A_1, A_2, Figure 5) extends from the Makarov Basin to the eastern slope of the ridge and crosses what bathymetrically appears to be a relatively uncomplicated zone. The main features of the section are the high-amplitude first arrivals with strongly varying apparent velocities and the prominent secondary event at about 15 s reduced travel time. From shot points A_1 and A_2, the crossover to velocities approaching 8 km/s appears at a distance of about 25 km, indicating an oceanic crustal section approximately 13 km thick (including water) beneath this area of the Makarov Basin. The last three traces show a lower apparent velocity and are interpreted as refracted-reflected events from the deepening transition to the Lomonosov Ridge.

The correlatable high-amplitude arrivals recorded at about 8 s after the first event at distances up to 60 km may be explained as the first multiple reflection between surface and Moho at near critical incidence. The primary reflection itself is evident within the tail cycles of the complex first arrival. The multiple provides a powerful constraint on the travel time through the oceanic crust and thus on the suitability of the models in general.

Profile B begins in the zone of transition from the Fram Basin to the ridge and thus the section from shot points B_1 and B_2 (Figure 6) is quite different from profile A. While first arrivals to a distance of about 40 km are consistent with a shallowing 4.7 km/s layer, first reflected arrivals from the base of the crust at a depth of about 27 km are only evident beyond about 65 km. The weaker first arrivals evident between 40 and 60 km, and perhaps in the emergent arrival at 70 km (Figure 6), are clearly unusual. They appear to fall into a partial shadow zone produced by midridge structural disruption of the 4.7-6.6 km/s transition. Possible interpretations of these events are that they are attenuated and delayed arrivals due to scattered refraction through the rifted structure of the Ridge [Overton, 1982] or that the events are diffractions from the structural offset of the 4.7-6.6 km/s transition.

Similarly, although the last three weaker first arrivals between 90 and 120 km on profile A (Figure 5) have been interpreted as energy refracted through the root structure of the ridge, the arrival times of events diffracted from root features may not differ greatly. Bolt and Gutdeutsch [1982] show that

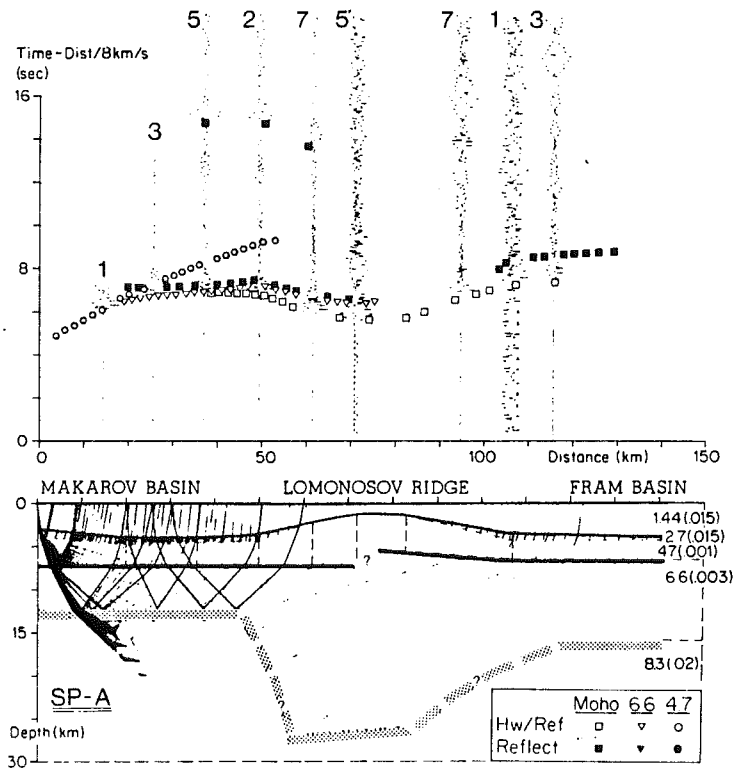

Fig. 5. Dip profile A from the Makarov Basin to the Fram Basin. A water velocity of 1.44 km/s with a vertical gradient of 0.015 s^{-1} was assumed.

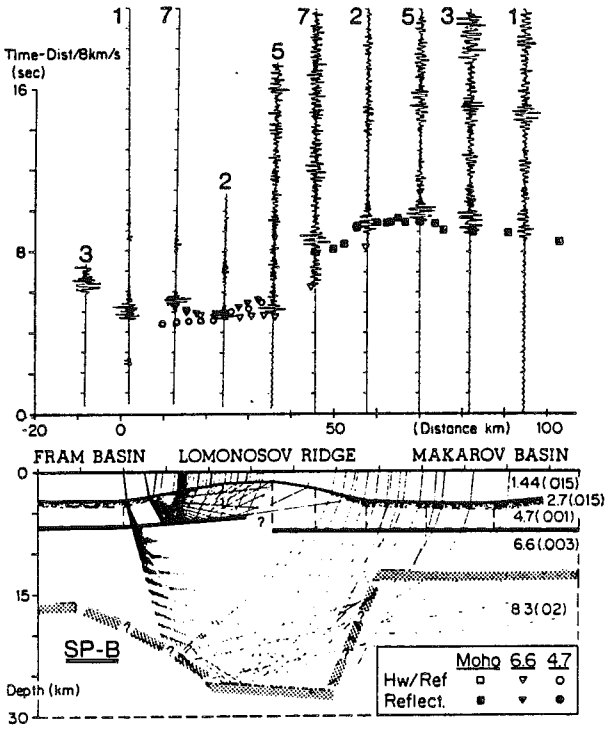

Fig. 6. Dip profile B from the Fram Basin to the Makarov Basin. Numbers in parentheses indicate velocity gradients within layers.

for a generalized root structure, with depths and dimensions similar to the present model, diffractions may be expected in the 80-140 km distance range, similar to the range of unusual arrivals here. However, no quantitative estimate of expected waveforms or amplitude differences are available for their models, and our profiles are not long enough to see energy clearly propagating beneath the ridge root for comparison with possible diffractions. Thus, while the difference in depth of the midcrustal 4.7-6.6 km/s discontinuity appears reasonable beneath the areas approaching shot points A and B, further details of structure beneath the ridge crust and of features of the ridge root remain undetermined.

Profile C (Figure 7) originates from shots about 140 km east of the ridge within the Fram Basin, and hence arrivals are all from below the crust-mantle transition. Instrument noise has affected most traces, but first breaks are reasonably distinguished to about 170 km. The model derived mainly on the basis of profiles A and B is supported by the travel times from shot point C. The later arrivals at distances beyond 140 km corroborate the interpretation of a thicker crust beneath the ridge crest.

Discussion

The crustal model provides travel times that satisfy the set of partly reversed observations from many shot points along and transverse to the ridge and provides a synthetic response which closely resembles the observed amplitudes along strike. The most pertinent features of

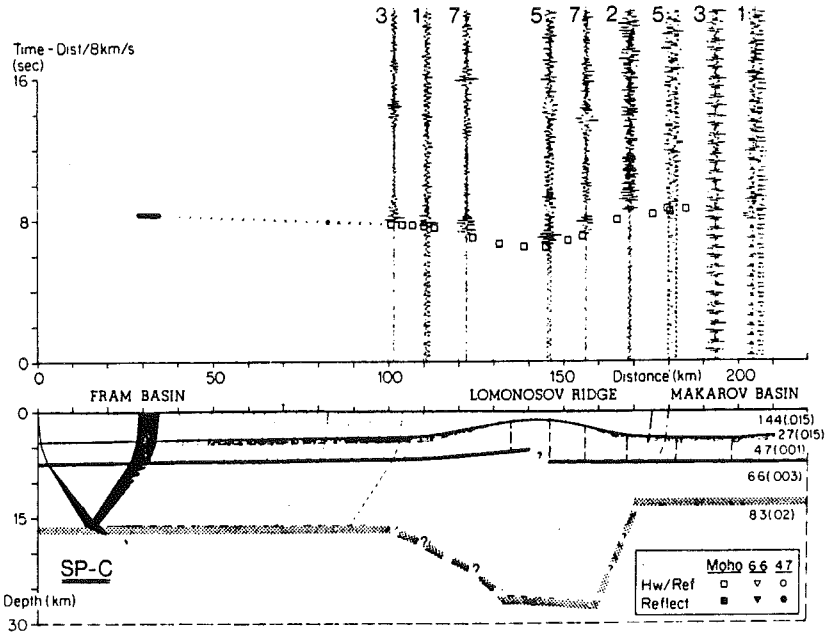

Fig. 7. Dip profile C from the Fram Basin to the Makarov Basin.

the model are the thicker crust beneath the Lomonosov Ridge and the generally asymmetric shape of the root structure.

The crustal structure and thickness beneath shot point C (Figure 7) in the Fram Basin are not well constrained. The crust could be thinner beneath this shot point, with a corresponding increase in thickness as it nears the Lomonosov Ridge, and still satisfy the seismic arrival times. As the crustal thickness of the Nansen-Gakkel Ridge is believed to be only about 4 km [Jackson et al., 1982], a regional dip of about 2° on the crust-mantle boundary from the spreading center to the Lomonosov Ridge is more reasonable than the horizontal layer modeled. The root structure would then be even more asymmetrical than as illustrated in Figure 7. The finer details of the root structure cannot be constrained with the present data set nor can the gross features of our model be claimed as typical of the ridge since the bathymetry suggests that the survey was conducted in the region of an anomalous offset from the ridge's general strike.

In comparing the strike and dip profiles, one notable feature is the difference in amplitudes of the first arrivals. Whereas the strike lines appear "normal" with lower-amplitude diving waves followed by larger-amplitude reflected events, the dip lines are characterized by strong, pulselike first arrivals followed by much weaker coda. This suggests that essentially all the dip line first arrivals beyond about 40 km are the result of refraction (with some possible diffractions) through dipping structures of the ridge root as opposed to refracted energy from the upper mantle. Significant energy with refracted travel times from beneath the root structure is either not produced or effectively scattered by the relatively dramatic structure. The dip lines are too short to distinguish clearly the crustal structure of the basins adjacent to the ridge from the ridge itself. Hence the modeling offers information on the ridge features but can only suggest basin crustal thicknesses in transition from the ridge. Conversely, the regular development of arrivals and the strong and persistent nature of multiple reflections on the strike lines suggest that the structure is generally continuous over the length of the Lomonosov Ridge studied.

Comparison of Seismic Results With Other Data

The possible explanation for the attenuated and delayed arrivals on the dip profiles in terms of fractures within the ridge as described by Overton [1982] from shallow seismic observations has been mentioned. The shallowing of high-velocity material beneath the bathymetric ravines near shot points G_1 and G_2 suggests fractures transverse to the ridge strike. Although the detailed magnetic profiles are not yet available (P. Hood, personal communication, 1983), Coles [1980] suggests that "short-wavelength magnetic highs along the upper ridge flanks and crest may indicate shallow igneous rocks." Although the designation of "igneous" is uncertain, the shallowing 6.6 km/s material suggested from the refraction results may be associated with the shorter-wavelength, high-amplitude magnetic anomalies.

Sweeney et al. [1982] have used the refraction model to reproduce the observed free air gravity field. The result was successful except in the Fram Basin, where the crustal thickness of 15-16 km suggested herein is too great. Since the present refraction study is heavily biased by ray paths on the ridge itself or in the area of transition to the ridge, a better estimate of crustal thickness beneath the Fram Basin proper may be the 12-13 km derived from the gravity modeling. The view of a thinner Fram Basin crust would tend to be supported by geothermal observations, which show a 20% higher heat flow in the Fram Basin than in the Makarov and thus a thinner lithosphere [Judge and Taylor, 1981]. It should be noted that like the seismic data, both the gravity and heat flow data are to some extent biased by their proximity to the Lomonosov Ridge. A definitive survey of the Fram Basin in the area of the north pole remains to be done.

Systematics of Crustal Types

Berckhemer et al. [1975] attempted to relate crustal models, interpreted from refraction data gathered on the Ethiopian Shield and the Afar region, within a general scheme of continental-tapnrogenic-oceanic crustal structures (Figure 8). The distinguishing features evident in this figure are the thinning of acidic rocks (velocities near 6 km/s) from thicknesses of 10-20 km in ancient continental shields to zero within oceanic crust, and the overall thinning of the total crustal sections.

Figure 9a indicates that a similar scheme can be obtained for arctic continental features grading into the oceanic crust of the Canada Basin. The two 6.3 km/s sections shown for the Sverdrup Basin indicate that limestone, encountered by deep drilling in this area and known to have this velocity, may overlie granitic rocks of similar velocity. Figure 9b indicates that the structures beneath the now shallow Barents and Kara seas and the Lomonosov Ridge do not follow Berckhemer et al.'s classification but appear to be related neither

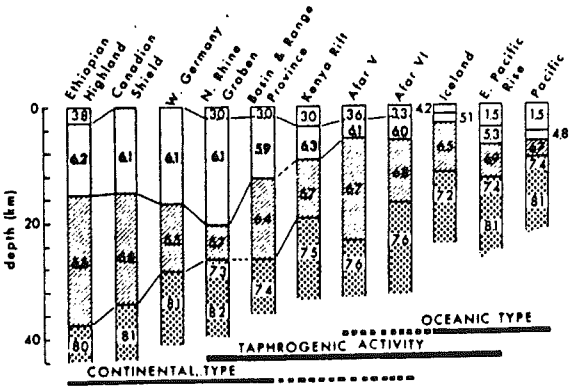

Fig. 8. Comparison of crustal structures from Berckhemer et al. [1975].

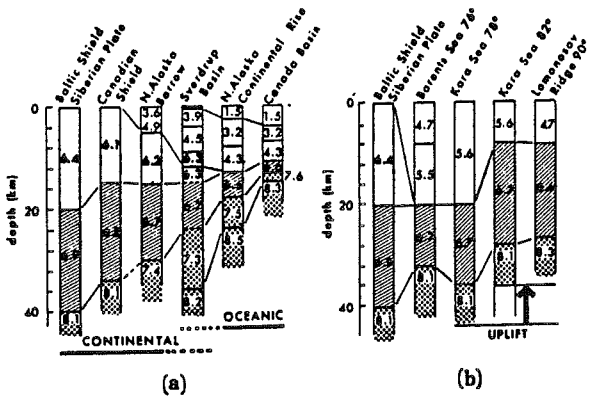

Fig. 9. Comparison of crustal structures grading into the Canada Basin with structures from the Lomonosov Ridge and to the Baltic Shield.

to ancient continental shields nor to modern ocean basins; that is, while the crusts are thick enough to be considered continental, they do not exhibit velocities typical of the acidic rocks. The Barents and Kara seas 78° sections may then represent an intermediate or "old shelf" type of crustal structure characterized by a 20-km-thick sedimentary section (p velocities near 5.5 km/s) deposited on an older oceanic crust. The structures below the Barents and Kara seas maybe the result of a very thick sedmentary section deposited upon a pre-Jurassic oceanic crust. Carlson et al. [1980] have reported on anomalous crustal features in ocean basins and also attempted to categorize them as having a continental or oceanic origin. Using

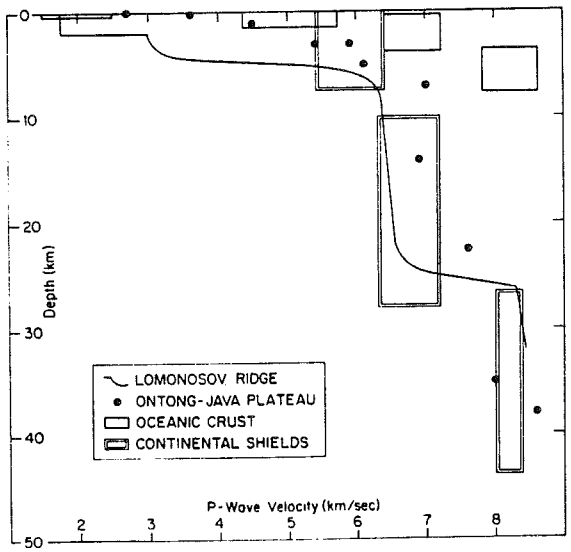

Fig. 10. Comparison of Lomonosov Ridge velocity structure with categorization from Carlson et al. [1980].

their classification (Figure 10), the velocity structure of the Lomonosov Ridge would favor a continental origin. However, as with the Ontong-Java plateau in the Carlson et al. study, the Lomonosov Ridge structure appears to have both continental and oceanic affinities.

The resemblance between the structure below the Kara Sea at 82°N and that of the Lomonosov Ridge at 90° in Figure 9b is striking granted that upper crustal velocity control is poor. Closing of the Fram and Nansen basins would place these structures together, and their similarity provides support for the suggestion (see, for example, Wilson [1963]) that the Lomonosov Ridge is a fragment rifted from the Baltic Shelf.

Conclusions

Partially reversed refraction profiles along strike and transverse to the Lomonosov Ridge show a signficantly different crustal section between the ridge and neighboring ocean basins.

Along strike the general velocity-depth profile shows a 5-km-thick upper crustal layer with a velocity of 4.7 km/s succeeded by a 15 to 20 km thick lower crustal layer of 6.6 km/s material. The upper mantle velocity is close to 8.3 km/s. A thin (1-2 km) and uneven veneer of sediments is suggested along the crest and margins of the ridge; however, control on shallow structural detail is poor in the data of this work.

Synthetic seismogram modeling of the crust-mantle transition (Moho) suggests that the region is characterized by a rapidly changing velocity over a depth interval of about 5 km. Both strike and dip line sections show clear first arrivals, strong primary reflections, and prominent multiples which provide important additional data to constrain the model.

Ray trace modeling of the dip line sections show a root structure extending to a depth of about 28 km. The Moho transition to a depth near 13 km beneath the Makarov Basin to the south is apparently more abrupt than the transition to near 16-km depth beneath the Fram Basin to the north.

A comparison of the crustal section for the Lomonosov Ridge with other crustal sections shows that the ridge section is transitional or intermediate between typical continental and oceanic types. The similarities between the crustal section of the ridge and the crust beneath the Barents and Kara seas support the idea that the Lomonosov Ridge is a rifted fragment from the Baltic Shelf.

Acknowledgements. The authors would like to thank A. Green, R. Haddon, and M. Berry for many constructive comments and helpful suggestions that improved the manuscript. We must also acknowledge the dedicated logistic support provided by the Polar Continental Shelf Project and in particular the personnel from Resolute Bay, N.W.T. We thank the Editor and referees provided by JGR for their positive and constructive comments on review. Contribution 948 of the Earth Physics Branch. LOREX contribution 015.

References

Berckhemer, J., B. Baier, H. Bartelsen, A. Behle, H. Burkhardt, H. Bebrande, J. Makris, H. Miller, and R. Vees, Deep seismic soundings in the Afar region and on the highland of Ethiopia. Afar depression of Ethiopia, Sci. Rep., 14, edited by A. Pilger and A. Rosler, pp. 89-107, Inter-union Commission on Geodynamics, Bad Bergzabern, 1975.

Bolt, B. A., and R. Gutdeutsch, Reinterpretation by ray tracing of a transverse refraction seismic profile through the California Sierra Nevada, I, Bull. Seismol. Soc. Am., 72, 889-900, 1982.

Carlson, R. L., N.I. Christensen, R. P. Moore, Anomalous crustal structures in ocean basins: continental fragments and oceanic plateaus, Earth Planet. Sci. lett., 51, 171-180, 1980.

Chapman, C. H., A new method for computing synthetic seismograms, Geophys. J. R. Astron. Soc., 53, 409-503, 1978.

Coles, R., The lorex magnetic gradient and total field experiment, Earth Phys. Branch 1979 Geomag. rep., 1-20, 1980.

Demenitskaya, R. M., and Y.G. Kiselev, The characteristic features of the structure, morphology and sedimentary cover of the central part of the Lomonosov Ridge based on seismic data, Geophys. Methods Explor. Appl. Arct., Engl. Transl., 5, 33-46, 1968.

Demenitskaya, R. M., A.M. Karasik, and Y.G. Kiselev, Structure of the Earth's Crust Under the Arctic (in Russian), pp. 114-121, Nauka, Moscow, 1964.

Forsytn, D. A., J.A. Mair, and I. Fraser, Crustal structure of the central Sverdrup Basin, Can. J. Earth Sci., 16, 1581-1598, 1979.

Gakkel', Y. Y., The submarine Lomonosov Range, Vokrug Sveta, 11, 4-7, 1954.

Gakkel', Y. Y., Evidence of recent submarine volcanism on the Lomonosov Ridge, Priroda Moscow, 4, 87-90, 1958.

Herron, E. M., J.F. Dewey, and W.C. Pitman, Plate tectonics model for the evolution of the Arctic, Geology, 2, 377-380, 1974.

Jackson, H. R., I. Reid, and R.K.H. Falconer, Crustal structure near the Arctic Mid-Ocean Ridge, J. Geophy. Res., 87, 1773-1783, 1982.

Judge, A., and A. Taylor, Heat flow in Arctic regions (abstract), in Program of Abstracts of the 21st General Assembly Meeting, July 1981. International Association of Seismologists and Physicists of the Earth's Interior, London, Ontario.

Leontiev, O. K., A Short Course in Marine Geology, 463 pp., Moscow University Press, Moscow, 1963.

Mair, J. A., and J.A. Lyons, Crustal structure and velocity anisotropy beneath the Beaufort Sea, Can. J. Earth Sci., 18, 724-741, 1981.

Ostrekin, M. Y., Recent study and exploration of the central Arctic, Priroda Moscow, Engl. Transl., 12, 3-12, 1954.

Overton, A., A seismic reflection profile across the Lomonosov Ridge, central Arctic ocean, in Technical Program, pp. 87-89, Society of Exploration Geophysicists Fifty-Second Annual International Meeting, Dallas, 1982.

Sweeney, J. F., J.R. Weber, and S.M. Blasco, Continental ridges in the Arctic Ocean: LOREX constraints, Tectonophysics, 89, 217-237, 1982.

Wilson, J. T., Hypothesis of the earth's behaviour, Nature, 198, 925-929, 1963.

Whittall, K. P., and R.M. Clowes, A simple, efficient method for the calculation of travel times and ray paths in laterally inhomogeneous media, J. Can. Soc. Explor. Geophys., 15, 21-29, 1979.

D. A. Forsyth, Division of Seismology and Geomagnetism, Energy, Mines and Resources, Canada, Earth Physics Branch, Ottawa, Ontario, Canada K1A 0Y3.

J. A. Mair, Dome Petroleum Ltd., P.O. Box 200, Calgary, Alberta, Canada T2P 2H8.

(Received April 8, 1983;
revised September 9, 1983;
accepted September 22, 1983.)

AN INTERACTIVE PROGRAM FOR ESTIMATING THE PARAMETERS OF MAGNETIC ANOMALY SOURCES

Project 780023

D.J. Teskey
Resource Geophysics and Geochemistry Division

Teskey, D.J., An interactive program for estimating the parameters of magnetic anomaly sources; in Current Research, Part A, Geological Survey of Canada, Paper 82-1A, p. 51-53, 1982.

Abstract

An interactive computer program for estimating the best-fit solution of the magnetization and geometric parameters of causative magnetic bodies using a Tektronix compatible terminal is now available. The required input parameters and options are requested sequentially during operation so that little advance experience or familiarity is required. An example of the use of the qualitative interpretation technique is presented utilizing an aeromagnetic profile across the Lomonosov Ridge.

Introduction

A number of quantitative interpretation computer programs for performing fits of magnetic anomalies are available (McGrath and Hood, 1973; Wells, 1979). However the first of these was developed primarily for batch use and the second is valid only for bodies of great strike extent (approximately four times the depth of burial) and does not include automated convergence procedures. Therefore a totally interactive program for use with a Tektronix type interactive terminal connected to a computer with adequate storage (70 K octal) capability and which could be used by geoscientists with little background in computing was developed. The particular features of this program are:

1. A 'best-fit' value of magnetization is calculated automatically for each source configuration.
2. Source geometries which have arbitrarily complex cross-sections can be represented.
3. A generating function is used which is applicable across the central profile of bodies which have finite strike extent, but are symmetrical through a vertical plane containing the profile. This model can also be used as a first approximation in cases where this symmetry is not present.
4. The position of points, outlining the cross-section of the causative bodies can be modified directly, or a nonlinear routine can be used to translate or rotate groups of points.

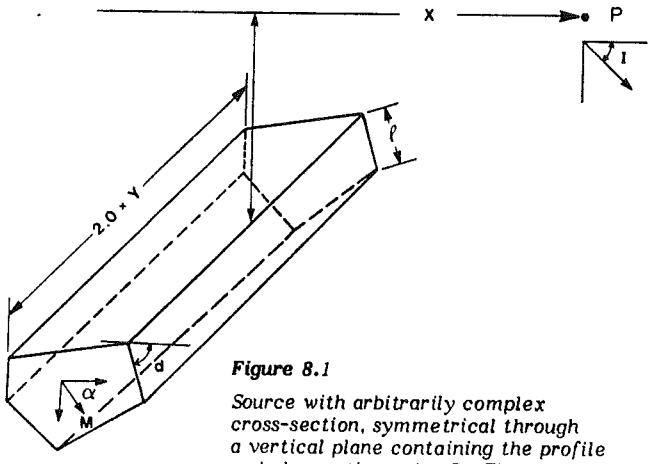

Figure 8.1

Source with arbitrarily complex cross-section, symmetrical through a vertical plane containing the profile and observation point P. The magnetic field is calculated as that due to the sum of the individual surfaces.

Generating Function

The formula for the vertical component of the total magnetic field ΔT at a point above the central profile across a 'pole sheet' at arbitrary dip (d) is given by:

$$\Delta T = M\left[\frac{1}{2}\sin d\left(\ell n\,\frac{A-Y}{A+Y} - \ell n\,\frac{B-Y}{B+Y}\right) + \cos d\left(\tan^{-1}\frac{Y(\ell + h\sin d - x\cos d)}{A(x\sin d + h\cos d)} - \tan^{-1}\frac{Y(h\sin d - x\cos d)}{B(x\sin d + h\cos d)}\right)\right] \quad (1)$$

where $A = \sqrt{(x - \ell\cos d)^2 + (h + \ell\sin d)^2 + Y^2}$

$B = \sqrt{x^2 + h^2 + Y^2}$

Y = 0.5 x strike extent

M = pole strength (normal component of magnetization)
(modified from Grant and West, 1965, p. 273-274)

The total field at any inclination can be calculated as only the relative angle (I - d) is important (Fig. 8.1). The field due to a source which is assumed to be symmetrical across a plane which contains the profile, can be calculated as the sum of that due to pole-sheets forming the surface of the source and with the pole strength on a given sheet proportional to the normal component of the magnetization vector to that sheet.

More than one body can be represented and a given sheet may form part of the boundary of a number of sources. Since the anomaly due to a given body is proportional to the magnetization strength of that body, the 'best fit' magnetization strength can be easily calculated and is done each time the anomaly is generated. An additive constant representing the earth's field and that due to deeper sources is also calculated automatically.

Interactive Fitting Program

A flow chart for the interactive fitting program is shown in Figure 8.2. Prior to running the program, the data points must be stored on a file, as the number of data points, followed by the values. The program starts by reading the

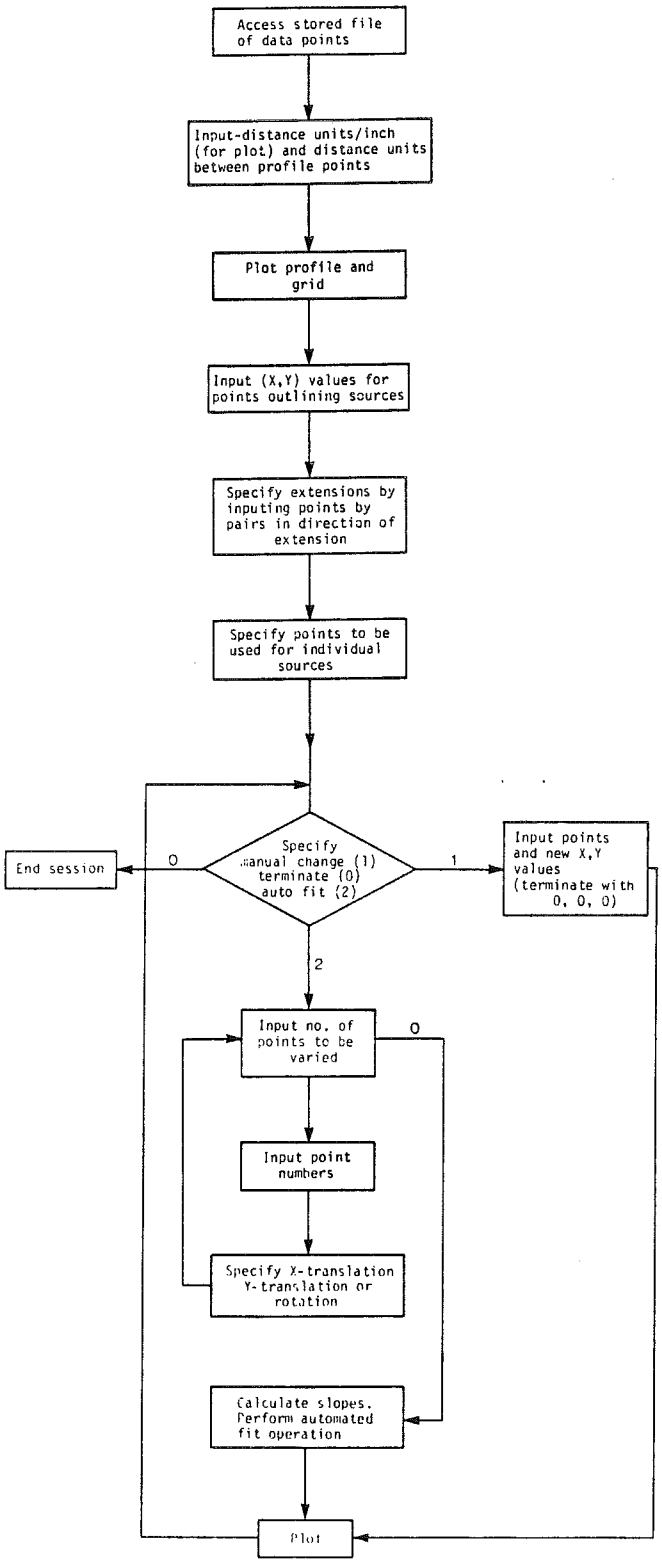

Figure 8.2. Flow chart for interactive fitting program.

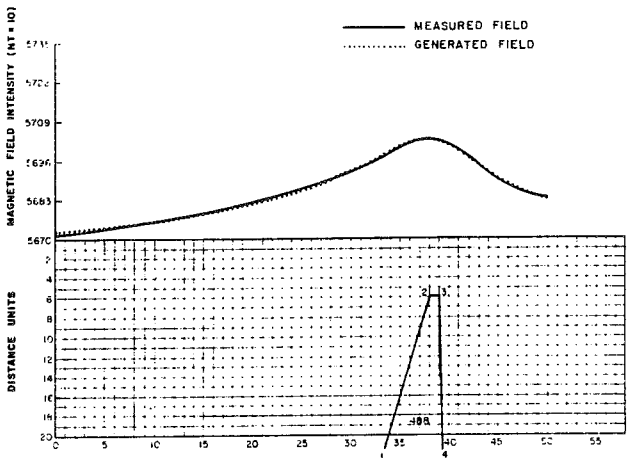

Figure 8.3. Calculated fit for an aeromagnetic profile across the Lomonosov Ridge.

data values and proceeds sequentially by requesting further information or options from the user. After receiving basic information, such as the scale (number of length units/inch) and the distance between profile points, the profile is plotted on the top half of the screen, with a square grid in length units on the lower half (Fig. 8.3). The user can then input the points, representing the cross-section of the magnetic sources, in any order, terminating with a zero entry. In the next step, selected sides can be extended by feeding in the two points in the order of the desired extension. This feature is used when it is necessary to represent a source with great depth extent. Finally the individual bodies are defined by inputing the number of points, the approximate strike extent (as estimated from the contour map), and a code to designate whether an open or closed source body is to be used, that is, whether the bottom surface will be considered during anomaly generation. The points that define the outline of each body are then specified in a clockwise direction. A point can, of course, be used in more than one body.

The program now proceeds in an iterative fashion with the operator deciding whether to modify points, enter an automated routine, plot, or terminate the session. These operations can be continued until the user decides that he has obtained the best fit possible and thus that the original hypothesis is possible or not. During the automated fit, the user first specifies the group of points to be varied, followed by an option for X translation, Y translation or rotation (rotation is about the first point entered). This process is continued until all desired movement modes for each group of points has been specified. The program then calculates the changes (slopes) in the 'sum-of-squares' difference between the generated and observed profile for each of the above specified movements. Movement then takes place along the maximum gradient in the least squares surface until a minimum in that direction is reached. The slopes are then recalculated and a new direction established. This process is continued until a minimum in the 'least squares' surface is reached or a specified number of iterations have been exceeded. After plotting the new fit the operator again chooses the appropriate action until an adequate fit has been achieved. This will, of course, usually be a matter of judgment.

Example

In 1980 and 1981, a set of parallel aeromagnetic profiles were flown over the Lomonosov Ridge near the North Pole as part of the Lorex project. The data were collected by the Convair 580 aircraft of the National Aeronautical Establishment, equipped with three rubidium vapour high resolution magnetometers (Hood and Bower, 1980). One particular profile from this set extending from 88°48'N, 164°42'W to 88°57'N, 164°06'E, a distance of 17 km was used as input to the modelling program (the actual profile extended farther north but was terminated to minimize interference from neighbouring anomalies). The result of the computer fit achieved with the described program is shown in Figure 8.3. The distance unit used corresponds to four seconds of aircraft travel which is approximately 340 m. Thus the source appears to be an intrusive body at a depth of approximately 2040 m below the aircraft or 1740 m below sea level. Bathymetric data indicate the depth to bottom at this point to be approximately 1750 ± 50 m.

In general it would be possible to fit the anomaly with a smoother source at shallower depth (clearly unlikely in this case).

Conclusions

This interactive fitting program can be used by persons with little computer experience as a simple technique for evaluating hypotheses concerning the sources of magnetic anomalies. Bodies with arbitrarily complex cross-sections can be represented and easily modified. The efficiency of the program will depend greatly on the experience of the user in postulating geologically reasonable geometries. Copies and demonstrations of the program can be obtained from the author.

References

Hood, P.J. and Bower, M.E.
1980: Aeromagnetic reconnaissance: Lorex Project (Abstract); American Geophysical Union Meeting, Toronto, May 22-27, 1980, EOS, v. 60 (17), p. 277.

Grant, F. and West, G.
1965: Interpretation Theory in Applied Geophysics; McGraw-Hill, New York.

McGrath, P.H. and Hood, P.J.
1973: An automatic least-squares multimodel method for magnetic interpretation; Geophysics, v. 38, p. 349-358.

Wells, I.
1979: A computer program to create two dimensional gravity and/or magnetic models; Geological Survey of Canada, Open File 597.

JOURNAL OF GEOPHYSICAL RESEARCH, VOL. 90, NO. B1, PAGES 663–677, JANUARY 10, 1985

Reinterpretation of Morphology and Crustal Structure in the Central Arctic Ocean Basin

J. R. WEBER AND J. F. SWEENEY[1]

Department of Energy, Mines and Resources, Earth Physics Branch, Gravity, Geothermics and Geodynamics Division Ottawa, Ontario

Ice station bathymetric profiles and submarine echograms reveal a steep escarpment at least 200 km long with up to 1700 m of relief subparallel to the Lomonosov Ridge. This feature, formerly called the Marvin Spur, is here interpreted as the Makarov-facing flank of the Alpha Ridge. East of the 160°W meridian the intervening Makarov Basin is a narrow grabenlike trough between 25 and 60 km wide filled with horizontally stratified sediments that were deposited largely after the Marvin Seamounts were constructed along the basin axis. The association of basement relief with geomagnetic field variations within the trough plus evidence of normal faulting on the Lomonosov Ridge suggest that this segment of the Makarov Basin is an extensional feature produced by other than typical seafloor-spreading processes. Gravity models indicate that the crust below the Makarov flank of the Alpha Ridge ranges in thickness between 16 and 20 km, considerably less than the 26 km known from seismic refraction work to exist below the Lomonosov Ridge. It is argued, on the basis of gravity data, that adjacent to the Lomonosov Ridge the Fram Basin crust, which is probably truly oceanic, is 3–4 km thinner than that of the Makarov Basin.

INTRODUCTION

Investigation into the nature and origin of the Lomonosov Ridge (see location map, Figure 1) by scientists from the Earth Physics Branch of the Canadian Department of Energy, Mines and Resources (EMR) began more than a decade ago. During the Second Canadian North Pole Expedition in 1969, plumb line deflection measurements and gravity observations were carried out in the vicinity of the north pole and across the nearby Lomonosov Ridge [*Lillestrand and Weber*, 1974]. The observed plumb line deflections were in good agreement with the values predicted from a model constructed assuming the ridge to be in isostatic equilibrium and composed of sedimentary rocks (densities between 2.2 and 2.5 Mg/m^3) underlain by a continental-type crust 27 km thick and a crust-mantle density contrast of 0.22 Mg/m^3. Gravity measurements were consistent with the free air gravity anomaly computed from the same model. Because the water depth in the Fram Basin (Figure 1) is 250 m deeper than in the Makarov Basin, it was concluded that the crust beneath the former is about 2 km thinner than beneath the latter. These early measurements supported the view, first put forward by *Heezen and Ewing* [1961] and later expanded by *Wilson* [1963], that the Lomonosov Ridge represents a rafted sliver of the Kara and Barents continental shelves [*Smith*, 1974].

During 1964 the ice island ARLIS II drifted across the Lomonosov Ridge some 450 km north of Ellesmere Island (drift path shown in Figure 9). Shallow seismic reflection and gravity measurements carried out over the ridge from ARLIS II [*Ostenso and Wold*, 1977] indicated that the ridge was made up of thick sedimentary sequences leaving "little doubt as to its continental origin." This was the first direct evidence for the continental nature of the Lomonosov Ridge.

In 1979, EMR undertook a large-scale, multidisciplinary project, code-named LOREX 79, to study the nature of the Lomonosov Ridge [*Weber*, 1979]. Observations taken included bathymetry and gravity plus shallow and intermediate reflection and crustal refraction seismic.

In this paper a structural interpretation of the ridge in the LOREX area near the north pole is presented based on depth soundings, gravity observations, and seismic data. A new interpretation of the ARLIS II shallow seismic and gravity data has been carried out. The resulting LOREX and ARLIS II crustal models are compared.

THE LOREX SURVEY

Bathymetry and Morphology

The first depth soundings and gravity measurements in the vicinity of the Lomonosov Ridge near the north pole were made during the First (1967) and Second (1969) Canadian North Pole Expeditions [*Lillestrand and Weber*, 1974; *Weber*, 1983]. Their drift track and the drift tracks of the LOREX main and two satellite camps are shown in Figure 2. The LOREX camp positions were determined in near real time from satellite Doppler navigation with an accuracy of about ±250 m. Navigational data were later reprocessed providing mean station positions for 3-hour intervals with horizontal precision of ±24 m and vertical uncertainty ±0.4 m [*Popelar et al.*, 1983]. All three camps were equipped with echo sounders and heavily damped LaCoste Romberg recording gravity meters. The spot measurements were carried out by helicopter equipped with a fourth LaCoste Romberg gravity meter and with the Global Navigational System, a very low frequency radio navigational aid, with an estimated positional accuracy of ±2000 m. The accuracy of the gravity readings depends on the prevailing magnitude of the wave motion of the ice and is estimated at better than ±1 mGal. Instrument drift was monitored and corrected for by frequently reading the mobile gravity meter side by side with the recording gravity meters and by establishing three ties to the gravity control station in Alert over the 2-month period of the experiment. Some additional water depths were obtained from the seismic crustal refraction survey [*Mair and Forsyth*, 1982]. Except for the soundings taken along the LOREX drift tracks all depths were deter-

[1] Now at Pacific Geoscience Centre, Sidney, British Columbia.

Paper number 4B1181.
0148-0227/85/004B-1181$05.00

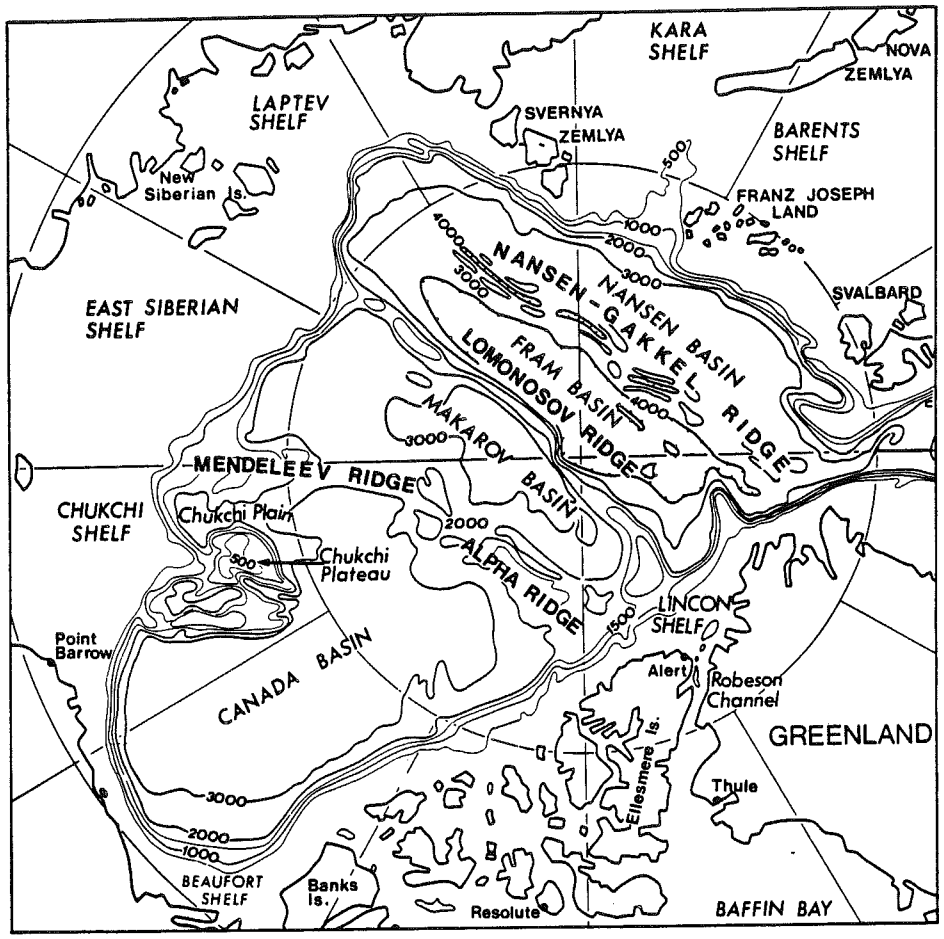

Fig. 1. Location map.

mined by the seismic reflection method. The accuracy of the depth determination is estimated at ±3m.

On the basis of all the sounding data a 100-m contour map of the seafloor was compiled (Figure 2) which extends from the Makarov Basin across the Lomonosov Ridge to the north pole in the Fram Basin. The shallowest and deepest depths recorded were 955 m at 88°43.6'N, 174°02'E and 4309 m at 89°30.50'N, 72°46'E, respectively. The Makarov Basin is some 250 m shallower than the Fram Basin and the Makarov-facing slope of the Lomonosov Ridge is much steeper than the Fram-facing slope. Comparison of the LOREX map with the *GEBCO* [1979] map of the Arctic Ocean reveals that the crest of the Lomonosov Ridge is up to 34 km farther south than is shown on the latest international map. On the other hand the 1954 Soviet map of the Arctic Ocean [*Burkhanov*, 1956], although more generalized, places the ridge in its correct position [*Weber*, 1983].

The seismic air gun profiles reveal that both the Makarov and Fram basins are floored by horizontal layers of well-stratified, unconsolidated sediments of up to 1 km thickness, which abut unconformably against the ridge flanks [*Blasco et al.*, 1979, Figure 12.7]. On the ridge, sediments are absent from the Makarov-facing flank where the average slope from near the base to near the crest of the ridge is as steep as 14°. The crest and the Fram-facing flank, whose slope does not exceed 6°, are covered with a thin veneer of stratified, unconsolidated sediments that lie conformably upon the underlying bedrock. This is illustrated in the shallow seismic profile in the Makarov Basin (Figure 3*a*) and on the top of the ridge (Figure 3*b*). The sawtoothed appearance of the crestal region with Fram-facing slopes covered by thin stratified sediments that are truncated by what appear to be scarps suggests that the ridge consists of en echelon fault blocks (see also Figure 4 of *Sweeney et al.*, [1982]).

The main camp was equipped with a cross-shaped seismic array, 600 m in diameter. Charges from 1 to 20 kg were fired at the center of the spread 2 or 3 times a day depending on the drift rate. Preliminary seismic reflection results [*Overton*, 1982] show a 20+ km wide trough containing at least 2.1 km of sediments with a well-defined subhorizontal reflector, detected also by air gun profiling at about 1 km below the seabed (Figure 4).

Two seamounts located some 40 km south of the Lomonosov Ridge crest (S_1 and S_2 on Figure 2) have been contoured on the basis of a few soundings only. Their presence is in part revealed by the seismic subbottom reflection profile which shows acoustic basement shallowing and protruding above the ocean floor (Figure 3*a*). There may be more basement relief in this part of the Makarov Basin, but the sounding density is too low to detect it. Submarine echograms [*Beal*, 1969] indicate seafloor relief at several points in the Makarov Basin. For example, the echogram of the *Sargo*, which in 1960 followed a course along the 170°W meridian (Figure 5), clearly outlines seamount S_2 (see Figure 2) and two other bathymetric features to the south that range in height from 70 to 700 m above the seafloor. The larger feature 50–60 km from the Lomonosov

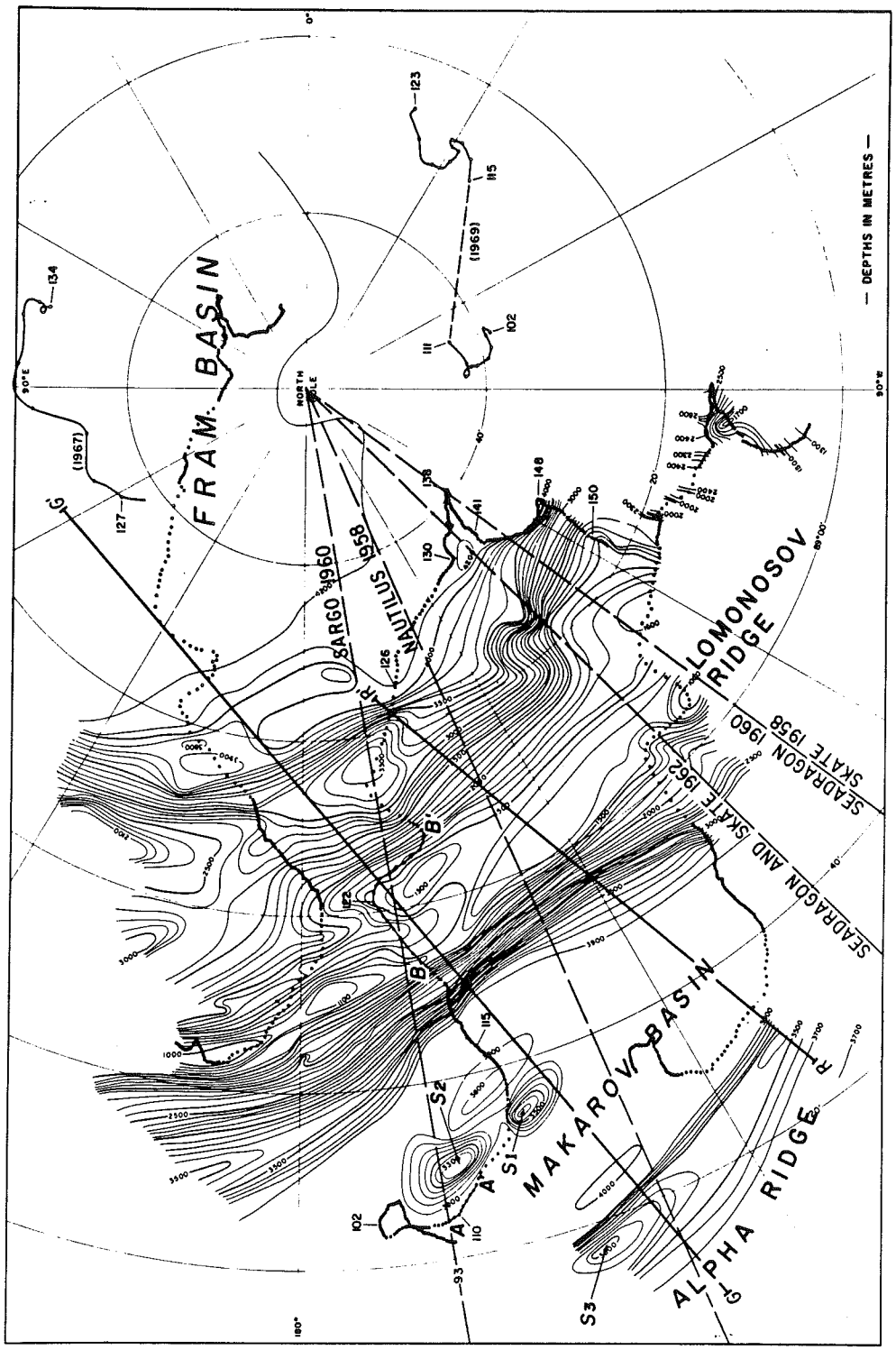

Fig. 2. LOREX bathymetric map. Contour interval 100 m. Dotted lines represent drift tracks of the LOREX main camp and two satellite camps with 3-hour intervals between dots; numbers represent Julian days. Drift track portion AA' and BB' represent sections of the subbottom profiles of Figures 3*a* and 3*b*. G-G' represents the profile location of the gravity model, and R-R' the location of the seismic refraction line transecting the ridge. For description of bathymetric features S_1, S_2, and S_3, see text. Drift paths of 1967 and 1969 Dominion Observatory polar expeditions are indicated. Also shown are tracks of six submarines whose echograms are illustrated in Figure 5.

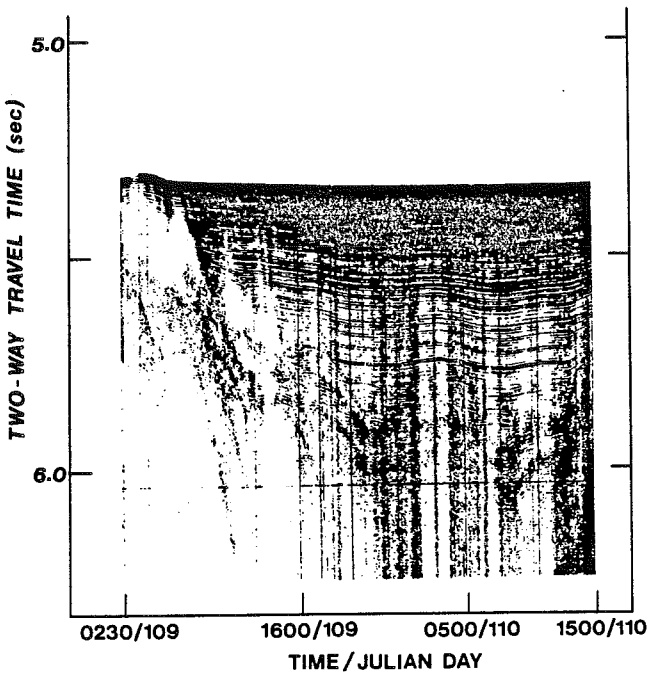

Fig. 3*a*. Subbottom profile in the Makarov Basin along section AA' in Figure 2. Profile length approximately 13 km.

Ridge is similar in relief to and is on strike with topographic feature S_3 (Figure 2), an indication that seafloor topography associated with S_3 continues to the west of the LOREX survey. The horizontally layered unconsolidated sediments which fill the Makarov Basin abut unconformably against the seamounts in Figure 3*a*, indicating that basement topography was formed before the sediments were laid down.

LOREX Gravity Model

The free air gravity anomaly field is dominated by a prominent positive anomaly of between 60 and 90 mGal centered along the crest of the Lomonosov Ridge (Figure 6). It is flanked by negative anomalies of between −20 and −50 mGal centered approximately along the 3900-m isobaths on either side of this ridge. Farther away from the ridge the free air anomaly field is generally positive over the Fram abyssal plain and negative over the Makarov Basin.

A generalized two-dimensional crustal density model was constructed from bathymetry and seismic information (Figure 7) using an algorithm developed by *Nagy* [1980]. This profile parallels closely the drift path of the main camp from the Makarov Basin across the Lomonosov Ridge which provides control for crustal density horizons from the LOREX seismic refraction results.

This LOREX gravity model was constructed to be consistent with the hypothesis that the Lomonosov Ridge is a fragment of continental crust flanked by an oceanic Fram crust to the north and a thicker Makarov crust of uncertain character to the south. Beneath the ridge the depth and shape of intracrustal boundaries and the Moho were taken from the *P* wave velocity model of *Mair and Forsyth* [1982] and *Forsyth et al.* [1983] except in the Fram Basin, as discussed below. Basement cover was modeled from shallow [*Blasco et al.*, 1979] and intermediate [*Overton*, 1982] reflection data (Figures 3 and 4). The upper crust beneath the ridge is assigned an average density of 2.50 Mg/m^3 based on gravity model calculations using ridge topography [*Sweeney*, 1980].

The basement relief at kilometers 35 and 65 of the crustal density model (Figure 7) corresponds to S_3 and S_1 of Figure 2. Both features antedate the sedimentation process, as indicated earlier. From gravity data analysis, however, it appears that the rocks beneath each have quite different densities, namely, 2.5 and 3.15 Mg/m^3, respectively. S_1 may represent an extinct volcano, while S_3 may represent a ridge of the same density material as the sedimentary or metasedimentary rocks of the Lomonosov Ridge. As we will propose in the discussion of the ARLIS II data, the Makarov-facing flank of S_3 may be part of a very long submarine escarpment that delineates the boundary between the Alpha Ridge and the Makarov Basin.

The 250-m greater depth of the Fram Basin may indicate that the crust there is up to 2.5 km thinner than that beneath the Makarov Basin, provided that seafloor sediment thicknesses and average crustal densities are about the same in each basin. As defined by the shallow and intermediate depth reflection data, basement cover near the ridge in each basin is about 1 km thick and locally much thicker in the Makarov Basin (Figure 4).

Mair and Forsyth [1982] obtained a crustal thickness (excluding water depth) of 9 km for the Makarov Basin and a thicker crust of 12 km for the Fram Basin. In his first preliminary interpretation of the LOREX gravity and seismic data, *Weber* [1980] was unable to reconcile the seismic crustal depths with the gravity data and, based on gravity information, estimated the Fram Basin crust adjoining the Lomonosov Ridge to be 8 km thick.

There is other evidence that the Fram Basin crust is quite thin. *Duckworth et al.* [1982] carrying out seismic refraction work in the Fram Basin near 89°30'N, 21°W (some 215 km from the Lomonosov Ridge crest and 285 km from the Nansen-Gakkel spreading center) during the FRAM II operation in 1980 found the crust to be about 7 km thick consisting of a 1.5- to 2-km-thick sediment blanket over a thin to nonexistent layer 2 with layer 3 extending to the Moho.

In their earlier crustal density model (which we will call model I), *Sweeney et al.* [1982] tried to reconcile the observed gravity field with the entire seismic crustal model from the Makarov Basin across the Lomonosov Ridge into the Fram Basin [*Sweeney et al.*, 1982, Figure 5]. While gravity and seismic data agreed reasonably well for the ridge and adjoining Makarov Basin, the seismically determined Fram

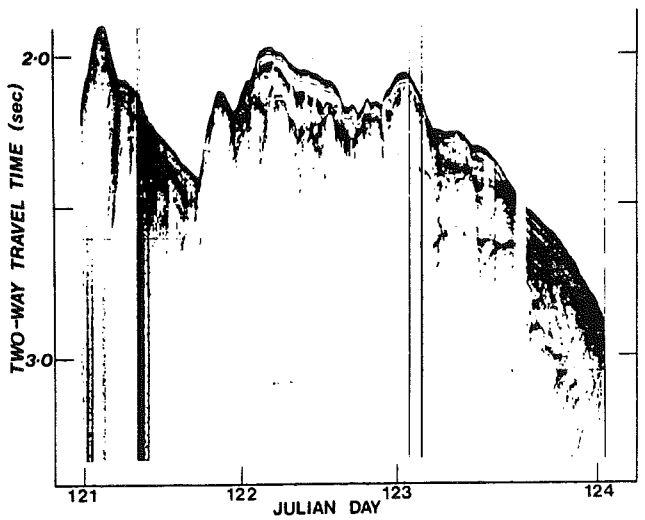

Fig. 3*b*. Subbottom profile across the crest of the Lomonosov Ridge along section BB' in Figure 2. Profile length approximately 28 km.

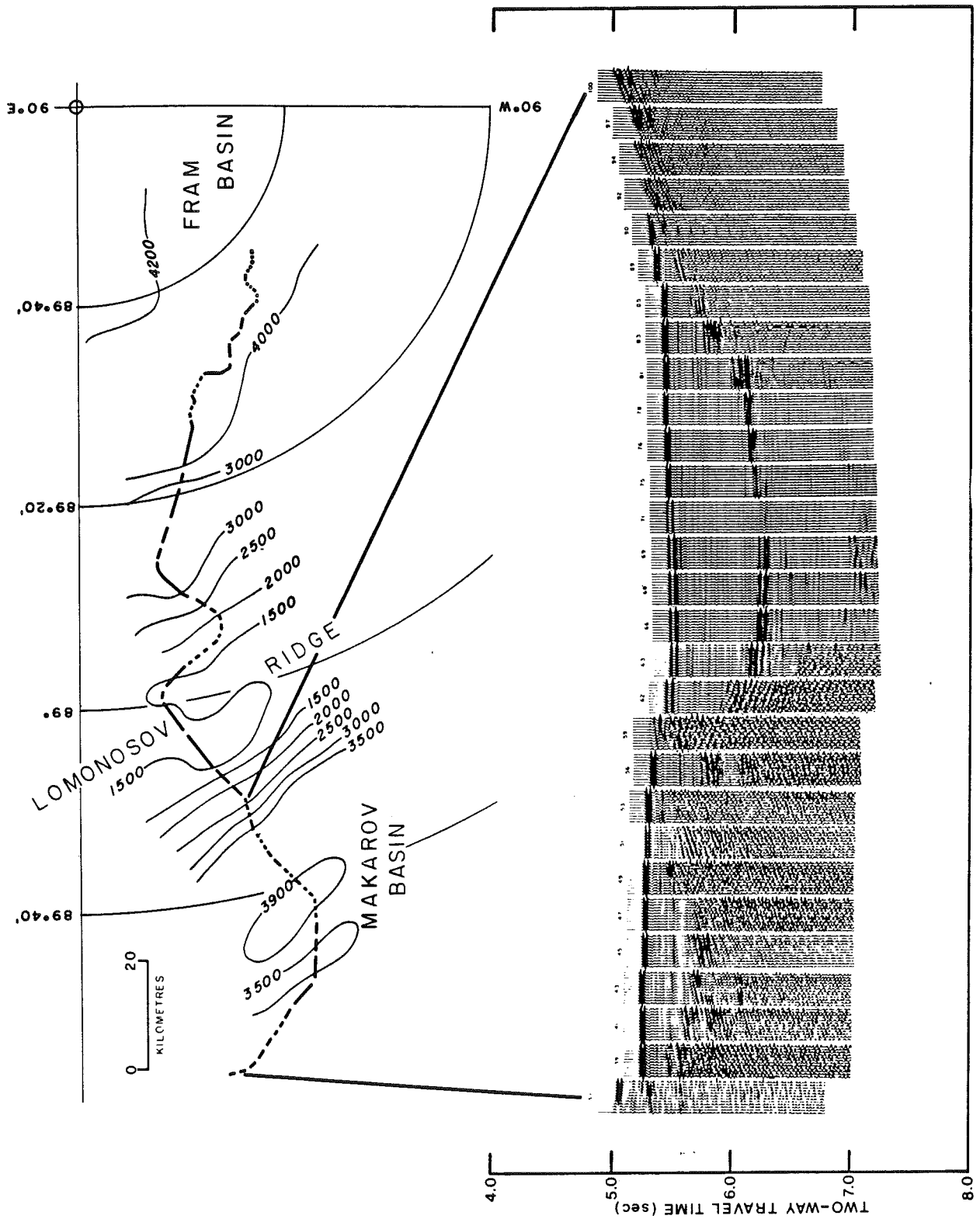

Fig. 4. Preliminary results of LOREX intermediate depth reflection seismic experiment across the Makarov Basin [from *Overton*, 1982].

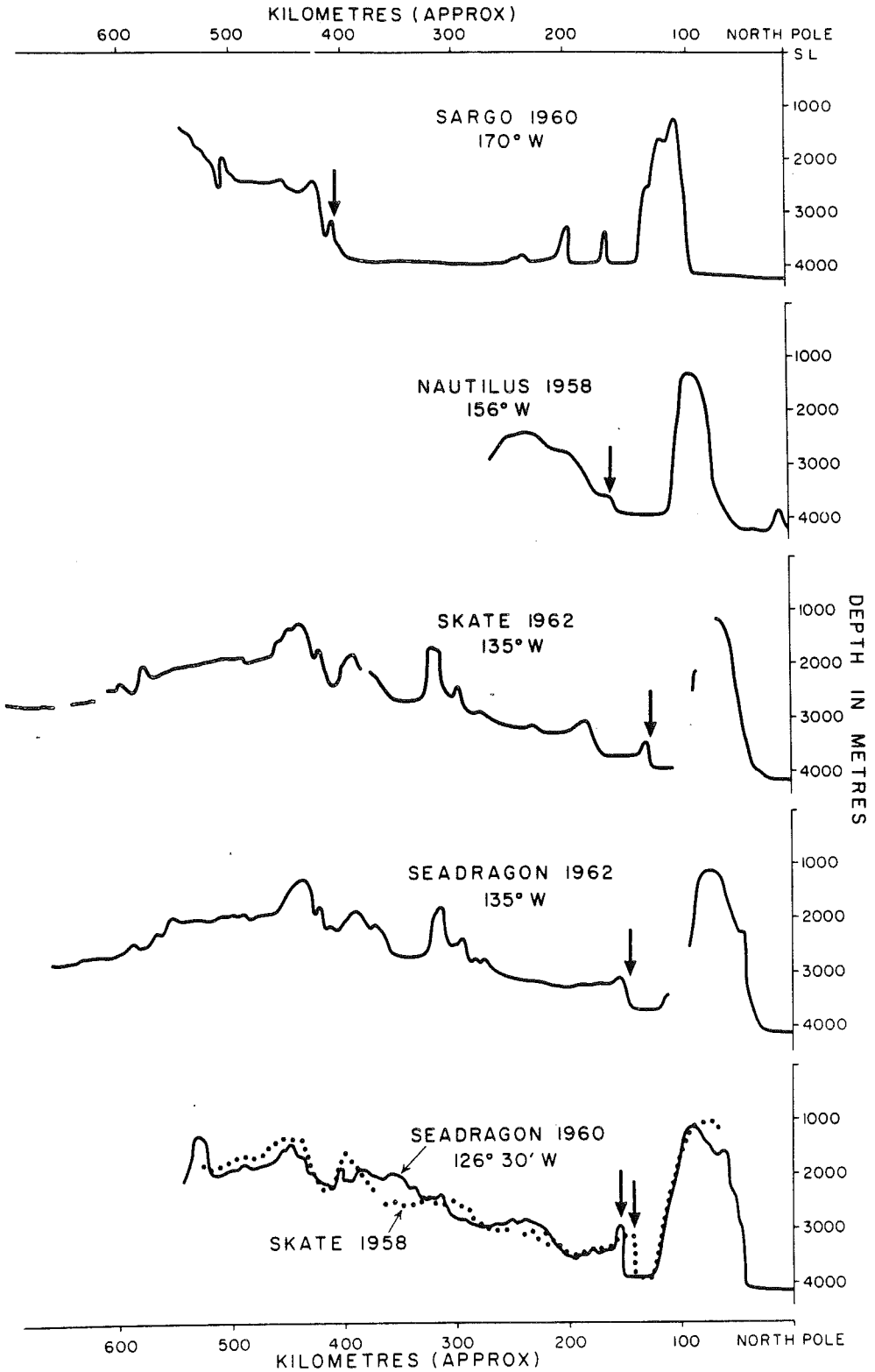

Fig. 5. Echogram of early U.S. submarine expeditions to the north pole along the 170°, 156°, 135° and 126°30′W meridians [from *Beal*, 1969]. Arrows indicate Makarov-facing flank of escarpment.

Basin crust appeared much too thick and could only be reconciled by assigning anomalously high-density values to the lowermost 4 km of Fram Basin crust.

Seismic refraction data for the Lomonosov Ridge are based on reversed arrivals and are well defined. Data for the adjoining basin structures, however, are more poorly defined because the refraction lines are single ended and may not extend far enough into either basin to obtain representative crustal thicknesses (D. A. Forsyth, personal communication, 1984).

The crustal density model of Figure 7 (model II) is based on a thin Fram Basin crust. By establishing, in the crustal density

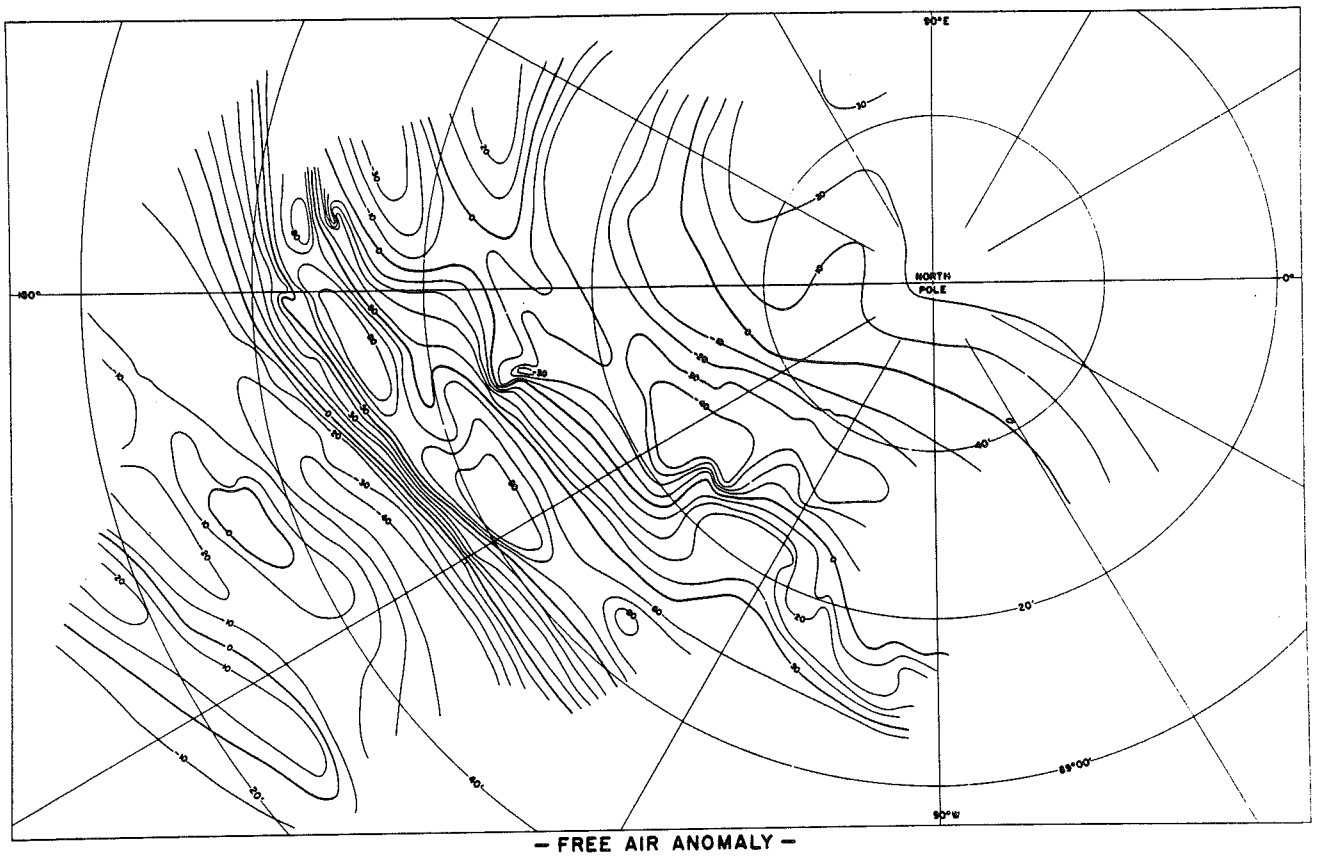

Fig. 6. LOREX free air gravity map [from *Sweeney et al.*, 1982]. Contour interval 10 mGal.

model, the thickness of the oceanic crust on the Fram side at 7 km and by assuming a uniform density for rocks within the crust of both basins and for the upper mantle, a crustal thickness of about 10.5 km is obtained for the Makarov side.

The assumption of a similar density structure on either side of the Lomonosov Ridge is speculative, but it confirms the thin Fram Basin crust hypothesis of *Duckworth et al.* [1982] and others [*Jackson et al.*, 1982]. Clearly, more seismic data for the Fram and Makarov basins are required.

THE ARLIS II SURVEY

Ostenso and Wold's Data Reduction

Ice island ARLIS II was occupied on July 1, 1961, 350 km northwest of Point Barrow, Alaska. During the next 46 months it drifted across the Arctic Ocean into the Greenland Sea and was abandoned on May 6, 1965, in Denmark Strait [*Wold*, 1973]. The scientific program conducted from the drifting station included depth measurements, gravity observations, and continuous seismic subbottom profiling. Positions of the ice island were obtained, weather permitting, by celestial fixes. The drift was interpolated between fixes on the basis of available meteorological information [*Wold*, 1973]. The maximum seismic penetration of the system is about 1.1-s two-way reflection time (corresponding to 1 km of sediments at a velocity of 1800 m/s). Instrumentation and methods used to retrieve and reduce the gravity and seismic data along with a discussion of accuracies are given by *Ostenso* [1968] and *Wold* [1973]. Navigation is considered to be accurate within 1 km, gravity to within 2 mGal, and bathymetry to within 1% of water depth.

The data in the section from the Alpha Ridge to the Morris Jessup Rise (November 1, 1963, to December 14, 1964) was reported by *Ostenso and Wold* [1977]. Ostenso and Wold divided the 409-day period into 79 segments, each corresponding to a magnetic tape of profiler data. Free air and Bouguer gravity anomalies and subbottom profiles were presented in 11 figures. The subbottom profiles of the section containing tapes 28 to 33 [*Ostenso and Wold*, 1977, Figure 6] are reproduced here in Figure 8. These seismic tapes were condensed and edited by Ostenso and Wold but not systematically adjusted for variations in the drift velocity of the ice island. Therefore the horizontal scale is in neither constant distance nor time units. These seismic records are reproduced linearly from left to right independent of complexities of the drift path. This can be misleading. For example between March 23 and April 17, ARLIS II drifted slowly westward while performing two 360° clockwise turns, followed by a 360° anticlockwise turn, all within a 6 by 12 km area above a narrow sediment-filled trough (kilometers 470–482 in profile EE', Figure 10*d*). In so doing, it recorded the same diapir 3 times while crossing it in the north-south, east-west, and south-north direction. Before the subbottom profiles can be used in any quantitative interpretation they need to be corrected for velocity variation of the ice island and put in a convenient coordinate frame.

Normalization of Subbottom Profiles

First, the drift path of ARLIS II from November 21, 1963, until May 19, 1964, was plotted; it consists of nearly 900 positions taken from *Wold* [1973]. The geographical positions marked on the subbottom profiles were identified on the plot; they divide the drift path into 65 segments of varying length.

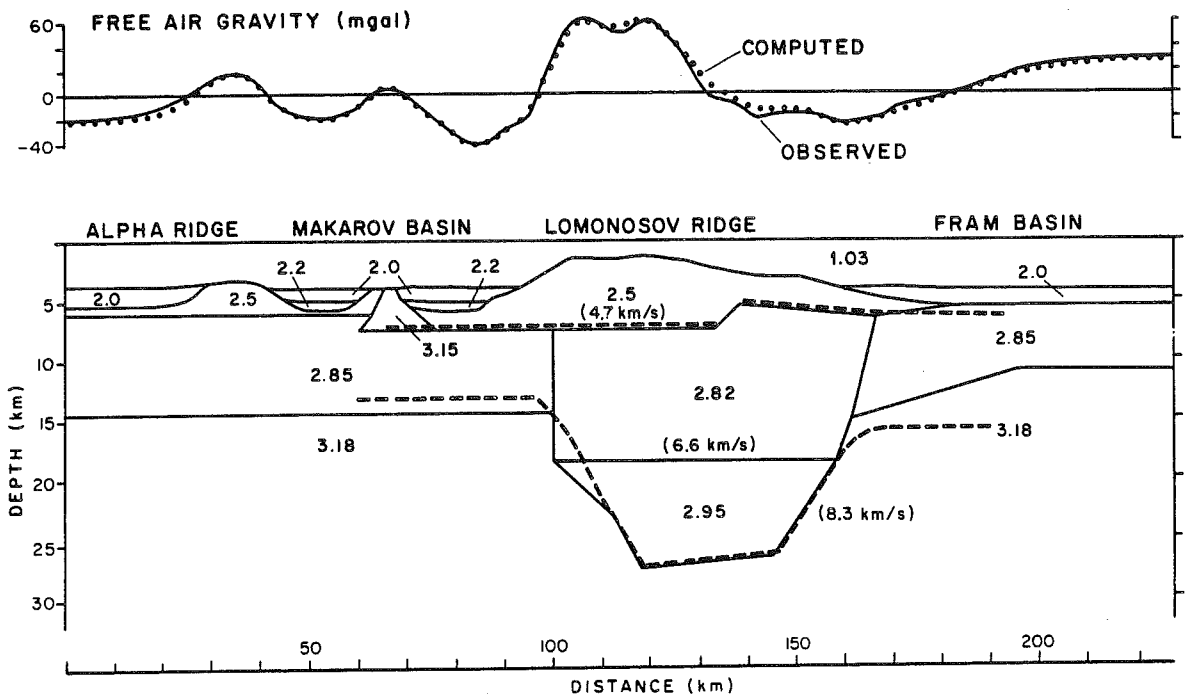

Fig. 7. Two-dimensional crustal density model along profile G–G′ of Figure 2. Densities are in megagrams per cubic meter. Dashed lines represent *Mair and Forsyth*'s [1982] seismic refraction results with an upper crustal velocity of 4.7 km/s, a lower crustal velocity of 6.6 km/s, and an upper mantle velocity of 6.3 km/s.

Next, the subbottom profiles for the same time period [*Ostenso and Wold*, 1977, Figures 3–6] were digitized by us using the identified geographical positions. The horizontal scale of each of the 65 segments was adjusted to agree with the length of the corresponding segment on the position plot. This presumes a constant average drift velocity of the ice island in each segment. The vertical scale was changed from two-way travel time in seconds to depth in meters using *Mathews*' [1939] tables. To remove variations in drift direction from this normalized subbottom profile, the drift track was projected onto six linear profiles AA′ to FF′ (Figure 9). Finally, multiple tracks produced by ARLIS II during periods of low drift were deleted, leaving only that part of the drift path illustrated in Figure 9.

The plot of the normalized and edited subbottom profiles along profiles AA′ to FF′ are shown in Figures 10*a*–10*d*. Also shown are free air gravity values and depth taken directly from *Wold* [1973]. Depth was recorded with an echo sounder separately from the subbottom profiles.

Bathymetry and Morphology

Profile AA′ (Figure 10*a*) starts at A with a ridge or seamount consisting partly of conformably folded sediments followed, after a 350-m drop, by a basin filled with a sequence of at least 600 ms (540 m) of largely undisturbed sediments. Between kilometers 77 and 101 the seismic tape is missing, but the depth sounder shows a rise from 3320 m at kilometer 45 to 2272 m at kilometer 94. At this point there is a gap in the soundings; the soundings continue again at kilometer 98 at a depth of 3925 m, indicating a very steep drop of 1650 m, which explains the failure of the sounder to resolve echos. The escarpment is seen in the gravity plot. Continuing with profile AA′, the next 12 km show horizontally stratified sediments, at least 530 ms (480 m) deep, abutting against the steep Makarov flank of the Lomonosov Ridge. The morphological sequence is similar to that found on LOREX except that here the Makarov Basin has narrowed to a 25-km-wide trough. The Lomonosov Ridge flank (kilometers 111–140), showing no indication of sediment cover, reaches a first plateau at 2400 m (profile BB′, Figure 10*b*). The plateau is covered with some 67 ms (60 m) of conformable sediments pierced by two outcrops. At kilometer 177 the seafloor rises again steeply, with no indication of sediment cover, to a second plateau at 1750 m which, from kilometer 220 on, rises gently toward the ridge crest. The subbottom records suggest some 300 ms (270 m) of conformable sediments on a very irregular basement. At this point, ARLIS II made a 110° turn and headed back toward the Makarov Basin to the first plateau (profile CC′, Figure 10*b*), where it changed course again and resumed its earlier direction (profile DD′, Figure 10*c*). Near D (kilometer 292) the ridge is covered with at least 560 ms (500 m) of fairly flat conformable sediments with no outcrops. The plateaus are suggestive of the block-faulted nature of the Lomonosov Ridge [*Sweeney et al.*, 1982, Figure 5]. At kilometer 305 a steep 1000-m escarpment is traversed as ARLIS II drifted obliquely across the flat crest of the ridge. Minimum water depth is 1062 m. The ridge top consists of stratified, conformable sediments at least 950 ms (850 m) thick. Elevation changes at kilometers 320 and 406 are caused by offsets between segments that are projected onto DD′. A short crestal cross section (profile FF′, Figure 10*d*) shows conformable folded sediments to a maximum depth of 600 ms (530 m) with individual reflectors 35 ms (32 m) apart on average.

The Fram-facing flank (profile EE′, Figure 10*d*) has a secondary ridge separated from the main ridge by a trough infilled with 700 ms (630 m) of sediments. The ridge tops are covered by sediments, while the flanks show no evidence of sediment cover. The uplifted sequence of sediments starting at kilometer 550 may be the edge of the Fram Basin. Unfortu-

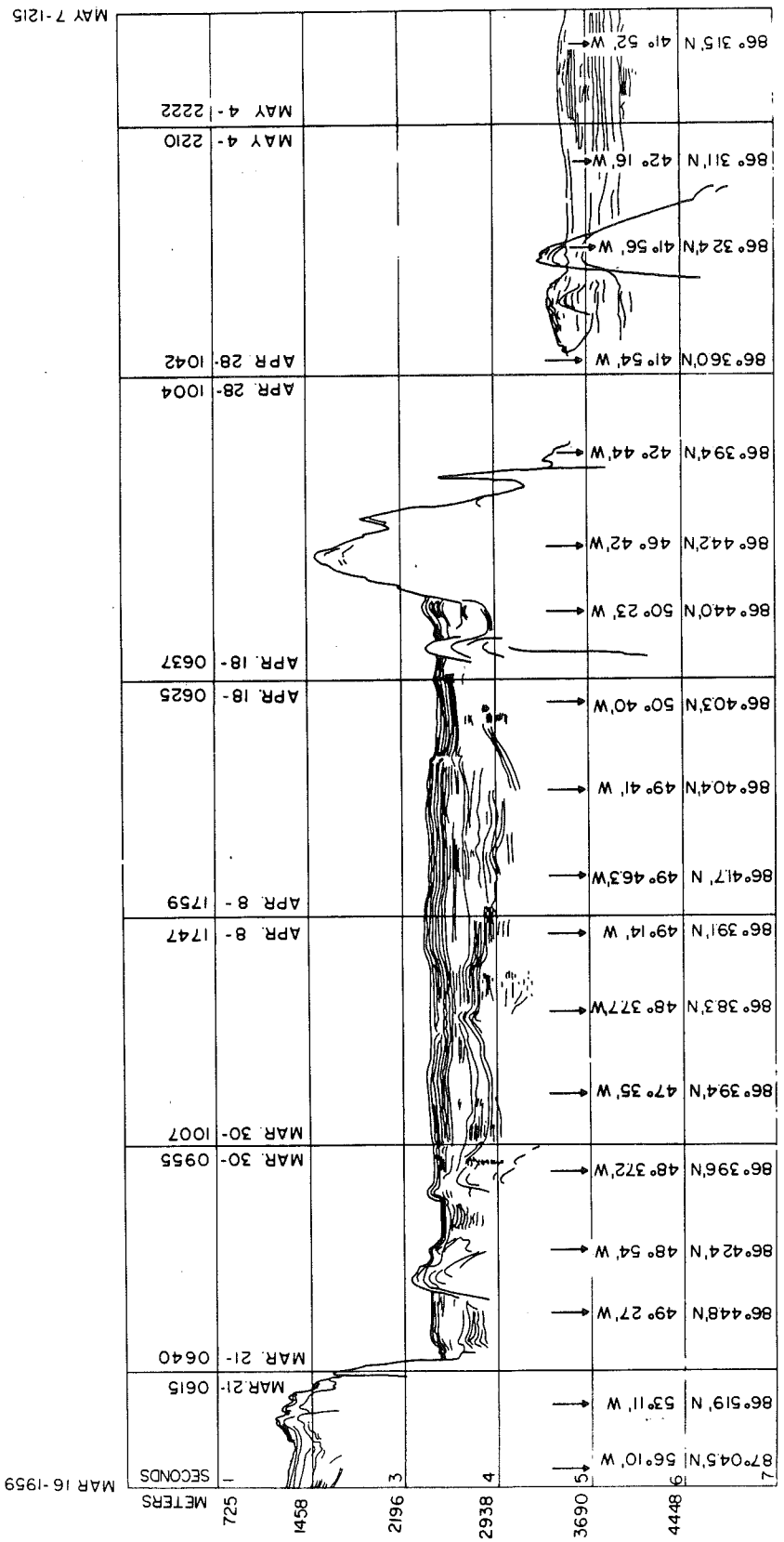

Fig. 8. ARLIS II subbottom profile over Fram flank of Lomonosov Ridge, profile EE' in Figure 9 (reproduced with permission from *Ostenso and Wold* [1973]). Horizontal scale is identified by geographical coordinates, date, and time. Time intervals divided by vertical lines represent seismic tapes. Intervals between geographical locations marked by arrows are referred to in this paper as segments. Vertical scale represents two-way travel time.

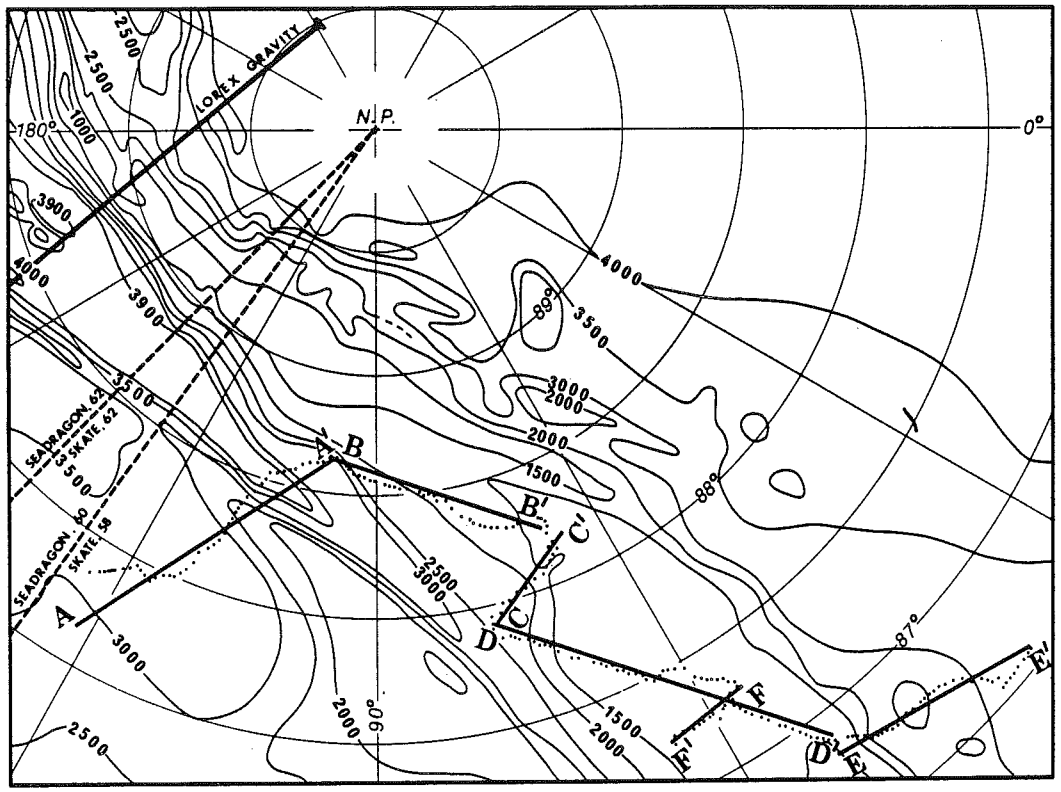

Fig. 9. Partial drift track of ARLIS II (dotted line from A to E') compiled from *Wold* [1973] and location of profiles AA' to EE' described in Figures 10*a*–10*d*. Drift convolutions and multiple tracks have been removed from the drift track. Also shown are the location of the LOREX gravity profile and the *Skate* and *Seadragon* submarine tracks of Figure 2. The background contour map was compiled from the LOREX and *Perry and Fleming* [1983] bathymetric maps.

nately, ARLIS II never entered the Fram Basin proper but skirted the Lomonosov flank to the Morris Jessup Rise.

The above description of the seabed topography of the normalized track differs from that given by *Ostenso and Wold* [1977] in that they regarded the Makarov-facing flank of the Lomonosov Ridge (kilometers 111–140, Figure 10*a*) as being the south flank of the Marvin Spur and the gap between kilometers 181 and 186 (Figure 10*b*) as concealing the north flank of Marvin Spur, the Makarov Basin, and the Makarov-facing flank of the Lomonosov Ridge. The excursion of the ice island back over the Makarov edge of the Lomonosov Ridge (kilometers 250–310, Figures 10*b* and 10*c*) was interpreted as an excursion over the Fram flank.

The basement relief located in the LOREX area about 60 km south of the Lomonosov Ridge (S_3 in Figure 2, kilometer 35 in Figure 7) has been interpreted as a ridgelike feature. It is clearly visible on each of the submarine echograms (arrows in Figure 5), and it is in line with the 1650 m near-vertical drop along the ARLIS II track about 25 km south of the Lomonosov Ridge (Figure 10*a*). The feature appears to diverge westward from the Lomonosov Ridge and is shown here to extend between at least 170°W and 100°W, a distance of over 200 km. Examination of the submarine echograms suggest that much of this escarpment is not a separate structure but belongs, morphologically, to the Alpha Ridge, forming its Makarov-facing boundary. It is separated from the Lomonosov Ridge by a grabenlike abyssal trough up to 60 km wide that between 140° and 150°W is underlain by thin (9 km) crust [*Mair and Forsyth*, 1982]. The seafloor to the south of the escarpment appears to rise irregularly toward the crest of the Alpha Ridge (Figure 5).

Crustal Density Model

The Lomonosov Ridge is a remarkably uniform, steep-sided, flat-topped feature, as illustrated in Figure 11, which shows the projection of the bottom topography and the free air anomalies of profiles BB', CC', DD', and FF' onto the extension of profile AA'. Of these overlapping profiles the whole of BB' and parts of DD' and FF' were used to construct a composite crustal model across the ridge along profile AA' and its extension eastward subparallel to the LOREX gravity profile GG' (Figure 2) nearly normal to the ridge crest (Figure 12). The block densities and depths are derived from the LOREX refraction and reflection seismic studies. Water depths over the Lomonosov Ridge and adjacent basins and the distribution of unconsolidated sediments are similar to those found in the LOREX area except that here the ridge is much wider (220 km compared to LOREX's 65 km) and the Makarov Basin is about half as wide.

Refraction seismic results from the FRAM II experiment [*Allen et al.*, 1980; *Duckworth et al.*, 1982] some 100 km to the east of E' (Figure 9) indicate that the Moho lies 11 km below the sea surface and that the Fram Basin crust is covered by 1.5–2 km of unconsolidated sediments and has no significant layer 2. In the composite gravity model (Figure 12) it is assumed that between the site of FRAM II and the Lomonosov Ridge the depth of the Moho increases to 12 km and the sediments, lying directly on layer 3, thicken to 2 km.

The Moho depth below the Lomonosov Ridge is taken from LOREX seismic results [*Mair and Forsyth*, 1982]. Sediment distribution and basement topography on the ridge are taken from ARLIS II subbottom profiles (Figure 10). The sedi-

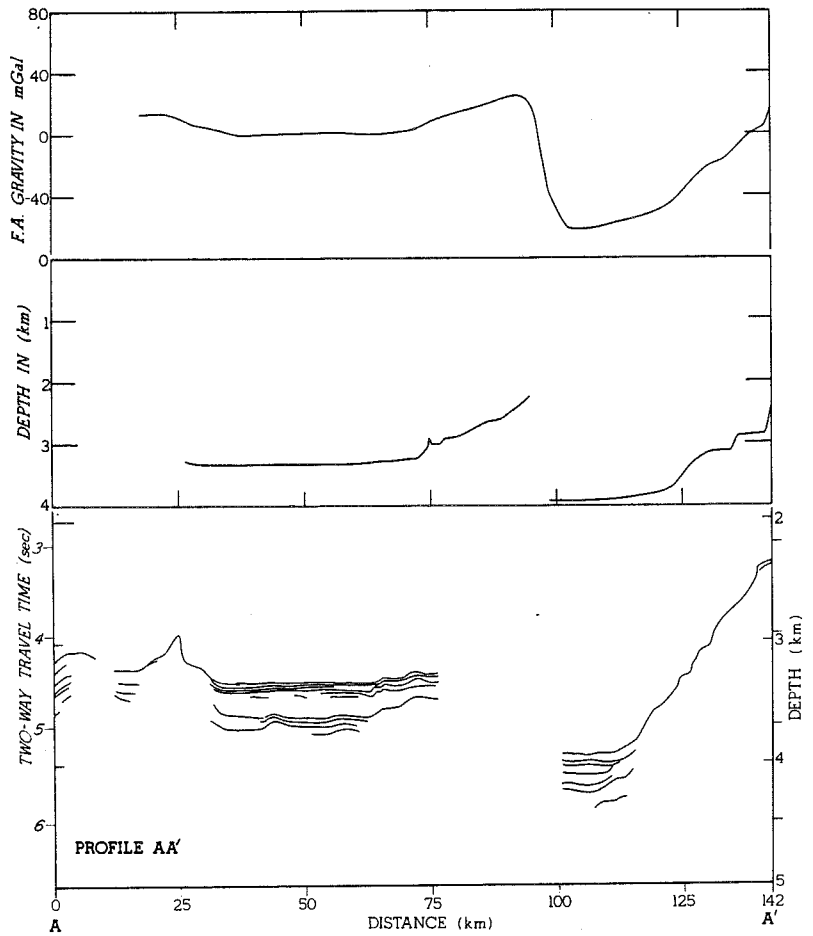

Fig. 10*a*. (Top) Free air gravity [from *Wold*, 1973]. (Middle) Water depth determined by echo sounder [from *Wold*, 1973]. (Bottom) Normalized and edited subbottom profiles [from *Ostenso and Wold*, 1977] along profile AA′ of Figure 9.

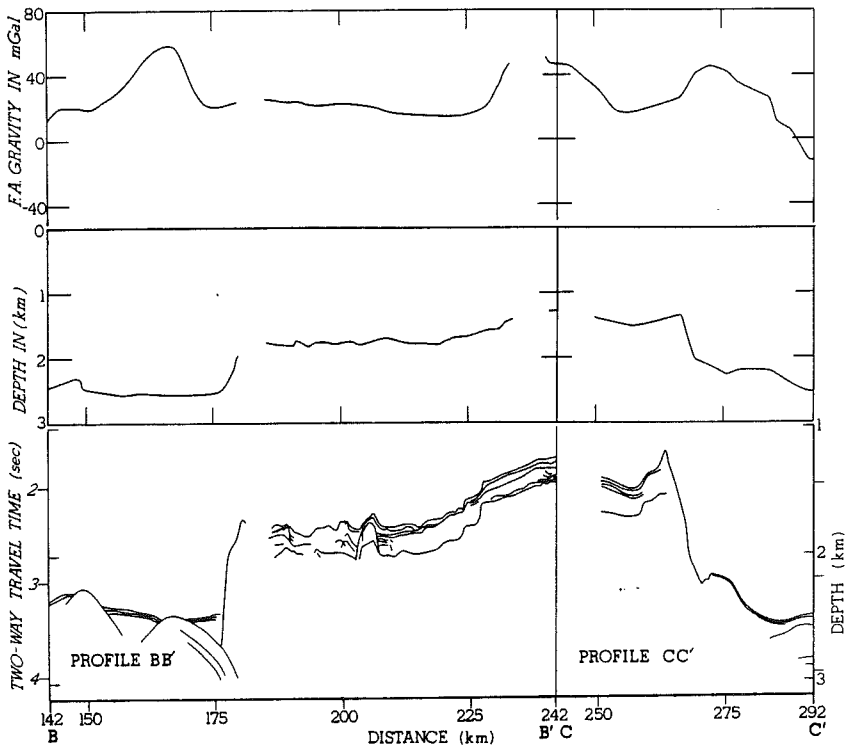

Fig. 10*b*. Same as Figure 10*a*; along profiles BB′ and CC′ of Figure 9.

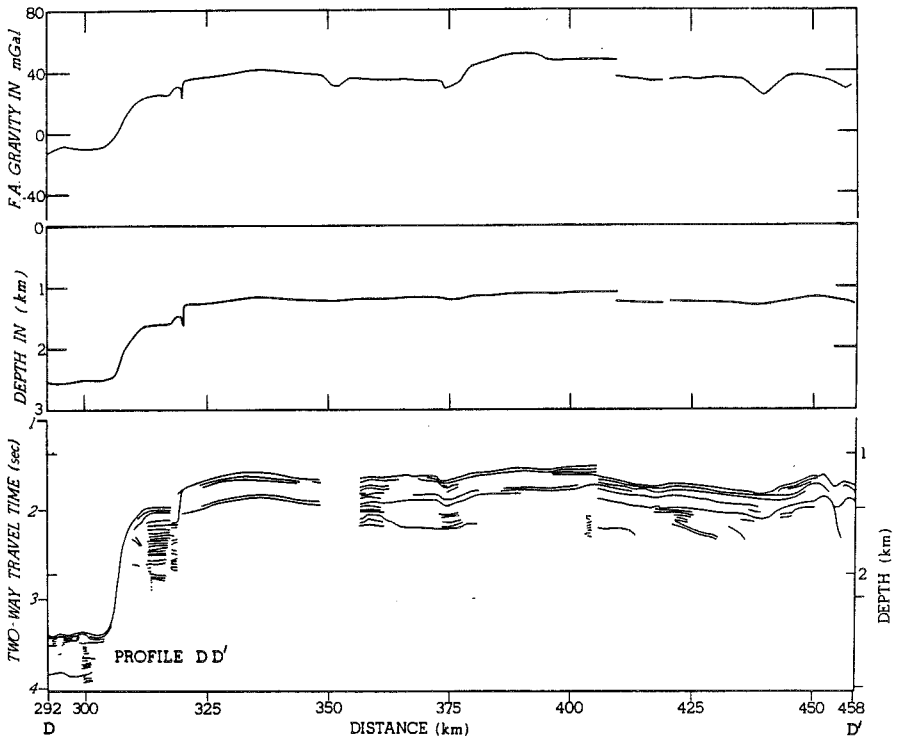

Fig. 10c. Same as Figure 10*a*; along profile DD' of Figure 9.

ments appear to have been deposited before the crest was faulted in the LOREX area [*Blasco et al.*, 1979]. In Figure 12 they are assigned a density of 2.2 Mg/m^3. The Makarov Basin is modeled using the crustal density structure established for the Fram Basin. This yields a crustal thickness for the Makarov Basin of about 10.5 km, similar to the thicknes derived in Figure 7.

On the basis of the submarine echograms (Figure 5) and the reworked ARLIS II data along profile AA' (Figure 10*a*), the Makarov-facing flank of the Alpha Ridge is represented by a steep escarpment of about 1700 m at kilometer 96 of the gravity model (Figure 12). This change in elevation is accompanied by a drop of 87 mGal in gravity with a gradient as steep as 22 mGal/km. The gravity gradient is somewhat larger than can be explained in reasonable geological and morphological terms. One reason for this may be that ARLIS II drifted over the escarpment at a greater speed than the average determined by this study for that particular drift segment.

The gravity high between kilometers 155 and 175 may be attributed to the effect of the two diapirs on profile BB' (kilometers 142–180, Figure 10*b*). However, the gravity gradients and amplitude are far too large to have been caused by density variations in the rocks only (a rock density of 7 Mg/m^3 would be required to cause such an anomaly through 2.5 km of water). The anomaly at kilometer 235 (Figure 10*b*) is similarly anomalous. The reasons for these anomalous gravity signatures are not known (R. J. Wold, personal communication, 1984), and accordingly, they are not modeled in Figure 12.

The density structure used below the Alpha Ridge closely matches that used beneath the Lomonosov Ridge on the presumption that the two features may once have been joined [*Mair and Forsyth*, 1982; *Sweeney et al.*, 1982]. A crustal thickness of 14–16 km for the northernmost part of the Alpha Ridge is thereby obtained, much thinner than the Lomonosov Ridge crust, to note, however, that there are few constraints on the density structure of the Alpha Ridge.

Discussion and Conclusions

The long, steep, and continuous escarpment along the western edge of the Makarov Basin is identified on older maps [e.g., *Heezen and Tharp*, 1975] as the Lomonosov-facing flank of the Marvin Spur, which was described by *Beal et al.* [1966] as a feature bisecting the Makarov Basin. Submarine echograms (Figure 5) and ARLIS II data reinterpreted here (Figures 10*a*–10*d*) indicate that the escarpment may be the Makarov-facing flank of the Alpha Ridge. It is distinct from *Sobczak*'s [1977] Marvin Seamounts to which S_1 and S_2 of Figure 1 belong. The LOREX gravity model (Figure 7) suggests that S_1 and S_2 are composed mainly of high-density rock. If this is so, then we may infer from their basement-sediment contacts (Figure 3*b*) that the Marvin Seamounts are volcanic features that were in place within the Makarov Basin early in its history before the onset of sediment deposition. The results presented here show that the Marvin Spur does not exist as a separate feature.

We have shown that in the region encompassed by the LOREX and ARLIS II surveys the Alpha Ridge is separated from the Lomonosov Ridge by a narrow grabenlike trough, part of the Makarov Basin, that appears to be a product of crustal extension judging from the structures present on the Lomonosov Ridge that indicate downfaulting toward the west. Within the trough, LOREX results show that linear magnetic anomaly highs are associated with basement relief close to the Lomonosov Ridge (P. Hood, personal communication, 1981). This part of the Makarov Basin, east of 160°W, may therefore not have been formed by typical seafloor spreading processes.

To the west of the 160°W meridian the Makarov Basin is

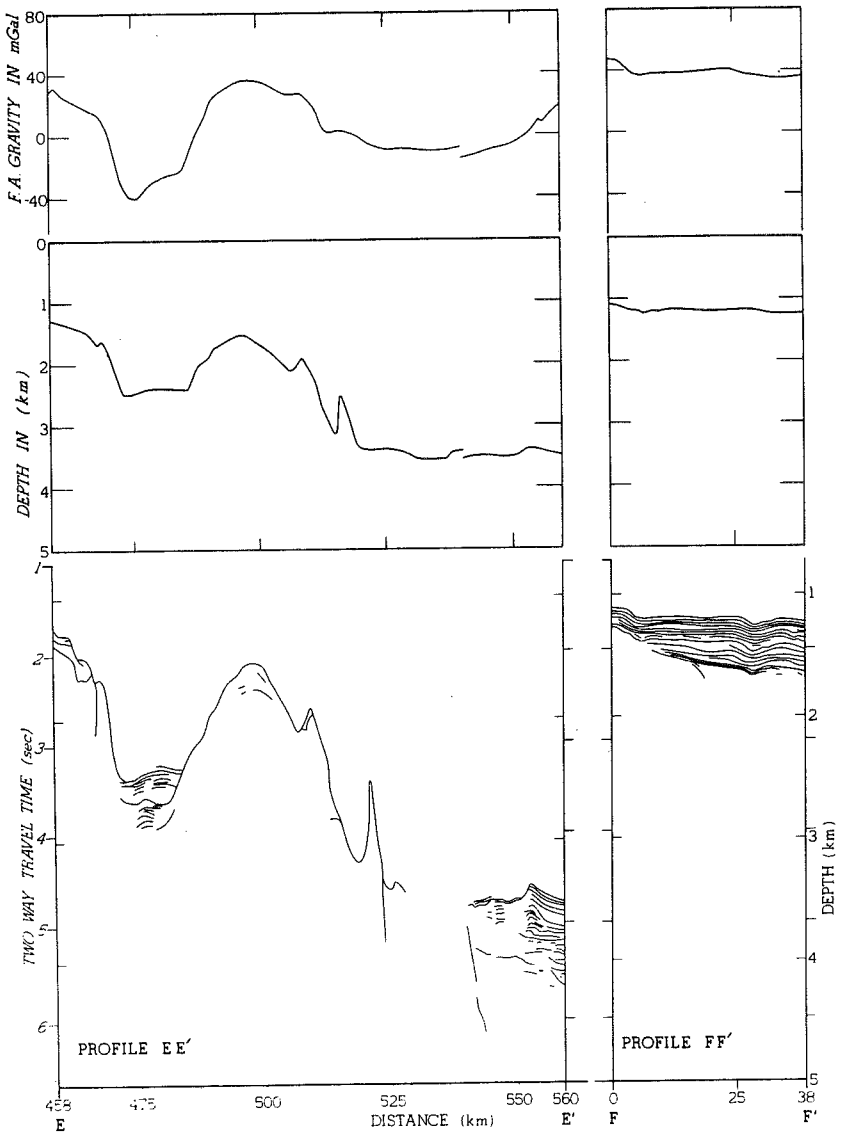

Fig. 10*d*. Same as Figure 10*a*; along profiles EE′ and FF′ of Figure 9.

appreciably broader (250 km wide on the *Sargo* echogram; Figure 5), and aeromagnetic data in this region show magnetic lineations that may represent a sequence of geomagnetic reversals associated with seafloor spreading [*Taylor et al.*, 1981]. Crustal thickness and structure are not known in this part of the basin, and *Vogt et al.* [1981] suggest that the magnetic lineations may be a topographic or structural effect.

The gravity interpretation of Figure 12 shows that a considerable difference in crustal thickness on opposite flanks of the Makarov Basin trough is produced if the Alpha and Lomonosov ridges are compositionally similar. The differences in Moho depth, if real, may indicate that a segment of the Alpha Ridge crust has been greatly stretched and thinned relative to the Lomonosov Ridge crust. This conclusion applies only to the Makarov-facing flank of the Alpha Ridge between 100° and 110°W (Figure 9), but the high intensity and, over short distances, the lineated character of the magnetic field over the entire Alpha Ridge relative to that over the Lomonosov Ridge [*Vogt and Avery*, 1974] may indicate that significant amounts

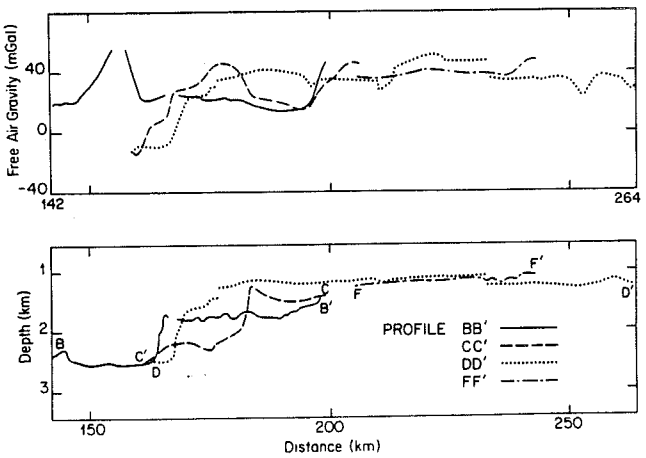

Fig. 11. Projection of seafloor topography and free air gravity anomalies of profiles BB′, CC′, DD′, and FF′ of Figure 9 onto the extension of profile AA′.

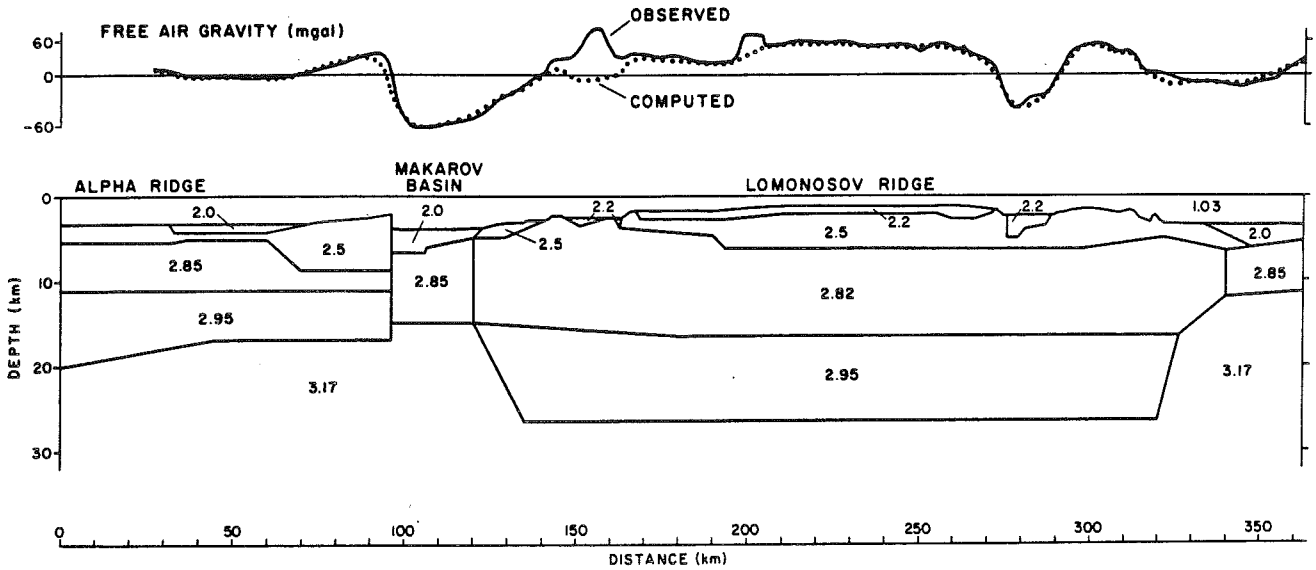

Fig. 12. Composite gravity density model across Lomonosov Ridge along profiles AA', BB', EE', and parts of CC' and FF' of Figure 9. Densities are in megagrams per cubic meter.

of mafic material have been injected into the Alpha Ridge as a whole along extensional faults during or after the time when the ridge was under tension. The Alpha Ridge could therefore be similar to the Lord Howe Rise northwest of New Zealand, as suggested by *Taylor* [1978] and *Taylor et al.* [1981] in that it is continental with abundant mafic volcanism.

The time of crustal stretching that created the Makarov Basin east of 160°W, faulted the Lomonosov Ridge, and, it is presumed, thinned the northernmost part of the Alpha Ridge is not known and more than one episode of extension may have taken place. It has been argued elsewhere [*Herron et al.*, 1974; *Sweeney et al.*, 1978] that for some period during the Cretaceous a compressional regime was produced in the Arctic when the pivot for the opening of the North Atlantic was located in northern Greenland. When the pivot position changed to the opposite side of the Arctic at the end of Mesozoic time [*Pitman and Talwani*, 1972], the north polar region was placed under tension. The extensional events that developed the central Arctic Basin may thereby be crudely restricted in time to post-Cretaceous and/or a distinctly earlier period prior to the opening of the North Atlantic.

Acknowledgments. Earth Physics Branch contribution 1131. LOREX contribution 21.

REFERENCES

Allen, B., J. Ardai, K. Hunkins, T. Lee, T. O. Manley, and W. Tiemann, Observations of position, ocean depths, and gravity taken from the FRAM II and Camp I drifting ice station, CU-13-80, *Tech. Rep. 13*, Lamont-Doherty Geol. Observ., Palisades, N. Y., Sept. 1980.

Beal, M. A., Bathymetry and structure of the Arctic Ocean, Ph.D. thesis, 205 pp., Oreg. State Univ., Corvallis, 1969.

Beal, M. A., F. Edvalson, K. Hunkins, A. Molloy, N. A. Ostenso, The floor of the Arctic Ocean: Geographic names, *Arctic*, *19*, 215–219, 1966.

Blasco, S. M., B. D. Bornhold, and C. F. M. Lewis, Preliminary results of surficial geology and geomorphology studies of the Lomonosov Ridge, Central Arctic Basin, *Current Res. Pap. 79-1C*, pp. 73–83, Geol. Surv. of Can., Ottawa, 1979.

Burkhanov, V., *New Soviet Discoveries in the Arctic*, 60 pp., Foreign Languages Publishing House, Moscow, 1956.

Duckworth, G. L., A. B. Beggeroer, and H. R. Jackson, Crustal structure measurements near FRAM II in the Pole Abyssal Plain, *Tectonophysics*, *89*, 173–216, 1982.

Forsyth, D. A., D. Dufresne, R. Jackson, and C. Pike, Crustal structure of Arctic Ocean floor ridges near the north pole (abstract), *Eos Trans. AGU*, *64*, 760, 1983.

GEBCO, General Bathymetric chart of the oceans, sheet 5.17; The Arctic Ocean, Can. Hydrogr. Serv., Ottawa, 1979.

Heezen, B. C., and M. Ewing, The mid-oceanic ridge and its extension through the Arctic Basin, in *Geology of the Arctic*, edited by G. O. Raash, pp. 622–642, University of Toronto Press, Toronto, 1961.

Heezen, B. C., and M. Tharp, American Geographic Society map of the Arctic region, Lamont-Doherty Geol. Observ., Palisades , N. Y., 1975.

Herron, E. M., J. F. Dewey, and W. C. Pitman, Plate tectonics model for the evolution of the Arctic, *Geology*, *2*, 377–380, 1974.

Jackson, H. R., I. Reid, R. K. H. Falconer, Crustal structure near the Arctic mid-ocean ridge, *J. Geophys. Res.*, *87*, 1773–1783, 1982.

Lillestrand, R. L., and J. R. Weber, Plumbline deflection near the north pole, *J. Geophys. Res.*, *79*, 3347–3352, 1974.

Mair, J. A., and D. A. Forsyth, Crustal structures of the Canada Basin near Alaska, the Lomonosov Ridge and adjoining basins near the north pole, *Tectonophysics*, *89*, 239–254, 1982.

Mathews, D. J., Tables of the velocity of sound in sea water for use in echo-sounding and sound ranging, *Admiralty Table HD 282*, Hydrogr. Dep., Admiralty, London, 1939.

Nagy, D., The gravitational effect of two-dimensional bodies of arbitrary shape, program writeup, Gravity and Geodyn. Div., Earth Phys. Branch Dep. of Energy, Mines and Resources, Ottawa, Aug. 1980.

Ostenso, N. A., Geophysical studies in the Greenland Sea, *Geol. Soc. Am. Bull.*, *79*, 107–132, 1968.

Ostenso, N. A., and R. J. Wold, A seismic and gravity profile across the Arctic Ocean Basin, *Tectonophysics*, *37*, 1–24, 1977.

Overton, A., A seismic reflection profile across the Lomonosov Ridge, Central Arctic Ocean, paper presented at the Soc. 52nd Annual Meeting, Soc. of Explor. Geophys., Dallas, Tex., Oct. 17–21, 1982.

Perry, R. K., and H. S. Fleming, Bathymetry of the Arctic Ocean, Polar sterographic projection, scale 1–4,704,075, Nav. Res. Lab., Office of Nav. Res., Arlington, Va., 1983.

Pitman, W. C., III, and M. Talwani, Seafloor spreading in the North Atlantic, *Geol. Soc. Am. Bull.*, *83*, 619–646, 1972.

Popelar, J., J. Kouba, and D. E. Wells, LOREX 79: Satellite positioning, *Internal Rep. 81-2*, Earth Phys. Branch, Dep. of Energy, Mines and Resour., Ottawa, 1983.

Smith, P. J., Plumbing at the north pole, *Nature*, *251*, 673–674, 1974.

Sobczak, L. W., Bathymetry of the Arctic Ocean north of 85°N latitude, *Tectonophysics*, *42*, T27–T33, 1977.

Sobczak, L. W., Bathymetry of the Arctic Ocean, *Publ. Earth Phys. Branch*, *45*, 67–73, 1978.

Sweeney, J. F. LOREX gravity: Implications for Lomonosov Ridge composition and compensation (abstract), *Eos Trans. AGU, 61*, 277, 1980.
Sweeney, J. F., E. Irving, and J. Geuer, Evolution of the Arctic Basin, *Publ. Earth Phys. Branch, 45*, 91–100, 1978.
Sweeney, J. F., J. R. Weber, and S. M. Blasco, Continental ridges in the Arctic Ocean: LOREX constraints, *Tectonophysics, 89*, 217–238, 1982.
Taylor, P. T., Low-level aeromagnetic data across the western Arctic Basin (abstract), *Eos Trans. AGU, 59*, 268–269, 1978.
Taylor, P. T., L. C. Kovacs, P. R. Vogt, and G. L. Johnson, Detailed aeromagnetic investigations of the Arctic Basin, 2, *J. Geophys. Res., 86*, 6323–6333, 1981.
Vogt, P. R., and O. E. Avery, Tectonic history of the Arctic basins: Partial solutions and unsolved mysteries, *Marine Geology and Oceanography of the Arctic Seas*, edited by Y. Herman, pp. 83–117, Springer-Verlag, New York, 1974.
Vogt, P. R., C. Bernero, L. Koracs, and P. Taylor, Structure and plate tectonic evolution of the marine Arctic as revealed by aeromagnetics, *Proc. Int.* Geol. Cong., *26th*, 25–40, 1981.
Weber, J. R., The Lomonosov Ridge Experiment: LOREX 79, *Eos Trans. AGU, 60*, 715–721, 1979.
Weber, J. R., Exploring the Arctic sea floor, *Geos, 9*, 2–7, 1980.
Weber, J. R., Maps of the Arctic Basin sea floor: A history of bathymetry and its interpretation, *Arctic, 36*, 121–141, 1983.
Wilson, J. T., Hypothesis of the earth's behaviour, *Nature, 198*, 925–929, 1963.
Wold, R. J., Gravity surveys of the Arctic Ocean Basin, final report, 222 pp., Univ. of Wis., Dep. of Geol. Sci., Milwaukee, 1973.

J. F. Sweeney, Pacific Geoscience Centre, Box 6000, Sidney, B. C., Canada V8L 4B2.
J. R. Weber, Department of Energy, Mines and Resources, Earth Physics Branch, Gravity, Geothermics and Geodynamics Division, 1 Observatory Cresent, Ottawa, Ontario, Canada K1A 0Y3.

(Received June 25, 1983;
revised August 9, 1984;
accepted August 24, 1984.)

PRELIMINARY RESULTS OF SURFICIAL GEOLOGY AND GEOMORPHOLOGY STUDIES OF THE LOMONOSOV RIDGE, CENTRAL ARCTIC BASIN

Project 780048

S.M. Blasco, B.D. Bornhold[1], and C.F.M. Lewis
Atlantic Geoscience Centre, Dartmouth

Blasco, S.M., Bornhold, B.D., and Lewis, C.F.M., Preliminary results of surficial geology and geomorphology studies of the Lomonosov Ridge, Central Arctic Basin; in Current Research, Part C, Geological Survey of Canada, Paper 79-1C, p. 73-83, 1979.

Abstract

Bathymetric subbottom and shallow seismic reflection profiling, sediment sampling, seabed photography and water column temperature and sound velocity profiling, as well as surface plankton tows, were conducted in April and May 1979 from the ice station ***LOREX*** *as it drifted over the Lomonosov Ridge close to the North Geographic Pole. These seabed geologic studies, in conjunction with other scientific programs, were undertaken to delineate the physical nature and origin of this little-known Arctic submarine feature. The Lomonosov Ridge has a relief of 2800 m and a width of 88 km along the drift path. Asymmetrical in cross-section, the Amerasian flank has slopes as steep as 12 whereas the Eurasian flank slopes are less than 7°. The ridge appears to consist of en echelon fault blocks that give the crest an irregular morphology. A thin veneer of unconsolidated sediments, primarily deposited on the fault block tops, is presently undergoing erosion by current action. These sediments were probably deposited prior to the assumed separation of the ridge from the Barents Continental Shelf. The presence of dinoflagellate* ***Luxadinium propalulum*** *in the surface material recovered from the ridge crest suggests that this separation was initiated no earlier than mid-Cretaceous. Observed thermal alteration of this species could have occurred during the early stages of spreading along the Nansen-Gakkel rift.*

Introduction

The Lomonosov Ridge, linear in form, aseismic in nature, extends across the floor of the Arctic Ocean a distance of 1800 km from the continental shelf adjacent to the New Siberian Islands and to the shelf north of Ellesmere Island and Greenland. This submarine ridge system separates the Amerasian and Eurasian basins as it rises some 3000 m from the abyssal plains to a depth of 1000 m below sea level. Ridge width varies from a maximum of 200 km in proximity to the continental shelves to a minimum of 25 km near the North Geographic Pole.

From March 29 to May 29, 1979, the writers participated in the Lomonosov Ridge Experiment (LOREX) located on a drifting ice floe some 90 km from the pole (Fig. 12.1). The objective of this Earth Physics Branch, multidisciplinary project was not only to define more clearly the geologic nature and origin of the Lomonosov Ridge, but to develop the Canadian expertise for conducting such research from a floating ice platform. The scope of the writers' participation was to conduct comprehensive seabed geological studies of this ridge feature and adjacent areas of the Makarov and Fram basins. This involved seabed photography and sediment sample recovery, acoustic profiling and surface plankton sampling.

With Transit satellite receivers and Omega navigation systems providing positioning control (with an accuracy of ± 100 m for the satellite fixes and ± 1 km for the Omega), the **LOREX** ice station drifted a net 160 km during the 62 day program. Drift rates varying from 0 to 1200 m per hour were recorded. The closest **LOREX** was to the pole was 35 km, reached on May 17. During the program the ice floe crossed the Lomonosov Ridge once, approaching approximately

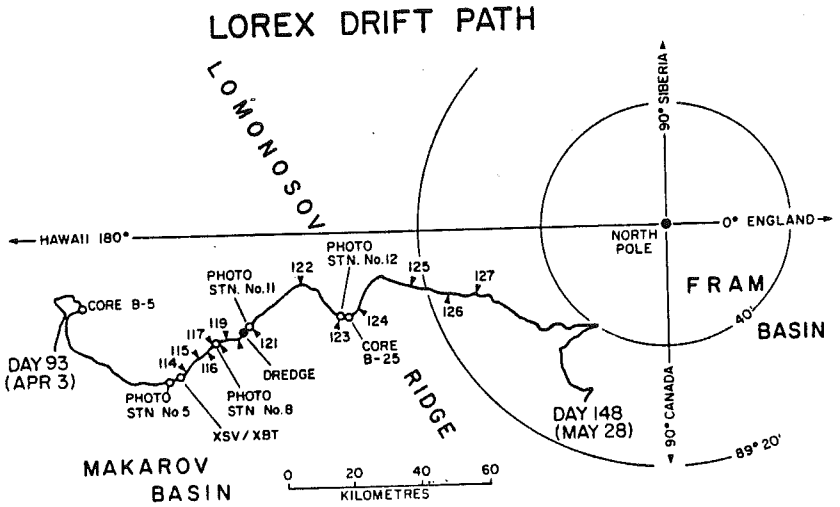

Figure 12.1. *Drift track of* ***LOREX*** *main ice camp from April 3 to May 28, 1979. Time is recorded in Julian days (GMT) and can be related to the bathymetric and seismic profiles (Fig. 12.6, 12.7). Core, dredge, photography and XSV/XBT stations referred to in the text are also located.*

[1]Regional and Economic Geology Division, Pacific Geoscience Centre, 9860 West Saamich Rd., Sidney, British Columbia, V8L 4B2

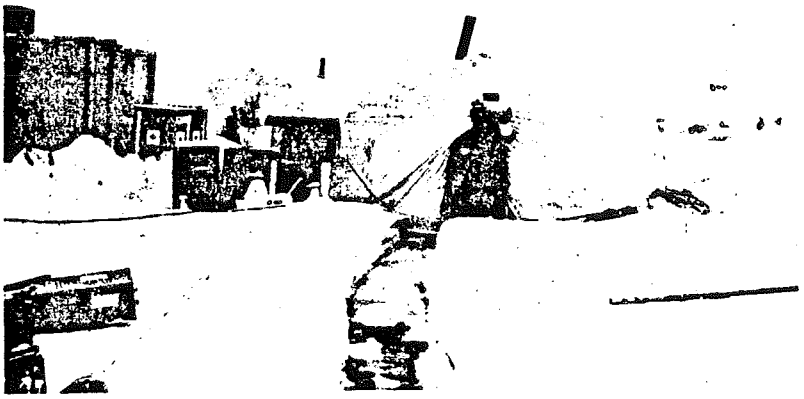

Figure 12.2

Following several hours of high winds in excess of 45 km/h cracks and leads opened up along and across the runways as well as under the marine geology camp. Part of this camp was relocated on more stable ice. (BIO Photo 5415-2).

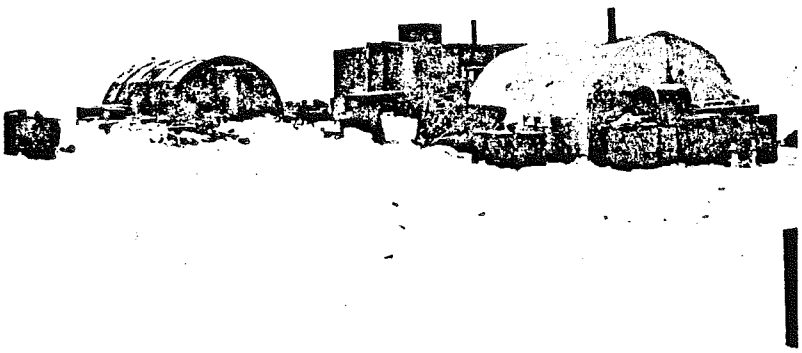

Figure 12.3

The longhouse tent, insulated plywood prefab and parcoll housed the equipment and facilities required for the marine geology program. This program used 1100 L of fuel (250 gal) per week for heat and power (BIO Photo 5300-28)

Figure 12.4

Undertaking the arduous task of cutting one of the four hydroholes needed for the operation. Augers (shown here), chain saws and ice chisels were employed. This process had to be repeated when the camp was moved (BIO Photo 5300-297)

normal to its axis from the Makarov basin, but trailing off at an angle to the axis towards the Fram basin (based on remote bathymetric observations from the main camp).

Having taken 9 days to set up and 3 days to break camp, the following data were collected from April 8 through May 26:

- 42 gravity cores (0.2 to 1.7 m long)
- 10 grab samples
- 4 dredge stations
- 14 seabed photography stations
- 1060 hours of continuous 3 kHz bathymetric, subbottom profiling
- 880 hours of continuous, high resolution, shallow seismic, airgun reflection profiling
- 31 expendable sound velocity profiles
- 11 expendable bathythermograph profiles, and
- 14 plankton tows.

Scientific activities were interrupted May 3 to 7 while the acoustic instrumentation and support facilities were transferred to a new location (Fig. 12.2). Unstable ice conditions made the original site unsafe for continued work.

Logistics and Instrumentation

The 'surficial marine geology' program occupied three heated enclosures (Fig. 12.3). A longhouse tent housed generator, compressor, winch hydraulics, workshop and a 1.5 m by 0.5 m hydrohole (Fig. 12.4) to accomodate the subbottom transducer array. An insulated plywood 'prefab' hut contained an array of sampling, photographic, and electronics equipment, and the winch assembly with 6000 m of 5 mm diameter Kevlar cable, sheave frame, and a 1 m diameter hydrohole through which instruments were lowered to the seafloor. A parcoll housed the acoustics instrumentation, a 0.5 m diameter hydrohole for the airgun electronics repair shop, photo lab, drafting table and quarters for two personnel who monitored the acoustics equipment. Bathymetric subbottom profiling instrumentation included an ORE 8 element transducer array and transceiver assembly interfaced with an EPC graphic recorder. The transducer array was mounted in a rigid aluminium frame and suspended in a hydrohole 3 m below ice surface. A central programmer fired the transducer on a one minute interval and triggered the recorder (on a one second sweep rate). This system was tuned to 3 kHz and operated at the 6 kW power rating. Both linear and time varying gain amplification were used.

One 164 cm^3 (10 cubic inch) Bolt airgun and a single active MIT designed hydrophone were the source-receiver equipment used for the high resolution, shallow seismic reflection profiling. Optimum source-receiver separation was determined by monitoring return signals while varying the geometry. This minimized the acoustic interference due to ghosting, camp and ice noise. The airgun was deployed through the hydrohole in the parcoll and tied off 5 m below ice surface. The hydrophone, located 34 m away from the airgun was suspended 6 m below ice surface through a 15 cm hydrohole. Attempts to keep this hole from freezing by filling it with diesel fuel were not very effective, and the hydrophone cable did freeze in. This coupling to the ice unfortunately increased the background noise level. The other hydroholes were kept open with standard lightbulbs suspended close to the base of the hole. A 210 L min^{-1} diesel driven Bauer compressor filled a bank of five, 8.5 m^3 capacity compressed air cylinders to 183 k/cm^2 (2600 psi). An additional 1.5 m^3 tank containing de-icer solution allowed the circulation of vapourized de-icer through the air hoses and airgun to prevent freezing in the intense cold, especially with slow firing rates. With the airgun firing at 113 kg/cm^2 (1600 psi) on a one minute interval, the compressor was needed twice daily for 2.5 hours per run.

Analog signal processing of the reflected pulse included linear pre-amplification followed by passband filtering of 125 Hz to 8 kHz and time varying gain amplification. The processed output was displayed on a second EPC graphic recorder while the 'raw' signal was recorded on a Racal tape transport. The central programmer, previously mentioned, fired the airgun 30 seconds after the subbottom system (to prevent interference) triggered the graphic recorder (on a 2 second sweep rate) and started the tape transport. A variety of source triggering rates was available to accommodate major variations in ice drift speed but the one minute interval was used throughout the survey. In addition, programmable time delay from 0 to 9.9 s was available in 100 ms increments to allow for the elimination of the water column on both acoustic records. The choice and arrangement of acoustics instrumentation for this type of operation was effective and reliable.

To provide for the accurate conversion of travel times to bathymetry, Sippican Corporation's new, 2000 m expendable sound velocimeters (XSV's) were used. These devices employ the 'sing-around' frequency principle and a known fall velocity. The system generates a profile of sound velocity versus depth with a velocity accuracy of ± 0.25 ms^{-1} and a depth accuracy of ± 2 per cent (Balboni and Walsh, 1978). These extended depth probes were released from a handheld launcher and dropped through the sampling hydrohole, taking approximately 6 minutes to fall 2000 m. Returning signals were fed into a processor and this output displayed on a Sippican strip chart recorder. Water column velocities used in this report were determined by analyzing these profiles.

In addition, the Sippican 1830 m expendable bathythermograph (XBT) probes were deployed in the same manner. The results were used to assess the relationship of sound velocity with temperature. Temperature readings had an accuracy of $\pm 0.2°C$ (Sippican Corporation, 1978).

Sediment sampling equipment included a 118 kg, Benthos gravity corer used with 2.4 m lengths of 67 mm (inside diameter) plastic liner sharpened at the end. This configuration, with controlled drop rates (approximately 1 ms^{-1}), provided optimum penetration in cohesive clays. Where less cohesive sediments were anticipated, a cutter and retainer were attached to the liner. In areas of unknown sediment cover, a steel barrel complete with cutter, retainer and liner were used. A 60 kg Shipek grab sampler was effective in retrieving surface sediment samples. A small 35 kg dredge with a 1 m^2 rectangular opening, was also deployed for periods of 4.5 to 6 hours. Plankton were retrieved in vertical tows from 300 m to surface at 30 m min^{-1}, in a 200 mesh net with a triangular 0.5 m^2 opening.

Seabed photography was accomplished by deploying the Bedford Institute's Arctic marine camera system (Fenerty, 1978). The camera and flash units were triggered when a compass-vane assembly, hanging 2.5 m below the camera frame, touched bottom. This contact interrupted signal transmissions from a 12 kHz pinger mounted on the frame. The pinger output was monitored on surface. With the lapse in signal the system operator stopped the winch. Raising and lowering the camera frame one metre or so, on a 10 to 60 second interval (depending on the ice drift rate) allowed for the generation of overlapping photographs of the seafloor. Each frame covered a 3.2 m^2 area of seafloor. Thirty-five millimetre black and white and colour photographs were taken. In a similar manner the National Geographic Society acquired still photographs and colour film footage.

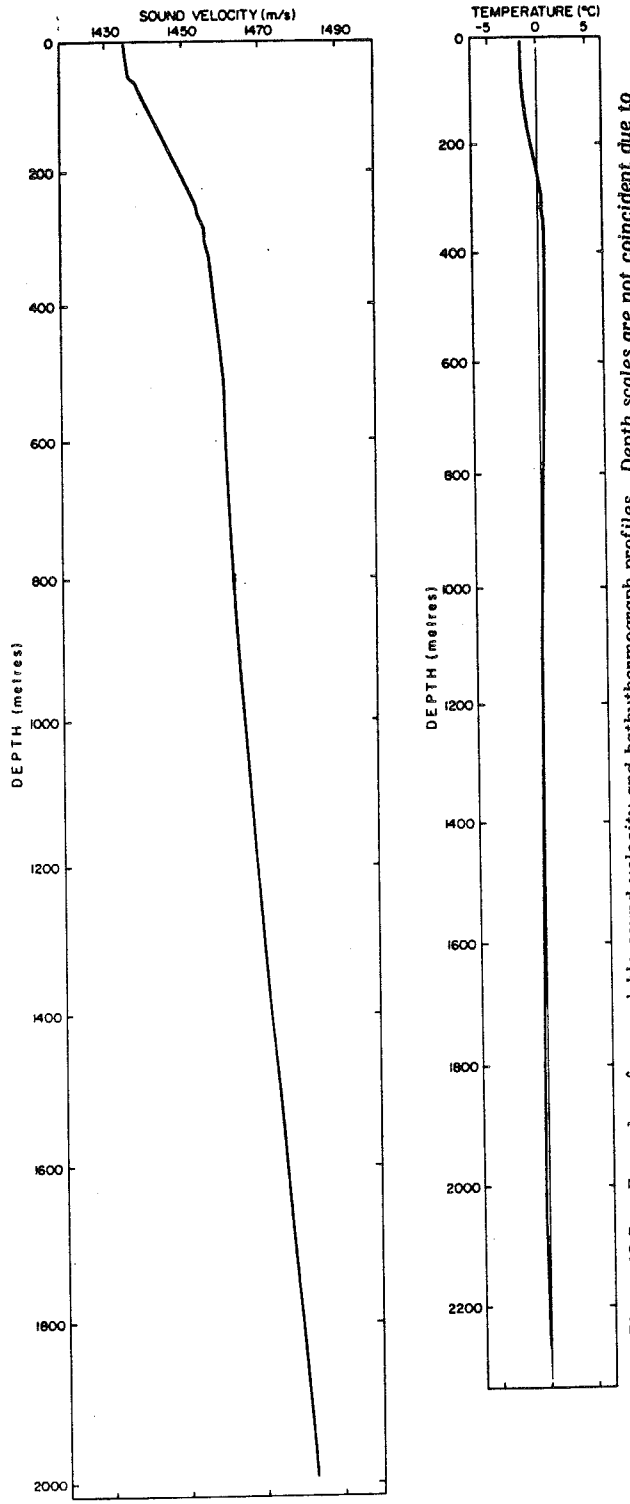

Figure 12.5. *Examples of expendable sound velocity and bathythermograph profiles. Depth scales are not coincident due to differing drop rates of the two probes.*

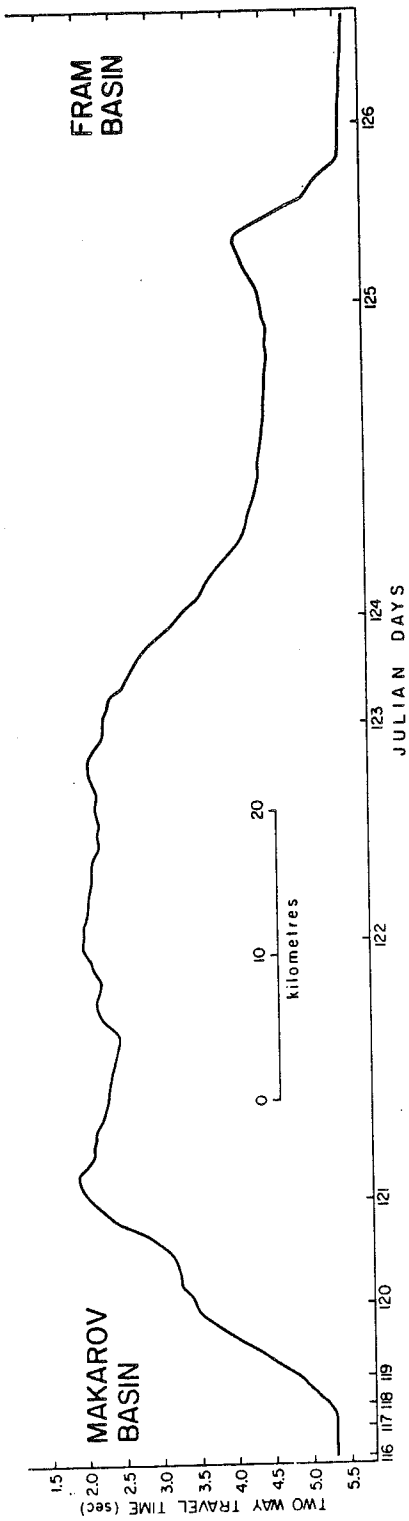

Figure 12.6. *Bathymetric profile of the Lomonosov Ridge along the drift path from the Makarov Basin to the Fram Basin. The profile has been corrected for variations in drift rate only.*

Observations

Bathythermograph and Sound Velocity Profiles

Although not all the XSV/SBT profiles have been analyzed, there appear to be only subtle differences between the Makarov and Fram profiles. Excellent examples of an XBT and XSV profile collected 240 m apart in the Makarov Basin (Fig. 12.1) in 3948 m of water are shown in Figure 12.5. The XBT profile extended to 2270 m before the probe sheared off. The temperature gradient increases evenly from a surface reading of -1.6°C to 0° at a depth of 245 m and to a maximum of 0.6° at 400 to 550 m. The temperature then decreases to 0° again at 1050 m and to a minimum of -0.3° at the base of the profile. The maximum temperature difference along the profile is 2.2°C. Surface temperatures are known to be -1.8°C (A.S. Judge, pers. comm., 1979). The recorded -1.6° is within the ±0.2° error of the XBT's. Also, contact of the XBT wire with the ice at the edge of the hydrohole caused premature termination of some of the profiles.

The XSV probe dropped to 1975 m before shearing off. Probe contact with seawater triggered the recorder but the sound velocity was not printed until 7 m. The reason(s) for this is unknown. Battery activation time and/or initial aeration on the transducer face are possible causes. Three distinct velocity 'zones' can be observed. From 7 to 58 m the velocity appears to increase slightly from 1435 to 1437 ms^{-1}, in response to pressure increase alone. The temperature is constant and probably salinity too in this mixed layer. From 58 m to 280 m the velocity gradient increases rapidly to 1455 ms^{-1}. With a maximum temperature difference of 2.2°C and the temperature and pressure gradients increasing evenly with depth, this increase in velocity is probably due to significant increases in salinity. R. Moore (pers. comm., 1979) confirms this. His **LOREX** salinity studies indicate an increase from approximately 30 to 34 parts per thousand in this zone. From 280 m to 1975 m the sound velocity increases primarily in response to increasing pressure. An integrated average velocity over this and other profiles to 2000 m was 1465 ms^{-1}. Assuming a linear increase in velocity to seabed an integrated average sound velocity from 0 to 4000 m was determined to be 1483 ms^{-1}.

Acoustics

Continuous bathymetric (Fig. 12.6) subbottom and shallow seismic reflection profiles were obtained over the Lomonosov Ridge from Makarov Basin to Fram Basin. The Makarov Basin itself, in close proximity to the ridge is flat with a consistent bathymetry of 5.325 s (3948 m at 1483 ms^{-1}). Local relief of 35 to 75 m on the seafloor reflects the presence of subbottom structures. Some 100 ms (75 m at 1500 ms^{-1} (Demenitskaya and Kiselev, 1968)) of well stratified, conformable, unconsolidated sediments are evident on the subbottom profile. Individual reflectors are 2 to 8 ms (1.5 to 6 m) apart, and some pinch out along the drift track. Variations in record intensity suggest differences in sediment density and/or texture. A minimum of 1.2 seconds (1080 m at 1800 ms^{-1} (Demenitskaya and Kiselev, 1968)) of these undisturbed, stratified sediments infills the Makarov basin adjacent to the ridge (Fig. 12.7). The underlying acoustic unit, bedrock, has an irregular morphology that is responsible for the local relief mentioned earlier. The unconsolidated sediments abut unconformably against these irregularities. The bedrock appears acoustically unstratified. The unit may be massive but more likely the limited output power of the small airgun coupled with the high frequency spectrum recorded prevented much resolution. This lower acoustic unit rises abruptly to form the core of the Lomonosov Ridge, the unconsolidated sediments abutting the flanks (Fig. 12.7).

The 'Makarov' flanks of the ridge rise steeply with 12° slopes to a peak at 1.907 seconds (1392 m at 1460 ms^{-1}) over a drift path of 36 km. Sediment thickness on these flanks is minimal, less than 2 ms on the subbottom profile. The morphology of the ridge crest is somewhat irregular (see Fig. 12.6). Three additional peaks at 2.157, 1.995 and 2.087 seconds were crossed. Unconsolidated sediments lie on the 'Fram'-facing flanks or slopes. These sediments are thin, 20 to 40 ms thick (18 to 36 m at 1800 ms^{-1}), are stratified and appear conformable with the underlying bedrock. The morphology of the 'Fram' flank is more variable, giving the ridge an assymetrical profile along the drift path. Slopes as great as 7° were observed on this flank. A transect normal to the ridge axis would still be assymetrical but less exaggerated.

Like the Makarov Basin, the unconsolidated sediments in the Fram Basin are well stratified, conformable and undisturbed. They also exceed 1.2 s (1080 m) in thickness and abut the ridge structure. However, no local relief due to high amplitude irregularities in the underlying bedrock was intersected, and the seafloor in the Fram Basin was consistently flat with a bathymetry of 5.668 s (4203 m at 1483 ms^{-1}). The maximum relief of the ridge is 2800 m. If the unconsolidated sediments flanking the ridge are ignored this relief is 3500 m. The apparent width of this feature along the drift path is 88 km, its true width at this location being somewhat less.

The acoustic profiles indicate the ridge consists of fault blocks, en echelon. The unconsolidated sediments are primarily associated with the block tops and not the fault faces, suggesting that these sediments were deposited prior to faulting.

Sediments

Sediments from the Makarov Basin include dense brown silts to sandy, clayey silts and firm, thinly layered grey brown clays. Core B-5, 166 cm long, recovered from 3948 m of water (see Fig. 12.1), was examined briefly in the field. Its stratigraphy consisted of 9 cm of soft homogeneous, dark brown silty clay at surface that graded into 87 cm of firm, thinly bedded, dark greyish brown clay. Underlying these units were 57 cm of interlayered dark greyish brown silt and olive brown clay in sharp contact with 13 cm of underlying dark brown, firm homogeneous clay. These distinct sediment types and their stratigraphic relationship are suggestive of interbedded pelagic and turbidite sequences, although grading and other diagnostic physical characteristics were not observed, and detailed sedimentological analyses have yet to be completed.

Sediments from the Fram Basin appear similar in stratigraphy and lithology except for a predominance of firm clays. Layering in these sediments is more obvious and is well defined by marked and abrupt changes in colour from light browns to grey browns. Sediment samples from the ridge itself have a greater proportion of coarse grained material, the sand sized fraction consisting primarily of quartz, with minor feldspar, dark minerals, lithic fragments, worm tubes, foraminifera tests and shell fragments. A 30 cm^3, botryoidal shaped manganese nodule (Fig. 12.8) and a 70 cm^3 subangular, manganese coated, recrystallized, dolomitized piece of chalk were recovered from a single dredge sample in 3190 m of water on the Makarov slopes of the ridge. Neither sample is thought to be 'in situ' and may have been moved into its present position as a result of slumping. The chalk fragment may have been ice rafted, but more probably, and significantly, its origin could be the ridge itself.

The organic-walled microfossils (palynomorphs) from the top 3 cm of core B-25 were briefly examined by J. Bujak of the Atlantic Geoscience Centre. The core was 154 cm

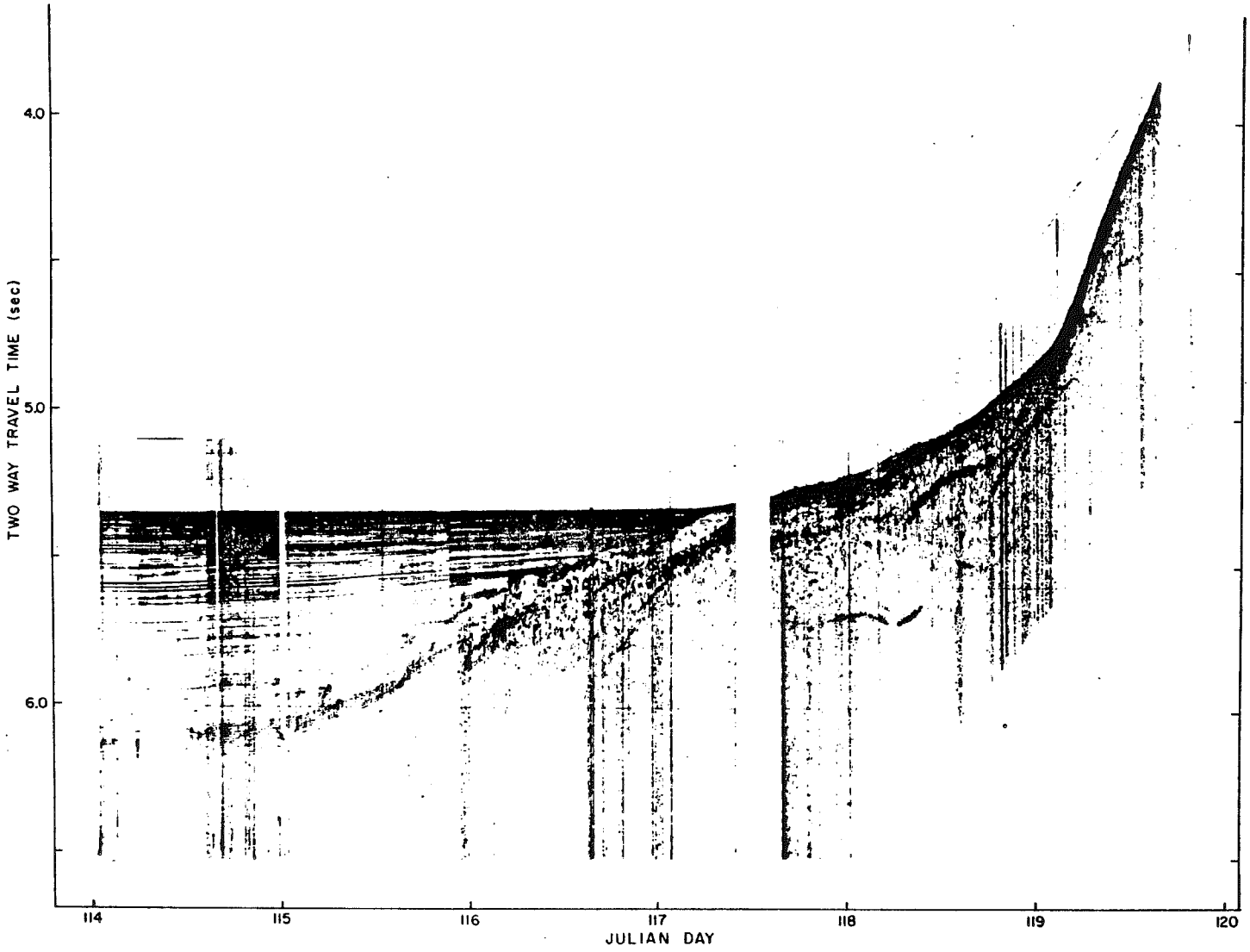

Figure 12.7. *Segment of the high resolution shallow seismic reflection profile adjacent to the Makarov flank of the Lomonosov Ridge. Blank area represents data loss due to equipment failure. The sediments thicken towards the centre of the Makarov Basin. The profile has not been corrected for variations in drift rate.*

long and was taken in 1721 m of water on the Fram flank of the ridge. Preliminary analysis revealed three distinct populations; disaccate pollen of Late Cenozoic age, spores and dinoflagellates (including the high latitude species **Luxadinium propalulum**) of mid-Cretaceous age and poorly preserved spore fragments of **Hystricosporites** or **Ancyrospora** of probable Devonian age. The relative abundance of the Cenozoic, Mesozoic and Paleozoic assemblages is roughly 1 to 7 to 2. The dinoflagellates and spores show significant thermal alteration whereas the Cenozoic pollen is unaltered.

Seabed Photography

Preliminary examination of the 900 black and white and 200 colour photographs of the seafloor provided a wide variety of benthic observations, some similar to those described by Hunkins et al. (1970). In the deepest waters of the Makarov and Fram basins, the soft sediments record several generations and types of winding biogenic tracks and trails some possibly generated by molluscs and bottom feeding fish (Fig. 12.9). In one frame the imprints of fin marks are found on either side of a track. Small mounds, depressions and burrows created by crustacea and other benthic organisms are also common features. In one photograph (Fig. 12.10) three crustacea, approximately 8 cm long, appear to be feeding off organic matter stirred up by previous trigger line impacts. Brittle stars, amphipods, sea anenomes (Coelenterates?), Tunicates, and Crinoids (?) were also observed on the bottom – perhaps indicating a more biologically productive environment than previously suspected. Small shell fragments, including bivalves, litter the seafloor in many places. Several photographs (Fig. 12.10) show ice rafted pebbles and cobbles resting on the soft mud bottom. Lack of accumulated sediments on these rocks indicates recent deposition or the presence of sufficient current action to keep them swept clean. The crest of the ridge appears to be exposed to current action as suggested by ripple marks, scouring and clean, coarse gravel pavements (Fig. 12.11, 12.12). In many cases the ridge floor is covered by gravelly sediments (the coarse fraction far too abundant to be totally ice rafted material). Colour photos reveal many of these pebbles and cobbles to be manganese coated (as were the rock specimens recovered from the dredge). Outcrops (Fig. 12.13) also appear on several ridge crest photographs. First thought to be solution-pitted carbonates or possibly volcanics, the subbottom and seismic records show bedrock to be 100 m below seabed. These outcrops appear to be an older, denser, more consolidated sediment substrate presently undergoing erosion by current action. These outcrops are clear of fine grained material and are more pitted on the upcurrent edge. The down-current periphery of these outcrops is generally less distinct. The observation of embedded cobbles in this substrate suggests that the gravelly sediments overlying it could represent lag deposits derived from the substrate.

Discussion

There is general agreement that the ridge is a linear fragment of the Barents Continental Shelf separated by the inception of spreading along the Nansen-Gakkel rift (Heezen and Ewing, 1961; Harland, 1965; Sweeney et al., 1978 and others). The initial timing of this event is not well defined but is thought to have occurred between 60 and 40 Ma (Osterso and Wold, 1973; Hall, 1973). However, Johnson and Vogt (1973) suggest the Nansen-Gakkel rift may have been active before this. The actual age of the ridge core itself is somewhat controversial and could be Early to Middle Paleozoic (Trettin, 1969; Meyerhoff, 1973 and Harland, 1973). This study has uncovered some evidence bearing on these events.

The reworked nature of the surficial sediments of core B-25 supports the idea that the sediments observed in the seabed photographs taken 1 km from the core site on the ridge crest are lag deposits. But it also appears these lag deposits have been derived from the associated older semiconsolidated substrate also noted in the photographs. The reworked Cretaceous palynomorphs could indicate the presence of mid-Cretaceous outcrops. Unconsolidated sediments of this age have been reported by Clark (1974) to occur elsewhere in the Arctic, in particular on the Alpha Cordillera. In addition, the acoustic evidence suggests that the stratified, unconsolidated sediments overlying the ridge were deposited prior to faulting (and hence ridge separation?). This stratigraphy implies that the sediments certainly are not recent, and in fact, a mid-Cretaceous age is quite acceptable in terms of the known history of the area. The separation of the Lomonosov Ridge could therefore be possibly not much older than mid-Cretaceous. It could however be younger and probably is, for two reasons; an unknown thickness of post mid-Cretaceous sediment may have been eroded after ridge separation, or the Cretaceous palynomorphs in the substrate may have been reworked more than once and hence have been incorporated into sediments of younger, possibly Cenozoic age. More detailed analysis of the **LOREX** sediment cores may or may not resolve these alternatives.

The Devonian spores may have been derived from the substrate or from other rocks. They may also have been reworked several times, but must have been originally derived from rocks of Devonian age. Whether this source was the ridge itself and whether the ridge is at least Devonian in age is difficult to say with such tenuous evidence. One could also speculate that the high degree of thermal alteration observed in these spores could have been the product of orogenesis known to have occurred during this time.

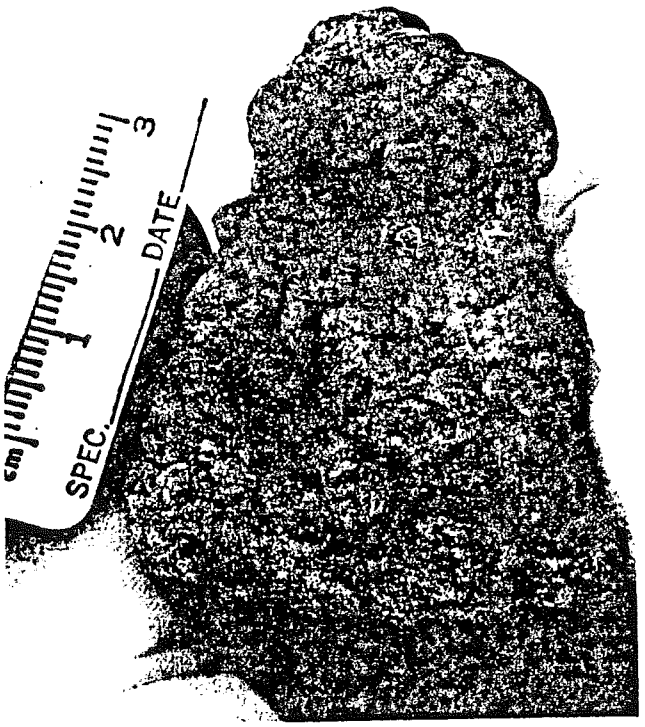

Figure 12.8. Manganese nodule recovered from 3160 m of water on the Makarov flank of the ridge. Other dredged rock samples were manganese coated as well. (BIO Photo 5413-100)

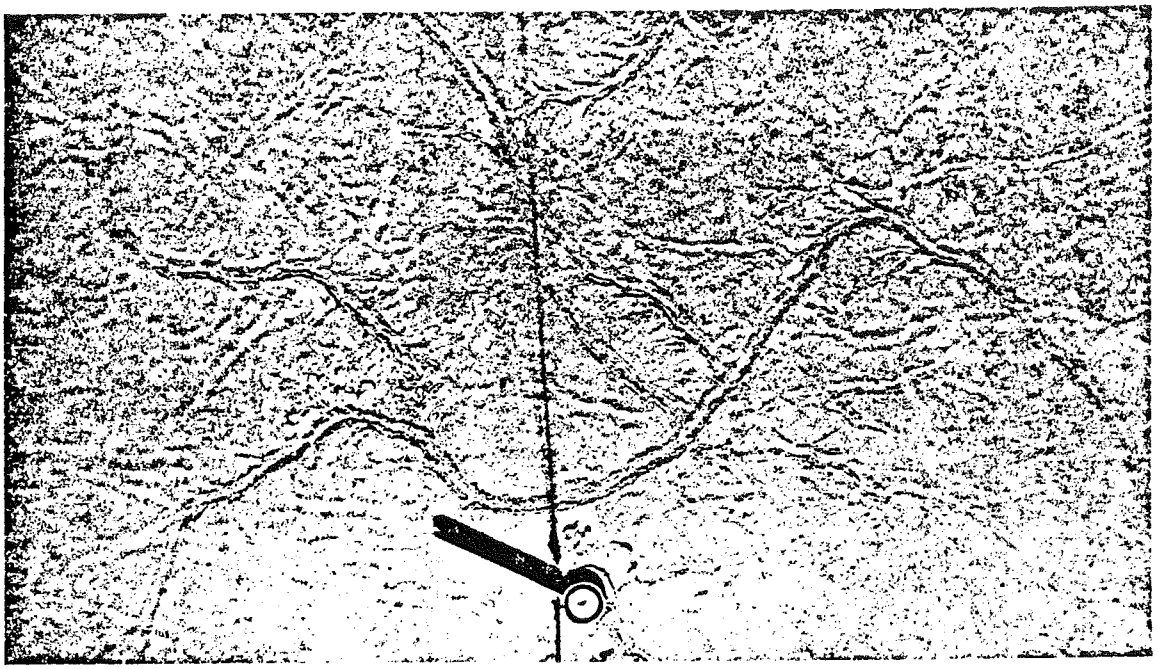

Figure 12.9. *Photo Station 5; 3948 m of water: The soft sediments record several generations of tracks and trails created by benthic fauna. Area covered by this and other photographs is approximately 2.7 m^2. The compass and vane assembly are 33 cm long. (N.E. Fenerty, BIO 5300-STN5)*

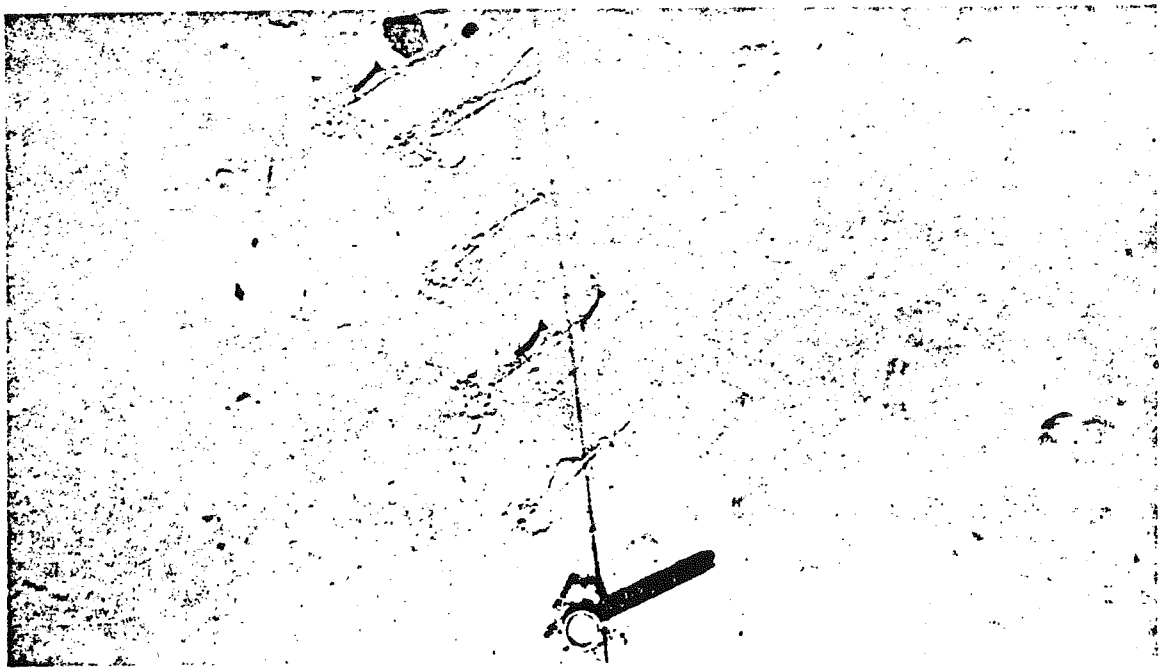

Figure 12.10. *Photo Station 8; 3896 m of water: Three crustacea apparently feeding on organic matter stirred up by previous compass impacts. Note the presence of ice rafted material and shell fragments on the bottom (white spots). (N.E. Fenerty, BIO 5300-STN8)*

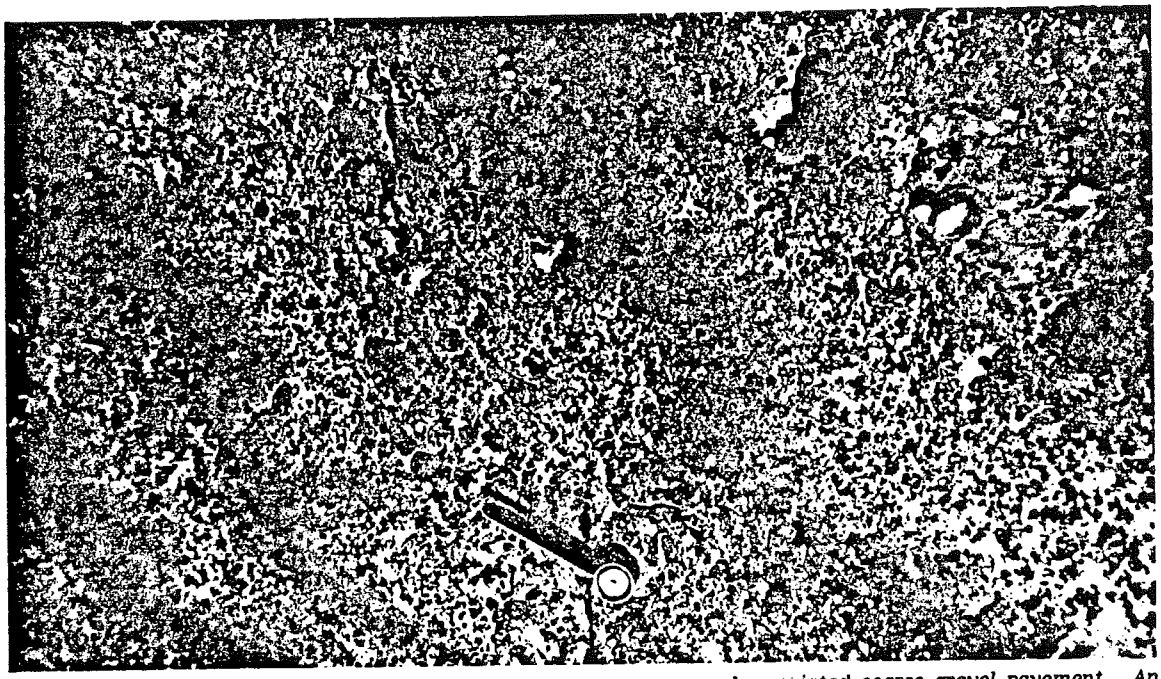

Figure 12.11. *Photo Station 11; 1830 m of water: Current scour and associated coarse gravel pavement. An outcrop of older semiconsolidated sediments is visable in the bottom left. The compass vane is aligned in the direction of current flow towards the bottom right. (N.E. Fenerty, BIO 5300-STN11)*

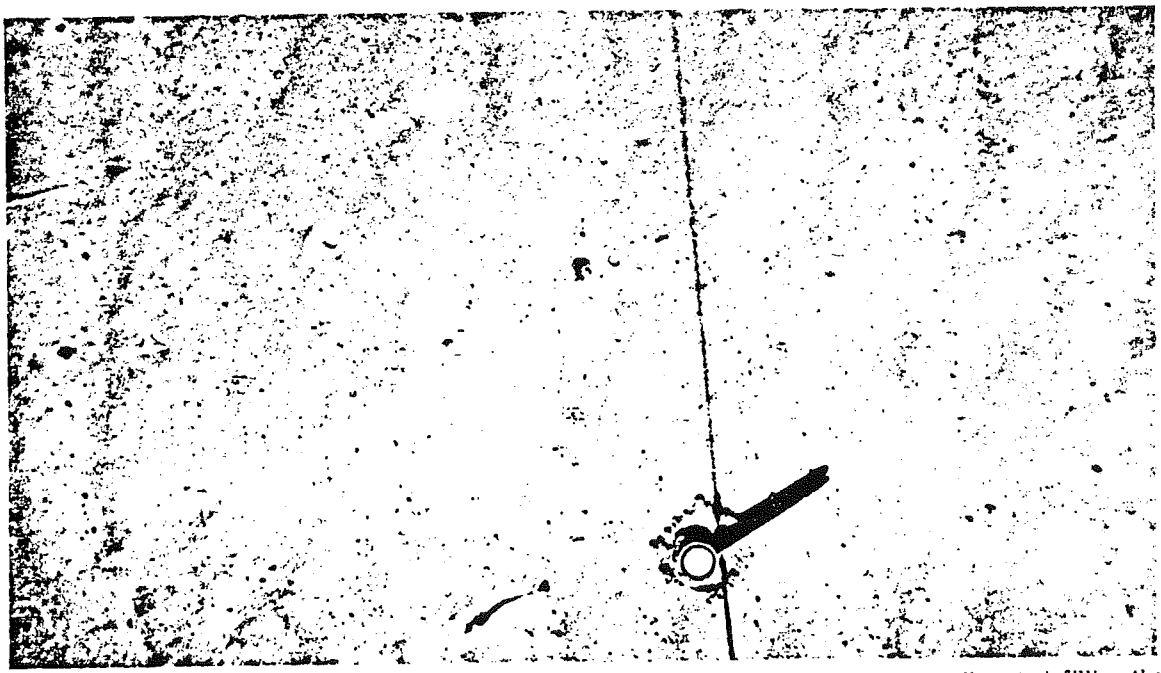

Figure 12.12. *Photo Station 12; 1697 m of water: Ripple marked seafloor with gravelly sediments infilling the troughs. Note the poorly focused crustacean swimming above the bottom; brittle star and burrow close by. (BIO 5300-STN12)*

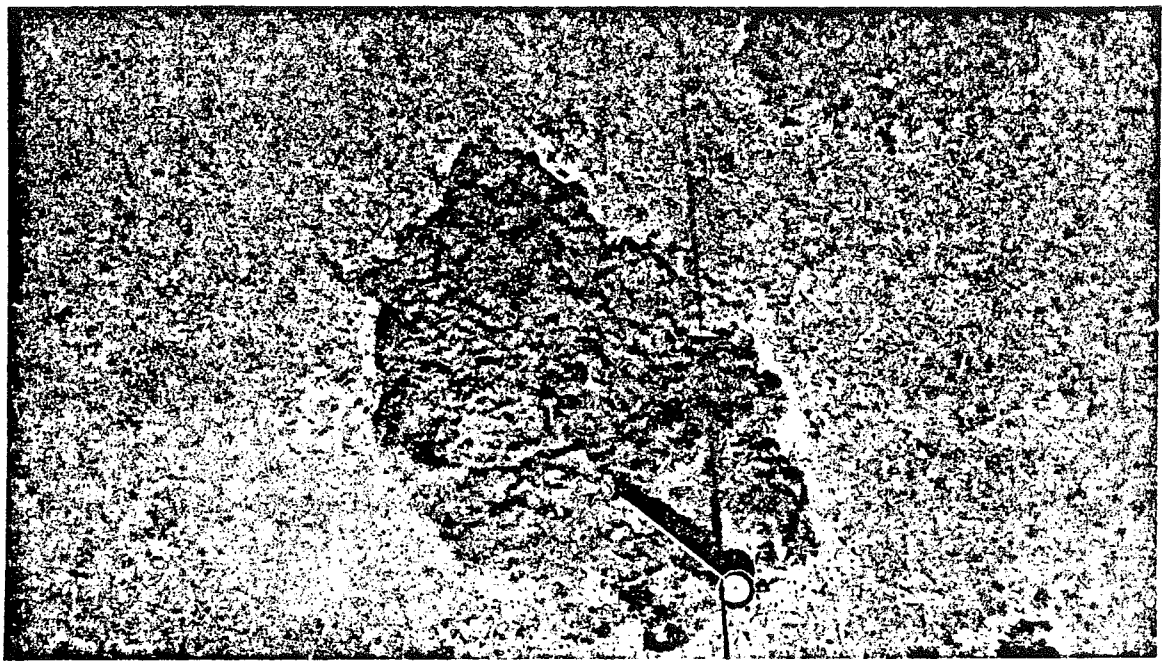

Figure 12.13. Photo Station 12; 1679 m of water: Three outcrops of older semiconsolidated sediments and the overlying lag deposits possibly derived from this substrate. Three brittle stars and three sea anenomes can also be seen associated with the outcrops. (BIO 5300-STN12)

The significance of the thermal alteration of the Cretaceous palynomorphs is also speculative. Only slightly anomalous heat flow values have been reported from the ridge (Churkin, 1973). It might be argued that if these sediments were in situ prior to faulting and probable ridge separation, this alteration could have resulted from the proximity of these sediments to the incipient Nansen-Gakkel rift during the early stages of spreading. (This process could also have affected the spore fragments as they have suffered a greater degree of thermal alteration.) Continued analyses of the LOREX data are necessary to reinforce or refute these interpretations.

Acknowledgments

Scientific programs for the **LOREX** expedition were coordinated by J.R. Weber of the Earth Physics Branch of EMR, and logistics support was provided through G.D. Hobson and the Polar Continental Shelf Project of EMR. The writers would like to thank J.R. Weber and G.D. Hobson for their efforts in making this phase of the **LOREX** program a success. N. Fenerty's Arctic seabed camera system was a definite asset to the program, and his participation is gratefully acknowledged. The assistance of F. Alt, F. Hunt, F. Jodrey and R. Jubb was greatly appreciated. F. Benoit's cuisine did much to sustain our enthusiasm during the expedition. G. Vilks kindly reviewed this manuscript, and C.S. Mulkins assisted in its preparation.

References

Balboni, M.J. and Walsh, W.E.
1978: The expendable sound velocimeter (XSV); Sea Technology, November, p. 38-42.

Churkin, M. Jr.
1973: Geologic concepts of Arctic Ocean Basin; in Arctic Geology, ed. M.G. Pitcher; American Association of Petroleum Geologists, Memoir 19, p. 490.

Clark, D.L.
1974: Late Mesozoic and Early Cenozoic sediment cores from the Arctic Ocean; Geology, v. 2, p. 42-44.

Demenitskaya, R.M. and Kiselev, Yu.G.
1968: The characteristic features of the structure, morphology and sedimentary cover of the central part of the Lomonosov Ridge based on seismic data; in Geophysical Methods of Exploration Applied in the Arctic; Arctic Geology Research Institute, Ministry of Geology, USSR, Leningrad, v. 5, p. 33-46.

Fenerty, N.
1978: Innovative photography pays off at World's largest Oceanographic complex; Canadian Photography, v. 9, no. 5, p. 25-33.

Hall, J.K.
1973: Geophysical evidence for ancient sea-floor spreading from Alpha cordillera and Mendelehev Ridge; in Arctic Geology, ed. M.G. Pitcher; American Association of Petroleum Geologists Memoir 19, p. 558-559.

Harland, W.B.
1973: Tectonic evolution of the Barents Shelf and related plates; in Arctic Geology, ed. M.G. Pitcher; American Association of Petroleum Geologists Memoir 19, p. 599-608.

Harland, W.B.
1965: Tectonic evolution of the Arctic-North Atlantic region; Royal Society of London, Philosophical Transactions Series A, v. 258, p. 59-75.

Heezen, B.C. and Ewing, M.
1961: The Mid-oceanic ridge and its extension through the Arctic Basin; in Geology of the Arctic, ed. G.O. Raasch; University of Toronto Press, v. 1, p. 662.

Hunkins, K., Mathieu, G., Teether, S., and Gill, A.
1970: The floor of the Arctic Ocean in Photographs; Arctic, v. 23, p. 175-189.

Johnson, G.L. and Vogt, P.R.
1973: Marine geology of Atlantic Ocean North of the Arctic circle; in Arctic Geology, ed. M.G. Pitcher; American Association of Petroleum Geology, Memoir 19, p. 169.

Meyerhoff, A.A.
1973: Origin of Arctic and North Atlantic Oceans; in Arctic Geology, ed. M.G. Pitcher; American Association of Petroleum Geology, Memoir 19, p. 569.

Ostenso, N.A., and Wold, R.J.
1973: Areomagnetic evidence for origin of Arctic Ocean Basin; in Arctic Geology, ed. M.G. Pitcher; American Association of Petroleum Geology, Memoir 19, p. 506-516.

Sippican Corporation
1978: Specification booklet on XSV/XBT products, Sippican Oceanographic Division, Marion, Mass.

Sweeney, J.F., Irving, E., and Geuer, J.W.
1978: Evolution of the Arctic Basin; in Arctic Geophysical Review, ed. J.F. Sweeney, Publication Earth Physics Branch, v. 45, no. 4, p. 91-100.

Trettin, H.P.
1969: A Paleozoic – Tertiary fold belt in northern most Ellesmere Island, aligned with the Lomonosov Ridge; Geological Society of America Bulletin, v. 80, p. 143-148.

Sediments of the Lomonosov Ridge and Makarov Basin: A Pleistocene stratigraphy for the North Pole

THOMAS H. MORRIS, DAVID L. CLARK } *Department of Geology and Geophysics, University of Wisconsin, Madison, Wisconsin 53706*
STEVEN M. BLASCO *Bedford Institute of Oceanography, Dartmouth, Nova Scotia B2Y 4A2*

ABSTRACT

Sediments of 16 short cores taken as part of the Lomonosov Ridge Experiment (LOREX) can be organized into the first Pleistocene stratigraphy for the North Polar region. This stratigraphy can be correlated with stratigraphic units described from the Alpha-Chukchi areas, ~300 km distant.

The LOREX cores include at least 12 sedimentary subunits differentiated by texture, color, and carbonate content. The units are silty and arenaceous lutites and are principally glacial-marine. Benthic and planktonic foraminifera, degree of bioturbation, and Fe-Mn micronodule abundance generally are positively correlated. Foraminifera in core B-8, from 3,956 m in the Makarov Basin, may have been affected by CCD fluctuations that did not affect fossils in core B-24, from 1,600 m on the crest of the Lomonosov Ridge.

The 12 stratigraphic units were deposited during the late Pleistocene and represent the same major sedimentary events as those of stratigraphic units K, L, and M of the Amerasian Basin. This correlation is excellent evidence for the remarkable and widespread uniform depositional style of glacial-marine sediment. Times of major glacial ice transport reflect deglaciation events in the central Arctic Ocean. Surface currents during deglaciation transport glacial ice in a more or less uniform pattern over at least 50% of the Arctic Ocean. Even thin sedimentary units deposited during relatively long time intervals are correlated over >500,000 km^2.

INTRODUCTION

Study of sediment cores from the Lomonosov Ridge and adjacent basins permits development of the first stratigraphy for the area around the North Pole. We report here the description and interpretation of sediment deposited during the past 700,000 yr on the Lomonosov Ridge and the adjacent Makarov Basin (Fig. 1) and its correlation and classification with sediments of the Chukchi–Alpha Ridge. This information, together with data from the Canada Basin (Campbell and Clark, 1977; Goldstein, 1983), the Alpha-Chukchi areas (Clark and others, 1980), and the eastern Alpha Ridge (Minicucci and Clark, 1983) provides a unique synthesis of central Arctic Ocean sedimentology and lithostratigraphy.

The Lomonosov Ridge Experiment (LOREX) was a multidisciplinary project of the Earth Physics Branch of the Geological Survey of Canada (Blasco and others, 1979). Multidisciplinary research was conducted on the ice from March 29 to May 29, 1979. The drift path of the LOREX ice station was 160 km long and crossed nearly perpendicular to the Lomonosov Ridge (Fig. 1). Its general direction was from the Makarov Basin over the crest of the Lomonosov Ridge and into the Fram Basin. On May 17, the ice station came within 35 km of the North Pole. Gravity cores, grab samples, dredge samples, plankton tows, seabed photographs, subbottom profiles, reflection profiles, velocity profiles, and bathythermograph profiles were collected during the LOREX drift. Along the drift path, 42 gravity cores, from 0.2 to 1.7 m long, were taken. These 67-mm-diameter gravity cores were recovered using a 118-kg Benthos gravity corer.

LOMONOSOV RIDGE

The Lomonosov Ridge is a linear aseismic plateau that rises above flanking abyssal plains in the Arctic Ocean. It is elevated ~3,000 m above the adjacent abyssal plains of the Amerasian Basin on its one flank and the Eurasian Basin on its opposite flank; hence, this ridge divides the Arctic Ocean into two separate and structurally distinct basins (Fig. 1). Pitman and Talwani (1972) concluded that active spreading has occurred along the Nansen-Gakkel Ridge (Eurasian Basin) for ~63 m.y. A paleoreconstruction of 63 m.y. ago places the Lomonosov Ridge against the Barents Shelf. Sweeney and Blasco (1982) suggested that the initial rifting of the Lomonosov Ridge from the Barents Shelf was in Late Cretaceous. He hypothesized a trans-Arctic, left-lateral offset system (possibly associated with the opening of Baffin Bay) that sheared the Lomonosov Ridge from the Barents Shelf.

Blasco and others (1979) presented a preliminary review of sediments from the Lomonosov Ridge. This included textural, mineralogic, and faunal/floral identifications that are here described in detail.

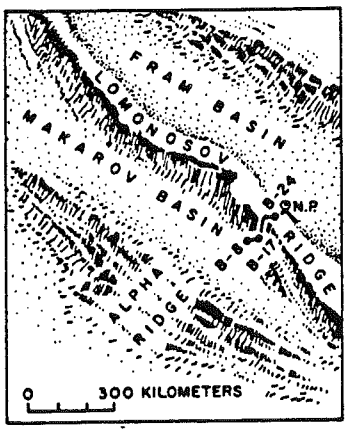

Figure 1. Index map of study area in the central Arctic Ocean. The Amerasian Basin is on the lower left side of the Lomonosov Ridge; the Eurasian Basin is on the upper right side. Core locations are as follows. Core B-8: lat. 88°29.72′ North, long. 167°07.83′ West. Core B-17: lat. 88°46.68′ North, long. 166°18.42′ West. Core B-24: lat. 89°05.00′ North, long. 168°29.50′ West. N.P. = North Pole.

Geological Society of America Bulletin, v. 96, p. 901–910, 11 figs., 1 table, July 1985.

STRATIGRAPHY

Introduction

Three cores selected for detailed study each represent a group of cores that can be visually correlated. Core B-8, from the Makarov Basin, was chosen because it apparently contains the most complete sediment record and can be easily correlated visually to at least four other LOREX cores (B-1, B-6, B-7, B-10). Core B-24, which is located on the crest of the Lomonosov Ridge and ~60 km north of core B-8, was chosen as representative of a group of seven cores which also can be visually correlated (B-20, B-21, B-22, B-23, B-24, B-25, B-26). Core B-17, located between cores B-8 and B-24 on the flank of the Lomonosov Ridge, was also studied and is representative of at least three other cores (B-16, B-18, B-19). Correlation among sixteen LOREX cores is therefore accomplished in this study.

The glacial-marine sediment represented by cores B-8, B-24, and B-17 are representative of the latest Cenozoic history of a minimum of 1,000 km^2 and perhaps several times this area. The sediment can be correlated with stratigraphic units defined for the Alpha Ridge, ~300 km distant, but there are some differences. It is proposed that the sediment represented by cores B-8, B-24, and B-17 be referred to as the "Makarov Basin Formation."

The Makarov Basin Formation is divisible into twelve members, in order of increasing age, designated Alpha to Mu. The members are best represented in core B-8, which is located in the Makarov Basin at a depth of 3,956 m. This core is defined as the stratotype. It is located at latitude 88°29.72′ north, longitude 167°7.83′ west. The core is 148 cm long (Fig. 2).

Generalized stratigraphic sections and sedimentary parameters of core B-8 and core B-24 are shown in Figures 2 and 3, respectively.

Alpha Member

The Alpha Member is the youngest sediment of the Makarov Basin Formation. It is dark brown (10YR 3/3), silty lutite. The Alpha Member is nonlaminated but is not bioturbated and has a gradational contact with the Beta Member below. The upper contact represents the top of the core.

The average coarse weight percent (>63 μ) of the Alpha Member in core B-8 is 8.04. Comparisons with other cores are shown in Table 1. Planktonic foraminifera abundance is higher in the Alpha Member than in any other member in the Makarov Basin Formation. Estimates range from 63,000 to >118,000 foraminifera per gram of coarse sediment on the basis of counts of quantitative sample splits of from 0.1 to 0.5 g. The diversity of benthonic foraminifera also is greatest in this member. Other microfossils include holothurian sclerites, ostracodes, and rare radiolaria. There are virtually no ferromanganese micronodules.

The Alpha Member is 5 cm thick in core B-8. The average thickness in the three cores studied is 4.33 cm.

TABLE 1. AVERAGE COARSE WEIGHT PERCENT OF EACH MEMBER FROM CORE B-8 AND CORE B-24

Member	B-8 avg	B-24 avg	B-17	Avg of cores
Alpha	8.04	59.03	21.01	29.36
Beta	3.98	32.28	19.12	18.46
Gamma	1	19.68	16.35	12.18
Delta	10.39	26.48	16.55	17.80
Epsilon	21.48	26.31	25.65	24.48
Zeta	20.21	26.44	12.31	19.65
Eta	7.54	15.3	23.75	15.53
Theta	7.66	30.1	16.49	18.08
Iota	8.07	31.63	8.44	12.04
Kappa	32.50	32.14		32.32
Lambda	5.71			
Nu	2.32			

Note: the coarse weight percent of a sample from each of the members from Core B-17 is also given

Beta Member

The Beta Member is a silty lutite. The color is yellowish brown but grades in shade from darker (10YR 5/4) yellowish brown at the top of the member to lighter (10YR 5/8) yellowish brown at the bottom contact. Color mottling is moderately intense. Dark brown splotches and light yellowish brown, sausage-shaped mottling (on the scale of a few millimetres) indicate bioturbation by *Chondrites* (Chamberlain, 1975). The Beta Member has gradational irregular contacts at both top and bottom.

The average coarse weight percent in the Beta Member of core B-8 is 3.98. The member has a high abundance of planktonic foraminifera ranging from an estimated 25,000 to 100,000 foraminifera per gram of coarse sediment. Benthonic foraminifera are also abundant and diverse relative to other members of the Makarov Basin Formation. Holothurian sclerites, ostracodes, radiolaria, and a fish tooth were also found in this member. Virtually no ferromanganese micronodules are present.

The Beta Member in core B-8 is 8 cm thick, and the average thickness in the three cores studied is 7 cm.

Gamma Member

The Gamma Member is a nonbioturbated, yellowish brown (10YR 5/4), silty lutite. The member grades to a lighter shade of yellowish brown at its bottom contact. The upper contact of the member is distinct, although irregular. The bottom contact is very sharp. The Gamma Member also exhibits very faint laminae on the order of 1 to 2 mm thick.

The coarse weight percent of the Gamma Member in core B-8 never reaches 1%. The planktonic foraminifera abundance is high relative to most of the other members in the core but fluctuates within the member. The top portion of the member has an estimated 21,000 foraminifera per gram of coarse sediment; the middle portion of the member has only 200 foraminifera per gram of coarse sediment. The bottom portion of the member, again, has abundant foraminifera, containing an estimated 58,000 per gram of coarse sediment. The abundance and diversity of benthonic foraminifera have been greatly reduced relative to the Alpha and Beta Members overlying it and the Delta Member underlying it. Preserved foraminifera tests are pitted and broken and probably are evidence of dissolution. Holothurian sclerites, unknown flakes possibly of siliceous composition, radiolaria, and echinoid fragments also occur. Ferromanganese micronodules constitute a large percentage of the coarse sediment within the Gamma Member. As much as 65% of the sand-sized material is composed of these micronodules.

The thickness of the Gamma Member in core B-8 is 13 cm. The average thickness in the three cores is 11.67 cm.

Delta Member

The Delta Member is dark yellowish brown (10YR 3/4). The larger part of the member is silty lutite, but a 1-cm interval near the base is areneaceous lutite. It is a nonbioturbated member with a sharp upper contact and a gradational, yet very distinctive, lower contact.

The average coarse weight percent in the Delta Member of core B-8 is 10.39. Coarse percentage generally increases from top to bottom within this member. The planktonic foraminifera abundance at the top of the member is an estimated 34,400 foraminifera per gram of coarse material.

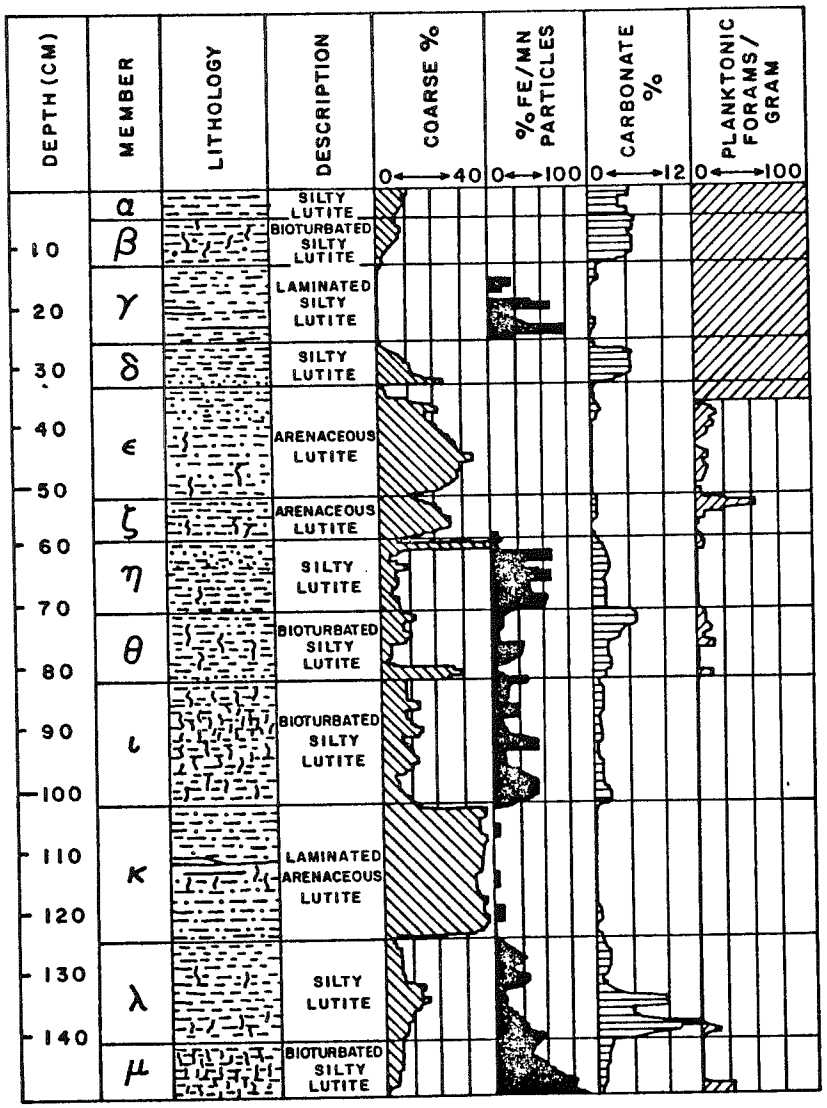

Figure 2. Stratigraphic section and sediment parameters of core B-8. Core B-8 is the stratotype of the Makarov Basin Formation.

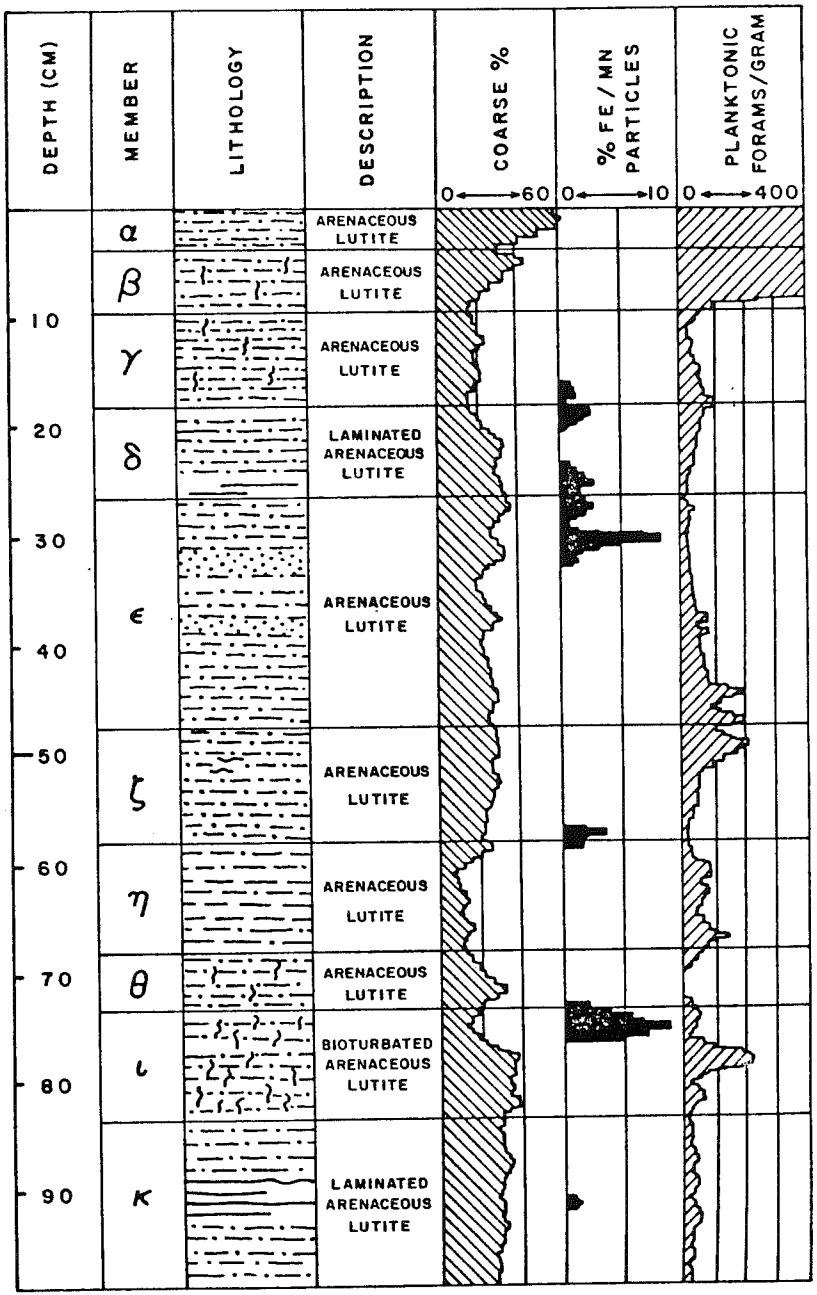

Figure 3. Stratigraphic section and sediment parameters of core B-24. Core B-24 is located on the crest of the Lomonosov Ridge.

This progressively decreases to an estimated 950 per gram of coarse material near the base of the member. Benthonics in the Delta Member are similar in maximum abundance to those in the Alpha Member (~1,500 per gram of coarse sediment). Ostracodes are present. There are virtually no ferromanganese micronodules within the Delta Member.

The Delta Member is 7 cm thick in core B-8. The average thickness of the member in the three cores studied is 7.56 cm.

Epsilon Member

The Epsilon Member is an arenaceous lutite and is variable in color. The uppermost centimetre is dark yellowish brown (10YR 4/4) and is followed by 3 cm of yellowish brown (10YR 5/4) and by 17 cm of olive brown (2.5Y 4/4) color. There is a distinctive arenaceous subunit within the upper portion of the Epsilon Member that can be correlated to other cores. It is considered a marker bed. The upper contact of the Epsilon Member is slightly gradational but very distinctive, especially in color change. The bottom contact is sharp but is characterized only by a slight color change. There are no laminations other than the arenaceous subunit. The lower third of the member is slightly mottled.

The average coarse weight percent in the Epsilon Member of core B-8 is 21.48. The abundance of planktonic foraminifera within the top 2 cm becomes greatly reduced relative to the other overlying members (Fig. 2). Few foraminifera are present below the Delta Member in core B-8. Estimated planktonic foraminifera per gram of coarse sediment within the Epsilon Member range up to 6,000 at the top. No benthonic foraminifera were found in this member from core B-8. Ferromanganese micronodules are absent.

The Epsilon Member of core B-8 is 19 cm thick. The average thickness of the member in the three cores studied is 21 cm.

Zeta Member

The Zeta Member is an arenaceous lutite. The upper 2 cm is yellowish brown (10YR 5/4), and the lower 4.5 cm is mottled olive brown (2.5Y 4/4). Although the upper contact with the Epsilon Member is distinctive, it is observable only by a slight color change. The bottom contact is very sharp and easily observable. The Zeta Member is distinct in core B-8 and core B-24 but indistinct in core B-17. The bioturbation of the lower two-thirds of the member is moderately intense. Laminations are suggested in X-radiograph negatives: these show a dark band in the upper 2 cm and a light band in the lower 4.5 cm of the member.

The average coarse weight percent in core B-8 is 20.21. Planktonic foraminifera are greatly reduced, ranging from an estimated 50 foraminifera per gram of coarse material to zero. Benthonic foraminifera are not present. There are traces of ferromanganese micronodules throughout the Zeta Member, but they constitute < 1% of the coarse fraction.

The thickness of the Zeta Member in core B-8 is 7 cm. The average thickness of the member in the three cores studied is 10.34 cm.

Eta Member

Except for 1 cm of arenaceous lutite near the top, the Eta Member is a silty lutite. The arenaceous lutite is the coarsest sediment of core B-8 (46.2 coarse weight percent). Another thin (~2 mm) subunit of sand is 2 cm below this sandy subunit. The color of the Eta Member darkens slightly from top to bottom but for the most part is brown (10YR 4/3). Very slight mottling is observable in the lower one-third of the member. The top contact is sharp; the lower contact is very gradational. X-radiography reveals a "four-striped" pattern of dark-light-dark-light within the Eta Member. This same distinct pattern can be observed from X-radiographs of core B-24. In core B-8, this pattern of subtle laminations is better developed.

The average coarse weight percent of the Eta Member in core B-8 is 7.54. The Eta Member contains few planktonic foraminifera; abundances range from six to zero foraminifera per gram of coarse sediment. No benthonic foraminifera were found. Estimates from the coarse fraction of the percent of ferromanganese micronodules range from 2% to 55% of the coarse material.

The Eta Member in core B-8 is 12 cm thick. The average thickness of the member in the three cores studied is 12.5 cm.

Theta Member

The Theta Member is largely a silty lutite. The bottom 2 cm, however, is much coarser and consists of arenaceous lutite. The top 3 cm is mottled light yellowish brown (10YR 6/4) with some white (10YR 8/1) splotches. These almost obscure whitish blotches are extremely significant. They occur in Amerasian Basin sediment at one to three correlatable horizons and have been termed "pink-white" layers (Clark and others, 1980). The single occurrence in the Makarov Basin Formation apparently is the second, or basal unit "M," correlative. The next 6 cm ranges from dark grayish brown (10YR 4/2) to dark brown (10YR 3/3). This part is lighter near the contact of the arenaceous lutite at the base. The arenaceous lutite is olive brown (10YR 3/3). The upper contact of the Theta Member is very gradational; the lower contact is very sharp. There are no laminations other than the rather indistinct arenaceous lutite at the base.

The average coarse weight percent of the Theta Member in core B-8 is 7.66. There are a few planktonic foraminifera present (Fig. 2), ranging in number from 14.3 to zero per gram of coarse sediment. No benthonic foraminifera were found. Other microfossils include an echinoid fragment and possible rind burrows (Chamberlain, 1975). Ferromanganese micronodules are fairly abundant, constituting an estimated 2% to 30% of the coarse fraction.

The Theta Member is 11 cm thick in core B-8. The thickness of the Theta Member averages 9.17 cm in the three cores studied.

Iota Member

The Iota Member is a mottled silty lutite. The top 2 cm is dark brown (10YR 3/3) with light splotches, giving it a mottled appearance. The next 2 cm is lighter brown with dark brown splotches and is also mottled. The next 10 cm is dark brown (10YR 3/3) with light brown mottling. The basal 6 cm is also mottled and is light olive brown (2.5Y 5/4). The upper contact is very sharp against the arenaceous lutite of the Theta Member. The lower contact is very gradational, marked only by the loss of bioturbation.

The average coarse weight percent of the Iota Member in core B-8 is 8.07. There are no planktonic foraminifera in the Iota Member (Fig. 2). Benthonic foraminifera are also absent, with the possible exception of one ferromanganese encrustation that has obvious interior chambers. Rind burrows are present. Ferromanganese micronodules are abundant, constituting an estimated 3% to 40% of the coarse fraction.

The Iota Member is 20 cm thick in core B-8. It averages 13.34 cm in the three cores studied.

Kappa Member

The Kappa Member is an arenaceous lutite. It has more sand-sized sediment than does any other member in the Makarov Basin Formation. It

is olive brown (2.5Y 4/4). Dark laminations are a key marker in this member. These laminations occur near the middle of the Member in core B-8. The laminations are ~1–2 mm thick. In core B-8, there is only one dark lamination; this is underlain by two very faint laminations. In core B-24, there are four obvious dark laminations. The laminations consist of a concentration of ferromanganese micronodules. Below the laminations, very slight bioturbation has occurred. The upper contact of the Kappa Member is gradational. The lower contact is distinct but is characterized only by a color that is slightly darker than the underlying member.

The average coarse weight percent of the Kappa Member in core B-8 is 32.50. No planktonic foraminifera are present (Fig. 2). Ferromanganese micronodules are found throughout the member but are only in trace amounts up to an estimated 1% of the coarse-sediment fraction.

The Kappa Member thickness in core B-8 is 23 cm, but in core B-24, its thickness is 13 cm. The thickness in core B-24 is incomplete due to the termination of the core; however, the upper portion of the member is expanded in core B-8 relative to core B-24.

Lambda Member

The Lambda Member is a silty lutite. The upper 8 cm is unmottled and light olive brown (2.5Y 5/4). The lower 11 cm is olive brown (2.5Y 4/4) and moderately mottled with darker brown splotches. There are also pinkish splotches in this lower portion of the member that could represent either a layer similar to that seen in unit J of the Alpha Ridge or a unique occurrence. The upper contact is irregular and occurs at a color change. The lower contact is sharp.

The average coarse weight percent of the Lambda Member in core B-8 is 5.71. The Lambda Member is not present in cores B-24 or B-17.

Only 5 planktonic foraminifera were found in a 2-cm interval. Numerous benthonic foraminifera, either as whole or partial tests, are present. Ferromanganese micronodules are very abundant, consisting of an estimated 1% to 40% of the coarse-sediment fraction.

The Lambda Member in core B-8 is 17 cm thick.

Mu Member

The Mu Member is a silty lutite. This member represents the oldest sediment of core B-8 and is probably the oldest sediment of any of the LOREX cores. Members Lambda and Mu are not found in either cores B-24 or B-17. The upper 3 cm is dark brown (10YR 3/3). The lower 3 cm is light olive brown (2.5Y 5/4). The entire member is intensely bioturbated. The upper contact is sharp.

The average coarse weight percent of the Mu Member in core B-8 is 2.32. One planktonic foraminifera was observed in the bottom 1 cm of the member. Only a few possible benthonic agglutinated foraminifera were noted. Of all members, this member contains the greatest abundance of ferromanganese micronodules. They constitute 40% to 80% of the coarse sediment. In B-8, only 6 cm of Mu Member is preserved.

SEDIMENTARY PARAMETERS

Introduction

Texture, degree of bioturbation, bulk carbonate analysis, Fe-Mn micronodule concentration, skeletal content, and, to a lesser degree, general mineralogy, are factors that are important in understanding the environment of deposition of the Makarov Basin Formation. Here, we summarize the most important of these sedimentary parameters and their interpretation.

Texture

The division between sand-sized material (>63 μ), here referred to as "coarse" sediment, and finer silt- and clay-sized sediment is fundamental to environmental interpretations. Arctic sediment is principally glacial-marine, most of it ice-rafted (Clark and Hanson, 1983). The frozen sea water (= pack ice) transports fine-grained sediment that is deposited from the atmosphere or is mobilized by storm action in shallow shelf areas and incorporated into the pack ice as it is formed in the fall of the year. Icebergs, derived from the Arctic Islands and from Greenland, transport clays and silts as well as the coarse sediment that ranges up to boulder size (Clark and Hanson, 1983). During the late Cenozoic, there was considerable variation in the magnitude of these two ice-transport systems, and the result has been alternate deposition of coarser material during late stages of glacial surges, as well as more important deglaciation, and deposition of more silt and clay between deglaciations (Clark and others, 1980; Clark and Hanson, 1983; Minicucci and Clark, 1983). The variability of coarse weight percent sediment in the Makarov Basin Formation reflects these same conditions. The Epsilon, Zeta, and Kappa Members reflect active iceberg transport (= deglaciations), and the other members represent pack-ice and iceberg transport that followed active deglaciations. Correlation of interglacial and deglaciation events across the Amerasian Basin has been accomplished, and a tentative correlation of the marine cycles with glacial tills and interglacial deposits on land appears possible (Clark and others, 1984).

In addition to this textural variation resulting from ice-transport mechanisms, there are significant differences in texture of the Makarov Basin Members formed on the Lomonosov Ridge crest and the adjacent flanks and basin (Fig. 4).

Of the ten comparable formation members, seven are thinner on the Lomonosov Ridge crest (B-24) than in the basin (B-8), and most of the members on the crest (B-24) are coarser. Current velocities measured by Aagaard (1981) as part of LOREX are sufficient to explain this pattern. Evidently, the pulsating currents directed from the Fram Basin across the Lomonosov Ridge into the Makarov Basin mobilize clays and silts on the Ridge (or prohibit their deposition there) and deposit the finer-grained material on the flanks and adjacent Makarov Basin (Fig. 1). Such currents

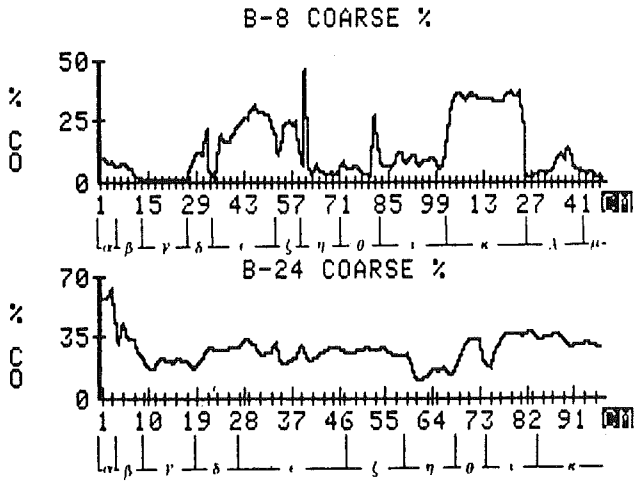

Figure 4. Comparison between coarse weight percent of core B-8 and core B-24; 1 = core top.

permit concentration of coarse-grained material on the Ridge and have been active across the Ridge almost continually during at least the past 700,000 yr.

Bioturbation

The record of both infaunal and epifaunal activity and consequent diagenesis can be interpreted from the degree of bioturbation as indicated by burrows and color mottling. Intensive bioturbation in finer-grained sediment (= slower accumulation rate) has been noted for central Arctic sediment (Clark and others, 1980; Minicucci and Clark, 1983). Bioturbation characterizes the Beta, Epsilon, Zeta, Theta, Iota, and Mu Members to a greater degree than it does other members of the formation. There is a general abundance of fossils and Fe-Mn micronodules in the bioturbated members. Lower sedimentation rates, typical of post-deglaciation intervals, encourage the development of bioturbation and related activity.

Carbonate Content

Samples from each 1-cm interval of core B-8 were analyzed for bulk carbonate percent by G. A. Jones at the Lamont-Doherty Geological Observatory (Jones and Kaiteris, 1983). A vacuum-gasometric carbonate analyzer was used. Comparison of bulk carbonate percent and coarse percent can be seen from Figure 5. The bulk carbonate analysis shows four peaks in carbonate percent. The uppermost peak in the core corresponds to Members Alpha and Beta which have extremely high abundances of planktonic foraminifera. There are more foraminifera tests in these members than there are sand-sized clastic grains. To determine what proportion of the carbonate peak can be accounted for by the planktonic foraminifera tests, 100 randomly chosen tests from the Alpha Member were weighed. The average weight recorded was 0.000004 g per test. Using this figure and the approximate numbers of foraminifera, a calculation of ~3.88% of the bulk sample could be attributed to the planktonic foraminifera tests within the Alpha Member. A conservative calculation of 3.17% was recorded for the Delta Member. It is apparent that much of these two carbonate peaks may be explained by the abundance of calcareous foraminifera tests alone.

Neither the third carbonate peak (at the Eta-Theta boundary) nor the fourth peak (within the Lambda Member) is associated with abundance peaks of calcareous microfauna. They may reflect increased glacial-marine transport and deposition of carbonate rocks that were being exposed and eroded from continental source areas. Ellesmere Island has both Paleozoic and Mesozoic carbonates and is currently contributing much of the glacial ice to the Arctic (Clark and Hanson, 1983).

Fe-Mn Micronodules

Ferromanganese micronodules occur in most parts of the Makarov Basin Formation, but the distribution is irregular (Fig. 6). The greatest concentration is in the oldest parts of the core.

The majority of ferromanganese micronodules are in the fine sand-sized range (125 to 250 μ) and have quartz grains as nuclei. These nuclei range in size but are primarily very fine sand-sized (~63 μ) to silt-sized particles. The nodules are rounded to subangular. Many particles are globose or botryoidal in shape. Very rarely, there are ferromanganese coatings around foraminifera tests, but this is observable in only a very small fraction of the micronodules.

Core B-8 has a large percentage of ferromanganese micronodules in the finer-textured members (Fig. 2), and there is an inverse correlation between coarse percentage and the percentage of ferromanganese micronodules (Fig. 7). A simple statistical linear technique (Huntsberger and Billingsley, 1981), using the average coarse weight percent of each member against the average estimated ferromanganese micronodule percent, gave a correlation coefficient of −0.5514.

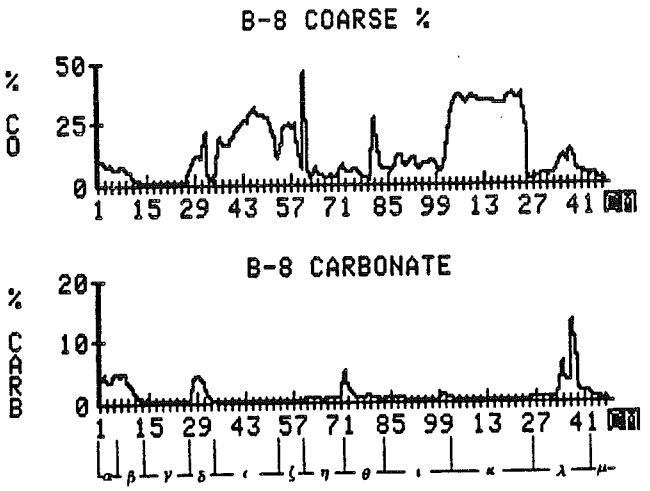

Figure 5. Comparison between coarse weight percent and bulk carbonate percent in core B-8; 1 = core top.

Core B-24 is characterized by a greatly reduced percent of ferromanganese micronodules relative to core B-8 (Fig. 6). Estimated maximum abundance reaches only 8% of the coarse sediment, and this is found in only 2 intervals. The association of high ferromanganese micronodule percent with silty lutites has been found elsewhere in the Arctic Ocean (Clark and others, 1980; Herman, 1974). Silty lutites indicate periods of lower sedimentation rates (that is, reduced glacial ice-rafting), and ferromanganese micronodule growth may occur with long exposure to the ocean bottom water.

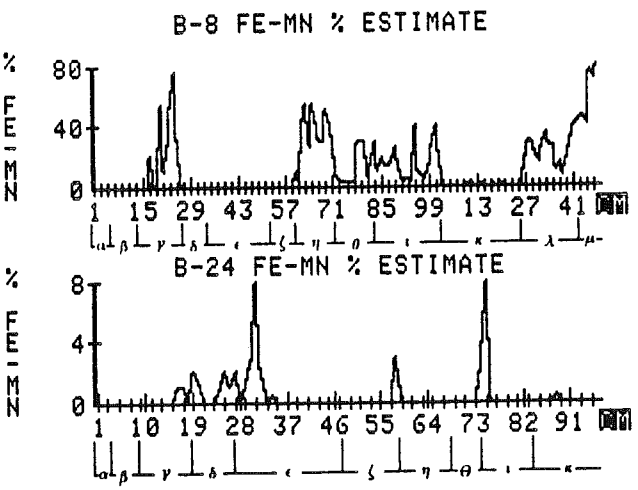

Figure 6. Comparison between estimated percent of ferromanganese micronodules of core B-8 and core B-24; 1 = core top. Note difference in vertical scales.

Core B-8 shows correlation between ferromanganese micronodule percentages and bioturbation. Furthermore, core B-24, which is from the higher current-velocity regime of the Lomonosov Ridge, shows greatly reduced ferromanganese micronodule percentages. The dark laminations in the arenaceous lutite of the Kappa Member of core B-8 consist of a concentration of ferromanganese micronodules.

In summary, Fe-Mn micronodules are interpreted as indicating intervals of slow sedimentation and are associated with silty lutites and bioturbation.

Foraminifera

Occurrence of Foraminifera is shown in Figure 8. Foraminifera are most abundant in the Alpha through upper Epsilon Members. Planktonic foraminifera include abundant *Neogloboquadrina pachyderma* and fewer numbers of *Globigerina quinqueloba.* Benthonic species are the same as those reported by Lagoe (1977) and O'Neill (1981). Differences in abundances between Lomonosov Ridge sediment (B-24) and the adjacent basin (B-8) are attributed to fluctuations in the CCD and exposure to corrosive bottom-water conditions.

Mineralogy

We have made only a cursory study of the mineralogy. Smear slide analysis of selected intervals shows that quartz and feldspar are the dominant minerals; 5%–20% are lithic fragments, and there are fewer opaque minerals present. No significant differences from the mineralogy of other Amerasian Basin sediment are apparent (for example, Clark and others, 1980).

Summary of Sedimentary Parameters

The 12 members of the Makarov Basin Formation recognized in LOREX cores consist of glacial-marine sediment with texture, mineralogy, and fossils similar to that in sediment of the Chukchi–Alpha Ridge areas. Significant variation in Lomonosov Ridge crest cores and cores from the adjacent basin is apparent. Core B-8 (basin) contains 98 cm of silty lutite and 50 cm of arenaceous lutite. The average coarse weight percent of the entire core is 10.68. In contrast, core B-24 has 90 cm of arenaceous lutite and only 6 cm of silty lutite. It has an average coarse weight percent of 34.69.

An inverse correlation exists between coarse weight percent and estimated percentages of ferromanganese micronodules in core B-8 (Fig. 7). Ferromanganese micronodules constitute >40% of the coarse sediment in a number of silty lutite members of core B-8. Conversely, micronodules reach only 8% in core B-24, and this percentage is found in only two 1-cm intervals (Fig. 6).

The two planktonic foraminifera, *Neogloboquadrina pachyderma* and *Globogerina quinqueloba,* are extremely abundant (maximum of >118,000 foraminifera per gram of coarse sediment) in the upper 36 cm of core B-8. Significant abundances are not present below 36 cm. This is also true of calcareous benthonic diversity and numbers in core B-8. In contrast, core B-24 has maximum foraminifera abundance in the upper 8 cm (maximum of >16,000 foraminifera per gram of coarse sediment) and also records significant fluctuating abundances throughout its length (Fig. 8). Furthermore, calcareous benthonic foraminifera are found throughout the core, except for the bottommost 13 cm.

Four carbonate peaks are evident from the bulk carbonate analysis of core B-8. The youngest two peaks primarily reflect abundances of calcareous foraminifera; the oldest two peaks primarily represent detrital carbonate (Fig. 5).

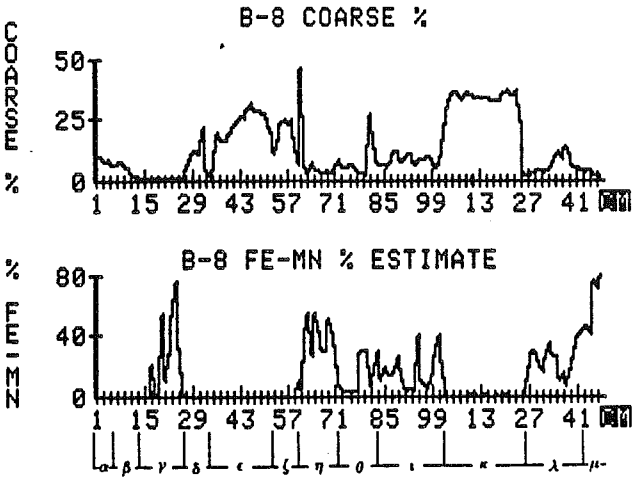

Figure 7. Comparison between coarse weight percent and estimated ferromanganese micronodule percent in core B-8; 1 = core top.

AGE OF MAKAROV BASIN FORMATION

In order to determine the age of the oldest sediment of core B-8 and core B-24, several techniques were used. One sample from each 10-cm interval of core B-8 was analyzed for magnetic reversals using the Princeton Spinner Magnetometer Model SM-2. No magnetic reversals were recorded. Similar (unpublished) magnetic data were obtained from several LOREX cores by the Bedford Institute of Oceanography–University of Dalhousie, and no reversals were found. This suggests that the sediment is younger than 730,000 yr B.P.

Lin' Kova (1965) recorded magnetic reversals in cores taken from near the crest of the Marvin Ridge adjacent to the Lomonosov Ridge. The Brunhes/Matuyama boundary was recorded ~105 cm from the top of the cores, giving a sedimentation rate of 1.5 mm/1,000 yr. Extrapolating,

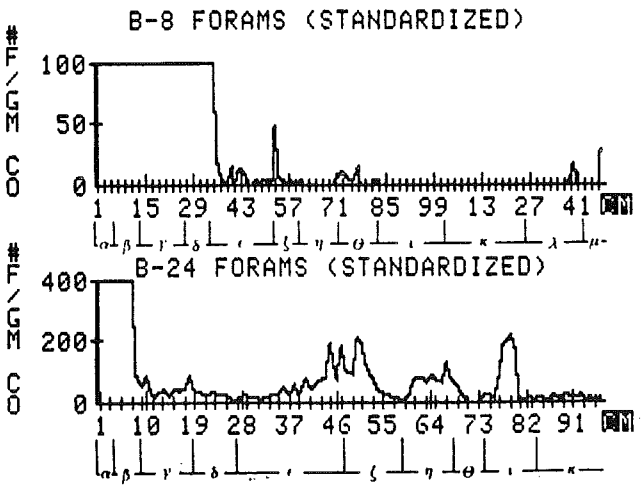

Figure 8. Comparison between standardized foraminifera abundance of core B-8 and core B-24; 1 = core top.

because of the short distance from the Marvin Ridge, and using this sedimentation rate, a date of 640,000 yr B.P. could be reasonable for the oldest sediment of the Kappa Member in core B-24.

Foraminifera were not of much help in resolving the age of the LOREX cores. All species of foraminifera that were identified range through the Pleistocene to the Holocene, except for the arenaceous *Reophax nodulosus*. According to O'Neill's (1981) study of 11 Amerasian Basin cores, this species ranges only to the latest early Pleistocene (within the Matuyama magnetic reversal). The magnetic data are preferred.

In addition, absence of calcareous dinoflagellates (Gilbert and Clark, 1983) may be important. *Thoracosphaera arctica* Gilbert and Clark is abundant in Arctic sediment prior to 730,000 yr B.P. (Gilbert and Clark, 1983). Their absence in cores B-8 and B-24 is negative evidence suggesting an age of younger than 730,000 yr B.P.

Magnetic signatures, foraminifera, and the absence of *Thoracosphaera arctica* together give weak evidence that the Makarov Basin Formation is <730,000 yr old. Confirmation of this age is obtained from conventional lithologic correlations, specifically, correlation with the stratigraphic units described for the late Cenozoic sediment of the Chukchi–Alpha Ridge areas (Clark and others, 1980; Minicucci and Clark, 1983). The correlation is dependent on texture, color, and key bed identification

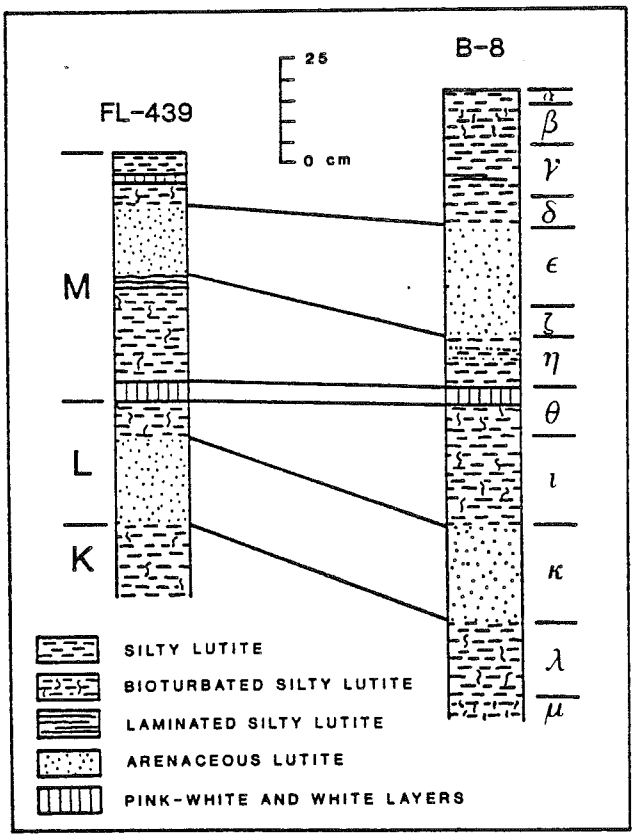

Figure 9. Correlation of core F1-439 (on the Alpha Cordillera) and core B-8 (Makarov Basin). Base of M = 400 k.y. (Boyd and others, 1984); mid-K = 730 k.y. (Clark and others, 1980).

for sediments of the two areas. This is diagrammed in Figure 9. For example, the members of the Makarov Basin Formation have the same textures as described for the upper half of unit K and units L and M of the Alpha Cordillera (Fig. 9). Equivalents of the Delta Member, a dark brown, silty lutite, cannot be distinguished in the Alpha Cordillera cores. Comparison of textural data between the areas shows similar trends, except for the missing Delta Member and a missing white layer in the Makarov Basin Formation that is present in the upper portion of unit M of Clark and others (1980). The basal pink-white layer that is present in unit M of the Alpha Ridge lithostratigraphy is recognized in the Theta Member of the Makarov Basin Formation. Although it is more weakly developed in the Theta Member, it is a key marker for correlation. The pink-white layer of B-8 is the first detrital carbonate peak of the core. The pink-white and white layers of Clark and others (1980) and Minicucci and Clark (1983) are also high in detrital carbonate.

The upper portion of unit L (Clark and others, 1980) was described as a highly bioturbated silty lutite, as is the Iota Member of the Makarov Basin Formation. The diameters of the larger burrows in unit L were described as being from 3 to 15 mm, whereas in the Iota Member, diameters reached a maximum of ~5 mm. The lower and major portion of unit L is nearly identical in color and texture to the arenaceous lutite of the Kappa Member, except that it lacks the ferromanganese micronodule laminations found in the Kappa Member. Most Alpha cores, however, have a faint dark lamination similar in appearance to the laminations of the Kappa Member (Minicucci and Clark, 1983).

The K unit of the Alpha Cordillera is nearly identical to the Lambda and Mu Members of the Makarov Basin Formation in both appearance and texture.

The percentage trends of ferromanganese micronodules are very similar between members of the Makarov Basin Formation (in core B-8) and the units described from the Alpha Cordillera. There is a high percentage in unit K which corresponds to the high percentage found in the Mu and Lambda Members. Percentages are much smaller in the lower part of unit L, corresponding to a similar abundance in the Kappa Member. Percentages rise again in the upper part of unit L and are high through the middle of the M unit, which corresponds to the high percentages in the Iota through Eta Members. Percentages are generally reduced in the upper part of unit M, as are percentages in the Zeta through Alpha Members, with the exception of one high peak recorded in the Gamma Member.

Foraminifera abundances do not show a close similarity between core B-8, which has very few specimens below the Delta Member, and Alpha Ridge cores (Clark and others, 1980).

Figure 9 summarizes the lithologic based correlations of the Alpha Ridge cores and core B-8. Because unit K of the Alpha Ridge contains the Brunhes/Matuyama boundary, this correlation indicates that the oldest member of the Makarov Basin Formation (Mu) is somewhat <730,000 yr old. All of the lithologic and magnetic work is consistent in this interpretation.

Assuming that the correlations based on lithologic characteristics, the absence of magnetic polarity reversals, and so forth, are valid (Fig. 9), a crude time scale for cores B-8 and B-24 can be constructed. This relies completely on the correlation of the base of unit M (pink-white layer), dated at 400 ka (Boyd and others, 1984), with the top of member Theta, and unit K (with the 730,000-yr magnetic boundary) with members Lambda and Mu (Fig. 9).

An unconventional check on the validity of these sedimentation rates can be made by the use of spectral analysis. Our program calculates autocorrelation functions and then performs a Fourier transformation of

the data (Panofsky and Brier, 1963). The output of frequency and period can be used with any time scale. The time scale which we used relies on a 4.7-k.y. interval for B-8 (Fig. 10) and a 6.3 k.y. interval for B-24. If this assumption of age is in error, spectral analysis could not be expected to identify the known orbital frequencies that have previously been established in the Arctic sediment record (Boyd and others, 1984). Core B-8 (Fig. 10) shows a strong concentration of power at 94 k.y. and 282 k.y., interpreted as being the 100–400-k.y. power eccentricity peak. The textural data for B-24, strongly affected by current transport, do not show the peaks developed in B-8 (Fig. 11), but the foraminifera record for this core (Fig. 11) has concentrations of power at approximately the expected orbital frequencies of 400–100 k.y. with hints of the 40- and 20-k.y. periods. Foraminifera accumulation on the Lomonosov Ridge was not affected by currents to the same degree as were the other sedimentary parameters. The concentration of power and the percentage of variance explained at the various peaks is in accord with previous oceanic sediment interpretations and is particularly useful for the LOREX material, because it supports the sedimentation rates interpreted from lithologic correlations.

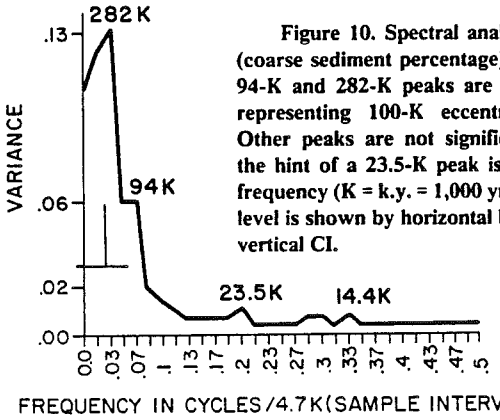

Figure 10. Spectral analysis of >63 μ (coarse sediment percentage) for core B-8. 94-K and 282-K peaks are interpreted as representing 100-K eccentricity forcing. Other peaks are not significant, although the hint of a 23.5-K peak is at precession frequency (K = k.y. = 1,000 yr). White noise level is shown by horizontal bar below 95% vertical CI.

LOREX CORRELATIONS

The stratigraphy of the Makarov Basin Formation can be recognized in 16 of the 42 LOREX cores (B-1, B-6, B-7, B-8, B-10, B-16, B-17, B-18, B-19, B-20, B-21, B-22, B-23, B-24, B-25, and B-26). These cores are located in the Makarov Basin and on the flanks and crest of the Lomonosov Ridge (Fig. 1). Other basin and ridge cores (B-2, B-3, B-4, and so forth) have at least superficial differences that have not been studied. Cores from the Fram Basin on the "east" side of the Ridge have significant differences, and the thin lithologic members of the Makarov Basin Formation cannot be visually correlated with the sediment of the Fram Basin (cores B-27 to B-42). Core B-31, from the Fram Basin, exhibits two zones of dark gray sediment unlike any sediment seen in cores of the Lomonosov Ridge or the Makarov Basin. These gray units are 15 cm and 10 cm thick; however, the sediment above, between, and below these gray units resembles the sediment of the Makarov Basin Formation in color but shows little evidence of color mottling (bioturbation) that is characteristic of many of the members of the Lomonosov Ridge and Makarov Basin cores. Faint rust-colored laminations are much more abundant within the brown sediments of the Fram Basin. The upper 15 cm of core B-31 resembles the Alpha Member of the Makarov Basin Formation; however, no other members can be visually correlated.

SUMMARY AND CONCLUSIONS

Glacial-marine sediment has been continuously deposited on the Lomonosov Ridge and in the Makarov Basin for at least the past 600,000–700,000 yr. The interbedded arenaceous and silty lutites record times of greater and lower influx of ice-rafted sediment. Differences in sediment accumulation, such as those described for the Makarov Basin and Fram Basin, suggest local sedimentary controls. This reflects the difference in either bottom-water chemistry or sedimentary processes, or both, between these basins. Probably, the Lomonosov Ridge acts as a dynamic

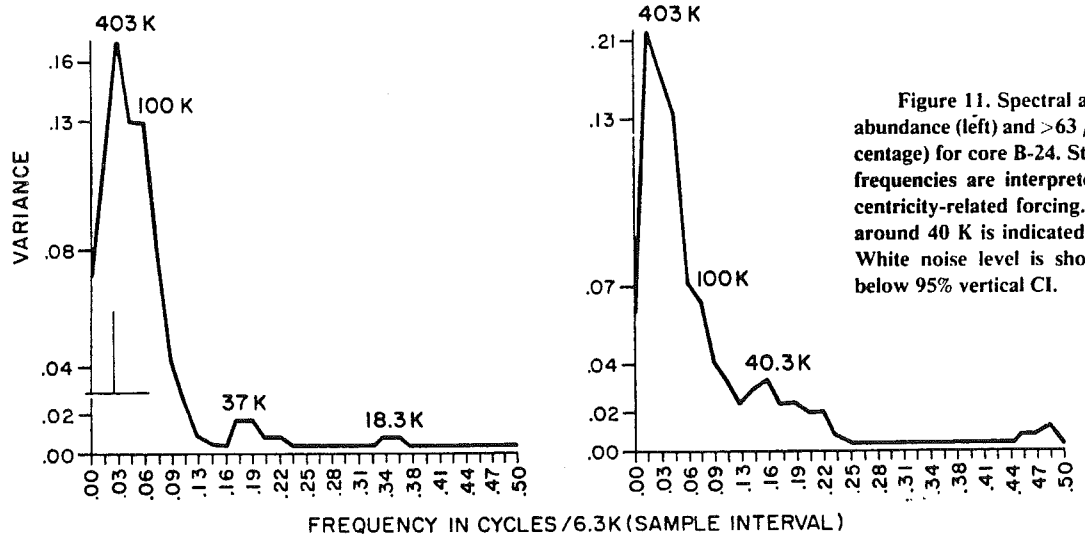

Figure 11. Spectral analysis of foraminifera abundance (left) and >63 μ (coarse sediment percentage) for core B-24. Strong 400-K and 100-K frequencies are interpreted as representing eccentricity-related forcing. Hint of tilt frequency around 40 K is indicated (K = k.y. = 1,000 yr). White noise level is shown by horizontal bar below 95% vertical CI.

barrier between processes affecting the Fram Basin and processes affecting the Markarov Basin; furthermore, the sediments on the crest of the Lomonosov Ridge can be readily correlated to the sediments in the Makarov Basin but not in the Fram Basin.

Our study permits the following conclusions. (1) A stratigraphy can be established for sedimentary units of the Lomonosov Ridge crest and the Makarov Basin. The sediment recovered permits division of the Makarov Basin Formation into twelve members. (2) The Makarov Basin Formation has a stratigraphy distinctly different from that of the sediment of the Fram Basin. (3) The Makarov Basin Formation can be correlated with the younger stratigraphic units established for the Alpha Cordillera–Chukchi area. (4) The age of the oldest sediment of the Makarov Basin Formation is between 600,000 and 700,000 yr. (5) Ferromanganese micronodule abundances in the Makarov Basin are associated with silty lutite and bioturbated silty lutite. (6) The Makarov Basin has been the depositional sink of a significant proportion of the silt-sized and clay-sized particles that have passed through the water column above the Lomonosov Ridge throughout much of the late Pleistocene and Holocene Epochs.

ACKNOWLEDGMENTS

We acknowledge all those involved with the Lomonosov Ridge Experiment (LOREX) for the assistance in obtaining the sediment cores. LOREX was sponsored by the Earth Physics Branch of the Geological Survey of Canada. We acknowledge the Office of Naval Research, under Contract No. 00014-67-A0238-0002, for support of this research.

G. A. Jones, Woods Hole Oceanographic Institution; Steven Carey, Bob Goldstein, Randy Marquard, J. A. Kitchell, and Lisa Morris, University of Wisconsin, aided in many ways.

REFERENCES CITED

Aagaard, K., 1981, On deep sea circulation in the Arctic Ocean: Deep-Sea Research, v. 28, Pt. A, no. 3, p. 251–268.

Blasco, S. M., Bornhold, B. D., and Lewis, C.F.M., 1979, Preliminary results of surficial geology and geomorphology studies of the Lomonosov Ridge, Central Arctic Basin: Current research, Part C, Geological Survey of Canada Paper 79-1C, p. 73–83.

Boyd, R. F., Clark, D. L., Jones, Glenn, Ruddiman, W. F., McIntyre, Andrew, and Pisias, N. G., 1984, Central Arctic Ocean response to Pleistocene Earth orbital variations: Quaternary Research, v. 22, p. 121–128.

Campbell, J. S., and Clark, D. L., 1977, Pleistocene turbidites of the Canada Abyssal Plain of the Arctic Ocean: Journal of Sedimentary Petrology, v. 47, p. 657–670.

Chamberlain, C. K., 1975, Trace fossils in DSDP cores of the Pacific: Paleontology, v. 47, p. 1074–1996.

Clark, D. L., and Hansen, Arnold, 1983, Central Arctic Ocean sediment texture: A key to ice-transport mechanism, *in* Molnia, B., ed., Glacial-marine sedimentation: New York, Plenum Press, p. 301–330.

Clark, D. L., Whitman, R. R., Morgan, K. A., and Mackey, S. D., 1980, Stratigraphy and glacial-marine sediments of the Amerasian Basin, central Arctic Ocean: Geological Society of America Special Paper 181, 57 p.

Clark, D. L., Vincent, Jean J.-S., Jones, G. A., and Morris, W. A., 1984, Correlation of marine and continental glacial and interglacial events, Arctic Ocean and Banks Island: Nature, v. 311, p. 147–149.

Galt, J. A., 1973, A numerical investigation of Arctic Ocean dynamics: Journal of Physical Oceanography, v. 3, p. 379–396.

Gilbert, M. W., and Clark, D. L., 1983, Central Arctic Ocean paleoceanographic interpretations based on late Cenozoic calcareous dinoflagellates: Marine Micropaleontology, v. 7, p. 385–401.

Goldstein, R. H., 1983, Stratigraphy and sedimentology of ice-rafted and turbidite sediment, Canada Basin, Arctic Ocean, *in* Molina, B., ed., Glacial-marine sedimentation, New York, Plenum Press, p. 367–460.

Herman, Y., 1974, Arctic Ocean sediments, microfauna, and the climatic record in late Cenozoic time, *in* Herman, Y., ed., Marine geology and oceanography of the Arctic Seas, New York, Springer-Verlag, p. 283–348.

Huntsberger, D. V., and Billingsley, P., 1981, Elements of statistical inference, (5th edition): Boston, Allyn and Bacon, 505 p.

Jones, G. A., and Kaiteris, P., 1983, A vacuum-gasometric technique for rapid and precise analysis of calcium carbonate in sediment and soils: Journal of Sedimentary Petrology, v. 53, p. 655–660.

Lagoe, M. B., 1977, Recent benthic foraminifera from the central Arctic Ocean: Journal of Foraminiferal Research, v. 7, p. 106–129.

Lin' Kova, T. I., 1965, Some results of paleomagnetic study of Arctic Ocean floor sediments, *in* Nastoyashcheye i prosuloye magnitnogo polia zemli (The present and the past of the geomagnetic field): Moscow, Nauka Press, p. 279–291.

Minicucci, D. A., and Clark, D. L., 1983, A late Cenozoic stratigraphy for glacial-marine sediments of Eastern Alpha Cordillera, central Arctic Ocean, *in* Molnia, B., ed., Glacial-marine sedimentation: New York, Plenum Press, p. 331–366.

O'Neill, B. J., 1981, Pliocene and Pleistocene benthonic foraminifera from the central Arctic Ocean: Journal of Paleontology, v. 55, no. 6, p. 1141–1170.

Panofsky, H. A., and Brier, G. W., 1963, Some applications of statistics to meteorology: University Park, Pennsylvania, Pennsylvania State University, p. 140–158.

Pitman, W. C., III, and Talwani, M., 1972, Seafloor spreading in the North Atlantic: Geological Society of America Bulletin, v. 83, p. 619–646.

Sweeney, J. F., and Blasco, S. M., 1982, Continental ridges in the Arctic Ocean. LOREX constraints, *in* Johnson, G. L., and Sweeney, J. F., eds., Structure of the Arctic: Tectonophysics, v. 89, p. 217–237.

Manuscript Received by the Society June 25, 1984
Revised Manuscript Received October 15, 1984
Manuscript Accepted December 24, 1984

Printed in U.S.A.

PALEOCEANOGRAPHY, VOL. 1, NO. 2, PAGES 181-195, JUNE 1986

PLEISTOCENE CALCITE LYSOCLINE AND PALEOCURRENTS OF THE CENTRAL ARCTIC OCEAN AND THEIR PALEOCLIMATIC SIGNIFICANCE

Thomas H. Morris and David L. Clark

Department of Geology and Geophysics,
University of Wisconsin, Madison

Abstract. Most previous references to the depth of the Arctic Ocean calcite lysocline have been based on comparison with the known North Atlantic carbonate compensation depth. Foraminifera from cores taken at depths ranging from 2316 to 3956 m provide the first firm calcite lysocline constraints for the central Arctic Ocean. These data suggest progressive lowering of the calcite lysocline to at least 3956 m during the past ~1.5 m.y., interrupted by 300-m rises of the lysocline level that apparently correspond with interglacial and early glacial climate conditions. Most cores from less than 2450 m indicate variable foraminifera abundance but continual presence of foraminifera for the past ~1.5 m.y. Low abundances commonly occur in coarse-textured sediment and are interpreted to represent low productivity during major deglaciations. Within certain equivalent lithostratigraphic units representing the past ~1.5 m.y. there is an absence of foraminifera in cores from depths greater than 2450 m. This absence of foraminifera is interpreted to be due to dissolution. Dissolution intervals are associated with fine-grain sediments interpreted to represent interglacial and early glacial climate conditions. The interpretation of a rise in the lysocline level during interglacials is in apparent disagreement with studies reported from lower latitudes in the Atlantic Ocean but is complementary with the hypothesis that formation of Norwegian-Greenland Sea Deep Water (NGDW) and cold Canada Basin Deep Water occurs during interglacials. Paleocurrent data from the Lomonosov Ridge and the adjacent Makarov Basin are interpreted to indicate that during periods of increased glacial ice influx into the Arctic Ocean system there was reduced current activity in the bottom and intermediate water masses relative to periods when little glacial ice was present. This is in accord with the idea that NGDW affects intermediate and deep water circulation in the central Arctic Ocean and hence the calcite lysocline level.

Paper number 6P0137.
0883-8305/86/006P-0137$10.00

INTRODUCTION

The Arctic Ocean is divided into two structurally distinct basins, the Amerasian and the Eurasian. Although the Lomonosov Ridge acts as a dynamic barrier between the two basins by reducing flow, intermediate water exchange does occur [Aagaard, 1981]. There is a direct deep water connection between the Arctic Ocean and the North Atlantic Ocean (Norwegian and Greenland Sea), the Fram Strait (Figure 1). This connection permitted continued water exchange during the late

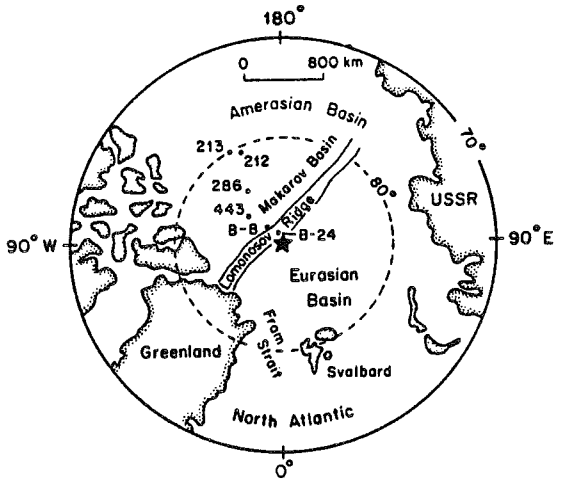

Fig. 1. Arctic Ocean, divided by Lomonosov Ridge into Amerasian and Eurasian basins. Fram Strait is the deepwater connection to the Greenland Sea and North Atlantic Ocean, and this connection was in existence during the late Cenozoic. Makarov Basin adjacent to Lomonosov Ridge is the site of deep core B-8. Core locations are as follows: B-8, 88°29.72'N, 167°07.83'W (water depth of 3956 m); B-24, 89°05'N, 168°29.50'W (water depth of 1600 m); Fl-212, 80°29.59'N, 159°37.96'W (water depth of 3642 m); Fl-213, 80°24.51'N, 159°27.47'W (water depth of 3349 m); Fl-286, 84°00.84'N, 144°02.17'W (water depth of 2316 m); Fl-443, 85°57.96'N, 121°07.71'W (water depth of 2436 m).

Cenozoic and also resulted in some similarities in the paleoceanographic conditions for the two ocean basins. It could be expected that the production of deep water in the Norwegian and Greenland seas would leave some record in the Arctic Ocean [e.g., Aagaard et al., 1985].

Our objectives in this study are to (1) present data that provide constraints for the depth of the calcite lysocline in the central Arctic Ocean for the last ~1.5 m.y. by recognition of foraminifera dissolution intervals, (2) present sediment texture interpretations from equivalent stratigraphic units of the Makarov Basin Formation (Lomonosov Ridge area) and show how this provides the first paleocurrent data for the central Arctic Ocean, and (3) interpret the impact of the production and interchange of Norwegian-Greenland Sea Deep Water (NGDW) for the Arctic Ocean during interglacial and glacial periods.

CHRONOLOGY

These objectives can only be achieved in the context of a workable lithostratigraphy and a reliable time scale for the central Arctic Ocean sediment. A late Cenozoic lithostratigraphy based on sediment texture, color, degree of bioturbation, abundance of Fe-Mn micronodules, and microfossils has been established [Clark et al., 1980]. This lithostratigraphic system organized the late Miocene or early Pliocene through Holocene sediment of the central Arctic Ocean (Alpha Ridge to Chukchi area) into 13 units designated A to M, from oldest to youngest [Clark et al., 1980] (Figure 2). The stratigraphy is widely used in central Arctic Ocean sediment studies [O'Neill,

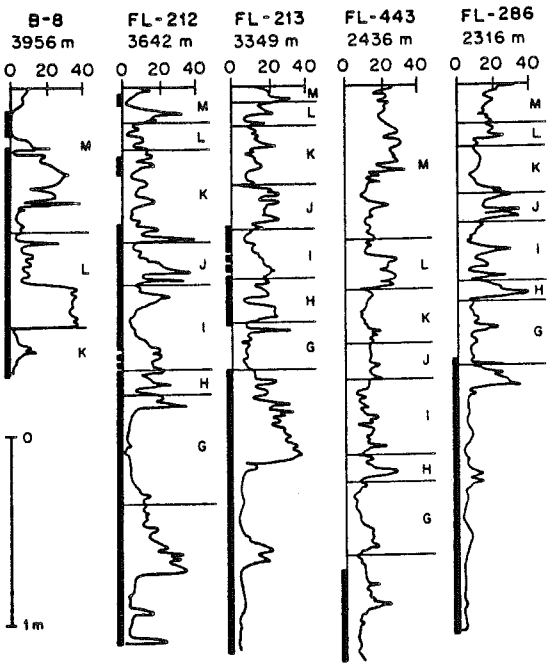

Fig. 2. Textural and foraminifera content of central Arctic Ocean sediment cores. The percentage of coarse fraction (>63μ) is indicated by 0-40% scale. Intervals barren of foraminifera are indicated by solid bars. Amerasian Basin stratigraphy (M, L, etc.) is indicated. The Brunhes/Matuyama magnetic reversal is in the middle of unit K (730 kyr).

1981; Minicucci and Clark, 1983; Gilbert and Clark, 1983; Boyd et al., 1984; Clark et al., 1984; Goldstein, 1983; Mudie and Blasco, 1985; Aksu, 1985a, b; Mudie, 1985].

The younger lithostratigraphic units have also been correlated with the Makarov Basin Formation of the Lomonosov Ridge area [Morris et al., 1985]. Since the publication of the Alpha-Chukchi stratigraphy, additional work in different parts of the central Arctic Ocean has documented facies changes in some of the stratigraphic units, particularly the older A to F units [Minicucci and Clark, 1983]. The Canadian Expedition to Study the Alpha Ridge (CESAR) research confirmed the validity of the stratigraphy as well as the facies differences in the older units [e.g., Mudie and Blasco, 1985]. All of the above cited work provides documentation of the reliability of correlation of the A to M stratigraphy over almost one half of the Arctic Ocean.

The ages of the stratigraphic units were first determined on the basis of magnetic measurements and extrapolation of sedimentation rates from major magnetic reversals [Steuerwald et al., 1968; Clark et al., 1980]. These ages were in agreement with sedimentation rates established on U-Th and ^{14}C studies [Olsen and Broecker, 1961; Hunkins and Kutschale, 1967; Ku and Broecker, 1967]. Additional paleomagnetic work in different labs was consistent with ages determined from radiometric techniques as well as the original paleomagnetic measurements [Lín Kova, 1965; Hunkins et al., 1971].

Recently, the validity of the sedimentation rates and, consequently, the age of the lithostratigraphic units was challenged by study of amino acid diagenesis [Sejrup et al., 1984]. The amino acid work was based on foraminifera from some of the cores that could be correlated with the established lithostratigraphy. The amino acid dates suggested that the oldest part of one Arctic core, magnetically interpreted to be several million years old, was less than 0.2 Ma and perhaps only ~72 kyr [Sejrup et al. 1984]. In addition, a short $\delta^{18}O$ stratigraphy, interpreted from sediment collected in the Greenland Sea between Greenland and Svalbard, had been interpreted to suggest that the central Arctic Ocean stratigraphic ages are too old [Zahn et al., 1985].

Because of these reports, a thorough reexamination of all of the evidence for the age of Arctic Ocean sediment was clearly called for and was accomplished as one of the principal contributions of the Canadian CESAR research [Jackson et al., 1985]. The results of this study, directed toward sediment cores taken in approximately the same part of the Arctic Ocean from which the lithostratigraphy was originally established, were positive for the validity and age of the established A to M stratigraphy. The study included a new and rather complete magnetostratigraphy, a new dinoflagellate stratigraphy for the Arctic Ocean (but based on well-dated dinoflagellate sequences in Subarctic areas) and provided additional oxygen isotope evidence for age assignments [Mudie and Blasco, 1985; Aksu, 1985a, b; Mudie, 1985; Aksu and Mudie, 1985]. In addition to supporting the validity of the earlier correlation and age assignments, the CESAR data also are consistent with new accelerator ^{14}C dating of central Arctic Ocean sediment that supports the validity of the ages of the established A to M lithostratigraphy [Clark et al., 1986]. Certainly, the amino acid diagenesis data must be re-evaluated in the face of this massive evidence for the validity of the earlier established ages of the central Arctic Ocean lithostratigraphy.

The $\delta^{18}O$ stratigraphy for the short cores taken between Greenland and Svalbard indicated that the sediment in this area was deposited up to 10 times as fast as that of the central Arctic Ocean [Zahn et al., 1985]. We are in agreement with this and base our agreement on $\delta^{18}O$ work now largely completed in our lab on core YMER MG-123, from the same area as the cores reported by Zahn et al. [1985]. We are not in agreement with the suggestion of Zahn et al. [1985] that the central Arctic Ocean chronology should be reinterpreted using a high sedimentation rate model based on the Greenland sea core. Evidence is available that the two areas simply have different sedimentation rates. For example, there is a greater rate of accumulation of glacial-marine sediment that is transported by the East Greenland current, and in addition, turbidite accumulation in the Greenland Sea is not matched in the A to M stratigraphy. The high sedimentation rates in the Greenland Sea are real but are controlled by different oceanographic conditions than those of the central Arctic Ocean.

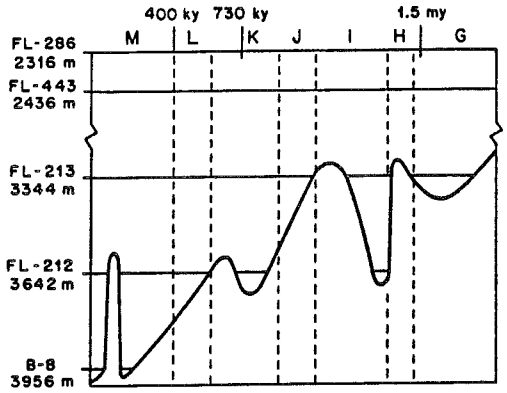

Fig. 3. Lysocline curve for the central Arctic Ocean. The drop from the ~3300-m level, 1.5 Ma, to the present level (top of unit M), with 300-m rises, is indicated. Stratigraphy and approximate absolute ages are shown. Core localities are shown in Figure 1. Foraminifera barren zones are shown in Figure 2.

THE CENTRAL ARCTIC OCEAN LYSOCLINE

Introduction

The conventional approach to interpretation of the carbonate dissolution history of any ocean basin is to first establish the modern location of the lysocline and carbonate compensation depth (CCD), including factors controlling their distribution, and then work back in time to formulate a historical sequence of events. Unfortunately, the limited data base for the central Arctic Ocean and the logistical problems of doing research in an ice-covered ocean have precluded this approach for us. Instead, we base our interpretations on data available from an incomplete sediment record obtained during two Arctic Ocean research programs, that of the drift of ice island T-3 from 1963 to 1974, and the Canadian Lomonosov Ridge Experiment (LOREX) ice pack drift during a few weeks in 1979. The results may be less than perfect for normal oceanic research but represent almost all that is available for the ice-covered central Arctic Ocean.

The calcite lysocline and the carbonate compensation depth are not distinguished in this study for two reasons: (1) our depth resolution is insufficient to distinguish between the calcite lysocline and the CCD, and (2) relatively abundant and diverse foraminiferal assemblages are required for complete lysocline interpretations. During the Pleistocene there were only two important species of central Arctic Ocean planktonic foraminifera, and benthonic species are uncommon. For these reasons we refer to the level of obvious dissolution as the calcite lysocline. Theoretically, this level lies above the CCD. It is also important to note that the depth resolution of this study permits calculation of only an average rate for the changes in depth of the calcite lysocline during the late Pleistocene. Rises of less than 300 m have not been documented. Extrapolation from our calcite lysocline curve (Figure 3) places the present lysocline between 4050 m and 4150 m. We cannot confirm this because there are no Arctic Ocean sediment cores taken at these depths. It is entirely possible that fluctuations for the last 60,000 years (through the last major glacial-deglacial stage) have been greater and that the calcite lysocline has again risen during the present interglacial. We only know that the present depth of the calcite lysocline is deeper than 3956 m.

The Data

The abundance of calcareous planktonic foraminifera (i.e., Neogloboquadrina pachyderma and Globigerina quinqueloba) and the percentage of coarse sediment from six central Arctic Ocean cores have been analyzed at 1-cm intervals (Figure 2). Using the lithostratigraphy of Clark et al. [1980] and Morris et al. [1985] and feeling secure in the validity of this because of the results of CESAR [Jackson et al., 1985], foraminifera abundance may be compared among time equivalent units from different depths. In general, coarse-grain-textured units (>63μ) tend to have lower foraminifera abundances than do fine-grain units. Coarse-grain sedimentation occurs during late glacial as well as deglacial stages when the rate of glacial ice flux into the Arctic Ocean is accelerated (Figure 4). During these periods the upper water photic zone has a reduced salinity and greater turbidity and may be more turbulent. These factors may result in a decline of foraminifera productivity [Lewis et al., 1984]. The increased amount of glacial ice-rafted sediment also increases the sedimentation rate and thereby affects apparent foraminifera abundances in the cores.

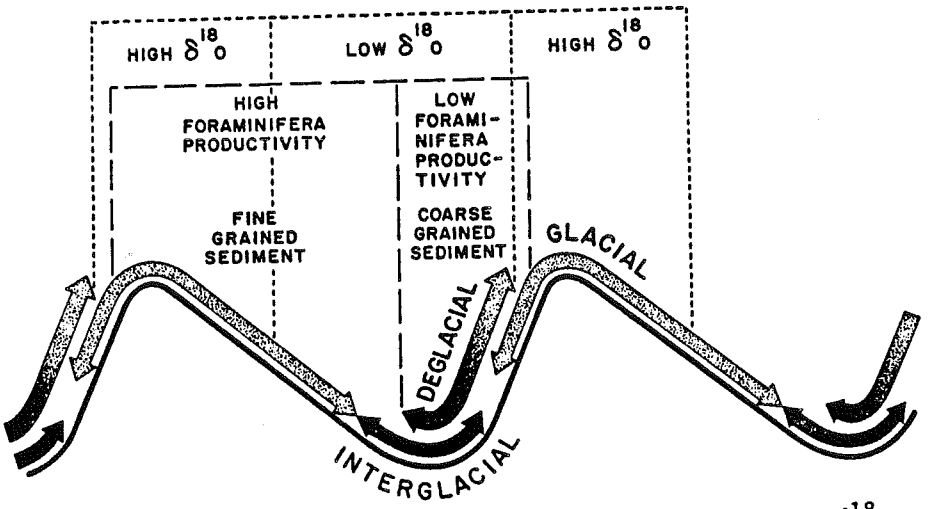

Fig. 4. Climate curve for Arctic Ocean showing relationship among $\delta^{18}O$ values, foraminifera productivity, and sediment texture. Note that productivity and $\delta^{18}O$ values are out of phase on the climate curve (after Clark and Morris [1985]).

Cores taken from relatively shallow depths (FL-286 from 2316 m and FL-443 from 2436 m) show different abundances of foraminifera, yet the calcareous fossils are consistently present in sediments younger than basal unit G, which is dated at approximately 1.5 Ma (Figure 2).

Core FL-213, from 3349-m depth, has barren intervals in the upper part of unit I and in unit H with an interval of low abundance between I and H (Figure 2). A zone from basal K to uppermost I also has a low abundance of foraminifera and may represent a time when the calcite lysocline was at this depth. Below the middle of unit G, no calcareous foraminifera are present.

Core FL-212, from 3642-m depth, has barren intervals within unit M and the upper part of unit K (Figure 2). Calcareous foraminifera are absent below the lowermost part of unit K, except for a low-abundance interval in the lower part of unit I. Approximately 50% of the foraminifera tests in the low-abundance interval of unit I are pitted.

Core B-8, from 3956 m, the deepest sediment core taken in the Canadian (Amerasian) Basin, has foraminifera in only the upper one half of unit M equivalents (Figure 2). This interval includes members Alpha through Delta of the Makarov Basin formation [Morris et al., 1985]. Member Gamma has a drastically reduced faunal abundance relative to the adjacent members (Figures 2 and 5). Foraminifera in the Gamma member are pitted. The ratio of fragmented tests to the total number of tests is greater than 0.5 for most samples within this member. This is much higher than the ratio in adjacent members (Table 1).

Interpretations

Although correlation among the various lithostratigraphic units is quite easily accomplished [Clark et al., 1980; Morris et al., 1985], precise dating of the barren intervals is more difficult. Sedimentation rates are estimated by

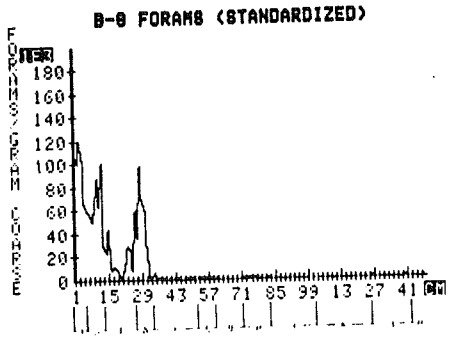

Fig. 5. Foraminifera abundance (x1000) for B-8. Note reduced abundance in Gamma member interpreted to be isotopic stages 5 and (most of) 4.

TABLE 1. Number of Whole and Fragmented Neogloboquadrina pachyderma From Core B-8 (3956 m)

Member	Sample	Whole	Fragmented	Fragmented/Total
Alpha	1	10,215	563	0.05
	2	11,970	765	0.06
	3	12,128	900	0.07
	4	13,703	495	0.03
	5	7,515	360	0.05
Beta	6	8,235	270	0.03
	7	12,060	360	0.03
	8	6,975	383	0.05
	9	7,245	293	0.04
	10	11,768	495	0.04
	11	3,600	135	0.04
	12	2,871	153	0.05
	13	284	233	0.45
Gamma	14	66	250	0.79
	15	164	268	0.62
	16	11	62	0.85
	17	25	79	0.76
	18	15	58	0.79
	19	3	29	0.91
	20	0	2	1
	21	0	5	1
	22	7	153	0.96
	23	273	303	0.53
	24	182	58	0.24
	25	12	56	0.82
	26	468	112	0.19
Delta	27	7,178	1,080	0.13
	28	17,753	2,610	0.13
	29	19,125	3,240	0.14
	30	16,200	3,375	0.17
	31	6,365	1,383	0.18
	32	372	128	0.26
	33	96	28	0.23
Epsilon	34	93	26	0.22
	35	44	10	0.19

The ratio of fragmented tests to the total number of tests is the measure of dissolution.

extrapolation from magnetic reversals when isotopic data are unavailable. The Brunhes-Matuyama reversal has been recognized in over 200 central Arctic sediment cores [Clark et al., 1980; Aksu and Mudie, 1985]. The reversal is always found within unit K and is usually in the upper middle portion of the unit. Extrapolating from this reversal, sedimentation rates were estimated for cores FL-212 and FL-213, and approximate age determinations were made for intervals barren of foraminifera (Figure 3). Isotopic data from the planktonic foraminifera Neogloboquadrina pachyderma are available for Makarov Basin Formation core B-24 from 1600-m depth. This core is located approximately 60 km to the north of B-8 on the crest of the Lomonosov Ridge. Although the isotopic data suggest a significant salinity

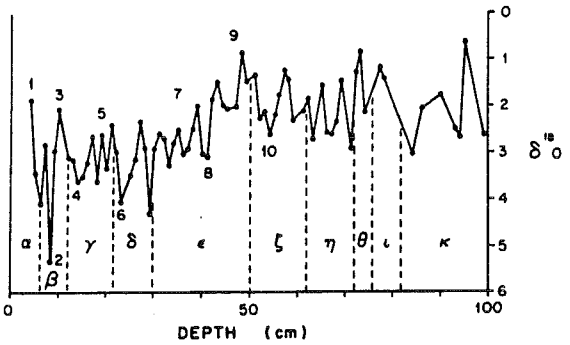

Fig. 6. Plot of $\delta^{18}O$ values of the planktonic foraminifera Neogloboquadrina pachyderma for core B-24 (see Figure 1). Makarov Basin formation stratigraphy is indicated [Morris et al., 1985]. Isotopic stage designations are indicated.

contribution to the overall signal, stage assignments can be made when analyzed in conjunction with sedimentation rates extrapolated from Lomonosov Ridge paleomagnetic data [Lińa Kova, 1965; Morris et al., 1985] as well as comparison with several unpublished central Arctic Ocean oxygen and carbon isotope curves. (A complete isotope stratigraphy for the late Cenozoic central Arctic is our current area of research). The isotopic data now available (Figure 6) are interpreted to indicate that the Gamma member represents isotopic stage 5 and most of stage 4. If accurate, this places the age span of the Gamma member at approximately 128 kyr to 70 kyr [Shackleton and Opdyke, 1973). Correlating from B-24 yields a sedimentation rate of 1.875 mm/1000 years for core B-8. This corresponds to an age range of 139 kyr to 69 kyr for the Gamma member in core B-8. We suggest that the uppermost barren interval of FL-212 (Figure 2) probably represents this same time interval. Using these ages, a crude time model of the lysocline activity in the Arctic Ocean is constructed (Figure 3). We emphasize that the details of the rise and fall of the lysocline are less clear than the progressive drop from 3349 m prior to deposition of unit G (~1.5 m.y.) to ~4000 m during deposition of the youngest Arctic sediment, unit M.

Unit G is considered to be approximately 1.5 Ma, and this is the time of first occurrence of abundant calcareous plankton in central Arctic Ocean sediment. A few cores taken in water depths of less than 2300 m have occasional intervals of few or no foraminifera even in sediment younger than unit G. Periodic times of low productivity or diagenetic factors (such as undersaturated shelf waters sinking to isopycnic levels and spreading laterally) may explain these unusual occurrences.

More important to note is that overall, coarse-grain units generally have fewer foraminifera than fine-grain units, at least in the G to L portions of the cores. Not only do the environmental conditions associated with deposition of coarse-grain sediment (i.e., deglaciation) influence general productivity of foraminifera, but the greater rate of accumulation of coarse-grain sediment probably dilutes foraminifera concentration. Finer-grain units represent more favorable environmental conditions, and greatest concentrations of calcareous plankton always occur in these units [e.g., Gilbert and Clark, 1983].

All of the barren intervals in our cores that are interpreted to represent periods of dissolution are associated with fine-grain sedimentary units whose shallower depth equivalents contain abundant calcareous plankton. We interpret this as an indication of the validity of these intervals as dissolution zones. Tests are pitted, and the proportion of fragmented tests rises in these depleted fine-grain intervals (Table 1). A single exception is a short coarse-grain interval within unit H of core FL-213, but even in this barren zone its base is associated with very fine grain sediment. The Gamma member of core B-8 has virtually no sand-sized (i.e., glacial ice-rafted) material in it. This is also true of the most recent barren zone of core FL-212 (Figure 2). Silty lutite is deposited during interglacial and early glacial stages, mostly by pack ice [Clark and Hanson, 1983].

ARCTIC OCEAN PALEOCURRENTS

Lomonosov Ridge and Makarov Basin

What is the effect of currents on the lysocline [e.g., Berger, 1977]? Unfortunately, paleocurrent data are virtually lacking for the central Arctic Ocean, but we have identified one area that yields some data. Core B-8, at 3956-m depth within the Makarov Basin, and core B-24, at 1600-m depth upon the crest of the Lomonosov Ridge, are representative of the Makarov Basin Formation [Morris et al.,

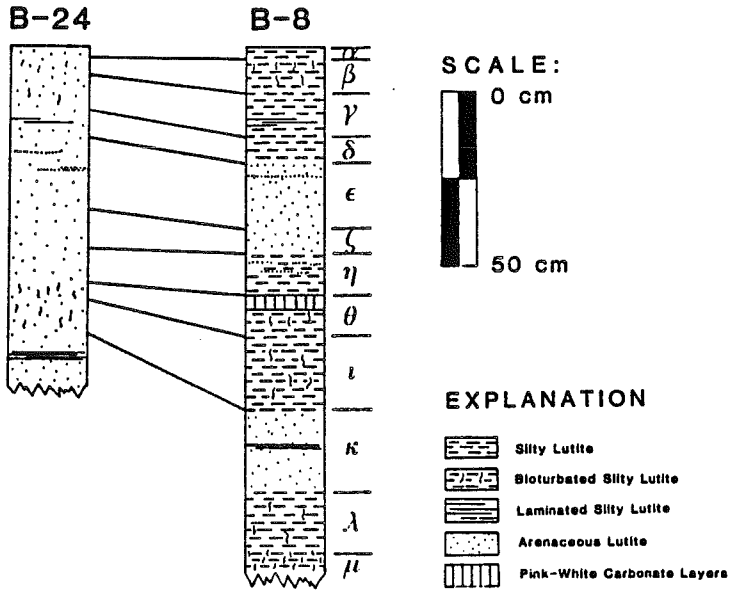

Fig. 7. Correlations of B-24 and B-8. Arenaceous muds are defined as >15% coarse sediment by weight. Note that units on Lomonosov Ridge crest (B-24) are thinner and coarser than equivalent units in Makarov Basin (B-8).

1985] (Figure 7). These two cores are uniquely situated to compare textural changes in the sediment between the basin and the ridge crest. There is high variability in weight percent of the coarse sediment fraction among the 12 sedimentary members (Figure 8). This is particularly true of B-8, whose members range in coarse weight percent from 3 to 32. The average coarse weight percent is 10.68.

In contrast, percent coarse sediment by weight in B-24 (Lomonosov Ridge) is higher and generally less variable (Figure 8). With the exception of the Alpha member, which has an average coarse weight percent of 59.0, all of the members of B-24 have average coarse weight percent between 15.3 and 32.3. The average coarse weight percent of all of the members of B-24 is 34.7. Table 2 illustrates the fact that equivalent members of the formation are coarser (on the average) on the Lomonosov Ridge than in the Makarov Basin.

Geographical and bathymetric differences are important when comparing the sediment of the cores. B-8 was recovered 60 km south of B-24, from water 2356 m deeper. B-24 does not include members Lambda or Mu but only the upper ten members of the Makarov Basin formation (Figure 7). Seven of the ten comparable members are thinner on the crest than in the basin. Two of the three remaining members are within 2 cm of being equal in length and are approximately equal in coarse weight percent. The stratigraphic units can be easily correlated both visually (using color, degree of bioturbation, ferromanganese concentration along laminae, sharpness of boundary contacts, etc.) and also with x-radiography [Morris et al., 1985]. Only the foraminifera abundance and coarse weight percent show important differences.

Interpretations

Currents could result in transportation of a significant proportion of silt- and clay-sized particles away from the Lomonosov Ridge and produce stratigraphic units that are thinner and coarser on the ridge crest. According to Stokes Law, large silt-sized particles (0.06 mm) have a settling velocity of less than 0.2 cm/s in water with a temperature of 0°C [Blatt et al., 1980]. Such particles, when affected by a horizontal current of 10 cm/s could be displaced horizontally more than 500 m for every 10 m of settling in the water column. Any turbulence would enhance the lateral component by inhibiting settling. These data are significant

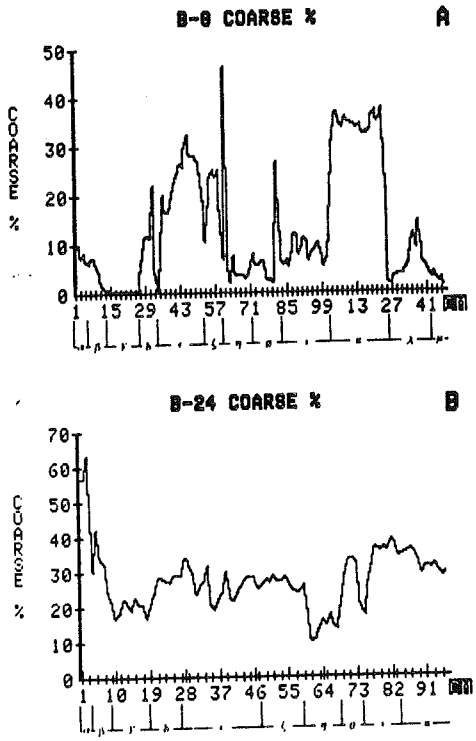

Fig. 8. Percentage coarse sediment (>63μ) in (a) B-8 and (b) B-24 (localities are shown in Figure 1).

because central Arctic Ocean water temperature ranges from at least -2.0°C to 0°C [Coachman and Aagaard, 1974].

Aagaard [1981] recorded fluctuations in current velocities 25 m above the surface of the Lomonosov Ridge with a mean velocity of only 2.7 cm/s. However, a maximum velocity of 12.2 cm/s was recorded, and this is sufficient to transport silt- and clay-sized particles. Two hundred meters above the sediment surface, a maximum velocity of 9.6 cm/s was recorded. These pulsating current velocities are directed obliquely (approximately 30° to the isobaths) from the Fram Basin across the Lomonosov Ridge into the Makarov Basin. Fluctuating velocities of this magnitude should permit deposition of silt- and clay-sized particles during low-velocity pulses but inhibit deposition of particles during higher-velocity pulses (12.2 cm/s). We assume that there have been times during the Pleistocene, such as those of the present, when such current sorting would produce coarser sediment and thinner units on the ridge crest, and less coarse sediment but thicker units in the adjacent basin. This can be verified by comparing the average coarse weight percent of each member of Pleistocene cores B-8 and B-24. The difference between the average percent >63 μ sediment of equivalent units on the ridge crest and the adjacent basin can be taken as an index of the strength or persistence of currents over the ridge crest relative to the basin (Figure 9). This paleocurrent index plot is interpreted as follows: the greater the index number, the greater or more persistent were the current velocities on the Lomonosov Ridge during deposition of a particular member. The highest value recorded is for the Alpha (i.e., youngest) member. It is

TABLE 2. Average Coarse Weight Percent of Each Member From B-8 and B-24

Member	B-8 Average	B-24 Average	Average of cores
Alpha	8.04	59.03	33.54
Beta	3.98	32.28	18.13
Gamma	1	19.68	10.34
Delta	10.39	26.48	18.44
Epsilon	21.48	26.31	23.9
Zeta	20.21	26.4	23.33
Eta	7.54	15.3	11.42
Theta	7.66	30.1	18.88
Iota	8.07	31.63	19.85
Kappa	32.50	32.14	32.32
Lambda	5.71	---	---
Mu	2.32	---	---

The average for each member of cores is shown.

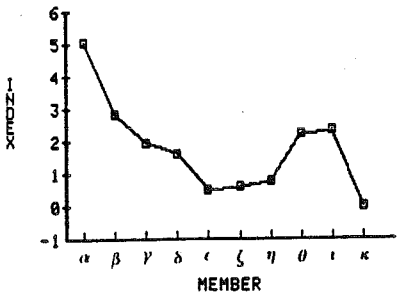

Fig. 9. Paleocurrent index as measure of difference in coarse-weight percent of equivalent members, Lomonosov Ridge and Makarov Basin. The greater the index number, the greater or more persistent were the currents over the ridge during deposition of any particular member.

recognized that this uppermost unit could have been affected by blowoff during the coring process, resulting in winnowing of clay and silt. However, even if blowoff occurred, the data from the underlying Beta member suggest that recent currents over the Lomonosov Ridge are greater than have existed since deposition of member Theta. Especially noteworthy is the fact that the obvious coarse members (Epsilon, Zeta, and Kappa of core B-8) have minimal coarse weight percent differences (Figure 9) and minimal thickness differences (Figure 10). These members must be the result of periods of increased glacial ice influx into the Arctic system. Glacial ice carries much fine-grain material (e.g., rock flour, etc.) as well as coarse-grain material, and it is likely that during periods of increased glacial ice the Arctic Ocean water column would be more turbid than during periods when less glacial ice was present. Deposition of "coarse" sediment also involves 50% or more silt- and clay-sized particles; hence under constant current velocities the greatest textural differences between equivalent sedimentary members would be expected to occur during time of increased glacial ice influx. The absence of such differences in units Epsilon, Zeta, and Kappa may indicate that average current conditions (surface, middepth, and bottom currents) over the Lomonosov Ridge were reduced during periods of abundant glacial ice in the Arctic surface waters.

All of these considerations are based on the idea that source area, transportation processes, and all related factors during the Pleistocene remained within the range presently understood for the area. The bathymetric and paleoceanographic configurations of the deep Arctic Ocean have changed little during the past few million years, and it is not surprising that modern Arctic Ocean current measurements show values that are sufficient to explain sedimentary differences during the Pleistocene as well. The significance of these presently isolated interpretations will increase as circulation patterns of the world ocean during glacial and interglacial stages are better understood and as the ventilation of the Arctic Ocean is reexamined [e.g., Aagaard et al., 1985].

NGDW/CENTRAL ARCTIC OCEAN CIRCULATION AND LYSOCLINE RESPONSE

Introduction

Numerous carbonate dissolution studies from various parts of the North Atlantic Ocean have shown that the lysocline is higher and that dissolution maxima occur during major glaciations. Damuth [1975] suggested that circulation increased during glacial periods for the western equatorial Atlantic. Bé et al. [1976] suggested that this held true for the eastern equatorial Atlantic as well and suggested that the probable source for this increased water mass circulation was increased Antarctic Bottom Water produc-

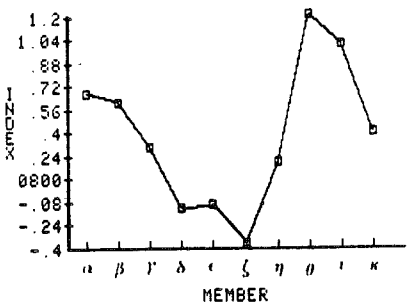

Fig. 10. Paleocurrent index as measure of the difference in thickness of equivalent members, Lomonosov Ridge and Makarov Basin. The index number represents the thickness difference divided by the thickness of the respective member in core B-8. The greater the index number, the greater or more persistent were the currents over the ridge during deposition of any particular member. Note similarity to Figure 9.

tion. Thunell [1976] noted greater dissolution in shallow cores of the western Gulf of Mexico during glacials, but he proposed that dissolution resulted from increased organic oxidation from continual runoff during low stands of sea level. Crowley [1983; 1985] noted that in the central North Atlantic this general pattern held, but there was not a simple linear relationship between dissolution and ice volume. Three deeper cores from his study showed greater dissolution during isotopic stage 5. Hence for various reasons, dissolution has been correlated with glacial periods in the Atlantic Ocean (with some exceptions) but for reasons not totally related to either NGDW or North Atlantic Deep Water production.

Discussion

The fact that the Arctic Ocean contributes to the formation of the world ocean deep water has only recently been demonstrated [Aagaard et al., 1985]. The interchange of NGDW with the Arctic is not much better known. Our data suggest that dissolution in the central Arctic Ocean is enhanced during both interglacial and early glacial stages and probably is related to the formation of dense brine on the Arctic Ocean shelf areas as well as to production of NGDW [McIntyre and Kipp, 1976; Kellogg et al., 1978; Duplessy and Shackleton, 1985; Aagaard et al., 1985]. Brine expulsion during freezing of water on the broad Arctic shelves during interglacial and early glacial stages is the driving mechanism for deep water circulation in the Canada or Amerasian Basin of the Arctic Ocean [Aagaard et al., 1985]. The result of this is water with sufficient density to displace existing deep water of the Canada Basin. When this occurs, displaced Canadian Basin Deep Water (CBDW), undersaturated with respect to calcium carbonate, could raise the level of the calcite lysocline. As brine formation on the Arctic shelf is taking place, NGDW production increases because of pack ice reduction. This has recently been documented for the Norwegian and Greenland seas during interglacial time [Streeter et al., 1982; Broecker et al., 1985; Duplessy and Shackleton, 1985]. The NGDW is largely equivalent to the Arctic Intermediate Water (AIW), and this NGDW-AIW circulation complements the processes responsible for brine formation on the Arctic shelves [Aagaard et al., 1985]. According to these observations the process of lysocline elevation is related both to brine formation on the Arctic shelves and to circulation of NGDW and AIW during interglacial and probably early glacial stages. Bottom traction flow along the shelf and slope may oxidize organic materials and add more CO_2 to this cold dense water. Studies have documented interglacial NGDW as being colder than glacial NGDW [e.g. Duplessy et al., 1975].

During peak glacial and deglacial stages there is less NGDW actively produced (and therefore less exchange with its AIW equivalent), and NGDW is probably warmer. In addition, glacial meltwater flux into the Arctic Ocean probably is saturated with $CaCO_3$. These factors together should produce a lowering of the calcite lysocline. Because CBDW circulates internally, during times of reduced vertical flux and lower brine formation, much of the deep water should remain undisturbed, and this should produce a more stable, lower-level lysocline than during interglacial stages.

Interpretations

The Pleistocene Norwegian-Greenland Sea/Arctic Ocean circulation model is consistent with our core data in that all of the foraminifera barren zones that we have interpreted to represent rises of the calcite lysocline are initiated during periods when little glacial ice was present in the Arctic Ocean. These intervals represent the interglacial and early glacial climate stages when little ice-rafted sediment was being deposited and the predominant sediment is silty lutite. Coarse-grain sediment represents peak glacial and deglacial conditions, and times of reduced intermediate and deep water circulation in the central Arctic Ocean (as documented over the Lomonosov Ridge). The sum of these data lead to the following climate cycle/lysocline scenario:

During interglacial and early glacial stages there is reduced glacial ice in the Arctic Ocean, and silty lutite is the dominant sediment deposited. At this time the production of NGDW is greater [Broecker et al., 1985; Duplessy and Shackleton, 1985; Ruddiman and McIntyre, 1981], and the increased production of the NGDW circulating with the AIW works in combination with brine formation processes on the Arctic shelves to increase inter-

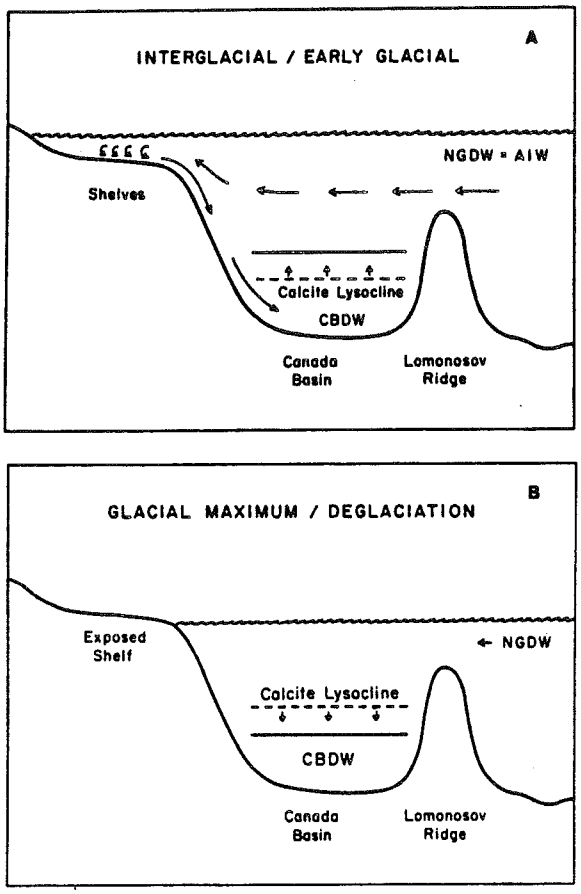

Fig. 11. Paleocirculation Model. (a) During interglacials and early glacials, relatively saline Arctic Intermediate Water formed largely from the Norwegian-Greenland Sea Deep Water, impinges on the shelves resulting in brine formation during freezing of seawater. Brines sink and displace undersaturated Canada Basin Deep Water and the calcite lysocline rises. (b) During full glacials, brine formation is minimal, hence CBDW stabilizes and sinks. During deglacials, shelves are flooded with low-salinity meltwater and brines do not form.

mediate and deep water thermohaline circulation. This produces a greater amount of dense shelf water, which sinks into the Canada Basin and causes the level of the calcite lysocline to rise (Figure 11).

During peak glaciation and deglaciation, when more shelf area is subaerially exposed, shelf waters are less saline because of meltwater runoff. Reduction in shelf areas and lower salinities reduce brine production. Glacial ice flux and meltwater into the Arctic system ultimately affect the surface water of the Norwegian and Greenland seas. As this progresses, the production of the NGDW is reduced [Broecker et al., 1985], thermohaline circulation decreases, and the calcite lysocline sinks (Figure 11).

Summary

The progressive lowering of the lysocline in the Arctic Ocean during the past ~1.5 m.y. is analogous to the general late Cenozoic lowering of the lysocline in the world ocean [e.g., Van Andel, 1975]. Reasons for the lowering are complicated and involve both regional and ocean-wide factors, the most important of which are amount of dissolved carbonate delivered to the oceans, ocean water temperature, and ocean water CO_2 levels. Which of these factors was most important for the Arctic Ocean? Because there appears to have been an increase in Arctic to Subarctic circulation during the late Cenozoic due to increased spreading of the North Atlantic/Nansen Ridge system, a general warming of the Arctic Ocean may have been a factor for the development of the lysocline. A model suggesting a very cold and sterile Arctic Ocean during the middle Cenozoic changing during the Pleistocene to conditions of modest productivity may be supported by the sudden appearance of calcareous plankton approximately 1.5 Ma. Alternately, the 1.5 Ma age may only indicate the time of initial preservation of the fossils. The real question is, was this a time when waters became more hospitable or does this date only mark the beginning of $CaCO_3$ preservation when the lysocline reached a depth that could accommodate preservation? Both are plausible causes and both suggest increased ventilation of the Arctic Ocean. A model could be developed for a progressive warming during the Pliocene and Pleistocene based on an evolution from an older, cold, isolated Arctic Ocean that became relatively warmer as NGDW and Pacific circulation developed in response to high-latitude plate movement. A "warming model" may be more difficult to defend than a model that relates the lowering of the lysocline to an increase in the amount of carbonate delivered to the Arctic during deglacial cycles and increased NGDW circulation. The greater saturation of the water mass with car-

bonate is more in line with traditional ideas on lysocline lowering in other oceans [Van Andel, 1975; Broecker and Peng, 1982]. For the central Arctic Ocean both an increase in the amount of dissolved carbonate and relative warming may be important, but data at hand are not sufficient to resolve the question.

CONCLUSIONS

Study of foraminifera barren zones and sediment texture from six central Arctic Ocean cores permits the following conclusions:

1. There has been a progressive lowering of the calcite lysocline in the central Arctic Ocean for at least the past 1.5 m.y. This may be a result of increased circulation between the NGDW (warm and rich in carbonate relative to the Arctic) and the central Arctic Ocean. The history of the lysocline previous to 1.5 Ma is unknown. The lysocline level is presently below 3956 m.

2. Overprinted on the progressive lowering of the calcite lysocline have been at least two intervals during which the lysocline rose ~300 m. These rises are associated with fine-grain sediment (silty lutite) interpreted to represent interglacial and early glacial conditions. This is best illustrated in the uppermost barren zones of cores B-8 and F1-212 which are apparently associated with isotopic stages 5 and 4.

3. Differences in the coarse weight percent and thickness of time equivalent units of the Lomonosov Ridge and Makarov Basin are variable for approximately the last 640 kyr. We interpret these differences to represent variable strength or persistence of currents in the water column above the Lomonosov Ridge. Greater textural differences are seen in the fine-grain silty lutites, suggesting that average current strength or persistence was stronger during periods when there was less glacial ice in the Arctic Ocean surface waters. We suggest that glacial ice and meltwater in the Arctic Ocean may add impetus to reducing NGDW production in the Norwegian and Greenland seas. This, in combination with the lack of ice formation, on the broad Arctic shelves reduces horizontal and vertical circulation in the Arctic Ocean, thereby lowering the level of the calcite lysocline in the Canada Basin.

4. During interglacial and early glacial periods, brine formation on the broad Arctic Ocean shelves, in combination with increased NGDW production, displaces Canada Basin Deep Water and the calcite lysocline rises.

5. During peak glacial and deglacial stages, reduced shallow shelf area, low-salinity meltwater, and reduced NGDW interchange limits brine formation and mixing with CBDW. This results in a lowering of the lysocline.

Acknowledgments. This research was supported by the Office of Naval Research, G. Leonard Johnson, program director for contract N00014-82K-003. We are grateful for the Canadian LOREX experiment and all of those involved with this research. S. M. Blasco, Bedford Institute of Oceanography, Dartmouth, Nova Scotia, arranged for study of the sediment cores taken during LOREX and has been helpful in many ways. R. K. Matthews, Brown University, provided the $\delta^{18}O$ data for core B-24. G. A. Jones, Woods Hole Oceanographic Institute, Knut Aagaard, University of Washington; and R. H. Dott, Jr., and Jennifer Hogler, University of Wisconsin, were very helpful.

REFERENCES

Aagaard, K., On deep sea circulation in the Arctic Ocean, Deep Sea Res., Part A, 28(3), 251-268, 1981.

Aagaard, K., J. H. Swift, and E. C. Carmack, Thermohaline circulation in the Arctic Mediterranean seas, J. Geophys. Res., 90(C3), 4833-4846, 1985.

Aksu, A. E., Paleomagnetic stratigraphy of the CESAR cores, Geol. Surv. Pap., Geol. Surv. Can., 84-22, 101-114, 1985a.

Aksu, A. E., Planktonic foraminifera and oxygen isotope stratigraphy of CESAR cores 102 and 103: Preliminary results, Geol. Surv. Pap., Geol. Surv. Can., 84-22, 115-124, 1985b.

Aksu, A. E., and P. J. Mudie, Magnetic stratigraphy and palynology demonstrate at least 4 million years of Arctic Ocean sedimentation, Nature, 318, 280-283, 1985.

Bé, A. W. H., J. E. Damuth, L. Lott, and R. Free, Late Quaternary climate record in western equatorial Atlantic sediment, Mem. Geol. Soc. Am., 145, 165-200, 1976.

Berger, W., Deep-sea carbonate and the deglacial preservation spike in pteropods and foraminifera, Nature, 269, 301-304, 1977.

Blatt, H., G. Middleton, and R. Murray, Origin of Sedimentary Rocks, 2nd ed., 782 pp., Prentice-Hall, Englewood Cliffs, N.J. 1980.

Boyd, R. F., D. L. Clark, G. Jones, W. F. Ruddiman, A. McIntyre, and N. G. Pisias, Central Arctic Ocean response to Pleistocene earth-orbital variations, Quat. Res., 22, 121-128, 1984.

Broecker, W. S., and T.-S. Peng, Tracers in the Sea, 690 pp., Lamont-Doherty Geological Observatory, Palisades, N.Y., 1982.

Broecker, W., D. M. Peteet, and D. Rind, Does the ocean-atmosphere system have more than one stable mode of operation?, Nature, 315, 21-26, 1985.

Clark, D. L., M. Andree, W. S. Broecker, A. C. Mix, G. Bonani, H. J. Hofmann, E. Morenzoni, M. Nessi, M. Suter and W. Woelfli, Arctic Ocean chronology confirmed by accelerator ^{14}C dating, Geophys. Res. Lett., 13, 319-321, 1986.

Clark, D. L., and A. Hanson, Central Arctic Ocean sediment texture: A key to ice transport mechanisms, in Glacial-Marine Sedimentation, edited by B. F. Molnia, pp. 301-330, Plenum, New York, 1983.

Clark, D. L., and T. H. Morris, Arctic Ocean sediment texture and the Pleistocene climate cycles, Geol. Soc. Am. Abstr. Programs, 17(7), 547, 1985.

Clark, D. L., R. R. Whitman, K. A. Morgan, and S. D. Mackay, Stratigraphy and glacial-marine sediments of the Amerasian Basin, central Arctic Ocean, Spec. Pap. Geol. Soc. Am., 181, 57 pp., 1980.

Clark, D. L., J.-S. Vincent, G. A. Jones, and W. A. Morris, Correlation of marine and continental glacial and interglacial events, Arctic Ocean and Banks Island, Nature, 311, 147-149, 1984.

Coachman, L. K., and K. Aagaard, Physical oceanography of Arctic and Subarctic seas, in Marine Geology and Oceanography of the Arctic Seas, edited by Y. Herman, 397 pp., Springer-Verlag, New York, 1974.

Crowley, T. J., Calcium-carbonate preservation patterns in the central North Atlantic during the last 150,000 years, Mar. Geol., 51, 1-14, 1983.

Crowley, T. J., Late Quaternary carbonate changes in the North Atlantic and Atlantic/Pacific comparisons, in The Carbon Cycle and Atmospheric CO_2: Natural Variations Archean to Present, Geophys. Monogr. Ser., vol. 32, edited by E. T. Sundquist and W. S. Broecker, pp. 271-284, AGU, Washington, D.C., 1985.

Damuth, J. E., Quaternary climate change as revealed by calcium-carbonate fluctuations in western equatorial Atlantic sediments, Deep Sea Res., 22, 725-743, 1975.

Duplessy, J.-C., and N. J. Shackleton, Response of global deep-water circulation to Earth's climate change of 135,000-107,000 years ago, Nature, 316, 500-507, 1985.

Duplessy, J.-C., L. Chenouard, and F. Vila, Weyl's theory of glaciation supported by isotopic study of Norwegian core K 11, Science, 188, 1208, 1975.

Gilbert, M. W. and D. L. Clark, Central Arctic Ocean paleoceanographic interpretations based on late Cenozoic calcareous dinoflagellates, Mar. Micropaleontol., 7, 385-401, 1983.

Goldstein, R. H., Stratigraphy and sedimentology of ice-rafted and turbidite sediment, Canada Basin, Arctic Ocean, in Glacial-Marine Sedimentation, edited by B. F. Molnia, pp. 367-400, Plenum, New York, 1983.

Hunkins, K. L. and H. W. Kutschale, Quaternary sedimentation in the Arctic Ocean, in Prog. Oceanogr., 4, 89-94, 1967.

Hunkins, K. L., A. W. Bé, and N. D. Opdyke, The Late Cenozoic History of the Arctic Ocean, in The Late Cenozoic Glacial Ages, edited by K. K. Turekian, pp. 215-237, Yale University Press, New Haven, Conn., 1971.

Jackson, H. R., P. J. Mudie, and S. M. Blasco, (Eds.), Initial Geological Report on CESAR--The Canadian Expedition to Study the Alpha Ridge, Geol. Surv. Pap., Geol. Surv. of Can., 84-22, 177 pp., 1985.

Kellogg, T. B., J.-C. Duplessy, and N. J. Shackleton, Planktonic foraminifera oxygen isotopic stratigraphy and paleoclimatology of Norwegian Sea deep-sea cores, Boreas, 7, 61-73, 1978.

Ku, T. L. and W. S. Broecker, Rates of sedimentation in the Arctic Ocean, Prog. Oceanogr., 4, 95-104, 1967.

Lewis, M. R., E. P. Horne, J. J. Cullen, N. S. Oakey, and T. Platt, Turbulent motions may control phytoplankton photosynthesis in upper ocean, Nature, 311, 49-50, 1984.

Lín Kova, T. I., Some results of paleo-

magnetic study of Arctic Ocean floor sediments, (in Russian), Nastoyashcheye i Proshloye Magnitnogo Polia Zemli, Moscow, pp. 279-281, 1965, translated from Russian by E. R. Hope, pp. 1-4, Directorate of Scientific Information Services, DRB Canada.

McIntyre, A., and N. G. Kipp, Glacial North Atlantic 18,000 years ago: A CLIMAP reconstruction, Mem. Geol. Soc. Am., 145, 43-76, 1976.

Minicucci, D. A. and D. L. Clark, A Late Cenozoic stratigraphy for glacial-marine sediments of the eastern Alpha Cordillera, central Arctic Ocean, in Glacial-Marine Sedimentation, edited by B. F. Molnia, pp. 331-365, Plenum, New York, 1983.

Morris, T. H., D. L. Clark, and S. M. Blasco, Sediments of the Lomonosov Ridge and Makarov Basin: A Pleistocene stratigraphy for the north pole, Geol. Soc. Am. Bull., 96, 901-910, 1985.

Mudie, P. J., Palynology of the CESAR cores, Alpha Ridge, Geol. Surv. Pap., Geol. Surv. Can., 84-22, 149-174, 1985.

Mudie, P. J. and S. M. Blasco, Lithostratigraphy of the CESAR cores, Geol. Surv. Pap., Geol. Surv. Can., 84-22, 59-99, 1985.

Olsen, E. A. and W. S. Broecker, Lamont natural radiocarbon measurements VII, Radiocarbon, 3, 141-175, 1961.

O'Neill, B. J., Pliocene and Pleistocene benthic foraminifera from the central Arctic Ocean, J. Paleontol., 55(6), 1141-1170, 1981.

Ruddiman, W. F., and A. McIntyre, Oceanic mechanisms for amplification of the 23,000-year ice-volume cycle, Science, 212, 617-627, 1981.

Sejrup, H. P., G. H. Miller, J. B. Grette, R. Lovlie, and D. Hopkins, Amino acid epimerization implies rapid sedimentation rates in the Arctic Ocean, Nature, 310, 772-775, 1984.

Shackleton, N. J., and N. D. Opdyke, Oxygen isotope and paleomagnetic stratigraphy of equatorial Pacific core V.28-238: Oxygen isotope temperature on a 10^5 year and 10^6 year scale, Quat. Res., 3, 39-55, 1973.

Steuerwald, B. A., D. L. Clark, and J. A. Andrew, Magnetic stratigraphy and faunal patterns in Arctic Ocean sediments, Earth Planet. Sci. Lett., 5, 79-85, 1968.

Streeter, S. S., P. E. Belanger, T. B. Kellogg, and J.-C. Duplessy, Late Pleistocene paleo-oceanography of the Norwegian-Greenland Sea: Benthic foraminiferal evidence, Quat. Res., 18(1), 72-90, 1982.

Thunell, R. C., Calcium carbonate dissolution history of late Quaternary deep-sea sediments, western Gulf of Mexico, Quat. Res., 16(2), 281-297, 1976.

Van Andel, T. H., Mesozoic/Cenozoic calcite compensation depth and the global distribution of calcareous sediments, Earth Planet. Sci. Lett., 26, 187-194, 1975.

Zahn, R., B. Markussen, and J. Theide, Stable isotope data and depositional environments in the late Quaternary Arctic Ocean, Nature, 314, 433-435, 1985.

D. L. Clark and T. H. Morris, Department of Geology and Geophysics, University of Wisconsin, Madison, WI 53706.

(Received October 9, 1985;
revised March 3, 1986;
accepted March 5, 1986.)

Satellite Doppler Determination of Differential Sea Ice Motion in the Vicinity of the North Pole*

J. Popelar

J. Kouba

Department of Energy, Mines & Resources
Earth Physics Branch
Gravity, Geothermics & Geodynamics Division
1 Observatory Crescent
Ottawa, Canada K1A OY3

Abstract During April and May 1979 multidisciplinary observations were conducted in the central Arctic Ocean from three manned ice stations to explore the nature of the submarine Lomonosov Ridge (Weber, 1979). Positions of the LOREX (Lomonosov Ridge Experiment) ice camps were monitored continuously using geodetic satellite doppler receivers and the U.S. Navy Navigation Satellite System. Near real-time doppler data reduction on the ice using broadcast satellite ephemeris provided operational horizontal positions with accuracies of about ± 250 m. A precise geodetic satellite doppler reduction program has been adapted to accommodate linear station motion in a simul-

*Contribution of the Earth Physics Branch No. 1036; Lorex Contribution No. 14.

Marine Geodesy Vol. 7, Number 1-4
0149-0419/83/030171-00$02.00/0

taneous multistation, three-dimensional adjustment in phases using postfitted precise satellite ephemeris, if available. Complete reprocessing of the LOREX doppler data set has produced average errors of ± 48 m for single pass solution and ± 24 m for mean three-four horizontal station positions. The station ellipsoidal heights show strongly correlated variations in excess of 5 m, with the average error of ± 0.45 m. Station velocities are also strongly correlated, with the mean of about 225 m/h and the maximum of 1,240 m/h. Total strain and hourly strain rate components of sea ice have been evaluated for a homogeneous two-dimensional strain model. The configuration of the ice camps provides a unique solution for mesoscale strain, indicating a major change in the pattern of pack ice deformation over the Lomonosov Ridge. The total strain reflects plastic deformation, which takes place mainly in episodic events. The strain rate also indicates nearly diurnal oscillations, with amplitudes an order of magnitude smaller than those corresponding to the major deformation events.

Introduction

The Lomonosov Ridge Experiment code, named LOREX 79, was organized by the Earth Physics Branch in cooperation with the Polar Continental Shelf Project. This multidisciplinary expedition to explore the nature and origin of the major submarine mountain ridge bisecting the Arctic Ocean between the Canadian and Siberian continental shelves took place in the spring of 1979 when geophysicists, geologists, and oceanographers carried out measurements from the drifting sea ice, took samples, and studied the ocean floor in the vicinity of the geographical North Pole. Three permanent ice camps—the Base Camp, Snowsnake, and Iceman—forming approximately an isosceles triangle with sides of about 60-km long and a 100-km base served as operation bases during the experiment (Weber, 1979). The ice camps were established upstream of the narrowest portion of the Lomonosov Ridge, and it was expected that the Transpolar Current would carry them across the ridge with an average speed of about 5 km per day. With known irregularities of sea ice drift it was essential to the success of the expedition to provide reliable all-weather positioning of the ice camps with the highest achievable accuracy. The Navy Navi-

gation Satellite System, also known as Transit, was the only system capable of providing real-time navigation to support field operations at the ice camps with a potential for further substantial improvement of the positional accuracy using postfitted precise satellite ephemeris and highly refined doppler data reduction software.

Although the Transit system facilitates accurate navigation of vessels on high seas and precise geodetic positioning of points on the earth's surface at latitudes up to 70°, the polar orbits of the Transit satellites give rise to two undesirable effects in the vicinity of the geographic poles: (1) every orbit of every satellite of the system is visible, producing at times severe mutual interference degrading the data quality; and (2) all the satellites pass nearly overhead, resulting in poor fix geometry and, moreover, frequent loss of signal at closest approach due to the tracking antennae gain pattern. These effects are particularly severe during unattended operation of standard Transit satellite receivers.

Satellite positions of the LOREX Base Camp were evaluated in real time with the satellite receiver on line to a disc-based minicomputer system most of the time. Raw satellite data from Snowsnake and Iceman camps were recorded on magnetic cassettes, which were then processed on the main camp computer with a three- to seven-day delay. The two-dimensional satellite fix evaluation software developed for BIONAV has been used to process the data on the ice during the expedition (Wells, 1976; Wells and Grant, 1977). At the same time copies of the raw and majority voted data files have been preserved on seven-track magnetic tapes for further analysis and postprocessing (Popelar et al., 1981).

A precise geodetic satellite positioning software package GEODOP (Kouba and Boal, 1976) has been modified extensively to accommodate sequential simultaneous positioning of slowly moving stations. The program employs higher order modeling of environmenal and instrumental effects, reflects time and space correlation of model parameters during simultaneous tracking from several stations, and takes advantage of the availability of postfitted precise satellite orbits. Thus, much improved positions of the LOREX camps have been obtained in three dimensions to satisfy the precision requirements of the plumb-line deflection ex-

periment (Johnson, 1982). The improved positions have made it possible to evaluate differential motion of the three stations and provide a unique solution for two-dimensional strain of the sea ice during the LOREX expedition. The results are particularly valuable, since for the first time variations of ellipsoidal height for the ice stations can be correlated with horizontal sea ice strain components. Analysis of the vertical coordinate provides information on variations of sea surface topography in the central Arctic Ocean.

Satellite Dynamic Positioning

Although the real-time satellite navigation satisfied well the operational requirements on the ice and provided positions acceptable for most of the scientific projects carried out during the LOREX expedition, the plumb-line deflection experiment required satellite positions to about ± 30 m to match the expected accuracy of astro fixes. High-precision satellite doppler positions are routinely obtained by multipass multistation solutions, based on postfitted satellite ephemeris, at 1 to 2 m level for geodetic purposes. However, geodetic models assume earth-fixed stations, whereas motion of an ice station can be appreciable and has to be modeled accordingly.

The new dynamic doppler reduction program GERDOP uses comprehensive error modeling of instrumental, orbital, and environmental effects for simultaneous multistation three-dimensional adjustment in phases (Kouba, 1979, 1981). Several program modules have been modified or completely rewritten to accommodate station position and velocity variations under the assumption of linear station motion over specified equal-length time intervals. Selection of the time interval is crucial; it has to be short enough to permit a linear approximation of the true motion and provide for accumulation of sufficient number of satellite passes to determine mean station positions and linear velocities. The station motion is modeled by three independent linear fits to successive station latitude, longitude, and height coordinates weighted according to their formal errors. A new linear fit is initiated at the beginning of each interval, and departures from the least-

squares line are modeled as exponentially correlated time processes in both the station coordinates and velocities to reflect the strong positive correlation of station positions over short time intervals. The doppler data reduction model accepts only dual-frequency data, corrects for higher order ionospheric effects, and respects the time and space correlation of the tropospheric refraction scaling factors and correlation between doppler data and model parameters during simultaneous tracking from several stations. Reference orbit bias is obtained from the simultaneous solution for each satellite pass, with parameter weights providing desirable constraints. A sequential adjustment procedure is used to update station positions, velocities, model bias parameters, and corresponding variance–covariance matrices after each pass. In this way only new observations are processed to update results of previous solutions without the loss of continuity, thus greatly increasing the economy of computation. Linear extrapolation is used to initialize interval mean station positions and velocities, using time- and space-dependent exponential correlation functions.

Postprocessing of the LOREX satellite doppler data is based on majority-voted output obtained during the real-time navigation preprocessing. Table 1 gives statistics for the LOREX dynamic positioning. The total of 4,920 passes from the three stations that have passed the preprocessing data quality checks represents 2,700 passes of one of the five operational satellites. This means that each accepted satellite pass was tracked at an average by two of the three LOREX stations, thus effectively taking advantage of the simultaneous multistation solution. The very low pass rejection rate increases by 20% the overall data recovery in comparison with the real-time navigation. Orbital data for satellites 12 and 20 (1,064 passes) have been derived from the broadcast message in a similar way as for the navigation processing, whereas precise postfitted orbits provided by the U.S. Defense Mapping Agency have been used for satellites 13, 14, and 19 (1,636 passes). This has significant impact on the point-positioning accuracy: the predicted broadcast orbits provide satellite positions in ± 20–30 m range, whereas the accuracy of the precise ephemeris is ± 2 m. The sequential adjustment of consecutive passes for which ground tracks change direction rapidly in the vicinity of the geographic pole

Table 1
Summary of LOREX dynamic positioning.

	Main Camp	*Snowsnake*	*Iceman*	*Total*
Station ID	S0	S1	S2	
Passes tracked	3,352	2,153	1,940	7,445
computed	2,189	1,368	1,363	4,920
accepted	2,162	1,334	1,340	4,836
Accepted per day	37.2	29.9	30.5	97.6
Data recovery	64%	62%	69%	65%
Pass rejection rate	1.2%	2.5%	1.7%	1.7%

practically eliminates the effect of larger cross-track errors produced by the overhead geometry. Moreover, the simultaneous multistation solution increases the accuracy of relative station positions, which is significant for evaluation of the differential station motion and studies of pack ice dynamics.

Mean polar stereographic coordinates of the LOREX stations as obtained by the dynamic positioning software for three-hour intervals are shown in Figure 1. The overall average error of the mean positions is ± 24 m in latitude and longitude and ± 0.42 m in ellipsoidal height. These estimates are somewhat conservative, since the first ten days of doppler data (day 92 to day 102) show much higher noise due to an initial oscillator instability producing much greater formal errors; the height solution is most sensitive and had to be practically fixed for that period. It is correct to say that errors in mean positions vary from interval to interval depending on the amount of data, pass geometry, and character of ice motion; errors under ± 15 m are encountered about 40% of the time.

Figure 2 displays the station velocities and their directions rections with respect to the Greenwich meridian. It is apparent that motion of the three stations is strongly correlated, reflecting relative rigidity of the sea ice cover at scales of 100 km. The average station velocity during LOREX was about 225 m/h reaching a maximum of 1,240 m/h on day 124. The direction of motion changed rapidly at times showing rather large scatter for low velocities, but the prevailing direction was about 190° with respect to the Greenwich meridian. Accumulated track length for the Main

Camp was 304.6 km, whereas Snowsnake and Iceman track lengths were 241.4 km and 240.6 km, respectively. The direct separations between the starting and terminal points for the three stations are 149.8 km, 140.6 km, and 158.6 km. The LOREX pass summary file is available on magnetic tape and lists receiver frequency offset, cartesian and geodetic coordinates, velocity, and separation between stations from simultaneous tracking for the 4,836 individual pass station solutions.

The standard errors for latitude, longitude, height, and station separation are derived directly from the solution variance-covariance matrix, which also reflects in addition to data quality and pass geometry the constraints imposed by the time- and space-dependent exponential correlation functions used for modeling physically realistic conditions from pass to pass. The mean errors for the pass solutions are about ± 48 m for latitude and longitude, ± 0.45 m for height, and ± 43 m for station sep-

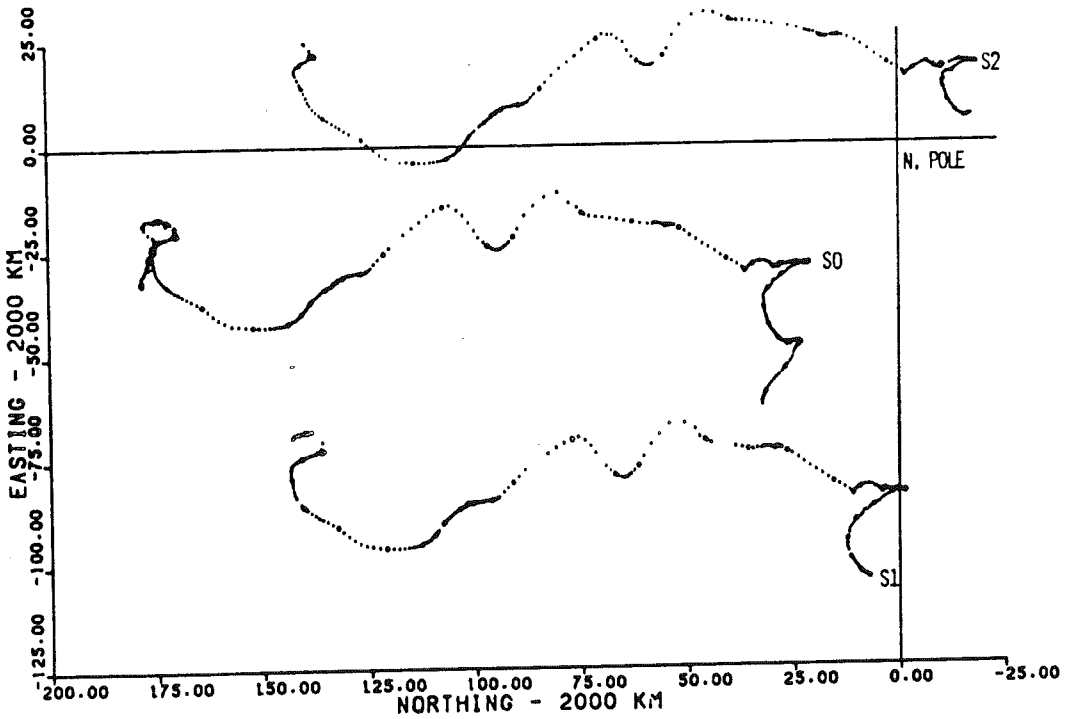

Figure 1. Mean three-hour LOREX ice camp positions. S0 = Main Camp, S1 = Snowsnake, S2 = Iceman.

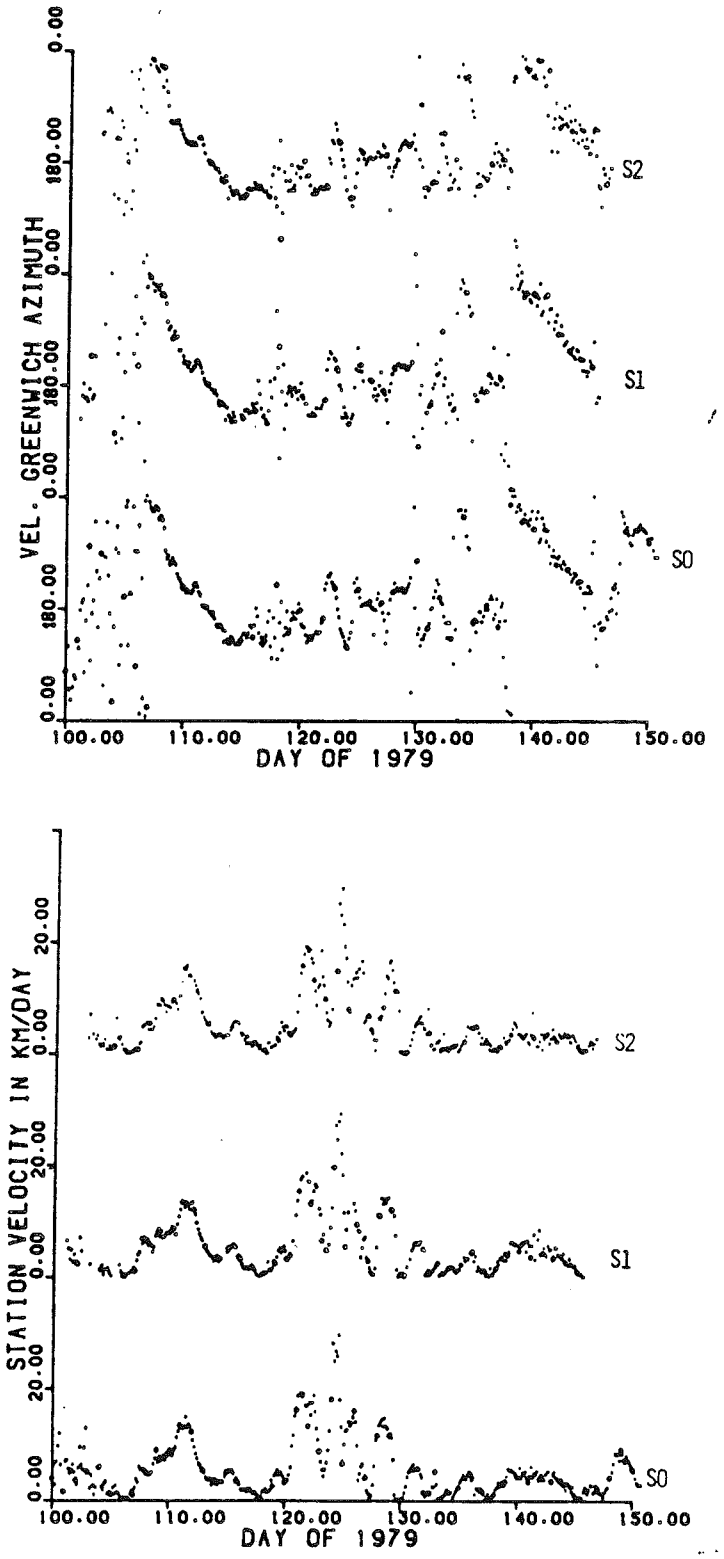

Figure 2. LOREX station velocity plots.

aration. These figures are again somewhat conservative due to the inclusion of the noisy data from the first ten days of the expedition, but they agree well with the errors given above for the three-hour mean positions. The slightly smaller error for station separation provides an independent check, as the accuracy of the relative station positions is free of orbit-related biases. The station velocities and the Greenwich azimuths of the motion have been evaluated as a three-pass running average based on consecutive station pass solutions. They show a higher mean value of about 270 m/h compared to 225 m/h derived from the station mean positions. This very likely reflects the short-period variation in ice motion, which is probably a major factor limiting the achievable accuracy of the results.

Ellipsoidal Heights

The simultaneous three-dimensional solution provides geometrical heights of the electrical centers of receiving antennae above the reference ellipsoid. The height time series (Figure 3) show a remarkable correlation of station height variations from day 109 on. These have amplitudes from 0.2 to about 4 m and range from one-day events to systematic trends clearly dominating any changes in height differences between the stations. Figure 3 does not contain any correction for antenna height, and it seems to reflect clearly the fact that the antenna at the Main Camp (S0) was located on the roof of the navigation hut about 2.30 m above the ice surface, whereas the Iceman antenna (S2) was placed on a small transport box only about 0.45 m high. Since it had not been anticipated that station ellipsoidal heights could be evaluated from satellite data, the antenna heights above water were not measured in the field. Approximate heights above ice have been determined from photographs of the antennae taken in the field, and it is estimated that the uncertainty of the height above water is less than 0.3 m.

The maximum sea surface slope and its Greenwich azimuth have been evaluated from the corrected mean three-hour ellipsoidal heights of the LOREX stations (Figure 4). This regional sea-surface slope with respect to the reference ellipsoid shows rather small variations between 5″ and 15″, with the mean Greenwich azi-

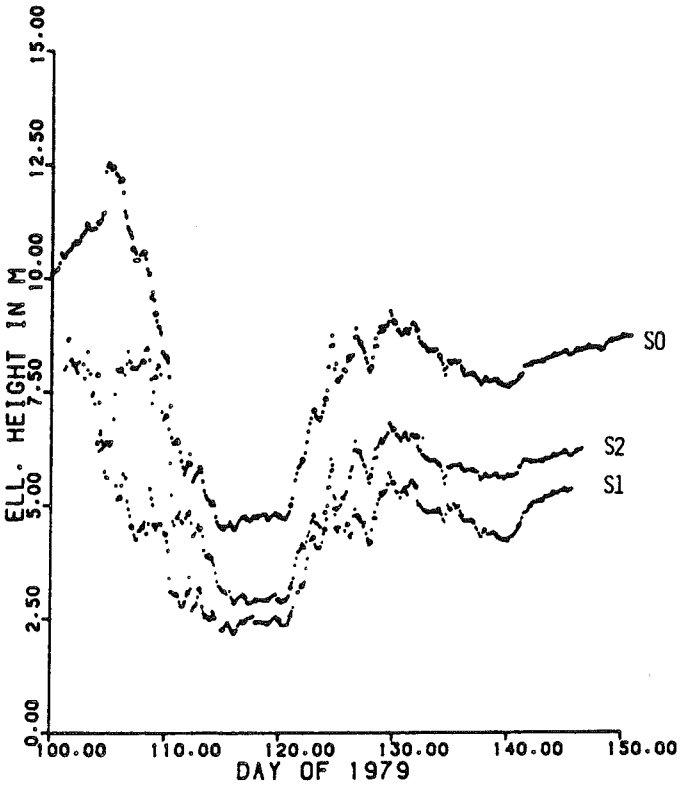

Figure 3. Mean three-hour ellipsoidal heights of LOREX ice camps.

muth of about 37°. However, such a slope would produce a general reduction of ellipsoidal heights for the LOREX stations along their paths, which is inconsistent with the results showing significant increase after day 121 (Figure 3). The discrepancy indicates the presence of a large time-varying component of the computed ellipsoidal heights common to the three stations. There are two possible sources of such variations: (1) the first relates to variations of the instantaneous sea ice surface resulting from dynamics of the ocean, atmosphere, and pack ice; and (2) the second would reflect systematic effects due to satellite orbital biases and data-reduction model deficiencies. While the former group would be of considerable interest to oceanographic studies, the latter represents disturbances that cannot be eliminated easily in the present data set. However, satellite-related effects are considered small, since precise orbits have been used for three of the five satellites,

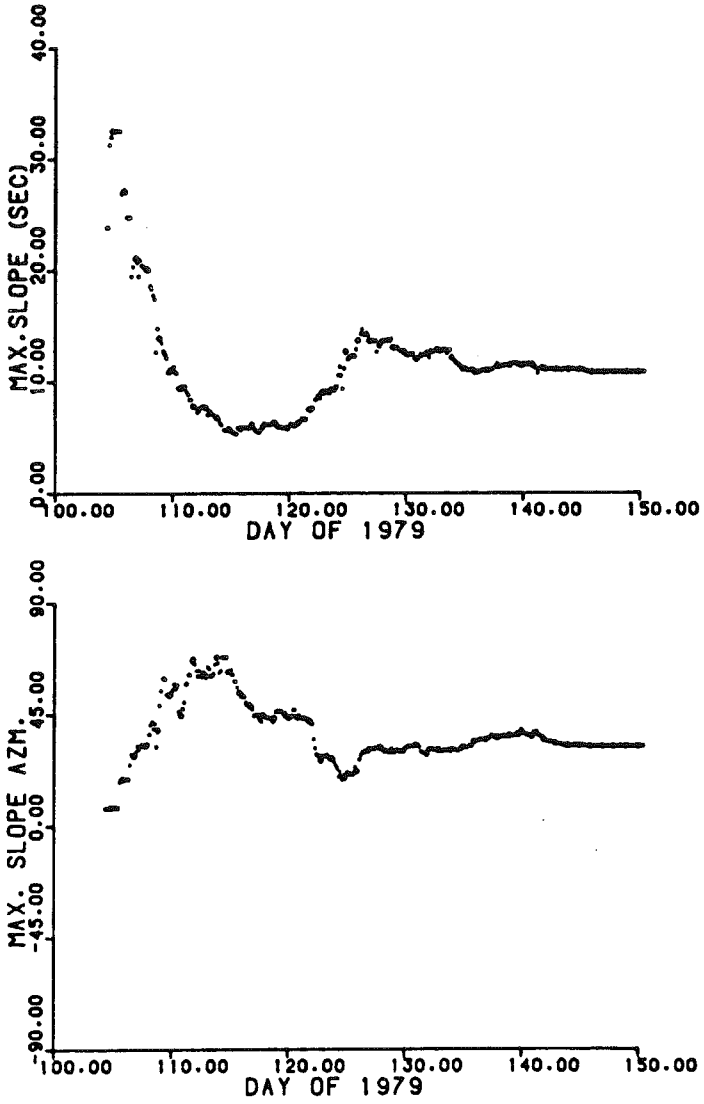

Figure 4. Regional sea-surface slope with respect to the reference ellipsoid.

and the error-modeling procedures have produced consistently high precision results for routine geodetic satellite surveys in similar circumstances. Only the possibility of highly anomalous ionospheric conditions in the polar region may be of some concern; it would be therefore highly desirable to include one or two land stations in future adjustments of sea ice stations and properly constrain the height solution.

Many short-term variations in ellipsoidal height can be correlated with changes in horizontal station velocities (Figure 2) and the horizontal pack ice strain discussed below. The sudden increase of the station ellipsoidal heights starting on day 121 correlates with a sharp decrease of the surface water salinity and a small increase in water temperature reported at Iceman by Pounder (1980).

Differential Station Motion and Sea Ice Deformation Model

It is apparent from the shapes of the LOREX triangle as shown for day 109 and 145 in Figure 5 that considerable deformation and rotation have taken place. The nature of the deformation is revealed by changes in relative station positions as given by lengths and orientation of the sides of the triangle (Figure 6). The side connecting the Main Camp and Snowsnake (S0–S1) shows little change in station separation before day 118 and after day 127, while nearly 2-km extension followed by about 4-km contraction took place in between; it is of interest that the side was approximately parallel with and crossing the Lomonosov Ridge at the time. The side also shows rather steady clockwise rotation of more than 15°. The other two sides clearly indicate episodic extension taking place in the direction roughly perpendicular to the Lomonosov Ridge with a generally smaller rotation.

Sea ice deformation includes opening of leads, formation of pressure ridges, and shear displacement along cracks and leads. These approximately linear features display locally large velocity variations and discontinuities. However, on a sufficiently large scale the pack ice sheet can be treated as a continuum, assuming large numbers of floe-to-floe discontinuities with no single one excessively long (Maykut et al., 1972; Coon et al., 1974; Thorndike and Cheung, 1977). The pack ice sheet deformations are evaluated in two-dimensions due to the great difference between horizontal scales (~1,000 km) and vertical scales (~10 m), and because horizontal velocities are basically constant throughout the thickness of any particular ice floe. The polar stereographic co-

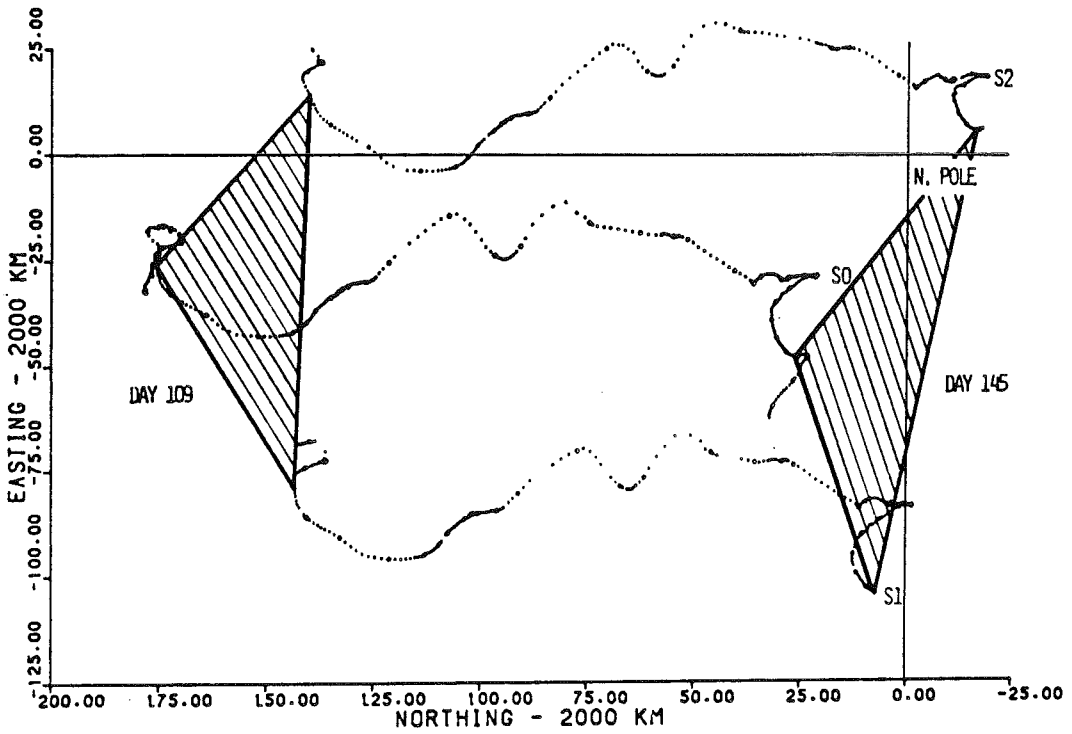

Figure 5. LOREX triangle deformation due to differential sea ice drift between days 109 and 145 of 1979.

ordinates X-northing and Y-easting have been used for the strain analysis.

The following mathematical model has been adopted to express displacements v_{xj} and v_{yj} of station j in the X and Y coordinates:

$$v_{xj} = \frac{\partial v_x}{\partial x} {}_jx_i + \frac{\partial v_x}{\partial y} {}_jy_i + X_{oj}$$

$$v_{yj} = \frac{\partial v_y}{\partial x} {}_jx_i + \frac{\partial v_y}{\partial y} {}_jy_i + Y_{oj} \qquad (1)$$

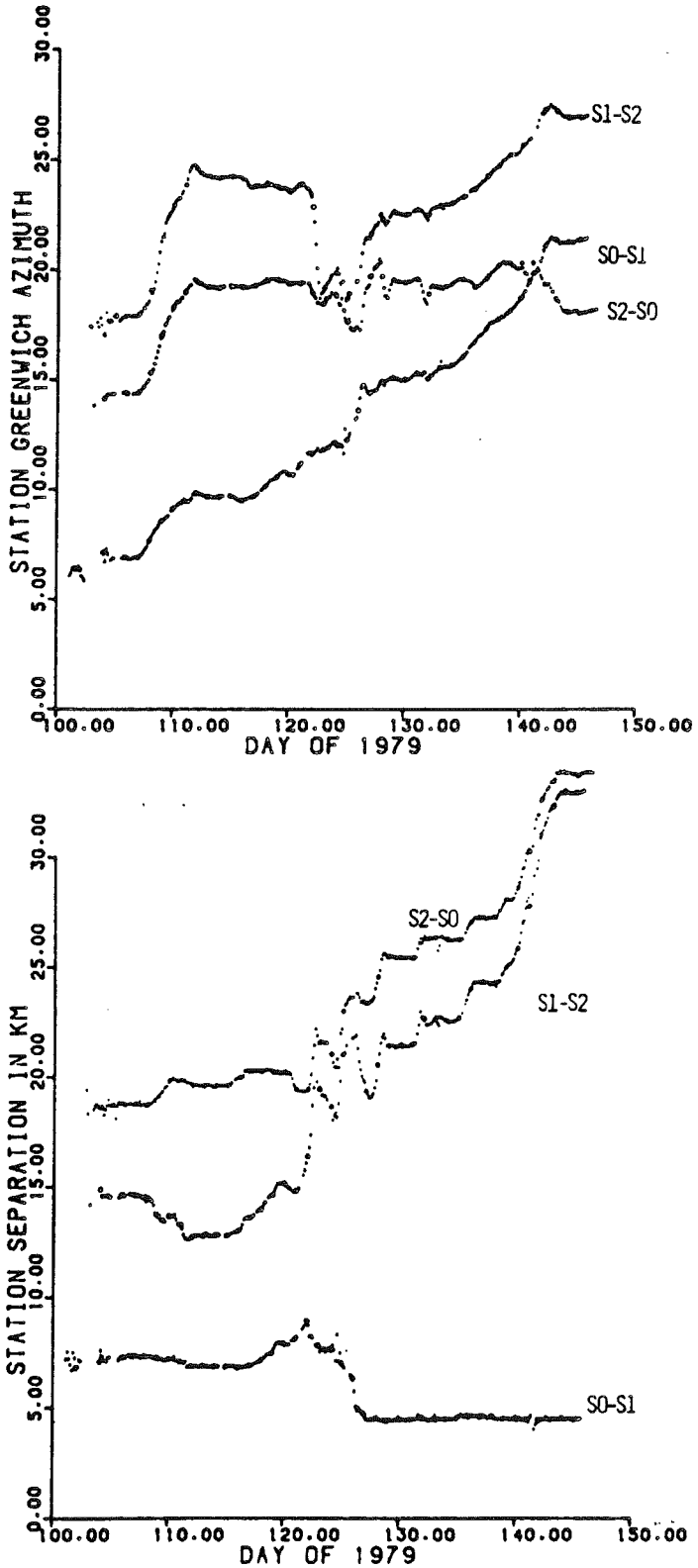

Figure 6. Relative changes of the LOREX triangle side lengths and orientation.

where

$v_{xj} = X_j(t) - X_j(0)$
$v_{yj} = Y_j(t) - Y_j(0)$
$x_i = X_i(0) - X_j(0)$
$y_i = Y_i(0) - Y_j(0)$
$i, j = 1, 2, \ldots, n$ number of stations

$[(X_j(t), Y_j(t)]$ and $[X_j(0), Y_j(0)]$ represent the current and initial positions of station j

$\partial v_x/\partial x$, $\partial v_y/\partial x$, $\partial v_x/\partial y$, $\partial v_y/\partial y$ are corresponding displacement gradients

X_{oj}, Y_{oj} are constants representing the translation

Equation (1) can be expressed as

$$v_j = e r_i + c_j \tag{2}$$

where

v_j is the displacement vector, r_i is the position vector, c_j is the translation component of the displacement vector and e represents the deformation tensor matrix. Thus, according to Equation (2), e serves as a transformation matrix from the position vector to the displacement vector and represents a distortion and/or rotation of a body. Elements of the deformation tensor and the translation components are obtained from the two sets of linear Equations (1), providing coordinates and displacements of at least three suitably distributed stations are known. If more than three stations are involved, a least-squares solution can be obtained assuming homogeneous strain in the region under consideration.

The nontranslational deformation tensor e defined by the displacement gradients can be expressed as the sum of a symmetrical and an asymmetrical tensor

$$e = \epsilon + \omega$$

with elements

$$\epsilon_{kl} = \tfrac{1}{2}(e_{lk} + e_{kl}) = \epsilon_{lk}$$

$$\omega_{kl} = \tfrac{1}{2}(e_{lk} - e_{kl}) = -\omega_{lk}$$

The first part defines the symmetric strain tensor

$$\underline{\varepsilon} = \begin{bmatrix} \varepsilon_{xx} & \varepsilon_{xy} \\ \varepsilon_{xy} & \varepsilon_{yy} \end{bmatrix} = \begin{bmatrix} \frac{\partial v_x}{\partial x} & \frac{1}{2}\left(\frac{\partial v_x}{\partial y} + \frac{\partial v_y}{\partial x}\right) \\ \frac{1}{2}\left(\frac{\partial v_x}{\partial y} + \frac{\partial v_y}{\partial x}\right) & \frac{\partial v_y}{\partial y} \end{bmatrix} \quad (3)$$

and the second part is the pure rotation

$$\underline{\omega} = \begin{bmatrix} 0 & \omega \\ -\omega & 0 \end{bmatrix} = \begin{bmatrix} 0 & \frac{1}{2}\left(\frac{\partial v_x}{\partial y} - \frac{\partial v_y}{\partial x}\right) \\ -\frac{1}{2}\left(\frac{\partial v_x}{\partial y} - \frac{\partial v_y}{\partial x}\right) & 0 \end{bmatrix} \quad (4)$$

The ϵ_{xx} and ϵ_{yy} strain components represent extension along the X and Y axes, whereas $2\epsilon_{xy}$ gives the simple shear. Characteristics values (the eigen values) of the strain tensor ϵ define the maximum and minimum strain, also called principal strains and their directions. These coincide with axes of the strain ellipse representing the irrotational part of the nontranslational two-dimensional deformation. Strain invariants are given by

$$\epsilon_I = \epsilon_{xx} + \epsilon_{yy} \quad (5)$$

called dilatation (or divergence) and

$$\epsilon_{II} = [(\epsilon_{xx} - \epsilon_{yy})^2 + 4\epsilon_{xy}^2]^{1/2} \quad (6)$$

representing maximum shear.

The above theory holds for infinitesimal strain characterized by small displacement gradients for which the squares and products are negligible. However, progressive pack ice deformation shows

considerable displacement gradients even for incremental strain over time intervals of a few hours. Therefore, the general linear transformation

$$\begin{bmatrix} x' \\ y' \end{bmatrix} = \begin{bmatrix} a & b \\ c & d \end{bmatrix} \begin{bmatrix} x \\ y \end{bmatrix} \tag{7}$$

is used to relate the final position (x', y') of a particle after deformation to its initial position (x, y). It is easy to show that the strain components can be expressed in terms of the transformation matrix elements as follows:

$$\begin{aligned} \epsilon_{xx} &= a - 1 \\ \epsilon_{xy} &= \tfrac{1}{2}(b + c) \\ \epsilon_{yy} &= d - 1 \\ \omega &= \tfrac{1}{2}(b - c) \end{aligned} \tag{8}$$

The finite homogeneous strain components are then evaluated from the following expressions:

$$\begin{aligned} \text{dilatation:}\quad & \epsilon_{I} = ad - bc - 1 \\ \text{max. shear:}\quad & \epsilon_{II} = \left[(a-d)^2 + (b+c)^2\right]^{\frac{1}{2}} \\ \text{max. strain:}\quad & \epsilon_{MX} = \tfrac{1}{2}\left[a+d + \left[(a-d)^2 + (b+c)^2\right]^{\frac{1}{2}}\right] - 1 \\ \text{min. strain:}\quad & \epsilon_{MN} = \tfrac{1}{2}\left[a+d - \left[(a-d)^2 + (b+c)^2\right]^{\frac{1}{2}}\right] - 1 \\ \text{MX direction:}\quad & \Phi = \tan^{-1}\left[\frac{b+c}{a-d + \left[(a-d)^2 + (b+c)^2\right]^{\frac{1}{2}}}\right] \end{aligned} \tag{9}$$

The mean three-hour station positions have been used for evaluating strain components. The polar stereographic station coor-

dinates for day 105 at 15/ UT define the initial "undeformed" triangle configuration. At that moment reliable continuous satellite doppler data became available from all three LOREX stations. The strain monitoring continued until day 145 at 15/ UT when the Snowsnake station satellite tracking terminated.

Progressive Sea Ice Deformation—Total Strain

The total strain components for the LOREX triangle have been obtained by comparing station configurations with the initial "undeformed" state, using the expressions (7) to (9) for finite homogeneous strain. Figure 7 shows the nonrotational strain components with respect to the polar stereographic axes. Direction of the maximum strain and the principal strains are shown in Figure 8, whereas the pure rotation, maximum shear, and dilatation are plotted in Figure 9. The progressive pack ice and deformation is well defined from the LOREX triangle, and two distinct deformation patterns can be identified. The first between day 110 and 120 is characterized by relatively small deformations with direction of the maximum strain nearly parallel with the Greenwich meridian. The second pattern from day 127 on displays progressive steplike extension in the direction approximately perpendicular to the Lomonosov Ridge with increasing dilatation. The two transition periods (before day 110 and between day 120 and 127) show rapidly changing direction of the axis of the maximum strain, and while the first transition indicates significant dilatation the second displays just the opposite, i.e., divergence of about the same magnitude. Systematic rotation by several degrees in opposite directions is also observed during the two transitions. Day 121 marks the most dramatic changes, and interestingly enough it coincides with the breakup of the Main Camp that was crossing the crest of the Lomonosov Ridge at the time. Moreover, as mentioned above, a significant drop in surface water salinity was recorded at Iceman, and a major increase of sea surface heights occurred at all three stations (Figure 3). These facts can be interpreted in terms of distinctly different hydrographic regimes in the Canadian and Eurasian basins adjacent to the Lomonosov Ridge (Aagaard, 1981). However, one cannot rule out a transient event

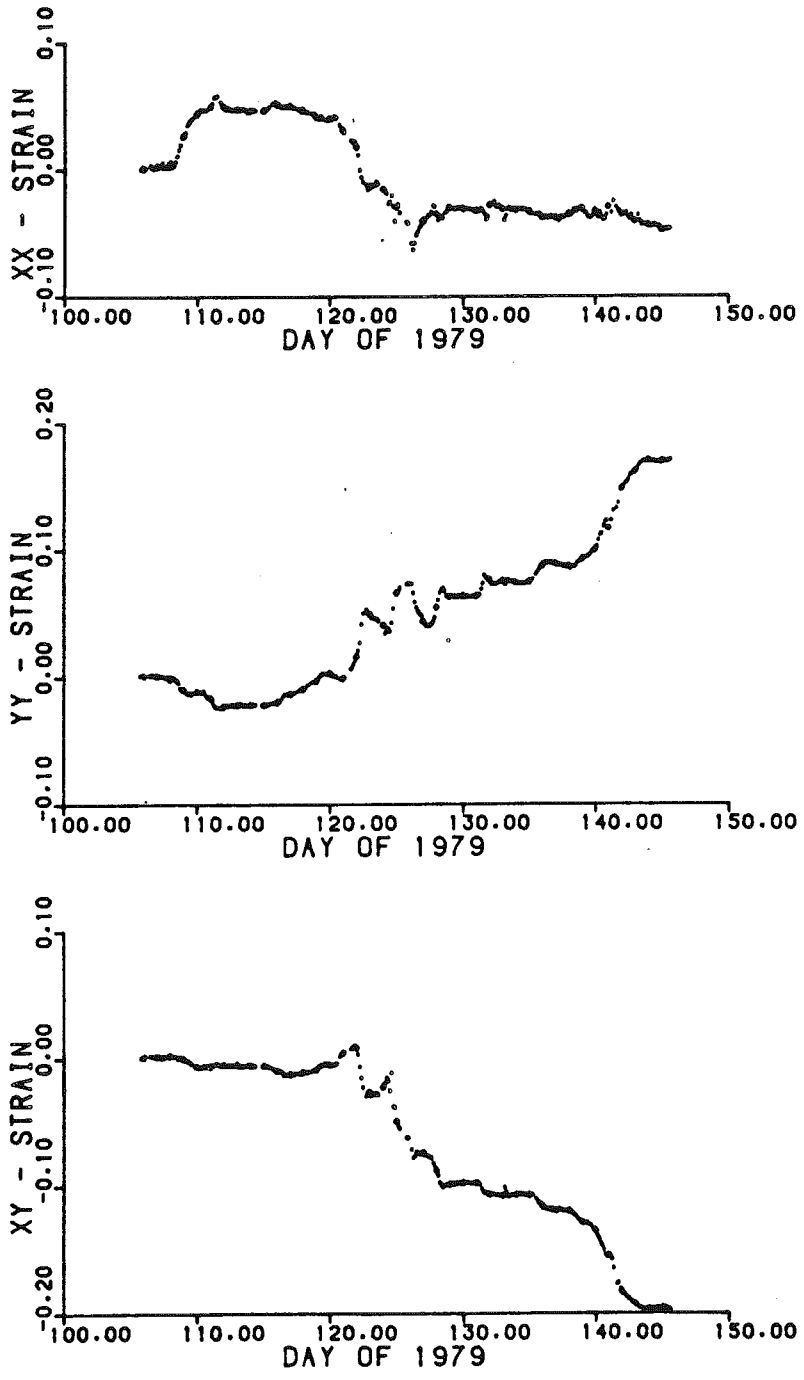

Figure 7. Nonrotational total strain components.

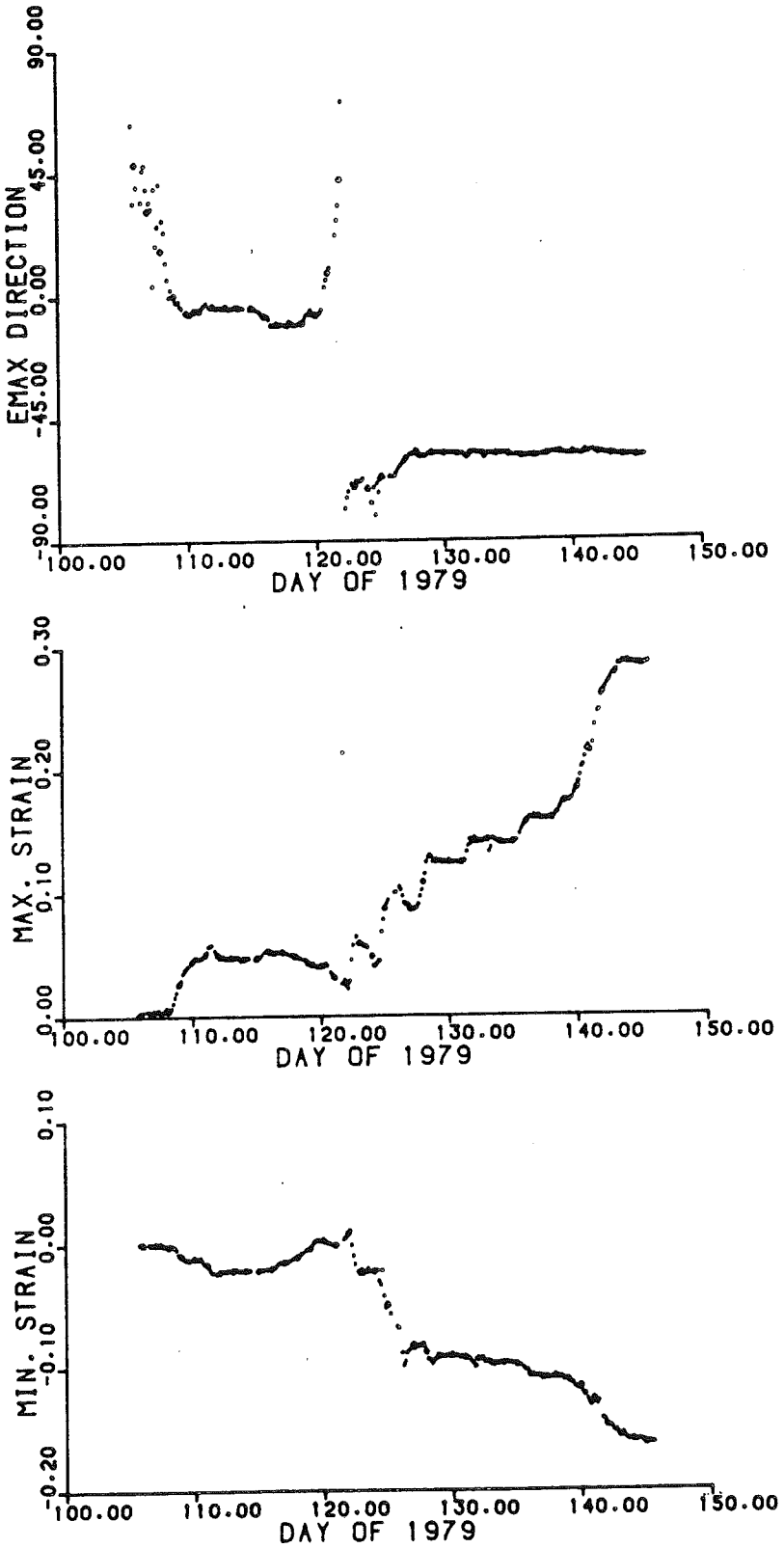

Figure 8. Principal total strain components and their orientation.

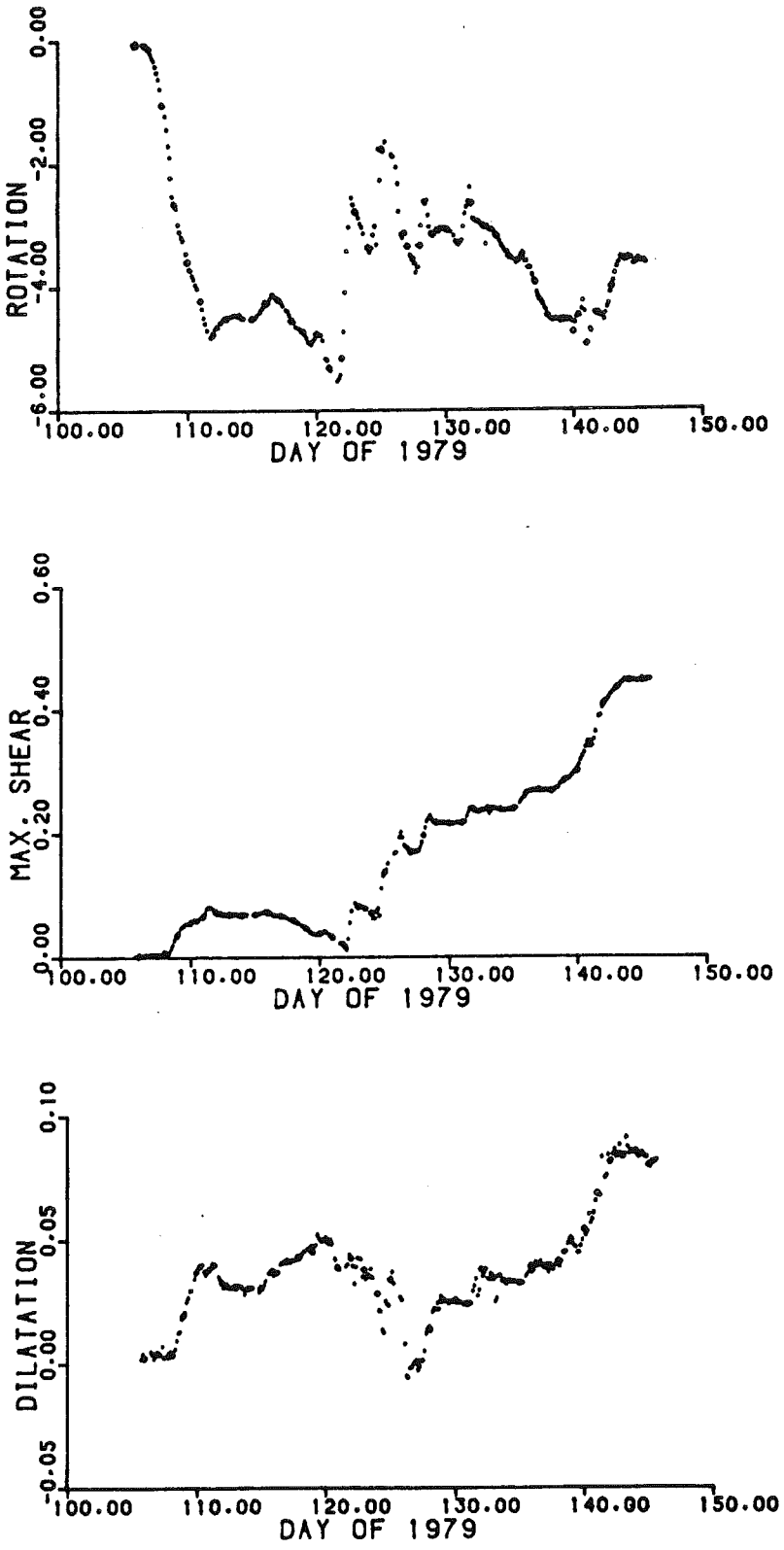

Figure 9. Pure rotation, maximum shear, and dilatation for total deformation.

as a possible source no matter how unlikely the coincidence with crossing of the ridge might be. Only additional new data could resolve the ambiguity.

In general, the total deformation during the 40-day period is considerable and reaches nearly 30% for maximum strain, exceeds 8% for dilatation, and shows pure rotation up to 5.5°.

Incremental Sea Ice Deformation — Strain Rate

The strain rate calculations are based on differences of consecutive mean three-hour station positions. Since the magnitude of differential strain effects for three-hour intervals is only marginally larger than the uncertainty in the mean station positions and both can vary a great deal, it is important to consider the known formal position errors when evaluating the strain rate components. This has been done by independent least-squares cubic spline smoothing of the elements of the transformation matrix in Equation (7), with weights reflecting the formal errors of station positions. The incremental strain components computed from the expressions (8) and (9) have been scaled to represent strain rates per hour, and these are shown in Figure 10 for the nonrotational components, whereas Figures 11 and 12 show the principal strain rates, hourly changes in dilatation, maximum shear, and pure rotation.

The major events reflecting large-scale permanent deformations clearly defined by the total strain (Figures 8 and 9) are expressed by conspicuous narrow anomalies of the strain-rate components, which permit more accurate determination of their timing and character. Often rapid, large changes in one direction are followed by somewhat lesser change in the opposite direction. Under close examination regular, nearly diurnal variations of the strain rate components can be observed between the major events. Most noticeable are these variations in the dilatation rate between day 112 and 120. Some correlation between strain rate components and the fine submeter ellipsoidal height variations (Figure 3) also can be observed. Detailed strain and tilt observations on a single large ice floe should be considered in the future to determine if this oscillation is related to elastic ice deformation due to tidal forces. In any case, additional observations are necessary to establish the

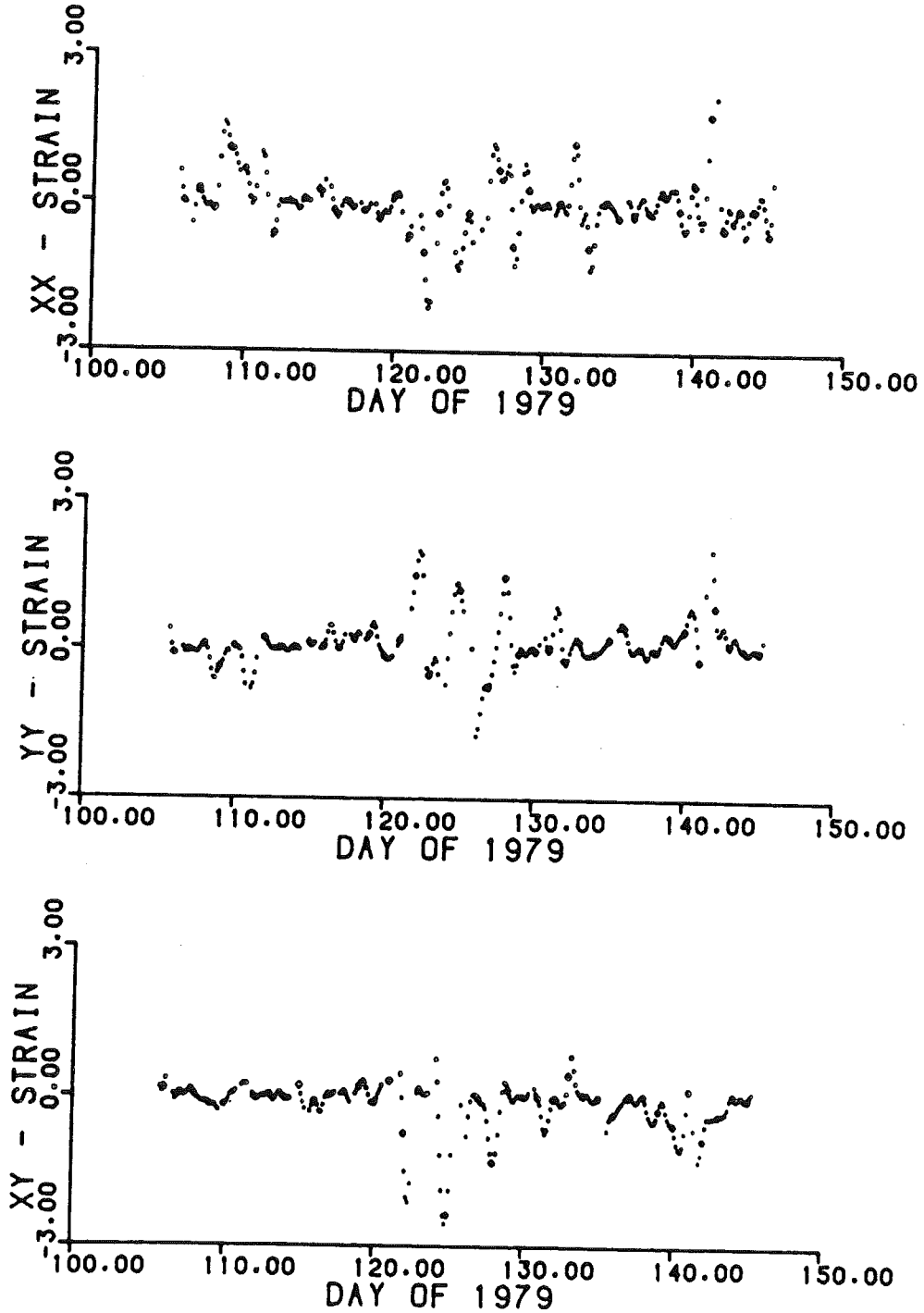

Figure 10. Nonrotational strain rate per hour (units of 10^{-1}).

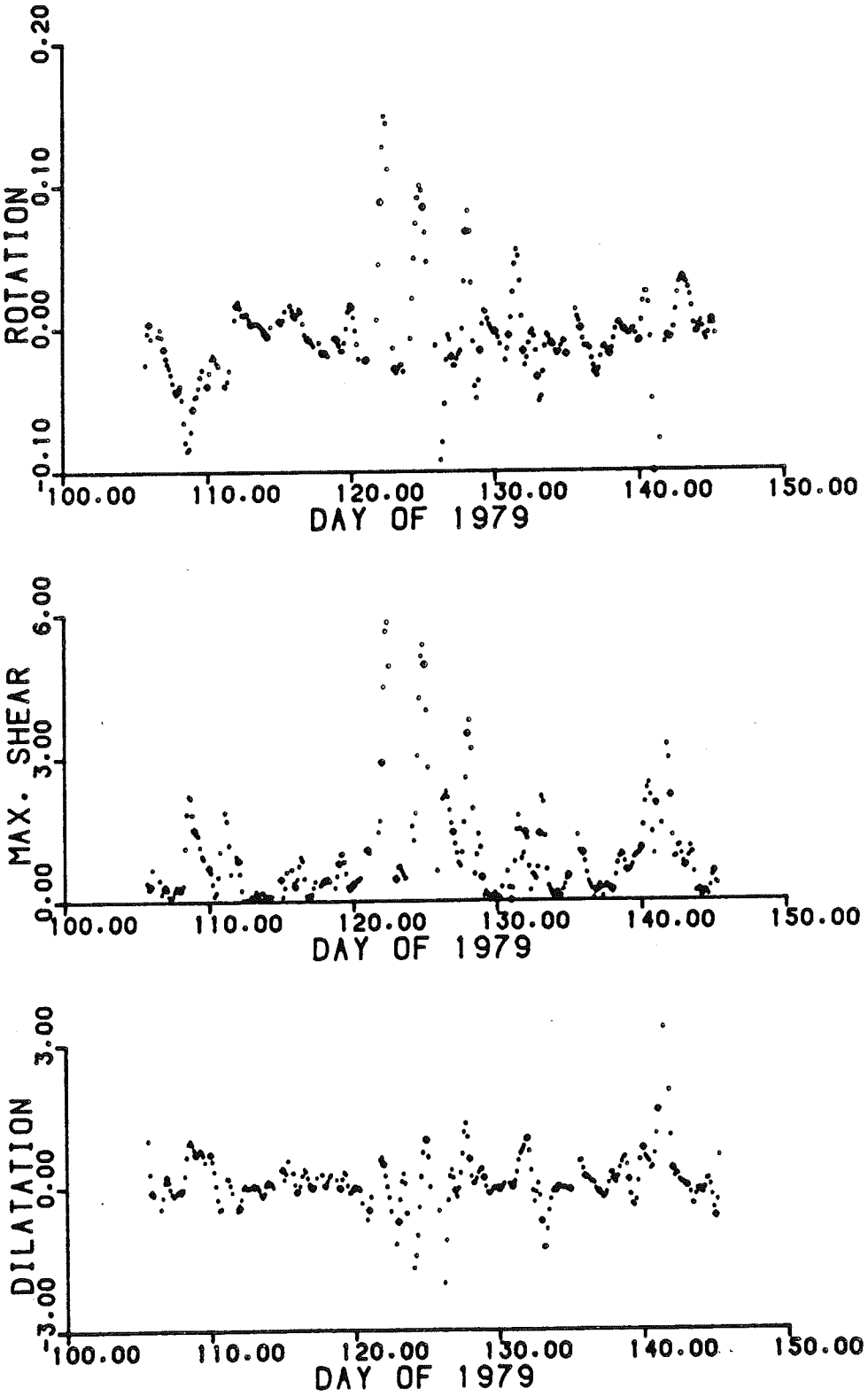

Figure 11. Hourly rates of pure rotation (in degrees), maximum shear, and dilatation (units of 10^{-3}).

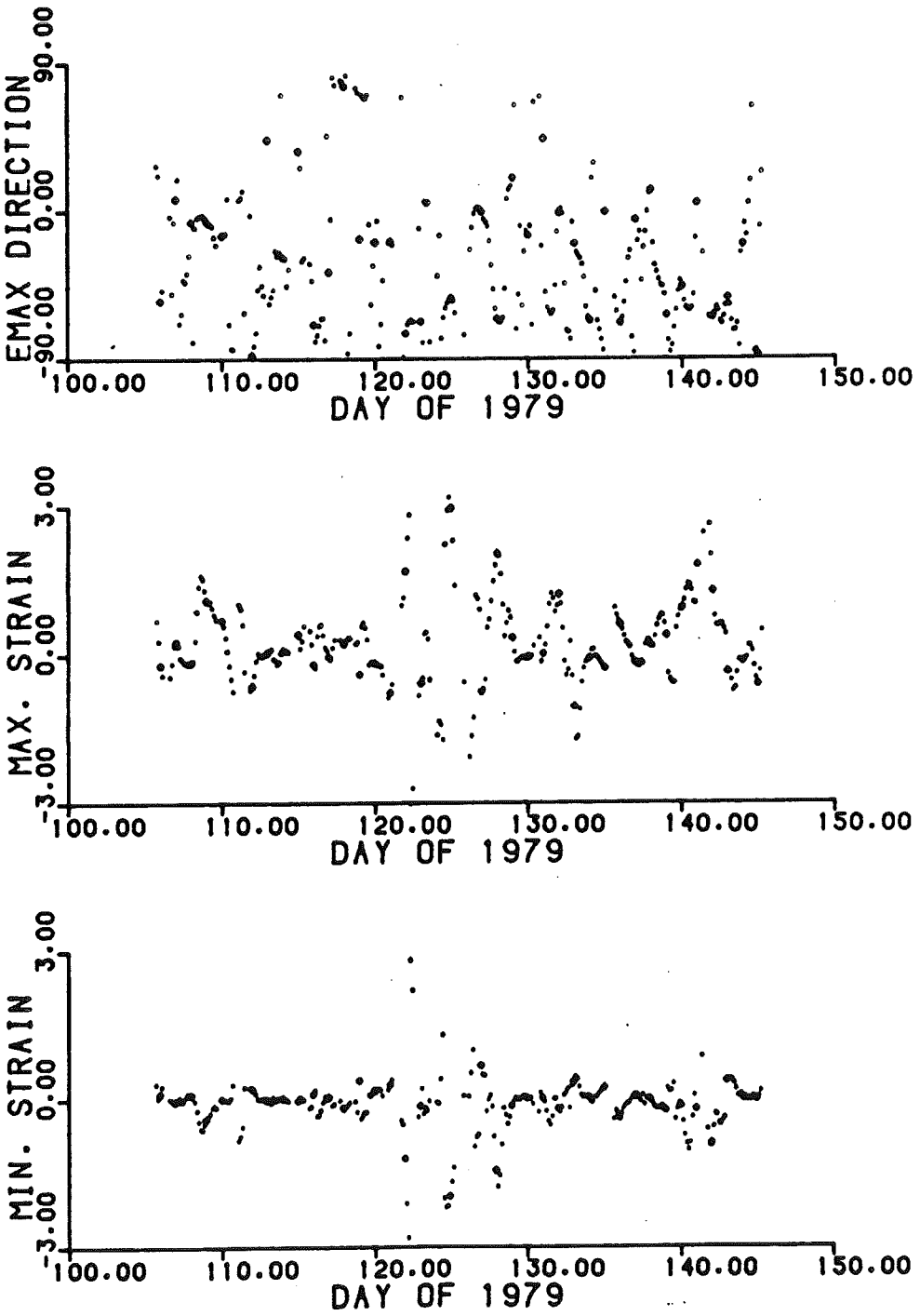

Figure 12. Principal strain rates per hour (units of 10^{-3}) and their orientation.

suitability of the two-dimensional homogeneous strain model and evaluate the effect of large discontinuities between the floes on the computed strain components.

The anomalous hourly changes have reached about 0.3% for maximum strain and dilatation, whereas maximum hourly change in pure rotation has been 0.15°. The above-mentioned nearly diurnal variations of the same components show amplitudes about an order of magnitude smaller. The greatest variance is displayed by the direction of maximum strain, which shows signs of discontinuous systematic trends, particularly in the second half of the experiment. An analysis of statistical frequency produces two peaks: one around −65° and one somewhat broader and smaller around −10°. The average hourly changes over the duration of the experiment amount to 0.024% extension for maximum strain and 0.011% dilatation, which is consistent with the total deformation results.

Conclusions

The Navy Navigation Satellite System facilitates reliable real-time navigation for drifting ice stations in the vicinity of the geographic North Pole. The positional accuracy can be improved significantly using postfitted precise satellite ephemeris and the newly developed dynamic doppler data reduction software. The new software accommodates multistation three-dimensional sequential positioning of slowly moving platforms under the assumption of linear motion over specified equal-length time intervals. It reflects time and space correlation of model parameters, including environmental and instrumental effects, station coordinates, and mean interval velocities. The sequential adjustment scheme updates all model parameters and corresponding variance–covariance matrices after each satellite pass, assuring data manageability and exceptional economy of computations. In this way all 2,700 satellite passes have been reduced in one computer run, using three-hour intervals to approximate station drift by linear motion. The overall average error of the mean three-hour station positions is less than ± 25 m in horizontal coordinates and about ± .4 m in ellipsoidal height, while the average station velocity was about 225

m/h with the maximum of 1,240 m/h. The average error of the 4,836 individual pass-station solutions derived directly from the variance–covariance matrices is less than ± 50 m in horizontal coordinates and ± .45 m in height, probably reflecting the high frequency ice jerk.

The positional accuracy is sufficient to monitor progressive pack ice deformation using a two-dimensional homogeneous strain model. The configuration of the three LOREX ice camps provides a unique solution for total mesoscale strain, indicating that a major change in the ice deformation pattern takes place above the Lomonosov Ridge in the vicinity of the North Pole. It is characterized by a change in the direction of maximum strain of more than 50° and clear divergence when crossing the ridge. The total strain reflects mostly plastic deformation, which takes place mainly in episodic events when the ice yields under the effects of shear and vertical stress.

Analysis of strain rate can be enhanced by smoothing of observations, which takes into account formal errors of individual mean station positions. The strain rate components produce conspicuous anomalies corresponding to the major deformation events. Moreover, nearly diurnal oscillations with an order of magnitude smaller amplitude are quite apparent. However, their interpretation would have to include detailed analysis of the suitability of a two-dimensional homogeneous strain model for pack ice deformation studies, which can only be based on presently unavailable redundant observations.

Similarly, the interpretation of ellipsoidal heights would require at least one land-based station to be included with the ice stations in the simultaneous adjustment to constrain the height solution. Additional monitoring of oceanographic and meteorological parameters is necessary to identify sources of pack ice motion and deformation. Future expeditions could provide more information by optimizing satellite-observing strategy to assure sufficient redundancy of measurements and by obtaining complementary geodetic, oceanographic, and meteorological data to study the interactions between the ocean and atmosphere, which determine ice conditions. This would also be beneficial to other scientific projects and contribute greatly to the safety of operations.

Acknowledgments

The authors are deeply obliged to Dr. D. Wells who conceived and set up the satellite navigation and the near real-time fix evaluation on the ice with support from F. Muise and S. Spencer of the Bedford Institute of Oceanography. Many thanks go to the LOREX Chief Scientist, Dr. J. R. Weber, and to the management of the Earth Physics Branch for advice, support, and encouragement, which have made the work possible. The cooperation of the U.S. Defense Mapping Agency Topographic and Hydrographic Center in providing the precise postfitted satellite ephemeris is gratefully acknowledged.

References

Aagaard, K. 1981. On the Deep Circulation in the Arctic Ocean. *Deep-Sea Research*, 28A (3).

Coon, M. D., Maykut, G. A., Pritchard, R. S., Rothrock, D. A., and Thorndike, A. S. 1974. Modelling the Ice Pack as an Elastic-Plastic Material. *AIDJEX Bull.* No. 24.

Johnson, G. W. 1982. Astronavigation for the Lomonosov Ridge Experiment. Manuscript.

Kouba, J. 1979. Improvements in Canadian Geodetic Doppler Programs. *Proc. 2nd Symp. on Satellite Doppler Positioning*, Las Cruces.

Kouba, J. 1981. Satellite Doppler Positioning for Geodynamics. *Proc. Symp. on Space Geodesy, Annales de Geophysique*, 37, (1).

Kouba, J., and Boal, J. D. 1976. Program GEODOP. Publ. Surveys and Mapping Branch, Ottawa.

Maykut, G. A., Thorndike, A. S., and Untersteiner, W. 1972. Aidjex Scientific Plan. *AIDJEX Bull.* No. 15.

Popelar, J., Kouba, J., and Wells, D. E. 1981. LOREX 79 Satellite Positioning. Internal Report 81-2, Gravity & Geodynamics Division, Earth Physics Branch, E.M.R.

Pounder, E. R. 1980. Physical Oceanography in the Central Arctic. Manuscript.

Thorndike, A. S., and Cheung, J. Y. 1977. AIDJEX Measurement of Sea Ice Motion 11 April 1975 to 14 May 1976. *AIDJEX Bull.* No. 35.

Weber, J. R. 1979. The Lomonosov Ridge Experiment: LOREX 79. *Trans. AGU*, No. 42.

Wells, D. E. 1976. Improved Marine Navigation Error Modelling Through System Integration. *CGU Symposium on Modern Trends in Geodesy*, Quebec.

Wells, D. E., and Grant, S. T. 1977. Reliable Navigation Through System Integration. *Proc. 16th Can. Hydrographic Conference*, Burlington.

Astronavigation for the Lomonosov Ridge Experiment

[LOREX Contribution No. 16]

by Gerald W. Johnson, Ph.D.

Abstract. The Lomonosov Ridge is an aseismic submarine mountain range that bisects the Arctic Ocean in the immediate vicinity of the North Pole. In the spring of 1979 the Canadian Department of Energy, Mines and Resources (EMR) undertook a large-scale multidisciplinary project to study its nature and origin. One research objective of the project was to use deflections of the vertical derived from astronomically determined latitudes and longitudes to help define a model of the density structure of the Ridge. During a 30-day period approximately 1,200 daylight star observations were made and 87 astronomic position fixes established as the *three* project camps drifted across the Ridge *between latitudes 88°20' and 89°07' North.*

Introduction

In the spring of 1979 the Canadian Department of Energy, Mines and Resources (EMR) undertook a large-scale, multidisciplinary project to study the nature and origin of the Lomonosov Ridge. The scientific program was planned and coordinated by the Earth Physics Branch, and the logistic support was provided by the Polar Continental Shelf Project. Scientists from several branches of EMR, from the Department of Fisheries and Oceans, and from several universities in Canada and the United States took part in the project, code-named LOREX.

The Lomonsov Ridge (see Fig. 1) is an aseismic submarine mountain range that bisects the Arctic Ocean. It rises sharply to a height of some 3 km above the adjacent abyssal plains, the Makarov Basin to the west and the Fram Basin to the east. It is close to 200 km wide where it approaches the North American and Eurasian continental shelves but narrows to 25 km at its midpoint near the North Pole. Some geophysicists theorize that the Ridge was once part of the continental shelf and was rafted to its present position by the process of sea floor spreading some 40 to 70 million years ago. However, since the available geophysical, geological, and bathymetric data are relatively sparse and often of doubtful quality (because of the enormously difficult operating conditions), the continental nature of the Ridge has never been unambiguously demonstrated, and some scientists suggest that it could have been formed by other processes.

In 1967 and again in 1969 the Earth Physics Branch—then the Dominion Observatory—of EMR carried out two expeditions with the Polar Continental Shelf Project to the vicinity of the North Pole. The prime objective of these surveys was to establish a line of gravity stations from Ellesmere Island to the Pole and to obtain as many gravity observations as possible in the vicinity of the Pole and across the Lomonosov Ridge. Gravity observations and deflections of the vertical obtained during during these two expeditions provided the basis for compiling a preliminary structural model of the Ridge. (Lillestrand and Weber, 1974) There was still a need, however, for more extensive research, and based on experience gained in these projects a plan was developed for a concentrated study of the Ridge. It would be conducted in the vicinity of the Pole and would include bathymetry, gravity, and deflection of the vertical measurements, sub-bottom profiling, shallow, intermediate, and deep crustal seismic observations, coring and dredging, bottom photography, heat flow measurements, geomagnetic and magnetotel-

Dr. Johnson is with the Dept. of Civil and Mineral Engineering, University of Minnesota, Minneapolis, Minnesota 55455.

Surveying and Mapping, Vol. 44, No. 3, 1984 pp. 237-245

luric soundings, and physical and chemical oceanography.

The basic plan was to establish a main camp and two satellite camps on the drifting pack ice upstream of the Ridge and let the transpolar current transport the camps across it. From the scientific point of view, the most desirable location was near the North Pole where the Ridge is narrowest and the chances best for drifting across the entire structure from the Makarov to the Fram Basin. The time period for the operation was defined by a 3-month window starting when daylight conditions in the polar region were adequate for aircraft landing on the ice and ending well before the onset of the melt season. On this basis it was estimated that March 14 was the earliest possible date on which a search for possible sites could begin and that the evacuation should be completed not later than June 15. Taking into account the time required for the search, the time required for the airlift, and the time required for delays caused by weather and other unforeseen circumstances, the scientific program was planned to last for 60 days.

By studying the paths of earlier stations that had drifted on the Arctic Ocean, it was estimated that in the springtime the ice would drift at an average speed of 5 km/day. Thus, there was a reasonable expectation that the camps would drift over the Ridge during the 2-month period of the scientific program. On March 21, after several days of searching, the eventual LOREX site was located at 88°38′ N latitude and 172° W longitude. It consisted of a thick multiyear ice flow adjacent to an area of 2 m-thick, first-year ice large enough to accommodate both an aircraft runway and a supply drop area. The airlift began on March 23, and on April 1 the buildup of the main camp was completed. Three days later the airlift to establish the two satellite camps, code-named Snowsnake and Iceman, was completed.

The camps drifted for more than 2 months along irregular drift paths that carried them across the Ridge (Fig. 2.). They

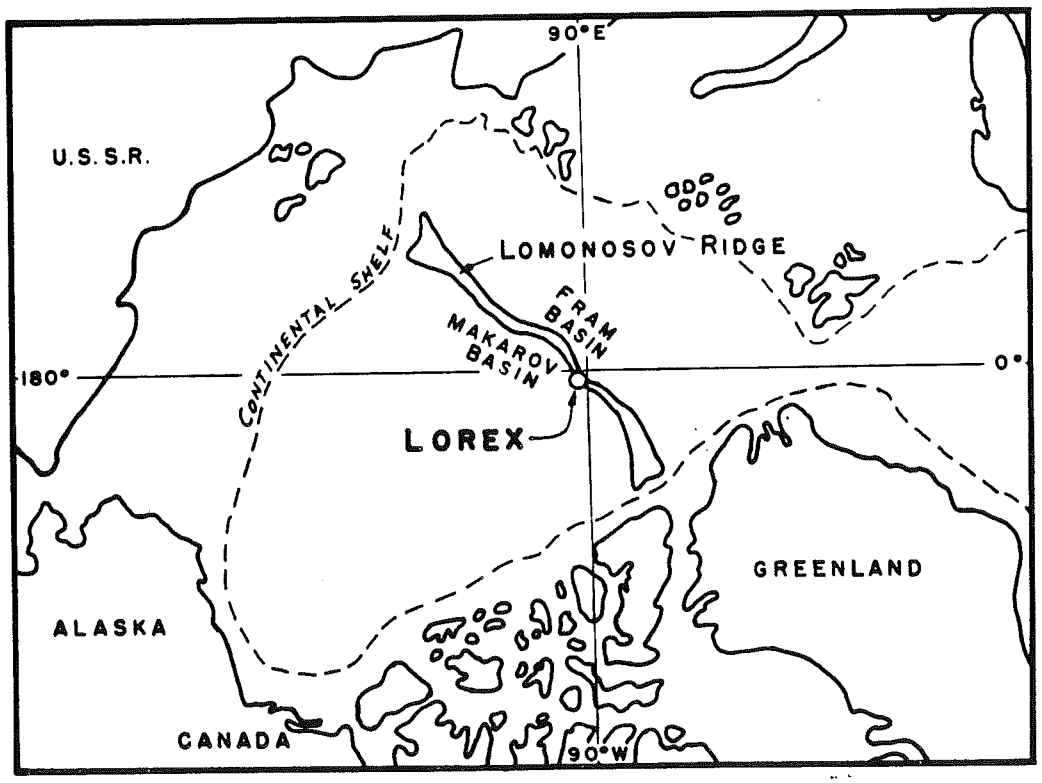

Figure 1. Arctic Ocean.

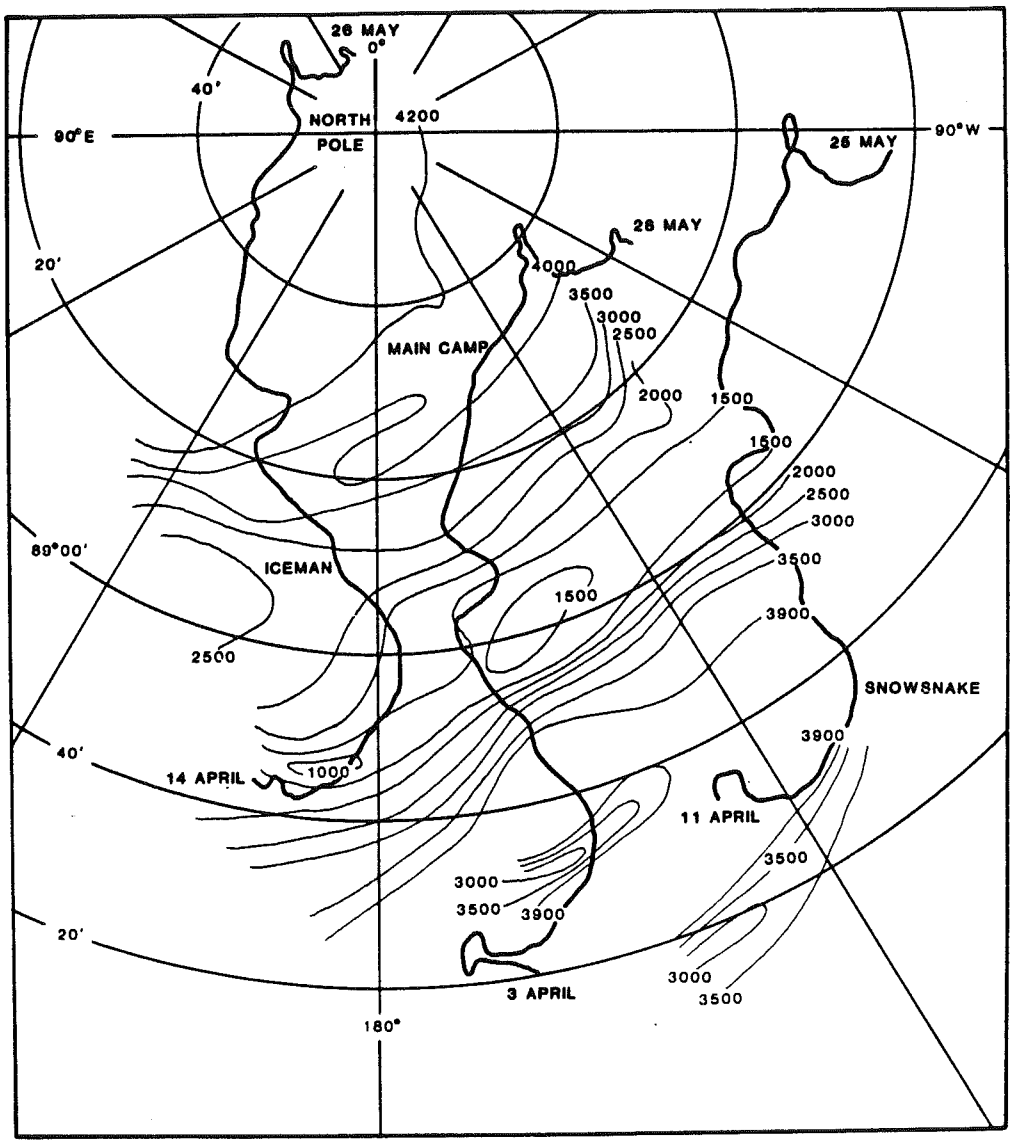

Figure 2. LOREX Drift Paths.

were manned until early June when ice melt and breakup required a termination of all research projects. Personnel and equipment were airlifted from the camps with the final flight leaving the ice on June 10. For an overall summary of LOREX, see Weber (1981).

Deflections of the Vertical

One objective of the LOREX research program is to derive a model of the density structure of the Ridge. Gravity measurements supplemented by measurements of deflections of the vertical will be the primary source of data for this. A deflection of the vertical, also called plumb line deflection, is the angle between the direction of gravity and the normal to the ellipsoid, or the angle between the ellipsoid and the geoid, at a particular point. The spirit levels used in leveling a theodolite align the vertical axis of the instrument with the local direction of gravity, and angles measured with the instrument are thereby influenced by local gravity anomalies. A latitude and longitude determined

astronomically from observations made with a theodolite thus contain the effect of these anomalies. When compared to a corresponding geodetic latitude and longitude the difference between the astronomic and geodetic values leads to a quantitative measure of the deflection of the vertical. This is used in conjunction with related gravity data to develop a model of the earth's underlying density structure.

Geodetic latitudes and longitudes for LOREX were obtained by transit satellite receivers located at the three camps. Preliminary positions were computed on-line using an HP 2100 computer. Positional data for the deflection of the vertical computations were refined, adjusted, and analyzed following completion of the field work.

Astronavigation

Astronomic latitudes and longitudes for deflection of the vertical computations were determined by the classic line-of-position (LOP) method. Although in the Arctic one's ability to obtain a position at any given time may be limited by environmental conditions, this method continues to be used successfully. (See, for example, Lillestrand and Johnson (1971) and Lillestrand and Weber (1974).)

The instrument used for the observations was a Wild T-4. It was mounted on a specially constructed aluminum base that was permanently frozen in the ice and was surrounded by a nylon wind screen supported by an aluminum frame. Sections of the screen could be raised or lowered depending on the intensity and direction of the wind. (Fig. 3.)

Accuracy requirements necessitated the use of stars for the observations, and prior to the expedition a list of usable stars was compiled using the following criteria:

- Angular distance from the sun, at least 45°.
- Angular distance above the horizon, at least 15°.
- Angular distance from the zenith, at least 5°.
- Magnitude, less than 2.5.

A total of 13 stars met this criteria, and of these, seven were usually selected for any one set of observations. Two factors governed the final choice. First, it was desirable to have a balanced LOP configuration, remembering that the sun eliminated a good part of one quadrant; and second, the dimmer stars, magnitude 2.0 and above, were not likely to be visible when atmospheric conditions were less than optimum. Early field experience led to an observing program that utilized the same six stars—Vega, Arcturus, Dubhe, Capella, Pollux, and Deneb—plus one of three additional stars—Alioth, Alphecca, or Mirfac. (Fig. 4.)

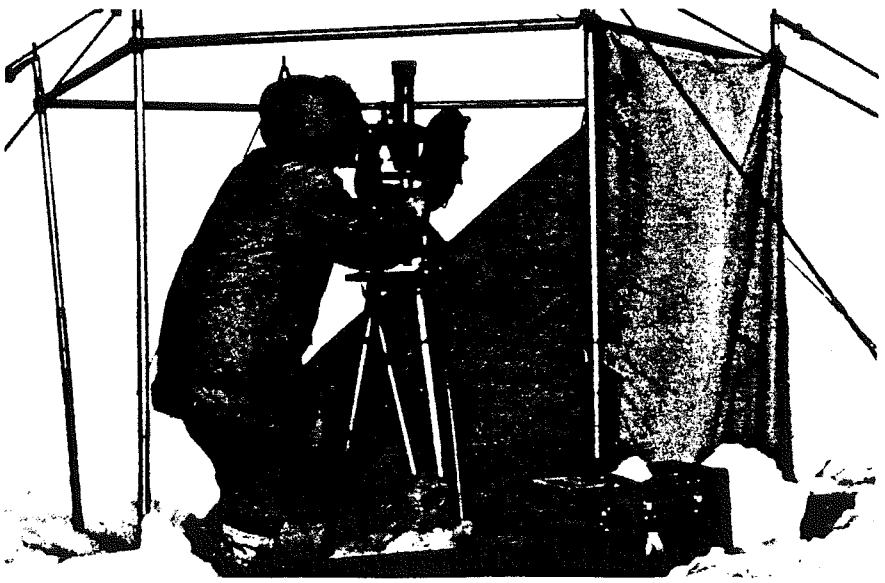

Figure 3. Observing Station.

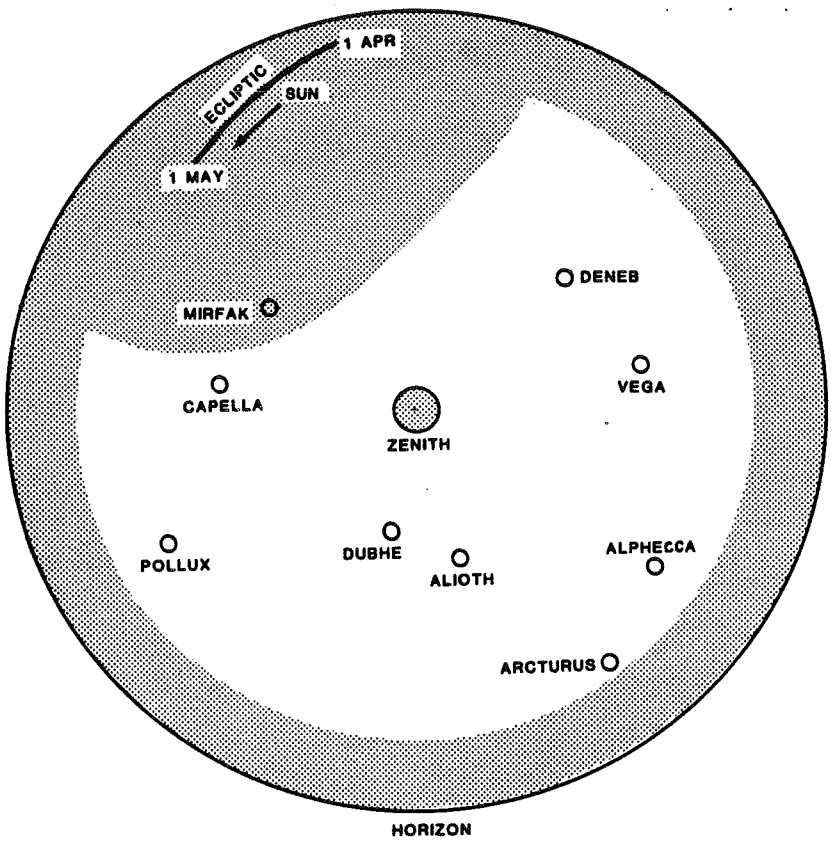

Figure 4. LOREX Navigation Stars.

With the sun above the horizon 24 hours a day, there was no twilight or nighttime during which the stars could be seen with the naked eye. It was, therefore, necessary to precompute the approximate zenith and azimuth angles of each star for the time of the observation. This computation was based on sidereal time and used a chronometer set to local sidereal time. In addition, it was necessary to know the approximate latitude and longitude of the station and the azimuth to a reference point established on the perimeter of the camp. An estimated latitude and longitude were obtained either by updating a previous astro fix or from a current satellite fix, and an updated azimuth for the reference point was computed after each series of observations. These precomputations were made with a programmable hand calculator immediately prior to each observation.

A small igloo-type tent, located about 4 m from the instrument, permitted the person doing the computing and recording to remain inside during the observations. When possible, one person made all the observations for a set. If, however, atmospheric conditions were less than optimum, increasing the time required to detect the stars, or if the wind and/or temperature were particularly severe, the observer and recorder exchanged jobs midway through a set.

In planning for LOREX it was necessary to decide how many pairs of observations should be taken for each position fix. Geometrically, two LOP's are sufficient to provide a fix, but to obtain a measure of the accuracy (precision) of the fix it is necessary to have at least three LOP's.

The accuracy of the position fixes required for LOREX was particularly important. Anticipating that the magnitude of the deflections of the vertical would be 0 to 10 arc seconds, it was necessary to achieve positional accuracies of 1 to 2 arc seconds.

Table 1. Precision of an Astro Fix for Various Star Sets and LOP Errors.

Set	Stars			LOP Errors (arc seconds)	Error Ellipse of Position Fix	
	Name	Magnitude	LOP Geometry		Semimajor Axis (arc seconds)	Semiminor Axis (arc seconds)
I	Vega (V) Arcturus (A) Dubhe (D)	0.1 0.2 2.0	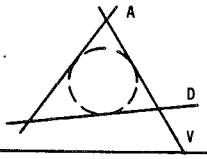	1.0	0.6	0.5
				2.0	1.2	1.1
				3.0	1.8	1.6
II	Vega (V) Arcturus (A) Dubhe (D) Capella (C) Pollux (P)	0.1 0.2 2.0 0.2 1.2	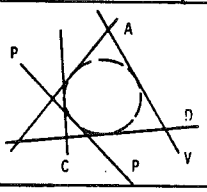	1.0	0.5	0.4
				2.0	1.0	0.8
				3.0	1.5	1.2
III	Vega (V) Arcturus (A) Dubhe (D) Capella (C) Pollux (P) Deneb (De) Mirfak (M)	0.1 0.2 2.0 0.2 1.1 1.3 1.9	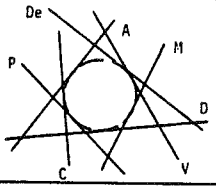	1.0	0.4	0.3
				2.0	0.8	0.7
				3.0	1.2	1.0

Working in the high latitudes of the Arctic induces two factors not normally encountered in other parts of the world. First, there is the environment itself. The temperature and/or wind limit the amount of time that an individual can spend taking observations and also reduce his effectiveness in handling, sighting, and reading the instrument. Beyond any direct physical impairment, there is often a psychological factor induced by the cold. The net result of these is to produce a higher error than would normally be expected from a given instrument and observer. Second, the movement of the sea ice is a factor. The observations have to be taken from a continually moving ice platform for which the rotation and short-term rate and direction of movement are unknown. In addition to inducing an unknown error is a set of observations, this requires that the set be completed in a reasonable amount of time. It is not possible to return at some later time and complete the set. Once begun, a fix is limited to the observations that can be completed at that time.

There are several ways to improve the accuracy of a fix: Decrease the residual errors of the LOP's by reducing the various input errors, increase the number of LOP's, and/or improve the geometry of the LOP's by using different star combinations. Depending on the circumstances, any or all of these can be used. With respect to the LOREX requirements, a sufficient number of observations had to be obtained to get the required positional accuracy, but the number could not be so great that the time became excessive. An error analysis program previously developed for Arctic astronavigation by Johnson and Clapp (1971(a)) was used to help determine how many pairs of observations would be used. Table 1 lists results from an analysis of three sets of observations using stars selected by the criteria outlined above. For each of the three analyses the semi-major and semiminor axis of the positional error ellipse are listed for an observing error of 1 arc second, 2 arc seconds, and 3 arc seconds. This analysis led to the following conclusions: If the combined observing errors were approximately 1 arc second, then three pairs of observations would be sufficient to obtain the desired accuracy, and if the combined observing errors were approximately 2 arc seconds, then five pairs of observations would be sufficient. If, however, the combined observing errors

Table 2. Typical Position Fixes and Errors.

Station	Fix Number	Date	Number of Pairs of Observations	LOP Errors	Position Fixes and Errors	
					Latitude (N)	Longitude (W)
Main Camp	95-1	5 April	6	2.2"	88° 22' 44.0" ± 1.0"	170° 40' 08.1" ± 1.0"
	95-2	5 April	8	3.1	88 22 59.2 1.3	170 56 23.8 1.4
	96-1	6 April	4	3.9	88 23 21.2 2.8	171 06 35.6 2.0
	97-1	7 April	7	3.1	88 23 42.4 1.3	171 55 12.9 1.2
	97-2	7 April	7	2.4	88 23 56.6 1.1	172 02 18.0 1.1
Iceman	108-2	18 April	7	3.1	88 42 45.2 1.3	186 57 55.0 1.4
	108-3	18 April	6	2.8	88 43 18.6 1.1	186 26 04.5 1.5
	109-1	19 April	7	2.2	88 43 51.3 1.0	185 35 09.4 0.8
	109-2	19 April	8	2.3	88 44 09.1 1.1	185 12 33.0 1.3
	109-3	19 April	6	2.1	88 45 21.0 0.9	183 51 08.1 1.2
	109-5	19 April	8	2.4	88 46 15.4 1.0	183 19 01.1 0.9
	110-1	20 April	6	4.0	88 46 59.7 2.1	182 59 32.8 1.6
	112-3	22 April	6	2.0	89 02 12.2 0.8	178 18 17.6 1.0
	112-4	22 April	7	2.5	89 02 43.2 1.2	178 31 02.8 0.9
	113-5	23 April	5	3.8	89 03 01.3 1.8	178 38 33.7 1.9
Main Camp	122-1	2 May	7	3.1	89 05 09.1 1.1	168 43 11.8 1.4
	122-2	2 May	7	3.0	89 05 51.3 1.4	167 11 33.7 1.2
	122-3	2 May	8	4.0	89 06 08.7 1.7	166 39 44.3 1.3
	123-1	3 May	8	2.3	89 06 39.7 0.8	165 58 52.0 1.1

were approximately 3 arc seconds, then seven pairs of observations would be necessary. Based on this analysis, pre-expedition plans called for three pairs of observations per fix and a fix every 2 hours.

Upon arrival at camp it was discovered that the fluid in the vertical index level of the Wild T-4 had been "lost" during shipment of the equipment. A replacement level was not readily available, and this meant the observer had to rely entirely on the plate levels of the instrument. This reduction of the instrument's precision plus early field experience caused the original observing plan to be modified, and the final operational schedule called for a set of observations every 3 to 4 hours, weather permitting, with the exclusion of one 8-hour period. Ideally the set consisted of 16 observations, eight pairs of direct and reverse readings, using seven stars and a repeated pair of observations on the initial star Vega, the brightest star. The average length of time necessary to make the observations was slightly more than 30 minutes, although the time varied from 16 minutes to 50 minutes. The shorter times came toward the end of the project and were the result of the increasing proficiency of the operators, combined with favorable viewing conditions.

Observations began on April 4 and continued through May 3, 1979, with 2 days being taken up moving observers and equipment from the main camp to the satellite camp and back again. At least one fix was obtained on 26 of the 30 days and, in all, 87 fixes were obtained.

Data Reduction

Preliminary position fixes were determined in the field as needed using a programmable hand calculator, but final data reduction and position determinations were made after completion of the field work and upon return from the Arctic. Reduction was by means of a computer program using a least squares solution of the classic two unknown (latitude and longitude) navigation problem. (Johnson and Clapp, 1971(a)) The program also included an option for analyzing systematic input errors. (Johnson, 1974)

Representative fixes from the main camp and the satellite camp, Iceman, are tabulated in Table 2. These 19 fixes are typical of the 87 fixes obtained during the 30 days of observing. The times between sets range from 2 to 6 hours, reflecting the 3- to 4-hour spacing called for in the final operational plan.

Forty-two of the fixes are initially being used to determine deflections of the vertical. The errors in latitude and longitude, expressed in the prime vertical, of the fixes selected for the study vary from ±0.6 to 1.6 arc seconds. Thus, the mean accuracy of the position fixes is ±1.1 arc seconds or about ±33 m.

Forty-five fixes are not currently being used for determining deflections of the vertical. In some cases these fixes did not occur at locations for which deflections were being computed, and in other cases one or both of the errors were in excess of 2.0 arc seconds.

Error Analysis

The 42 fixes used in the deflection study have an average error of the LOP's of ±2.6 arc seconds. This is not the positional error, but the average error of the individual LOP's relative to the final fix position. It effectively represents the combined random input errors from all sources including the following: leveling errors, pointing and reading errors, timing errors, refraction errors, and errors resulting from movement of the ice during a set of observations.

As previously stated, the vertical circle index level went dry during shipment of the Wild T-4 and it was, therefore, not possible to adjust the vertical circle prior to each reading. Limited field tests indicate that the error from this source was 1 to 2 arc seconds.

The combined pointing and reading error is estimated at 1 to 2 arc seconds. This is higher than would be expected from a T-4 under normal operating conditions, but it is a direct reflection of the environmental conditions under which the LOREX observations were made.

Time was recorded to the nearest half second and, given the ear/eye method used for the observations, the errors are estimated at 0.5 second of time. For the latitudes at which the observations were made, the equivalent residual error is no more than 0.2 arc seconds.

Refraction in the polar regions is thought by some to be unreliable. While not doubting reported cases of large refraction anomalies, it seems likely that these are the exception rather than the rule. Two detailed studies of Arctic refraction, one by Johnson and Clapp (1971(b)) and another by Johnson (1976), have shown that with the exception of extremely low altitudes, 5° or less, the Garfinkel refraction model is accurate to a few tenths of an arc second.

The error due to sea ice drift is a function of three parameters: the rate of drift, the direction of the drift relative to the star's azimuth, and the length of time necessary to complete a set of observsations. Based on typical values for these parameters, the error introduced by not taking them into account is in the range of 0.1 to 0.5 arc second, and for the 42 fixes used in the study the error from this source is likely in that range. Given the uncertainty of the parameters, however, the error could be larger and in some cases a contributing factor in those fixes that were rejected because of the size of their position errors.

These errors are tabulated in Table 3 along with their combined total, 1.4 to 2.9 sec-

Table 3. Estimated Errors in Observations.

Error Source	Estimated Magnitude (arc seconds)
1. Instrument/Observer	
Leveling	1.0 - 2.0
Pointing & Reading	1.0 - 2.0
Timing	0.2 - 0.2
2. Refraction	0.1 - 0.2
3. Sea Ice Drift	0.1 - 0.5
Combined Total	1.4 - 2.9

onds. The average, 2.2 arc seconds, of these estimated values can be compared with the average value, 2.6 arc seconds, of the 42 fixes being used in the deflection study. It can also be compared with the LOP errors tabulated in Table 2. Although somewhat smaller the estimated values seem to be of a correct magnitude.

Summary

The operational problems encountered in carrying out astronavigation on the Arctic Ocean are somewhat unique. First, the stars cannot be seen with the naked eye during the 24 hours of daylight, therefore their position must be precomputed with some accuracy. This requires that a reliable estimated position be obtained, either by dead reckoning from a previous astro fix or by supplemental means such as satellite positioning. The accuracy of the assumed position depends on such factors as time since the previous fix and the movement of the sea ice during that time. Other important factors in detecting a star are its magnitude and the atmospheric conditions at the time of the observation. Under some conditions a star of a given magnitude will be visible and a star of greater magnitude will not be visible. The next day both stars may be visible or neither star may be visible.

To minimize the detection problem it is desirable to use the best equipment available for making the observations. A Wild T-4 or comparable instrument is recommended. For LOREX the T-4 was chosen for its superior optics, ease of setting to precomputed zenith and azimuth angles, and ease of operator viewing and reading, all of which take on added, often critical, significance when the temperature drops to -40 C/F. some of its refined operational capabilities, eyepiece micrometer, automatic timing, etc., were nor utilized, and "loss" of the vertical circle index level bubble during shipments reduced its accuracy, but overall it maximized the operator's ability to locate daylight stars.

Seventy years after it was used by Peary to reach the North Pole, it is worthwhile to note that astronavigation is still helping unlock the mysteries of that remote part of the world. Of all the scientific experiments undertaken during LOREX, astronavigation was probably the most dependent on weather and, in an environment not known for its hospitable nature, there was always a question as to the limitations that it might impose. Through a combination of favorable weather, only minor equipment malfunctions, and excellent logistic support, approximately 1,200 observations (600 pairs of direct and reverse readings) were obtained over a 30-day period. Forty-two fixes are currently being used in conjunction with geodetic fixes obtained with a transit satellite receeiver to obtain deflections of the vertical in the vicinity of the Lomonosov Ridge. These represent a unique combination of one of the oldest and one of the newest methods of navigation.

ACKNOWLEDGMENT

The scientific director for LOREX was Dr. J. R. Weber of the Earth Physics Branch of EMR. Gordon Corcoran of the Geodetic Survey of Canada and the writer served as principal investigators, and the observations were made by Larry Hennessey and Brian Mousseau of the Geodetic Survey of Canada.

REFERENCES

Johnson, G. W. (1976), "Arctic Refraction Study," *Journal of the Surveying and Mapping Division*, ASCE, Vol. 102, No. SU1, Proc. Paper 12602, Dec., pp. 1-7.

Johnson, G. W. (1974), "Systematic Errors in High Latitude Astronavigation," *Journal of the Surveying and Mapping Division*, ASCE, Vol. 100, No. SU2, Nov., pp. 183-187.

Johnson, G. W. and J. L. Clapp (1971(b)), "Reliability of Refraction in Polar Astronavigation," *Journal of the Surveying and Mapping Division*, ASCE, Vol. 97, No. SU2, Proc. Paper 8502, Nov., pp. 165-171.

Johnson, G. W. and J. L. Clapp (1971(a)), "Solar Astronavigation in High Latitudes," *Journal of the Surveying and Mapping Division*, ASCE, Vol. 97, No. SU1, Proc. Paper 8139, May, pp. 27-38.

Lillestrand, R. L. and G. W. Johnson (1971), "Cartography of North Greenland," *Surveying and Mapping*, ACSM, Vol. XXXI, No. 2, June, pp. 233-250.

Lillestrand, R. L. and J. R. Weber (1974), "Plumb Line Deflection Near the North Pole," *Journal of Geophysical Research*, AGU, Vol. 79, No. 23, Aug. 10, pp. 3347-3352.

Weber, J. R. (1981), "Exploring the Arctic Sea floor," *GEOS*, EMR, Summer, pp. 2-7. ■

Deep-Sea Research, Vol. 28A, No. 3, pp. 251–268, 1981.
Printed in Great Britain.

0198-0149/81/030251-18 $02.00/0

On the deep circulation in the Arctic Ocean*

KNUT AAGAARD†

(*Received* 13 *June* 1980; *accepted* 27 *August* 1980; *final revision received* 24 *September* 1980)

Abstract—New measurements show that the deep water of the Arctic Ocean is not simply a uniform body of water but has an internal structure in its hydrography, mixing history and motion. A primary distinction can be made between the upper deep water, less saline than 34.92 to 34.93, which may derive rather directly from the Greenland or Norwegian Sea, and the lower deep water, which has had its salinity augmented within the Arctic Ocean. The relatively sharp interface between the two is centered near 1500 m, but its depth varies considerably.

Both the upper and lower deep waters cross the Lomonosov Ridge. In the vicinity of the Pole, the deep overflow moves diagonally up the ridge in a pulsating manner, with peak speeds exceeding 12 cm s^{-1}. There are indications that oscillations with periods exceeding about two days are bottom-trapped.

Flow in the abyss is generally less than 1 cm s^{-1}, but more energetic episodes with speeds of 2 to 4 cm s^{-1} occur, typically 5 to 10 days apart.

Below the upper few hundred meters, the circulation in both the Eurasian and Canadian basins appears to be cyclonic, and in most areas it is counter to the upper flow regime.

INFERENCES FROM THE HYDROGRAPHY

THE DEEP WATER of the Arctic Ocean, which we can somewhat arbitrarily define as lying below the lower 0°C isotherm, constitutes some 60% of the water in the Polar Basin. While the deep water is remarkably uniform in temperature and salinity, there are nonetheless two distinct features of the hydrography (Fig. 1) that have important implications for the deep circulation. These are (a) the difference in deep temperatures between the Eurasian and Canadian basins, with the Eurasian Basin being colder by about 0.5°C, and (b) the relatively high deep salinities, which throughout the Polar Basin are in the range 34.94 to 34.95 and in most of the basin form a slight maximum in the vertical.

The existence of the deep temperature difference was first shown by WORTHINGTON (1953), who attributed it to the presence of an as-yet uncharted submarine ridge. Since then the deep temperature structure has been discussed by a number of investigators (e.g., COACHMAN, 1963). The resulting conceptual model has the Canadian Basin filled by water coming over the Lomonosov Ridge and sinking adiabatically. NIKIFOROV, BELYSHEVA and BLINOV (1966) proposed that overflow occurs principally in the vicinity of the Pole and through the gap in the ridge north of the New Siberian Islands, near 81°N.

The existence of a deep salinity maximum has to my knowledge never been discussed as such in the literature. While the details of the maximum are unknown (e.g., whether the salinity increases monotonically to the bottom), it is clear that the highest salinities in the

* Contribution No. 1168 from the Department of Oceanography, University of Washington, Seattle, WA 98195, U.S.A. LOREX Contribution No. 3.

† Department of Oceanography, University of Washington, Seattle, WA 98195, U.S.A.

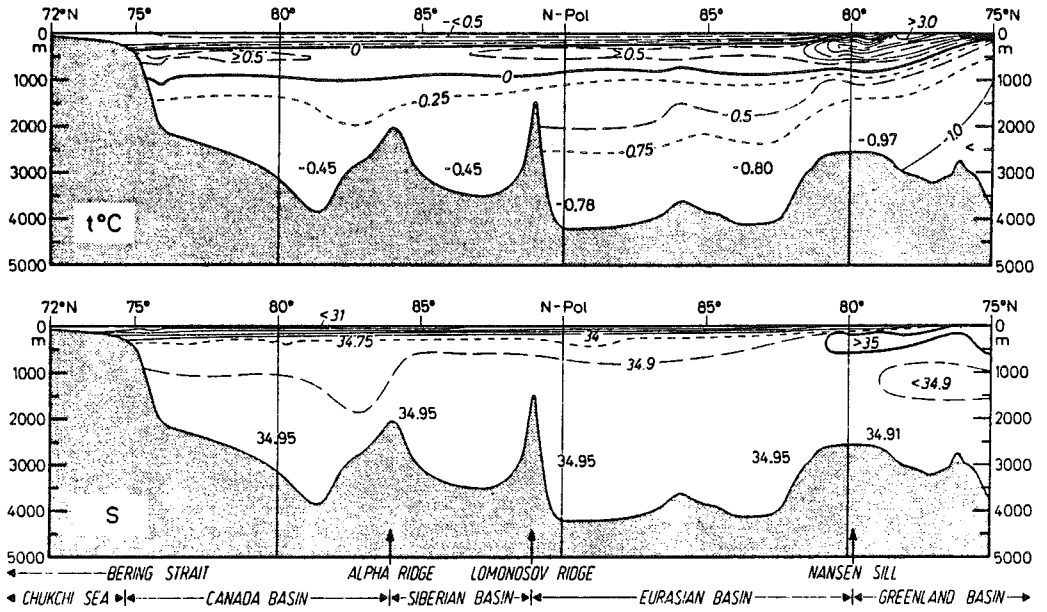

Fig. 1. Longitudinal section of temperature and salinity from the Greenland Sea over the North Pole to the Chukchi Sea (from COACHMAN and AAGAARD, 1974).

water column are below about 1300 to 1700 m (Figs 1, 2). The vertical salinity maximum is also a horizontal maximum, with deep salinities in the seas to the south not exceeding about 34.92 (compare Fig. 1). This is extremely important in that it is in the Greenland and Norwegian seas that the deep water of the Arctic Ocean is believed to have its origin, a view that originated with NANSEN (1902) and has never been seriously challenged. If the deep water of the Greenland Sea is also to supply the Polar Basin, then in so doing the Greenland Sea deep water must in some way mix with a more saline source. The effect of this salt source is to increase the salinity of the lower waters of the Arctic Ocean, roughly those lying deeper than 1300 to 1400 m, by a few hundredths of a part per thousand.

During March to May 1979, a geophysical program was conducted in the central Arctic Ocean. Dubbed LOREX (Lomonosov Ridge Experiment, WEBER, 1979), it included hydrographic casts and measurements from moored current meters. The observations have increased our knowledge of the deep circulation considerably. Figure 2 shows all LOREX salinity measurements from 500 m down. Below about 1500 m the salinity gradients decrease drastically, suggesting that waters above and below this depth have different sources or mixing histories. A second feature of Fig. 2 is the near-total lack of salinity observations in the range 34.92 to 34.93. That this is not simply an observational fluke is indicated by Fig. 3, showing the number of samples over the total depth and salinity ranges of interest. From Fig. 2 we should expect to find salinities of 34.92 to 34.93 in the depth interval 1200 to 1600 m. Figure 3 shows that this depth interval was not undersampled and it also suggests that there are at least two distinct salinity populations, one 34.92 or less, and the other greater than 34.93. The lack of salinity observations in the interval 34.92 to 34.93 can only mean that a rather sharp salinity gradient must exist immediately below 34.92. This is also suggested by the fact that by far the greatest salinity variation at any

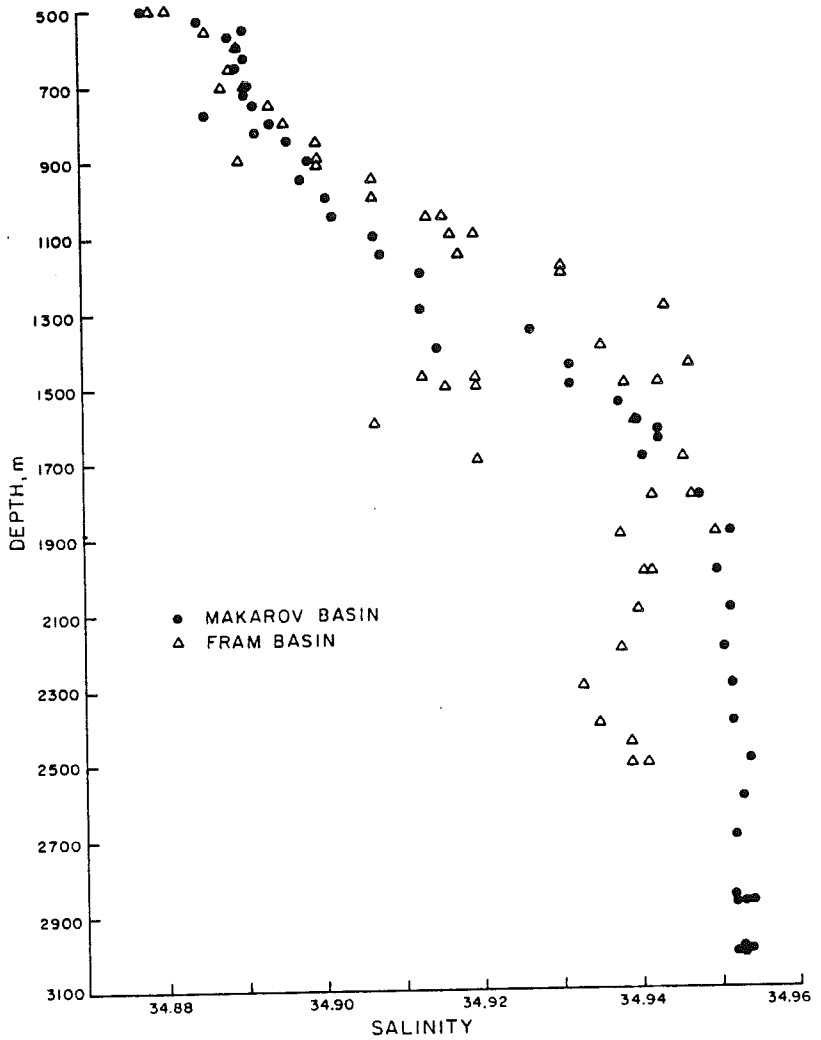

Fig. 2. All LOREX salinities from below 500 m. The Makarov Basin is on the Canadian side of the Lomonosov Ridge, the Fram Basin on the Eurasian side. The Fram Basin data are restricted to the north slope of the Lomonosov Ridge above 2600 m. All the observations were made by ROBERT MOORE and MALCOLM LOWINGS.

depth is centered around 1500 m, as would be observed for a salinity gradient which in some manner oscillated about this mean depth. I return to this matter in connection with the temperatures observed at the current meter moorings, emphasizing for the present only that the depth of the salinity gradient can vary by at least 600 m.

Where might we expect the source of salt for the deep water below the salinity gradient? There are two possibilities, one the overlying Atlantic water and the other brine rejection on freezing. If the Atlantic water is the source, then the salt transfer would have to occur in the Eurasian Basin and probably relatively close to the point of inflow. Certainly in the

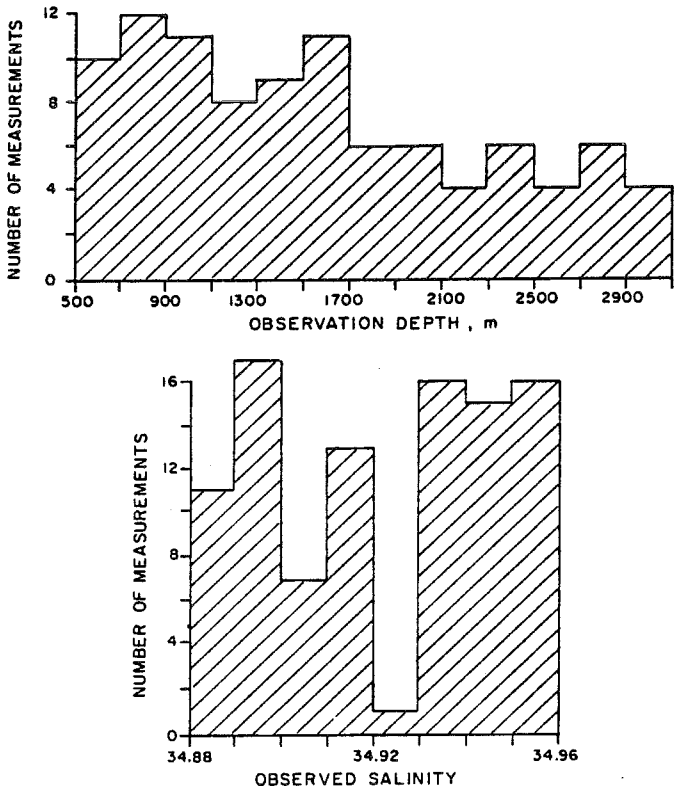

Fig. 3. Distribution of measurements in Fig. 2 by depth and salinity intervals.

Canadian Basin the salinity in the core of the Atlantic water is considerably lower than in the deep water. If the Atlantic water is in fact a source of salt for the deep water, one might, for example, suspect salt fingering below the core as part of the mixing process. It is also conceivable that upwelling of Atlantic water on to the shelves, followed by cooling, might form water of a density sufficient to let it feed into the abyss. While such upwelling has been observed in the Beaufort Sea (AAGAARD and TRIPP, 1978), the core salinities there are too low for the process to contribute to the more saline deep water. Only adjacent to the Eurasian Basin, most notably in the Barents and Kara seas, could such a mechanism conceivably constitute the salt source.

The other possible salt source is brine rejection. This would have to occur in selected areas on the adjoining shelves because the Arctic Ocean is generally well stratified. Water on the open shelf in the Chukchi Sea has in fact been observed in winter with salinities near the bottom as high as 34.99 and at the freezing point (AAGAARD and TRIPP, 1978). So far, however, this is exceptional, with normal winter shelf salinities appearing to be considerably lower.

We are left, then, with rather fragmentary but provocative evidence that the deep water in the Arctic Ocean represents at least two different advection and mixing histories. Water less saline than about 34.92, which we might call the upper deep water, may be connected with the Greenland Sea by a relatively direct advective link, as first suggested by NANSEN

(1902). However, water more saline than 34.92 to 34.93 (the lower deep water) has probably had to form by mixing of upper deep water with an even more saline water; both the salt source and the manner of the mixing are unknown. Considering the differences between the waters above and below the 34.92 to 34.93 isohaline, one might also expect gradients in other water properties across this interface. The interface itself is centered near 1500 m but undergoes vertical excursions of many hundreds of meters, so that salinity or, nearly equivalently, density is a more useful coordinate than depth.

CURRENT MEASUREMENTS

A total of seven previous bottom-referenced current measurements in the deep water have been reported by GALT (1967) and by HUNKINS, THORNDIKE and MATHIEU (1969). All were spot measurements representing motion immediately above the bottom over periods ranging up to about 30 min. Galt's two measurements were made over the Canada Abyssal Plain, as was one of those by HUNKINS *et al.* (1969), the other four being on the Mendeleyev Ridge. Over the abyssal plain the currents were 2.6, 1.5, and less than 1 cm s^{-1}, while the four ridge measurements were in the range 4 to 6 cm s^{-1}. Based on these measurements and on their comparison with measurements at higher levels made by instruments suspended from drifting stations (NIKITIN and DEM'YANOV, 1965; GALT, 1967), COACHMAN and AAGAARD (1974) concluded that "averaged over time the whole Arctic Ocean water column below about 400 m . . . moves as a unit without significant shear".

The deep current measurements made during the LOREX are the first Eulerian time series from the Polar Basin. The deployment and recovery techniques for moorings in ice-covered waters have been discussed by AAGAARD, DARNALL and KARIG (1978); the procedures used in obtaining the LOREX measurements correspond closely to those described earlier. Figure 4 shows the locations of the two moorings: L1 was just north of the ridge crest in 1440 m of water, and L2 was at the base of the northern flank in 3565 m. In each case Aanderaa current meters were mounted 25 and 200 m above the bottom, i.e., at 1415 and 1240 m for L1 and at 3540 and 3365 m for L2. Unfortunately, the lower current meter at L2, at 3540 m, malfunctioned electronically and yielded a data tape so noisy that we have been unable to use it. The records from the other three instruments were shortened by various amounts because of battery failure. Table 1 gives details of the moorings and current meter records.

First briefly consider the temperature records, some features of which are shown in Table 2. The potential temperatures recorded at L2 upper are consonant with the deep temperature field in the Eurasian Basin, based on spot measurements, depicted by COACHMAN and AAGAARD (1974, their Fig. 20). The temperature ranges at L1 upper and lower are indicated in Fig. 5 in which are also plotted all deep-water potential temperature salinity observations from the LOREX. Figure 5 suggests that the water at the L1 instruments is representative of the water at deeper levels in the Canadian Basin, which has spilled over from the Eurasian Basin. For example, all potential temperatures observed below 1450 m within the Canadian Basin were within the temperature range recorded by L1 lower. From the thermal record, then, L1 was in a position to have recorded overflow. The larger temperature range recorded at the lower instrument suggests considerable and variable vertical excursions of the water moving past the instrument. The temporal temperature range corresponds to vertical excursions of perhaps 400 to 600 m, based on gradient estimates from individual LOREX temperature observations. In this

Table 1. LOREX moorings and current meter records

Mooring	Latitude (°N)	Longitude (°W)	Sounding (m)	Deployed (Z)	Recovered (Z)
L1	89°10.6′	141°30.2′	1440	6 April 1979	31 May 1979
L2	89°24.6′	136°38.7′	3565	6 April 1979	27 May 1979

Current meter	Depth (m)	First valid record (Z)	Last valid record (Z)	Maximum velocity (cm s^{-1} at °T)	Vector mean velocity (cm s^{-1} at °T)	Mean temperature (°C)
L1 upper	1240	0130 6 April 1979	1640 13 May 1979	9.6 toward 113 (8 May)	2.1 toward 122	−0.34
L1 lower	1415	0130 6 April 1979	2100 16 May 1979	12.2 toward 098 (9 May)	2.7 toward 105	−0.39
L2 upper	3365	2230 6 April 1979	0510 9 May 1979	3.8 toward 043 (8 April)	0.4 toward 053	−0.75

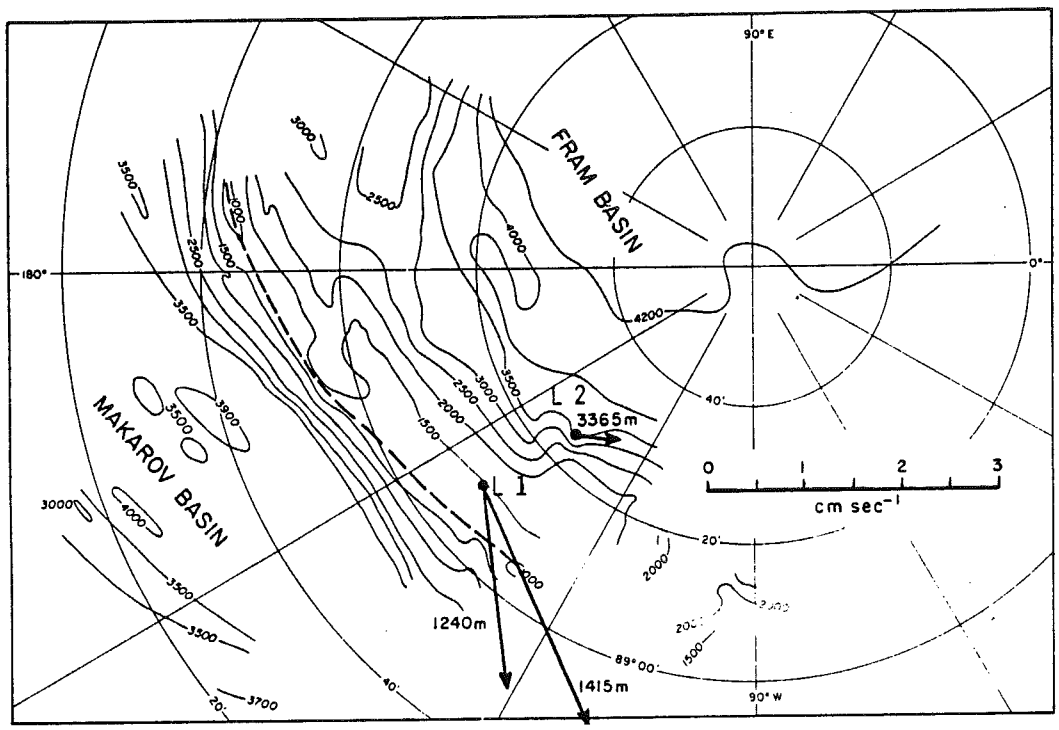

Fig. 4. Bathymetry in the LOREX area and mean currents at the mooring sites. Depths are in meters. The dashed line denotes the ridge axis. Bathymetry prepared by the Department of Energy, Mines and Resources, Ottawa.

connection recall that considerable scatter in salinity was observed centered near this depth at the hydrographic stations occupied in the Eurasian Basin during the LOREX (Fig. 2, Fram Basin), again suggesting vertical motions over 600 m.

The mean flow during the total recording time at each instrument (varying from 34 to 41 days) is shown in Table 1 and in Fig. 4. Before discussing the possible overflow registered at L1, I will briefly summarize the motion at L2. Current meter L2 upper appears to have been near a sharp turning point in the bathymetry so that the local isobath trend is somewhat uncertain, but the mean flow towards the northeast is probably not far from being aligned with the isobaths; it is quite slow, being less than 0.5 cm s^{-1}. The daily mean vectors are shown in Fig. 6. Examination of the original record shows several different flow modes. During most of the record, the current was below the threshold (< 1 cm s^{-1} for that

*Table 2. Potential temperatures**

Current meter	Depth (m)	Range of θ (C)	Mean θ (C)
L1 upper	1240	−0.37 to −0.43	−0.40
L1 lower	1415	−0.41 to −0.57	−0.46
L2 upper	3365	−0.94 to −0.99	−0.97

* The potential temperatures have in each case been calculated for an assumed salinity of 34.95.

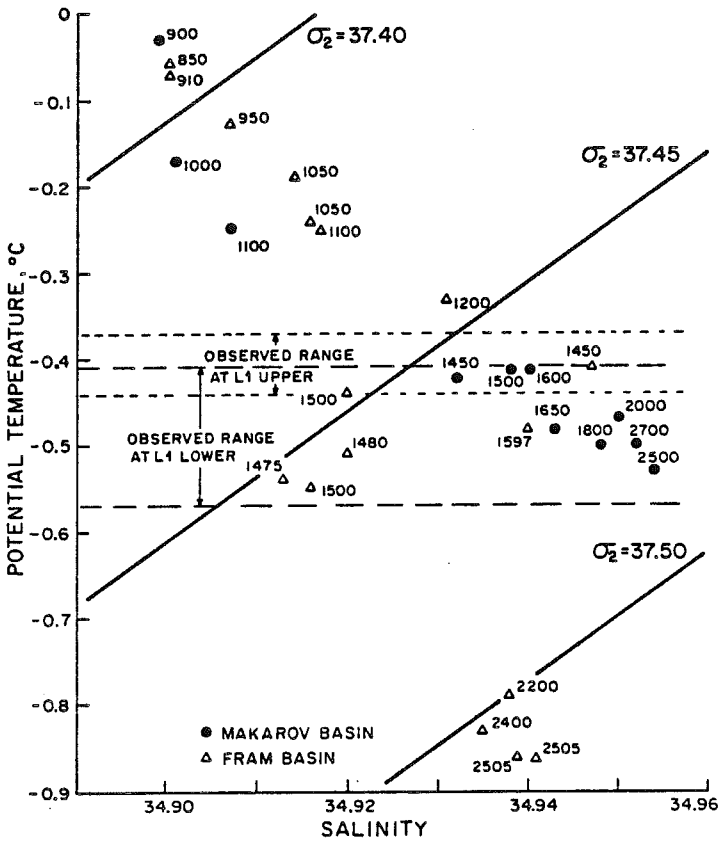

Fig. 5. All LOREX potential temperature–salinity observations from below 850 m and potential temperature ranges observed at mooring L1. The lines of equal density are for 2000 dbar. Hydrographic observations were by ROBERT MOORE and MALCOLM LOWINGS.

instrument), but systematic changes in the direction suggest a very weak NE flow on which was superimposed an even weaker semi-diurnal tidal oscillation. On four separate occasions, major bursts of speed in the range 2 to 4 cm s^{-1} were registered. Each lasted 1 to 2 days, and while three of them were directed NE, the last one was SE. Four smaller and shorter bursts also occurred, generally less than 1.5 cm s^{-1} and all but one toward NE.

At L1 the motion was substantially different; it was faster, it had a mean component directed across isobaths, and it was of a different temporal nature. Speeds at L1 reached over 12 cm s^{-1}, with vector means being in the neighborhood of 2.5 cm s^{-1} (Table 1). Particularly striking is the vertical shear, with the mean flow increasing downward. The difference in mean speed over the 175 m separating the upper and lower current meters was 0.6 cm s^{-1}. The LOREX hydrographic data suggest a density gradient in this depth range of about 6×10^{-10} g cm^{-4}, corresponding to a density difference between the two instrument levels of 0.01 in σ. Geostrophically to sustain the mean shear requires an isopycnal slope of 9×10^{-3} upward toward the ridge crest. For reference, the bottom slope on the north face of the ridge is about six times this, or 5.4×10^{-2}. Comparison with baroclinic instability models (SMITH, 1976) shows that under these circumstances the mean

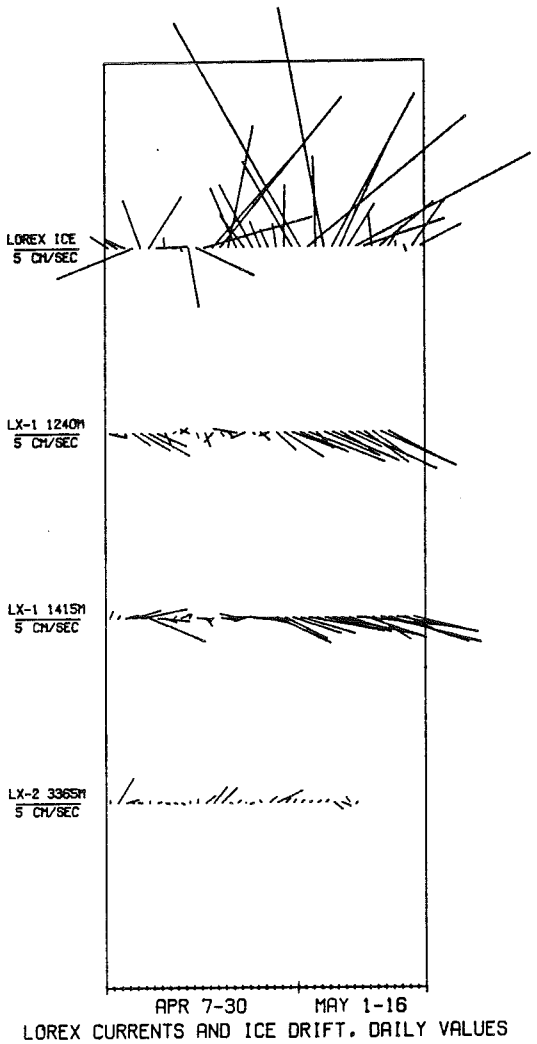

Fig. 6. Daily mean currents and ice drift, 7 April to 16 May 1979. North is toward the top. Ice drift calculations were made by D. WELLS and J. POPELAR.

flow is baroclinically stable. Only on a few occasions did the shears achieve sufficiently high values (3 to 4 cm s^{-1} over 175 m) possibly to approach unstable conditions, but the shears were not sustained for any length of time. There would thus seem little doubt that the observed flow was stable.

Figure 4 shows the mean currents at L1 to be directed upslope at angles of 20 to 40° relative to the isobaths. The compasses were calibrated both before and after deployment, and examination of the calibrations shows it unlikely that the compass error exceeded ± 5°. The magnetic declination (180° at L1) is based on Canadian airborne magnetic surveys updated for secular variations by observations at Alert. The declination is almost certainly also correct within ± 5°. It is therefore highly likely that the partially uphill

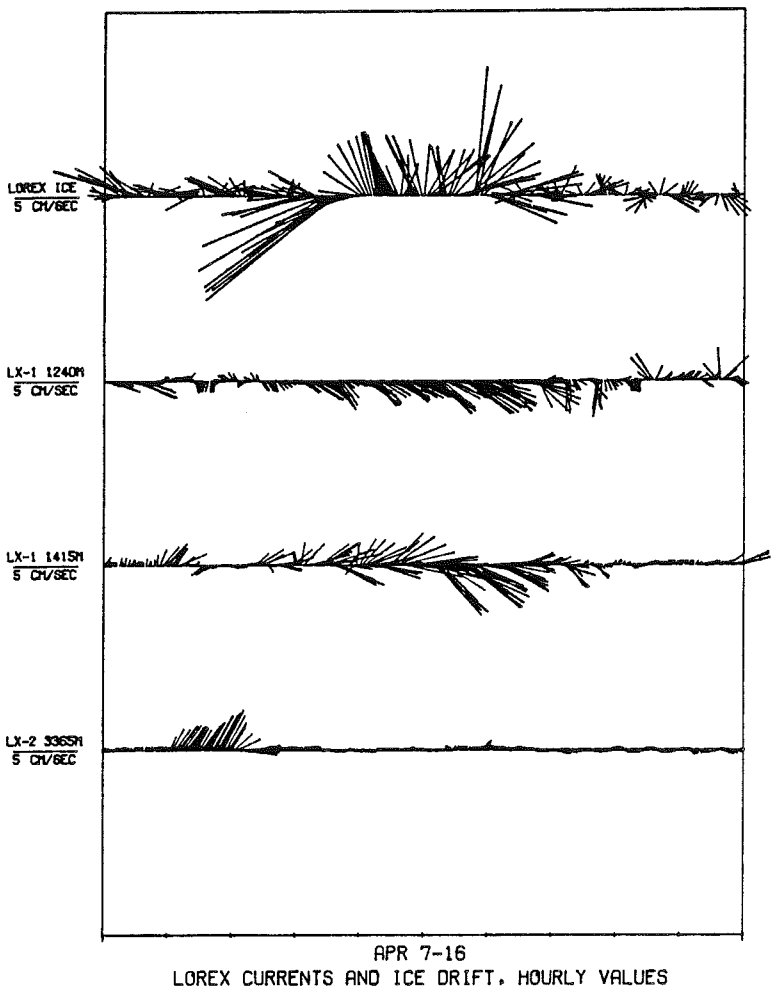

Fig. 7. Hourly mean currents and ice drift, 7 to 16 April 1979.

vector orientation is in fact real and that the meter recorded overflow across the Lomonosov Ridge.

What is the nature of the overflow? Figure 6 shows that it occurred as a series of pulses directed ESE, principally during May, but with one large event in mid-April. (At the mooring location the ridge axis lies nearly E–W, i.e., nearly parallel with the time axis.) The daily vector mean during the events was of order 5 cm s^{-1}. The hourly vector plots (Figs 7–10) illustrate the situation further. The first large overflow event, occurring the second week in April, lasted 2 to 3 days and had peak speeds of about 5 cm s^{-1}. The period 17 to 26 April was relatively quiet, and tidal currents of 1 to 3 cm s^{-1} rotating clockwise are readily apparent in the record. Beginning about 28 April, there was a series of increasingly strong pulses toward ESE of amplitude 5 to 10 cm s^{-1} and a fairly regular period of about 3 days. These continued to the end of the current record, but with decreasing amplitude the

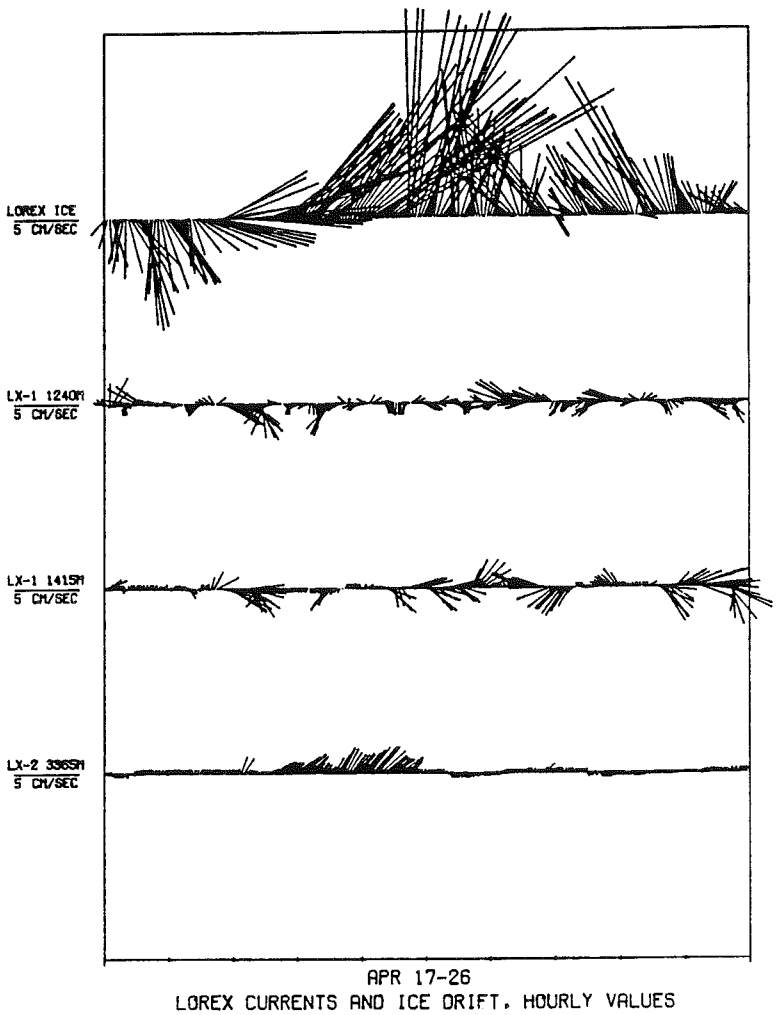

Fig. 8. Hourly mean currents and ice drift, 17 to 26 April 1979.

last several cycles. The signal is also obvious in the serial velocity component plots (Fig. 11).

The energy spectra (Figs 12, 13) also show many of these features, including the peak at 3 days. For frequencies lower than the semi-diurnal, the zonal component, i.e., along the ridge, is the more energetic. The opposite is true in the semi-diurnal band, which the spectral estimates show quite clearly to represent principally the M_2 tide; it co-oscillates with the North Atlantic and propagates across the ridge. [The energy and phase spectra yield M_2 current ellipses oriented N–S, with maximum amplitudes of 2 to 2.5 cm s^{-1}, and a minor axis slightly over one-half the major axis. The M_2 tidal current rotates clockwise; it diminishes only slightly toward the bottom. The agreement with the recent numerical tidal model of KOWALIK and UNTERSTEINER (1978) is quite good.]

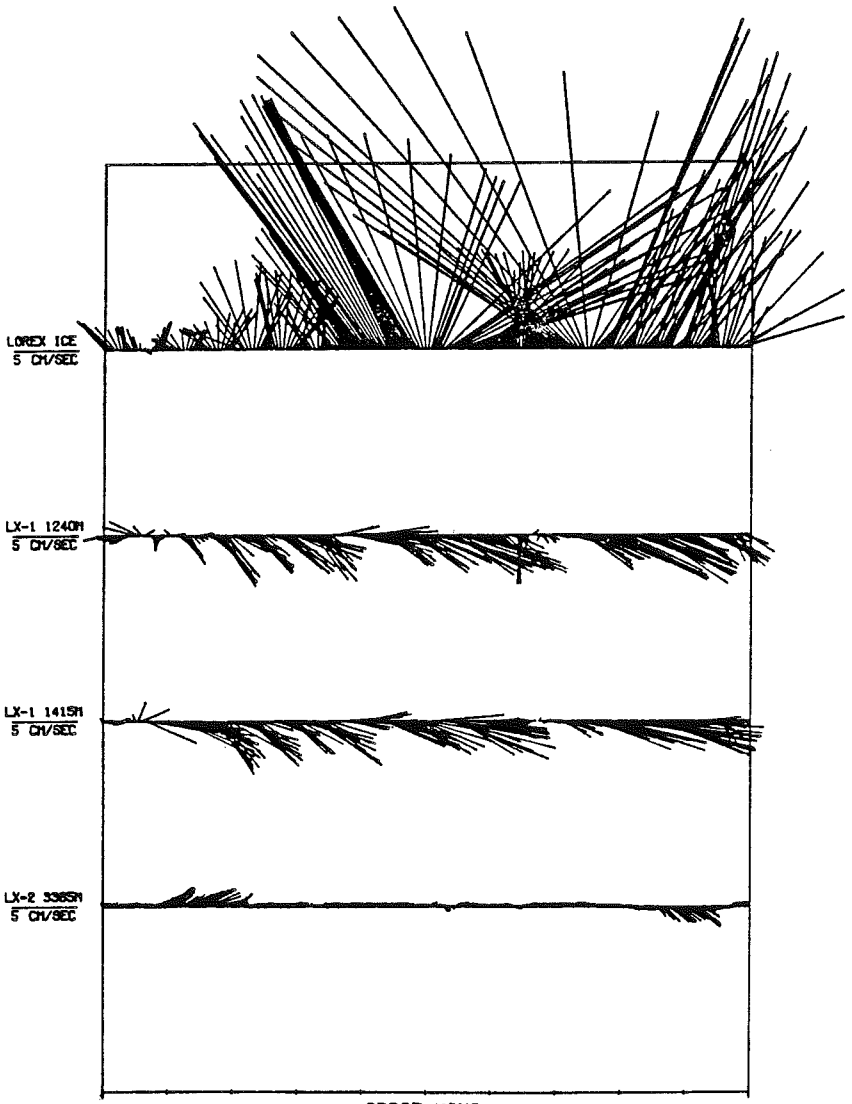

Fig. 9. Hourly mean currents and ice drift, 27 April to 6 May 1979.

The spectra also suggest that the low-frequency motion is more energetic at the lower meter than it is at the upper particularly for the east component (Fig. 13). However, the 95% confidence limits do not distinguish between the relative amplitudes of the two peaks, so that statistically we cannot be certain that there is a shear. If we use the spectra to estimate the mean characteristics of the low-frequency peak, we find the motion (a) to have a period of very nearly 3 days, (b) to have north and east components nearly out of phase, i.e., the oscillation is essentially rectilinear, (c) to have amplitude increasing from about

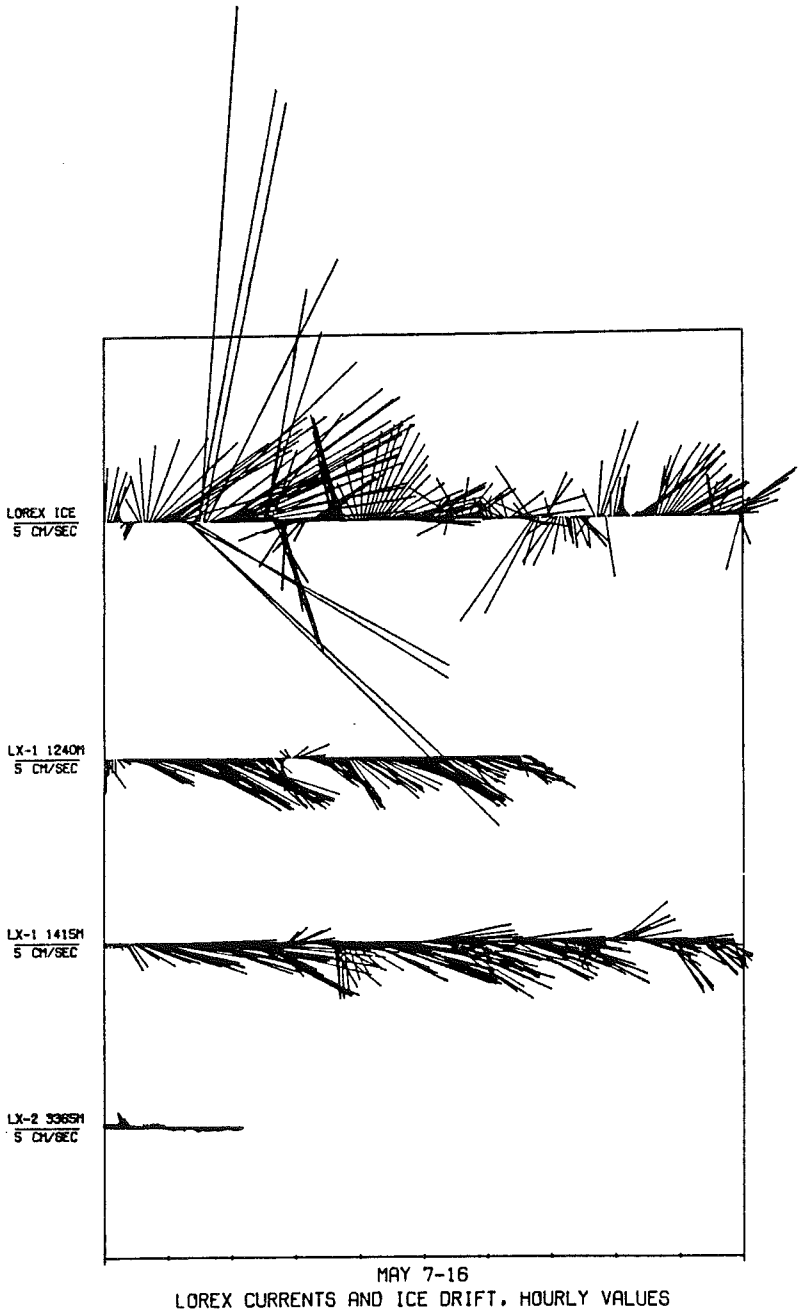

Fig. 10. Hourly mean currents and ice drift, 7 to 16 May 1979.

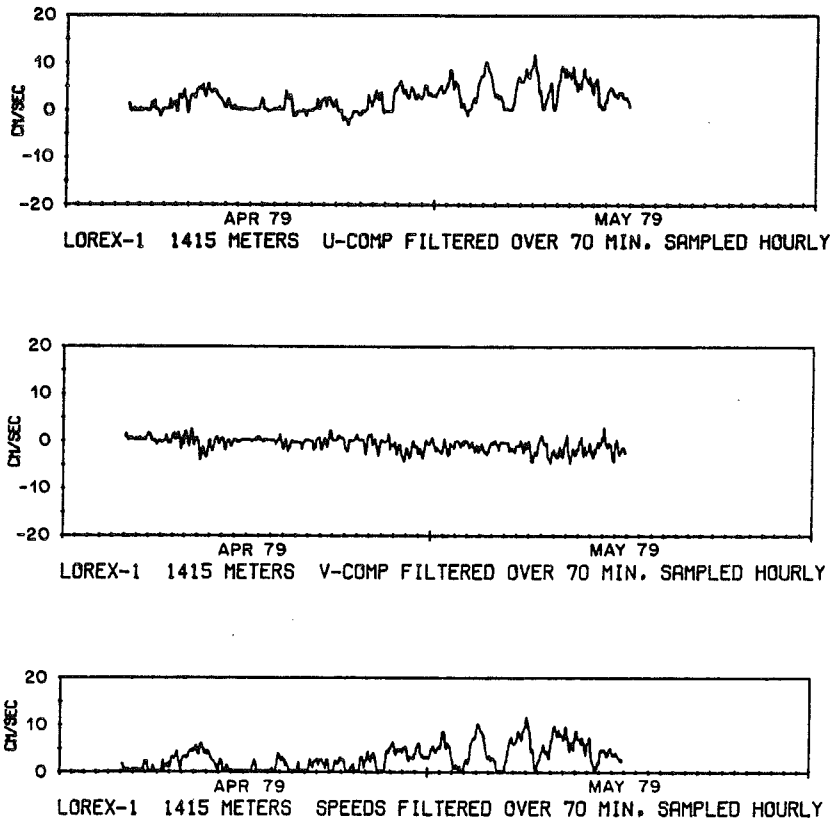

Fig. 11. Hourly running means of u (east)- and v (north)-components of velocity and speed at current meter L1 lower, 6 April to 16 May 1979.

2.2 cm s^{-1} at 1240 m to 3.2 cm s^{-1} at 1415 m, and (d) to be directed about ESE (116°T at 1240 m and 104°T at 1415 m).

Apart from the mean motion, the principal contribution to the flow across the ridge is thus seen to be a low-frequency (3-day period) motion, probably intensifying toward the bottom, but baroclinically stable. Furthermore, we have previously noted that the largest temperature variations also occurred close to the bottom. The characteristics suggest bottom-trapped buoyancy oscillations (RHINES, 1970), in which the motion decays exponentially away from the bottom.

For short wavelengths, the highest possible frequency of such oscillations is $\omega = \alpha N \sin \theta$, where α is the bottom slope, N the buoyancy frequency, and θ the angle between isobaths and principal current axis. Six of the LOREX hydrographic casts were averaged to give $N = 7.6 \times 10^{-4}$ s^{-1}, between 1000 and 2000 m. The angle θ is in the neighborhood of 30° and α is about 100 m per nautical mile, or 0.054. The values give a maximum frequency corresponding to a period of just over 3.5 days. The period of the low-frequency spectral peak is about 3.0 days, in reasonably close agreement with the calculated high-frequency cutoff. The spectra also show peaks at about 1.8 days, and the signal is particularly marked in the north component at the deeper meter, as would be the case for

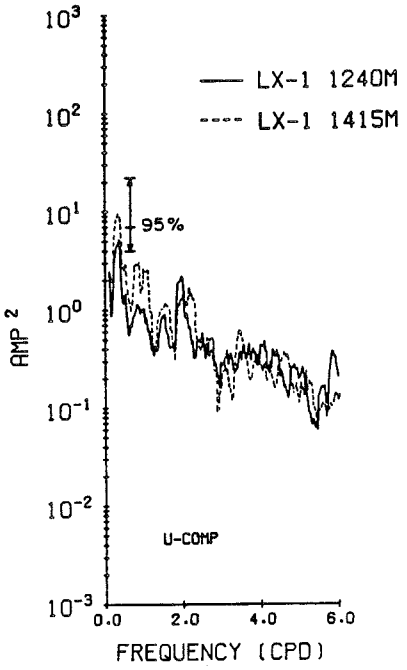

Fig. 12. Energy-conserving spectra of u (east)-components of velocity at mooring L1.

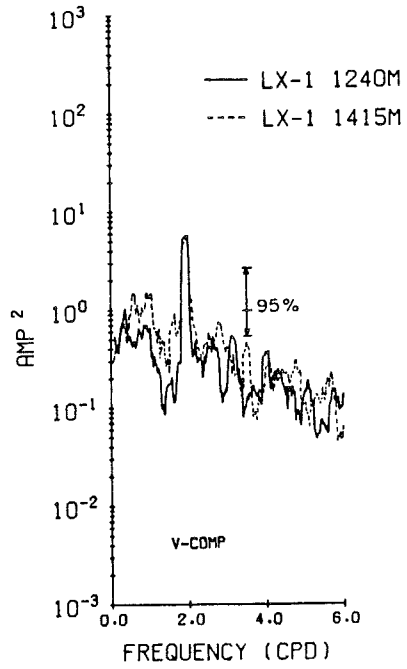

Fig. 13. Energy-conserving spectra of v (north)-components of velocity at mooring L1.

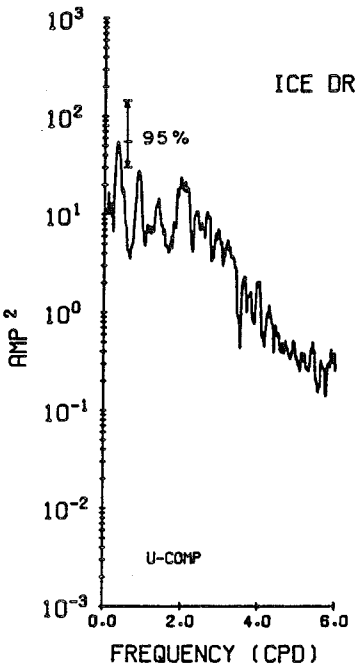

Fig. 14. Energy-conserving spectrum of u (east)-component of ice drift.

trapped oscillations directed approximately up-slope. A period of 1.8 days is in fact identical with the high-frequency cutoff calculated for $\theta = 90°$. With the present limited observations of the density and velocity fields, it is difficult to explore the application of the model much further, and in the absence of statistically clear evidence, bottom trapping along the ridge remains a hypothesis.

It should be noted, however, that the ice motion also exhibits a spectral peak at a period of 3 days, as shown in Fig. 14 for the east component. The amplitude of oscillation in the ice drift is over twice that in the record from the near-bottom instrument at L1, but we do not, of course, know the magnitude of the corresponding oscillation in the upper part of the water column. However, the east components of the ice drift and deep current are quite coherent at this frequency, so that we may be seeing evidence of barotropic disturbances which, when they reach the ridge, are bottom-trapped. The waves then align themselves with the bottom slope at the angle appropriate to their forcing frequency.

DISCUSSION

How do these pieces of evidence contribute toward a better understanding of the deep circulation? First, the deep water of the Polar Basin is not a uniform body of water in terms of hydrography, mixing history, or motion. Rather, we can at a minimum distinguish between an upper deep water less saline than 34.92 to 34.93 and a more saline lower deep water. While both may ultimately derive from the Greenland Sea or the Norwegian Sea, only the upper deep water can do so fairly directly. The more saline lower part has to be augmented by a salt source, probably to be found either in the Atlantic water or on the

shelves. The interface between the two deep waters is relatively sharp, and while it is nominally centered near 1500 m, its depth varies by many hundreds of meters, probably both as a function of position and time.

The flow measured at the LOREX moorings is consonant with a deep cyclonic circulation in the Eurasian Basin, in the same sense as the Atlantic water circulation. Such a deep circulation has in fact been suggested earlier for the Canadian Basin by HUNKINS *et al.* (1969); again this circulation would be in the same sense as that of the overlying Atlantic water. Nothing is known about possible short circuits of such basin-wide deep cyclonic gyres. Over most of the Polar Basin an intermediate and deep cyclonic circulation would run counter to the flow in the upper few hundred meters.

The flow in the abyss is relatively slow, probably typically of order 1 cm s^{-1} or less but with faster episodes, say 2 to 4 cm s^{-1}, typically 5 to 10 days apart. Along major topographic slopes speeds are considerably higher, certainly capable of reaching 10 cm s^{-1} or more. Over the Lomonosov Ridge, the semi-diurnal tide alone has an amplitude of 2 to 3 cm s^{-1}. One would thus expect quite active sediment movement in these areas. The currents are quite variable, and there are indications of bottom trapping of oscillations with periods of a few days or more.

Both the upper and lower deep waters cross the Lomonosov Ridge, but only the more saline part will sink any significant distance to fill the Canadian Basin below about 1500 m. Near the pole the deep overflow moves diagonally up the Eurasian side of the ridge and has been observed to cross the isobaths at an angle of about 30 . It is highly time-dependent, and one should therefore expect that the flow down the Canadian flank of the ridge will occur in pulses, even if it is baroclinically stable. Rotational effects would constrain the flow to be directed nearly along the isobaths and toward the left, for an observer looking uphill.

Acknowledgements—I thank HANS WEBER for the opportunity to participate in LOREX, ROBERT MOORE and MALCOLM LOWINGS for the hydrographic data, ADRIAN CAMFIELD, J. JOHNSON, DAVID WELLS, J. POPELAR, HELLA LEE and R. B. TRIPP for technical assistance, EDDY CARMACK and L. K. COACHMAN for their careful review of an earlier version of this paper, and the many people who gave freely of their time and efforts on the ice. I especially thank CLARK DARNALL and S. HARDING, with whom I had the pleasure and privilege of making the current measurements.

The work was supported financially by the Office of Naval Research under Contract N00014 75 C 0893 and logistically by the Polar Continental Shelf Project, Department of Energy, Mines and Resources, Canada.

REFERENCES

AAGAARD K., C. DARNALL and F. KARIG (1978) Measurements with moored instruments in ice-covered waters. *Deep-Sea Research*, **25**, 127 128.

AAGAARD K. and R. B. TRIPP (1978) Saline water on the northern Alaskan shelves. *Transactions of the American Geophysical Union*, **59**, 1091.

COACHMAN L. K. (1963) Water masses of the Arctic. In: *Proceedings of the Arctic Basin Symposium*. Arctic Institute of North America, Washington, D.C., pp. 143 167.

COACHMAN L. K. and K. AAGAARD (1974) Physical oceanography of arctic and subarctic seas. In: *Marine geology and oceanography of the Arctic seas*, Springer-Verlag, New York, pp. 1 72.

GALT J. A. (1967) Current measurements in the Canadian Basin of the Arctic Ocean, summer 1965. University of Washington Department of Oceanography Technical Report 184, 17 pp.

HUNKINS K., E. M. THORNDIKE and G. MATHIEU (1969) Nepheloid layers and bottom currents in the Arctic Ocean. *Journal of Geophysical Research*, **74**, 6995 7008.

KOWALIK Z. and N. UNTERSTEINER (1978) A study of the M_2 tide in the Arctic Ocean. *Deutsche Hydrographische Zeitschrift*, **31**, 216 229.

NANSEN F. (1902) Oceanography of the North Polar Basin. *The Norwegian North Polar Expedition*, 1893 1896, *Scientific Results*, **3**(9), 427 pp.

NIKIFOROV YE. G., YE. V. BELYSHEVA and N. I. BLINOV (1966) The structure of water masses in the eastern part of the Arctic Basin. *Oceanology*, **6**, 59–64.
NIKITIN M. M. and N. I. DEM'YANOV (1965) O glubinnikh techeniyakh Arkticheskogo Basseina. *Okeanologiya*, **5**, 261–263.
RHINES P. (1970) Edge-, bottom-, and Rossby waves in a rotating stratified fluid. *Geophysical Fluid Dynamics*, **1**, 273–302.
SMITH P. C. (1976) Baroclinic instability in the Denmark Strait overflow. *Journal of Physical Oceanography*, **6**, 355–371.
WEBER J. R. (1979) The Lomonosov Ridge Experiment: 'LOREX 79'. *EOS Transactions of the American Geophysical Union*, **60**, 715–720.
WORTHINGTON L. V. (1953) Oceanographic results of project Skijump 1 and Skijump 2 in the Polar Sea, 1951–1952. *Transactions of the American Geophysical Union*, **34**, 543.

JOURNAL OF GEOPHYSICAL RESEARCH, VOL. 91, NO. C10, PAGES 11,763–11,773, OCTOBER 15, 1986

Physical Oceanography Near the North Pole

E. R. POUNDER

Institute of Oceanography, McGill University, Montreal, Quebec, Canada

As part of LOREX 79, observations of current, conductivity, temperature and depth were made for 40 days from an ice floe which drifted in the area within 1.5° of the north pole. Daily profiles were taken to a maximum depth of 1400 m. Observations were analyzed to give profiles of S, T and σ_T and of water speed and true direction. The water column was stable at all stations; density increased with depth. Observations of the under-ice mixed layer showed it to become both thinner and warmer during northward drift of the floe. Downward motion and cooling of Atlantic water advected southward were observed. Near the middle of the drift period the surface salinity dropped abruptly by 1‰, indicating passage into a different water mass. A rough calculation showed only small water transport over the Lomonosov Ridge where the drift track crossed it.

INTRODUCTION

The Lomonosov Ridge Experiment (LOREX 79) was a major field program organized by the Department of Energy, Mines and Resources of Canada (DEMR) to study the ridge, using a variety of geophysical techniques including seismic soundings, gravity profiles, heat conduction measurements, etc. The objective was to try to establish the nature of the ridge, i.e., whether it is a purely marine phenomenon or whether it could have been part of a land mass which had separated and moved to its present position through continental drift. Teams for the experiment were drawn from a number of Canadian governmental agencies and several universities.

LOREX also provided the McGill group with an opportunity to continue its work in Arctic oceanography, although available resources permitted observations from a single drifting station only. A series of physical oceanographic measurements was made for 40 days from a drifting ice floe, code named ICEMAN. This station was established on April 4, 1979, at 88°41'N, 175°43'E and operated until May 28 (89°52.3'N, 48°26'E). The observations commenced on April 14 (day 104). (A Julian calendar date with January 1, 1979 = Jday1 was used.) During the first few days of the drift ICEMAN passed over the Lomonosov Ridge, recording a minimum depth of 956 m. Figure 1 shows the drift track of ICEMAN superimposed on a contour map of the sea floor. It was supplied by J. R. Weber and is an updated combination of two figures in *Weber* [1979]. All data in this paper are derived from the drift of ICEMAN, the most westerly dotted curve in Figure 1, but for completeness the other two drift tracks of LOREX stations are shown (two other dotted curves) as well as the tracks of two earlier drifting stations set up by the Earth Physics Branch of DEMR (1969, 1971), the organizer of LOREX. The McGill group [*Johannessen*, 1970] took part in the 1969 expedition.

A review of the oceanography and bathymetry of the Arctic Ocean can be found in *Coachman and Aagaard* [1974]. Only a brief summary will be given here. The principal bathymetric feature is the Lomonosov Ridge, a submerged range which runs from about Greenland, almost under the north pole, to the entrance to the Laptev Sea. The average depth of the ridge crest is about 1400 m. It divides the Ocean into two main, deep basins, the Amerasia and the Eurasia Basins (respectively to the lower left and the upper right in Figure 1). These basins are about 3800 m and 4200 m deep. Other major bathymetric features such as the Alpha Ridge (in the Amerasia Basin) and the Nansen-Gakkel Ridge (on the Eurasian side) are at considerably greater depths than the Lomonosov Ridge.

The surface circulation of the Arctic Ocean shows two dominating features, a large clockwise circulation in the Amerasia Basin called the Beaufort Gyre and the Transpolar Drift Stream which runs on the Eurasian side from Western Siberia toward the north pole and then (more rapidly) north of Greenland to form part of the East Greenland Current. This is the main route for export of water and ice from the Arctic. The original siting of the three LOREX stations was towards the Siberian side of the north pole so that they should (and did) drift across the Lomonosov Ridge.

Fresh or nearly fresh water enters the Arctic Ocean by drainage from the surrounding land masses, principally through the discharge of the main rivers such as the Mackenzie, Yukon, Lena, etc., and by the melting of the low-salinity surface layers of ice floes. Precipitation and evaporation have negligible effects on the water budget. There results a low-salinity layer immediately under the ice and overlying a rather sharp pycnocline. This layer is often called Arctic water and its salinity and depth vary both seasonally and geographically. Typical values are 30‰ and 30–100 m. A small amount of Pacific water enters through the Bering Strait, cools as it passes over the shallow Chukchi Sea and sinks, after considerable mixing with surface water, below the surface layer. The Canada Basin (the southeastern part of the Amerasian) is often described as a three-layer system: Arctic water ($0 \approx 50$ m), modified Pacific water (≈ 50–200 m), and modified Atlantic water below 200 m. Water below 900 m is referred to as deep water; it is very uniform in salinity and temperature. The largest input to the Arctic is of relatively warm, highly saline surface water from the Atlantic via the Norwegian-Greenland Seas. This denser water sinks slowly and cools by conduction of heat to both the Arctic layer and the deeper water. The TS diagram shown in Figure 14 of *Coachman and Aagaard* [1974] shows how the characteristics of the Atlantic water are modified as it flows from Spitzbergen to the southern Beaufort Sea. No indication of Pacific water is found in the Eurasia Basin, which is a two-layer system.

The drift track of ICEMAN was almost entirely over the Eurasia Basin, and this paper is a study of the variations in water properties along this track.

Paper number 6C0360.
0148-0227/86/006C-0360$05.00

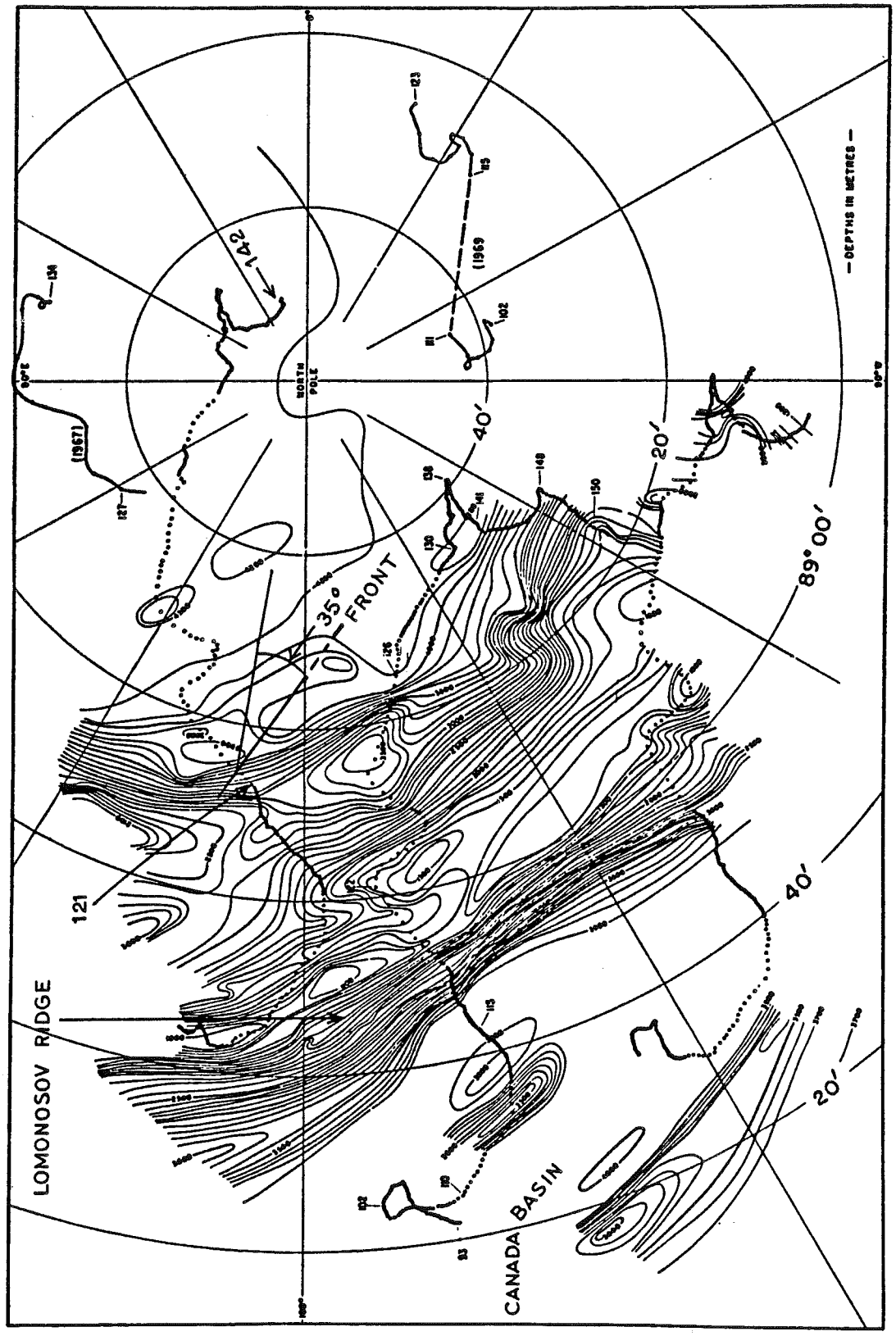

Fig. 1. Bottom contour map of the LOREX area showing the drift tracks of the three stations, that of ICEMAN being the most westerly. Except for a brief period of a few days early in April the track of ICEMAN lay entirely in the eastern hemisphere. The line marked FRONT shows the location where the drift track crossed a frontal zone, as well as the probable direction of the front at that time.

INSTRUMENTATION

The main instrument was an RCM-4 Aanderaa current meter equipped with conductivity (C), temperature (T), and depth (D) sensors. This device was lowered daily to the bottom or to a maximum depth of 1400 m to yield CTD and current profiles. Each cast took about 8 hours. A similar Aanderaa meter was mast-mounted 5 m below the lower ice surface, and recordings of C, T and velocity were made every 10 min throughout the experiment. Comparisons as the profiling meter passed through the 5-m level were useful and, as well, an important role of the fixed meter was to provide a number of absolute values of the current direction by comparison with independent astronomical observations.

ANALYSIS

The output data from the two Aanderaa meters were processed to provide time series of C, T, D, current speed and, using an assumed value of magnetic variation, true direction. Pressure corrections were applied to obtain salinity S and density, ρ, in the form of σ_T. The choice of the magnetic variation to be used presented a problem. Because the magnetic pole is currently near Melville Island, some 24° of latitude from the geographic pole, the variation changes very rapidly over the surface near the latter. During the drift of about 180 km the variation changed from approximately 145°E to 30°E. The best information available appeared to be Admiralty Chart 5384 showing variations in the polar regions in 1975. This chart was not based on actual measurements in these regions but on the mean of two world models IGS 75 (UK) and AWC 75 (US). Past comparisons with observations at stations between 80°N and 80°S have given a mean difference of 0.02° from the model data.

Additional calibration on magnetic variation was available from a series of 28 sun shots taken by Barry Allen of the Lamont-Doherty Geophysical Observatory of Columbia University. Unfortunately, overcast conditions limited these observations to the periods April 12–20 and May 3–20. Each sun shot gave the azimuth of the sun and hence the direction of true north. Comparison with the compass reading on the 5-m mast gave a fairly accurate magnetic variation. The variations used in the calculations of true-velocity directions were based on Allen's azimuths combined with interpolations from the Admiralty Chart.

A further complication is that with small directive fields (<3000 gammas at the LOREX sites) the compass on the Aanderaa may have a declination error as large as 15° on some headings. This has been investigated by *Keenan* [1979] and his suggested calibration curve for a field of 3000 gammas was applied to the magnetic variations chosen as described above.

Some indication of the reliability of the Aanderaa instruments under these conditions can be obtained by comparisons between the fixed-mast readings and those of the profiling current meter at the 5-m level. Comparisons were possible on 38 occasions. The mean and maximum differences in temperature and salinity were $\Delta T < 0.02$ and $\Delta T = 0.04$°C, and $\Delta S = 0.09$ and 0.18‰. The mean speed difference, Δv, was 1 cm s^{-1} and the mean azimuth difference, $\Delta\phi$, 4°. This is encouraging but it should be noted that $\Delta v > 3$ cm s^{-1} occurred nine times while $\Delta\phi > 25°$ ten times.

The currents calculated as above were, of course, relative to the moving ice floe. Dave Wells of Bedford Institute of Oceanography supplied us with the navigational data for ICEMAN in the form of position and mean ice velocity on both an hourly and a 6-hourly basis. The latter velocity was subtracted vectorially from the observed velocity to give the true velocity relative to the earth's surface.

Errors. The two Aanderaa current meters were calibrated in January 1979 by the manufacturer and recalibrated in March 1981. The profiling meter (serial number 1911 with temperature sensor S/N 1227 and conductivity cell S/N 2871) had the same sensors in both calibrations: maximum temperature difference was 0.02°C and maximum salinity difference 0.01‰. The conductivity cell in the fixed-mast meter (S/N 114) developed a leak after LOREX and had to be replaced, but the same temperature sensor was tested in the two calibrations. The maximum temperature difference was 0.02°C. A 3-month stability test was made by Aanderaa on the type of conductivity cell used on LOREX: the maximum drift observed was 0.02‰.

The conductivity cells had a narrow range of 21–30 mmhos with a nominal accuracy of $\pm 0.1\%$ of range, i.e., ≈ 0.01 mhos, corresponding to an uncertainty in S of $\approx \pm 0.01$‰. The temperature sensors had a range of $-2.4°$ to $+21.48$°C with a nominal accuracy of ± 0.15°C. The pressure sensor on the "deep" instrument had a range of 0–3000 psi $\pm 1\%$ of range or ± 30 psi, corresponding to $\approx \pm 20$ m. In view of the discussion above of intercomparison tests of the meters and the results of the two calibrations it seems safe to conclude that salinity data given have a relative accuracy of about 0.02‰ with an absolute accuracy of better than 0.05‰ and that the corresponding figures for temperature are 0.02 and 0.15°C.

Nominal accuracy of current speeds was ± 1 cm s^{-1} with a starting speed of 2 cm s^{-1}. Observed speeds of 2 cm s^{-1} or less were disregarded. Nominal accuracy for current direction was quoted as $\pm 7.5°$ for speeds 2.5 cm s^{-1} and $\pm 5°$ for higher speeds. In the intercomparison tests of the two meters this accuracy was not achieved in one third of the tests. In calculating true azimuths there is also an unknown, possibly systematic, error in the magnetic variations used. It seems a reasonable estimate that true azimuths were correct to $\pm 15°$.

RESULTS

Figure 2 shows the water characteristics measured from a shallow station over the Ridge (on April 19). The water column was quite stable to a depth of about 300 m, and had only slight positive stability below that depth. In all, 40 similar T, S and σ_T profiles were plotted, the first few in shallower water but most over depths >3 km. All show similar stability patterns, with the density below 300 m increasing by about 0.01% per km of depth. The mixed layer of uniform temperature and salinity shows clearly in Figure 2. Another feature is the broad high-temperature layer centred at about 420 m, presumably the core of Atlantic water. Figure 3 shows the calculated true water velocity. Two features may be noted. There is a current speed maximum at about 380 m; below this the speed decreases in a fairly regular manner and the direction rotates very slowly in a clockwise direction.

Figures 4, 5 and 6, 7 show similar data for the casts on days 122 (May 2) and 126, respectively. Water depth was about 4.2 km in each case. The mixed layer is much less well defined, the maximum temperature peaks are quite sharp, and the clockwise rotation of current direction is slightly more pronounced on day 122 and much more so on day 126, compared with data from day 109. Currents in the top 100 m on day 122 were the largest (the speed scale on Figure 5 is compressed) and most erratic observed.

Data from all 40 profiles will be on file at the Marine Environmental Data Service, Ottawa.

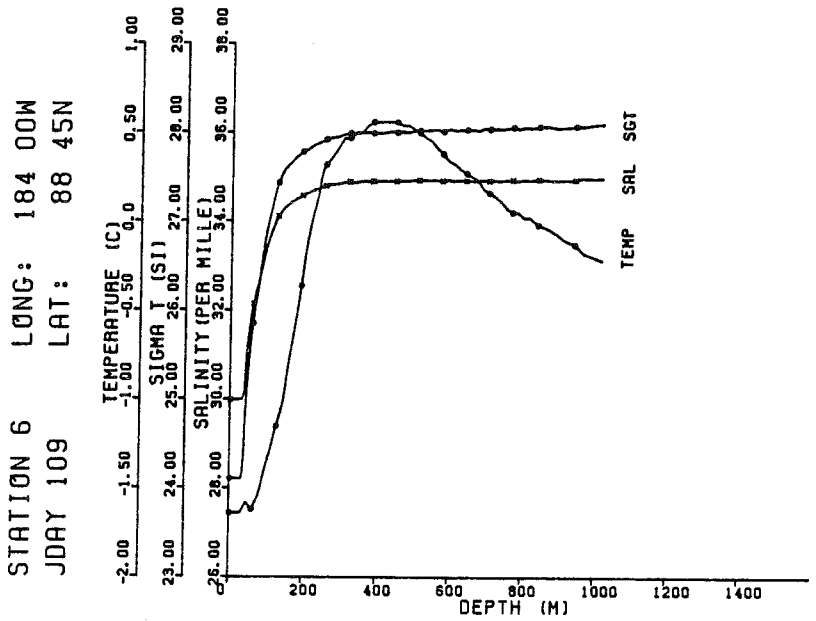

Fig. 2. Water characteristics over the ridge on April 19, 1979. Water depth was 1.01 km.

Mixed layer. For the first 8 days there was a well-defined mixed layer about 38 m thick, with mean values of $T = -1.62$°C and $S = 29.94$‰. From then on as the station drifted northward the definition of the layer became less clear. Small gradients of salinity (salinity increasing with depth) became more pronounced day-by-day and the bottom of the layer had to be identified from the thermocline. Eventually a small gradient of temperature (warming with depth) developed and after day 132 it was difficult to identify the layer. Between days 113 and 132 the mixed layer appeared to become thinner (to about 23 m), and both the salinity at the surface and at the bottom of the mixed layer decreased to 28.6‰ and 29.1‰, respectively. (Confirming evidence for the reduction in salinity will be discussed below.) There also appeared to be a slight warming trend (to −1.55°C on day 132). The observed changes in temperature and depth are smaller than the accuracy limits of the sensors but the regularity of the day-to-day observations lends some support to these tentative conclusions.

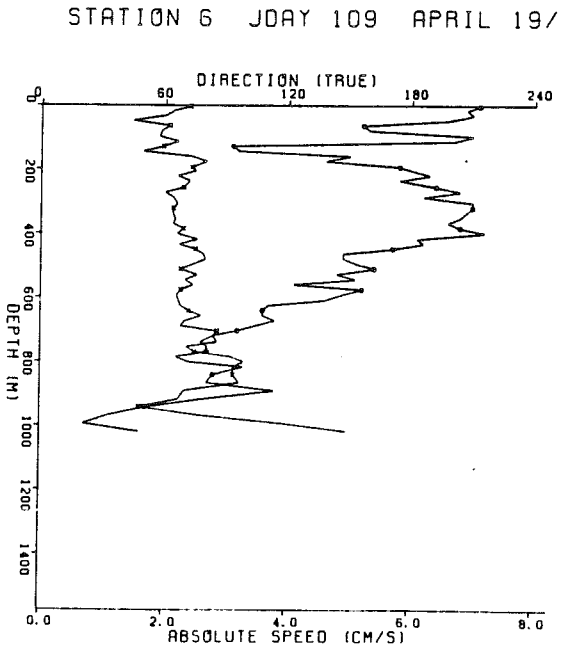

Fig. 3. True water speed and direction for the same profiling run as in Figure 2. Speed plot is marked with dots, direction plot with crosses, every fourth data point being marked.

The existence of such a sub-ice mixed layer is a characteristic feature of the Arctic Ocean in winter and "spring" months. During AIDJEX (Arctic Ice Dynamics Joint Experiment) in 1975–1976 the properties of the mixed layer were studied at three stations for a full calendar year [*Dixit*, 1978]. The principal cause of the formation and growth of the layer seems to be the rejection of brine on the freezing of salt water to ice. The heavier brine sinks, setting up a convective process between the lower ice surface and the upper layers of the pycnocline. On AIDJEX (at about 75°N) the mixed layer developed near the end of August and gradually increased in thickness (presumably by incorporating water from the pycnocline) until about the end of May. After this, with the melting and runoff of the surface snow and ice the mixed layer evolved into a more complex, stratified system.

The LOREX observations above do not fit this pattern. Melting cannot be invoked to explain the thinning, warming and lower salinity, and another explanation must be sought.

Atlantic water. If one identifies the depth of the temperature maximum as the core of the Atlantic water, this water mass showed maximum modification at the beginning of the drift and progressively less as the floe moved northward. Calling T_M the maximum temperature and d_M the corresponding depth, Figure 8 shows the variation in these parameters plotted along the approximate direction of advection of the Atlantic water. The current direction at d_M varied wildly, from 015° clockwise to 349° with an average azimuth of 139° (this

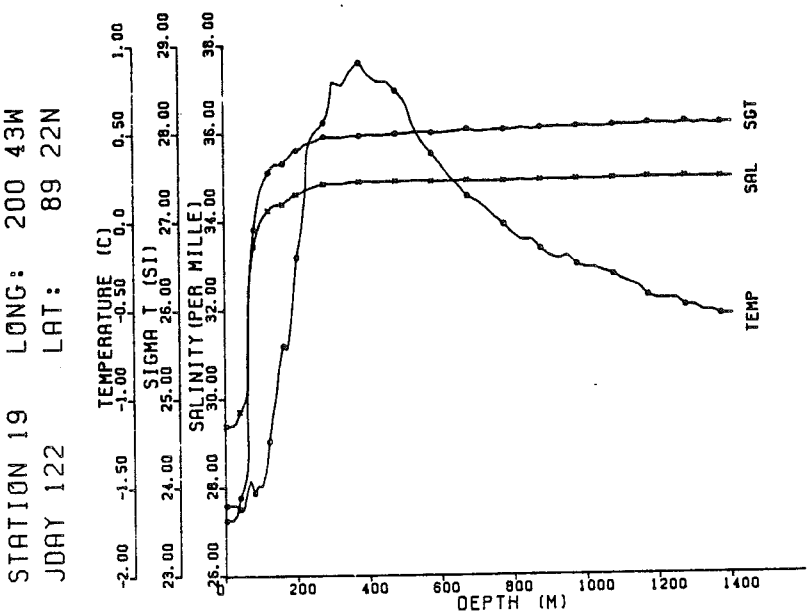

Fig. 4. *S*, *T*, *D* (salinity, temperature, density) plots for May 2, 1979. Water depth was 4.18 km.

average was not weighted for current speeds), indicating an average flow with a component toward the ridge.

Figure 8 shows that the major changes in T_M and d_M were observed between days 119 and 124. This will be shown later to be the period when the floe drifted across a "frontal zone" between two different water masses: a northern one, warmer and less saline (in the upper levels) than the water to the south. The graphs are consistent with the Atlantic water being forced to greater depths in the frontal zone, undergoing considerable cooling, by mixing with the colder, deeper water, in the process. This downward deflection must have been mechanical, when the Atlantic water impinged on the southern water mass; subsidance caused by cooling can not explain it because at these low temperatures density is almost totally controlled by salinity, and the σ_T and S curves show no maxima on any of the vertical profiles. Figure 8 shows no

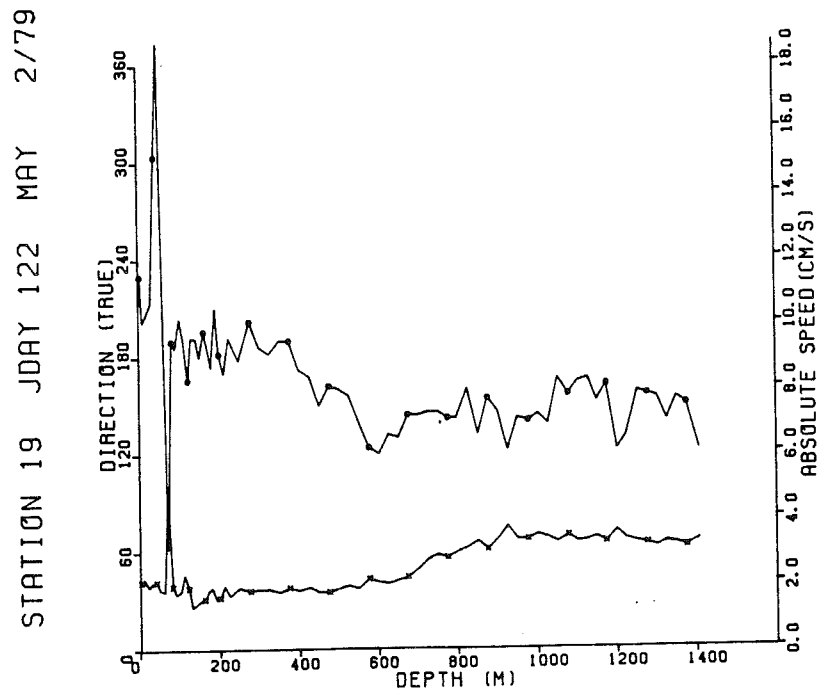

Fig. 5. True water speed and direction on May 2. Coding is as in Figure 3 but speed scale has been compressed.

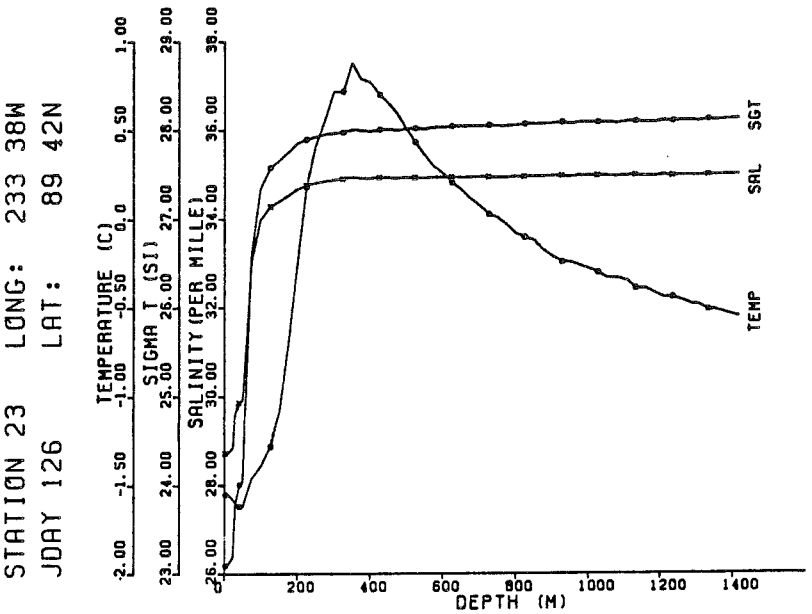

Fig. 6. *S*, *T*, *D* plots for May 6, 1979. Water depth was 3.19 km.

consistent trends in either T_M or d_M on either side of the frontal zone, but the profile curves of density show a gradual broadening in depth of the Atlantic "plume" as it advected southward. This presumably resulted from heat conduction to colder water above and below, and to mixing with the water below; mixing with the Arctic layer must have been at most slight because of the very sharp pycnocline.

Mast data. Figure 9 shows the results obtained from the meter attached to the fixed mast at 5 m below the ice. Parts of the second curve from the top (true water speed) show a noticeable periodicity of about 12 hours which is the inertial period at these very high latitudes, and also the approximate period of the M2 and S2 tidal components. The same curve shows maximum speeds (with the exception of a single peak on day 135) during the interval from day 121 to day 128 (May 1–8). The lowest curve shows that the surface salinity dropped sharply from about 30‰ to just under 29‰ in the interval May 1 to 5.

This behavior was investigated further by taking from the daily profiles the salinities at 25, 50, 100, 125, 200 and 400 m.

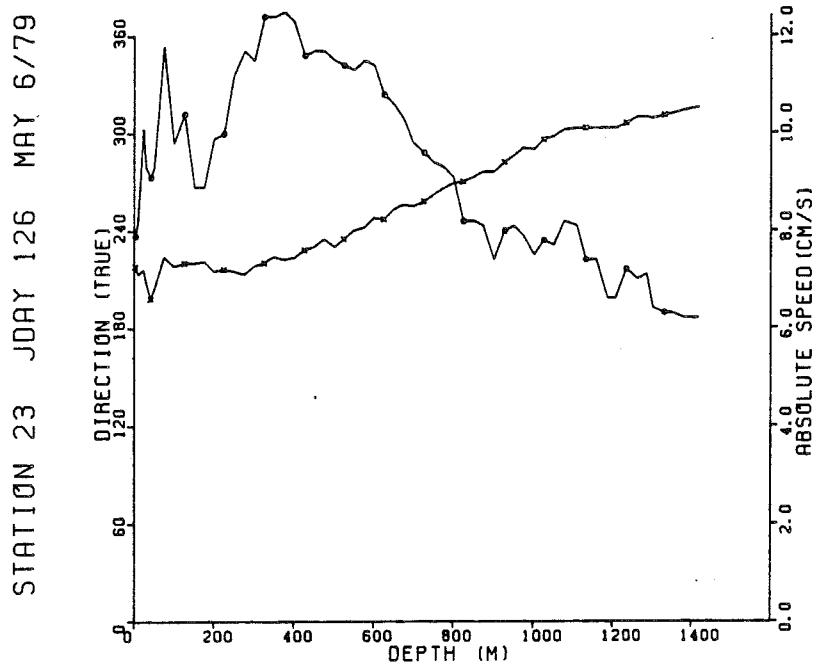

Fig. 7. True water speed and direction on May 6. Coding is as in Figure 3.

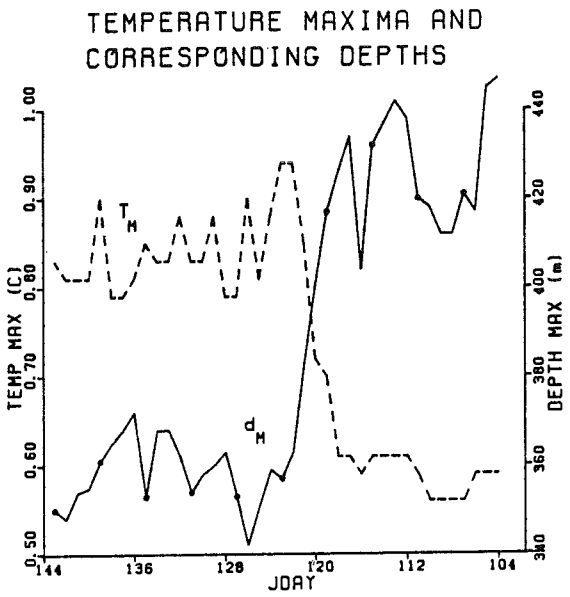

Fig. 8. Time plots of temperature maxima (dashed line) and corresponding depths (solid line).

Figure 10 shows plots of salinity vs time for the first three of these depths as well as for 5 m, taking the data from Figure 9 for the latter. It is seen that the 5-m and 25-m plots are virtually identical between days 104 and 125. After this date the 25-m plot shows a slight increase in salinity rising to 29.5‰ by day 143. There is also a hint of this behavior in the salinity curve of Figure 9. The 50-m plot has higher salinities throughout but shows a similar sharp drop about day 121 from an average salinity of 31.2‰ to a new, fairly steady value of 29.9‰. A similar but reverse change occurs on the 100-m plot at the same time with an increase from 33.4‰ to 34.0‰. The 125-m plot (not shown) resembles that at 100 m with a similar but smaller increase from 34.1 to 34.3‰. The deeper plots at 200 m and 400 m show almost uniform salinities of 34.6‰ and 34.9‰, respectively, with small decreases ($\approx$0.1‰) at 200 m between days 119 and 121 and at 400 m between days 115 and 121. These decreases are real, being an order of magnitude greater than the resolution of the salinity sensor, but their relation to the characteristics of the water mass at lesser depths is not known.

Oceanographic front. It seems clear that between days 121 (May 1) and 126 the floe drifted across an oceanographic front into a significantly different water mass. Oceanographic fronts, like their atmospheric counterparts, are boundaries where some property of the medium (in this case, surface salinity) changes very rapidly, almost discontinuously. They are discussed in many texts [e.g., *Defant*, 1961; *Neumann and Pierson*, 1966; *von Arx*, 1962]. Fronts, typically, are rather shallow with slopes of order 10^{-3}.

In a single-pass experiment such as this it is difficult to obtain much information about the extent of this new water mass. If we assume that the floe was leaving this mass on day 142 (May 22), as suggested by the slight increase in near-surface salinity at that time, we can obtain the length of one transect of the mass as measured from the floe. The great circle distance between the floe positions on May 2 and May 22 was about 90 km, but the actual length of the transect in the water mass was considerably greater since the water was moving more or less southward at a rate of a few kilometers per day and the floe was drifting to the northwest at about 4.5 km/day.

Vector plots of velocity vs time were made for 16 depths: 5 m, every 10 m from 10 to 100 m, 125 m, and every 200 m from 200 to 800 m. There is a great deal of scatter in velocity on each plot, probably because the data are limited to a single value per day at each depth. The rate of descent of the probe was about 175 m/hr so that the observations at 400 m were made about 2 hours later each day than the surface ones. This does not appear to be a serious limitation since there was some degree of coherence, most marked in the frontal zone, in velocity vs depth in the top 400 m. It was observable in both water masses. Table 1 lists the velocities at various depths for selected days. On day 112 the floe was over the southern (more saline) mass, on day 136 over the northern one and days 122 and 126 bracket the passage through the frontal zone.

Figure 11 shows the velocity plots for depths of 20 and 125 m, which are reasonably typical of the top 400 m. Below this depth the coherence during the critical period, days 122 to 126, is not in evidence and the currents can best be described as random. This would suggest that the depth of the northern water mass was at least 400 m since marked velocity changes persisted to that depth, although salinity variations largely disappeared below 125 m.

The most striking feature of Figure 11 is the almost exactly 180° change in current direction between days 122 and 126. This feature appears on all but one of the other 11 velocity plots between 10 and 400 m. This is further evidence of the front-like character of the observed transition. The same figure shows that within the frontal zone the current direction rotated in a clockwise direction on successive days but at an irregular rate. Similar behavior is seen on the other velocity plots. The fact that the frontal zone seems to be bounded by days 121, 126 at all depths to 400 m indicates that the front was close to vertical. From Table 1 the average current direction on day 122 (omitting the 5-m reading and the apparently anomalous one at 70 m) is 037°. The average direction (10–400 m) on day 126 is 215°, or 178° greater, so that the horizontal direction of the front was about 035–215°, assuming it to be parallel to the flow on either side.

Figure 12 is an approximate isopycnal chart of the upper 140 m of water for 9 days including frontal passage. The approximation lies in plotting density against distance along a mean straight-line track. The floe actually drifted along a vaguely sinusoidal path. A straight line was drawn from the position on day 119 to approximate a mean track (bearing 340°) up to day 127. Table 2 lists the daily distances along this mean track. The maximum distance between the actual path and this mean track was 11 km, the average being about 4.5 km. Figures 10 and 12 naturally show many similarities, since density is almost exclusively dependent on salinity at these low temperatures.

Analysis of the behavior at the frontal "discontinuity" is complicated. Both the southern and, to a lesser degree, the northern water masses were sharply stratified two-layer systems, each of which must have given rise to a very sharp, nearly horizontal density gradient, and marked changes in current direction. This probably explains the erratic variations in current directions and speeds where the two masses impinged. If we treat the two water masses as a simple two-layer system we can use Figure 12 to check if the near-surface flow was approximately geostrophic. The isopycnals had a fairly regular slope from 10 to 30 m on days 121–125 with an

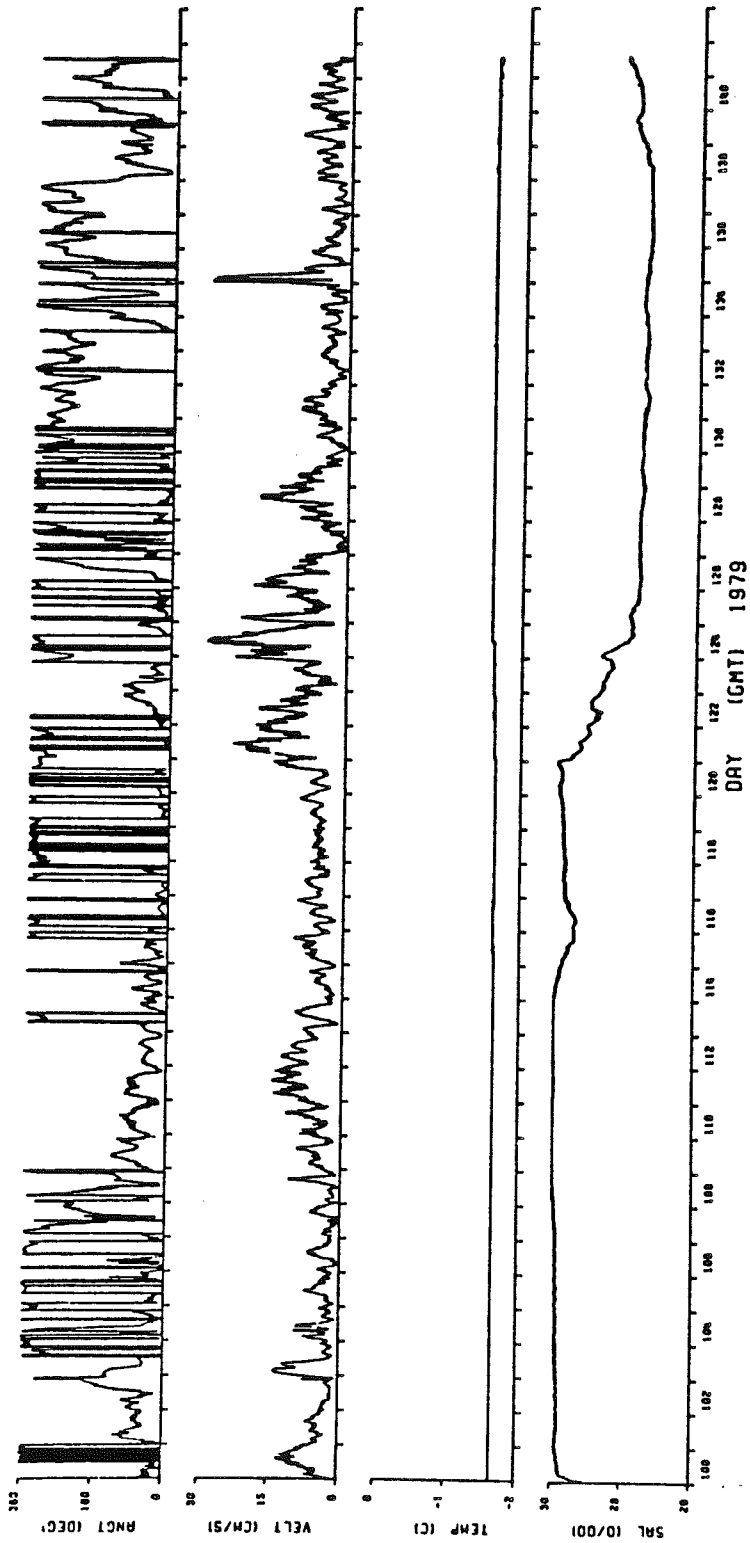

Fig. 9. Data from the mast-mounted meter at 5 m below the lower ice surface. The curves are, from the top, true water direction, true speed, temperature and salinity. Note the sharp drop in surface salinity from 30‰ to 29‰ during days 121–125 (May 1–5).

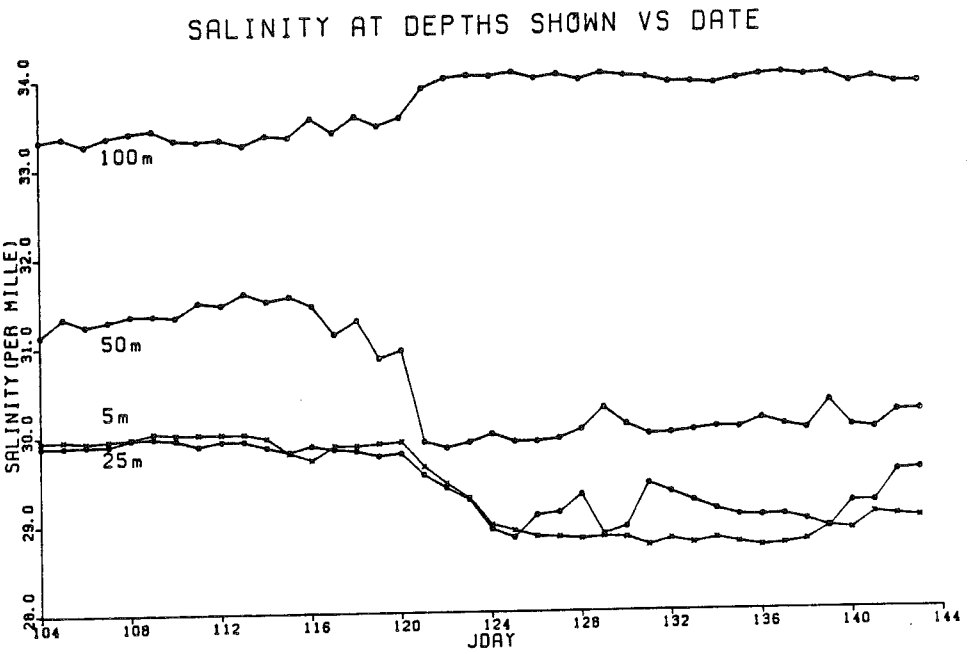

Fig. 10. Salinity vs time at various depths.

average value of $\tan \gamma' = -2.1 \times 10^{-3}$ for the three lowest densities, as measured along the mean track (340°). We need the slope $\tan \gamma$ along the front (035°). If p is the pressure and **s**, **n** unit vectors along the track and the horizontal projection of the front

$$\frac{\partial p}{\partial n} = \frac{\partial p}{\partial s}\frac{ds}{dn} = \frac{\partial p}{\partial s}\Big/\cos(\mathbf{n}, \mathbf{s}) = \frac{\partial p}{\partial s}\Big/\cos 55^\circ = 1.74\,\frac{\partial p}{\partial s}$$
$$\tan \gamma = 1.74 \tan \gamma' = -3.66 \times 10^{-3} \quad (1)$$

The standard equation for straight-line geostrophic flow is

$$\frac{1}{\rho}\frac{\partial p}{\partial n} = fc \quad (2)$$

where ρ is the density, f the Coriolis parameter, and c the velocity normal to the pressure gradient, i.e., along **n**. Let the subscripts 1 and 2 refer to the less dense (northern) water mass and the more dense one, respectively. Choosing a coordinate system so that y is along **n** and z is positive upward, $c = v_2$ and

$$\frac{1}{\rho}\frac{\Delta p}{\Delta n} = \frac{(\rho_2 - \rho_1)}{\rho} g \frac{\Delta z}{\Delta n} = g' \tan \gamma = f v_2 \quad (3)$$

where g', the reduced gravity $= (1023.64 - 1023.13)/1023 \times 9.81 = 4.89 \times 10^{-3}$ and $f = 1.46 \times 10^{-4}$ rad s^{-1} (the polar value). Solving equation (3),

$$v_2 = 4.89 \times 10^{-3} \times (-3.66 \times 10^{-3})/(1.46 \times 10^{-4})$$
$$= -0.12 \text{ m s}^{-1}$$

The observed mean value of v_2 over the range 10–30 m on day 126 was -10.2×10^{-2} m s^{-1}, so the agreement is close

TABLE 1. Water Velocity Versus Depth on Selected Days

Depth, m	Day 112		Day 122		Day 126		Day 136	
	S_p	D	S_p	D	S_p	D	S_p	D
5	6.6	0.45	14.4	048	8.7	192	3.0	307
10	7.0	051	10.0	045	8.8	210	1.6	084
20	5.1	052	10.5	039	12.4	213	4.4	121
30	5.0	027	10.7	041	9.3	208	4.7	118
40	2.8	040	15.6	040	9.2	200	4.8	123
50	4.2	012	18.7	037	9.3	204	3.9	115
60	3.2	020	13.0	034	8.8	218	4.3	085
70	0.6	020	3.1	101	10.3	223	2.2	062
80	1.4	339	10.0	040	9.0	222	5.2	233
90	2.6	012	9.3	034	10.7	211	2.4	315
100	1.6	037	10.7	035	9.8	220	0.2	075
125	2.0	061	8.6	035	10.3	220	2.2	079
200	3.0	160	9.1	032	9.9	215	3.2	295
400	3.1	109	8.9	035	12.3	224	0.8	134

S_p is speed in cm s^{-1}
D is direction in degrees east of true north.

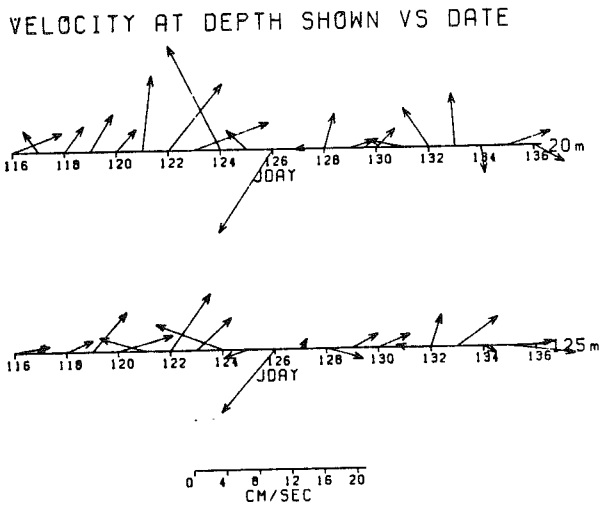

Fig. 11. True water velocity vs time at depths of 20 m, 125 m. The top of the page is the direction of true north.

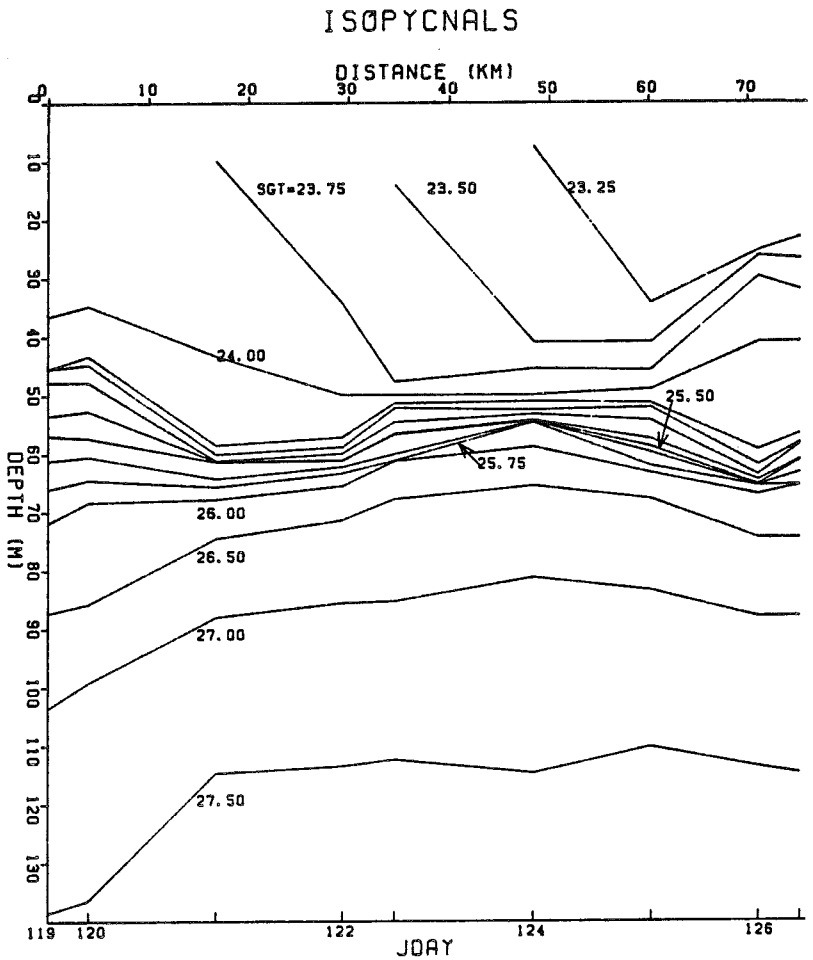

Fig. 12. Approximate isopycnal chart.

enough to say that the flow was approximately geostrophic. The Margules equation [*Neumann and Pierson*, 1966] is

$$\tan \gamma = -\frac{f(\rho_1 v_1 - \rho_2 v_2)}{g(\rho_1 - \rho_2)} \tag{4}$$

Over the same vertical range, on day 122 $\bar{v}_1 = 10.4 \times 10^{-2}$ m s^{-1} and equation (4) gives $\tan \gamma = -6.2 \times 10^{-3}$, the right order of magnitude, at least, compared with the observed value of equation (1).

Below 30 m, Figure 12 gives few clues to the slope of the front, other than the general conclusion that it must be greater since the density difference between the two masses decreases.

TABLE 2. Distances in Kilometers Along Mean Track

J Day	Distance
119	0
120	4.0
121	16.8
122	29.5
123	34.7
124	48.5
125	60.4
126	71.2
127	75.4

On the basis of the velocity plots as a function of depth, it was claimed earlier that the slope was close to the vertical. If this was indeed true the instruments used in calculating density were not accurate enough to verify it. The maximum accuracy of the salinity differences calculated was at best 0.02‰, corresponding to a $\Delta\rho \approx 1 \times 10^{-6}$ kg m^{-3}. From equation (4) this difference would give $\tan \gamma \approx -0.3$, $\gamma \approx -17°$.

Returning to the problem of the thinning of the mixed layer with distance along the track, it seems likely that this is, in part at least, another effect of the frontal system. The decrease in salinity in the upper layers has been discussed, and convergence in the frontal zone must have produced descending currents and turbulence. Figure 8 suggests a descending current of Atlantic water, from 360 to 420 m in about 4 days or about 0.02 cm/s downward motion. To investigate more quantitatively convergence in the upper layers, 5-day averages of current were calculated for the periods of days 116–120 and 126–130, i.e., before and after passage through the frontal zone. The calculations at the 5-m level showed no significant difference in the two periods, but when the averages were extended to cover the 10- to 100-m range the results were 7.3 cm/s toward 044° in the earlier period and 1.8 at 160° in the latter. At least the first of these averages is well above the experimental uncertainty in current values. If the frontal azimuth is taken as 035°, these results together show a net, horizontal convergent current of ≈ 3 cm s^{-1} toward the front.

The gradual thinning between days 113 and 121, if indeed it is not an artifact resulting from inaccuracies in the depth sensor, remains unexplained.

This isolated, (presumably) small, and less saline water mass was not a unique event. On the Fram I expedition taking place at the same time some 250 km off the northeast coast of Greenland, *Hunkins and Manley* [1980] noted a change $\Delta S = 1.0‰$ as the floe drifted across a frontal zone 10 km wide.

Water transport. A ballpark estimate of the water transport for station 6 (Figure 3), transverse and parallel to the Ridge, was made as follows. Smooth curves of speed and direction were drawn on Figure 3 and estimated mean values read for 50-m intervals. The Ridge at the crossing track bore about 63°W of N. Currents were resolved parallel and perpendicular to this direction. The mean velocity of the water over the depth of the ridge (1017 m) had components of 3.2 cm s^{-1} transverse to the ridge in a northeasterly direction and 3.1 cm s^{-1} parallel to the ridge to the southeast. These correspond to a transverse flow of about 30 m^3 s^{-1} per meter of horizontal length and a parallel flow of about the same size per meter of width (perpendicular to the ridge).

There are at least two serious flaws in this method: the more serious is the tacit but unrealistic assumption that the situation is static with currents constant at each level throughout the 5.6 hours of the cast; the other is the uncertainty about the true azimuths of the currents. Taking the results at face value, the transverse flow is from SW to NE, i.e., from the Canada Basin across to the Eurasian side. Since the net flow of Atlantic water must be into the Canada Basin (the TS diagrams of Beaufort Sea water show that most of it is of Atlantic origin), the 40 profiles were examined from the point of view of average azimuth over the depth of the station. It appears that 18 of them have a component velocity SW to NE (as at station 6), 13 have a component NE to SW, and the remaining 9 have either currents too weak to be significant or too mixed in current direction to draw conclusions. This suggests a picture of water sloshing back and forth across the shallow part of the ridge with the main transport of water to the Canada Basin occurring across deeper portions of the Ridge.

In another LOREX program *Aagaard* [1981] bottom-moored two current meters on the slope of the Ridge at 89°11'N, 141°31'W. At this location the crest of the ridge was at about 1400 m below sea level and its axis was almost east-west. Water depth at the site was 1440 m and the current meters were at 1240 and 1415 m. Vector averaging over the observation period of about 40 days gave the current at the lower meter as 2.7 cm s^{-1} toward 105° and at the upper meter as 2.1 to 122°. Averaging these two figures gives an approximate component to the south as 0.9 cm s^{-1}. The observed currents varied considerably and Aagaard concluded that flow over the Ridge into the Canada Basin occurred in pulses of a few days duration.

SUMMARY

The results of this experiment are quite consistent with the accepted view of the Eurasia Basin of the Arctic Ocean being a two-layer system. Numerical values of salinity and temperature are in good agreement with earlier results on near-surface waters of the Canada Basin. The principal point of interest is the discovery of a frontal zone, which the floe drifted over at about the midpoint (in time) of the observation period, and which resulted in rapid changes in most of the parameters studied. A number of questions remain unanswered, such as the apparent discrepancy between salinity and current data on the depth of the northern water mass. Another odd feature is that in this mass the salinities down to 60 m were smaller than in the southern water mass but then reversed this situation down to about 200 m.

Acknowledgments. This work was supported by the Polar Continental Shelf Project of the Department of Energy, Mines and Resources under DSS Contract OST78-00208. We are grateful to PCSP (G. D. Hobson) and the LOREX 79 organization (J. R. Weber) for financial and logistic support. P. Stalinski and P. Peltola carried out the field measurements and the latter carried out a major part of the data analysis. Thanks to Barry Allen for the astronomical data and for general assistance on ICEMAN, and to Dave Wells for the navigational data. Grant Ingram of the Institute of Oceanography contributed greatly to the data analysis and also helped with a critical review of this paper. Some of the computation was done by F. Diaz and F. Lim. Additional financial assistance was received from the Natural Sciences and Engineering Research Council under Grant A2669. Finally, I am grateful to reviewers whose pertinent comments have led, I am sure, to greater clarity in this paper. This is LOREX contribution 4.

REFERENCES

Aagaard, K., On the deep circulation in the Arctic Ocean, *Deep Sea Res., 28A*, 251–268, 1981.

Coachman, L. K., and K. Aagaard, Physical oceanography of Arctic and Subarctic Seas, in *Marine Geology and Oceanography of the Arctic Seas*, edited by Y. Herman, pp. 1–72, Springer-Verlag, New York, 1974.

Defant, A., *Physical Oceanography*, vol. 1, pp. 451–469, Pergamon, New York, 1961.

Dixit, B., Some mesoscale flow features in the Beaufort Sea during AIDJEX 75–76, Ph.D. thesis, pp. 180–192, McGill Univ., Montreal, 1978.

Hunkins, K. L., and T. O. Manley, Oceanographic measurements at the Fram I ice station (abstract), *Eos Trans. AGU, 61*, 278, 1980.

Johannessen, O., Note on some vertical profiles below ice floes in the Gulf of St. Lawrence and near the north pole, *J. Geophys. Res., 75*, 2857–2862, 1970.

Keenan, P. V., Sources of compass error within the Aanderaa recording current meter: revised 1979, *Rep. BI-R-79-6*, Bedford Inst. of Oceanogr., Dartmouth, N. S., 1979.

Neumann, G., and W. J. Pierson, Jr., *Principles of Physical Oceanography*, pp. 160–166, Prentice-Hall, New York, 1966.

von Arx, W. S., *Introduction to Physical Oceanography*, pp. 97–98, Addison-Wesley, Reading, Mass., 1962.

Weber, J. R., The Lomonosov Ridge experiment: "LOREX 79," *Eos Trans. AGU, 60*, 715–720, 1979.

E. R. Pounder, Institute of Oceanography, McGill University, Montreal, Quebec H3A 2T8, Canada.

(Received March 11, 1986;
accepted July 3, 1986.)

Geochimica et Cosmochimica Acta Vol. 45, pp. 2475 to 2482, 1981
Printed in Great Britain.

0016-7037/81/122475-08$02.00/0

Oceanographic distributions of zinc, cadmium, copper and aluminium in waters of the central Arctic*

R. M. MOORE
Department of Oceanography, Dalhousie University, Halifax, Nova Scotia, Canada B3H 4J1

(*Received* 11 *February* 1981; *accepted in revised form* 18 *August* 1981)

Abstract—Vertical profiles are presented of dissolved cadmium, zinc, copper and aluminium at the LOREX 79 site in the central Arctic Ocean. Cd, Zn and Cu show unusually high surface concentrations of 0.3, 3 and 5 nmol l^{-1} respectively; these levels are related to contributions from surface run-off and from the underlying nutrient-rich Bering Sea winter water. Al has lower surface concentrations than observed elsewhere and shows no correlation with the nutrients; the importance of aeolian supply is questioned and the results point to a major role for inorganic removal of Al at least in the Arctic Ocean.

INTRODUCTION

THE DIFFICULTIES of doing oceanographic work in the Arctic Ocean are such as to have limited investigations to quantities such as salinity and temperature and, to a lesser extent, those that are of value in ascertaining the source and history of water masses such as the nutrients and oxygen. There are, however, ways in which what is already known of certain peculiarities of the Arctic Ocean may be used to refine our knowledge of marine geochemistry as currently understood from studies of the other oceans. For instance, on account of the long Arctic night primary productivity must fall to zero over much of the ocean for up to half of the year, and this may be expected to modify the transport of nutrients and other trace elements from the surface to deeper waters. For those elements (e.g. Cu) whose speciation is affected by biological processes it is likely that this influence will be less than observed in the more productive lower latitude waters and also will vary more with the seasons. A number of trace elements (e.g. Cd, Ba and Zn) have been shown to have oceanic distributions very similar to those of the nutrients, phosphate and silicate, suggesting simultaneous incorporation of the elements into the tissue or skeletal material of the plankton and their subsequent release together in intermediate or deep waters (BOYLE *et al.*, 1976; BRULAND *et al.*, 1978a, b; BRULAND, 1980; CHAN *et al.*, 1977). While the importance of biological processes in the cycling of some trace elements is now well established, it is not known to what extent inorganic processes operate simultaneously nor is it known to what concentrations the trace metals can accumulate in a biologically inactive system before inorganic processes produce a steady state, though a study of the elements in the deep ocean can provide insight into this question as has been shown in the case of copper (BOYLE *et al.*, 1977). These are questions which detailed studies of Arctic Ocean chemistry should help to resolve. Of particular interest in this respect is the well-defined layer of nutrient-rich water fed by northward flow from the Pacific through the shallow Bering Strait, which is spread over much of the Arctic Ocean centred at a depth somewhere between 100 and 200 m depending on locality. It is below the euphotic zone so that the trace element composition is not affected by biological uptake, but can be influenced by respiration and by inorganic processes.

Atmospheric contributions of a number of trace metals to the Arctic Ocean are likely to be less than to the Atlantic; this is deduced from the lower atmospheric load of the metals Al and Cd in the Arctic atmosphere and from the lower deposition velocity applying in the Arctic (DUCE *et al.*, 1976; Rahn, 1980). Furthermore, if the residence time in the ocean surface layer of the atmospherically derived element is extremely short, of the order of months, the oceanic distribution at shallow depths would show a seasonal effect due to the winter ice coverage followed by ablation of the ice surface during the summer.

During the Lomonosov Ridge Experiment water samples were collected at stations north of 88°40′ for analysis of the trace metals: Zn, Cd, Cu and Al. The results are compared with data from other oceanic regions and are related to some of the characteristic features of the Arctic Ocean.

SAMPLING AND STORAGE

The locations of sampling stations are given by MOORE and LOWINGS (in preparation). The conditions under which the water samples were collected from the drift station were very much cleaner than those normally prevailing in ships, with little dust in the environment and relatively few metal surfaces exposed. Water samples for trace metal analysis were collected in 5 l. Go-flo bottles which were coated internally with Teflon and had metal parts coated with a plastic film. The bottles, which were suspended from new stainless steel cable, were washed with sea water before use. As they were low in particulate matter, the samples were not filtered and were stored in acid-washed

* LOREX Contribution No. 6.

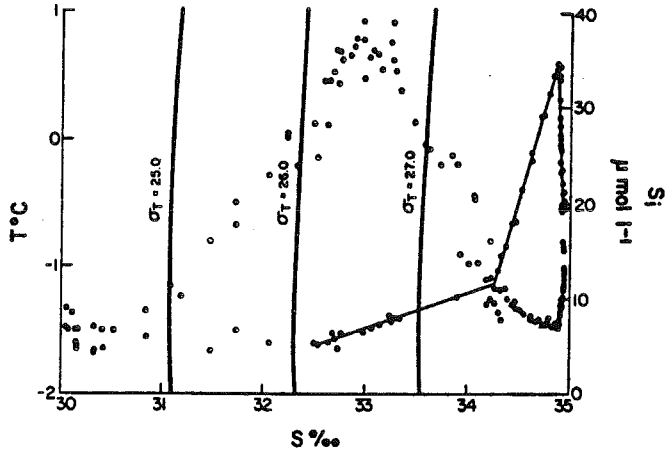

Fig. 1. Temperature–salinity relationship (filled circles) and silicate–salinity relationship (open circles) at the LOREX site.

polyethylene bottles and frozen immediately after collection. Before analysis, samples were thawed and acidified with Ultrex hydrochloric acid (12 M, 2 ml l^{-1}) in order to release metal adsorbed on the container walls during freezing and thawing. Samples used for Al analysis were not acidified but were used immediately after thawing.

ANALYTICAL METHODS

The method used for analysis of Zn, Cd and Cu was essentially that described by BRULAND *et al.* (1979). Modifications introduced had the object of reducing the blank, as obtained in this laboratory, to acceptable levels. This was done by reducing the quantity of acid necessary for destroying the organic matter and by cutting down the number of steps in the procedure.

After two chloroform extractions of the sample and chelating agents, the extracts in 7.5 ml quartz tubes were evaporated to dryness in a water bath. Ultrex hydrogen peroxide solution (0.1 ml, 30%) was added to the residue. After *ca.* 15 min, hydrochloric acid (1 ml, 0.1 M) was added to the tubes which were then covered, weighed and positioned 5 cm from an air-cooled 1000 W Hanovia medium pressure mercury discharge lamp with which they were irradiated for two ten-minute periods. Between the irradiations the tubes were removed and shaken. After irradiation the tubes were reweighed to ensure that there had been no significant evaporation during this procedure and the volumes were made up to 2.1 ml with 0.1 N HCl; the blank was left at 1.1 ml to facilitate measurement of the very low metal concentrations. This procedure gave average blanks for Cd, Zn and Cu of 0.006, 0.1 and 0.2 nmol l^{-1} respectively; such low values show that contamination was not a problem during analysis. The metals were determined by atomic absorption spectrophotometry using a Perkin–Elmer 403 spectrophotometer fitted with a Perkin–Elmer graphite furnace (HGA 2200).

The method used for measuring Al in seawater was essentially that described by HYDES and LISS (1976), the chief modification being the reduction of sample volume from 100 to 10 ml. The procedure gave a blank of 3 nmol l^{-1}.

SUMMARY OF HYDROGRAPHIC FEATURES

The following is intended as a brief description of those hydrographic features of the central Arctic Ocean that are pertinent to an understanding of the trace metal distributions; details of the hydrography will be presented elsewhere. Salinity, temperature, density and silicate data are summarized in Fig. 1.

Between the surface and about 50 m the water column is well mixed and has a salinity of *ca.* 30‰ and a potential temperature of −1.7°C. This layer is maintained at a low salinity by surface runoff and melt water; stable oxygen isotope measurements (MOORE and TAN, unpublished data) show the former to be of major importance.

Beneath the mixed layer salinity increases rapidly reaching 34‰ at about 150 m. In the halocline appears a thin layer of water, centered at around 110 m (σ_T, 26.5), with high nutrient concentrations: reactive silicate reaches 39 μmol l^{-1} and phosphate 1.9 μmol l^{-1}. This is identified as water that flows north through the shallow Bering Strait during winter and then spreads out as a thin subsurface layer extending over much of the Arctic Ocean.

A prominent feature on the *T–S* diagram is the temperature maximum at 400–500 m that marks the core of Atlantic water which enters the Arctic Ocean through Fram Strait. As seen from Fig. 1, silicate concentrations decrease until the core of this layer is reached and thereafter show a gradual increase with depth. The Arctic Bottom Water is defined arbitrarily as lying beneath the 0°C potential temperature surface; its relatively low nutrient concentrations may be accounted for by the low productivity of the overlying waters, by a short residence time, or by a combination of these factors.

RESULTS AND DISCUSSION

Cadmium

In spite of its extremely low oceanic concentrations, Cd is now one of the most thoroughly studied trace metals in marine environments (BOYLE *et al.*, 1976; BRULAND *et al.*, 1978a; BRULAND, 1980). The results of

Table 1

Trace metal and silicate concentrations at the LOREX 79 site.

Sample number	Depth m	Zn nmol ℓ^{-1}	Cd nmol ℓ^{-1}	Cu nmol ℓ^{-1}	Si μmol ℓ^{-1}
96	10	2.9, 3.5	.24, .32, .33	4.7, 4.7	6.6
98	20	2.3	.33	5.0	--
100	30	2.6, 3.2, 3.4	.28, .29, .34	4.2, 5.4	6.6
104	50	2.4	.33	4.7	11.2
106	60	2.6	.43, .32	5.2, 4.9	20.0
111	80	4.1	.37	5.4	28.2
113	90	4.9, 5.4, 5.5	.56, .61	4.1, 4.6, 4.7	36.4
115	100	6.1, 5.5	.53, .60	3.5, 3.9	35.0
122	135	3.4	.32	2.5	13.8
141	170	2.9, 3.5, 3.8	.20, .24, .30	3.1, 3.6	10.0
143	190	--	--	2.0	9.0
145	225	4.6, 3.5, 4.4	.20, .20, .21	2.8, 2.5	8.2
148	300	2.6, 1.7, 1.8	.20, .20	1.6, 2.0	8.0
150	350	2.3, 3.2, 2.9	.16, .17, .18	2.7, 2.2	7.1
152	400	3.5, 2.8	.19, .18	2.0, 1.9	7.5
159	475	2.3, 2.4, 2.6, 2.8	.15, .17, .18, .18	--	7.8
43	525	3.4, 3.7, 3.7	.26, .28, .22	2.0, 2.0, 3.0	7.0
161	550	3.4, 3.1	.15, .18	3.6, 4.1	7.5
47	625	--	.19	2.5	7.0
163	650	2.6, 2.3, 2.1	.13, .14, .18	2.0, 2.2, 2.8	7.6
50	725	3.2, 2.7	.20	3.9, 4.2	7.0
52	775	2.3, 2.6, 2.6	.20, .20, .20	3.9, 3.8, 3.9	7.1
166	800	1.5, 2.0, 2.0, 2.4	.19, .14, .18	4.4, 4.9, 4.7	7.7
54	825	2.4, 2.9	.15, .17	1.7, 2.4	7.5
168	900	1.7, 1.7, 2.3	.18	--	7.6
57	950	2.6	.20	1.7	7.6
170	1000	2.0, 1.2	.17, .17	0.8, 1.4	--
59	1050	2.6, 2.9, 2.9, 2.9	.20	4.1, 4.2, 3.8 4.9, 4.9	7.8
61	1150	4.0, 4.1	.17, .19	2.2, 2.5	8.3
173	1150	3.2, 2.8	.17, .19	2.7	8.8
175	1250	--	.16, .17, .20	--	9.4
65	1300	1.7, 2.0, 2.1	.16	4.2	9.3
67	1400	1.5	.18	1.4	9.9
69	1500	1.6	.16	2.0	10.5
72	1625	2.4, 3.1	.21	3.5, 3.3	11.1
74	1700	2.3	.15	1.7	11.7
76	1900	4.1, 4.1	.18	1.9, 2.0	12.1
79	2200	1.7, 1.7	.19, .19	5.5, 5.9	12.7
81	2400	3.1, 3.7	.18, .20	6.5, 8.7, 8.8	13.0
83	2600	3.7, 3.8, 4.1	.15, .20	4.9, 6.1, 6.1	13.0

this study given in Table 1 and Fig. 2 are compared with the distribution of the element in temperate ocean waters.

The surface concentration 0.3 nmol l^{-1} of the metal is high compared with the other oceans and immediately below the mixed layer the concentration increases to a maximum of 0.6 nmol l^{-1} at 90 m, the depth corresponding to the nutrient maximum. Beneath the maximum the concentration drops to around 0.2 nmol l^{-1} and shows little further variation with depth.

Cadmium has a depth distribution closely resembling that of both phosphate and silicate. The similarity of Cd and silicate profiles is chiefly the result of advection of the thin layer of water containing high concentrations of both elements from the Bering Sea into the Arctic waters, which are much lower in nutrients and cadmium, and have little depth variation in either quantity. The same argument may be applied to the Cd and phosphate profiles, though in this case the similarity has a more fundamental explanation in the tendency for these two elements to be cycled in unison (Boyle *et al.* 1976; Bruland *et al.*, 1978a; Bruland, 1980; Knauer and Martin, 1981), which accounts for why the components of the water column, e.g. Pacific and Atlantic waters, have their respective high and low phosphate and Cd values. The different water layers should tend to retain their original composition, at least for the components mentioned, because biological transport between the layers is low and the part of the water column between 50 and 250 m has strong density gradients that will inhibit mixing between the layers. With water masses originating in both North Atlantic and North Pacific as well as a surface water type with a marked freshwater component, it might be expected that the Arctic Ocean would not exhibit the excellent correlation shown between trace metals and nutrients that have been found for other oceanic regimes. This is particularly so since the vertical transport of these

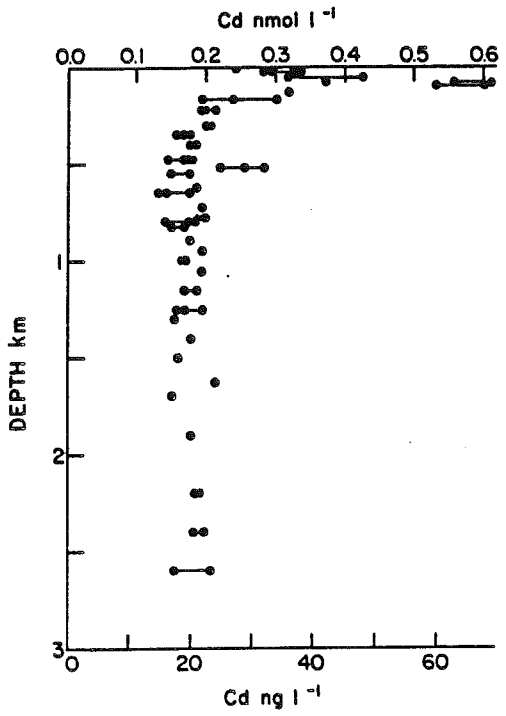

Fig. 2. Dissolved cadmium vs depth at LOREX station.

components in organic debris is much reduced in comparison with other oceanic regimes as indicated by the high surface nutrient levels which are clearly not being replenished by local active upwelling.

There is a question of to what extent the surface Cd concentrations are the result of surface runoff and to what extent they are a result of supply from the underlying waters. Similar questions also apply to the trace metals, Zn and Cu.

The supply of freshwater from surface runoff to the Arctic Ocean has been estimated (*SCOR*, 1979), it is equivalent to *ca.* 0.3 m yr^{-1}; this makes some contribution to the low salinity of the surface mixed layer. It is not possible to attribute the observed estuary-like salinity structure entirely to surface runoff since similar salinity characteristics may in principle result from the processes of ice formation and melting alone. Stable oxygen isotope data (VETSHTEYN *et al.*, 1974) do, however, distinguish between meteoric water and melt water and show the important contribution of the former to the surface mixed layer.

For Cd, Cu and Al a comparison is made (Table 2) of the amount supplied to the surface layer by the Arctic rivers and the amount which could be supplied by an annual upwelling of 2 m yr^{-1}. This figure, arrived at by a rough estimate of salt balance in the surface layer, should be considered arbitrary and of value only in making comparisons between the cycling of the different trace metals under consideration. It is derived from the quantity of water of salinity 34‰ (equivalent to a depth of 130–150 m) that must be added to the annual freshwater runoff of 0.26 m to give a mixed layer salinity of 30‰.

A further difficulty which should be stressed is the paucity of data on the dissolved trace metal composition of rivers which is acute for Arctic rivers and scarcely better for the world average river water.

The contributions of Atlantic and Bering Sea water to the upwelling flux are not known, accordingly a range of fluxes for each metal is given in Table 2, the extremes corresponding to total supply from each source. A single value results for aluminium since the two source waters contain essentially the same concentration of this metal. The term 'upwelling' is used here in the sense of a general compensation for sinking; though it might be the case that some addition of trace metals to the surface layer occurs through a more localized coastal upwelling.

In the case of Cd it appears that the high surface concentration is mainly due to the supply from underlying waters and the relatively low biological activity in the Arctic waters (RYTHER, 1963). For this metal a low, estimated river water concentration of 0.1 nmol l^{-1} (E. BOYLE, personal communication) has been assumed, but reliable data are at present still unavailable in spite of the fact that sufficiently sensitive analytical techniques are now available.

Table 2

A comparison of the magnitude of sources of Cd, Cu and Al to the surface mixed layer assuming an upwelling rate of 2 m y^{-1} and metal concentrations in upwelling water ranging from Atlantic layer to Bering winter layer values.

	River water concentration n mol ℓ^{-1}	River supply (a) to Arctic Ocean n mol m^{-2} y^{-1}	Upwelling supply n mol m^{-2} y^{-1}	River supply / Upwelling supply
Cd	0.1 (b)	26	400-1200	0.02-0.07
Cu	25 (c)	6.5×10^3	$4\text{-}10 \times 10^3$	0.7-1.6
Al	1.1×10^3 (d)	300×10^3	7×10^3	43

(a) River flow, 0.1×10^6 m^3 s^{-1} (SCOR, 1979)
Area of Arctic Ocean 12×10^{12} m^2.
(b) E. Boyle, personal communication.
(c) Boyle (1979).
(d) Rahn (1980).

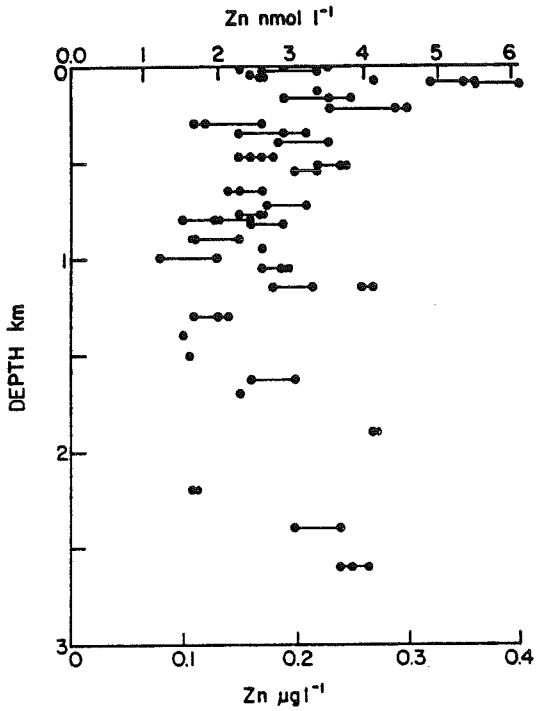

Fig. 3. Dissolved zinc vs depth at LOREX station.

Zinc

There is a general similarity between the findings for Cd and those for Zn (Table 1, Fig. 3), but the generally poorer analytical precision for zinc results in little extra information being derived from these data. Poor precision in the analysis of a single sample results in part from the fact that the sensitivity of the atomic absorption spectrophotometric method is not a linear function of Zn concentration; increasing Zn levels yield lower sensitivity. Disagreement between samples collected at the same or similar depths is thought to result from some contamination produced by the sampling bottles; a possible source being the Go-flo sampling bottle spigots that other workers have recommended be replaced with Teflon taps (BRULAND *et al.*, 1979).

A few points are worthy of note. Surface levels are higher than in the other oceans and there is a peak corresponding with the nutrient maximum at *ca.* 100 m. This is in accordance with the correlation reported by other workers (BRULAND *et al.*, 1978b; BRULAND, 1980) between Zn and silicate.

Below the nutrient maximum the zinc concentrations vary around a mean of 3 nmol l^{-1}. This is only about one third of the value reported for the northern Pacific (BRULAND, 1980), while the silicate levels are an order of magnitude lower in the deep Arctic Ocean compared with the Pacific. It remains to be established whether the correlations shown to exist between metals and nutrients at any given location are of general validity in widely differing oceanic regimes. This task might have to wait until it has been shown by inter-laboratory calibrations that different groups can produce concordant trace metal analyses.

No comparison has been made of the contributions of river water and subsurface water to the surface Zn concentration on account of lack of information on the concentration of Zn in river waters. It has been estimated, however, that the river concentration would be in the range 20–40 nmol l^{-1} for the river flux to be comparable to the upwelling flux.

Copper

There is scatter in the Cu concentrations of the deep samples which could possibly be natural, but is felt to be more probably the result of contamination from the sampling bottles, the deepest samples having spent longest in the bottles. For this reason Cu values are plotted only for the upper part of the water column where the data show smooth changes with depth (Fig. 4); all values are listed in Table 1. The results point to a significant difference between Cu and both Cd and Zn in that there is no increase in the metal in the nutrient maximum. Surface concentrations are high at 5 nmol l^{-1} and they show a decline at 100 m continuing to a depth of 300 m.

From Table 2 it is seen that for Cu the river water supply is potentially important. The depth profile shows that the subsurface waters alone cannot provide sufficient copper to maintain the surface layer at *ca.* 5 nmol l^{-1}. The pronounced surface maximum of copper in these waters is consistent with normal river supply coupled with inefficient scavenging of the metal due to low biological productivity.

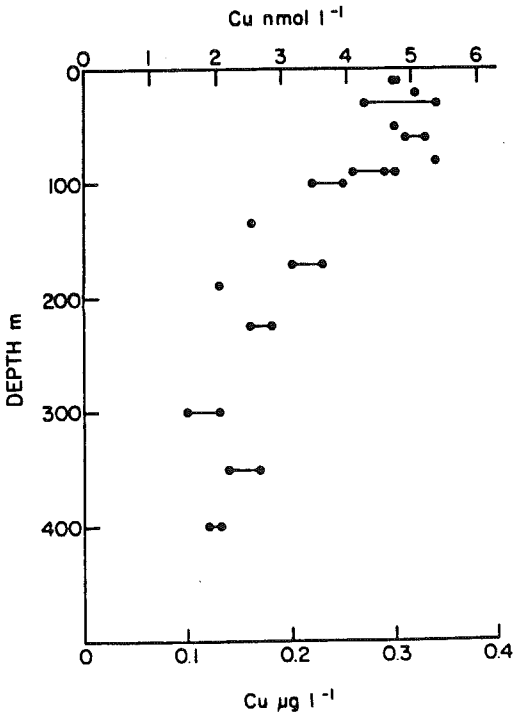

Fig. 4. Dissolved copper vs depth at LOREX station.

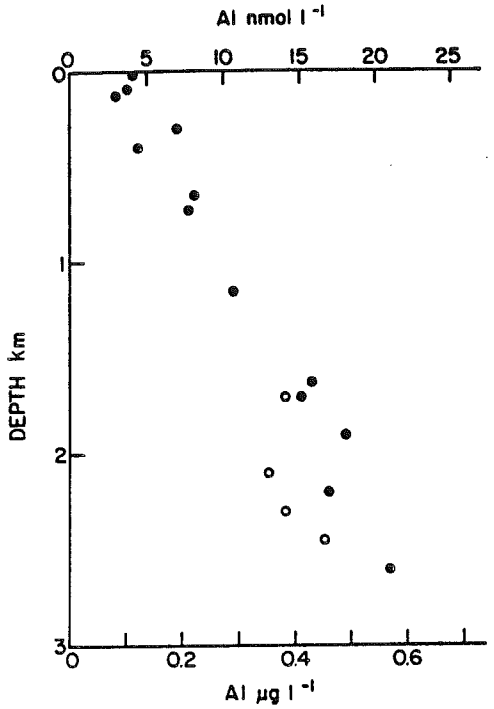

Fig. 5. Dissolved aluminium vs depth at LOREX station.

It has been shown that in the Pacific Cu is transported into deep waters more effectively than Zn, Cd and the nutrients (BRULAND, 1980), the reason for this being the additional downward transport transport process of intermediate and deep water scavenging of Cu. This fractionation of Cu and nutrients could allow the passage of shallow nutrient rich water from the Bering Sea into the Arctic without a large transport of dissolved Cu. It is a combination of this fact and the enhanced mixed layer concentration that can account for the different profiles observed for Cd and Cu. A process, well established in the deep ocean (BOYLE *et al.*, 1977), that might be of some importance in maintaining enhanced levels of Cu in the surface waters relative to Zn and Cd, is diffusion out of the extensive continental self sediments into the upper part of the water column.

Aluminium

The depth profile of Al (Fig. 5, Table 3)) shows a steady increase in concentration with depth from a near surface (20 m) value of 4.1 to 21 nmol l^{-1} at 2600 m. A sample taken from the nutrient maximum (90 m, Si, 36 μmol l^{-1}) had an Al concentration (3.7 nmol l^{-1}) very similar to that found in the mixed layer where the nutrient concentrations are much lower (Si, 6.9 μmol l^{-1}). Deep samples from both sides of the Lomonosov Ridge were analyzed and found to contain rather similar amounts of dissolved aluminium.

The data differ markedly from those presented by HYDES (1979) for the North Atlantic (40°51'N, 64°10'W) and those of CASCHETTO and WOLLAST (1979) for the western Mediterranean. As there is currently little information on dissolved Al in the oceans and there exist significant differences among the results it is worthwhile comparing these findings with those for the other areas that have been studied.

The absence of a peak in the dissolved Al profile at the depth of the nutrient maximum rules out the type of relationship that certain elements such as Cd and Zn have with the nutrients, phosphate and silicate.

Table 3

Dissolved aluminium and silicate concentrations from the LOREX drift path.

Depth	Al nmol ℓ^{-1}	Si µmol ℓ^{-1}
20	4.1	6.7
93	3.7	36.4
130	3.0	14.7
300	7.0	8.0
400	4.4	7.5
650	8.2	7.6
725	7.8	7.0
1150	10.7	8.3
1625	16.0	11.1
1700	15.2	11.7
*1700	14.1	11.6
1900	18.2	12.1
*2100	13.0	10.2
2200	18.5	12.7
*2300	14.5	10.0
*2450	16.7	10.3
2600	21.1	13.0

* - Samples from beneath the Lomonosov ridge crest (~1500 m) in the Fram Basin; all other deep samples from the Makarov Basin (Moore and Lowings, 1981).

This is not to say that simultaneous vertical transport of both components does not occur in biogenic particles, but rather that if such a mechanism exists it is in addition to a process, presumably inorganic, that permits a fractionation of Al and nutrients and which operates independently of biological activity.

From their work on the Mediterranean, CASCHETTO and WOLLAST (1979) pointed to some analogies in distribution and seasonal change between dissolved Al and silicate; they suggest that biological activity plays a dominant role in controlling dissolved Al. HYDES (1979) has already shown that a direct correlation between Al and silicate is not a general oceanic phenomenon and has pointed to evidence for an inverse relationship between these quantities.

Pronounced differences are apparent between this profile and one from the Northwestern Atlantic (HYDES, 1979); most significant amongst these is the absence in the Arctic profile of the enrichment to a depth of 1000 m observed in the Atlantic. Hydes interpreted the surface maximum as a result of an atmospheric input of particulate matter, some of which dissolves. If this were assumed to be the case, the argument might be extended to the case of the Arctic profile and the lower surface values there attributed to the lower flux of atmospherically derived Al, evidence for which has been provided by RAHN (1980).

A closer look at the question of an atmospherically derived contribution to the dissolved Al pool in the upper 1000 m of the Atlantic profile, reveals that it is unlikely to account for the feature in any simple way. The estimates given below of the particulate flux of Al to the ocean are necessarily crude, because of the variability of particulate Al in the atmosphere and because the deposition velocity is not well known.

Atmospheric concentration of Al in Bermuda $= 130\ \text{ng m}^{-3}$ (DUCE *et al.*, 1976).

Deposition velocity $= 1\ \text{cm sec}^{-1}$ (WALLACE *et al.*, 1977)

Flux $= 1.3\ \text{ng m}^{-2}\ \text{sec}^{-1}$
$= 41\ \text{mg m}^{-2}\ \text{yr}^{-1}$

% of particulate flux dissolving: *ca.* 1% (HODGE *et al.*, 1978)

Annual contribution to dissolved pool $= 0.4\ \text{mg m}^{-2}\ \text{yr}^{-1}$

If this were distributed over the top 200 m the addition would be equivalent to $2\ \text{ng l}^{-1}\ \text{yr}^{-1}$. The surface concentration is *ca.* $1000\ \text{ng l}^{-1}$, so if the Al were removed entirely by re-incorporation into particles the necessary residence time with respect to this process would be 500 yr. This has oversimplified the problem by omitting removal by downward mixing. A somewhat more rigorous treatment of the same profile which included a consideration of vertical mixing would require an even longer residence time for the enrichment in the upper waters to be maintained by the atmospheric source; the reason for this being the decrease in dissolved aluminium with depth to 1000 m. A residence time for Al in surface waters of *ca.* 500 yr is inconsistent with an estimated residence time for waters above the thermocline of 80 yr (BROECKER, 1974).

The shape of the Atlantic profile cannot be attributed in any significant degree to contributions made by natural particulate matter. The total particulate Al load as estimated from data given by WALLACE *et al.* (1977) for particulates between New England and Bermuda beyond the continental shelf is only *ca.* $80\ \text{ng l}^{-1}$: $3\ \text{nmol l}^{-1}$. Furthermore, the analytical method used by HYDES and LISS (1976) involves a mildly acidic medium (pH 5) which is unlikely to release the bulk of any particulate Al, present probably as clay particles.

These considerations suggest that the atmospheric flux of Al to the surface waters of the Atlantic does not play a dominant role in maintaining the surface concentration of dissolved aluminium at the observed excess over the water at 1000 m. Alternative explanations for the distribution may involve, separately or together, advection, an inorganic removal process occurring at intermediate depths, and more extensive dissolution of atmospherically derived particulate aluminium than reported by HODGE *et al.*, 1978.

It is interesting that the Arctic Ocean profile does not conform to what would be expected if there were a major influence of river-derived dissolved Al. Table 2 indicates that the river supply of dissolved Al to the ocean as a whole is potentially large compared with the supply from subsurface waters; and yet the surface concentrations are minimal. Two reasons may be suggested to account for this observation.

First, the river supply of dissolved Al might be overestimated because a particulate component has been included and secondly, inorganic removal processes might prevent the influence of river supply from extending to the centre of the ocean. HYDES and LISS have presented evidence that around 30% of the dissolved Al in river water can be removed in the estuary; they have also pointed out that the poor correlation between dissolved Al and salinity in the North Sea indicates that processes other than simple dilution have some control on the metal distribution.

In addition to the major difference between the Atlantic and Arctic Al profiles in near-surface waters there is also a general difference in the metal levels at greater depths. The Atlantic values increase from $22\ \text{nmol l}^{-1}$ at 1000 m to 29 nmol at 2500 m while the Arctic values are significantly lower: 10 nmol at 1000 m increasing to *ca.* 20 nmol at 2500 m. The simplest explanation of a distribution having this form would be the existence of a pressure dependent equilibrium between dissolved Al and a solid phase; this problem requires further study.

CONCLUSIONS

The concentration profiles of the dissolved metals Zn, Cd, Cu and Al in the central Arctic Ocean are

generally rather different from those of other oceanic regions, but in the case of Zn, Cd and Cu the features are apparently explicable in terms of the local hydrography and the geochemistry of these elements as understood from studies in the other regions of the World Ocean. The extent to which the relatively high concentration of these metals in surface waters are due to riverine inputs cannot be accurately assessed as there is a dearth of information on the concentrations of the elements in river water generally.

In the case of Al not only are the results dissimilar to those for other regions but also they demonstrate that the mechanisms invoked to explain observations elsewhere are not of general validity. It is suggested that inorganic removal processes play a prominant role in controlling the concentration of this element in sea water, at least in regions characterized by low biological productivity.

Acknowledgements—The author wishes to thank HANS WEBER of the Earth Physics Branch of Energy, Mines and Resources, Canada for permitting and facilitating participation in the LOREX programme, also members of EPB and the Polar Shelf Project for assistance in logistics. The help of M. G. LOWINGS during collection of the samples and of P. EGLI-STOFFYN with aluminium analysis are acknowledged with thanks, as are the helpful comments of reviewers.

REFERENCES

BOYLE E. A. (1979) Copper in natural waters. In *Copper in the Environment* (ed. J. O. Nriagu), pp. 77–78. Wiley-Interscience.

BOYLE E. A., SCLATER F. and EDMOND J. M. (1976) On the marine geochemistry of cadmium. *Nature* **263**, 42–44.

BOYLE E. A., SCLATER F. and EDMOND J. M. (1977) The distribution of dissolved copper in the Pacific. *Earth Planet. Sci. Lett.* **37**, 38–54.

BROECKER W. S. (1974) *Chemical Oceanography*. Harcourt Brace Jovanovitch.

BRULAND K. W. (1980) Oceanographic distributions of cadmium, zinc, nickel and copper in the North Pacific. *Earth Planet. Sci. Lett.* **47**, 176–198.

BRULAND K. W., KNAUER G. A. and MARTIN J. H. (1978a) Cadmium in northeast Pacific Waters. *Limnol. Oceanogr.* **23**, 618–625.

BRULAND K. W., KNAUER G. A. and MARTIN J. H. (1978b) Zinc in northeast Pacific water. *Nature* **271**, 741–743.

BRULAND K. W., FRANKS R. P., KNAUER G. A. and MARTIN J. H. (1979) Sampling and analytical methods for the determination of copper, cadmium, zinc, and nickel at the nanogram per litre level in seawater. *Anal. Chim. Acta* **10**, 233–245.

CASCHETTO S. and WOLLAST R. (1979) Vertical distribution of dissolved aluminium in the Mediterranean Sea. *Mar. Chem.* **7**, 141–155.

CHAN L. H., DRUMMOND D., EDMOND D., EDMOND J. M. and GRANT B. (1977) On the barium data from the Atlantic GEOSECS Expedition. *Deep-Sea Res.* **24**, 613–649.

DUCE R. A., RAY B. J., HOFFMAN G. L. and WALSH P. R. (1976) Trace metal concentration as a function of particle size in marine aerosols from Bermuda. *Geophys. Res. Lett.* **3**, 339–342.

HODGE V., JOHNSON S. R. and GOLDBERG E. D. (1978) Influence of atmospherically transported aerosols on surface ocean water composition. *Geochem. J.* **12**, 7–20.

HYDES D. J. (1979) Aluminium in seawater: control by inorganic processes. *Science* **205**, 1260–1262.

HYDES D. J. and LISS P. S. (1976) Fluorimetric method for the determination of low concentrations of dissolved aluminium in natural waters. *Analyst* **101**, 922–931.

HYDES D. J. and LISS P. S. (1977) The behaviour of dissolved aluminium in estuarine and coastal waters. *Estuarine Coastal Mar. Sci.* **5**, 755–769.

KNAUER G. A. and MARTIN J. H. (1981) Phosphorus–cadmium cycling in northeast Pacific waters. *J. Mar. Res.* **39**, 65–76.

MOORE R. M. and LOWINGS M. G. Hydrographic features and nutrients at the LOREX station in the central Arctic Ocean (in preparation).

RAHN K. A. (1980) Atmospheric, riverine and oceanic transport of trace elements to the Arctic Ocean. Paper presented at the Conference on the Arctic Ocean, London, 11–12 March, 1980.

RYTHER J. H. (1963) Geographic variations in productivity. In *The Sea* (ed. M. N. Hill), Vol. 2, pp. 347–380.

SCOR Working Group 58 (1979) *The Arctic Ocean Heat Budget*, Rep. No. 52.

VETSHTEYN V. YE., MALYUK G. A. and RUSANOV V. P. (1974) Oxygen-18 distribution in the central Arctic Ocean. *Oceanology* **14**, 514–519.

WALLACE G. T., HOFFMAN G. L. and DUCE R. A. (1977) The influence of organic matter and atmospheric deposition on the particulate trace metal concentration of northwest Atlantic surface seawater. *Mar. Chem.* **5**, 143–170.

From: TRACE METALS IN SEA WATER
Edited by Wong, Boyle, Bruland and Goldbert
(Plenum Publishing Corporation, 1983)

THE RELATIONSHIP BETWEEN DISTRIBUTIONS OF DISSOLVED CADMIUM, IRON AND ALUMINIUM AND HYDROGRAPHY IN THE CENTRAL ARCTIC OCEAN

Robert M. Moore

Department of Oceanography
Dalhousie University
Halifax, Nova Scotia
Canada B3H 4J1

INTRODUCTION

Over many years there has been considerable interest in the role of iron as a micronutrient element[1] with attention focussing on its solubility[2,3], speciation, both inorganic[3] and organic[4], its availability to plankton[5,6,7] and modification of its speciation by organisms[6,7,8,9], and the possible ecological effects of its concentration and chemical form.

Studies of the biological roles, solubility and speciation of iron in seawater have not, however, been matched by studies giving a coherent picture of the distribution of this element in the world ocean. The reasons for this are probably related to the ubiquitous terrestrial distribution of the element and its very low solubility in seawater which combine to give contamination problems equalled by few other elements. Added to this, the distribution of the metal between dissolved and particulate forms, with the latter strongly favoured, results in some difficulty in comparing data sets which make different divisions of the total iron pool. These divisions result from the procedures used for storage, filtration and analysis.

This paper describes the vertical distribution of iron in the central Arctic Ocean and compares this with profiles of Cd and Al, relating each to the hydrography.

Sampling, Storage and Analysis

Water samples were collected from a drifting ice station between 88° N, 139°50'W and 89°9'N, 97°7'W in the central Arctic Ocean (Fig. 1). The samples for trace metal analysis were taken with 5 l Go-flo bottles attached to a new stainless steel hydrographic wire. Samples were not filtered since this procedure is liable to contaminate them, also, for most of the elements analyzed the concentration of particulate matter in open ocean waters is too low to make a significant contribution to the total. This may not be the case for iron which probably has a colloidal form with uncertain behaviour on filtration. In view of this, measurement of the total iron in these waters should provide a useful starting point for understanding its geochemistry in the Arctic Ocean. Immediately after collection, the samples in acid washed polyethylene bottles were frozen for storage.

The analytical method is essentially the solvent extraction procedure described by Danielsson et al.[11] but with some modifications designed to reduce handling of the sample. A closely similar method was used for analyzing samples for Cd, Zn and Cu[9,12] The sample was thawed and to a 200 ml aliquot was added 1 ml of a solution containing sodium diethyldithiocarbamate (1% w/v) and ammonium pyrrolidine dithiocarbamate (1% w/v) in 1% ammonia solu-

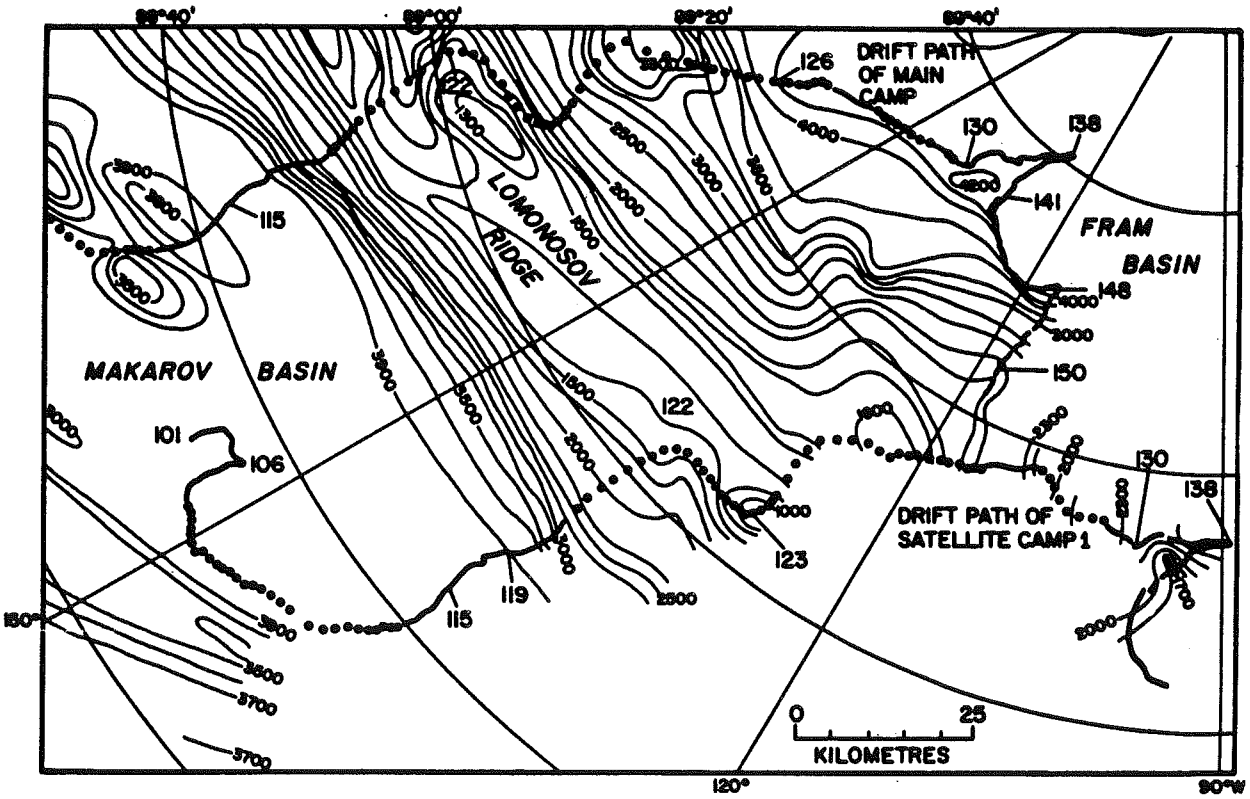

Fig. 1 Drift path of LOREX satellite camp 1. Numbers along path indicate Julian days.

tion, and 0.650 ml of 1 M hydrochloric acid to bring the pH to 4. The solution was extracted three times with 5 ml volumes of 1,1,2 trichloro-1,2,2 trifluorethane and the organic phase evaporated dryness in a silica vial and treated with 0.1 ml of Ultrex hydrogen peroxide (30%) to initiate the decomposition of organic matter present. After an hour or more, 0.5 ml of 0.1 M hydrochloric acid was added and the solution irradiated with a 1000 W Hanovia medium pressure mercury vapour discharge tube at a distance of 4 cm for 18 minutes. The iron in the concentrate was then compared with standards in 0.1 M hydrochloric acid using a Perkin-Elmer Model 403 Spectrophotometer fitted with a Perkin-Elmer graphite furnace (HGA 2200).

The blank, determined by repeating this procedure on extracted sea water, was typically 5 ng Fe, (equivalent to 25 ng l^{-1}).

The coefficient of variation of analyses was 21% for seven subsamples containing 1.6 nmol Fe l^{-1}, and 30% for eight subsamples at 0.6 nmol Fe l^{-1}. The detection limit was estimated to be 0.2 nmol Fe l^{-1}.

The efficiency of the extraction procedure was tested using sea water spiked with iron-59, which indicated a recovery of 97%, and with stable iron of 86%.

Aluminium analyses were made by a slightly modified version[12] of the procedure described by Hydes and Liss[13].

Results and discussion

Salinity, temperature and silicate profiles for the central Arctic Ocean are given in Figures 2-5. In the following discussion the distributions of iron, cadmium and aluminium, illustrated in Figures 6-8, are related to the hydrography and to addition and removal processes.

The central Arctic Ocean is characterized by a low salinity (ca. 30 $^{o}/oo$) well-mixed surface layer extending to about 50 m, below which the salinity increases very sharply (Fig. 2) reaching 34 $^{o}/oo$ by 130 m. Stable oxygen isotope ratios were linearly correlated with salinity, the relationship being described by the equation $\delta^{18}O = -23.2 + 0.656\ S\ ^{o}/oo$: this indicates that the fresh water component is primarily meteoric rather than sea ice meltwater (F. Tan, personal communication). The fresh water input comprises contributions from river flow and direct precipitation in a ratio of 3:1[14]. The trace metal composition of the surface water should therefore reflect that of Arctic river waters with modification by an atmospheric flux and by biological and inorganic removal processes.

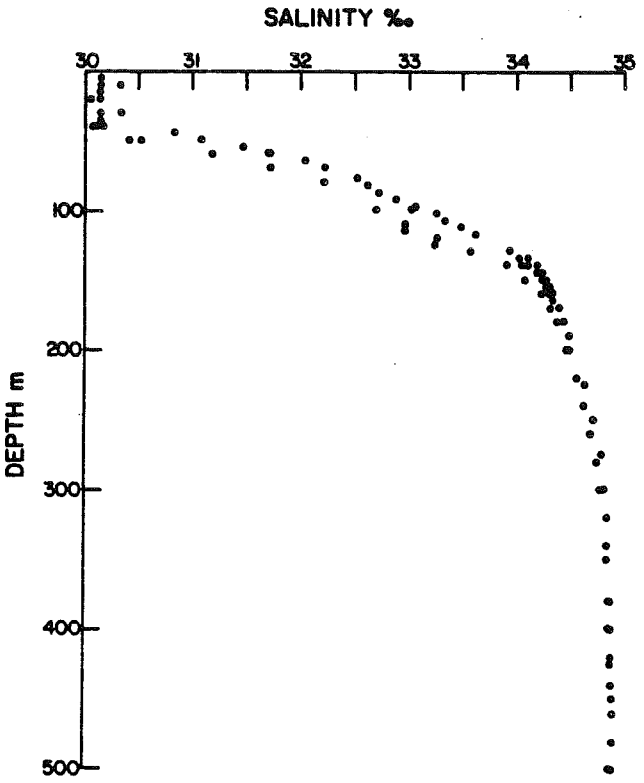

Fig. 2 Salinity profile to 500 m. Filled circles indicate profile from the Makarov Basin; open circles, profile from Fram Basin.

It is found that the surface layer has, relative to most surface ocean waters, high levels of silicate (7 μmol l^{-1}), phosphate (1 μmol l^{-1}) which are matched by relatively high cadmium (0.3 nmol l^{-1}). Unless the Arctic rivers carry unusually high concentrations of cadmium, the surface values must be accounted for by the admixture of the water that lies just beneath the mixed layer. This would also account for the surface silicon concentrations without needing a significant contribution from rivers. The high concentrations of both nutrients and those trace metals that are subject to biological control are allowed to persist in the surface waters on account of the very low primary productivity. This has been estimated by Ryther[15] to be only 1 g C m^{-2} yr^{-1}, much lower than even the oligotrophic waters of subtropical ocean regions (ca. 25 g C m^{-2} yr^{-1})[16], the reason is that the light flux is severely attenuated by the covering of ice.

Neither iron nor aluminium (Fig. 7, 8) show any enhancement of concentration in the surface waters that might be expected from the river inputs. In the case of aluminium it has been proposed[12] that the surface levels must be accounted for by an inorganic removal process possibly occurring in the nearshore or shallow

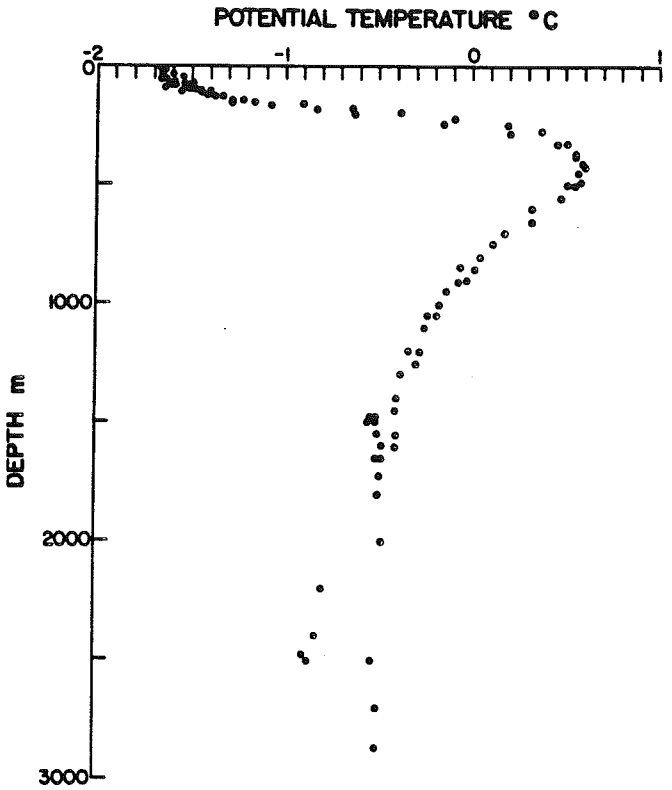

Fig. 3 Potential temperature profiles to 3000 m. Symbols as on Fig. 1.

continental shelf region. Similarly, in the absence of efficient biological stripping of trace elements from the surface waters, it may be argued that the iron levels are also controlled by inorganic removal processes. There is good evidence for inorganic removal of iron in the estuarine zone[17] but it is not yet clear whether similar processes continue to operate in the coastal zone.

Neither the iron nor aluminium distribution shows any sign of an atmospheric flux even though these elements are major components of atmospheric particles[18,19]. Some consideration should be given to the mechanism of atmospheric supply of elements to the Arctic Ocean. During much of the year there can be no addition of atmospherically derived trace elements to the water column on account of the complete ice cover. During the summer months the upper surface of the sea ice which has accumulated the atmospheric deposition of the foregoing winter is melted and the fresh water added to the surface layer with which it mixes. Additionally Rahn[14] suggests that a major part of the atmospheric deposition occurs in the summer, since most of the Arctic Ocean precipitation is rain. The atmospherically derived metals are therefore added in a pulse when temperatures rise above freezing and the addition continues until temperatures fall again below zero. Data available so far[20,21]

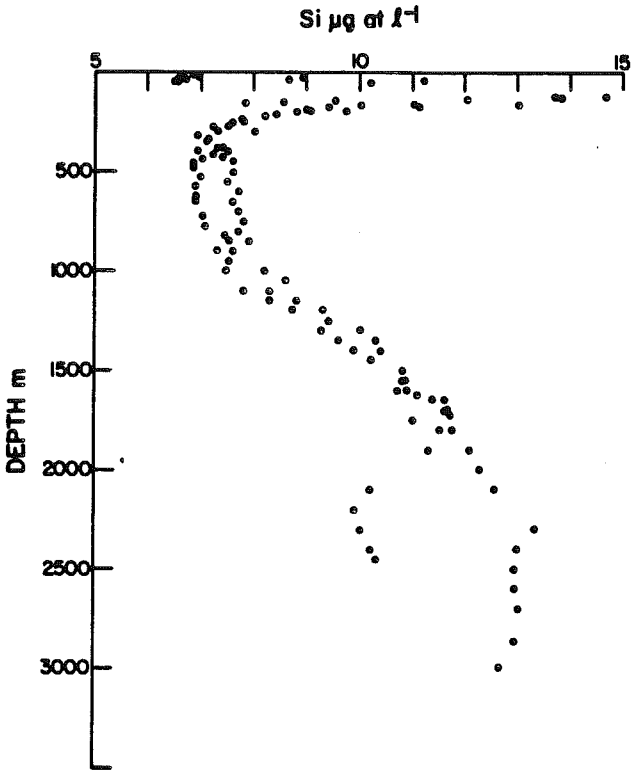

Fig. 4 Silicate profiles to 3000 m. Maximum values at ca. 100 m are not shown. Symbols as in Fig. 1.

would suggest that for both of the elements only a small fraction (1-4%) of the atmospheric flux is soluble.

A pronounced hydrographic feature below the surface mixed layer is a well-defined nutrient maximum centred at about 100 m (Fig. 4). This has been identified[22,10] as water originating in the Bering Sea entering the Arctic Ocean through the Bering Strait. Associated with the coincident silicate and phosphate maxima are peaks in the cadmium and zinc profiles[12]. This is in agreement with the association between these metals and nutrients which is well documented in the case of the Pacific Ocean[23,24].

Iron and aluminium profiles show no feature in the region of this advected water mass. This is in accordance with the suggestion that both elements have distributions strongly regulated by inorganic processes. It is worth mentioning at this point that radionuclide measurements[25] made on samples collected at the time of this work suggest that complete removal of Am-241 occurs while this water mass is in the shallow waters of the Bering Strait and adjoining shelf areas.

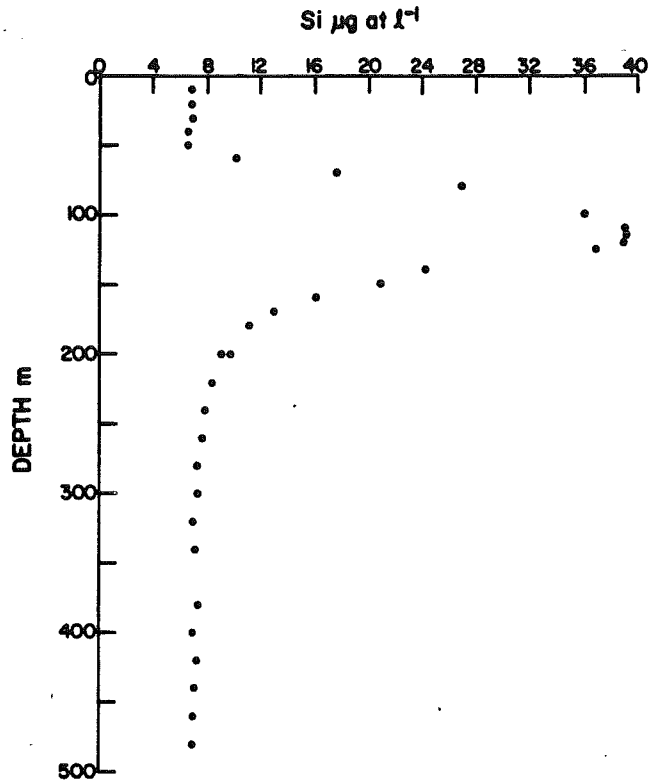

Fig. 5. Silicate profile to 500 m from Makarov Basin.

Below the layer of water from the Bering Sea lies a layer of Atlantic water characterized by a temperature maximum (Fig. 3), below this is Arctic Bottom Water arbitrarily defined by a potential temperature of below 0°. Cadmium levels drop sharply below the nutrient maximum and then show little variation with depth. This is consistent with the nutrient distribution in Atlantic and Arctic bottom water layers where there is only a gradual increase in nutrients with depth indicative of a low flux of biogenic material and moderate residence time of the deep water.

The increase in aluminium with depth, Fig. 8, is similar to that reported by Hydes[26] for depths below 1000 m in the North Atlantic. While such a profile can frequently be related to transport of the element concerned in biogenic material along with the nutrients, this simple explanation is inappropriate here since the shallow nutrient maximum is not matched by a maximum of dissolved aluminium.

The deep water concentrations of iron are not significantly different from the surface and intermediate water values. The samples analyzed for iron in this work were not filtered and so the measured concentrations of around 1×10^{-9} molar include an

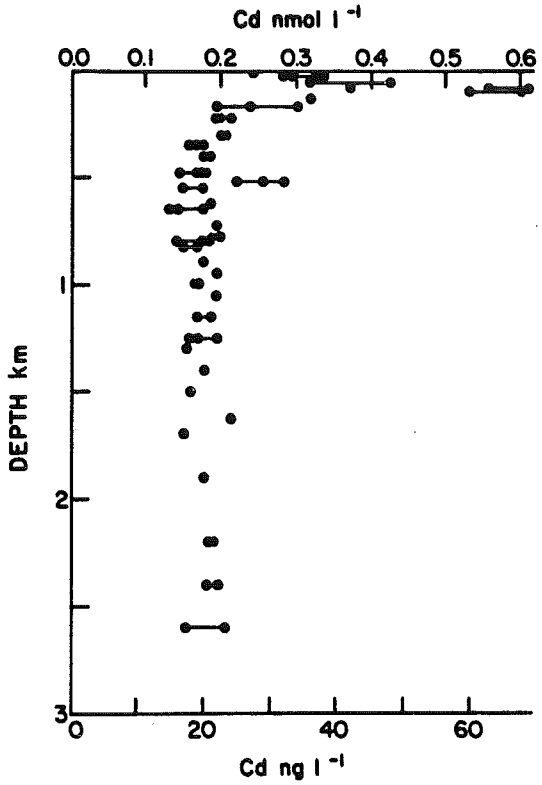

Fig. 6 Cadmium profile comprising samples from both sides of Lomonosov Ridge. From Moore (1981) with permission of Pergamon Press.

unknown contribution of reactive particulate iron. There appear to be no data on the distribution of particulate matter in the waters of the Arctic Ocean but in view of the low productivity of the waters and turbulence in the shelf regions reduced as a result of ice cover it may be supposed that the suspended load is relatively low, and that the particulate iron is correspondingly low.

CONCLUSIONS

A preliminary look at the distribution of reactive iron in the water column of the central Arctic Ocean indicates a marine geochemistry differing markedly from that of a number of trace metals that have been more thoroughly studied. Its distribution does not reflect the influence of river or atmospheric inputs nor the influence of advected water masses having quite different trace element compositions. It appears that inorganic processes are dominant in the removal of river-derived iron from the surface waters of the Arctic Ocean; this also applies to dissolved aluminium. The distribution of iron in the water column is consistent

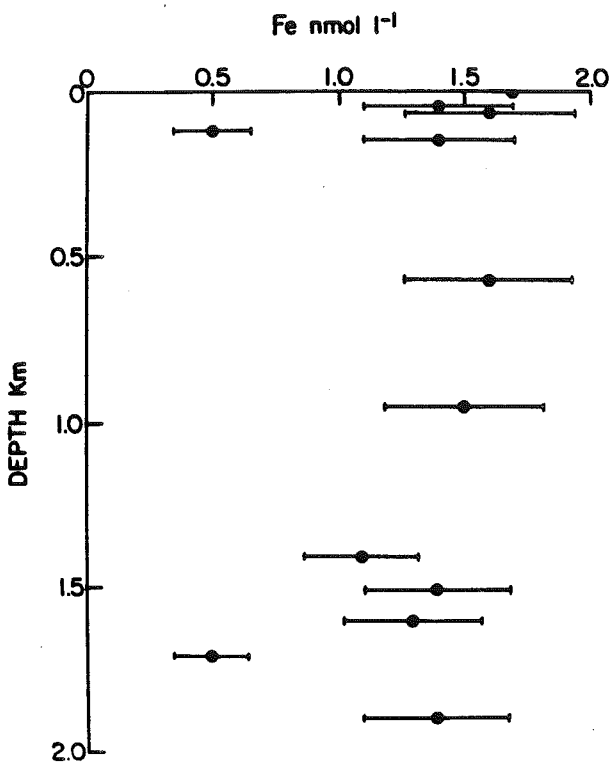

Fig. 7 Reactive iron concentrations, samples taken from both sides of Lomonosov Ridge. Error bars indicate ± 1 standard deviation.

with control by equilibrium with solid phases. Perhaps the simplest among the possible explanations for the dissolved aluminium profile is also equilibrium with a solid phase, though in this case a pressure dependence of the solubility of the controlling solid phase would be necessary to account for the increasing concentration with depth.

The observations of cadmium distribution are in accord with the interpretation of earlier studies of the metal in the other oceans; this work does, however, illustrate that the correlation between cadmium and phosphate can be maintained in shallow waters where inorganic removal processes are dominant.

It is not possible to ascertain how general are the conclusions that may be drawn from this specific study; the Arctic Ocean provides an environment differing greatly from the more temperate ice-free oceans, it is strongly stratified, has a large freshwater input, a periodic input of atmospherically derived materials, low productivity, unique light cycle and hence productivity cycle, and an unusually extensive shelf area. The study of trace element geochemistry in such an environment provides data that constrain the hypotheses constructed to explain observations made in more usual oceanic conditions.

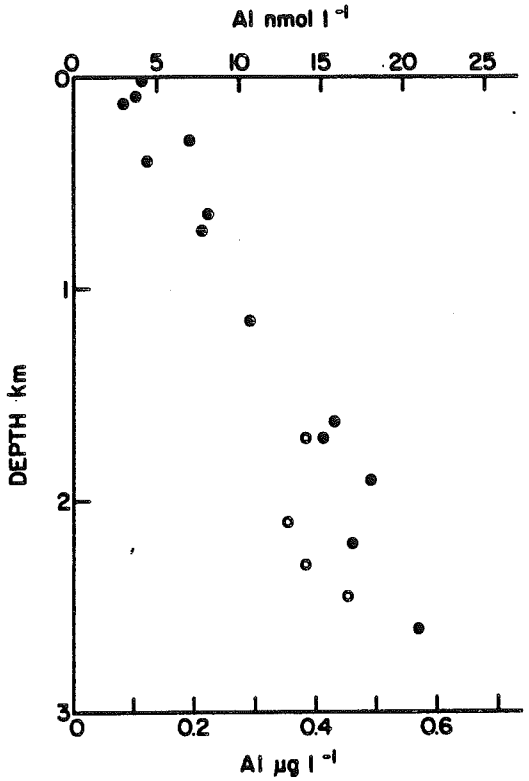

Fig. 8 Reactive aluminium concentrations. Open circles represent samples from below depth of ridge crest (ca. 1500 m) in the Fram Basin. From Moore (1981) with permission of Pergamon Press.

ACKNOWLEDGEMENTS

The valuable assistance of M.G. Lowings in the field work is gratefully acknowledged, also the support provided by the Natural Sciences and Engineering Research Council, Canada, the Earth Physics Branch of Energy, Mines and Resources, Canada, and the Polar Continental Shelf Project. The author wishes to thank H. Gote Ostlund of the tritium laboratory, University of Miami for his support of the project. This paper is LOREX contribution #8.

REFERENCES

1. Menzel, D.W. and J.H. Ryther, 1961: Nutrients limiting the production of phytoplankton in the Sargasso Sea, with special reference to iron. Deep-Sea Res., 7, 276-281.
2. Kester, D.R., T.P. O'Connor and R.H. Byrne, 1975: Solution chemistry, solubility, and adsorption equilibria of iron, cobalt and copper in marine systems. Thalassia Jugoslavica, 11, 121-134.

3. Byrne, R.H. and D.R. Kester, 1976: Solubility of hydrous ferric oxide and iron speciation in seawater. Mar. Chem., 4, 255-276.
4. Sugimura, Y., Y. Suzuki and Y. Miyake, 1978: The dissolved organic iron in seawater. Deep-Sea Res., 25, 309-314.
5. Levandowsky, M. and S.H. Hutner, 1975: Utilization of Fe^{3+} by the inshore colorless marine dinoflagellate Crypthecodinium cohnii. Annals New York Academy of Sciences, 245, 16-25.
6. Davies, A.G., 1970: Iron, chelation and the growth of marine phytoplankton 1. Growth kinetics and chlorophyll production in cultures of the euryhaline flagellate Dunalliela tertiolecta under iron-limiting conditions. J. Mar. Biol. Ass. U.K., 50, 65-86.
7. Lewin, J. and C.H. Chen, 1971: Available iron: a limiting factor for marine phytoplankton. Limnol. Oceanogr., 16, 670-675.
8. Sorokin, Y.I. and Y.A. Bogdanov, 1971: Transformation of iron during bacterial decomposition of planktonic organic matter. Hydrobiol. J., 7, 89-90.
9. Gonye, E.R. and E.J. Carpenter, 1974: Production of iron-binding compounds by marine microorganisms. Limnol. Oceanogr., 19, 840-842.
10. Moore, R.M. and M.G. Lowings, in preparation: Hydrographic features and nutrients at the LOREX station in the central Arctic Ocean.
11. Danielsson, L.-G., B. Magnusson and S. Westerlund, 1978: An improved metal extraction procedure for the determination of trace metals in sea water by atomic absorption with electrothermal atomization. Anal. Chim. Acta., 98, 47-57.
12. Moore, R.M., 1981: Oceanographic distributions of zinc, cadmium, copper and aluminium in waters of the central Arctic. Geochim. Cosmochim. Acta., 45, 2475-2482.
13. Hydes, D.J. and P.S. Liss, 1976: Fluorimetric method for the determination of low concentrations of dissolved aluminium in natural waters. Analyst, 101, 922-931.
14. Rahn, K.A.: Atmospheric, riverine and oceanic transport of trace elements to the Arctic Ocean. Paper presented at the Conference on the Arctic Ocean, London, 11-12 March, 1980 sponsored by the Arctic Committee of Monaco and the Royal Geographic Society.
15. Ryther, J.H.: Geographic variations in productivity. In, "The Sea", vol. 2. M.N. Hill (ed.) Interscience.
16. Koblentz-Mishke, O.J., V.V. Volkovinsky and J.G. Kabanova, 1970: Plankton primary production of the world ocean. In, "Scientific exploration of the South Pacific", W.S. Wooster (ed.), Washington, U.S. Nat. Acad. of Sciences.

17. Holliday, L.M. and P.S. Liss, 1976: The behaviour of dissolved iron, manganese and zinc in the Beaulieu Estuary. Estuarine Coastal Mar. Sci., 4, 349-353.
18. Chester, R. and J.H. Stoner, 1974: The distribution of Mn, Fe, Cu, Ni, Co, Ga, Cr, V, Ba, Sr, Sn, Zn, and Pb, in some soil-sized particulates from the lower troposphere over the world ocean. Mar. Chem., 2, 157-188.
19. Duce, R.A., B.J. Ray, G.L. Hoffman and P.R. Walsh, 1976: Trace metal concentration as a function of particle size in marine aerosols from Bermuda. Geophys. Res. Lett., 3, 339-342.
20. Hodge, V., S.R. Johnson and E.D. Goldberg, 1978: Influence of atmospherically transported aerosols on surface ocean water composition. Geochem. J., 12, 7-20.
21. Crecelius, E.A., 1980: The solubility of coal fly ash and marine aerosols in seawater. Mar. Chem., 8, 245-250.
22. Kinney, P., M.E. Arhelger and D.C. Burrell, 1970: Chemical characteristics of water masses in the Amerasian Basin of the Arctic Ocean. Geophys. Res., 75, 4097-4104.
23. Bruland, K.W., G.A. Knauer and J.H. Martin, 1978: Cadmium in northeast Pacific waters. Limnol. Oceanogr., 23, 618-625.
24. Bruland, K.W., G.A. Knauer and J.H. Martin, 1978: Zinc in northeast Pacific waters. Nature, 271, 741-743.
25. Livingston, H.D., S.L. Kupferman, V.T. Bowen and R.M. Moore: Vertical profile of artificial radionuclide concentrations in the Arctic Ocean. Submitted to Geochim. Cosmochim. Acta.
26. Hydes, D.J., 1979: Aluminium in seawater: control by inorganic processes. Science, 205, 1260-1262.

Geochimica et Cosmochimica Acta Vol. 48, pp. 2195–2203

0016-7037/84/$3.00 + .00

Vertical profile of artificial radionuclide concentrations in the Central Arctic Ocean

HUGH D. LIVINGSTON[1], STUART L. KUPFERMAN[2], VAUGHAN T. BOWEN[3] and R. M. MOORE[4]

[1]Woods Hole Oceanographic Institution, Woods Hole, Massachusetts 02543
[2]Sandia National Laboratories, Albuquerque, NM 87185
[3]652 Knox Road, Strafford, PA 19087
[4]Dalhousie University, Halifax, N.S. B3H 4J1, Canada

(*Received October* 6, 1981; *accepted in revised form July* 27, 1984)

Abstract—The artificial radionuclides ^{90}Sr, ^{137}Cs, ^{238}Pu, $^{239,240}Pu$ and ^{241}Am have been measured in eight water samples collected in 1979, at intervals from surface to bottom, through the ice at the LOREX satellite camp SS near the North Pole. Differences in the concentrations and ratios of these nuclides, compared with values measured, over time, in the various water masses that flow into the Arctic Ocean, can be used as semi-independent checks on rates of flow to the LOREX stations and on residence times in the Arctic Ocean. An unexpected finding was that water labelled with low-level liquid waste from the Windscale plant on the Irish Sea is a major component of the 1500 m LOREX sample, and has reached there in no more than eight to ten years. Even from this one station in the Polar Ocean, estimation of the inventories of the various radionuclides is good enough to emphasize the importance of horizontal advection of the various supply terms to the Arctic.

INTRODUCTION

DURING 1979, as part of the Lomonosov Ridge Experiment (LOREX; WEEER, 1979), water samples were collected in the Central Arctic Ocean for radiochemical analysis of artificial radionuclides. The collection and the hydrographic setting of these samples are reported by MOORE *et al.* (1983). Data concerning trace elements in the same set of profiles are reported by MOORE (1981).

There is considerable intrinsic interest in radionuclide distribution data from an ocean virtually unstudied in this respect. Furthermore, as discussed below, we had confidence that differences in nuclide ratios among the various source terms for the Arctic Ocean would enable such data to assist in choosing among hypothesis concerning Arctic circulation. A good deal of information is available concerning the Arctic Ocean source terms and the changes, with time, of the concentrations and ratios of artificial radionuclides in them. Furthermore, one can infer several aspects of the circulation history of a labelled water mass by looking for changes, along its trajectory, in the ratio of ^{137}Cs to ^{90}Sr, or among the actinide elements.

SAMPLES AND ANALYTICAL METHODS

Eight samples, collected at depths from 2 m to 3000 m were available for our radionuclide analyses. The collections were made over a four week period along the ice station's 200 km westward drift path across the Lomonosov Ridge at about 89°N. All, excepting the 1500 m and 2500 m samples, were collected over the Makarov Basin between 151°W and 138°W. The 1500 m sample was collected just over the ridge at 111°W and the 2500 m sample in the Fram Basin at 89°W. The area of the LOREX stations and the position of other stations discussed later are shown in Fig. 1.

Each sample, because of the large volume desired, represented a composite taken from several 30-l Niskin bottles (General Oceanics, Inc., Miami, FL 33127), the largest available on the ice. At all depths but 110 m, enough water was retrieved to make up a 200-l composite; each of these was acidified, and CO_2 extracted for ^{14}C analysis, before the solution was transferred to 19-l Cubitainers (Hedwig Corp., Baltimore, MD 21211) for shipment back to the shore-based laboratory. The 110 m sample was not intended for ^{14}C and was transferred directly to shipping containers. In Woods Hole, two or three Cubitainers were emptied, with acid rinsing, into 100-l drums for radiochemistry; actual sample sizes ranged from 40 to 63 kg.

Temperature, salinity and some nutrient data, useful for confirming the depths and water masses sampled, were obtained from thermometer-equipped 1.7-l Niskin bottles mounted above and below the 30-l bottles. Potential temperature, salinity and silicate values obtained by averaging these data were assigned to the large volume samples and are shown in Table 1.

Tritium data from some of the 1.7-l Niskin samples, and ^{14}C data from CO_2 extracted as noted above, have been reported by the University of Miami Tritium Laboratory, in Data Release #80-25 and by OSTLUND (1982). Some of these values are referred to in our discussion.

We present here the data from measurements in these water samples of ^{90}Sr, ^{137}Cs, Pu and Am. Our procedures for these analyses have been described, Sr and Cs following essentially those reported by WONG *et al.* (1970), and the actinides those reported by LIVINGSTON *et al.* (1975a). Discussions of, and references to publications of, our laboratory performance on standards or in interlaboratory analytical comparisons will be found in the literature (LIVINGSTON *et al.*, 1975a; BOWEN *et al.*, 1974, 1980).

In addition to the analyses of retrieved water samples, two very large amounts of Cs were collected by pumping 2 m water through chemisorbent cartridges loaded with resin beads impregnated with cupric ferrocyanide (MANN and CASSO, 1984). Through one absorber was pumped 4148 l, through the other 4860 l. The purpose of these collections was to obtain more sensitive and accurate measurements of the ratio, in the 2 m water, of ^{134}Cs to ^{137}Cs; measurement was done by Ge(Li) gamma spectrometry on the intact absorbent mass, placed in Marinelli beakers.

RESULTS

In Table 1 are set out the depths of the eight large volume samples, together with the potential temperatures, salinities,

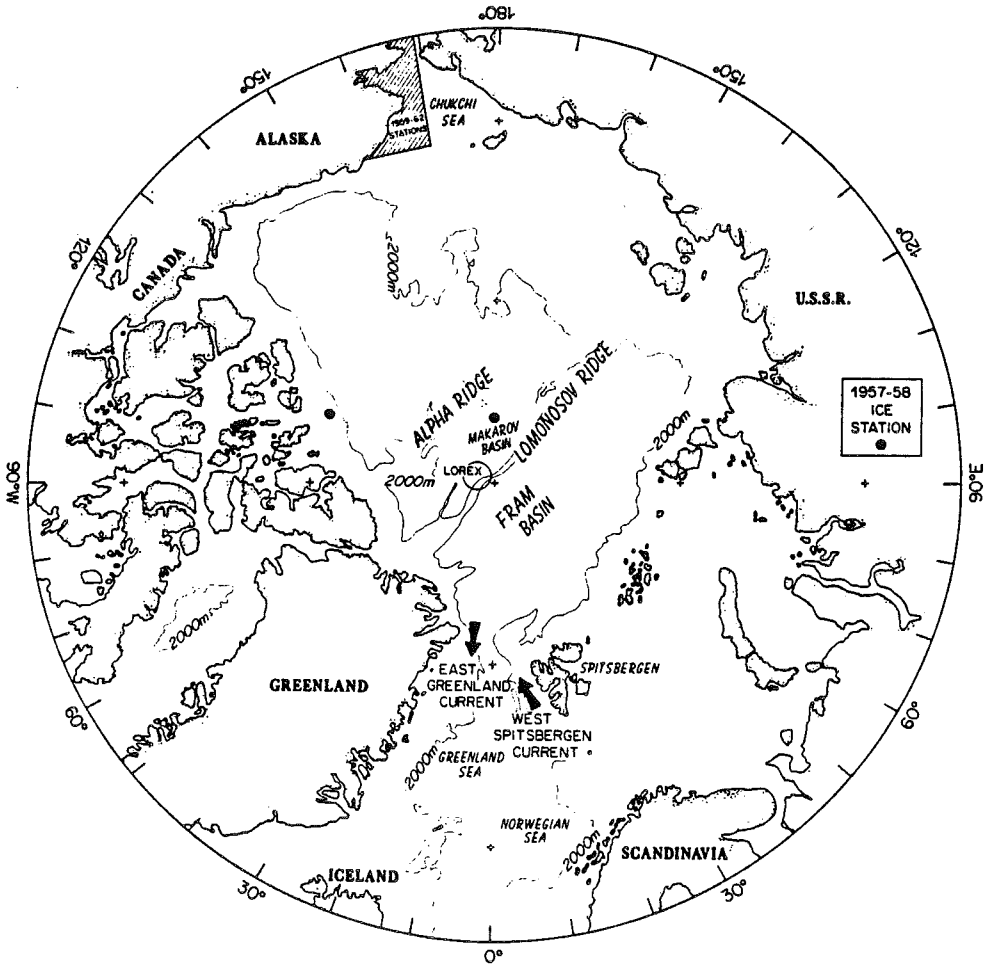

FIG. 1. Station positions, geography and bathymetry of sampling locations in Arctic Ocean.

and silicates and the water mass designations reported for them by MOORE *et al.* (1983). Against these are shown our measured concentrations of ^{90}Sr, ^{137}Cs, $^{239,240}Pu$, and ^{241}Am and the derived ratio $^{137}Cs/^{90}Sr$.

Attempts were made, using sensitive gamma spectrometry on the separated Cs, to evaluate the activity ratios of ^{134}Cs to ^{137}Cs in the three high-^{137}Cs near-surface samples. In each case, however, the ^{134}Cs was less than our detection limit. This was also true of the very large Cs collections from the chemisorbent cartridges. These yielded the following ratios in the respective volumes stripped:

Absorber No. 1: 4148 l, ^{134}Cs to ^{137}Cs activity ratio -0.003 ± 0.005

TABLE 1
LOREX 79 NORTH POLE STATION RADIONUCLIDE DATA

Water Mass	Sample Depth (m)	Salinity ‰	Potential Temp. °C	Si*	^{137}Cs**	^{90}Sr**	$\frac{^{137}Cs}{^{90}Sr}$	$^{239,240}Pu$**	^{241}Am**
Surface Mixed Layer	2	30	-1.6	6.9	39.2±0.5	31.6±0.7	1.24	0.082±0.013	0.042±0.011
Bering Sea Summer Layer	75	32	-1.6	20	33.6±0.4	33.1±4.4	1.02	0.098±0.012	0.031±0.007
Bering Sea Winter Layer	110	33.5	-1.5	29	25.5±0.5	25.5±1.0	1.00	0.045±0.008	-0.005±0.007
Atlantic Water	500	34.88	+0.51	7	7.3±0.4	4.5±0.1	1.63	0.11±0.01	0.025±0.006
Atlantic Water	1000	34.901	-0.17	7.5	6.6±0.3	3.8±0.3	1.74	0.061±0.014	0.019±0.005
Upper Deep Water	1500	34.920	-0.52	8.7	18.5±0.4	8.7±0.1	2.16	0.068±0.007	0.018±0.005
Arctic Bottom Water									
A) Eurasian Basin (FRAM)	2497	34.940	-0.85	10.3	7.3±0.2	4.8±0.7	1.52	0.035±0.006	0.003±0.002
B) Amerasian Basin (MAKAROV)	3000	34.953	-0.46	12.8	0.9±0.3	0.6±0.3	1.50	0.012±0.005	0.004±0.002

* Concentration in μg atoms per liter.

** Concentration in dpm per 100 kg.

Absorber No. 2: 4860 l, ^{134}Cs to ^{137}Cs activity ratio -0.001 ± 0.003.

DISCUSSION

The known sources of supply of artificial radionuclides to the Arctic Ocean in the region of the LOREX station may be listed as follows:

1. Direct Fallout (largely stratospheric) to the surface of the Arctic Ocean.
2. North Atlantic Ocean water inflow through Fram Strait and to the Siberian shelf.
3. North Pacific Ocean water flowing through the Bering Strait and Chukchi Sea.
4. Run-off and River Supply from the land masses that border the Arctic Ocean.

As we suggested earlier, it is reasonable to attempt to identify each of these by some aspects of its concentrations or ratios of the radionuclides we have measured, as well as of the time courses of the applicable delivery patterns. These aspects can be summarized for each of the above source terms as follows:

1. Direct Stratospheric Fallout should have been characterized by a ratio ^{137}Cs to ^{90}Sr very close to 1.45 (BOWEN *et al.*, 1974, 1980), by a ratio $^{239,240}Pu$ to ^{137}Cs about 0.012 (HARLEY, 1975), and by a ratio ^{241}Am to $^{239,240}Pu$ that varied with time as discussed by LIVINGSTON *et al.* (1975b). About one quarter of the total direct fallout to northern hemisphere points arrived in the period 1956–1960, and about three quarters in the period 1962–1966; after 1966 annual fallout increments ranged 2% or less of the accumulation at the beginning of each year (VOLCHOK and TOONKEL, 1974).
2. North Atlantic Ocean water exhibited the fallout ratios of ^{137}Cs to ^{90}Sr (BOWEN *et al.*, 1974) of about 1.45. Soluble nuclide concentrations in its upper layers did not diminish in parallel with the reduction in rates of fallout delivery (BOWEN *et al.*, 1969). Particle associating nuclides like Pu or Am did leave the upper water layers, Am more rapidly than Pu, diminishing their ratios to ^{137}Cs.

   In 1957, a new source began to release artificial radioactivity to the high latitudes of the North Atlantic. This resulted from northward transport of the stream of liquid low-level wastes from European nuclear fuel reprocessing activities, especially the U.K. fuel reprocessing plant at Windscale in Cumbria (LIVINGSTON *et al.*, 1982a). Early releases were small, but in 1969–70 the annual output of ^{137}Cs from this source exceeded 10% of the fallout inventory at latitudes north of 60°N in the Atlantic; in the period 1970–72 annual ^{137}Cs output continued high, at 20–25% of the fallout inventory, and in 1974–78 increased again, approaching 100% of the fallout inventory, and even, in 1975, exceeding it. During the whole period 1969–78 the Windscale contribution of ^{137}Cs amounted to about four times the fallout contribution in the Atlantic north of 60°N; other tracers were also contributed, ^{90}Sr in an amount equal to that from fallout, and $^{239,240}Pu$ and ^{241}Am in amounts greatly exceeding the fallout delivery. Furthermore, as discussed elsewhere by LIVINGSTON *et al.* (1982a) the Windscale stream contained both elapsed-time indicators and event markers in the forms of variously changing isotope or nuclide ratios. We return to this point below.
3. North Pacific Ocean Water has exhibited fallout ratios of ^{137}Cs to ^{90}Sr, but substantially elevated ratios of $^{239,240}Pu$ to ^{137}Cs (BOWEN *et al.*, 1980). The flow through the Chukchi Sea may have been characterized by large fluctuations of nuclide concentrations (BOWEN and SUGIHARA, 1964), and may also have been substantially purged of Am and some Pu, in the process of passing over shallow shelves in the vicinity of the Bering Strait.
4. Run-off and River Supply should have been characterized by ratios ^{137}Cs to ^{90}Sr much lower than those in fallout (BOWEN *et al.*, 1974), and to be even more depleted in Pu or Am. Earlier work has shown that coastal ocean waters rather generally show ratios ^{137}Cs to ^{90}Sr ranging about 1 (BOWEN *et al.*, 1974).

Estimates of the probable "ages" of the water masses represented in the LOREX profile, and of the sources and pathways of artificial radionuclides to the sampling site, can be made from this summary of the properties of the various sources of artificial radionuclides and from the very small amount of relevant data from analyses of other Arctic Ocean samples. These estimates can best be organized separately by water mass, as shown in Table 1. For convenience in visualization, the data are shown graphically in Fig 2.

Another approach to testing the various hypotheses set out below is by way of calculation of the water column inventories of the various nuclides. In the present case these calculations have been made difficult because of the limited number of sample depths available for analysis in each water mass. Because of this limitation, the values calculated should be assigned rather large uncertainties. In Table 2 are set out our best estimates of the artificial nuclide inventories at the LOREX station. In the water column above 1250 m, the calculations assumed that the measurements on each sample represented the average concentrations in the layer defined by the mid-points of the separations between sampling depths; these depth intervals are shown in the third column of Table 2. Although they do not exactly correspond to the hydrographically defined depths of the various layers, our uncertainty in interpolation between the sampling points made this approach seem the best compromise. Furthermore, examination of the distribution of values estimated shows that, in the upper water column, most of the estimates are not very sensitive to variations in these assumptions. Below 1250 m the situation is a little trickier. In recognition of the differences in nuclide content between the two very similar samples from 500 m and 1000 m, and the very different one from 1500 m, we have used the terms Atlantic Water (AW) for the first two, and Upper Deep Water (UDW) for the 1500 m representation. Following our understanding of the discussion by AAGAARD (1981), we have assumed that the 1500 m sample, collected over the Fram Basin, represented a layer between 1250 and 1750 m. Also, the 2500 m sample in this basin was taken to represent all the water below 1750 m. Over the Makarov Basin, however, we have assumed that the "1500 m water" had been cut off, close to this depth by passage over the Lomonosov Ridge (sill depth about 1300 m), and that from 1500 m to the bottom of this basin at 4000 m, the water resembled our 3000 m sample. It is apparent that, unlike the situation of the shallower

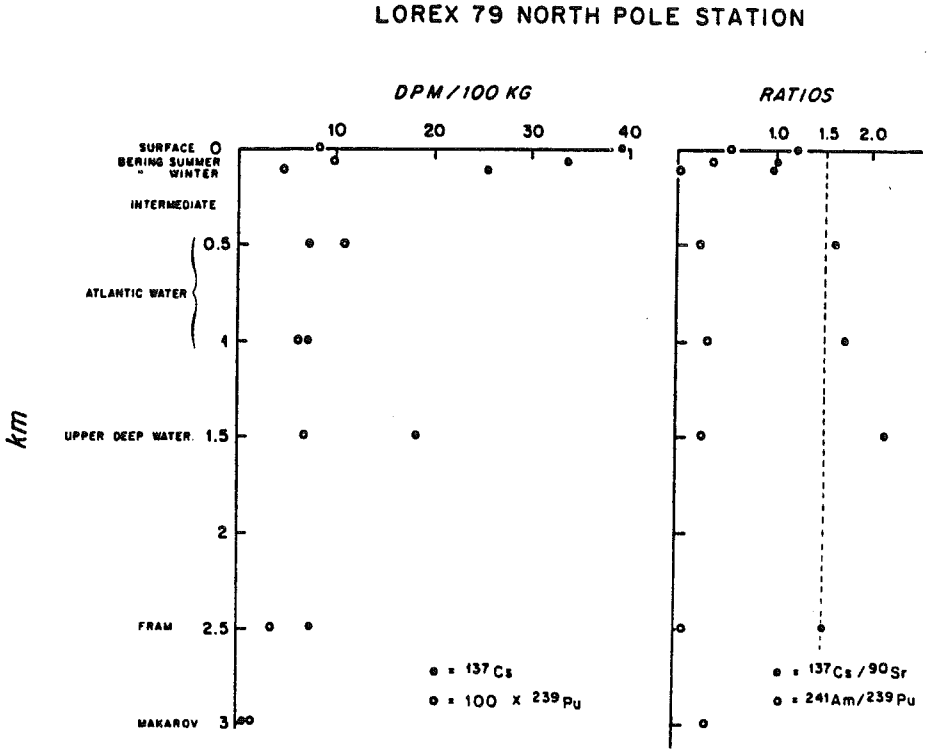

FIG. 2. Radionuclide concentrations and ratios measured in water sampled from various water masses from the LOREX site. The vertical dotted line in the ratio plot is the ^{137}Cs to ^{90}Sr ratio characteristic of nuclear fallout (1.5).

layers, these assumptions strongly influence the respective deep water inventory estimates, and the nature of the assumptions, as well as their unreliability, must be kept in mind in considering these values.

Now we proceed to consider each water mass sampled, in terms of what the radionuclide tracer data can be taken to suggest.

Surface mixed layer

BOWEN and SUGIHARA (1964) reported ^{90}Sr concentrations in low-salinity samples taken close under the Arctic ice in 1957 (2.3 dpm per 100 l) and in 1958 (5.3 dpm per 100 l). Unfortunately at that time these authors were unable to report data for ^{137}Cs or

TABLE 2
RADIONUCLIDE INVENTORIES AT LOREX STATION

Water Mass	Sample Depth (m)	Depth Interval Integrated (m)	Inventories in mCi/km^2 ^{90}Sr	^{137}Cs	$^{239,240}Pu$	^{241}Am
Surface Mixed Layer	2	0-39	5.6	6.9	0.014	0.005
Bering Sea Water	75	40-92	7.9	8.0	0.023	0.007
	110	93-305	24.5	24.5	0.043	0
Atlantic Water (Upper)	500	306-750	9.0	14.6	0.220	0.050
	1000	750-1250	9.9	14.9	0.137	0.043
INVENTORY TOTAL ABOVE 1250 m:			56.9	68.9	0.437	0.105
Upper Deep Water						
over FRAM Basin	1500	1250-1750	19.6	42.1	0.153	0.041
over MAKAROV Basin	1500	1250-1500	9.8	21.1	0.076	0.020
Arctic Bottom Water						
FRAM Basin	2500	1750-4000	48.7	74.1	0.356	0.030
MAKAROV Basin	3000	1500-4000	6.8	10.1	0.14	0.045
WATER COLUMN INVENTORY:						
FRAM Basin			125.2	185.1	0.946	0.176
MAKAROV Basin			73.5	100.1	0.653	0.170

for Pu, so no ratio information is available. If the ^{90}Sr in these samples originated from direct fallout accumulation, without additional input *via* advection or loss *via* downmixing, a prediction could be made of the concentration expected by the time of the LOREX sampling in 1979. This would follow from the pattern of annual fallout delivery by taking the *amount* delivered by 1957–58 as a fraction of the total delivered by 1979. From such a pattern as reported by NOSHKIN and BOWEN (1973) it may be calculated that, of the total deposit by 1970 (after which the total deposited fallout on the earth's surface increased minimally) less than 20% was delivered by mid-1958. Adjustment of the above 1957–58 ^{90}Sr concentrations by this factor leads to a predicted 1979 concentration in the range 12–27 dpm per 100 l. Although less than measured in the LOREX station 2 m sample, this prediction of ^{90}Sr concentration from a hypothesis of direct delivery is at first sight not completely impossible. On the other hand, assuming that the low salinity parts of the East Greenland and Canadian Archipelago Currents represent outflow of the near-surface waters of the Arctic Ocean, short residence times of this layer can be calculated. For example, if the low salinity outflow is taken to be 4×10^6 m^3/sec (WORTHINGTON, 1970) and the Arctic near surface layer volume as 10^7 m^3 (DORSEY and PETERSON, 1976), a residence time of eight years is obtained by dividing the volume by the outflow. This is not greatly different from the value of ten years estimated by AAGAARD and COACHMAN (1975) or of eleven years by OSTLUND (1982). These show the importance, in the Arctic Basin, of advection. As MOORE *et al.* (1983) note, advection is indicated as the source of silicate or phosphate in this water mass, indirectly by mixing upward from the nutrient-rich Bering Sea layer; consideration of the delta ^{18}O of the surface layer samples also suggests an important advection, as far as the LOREX station, of meteoric water delivered as run off at the edges of the basin. Advection is suggested also by the low ratio ^{137}Cs to ^{90}Sr (1.24 *vs.* the 1.45 characterizing fallout), and probably by the rather high concentrations of $^{239,240}Pu$ and ^{241}Am. The first point was addressed at some length in an earlier discussion (BOWEN *et al.*, 1974) that concluded that a number of processes must act together in near-shore ocean waters to reduce the ratio ^{137}Cs to ^{90}Sr from the fallout value to about 1. These processes have been shown to affect the upper water column off the west and east coasts of Greenland (BOWEN *et al.*, 1974; AARKROG and LIPPERT, 1977; AARKROG *et al.*, 1979), and we discuss below some other relevant evidence. Our belief is that the LOREX near-surface mixed layer must have been advected through near-shore environments, at least in part, to have reached the observed low ratio of ^{137}Cs to ^{90}Sr. Half of the ^{137}Cs and ^{90}Sr could thus have been supplied at the fallout ratio by direct delivery, to be mixed with advected and meteoric water of ^{137}Cs to ^{90}Sr ratio 1 or even less. Our data in this respect are quite consistent with the conclusion of MOORE *et al.* (1983) that "meteoric water makes a major contribution to the low salinity layer". The absence of measurable ^{134}Cs in this layer, noted above in the Results section, shows it to have little or no representation of recent Norwegian Sea surface water. At high latitudes the Norwegian and Greenland Seas have been receiving ^{134}Cs-containing wastes of Windscale origin (LIVINGSTON *et al.*, 1982b).

Bering Sea water layers

Although the temperature anomaly associated with the Bering Sea Summer Water was not observable at the LOREX station, we may, however, reasonably attribute both of our high-Si samples (75 m and 110 m depths) to N. Pacific Ocean water flowing through the Bering Sea and into the Arctic Ocean. Rather less information than one would like is available concerning artificial radionuclides in this source term, but the data available support some interesting inferences concerning travel times and geochemical history. BOWEN and SUGIHARA (1964) reported a few relevant analyses of water from the Chukchi Sea (*cf.* Fig. 1):

Aug. 30, 1959 Salinity 32.3‰;
^{90}Sr 21 ± 1 dpm/100 l

Aug. 1960 Salinity —;
^{90}Sr 35 ± 1.6 dpm/100 l

May 1962 Salinity 32.2‰;
^{90}Sr 54 ± 5 dpm/100 l.

BOWEN *et al.* (1980) reported a couple of other relevant samples:

Oct. 1973 Salinity 32.6‰;
^{137}Cs 39.5 ± 0.4; ^{90}Sr 23.6 ± 0.8 dpm/100 l

Oct. 1973 Salinity 33.07‰;
^{137}Cs 31 ± 1.2; ^{90}Sr 21.5 ± 0.9 dpm/100 l.

The first of these 1973 values represents N. Pacific surface water just south of the Aleutians, the second just north at 53°07'N. Both the curve of change with time of N. Atlantic Ocean surface water ^{90}Sr concentrations (BOWEN *et al.*, 1969) and the available Pacific Ocean data (VOLCHOK *et al.*, 1971) suggest that during the period 1962–72 N. Pacific surface water showed neither ^{137}Cs nor ^{90}Sr concentrations as low as those that characterized the 75 or 110 m samples of Table 1. The 75 m sample could well represent water, somewhat altered during advection as discussed below, passing the Bering Sea during the early 1960's or after mid-1973. The somewhat lower concentrations in the 110 m sample we believe are likely to reflect, as does the higher salinity, mixing during advection with an underlying water layer similar in

properties to the 500 m sample from the top of the Atlantic water. Unfortunately we do not yet have any samples either from the silicate maximum of the Bering Sea water, about 39 μg at m per l a little shallower than the 110 m sample of Table 1 (MOORE, 1981), or from the "Intermediate Layer" (between the Bering Sea Winter Layer and the top of the core of Atlantic Water), so the radionuclide properties of the water available for mixing remain conjectural.

The ratio ^{137}Cs to ^{90}Sr in the "Bering Sea water" should have approximated 1.5 as the water entered the Bering Sea (BOWEN *et al.*, 1980 and above). We believe a substantial history of advection through a coastal water regime would have been required to reduce this ratio to the low values observed in these samples. The Bering and Chukchi Seas almost certainly would provide the right conditions, but no confirming radionuclide data are available. The concentrations of Pu and of Am that were found in these two samples present some problems of interpretation. One might have expected Pu concentrations to be reduced well below those observed, by removal to the sediments, during passage through these shallow seas; the samples actualy contain 100% or 50% of the Pu that was found at 70 or 80 m at the two northernmost GEOSECS stations (BOWEN *et al.*, 1980). This observation is, of course, perfectly in accord with the hypothesis that much of the 70–80 m Pu at these stations is in a chemical/physical form that is not rapidly removed *via* particle association, as has been shown to be characteristic of the mid-depth Pacific high-Pu layer (BOWEN *et al.*, 1980). Like the 2 m sample, the 75 m LOREX sample, however, contained significantly more ^{241}Am than would be expected in a 1979 sample contaminated only by fallout from the 1961–63 test series (LIVINGSTON *et al.*, 1975b). Since the possibility of local supply of actinides by ice melting seems remote, their supply in the meteoric runoff water advected to the central Arctic Ocean seems the only remaining scenario. The data otherwise appear quite consistent with our preconception that during a long passage through very shallow seas, some of the actinides that were present in this current when it left the Pacific should have been lost to the sediments, Pu less effectively than Am in accordance both with the higher tendency for sediment association of Am, and the greater tendency for resolubilization of sediment Pu (BOWEN *et al.*, 1980). The fact that ^{241}Am supplied on sinking particles has not yet penetrated to 110 m depths must be an indication of the relative inefficiency of particle transport processes under the ice and the major role that horizontal advection plays in the transport of this water mass.

Evidence that the water represented by the 110-m sample can have had only a very few years to circulate since losing its Am (presumably during passage through the Bering and Chukchi Seas) is offered directly by the measured ^{241}Am: the zero concentration measured is distinctly different from the 0.005 dpm per 100 kg that would result from ingrowth, in as little as six to seven years, at the measured ^{239,240}Pu concentration if fallout ratios of ^{241}Pu to ^{239,240}Pu (LIVINGSTON *et al.*, 1975b) apply. This seems to counter the possibility of the LOREX Bering Sea water having left the N. Pacific as early as mid-1960, leaving only the mid-1973 (or later) possibility open. The higher salinity and Si in the 110-m sample are consistent with its representing largely Bering Sea winter water, and the lower salinity and Si of the 75-m sample with its representing largely summer water. The data are quite consistent with most of the observations and hypotheses of COACHMAN and BARNES (1961) concerning the contribution of Bering Sea water to the Arctic Ocean. Certainly the reduced ratio ^{137}Cs to ^{90}Sr, and the relatively high concentration of both these solute nuclides, are as we would have expected from their hypotheses. Unfortunately, the adoption of their estimate, 10–20% Bering Sea water to 80–90% intermediate shelf water (from the Siberian shelf), essentially wipes out our estimation of the date of passage of our samples through the Bering Strait; too little information is available concerning the possible range, and changes with time, of the concentrations of ^{137}Cs and ^{90}Sr in the major component of such a mixture. On the other hand, the Pu and Am concentrations we measured could be consistent with their (1961) estimated mixture "10–20% Bering Sea water and 80–90% Siberian shelf water" only if the latter is both richer in Pu than other shelf waters we have sampled, and more depleted in Am. More data will be needed to resolve this dilemma.

Atlantic and Upper Deep Water

The radionuclides in the two samples of Atlantic water, at 500 m and 1000 m, and in the 1500 m Upper Deep Water sample, offer a coherent but most surprising pattern. Rather than showing highest values at 500 m, the "core" of the Atlantic water layer (MOORE *et al.*, 1983), both ^{137}Cs and ^{90}Sr exhibit a strong concentration maximum at 1500 m, below the "Atlantic water," in the region which we have called the Upper Deep Water. Furthermore, the ratio of ^{137}Cs to ^{90}Sr at the peak is one we regard as reflecting Windscale effluent origin of relatively recent date, post-1969 certainly. LIVINGSTON *et al.* (1982a) have discussed at some length the use of nuclide ratio changes in the Windscale effluent stream as event-markers. It is true that the ratio observed, 2.16, lies within the range reported by BOWEN *et al.* (1974) for fallout-contaminated water samples from the open Atlantic Ocean; theirs was a relatively early data set, however, and more recent series of analyses, especially at nuclide concentrations as high as the LOREX samples show, have been much more closely clustered around the fallout mean, as BOWEN *et al.* (1980)

reported for their large series of 1973–74 Pacific Ocean analyses. Especially reinforced by the higher than fallout ratios observed at 500 m and 1000 m, we are confident that the high ratio at 1500 m is real and requires Windscale origin as the explanation. Further evidence that this water has recently had a prolonged experience as surface water comes from the high ^{14}C concentration reported in the same sample by University of Miami ($\Delta^{14}C$ of only −10.8‰, compared to −40 to −50 in the other Atlantic Water samples). The available tritium data, from nearby but not identical samples, do not show evidence of any anomaly in the 1400–1600 m depth ranges (UNIVERSITY OF MIAMI, 1980; OSTLUND, 1982), but samples that remain to be analyzed may still contribute. It is especially unfortunate that the ^{3}H data refer to different samples, collected at different depths and at different times along the ice-station's trajectory. Such separation makes it difficult even to use them to argue about the lateral extent of labeling in the layers examined. The shallower details of the tracer concentration profiles (Table 1 and Fig. 1) do appear to preclude this 1500 m sample being affected by either a pre-trip or sampler leakage during retrieval, two problems always in the minds of oceanographers taking large-volume samples; no water was collected shallower than 1500 m capable of providing anomalously high ^{137}Cs to ^{90}Sr ratios.

As LIVINGSTON *et al.* (1982a) summarized, the Windscale discharges in 1957, 1958 and 1961 were characterized by ratios of ^{137}Cs to ^{90}Sr of 2 or more, but the amounts discharged were not large compared to the annual delivery increments resulting from world-wide fallout; they concluded that the isotope ratio signals in these early Windscale discharges probably had been observed in the northwestern North Sea but were unlikely to have been observable much further downstream from their source. Beginning in 1969, however, as described above, the Windscale tracer signal became abruptly large enough to be readily detected; this has been consistently the case in each year since. The 1500 m water at the LOREX station is likely to have derived its high ratio of ^{137}Cs to ^{90}Sr from Windscale effluent. By assuming that the 500-m and 2500-m samples, essentially identical in respect to these two nuclides, (and to ^{3}H and ^{14}C) represent the "Windscale-free N. Atlantic signal", and that the 1500 m sample represents some simple mixture of this with Windscale contaminated water, the ratio ^{137}Cs to ^{90}Sr in the latter can be calculated. Dilution of a Windscale contaminated surface water mass by one and three volumes of "Windscale-free" N. Atlantic water in the Fram Basin would require the surface water to show ^{137}Cs concentrations of 29 and 52 dpm per 100 kg and ^{137}Cs to ^{90}Sr ratios of 2.3 and 2.5 respectively. In 1972, Barents Sea surface water was labelled with ^{137}Cs in this concentration range but at a ^{137}Cs to ^{90}Sr ratio around the fallout value of 1.5 (KAUTSKY, 1980). By 1979, this water was labelled with ^{137}Cs at substantially higher ^{137}Cs concentrations and ratios ^{137}Cs to ^{90}Sr (KAUTSKY, pers. commun.). This implies that the recent surface component of the 1500 m LOREX sample was in the Barents Sea in the time interval between 1973 and 1978. The latter part of this time period is consistent with the transport to the Barents Sea of Irish Sea water labelled with the increased Windscale ^{137}Cs releases in the 1970–72 interval (LIVINGSTON *et al.*, 1982a). So we envisage a scenario involving about five years travel time from the Irish Sea to the Barents Sea followed by a further three years for travel from the surface Barents Sea to the point sampled at 1500 m in 1979 at the LOREX site. In 1974 and for several years thereafter, the ^{137}Cs to ^{90}Sr ratio in the Windscale releases exceeded 10 and the ^{137}Cs released annually became very large, so we would expect an even more striking effect when post-1973 Windscale effluent arrives at depth in the Arctic.

In their discussion of the circulation of Atlantic water in the Arctic Ocean, COACHMAN and AAGAARD (1974) refer to its relatively rapid transit of the Arctic basin—at flow speeds of 1 to 3 cm sec^{-1} the water would take about three years to travel from north of Spitsbergen to the LOREX site. This length of time can be regarded as being consistent with the timeframe set by the Windscale ^{137}Cs signal for transport from the Barents sea to the LOREX site—the 1970–72 increase in ^{137}Cs release rate would not have reached the Barents Sea until 1976 at the earliest. So the Windscale tracer signal detection at the LOREX site in 1979 establishes an upper limit of three years for transport from the Barents Sea to the LOREX site at a depth of 1500 m.

Arctic Bottom Water

The two samples of Arctic Bottom Water, at 2500 m from the Eurasian Basin and at 3000 m from the Amerasian Basin (Fig. 2) exhibit unexpected differences in their concentrations of soluble radionuclides. In the Fram Basin (Eurasian) these concentrations are as high as those of the Atlantic Water. This was also true of the ^{3}H data (OSTLUND, 1982). The very low tracer concentrations in the Makarov Basin (Amerasian) are consistent with the high values in the Fram Basin only if the inferred pattern of supply of deep water from the latter into the former basin (AAGAARD, 1981) represents very small volume, or sporadic, incursion. From AAGAARD's (1981) analysis of the current meter and salinity data from LOREX, we would expect that detailed large-volume sampling about the Lomonosov Ridge would reveal a plume of deep Arctic Bottom Water, in the Makarov Basin, that would be easily identified by its radionuclide concentrations as having come from the Eurasin Basin. The shape and volume of such a plume, plus the distributions within it of tracer concentrations, would clarify greatly, we believe, the patterns and

rates of deep water movement across the Lomonosov Ridge.

Pu concentrations in these two deep water samples are substantially lower (20–50%) than those we have measured in the Greenland Sea at comparable depths—and at ^{137}Cs concentrations similar to the deep Fram Basin sample. The low values of Pu and Am in the Makarov Basin sample show that delivery processes involving particle sinking are not very active under the Arctic ice. On the other hand, the low values of the Fram Basin sample, when viewed in comparison with the substantial ^{137}Cs or ^{90}Sr concentrations in this sample, require that the transuranics must have been lost during transport to this location and depth—perhaps during passage over a shelf or slope region in which significant vertical fluxes of particles are found.

Inventory considerations: ^{137}Cs

As discussed above, for inventory calculation it was assumed that the available data from water samples taken at 1000 m and shallower represent equally both sides of the Lomonosov Ridge, but that the waters of the Fram and Makarov Basins are represented differently by the respective deeper samples. On these bases, as shown in Table 2, the water column inventory in the Fram Basin approximates 185 mCi $^{137}Cs/km^2$, and that in the Makarov Basin, 100 mCi $^{137}Cs/km^2$, only slightly exceeds half that value. When compared to estimates of fallout delivery to the area north of 80°N, these inventories are enormous indeed: SEYMOUR *et al.* (1975) put the direct delivery of fallout to this area at about 8 mCi $^{90}Sr/km^2$, corresponding to about 12 mCi $^{137}Cs/km^2$; it is well known that high latitude estimates of fallout are based on very little data, but few would entertain seriously the thought they are in error by factors much exceeding two. Clearly the first implication of this great excess of the inventory estimated from water column data over the delivery in fallout must be to emphasize the overwhelming significance of advection in the delivery of artificial radionuclides to the Arctic Ocean. The importance of advection has, of course, been argued in each of our earlier discussion sections; these inventory data neatly put the cap on those arguments.

Inventory considerations: Actinides

Inventory estimates of $^{239,240}Pu$ and ^{241}Am in the various Arctic water masses (Table 2) may be used to address the question of the sources of supply of these nuclides. Arguments presented earlier, based on near-surface concentrations and ratios, raised the possibility of several contributing processes and sources. On the other hand, when their completed inventories in the whole water column, in either basin, are compared with their expected delivery by direct fallout, substantial water column excesses of these nuclides are evident. The fallout delivery of Pu to this area derivable from conversion of 8 mCi/km^2 ^{90}Sr delivery, estimated (SEYMOUR *et al.*, 1975) using the fallout $^{239,240}Pu$ to ^{90}Sr ratio of 0.018 (HARLEY, 1975), is 0.14 mCi/km^2. This is substantially less than the 0.95 and 0.65 mCi/km^2 calculated for the Fram and Makarov basins respectively. We take this to mean that advection must be the major source of supply of Pu to the Arctic water column as it is for ^{137}Cs and ^{90}Sr. The ratios of the inventories of ^{241}Am and $^{239,240}Pu$ are sufficiently close to their ratios in fallout (LIVINGSTON *et al.*, 1975b) to support the conclusion that advection also supplies much Arctic ^{241}Am.

SUMMARY AND CONCLUSIONS

As we have usually observed to be the case in an initial examination of radiotracer data from a new oceanic environment, the LOREX radionuclide data raise more questions than they answer. They do fit into a good proportion of the widely held views concerning water supply to and circulation within the Arctic Ocean. We have considered the implications of our data set often in more detail than the sampling density can possibly justify; our purpose in this has been to illustrate how apt and how powerful a tool is offered to physical oceanographers by measurements of this sort. The effort of collecting the required samples is very substantial, as is the effort of making the analyses. We hope that the results will encourage others to begin establishing the wide ranging net of sampling sites that will be needed to exploit the information available from the tracer distributions that now obtain, and from the changes to be anticipated in the next decade.

The data lead to the following explicit conclusions:

a) The time scales of water movement to the center of the Arctic Ocean from the Bering Strait, from the Norwegian Coastal Current, from the Norwegian Sea, or from the surface Atlantic Ocean are consistent both with a residence-time estimate of about eight to eleven years for surface water, and with the short circulation time estimated for the Atlantic water in the Arctic basin (COACHMAN and AAGARD, 1974).

b) A substantial incursion of Windscale effluent labelled water has travelled from the Irish Sea and penetrated to 1500 m in the Arctic Ocean, where it is mixing with fallout-labelled Atlantic water lying above it, in the short time of about eight years.

c) Concentrations of soluble fallout tracers in the deep water of the Fram Basin indicate it receives an active and rapid supply, by downward advection, of Atlantic Ocean surface water; transfer of this water to the Makarov Basin is slow.

d) In most layers of the Arctic Ocean, with the possible exception of the surface mixed layer, a large input by advection of Pu and Am is required to explain their water column inventories.

Acknowledgements—In acknowledging the assistance of Malcolm Lowings in collecting the samples on which we report, it is appropriate that the first three authors acknowledge the activity of the fourth author (R. M. Moore) in planning the program, organizing the cooperation, and carrying out the work on the ice; especially the last required an expertise and vigor not possessed by the rest of us. The radiochemical analyses at WHOI depended on the skill and interest, especially, of L. Clarke, W. R. Clarke, T. E. Desrosiers and D. R. Mann. The LOREX program was organized and supported by the Physics Branch of the Department of Energy, Mines and Resources, and by the Polar Continental Shelf Project, both of the Canadian government. The radiochemical analyses and the preparation of this report were supported by the U.S. Department of Energy under contract DE-AC02-83ER60172 and earlier contracts and by the U.S. National Science Foundation under grant OCE-8300491; Kupferman's participation was supported by the U.S. National Science Foundation under grant OCE-7910542. We are grateful for the support of these agencies. This is Contribution 5704 from the Woods Hole Oceanographic Institution and Number 11 of the LOREX program.

REFERENCES

AAGAARD K. (1981) On the deep circulation in the Arctic Ocean. *Deep Sea Res.* **28a**, 251–268.

AAGAARD K. and COACHMAN L. K. (1975) Toward an ice-free Arctic Ocean. *EOS* **56**, 484–486.

AARKROG A. and LIPPERT J. (1977) Environmental Radioactivity in Greenland in 1976. Riso Rept. R-405 (Riso National Laboratory, Denmark).

AARKROG A., HANSEN H. and LIPPERT J. (1979) Environmental Radioactivity in Greenland in 1978. Riso Rept. R-405 (Riso National Laboratory, Denmark).

BOWEN V. T. and SUGIHARA T. T. (1964) Fission product concentrations in the Chukchi Sea. *Arctic* **17**, 198–203.

BOWEN V. T., NOSHKIN V. E., VOLCHOK H. L. and SUGIHARA T. T. (1969) Strontium-90: concentrations in surface waters in the Atlantic Ocean. *Science* **164**, 825–827.

BOWEN V. T., NOSHKIN V. E., VOLCHOK H. L., LIVINGSTON H. D. and WONG K. M. (1974) Cesium 137 to strontium 90 ratios in the Atlantic Ocean 1966 through 1972. *Limnol. Oceanogr.* **19**, 670–681.

BOWEN V. T., NOSHKIN, V. E., LIVINGSTON, H. D. and VOLCHOK H. L. (1980) Fallout radionuclides in the Pacific Ocean; vertical and horizontal distributions, largely from GEOSECS stations. *Earth Planet. Sci. Lett.* **48**, 411–434.

COACHMAN L. K. and BARNES C. A (1961) The contribution of Bering Sea water to the Arctic Ocean. *Arctic* **14**, 147–161.

COACHMAN L. K. and AAGAARD K. (1974) Physical oceanography of Arctic and Subarctic Sas. In *Marine Geology and Oceanography of the Arctic Seas* (ed. Y. HERMAN) pp. 1–72. Springer Verlag. New York.

DORSEY H. G. and PETERSON W. H. (1976) Tritium in the Arctic Ocean and East Greenland current. *Earth Planet. Sci. Lett.* **32**, 342–350.

HARLEY J. H. (1975) Transuranium elements on land. In *Energy Research Development Administration, Health and Safety Laboratory, Environmental Quarterly Rept. HASL-291*, pp. I-104–I-109.

KAUTSKY H. (1980) Distribution of radioactive fallout products in the water of the North Atlantic and Barents Sea during the year 1972. In *Isotope Marine Chemistry* (ed. E. D. GOLDBERG), Chap. 2, pp. 9–23. Uchida Rokakuho Pub. Co. Ltd., Tokyo, Japan.

LIVINGSTON H. D., MANN D. R. and BOWEN V. T. (1975a) Analytical procedures for transuranic elements in seawater and marine sediments. In *Analytical Methods in Oceanography, Advances in Chemistry Series No. 147* (ed. T. R. P. GIBB JR.), pp. 124–138. Amer. Chem. Soc., New York.

LIVINGSTON H. D., SCHNEIDER D. L. and BOWEN V. T. (1975b) ^{241}Pu in the marine environment by a radiochemical procedure. *Earth Planet. Sci. Lett.* **25**, 361–367.

LIVINGSTON H. D., BOWEN V. T. and KUPFERMAN S. L. (1982a) Radionuclides from Windscale discharges I: non-equilibrium tracer experiments in high-latitude oceanography. *J. Marine Res.* **40**, 253–272.

LIVINGSTON H. D., BOWEN V. T. and KUPFERMAN S. L. (1982b) Radionuclides from Windscale discharges II: Their dispersion in Scottish and Norwegian coastal circulation. *J. Marine Res.* **40**, 1227–1258.

MANN D. R. and CASSO S. A (1984) *In situ* chemisorption of radiocesium from seawater. *Mar. Chem.* **14**, 307–318.

MOORE R. M. (1981) Oceanographic distribution of zinc, cadmium, copper and aluminum in the central Arctic Ocean. *Geochim. Cosmochim. Acta* **45**, 2475–2482.

MOORE R. M., LOWINGS M. G. and TAN F. C. (1983) Geochemical profiles in the central Arctic Ocean: Their relation to freezing and shallow circulation. *J. Geophys. Res.* **88**, 2667–2674.

NOSHKIN V. E. and BOWEN V. T. (1973) Concentrations and distributions of long-lived fallout radionuclides in open ocean sediments. In *Radioactive Contamination of the Marine Environment*, pp. 671–686. IAEA, Vienna.

OSTLUND H. G. (1982) The residence time of the freshwater component of the Arctic Ocean. *J. Geophys. Res.* **87**, 2035–2043.

SEYMOUR A. H., BOWEN V. T., CALKINS J., FOREMAN R. E., FORSTER W. O., HARRISON F. L., OPHEL I. L., RICE T. R., SOLDAT J. F., VOLCHOK H. L. and BURROUGHS R. H. (1975) Aquatic environment. In *Long-Term Worldwide Effects of Multiple Nuclear Weapons Detonations*, pp. 102–161. NAS-NRC Washington.

UNIVERSITY OF MIAMI (1980) Lorex Tritium and Radiocarbon. Tritium Laboratory, Data Release 80-25 (Univ. Miami, Florida).

VOLCHOK H. L. and TOONKEL L. (1974) Worldwide deposition of Sr-90 through 1973. In *U.S. Atomic Energy Commission, Health and Safety Lab. Fallout Program Qtly. Summ. Rept. HASL-286*, pp. I-17–I-35.

VOLCHOK H. L., BOWEN V. T., FOLSOM T. R., BROECKER W. S., SCHUERT E. A. and BIEN G. S. (1971) Oceanic distributions of radionuclides from nuclear explosions. In *Radioactivity in the Marine Environment*, pp. 42–89. NAS-NRC, Washington.

WEBER J. R. (1979) The Lomonosov Ridge experiment: Lorex 79. *EOS* **60**, 715–721.

WONG K. M., NOSHKIN V. E. and BOWEN V. T. (1970) Radiochemical procedures for the analysis of strontium, antimony, rare earths, caesium and plutonium in seawater samples. In *Reference Methods for Marine Radioactivity Studies*. Tech. Rept. Series No. 118, pp. 119–127. IAEA, Vienna.

WORTHINGTON V. (1970) The Norwegian Sea as a Mediterannean Basin. *Deep Sea Res.* **17**, 77–84.

JOURNAL OF GEOPHYSICAL RESEARCH, VOL. 88, NO. C4, PAGES 2667–2674, MARCH 20, 1983

Geochemical Profiles in the Central Arctic Ocean: Their Relation to Freezing and Shallow Circulation

R. M. MOORE AND MALCOLM G. LOWINGS

Department of Oceanography, Dalhousie University, Halifax, Nova Scotia, Canada, B3H 4J1

F. C. TAN

Atlantic Oceanographic Laboratory, Bedford Institute of Oceanography, Dartmouth, Nova Scotia, Canada, B2Y 4A2

Temperature, salinity, nutrient, tritium, and oxygen isotope data collected during the Lomonosov Ridge Experiment along a drift track between the Makarov and Fram Basins over the Lomonosov Ridge are presented. The relationship of these quantities to the processes that maintain the halocline, in particular to the production of more saline waters by addition of brines formed during the freezing of seawater, is described. The results support the idea that the wide continental shelves of the Arctic Ocean play an important role in maintaining the halocline.

INTRODUCTION

Questions of particular interest pertaining to the Arctic Ocean relate to its important role as a region of heat exchange with the atmosphere, to the effects that ice cover has on mixing of the surface layer and on heat and gas exchange, to the unusual light cycle and its effect on productivity, and to the chemical and physical effects of freezing sea water. A comparison of this ocean, with its low productivity (at least during winter), with other oceanic regions should help to elucidate some of the effects of biological activity on marine chemistry, for example, trace metal cycling and speciation.

Aagaard et al. [1981] discussed the way in which the cold waters of the halocline which lie immediately below the surface mixed layer and extend to the top of the warm Atlantic layer could be produced on the wide continental margins surrounding the Arctic Ocean. The processes involve freezing with release of highly saline brines having a temperature close to the freezing point of surface sea water. This water flows over the shelves and into the central basin, sinking then to the appropriate density surface. The distributions of various chemical parameters will be affected in predictable ways by these processes.

As a part of the Lomonosov Ridge Experiment (LOREX), which ran from late March until the end of May 1979, a program was undertaken aimed at describing more accurately the hydrography of the central Arctic Ocean and studying the geochemistry of selected trace elements in this unusual environment. To this end, water samples were collected from a drifting ice station (LOREX satellite camp 1) for the measurement of salinity, silicate, phosphate, $\delta^{18}O$, trace metals [*Moore*, 1981, 1983], carbon-14, tritium, helium-3, caesium-137, caesium-134, strontium-90, plutonium, americium (H. D. Livingston et al., manuscript in preparation, 1983), alkalinity, and pH. Ice cores were collected to investigate the possibility of deducing the extent of temporal changes in the tritium content of the surface waters.

Paper number 2C1673.
0148-0227/83/002C-1673$05.00

During the period of sampling, April 13 to May 21 (days 103–141), the camp drifted from 88°40'N 139°50'W to 89°9'N 97°7'W. The drift track (Figure 1) extends from the Makarov Basin, a part of the Amerasian Basin with a water depth of ca. 4000 m, across the Lomonosov Ridge, where the depth decreased to about 1000 m, into the Fram Basin and depths of ca. 2500 m.

METHODS

Temperatures were measured using reversing thermometers on 1.7-l Niskin and 5-l Go-Flo bottles, and salinities were determined by using a portable Bissett-Berman inductively coupled salinometer.

Reactive silicate was determined spectrophotometrically by the method described by *Strickland and Parsons* [1972], involving a metol-reduced silicomolybdate complex. The determinations were normally carried out within about 24 hours of sample collection. Reactive phosphate was determined by the method of Strickland and Parsons, the samples being frozen immediately after collection and determined for phosphate within a few days. A Varian model 634 spectrophotometer was used for both of these analyses.

Measurements of $\delta^{18}O$ were made according to the methods given by *Tan and Strain* [1980], and tritium measurements were made by H. G. Ostlund [*Östlund*, 1982].

TEMPERATURE AND SALINITY

The first profile was sampled during the period April 16–29 (days 106–119) and was marked initially by very slow movement of the ice. The surface layer to a depth of about 50 m (Figure 2) is of low salinity, ca. 30 ‰, but fluctuations between 30.059 and 30.409 ‰ are apparent: because of the very few samples involved, no explanation will be proposed for this anomaly.

The second profile (Figure 2) comprises samples collected in the period May 3–15 (days 123–135). The near-surface salinities recorded during a period of more rapid ice movement (day 123) show an almost homogeneous layer to about 40 m. There is a slight decline in salinity from 30.152 ‰ at 5 m to 30.137 ‰ at 25 m consistent with an addition of salt at the surface: the salinity increases a small amount to 30.175 ‰ at 40 m. At about 40 m a steep rise in salinity begins (as much as 0.13 ‰ per m at 40 m) reaching 34 ‰ by 130 m. The

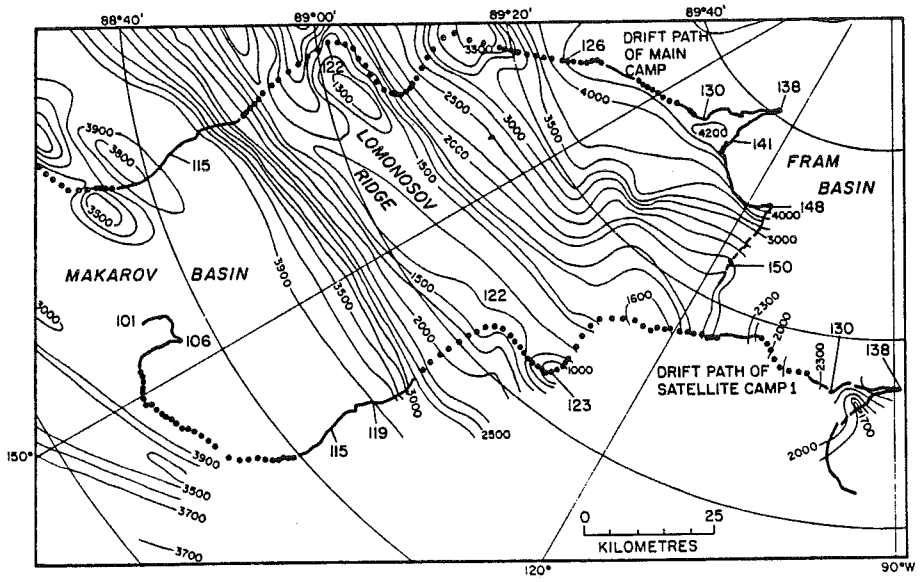

Fig. 1. LOREX satellite camp 1 drift path (Julian days indicated).

surface salinities reported here are at the lower limit of the range (30–32 ‰) reported by *Coachman and Barnes* [1962] and *Treshnikov et al.* [1977] for the central Arctic Ocean.

Between the bottom of the mixed layer and about 200 m the two profiles have a similar shape, but the salinities of the more westerly profile are displaced to greater depths by 10–15 m. At the core of the Atlantic water (ca. 450 m) as defined by the temperature maximum (Figures 3 and 4), the salinity was 34.89 ‰. Although there was generally good agreement between the salinities of different samples from similar depths in the deep water [*Aagaard*, 1981], there is some scatter at around 1500 m with salinities in the range 34.91–34.94. The salinities in this region have been dealt with in some detail by *Aagaard* [1981]. The number of salinity measurements below 2000 m is rather small, but they indicate that at least between 2000 and 2500 m the Makarov Basin salinities are slightly greater (by 0.01 ‰) than those of the Fram Basin at the same depth.

The T-S diagram (Figure 3) shows that the temperature remains constant and near freezing point to a depth of about 100 m, it then increases slightly over the depth range 100 to 160 m. At this point the diagram shows a marked inflection point and the temperature begins to rise sharply to a prominent maximum which is the characteristic of water originating in the Atlantic. This inflection point corresponds to that reported by *Kinney et al.* [1970] at *T3* (position ca. 80°–83°N, 160°W) at a depth of 230 m but at the same temperature and density, σ_T = 27.6. *Aagaard et al.* [1981] have pointed out that the waters lying between the mixed layer and the

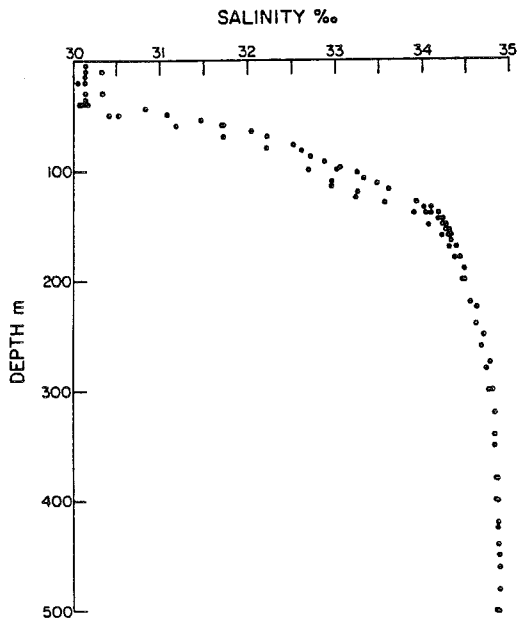

Fig. 2. Salinity versus depth at LOREX station. Solid circles, profile 1; open circles, profile 2.

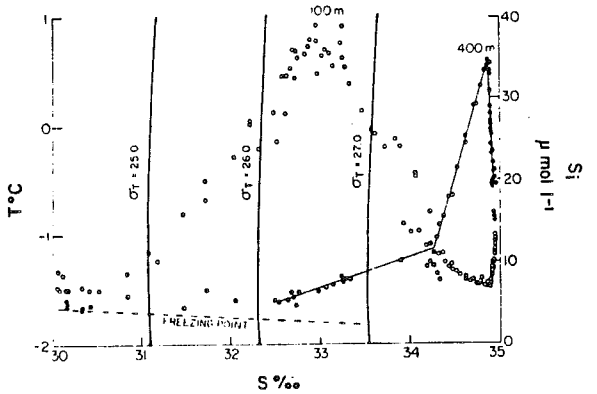

Fig. 3. Temperature-salinity relationship (solid circles) and silicate-salinity relationship (open circles) at the LOREX site; data from both profiles are included. Broken line indicates freezing point at atmospheric pressure.

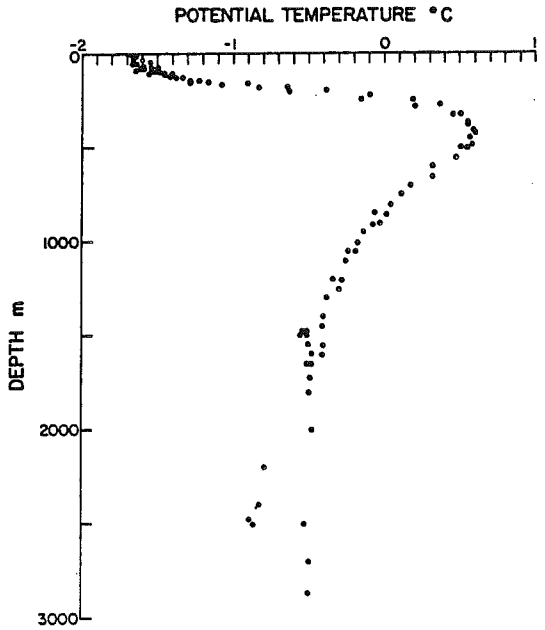

Fig. 4. Potential temperature, surface to 3000 m. Solid circles, profile 1; open circles, profile 2.

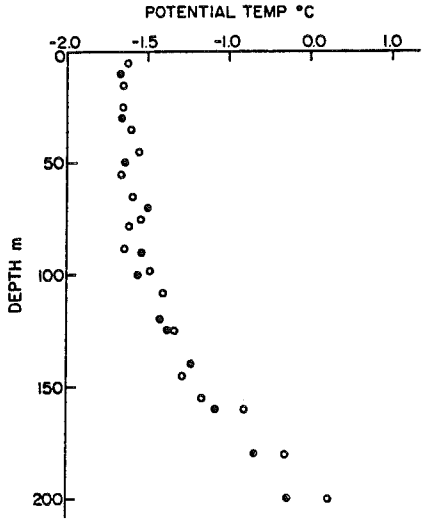

Fig. 5. Potential temperature, surface to 200 m. Solid circles, profile 1; open circles, profile 2.

temperature maximum cannot be produced simply by mixing surface water (0–50 m) and the relatively warm Atlantic water, and they suggest that these waters are produced over the shelves by a process involving freezing and salt addition. In the discussion of the silicate, tritium, and stable oxygen isotope ratios, it will be shown that their distributions are in accordance with this interpretation.

Coachman and Barnes [1962] give an alternative explanation of how cold saline water of the type described above may be formed by a process involving the submarine canyons of the continental slope which provide access for Atlantic water to the shelf regions where mixing with low salinity water and cooling occurs.

It is worth noting that the temperature maximum that is found in much of the Canada Basin in the halocline [*Coachman and Barnes*, 1961] is scarcely discernible at this region (Figures 3 and 5), at least during late winter.

Below 2000 m the two potential temperature profiles diverge (Figure 4), the higher temperatures occurring in the Makarov Basin. Data are available to 2900 m and 2500 m in the Makarov and Fram Basins, respectively; the temperature difference between the two basins becomes discernible at 2000 m and is marked at 2500 m.

SILICATE AND PHOSPHATE

While the T-S diagram (Figure 3) gives no indication of the presence of a well-defined water mass centered at about 100 m, the silicate profiles (Figures 6 and 7) show a well-defined maximum at this depth with silicon concentrations of almost 40 μmol l^{-1}. Beneath the peak the concentration falls rapidly, until at about 250 m it is near to the surface water value of 7 μmol l^{-1}. Below 800 m (Figure 7), concentrations increase again with depth reaching a maximum value of 13 μmol l^{-1} in the Makarov Basin at a depth of ca. 2300 m, then remaining almost constant to 3000 m (bottom depth 3380 m). At around 1800 m a marked divergence appears between the two profiles, the concentration of silicate decreasing with further increase in depth in the Fram Basin to a minimum at 2200 m followed by a small increase toward the bottom, which at this position was at a depth of 2600 m. The maximum in silicate at about 1700 m in the profile in the Fram Basin is apparently supplied by water in the Makarov Basin.

The silicate data, when plotted all together as in Figure 3, show considerable scatter; this is due to the presence of steep lateral gradients. If only those samples that were collected simultaneously are plotted together, well-defined relationships become apparent. In Figure 8, silicate values are plotted in this way against salinity for the depth range from just below the surface mixed layer to beneath the nutrient maximum.

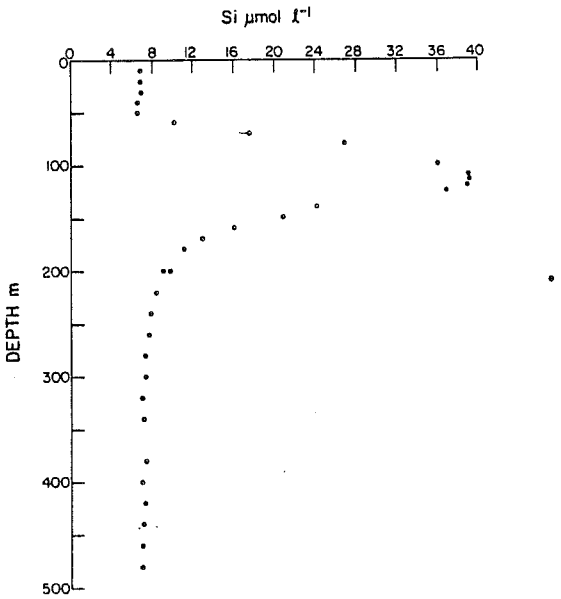

Fig. 6. Silicate against depth, surface to 500 m, profile 2.

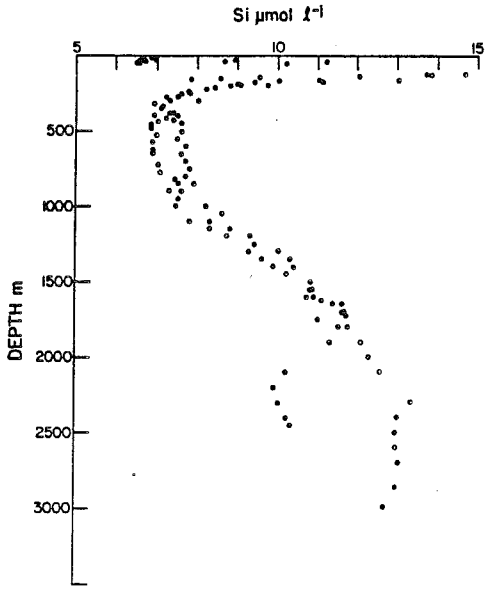

Fig. 7. Silicate against depth to 3000 m. Solid circles, profile 1; open circles, profile 2.

Considering first the waters lying between the surface mixed layer and the nutrient maximum, it is seen that generally the silicate and salinity values are appropriate to mixtures of waters from the nutrient maximum and water from just beneath the mixed layer rather than with the mixed layer itself. The Si-S characteristics of the mixed layer water (Figure 3) are appropriate to a mixture of the underlying layer with a fresh component, comprising meltwater and runoff, with the lower salinity of the surface layer demanding a freshwater component equivalent to only ca. 1% of its volume. Consequently, while the silicate concentration of runoff is unknown and could lie within a wide range [*Codispoti and Lowman*, 1973], the actual value will have little effect on the silicate concentration of the surface water. The water that lies immediately below the mixed layer may be expected to have a component of brine derived from freezing sea water. Figure 8 shows that the linear Si-S relationships above the nutrient maximum can have quite different slopes. The steeper slope can be accounted for by the introduction of water having similar Si concentration but higher salinity than that at 50 m, i.e., having a greater brine component than the ambient waters of similar silicate concentration. It will be seen that the tritium level of this water is also consistent with it being formed with a large brine component.

The water of the nutrient maximum is well established in the literature as coming from the Chukchi Sea region [*Kinney et al.*, 1970]. The elevated nutrient concentrations are then simply a reflection of the source of these waters in the Bering Sea; it is suggested here, however, that the prominence of this water type is the result primarily of the presence of the nutrient marker and that waters of similar salinity and temperature, hence density, are also produced in other continental shelf locations from where they flow to lie above, below, and perhaps to interleave the nutrient maximum water. It is worth noting that any waters that have been enriched in salinity by freezing in the marginal seas and flowed over the shallow shelf sediments to enter the central basin will have tended to accumulate nutrients that diffuse from the sediment surface. Such a process is likely to be enhanced in the Arctic Ocean on account of the unusually extensive continental shelves; it would be further enhanced by a strong density gradient near the bottom of the shelf seas, as this could confine the nutrients of sedimentary origin to a relatively thin layer of water and produce a correspondingly higher anomaly. Thus it may be the case that the nutrient-rich waters of the halocline have a wider origin than is immediately apparent. This would help to explain the observation that the temperature maximum which is normally attributed to water that has entered the Arctic Ocean from the Bering Strait during summer decays away more rapidly than the nutrient signal of the underlying water, the former being neutralized by cold water introduced at the same density, while the latter is weakened only to the extent that the waters added from other sources have lower nutrient levels.

Looking now at the waters lying beneath the Si maximum (Figure 3), it is seen that they mix with some water that is low in silicate and is considerably cooler than the Atlantic water. From Figure 9 it is seen that two Si profiles show a nonlinear Si-S relationship: the silicate maximum is one end-member, and the Atlantic water with its minimum silicate values constitutes a second component. There must be another component that produces this curvature, and one series of samples (Figure 9, crosses) clearly indicates a body of water having low Si concentrations but at a significantly lower salinity (34.3 ‰) than the Atlantic water (34.9 ‰) and also at much lower temperature. It is this water that marks the inflection point on the T-S diagram, the temperature rising steeply below this point (Figure 10). The similarity between this water and the Atlantic water in silicate concentration suggests that it may be modified Atlantic water. *Coachman and Barnes* [1962] have suggested how Atlantic water may be modified in temperature and salinity by a process involving submarine canyons on the continental shelves. *Aagaard et al.* [1981] have further commented on this process.

Phosphate data, available only for the Makarov Basin, and not detailed here, form a profile essentially like that of silica, though small variations in the water column are less readily resolved on account of the lower precision of the analysis.

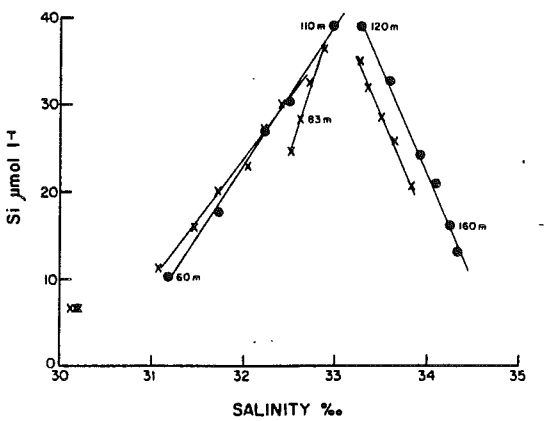

Fig. 8. Silicate versus salinity, 50–150 m. Solid circles, samples collected days 106–108; crosses, days 123–125.

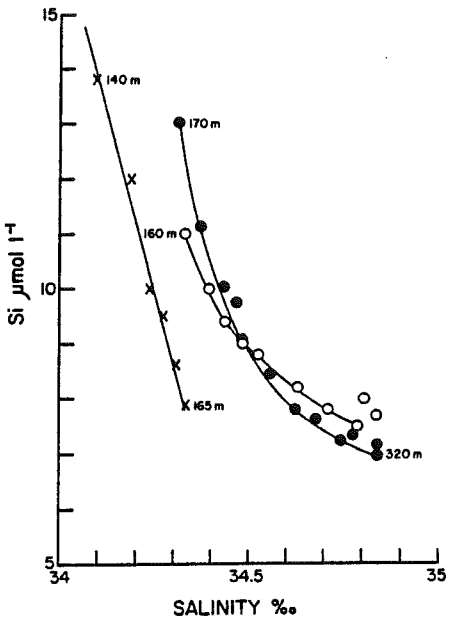

Fig. 9. Silicate versus salinity, 140–325 m. Solid circles, samples collected days 108–109; open circles, day 99: crosses, day 95.

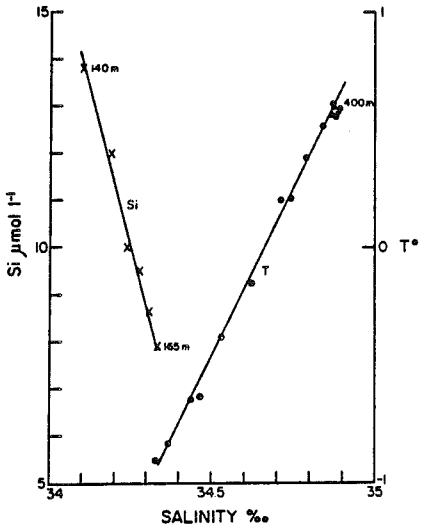

Fig. 10. Silicate versus salinity, 140–165 m, samples collected day 95 and temperature versus salinity for all samples 140–480 m.

An appendix giving raw data is available on microfiche.[1] The phosphate and silicate maxima are coincident in depth, as expected for an advective feature.

TRITIUM

Tritium samples were collected thoughout the duration of the project; the data described here are primarily from the upper 200 m of the water column. For treatment of the deeper samples reference should be made to *Östlund* [1982].

The data are shown in Figure 11. Tritium values for the depth range 200–3000 m are essentially consistent with the presence of a freshwater component having a tritium concentration of 675 TU [*Östlund*, 1982]. Figure 11 shows that between 50 and ca. 200 m tritium varies less steeply with salinity; extrapolation of a straight line through these points would yield a freshwater component containing ca. 150 TU. There are a number of samples containing somewhat higher tritium, and these will be dealt with separately. The mixed layer contains a markedly higher tritium concentration; this will be dealt with first.

In the same way that the silicate data in the surface mixed layer were interpreted as the result of an addition of a fresh component to water of the subsurface type, so do the tritium values fit this interpretation. But in this case it must be assumed that it is the meteoric component of the freshwater that accounts for the bulk of the tritium enhancement. The meltwater component would be expected to have a tritium level similar to that of the surface water from which it is ultimately derived, i.e., 30–35 TU [*Weston*, 1955]. Ice cores from the LOREX site confirm this estimate; though a few sections showed higher levels [*Östlund*, 1982], these are likely to contain a fraction of meteoric water which would be present on the surface as snow but could also be present within the core as a result either of freezing of meteoric water on the underside of the ice or of percolation of rain or melted snow through the ice during summer.

If the 50 m sample, S = 31.080 ‰, is taken as representative of the water immediately beneath the mixed layer and a tritium value is then calculated for the freshwater that must be added to give the mixed layer salinity, we get a value of ca. 450 TU. Then taking a figure of 675 TU for the meteoric component [*Östlund*, 1982] and 35 TU for meltwater, an estimate can be made of the proportions of each type needed to give a mixture of 450 TU. This calculation indicates a mixture of 35% meltwater and 65% meteoric water. This is in tolerable agreement with the ratio that would be calculated for the entire Arctic Ocean by using the value for precipitation and runoff of 0.45 m yr^{-1} [*SCOR Working Group 58*, 1979] and of 0.6 m yr^{-1} for ice melting [*Thorndike et al.*, 1975].

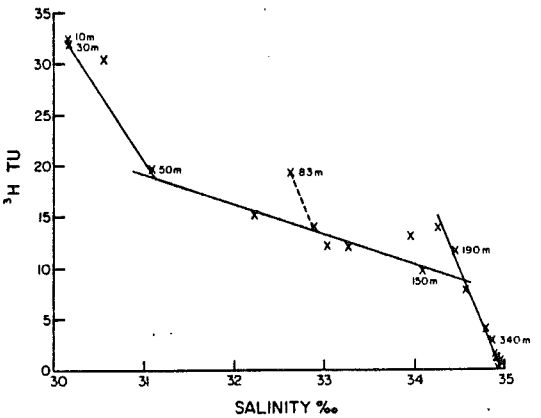

Fig. 11. ^3H versus salinity.

[1] Appendix table is available with entire article on microfiche. Order from the American Geophysical Union, 2000 Florida Avenue, N.W., Washington, D. C. 20009. Document C82-001; $2.50. Payment must accompany order.

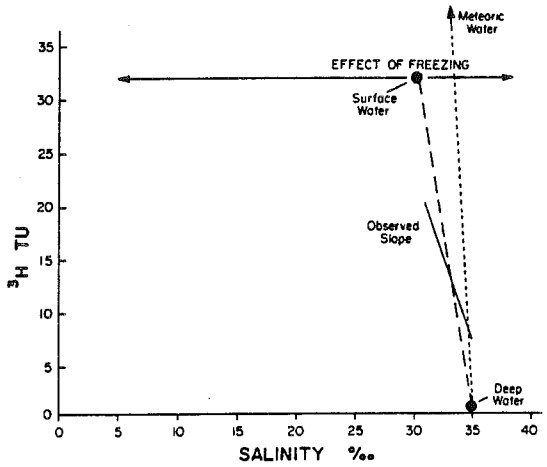

Fig. 12. Illustration of the way in which freezing and melting of surface water yields two components that can reduce the slope of the ^{3}H-S relation below that obtainable by mixing the three components deep, surface, and meteoric water.

A slightly more refined calculation takes into account the fact that the 50-m sample is slightly more saline than the water type that is contributing to both the overlying mixed layer and the underlying waters down to the nutrient maximum; this is demanded by the silica concentration of the mixed layer and of freshwater. The result is similar: the tritium of the freshwater addition becomes 480 TU, which is equivalent to 70% meteoric water and 30% meltwater.

It is now necessary to account for the rather slow decrease in tritium with salinity below the mixed layer to ca. 200 m. This is essentially due to the fact that these waters contain a significant component of laterally advected water, formed on the continental shelf from shallow, tritium-rich water to which brine has been added.

The slope of the ^{3}H-S line is then determined by the proportion of meteoric water and meltwater added with modification due to the addition of brine having a tritium content similar to that of surface water (ca. 35 TU). The plot of tritium against salinity (Figure 11) suggests that this process is significant to a depth of about 160–200 m, so it matches the depth range over which the T-S plot indicates advection of cool waters into the Arctic Basin.

The process described here is illustrated in Figure 12. The gradient of the ^{3}H-S line resulting from mixing surface and deep water is shown; also indicated is the steeper slope that would result from mixing meteoric water with deep water. It is observed, however, that an intermediate depth range alone exhibits a shallower gradient than these components can accommodate. Freezing and melting of the surface water produces two new components that have the appropriate properties to yield the observed gradient, provided that they are mixed in at different depths as their densities would demand.

The few samples that have anomalously high tritium levels represent traces of advected layers which have not yet completely mixed with the ambient water of the same density, so they retain a signature of elevated tritium and also a remnant of their original nutrient concentration. In the specific case of the sample from 83 m, this appears (Figure 8) as a low silicate value compared with the background of nutrient rich water having its origin in the Bering Sea. Also, between 150 and 200 m there are a few samples that have relatively high tritium levels. These are apparently associated with the water that advects at the density surface corresponding to the inflection point on the T-S plot. Water at this level (corresponding to about 160 m) has a tritium content of ca. 13 TU; this represents only a small decrease from the level at around 70 m even though the salinity has increased by ca. 2 ‰.

Below ca. 200 m the ^{3}H-S plot has a slope appropriate to the addition of meteoric water only, the ^{3}H-S relationship in this region being established outside the Arctic Ocean. Meltwater is not apparent at this location below a depth of about 200 m.

STABLE OXYGEN ISOTOPES

Since the processes that have been invoked to account for the distribution of T, S, Si, and tritium have an influence on the stable oxygen isotope composition of sea waters, it should be possible to relate the foregoing arguments to the $^{18}O/^{16}O$ ratios in the water column.

Measurements of $\delta^{18}O$ in Arctic Ocean waters have been reported by *Vetshteyn et al.* [1974] and *van Donk and Mathieu* [1969]. Owing to either the data being too sparce, particularly in the upper waters (0–400 m) or the vertical profiles being made up of samples from widely different sampling stations, these authors are unable to examine the processes of freezing and meteoric water addition that would affect the $\delta^{18}O$ distributions. In addition to the significance of $\delta^{18}O$ data in relation to the processes that have been discussed above, the presentation of detailed $\delta^{18}O$ data for the upper few hundred meters of the water column is also important in relation to Arctic paleoclimatology and paleoceanography. In order to understand the $\delta^{18}O$ record preserved by fossil forams, it is essential to have some knowledge of the present Arctic surface water and the relationships between $\delta^{18}O$ and salinity.

The data are shown in Figure 13. Compared with surface mixed layer water, the water lying immediately beneath (at 60 m) shows a similar $\delta^{18}O$ but higher salinity; this is in accordance with its formation by brine addition to a surface water type. Below this depth we should expect a relationship between $\delta^{18}O$ and salinity consistent with formation of the

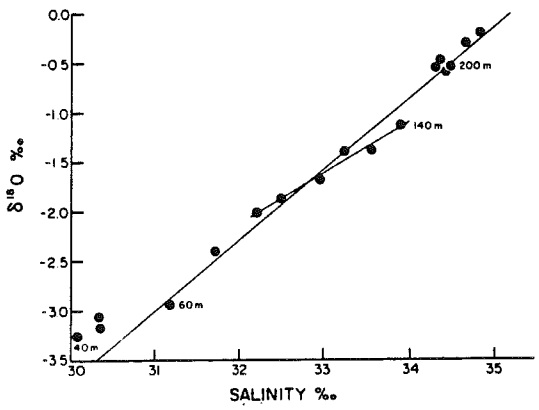

Fig. 13. $\delta^{18}O$ versus salinity, depth range surface to 320 m. Equation of line through all samples, $\delta^{18}O = -25.2 + 0.71S$. Equation of lines through samples in depth range 80–140 m, $\delta^{18}O = -18.6 + 0.52S$.

waters from a surface type with a component of brine and a component of the underlying water. It is possible to estimate the form of the $\delta^{18}O$-salinity relationships that would be observed in the extreme cases of (1) salinity modification by brine addition alone and (2) by mixing of surface water and water from beneath the halocline. Case (1) would have a gradient $d(\delta^{18}O)/dS$ of near zero because freezing produces only a small fractionation of oxygen isotopes. Case (2) would have a gradient dependent on the proportion of meteoric and meltwater being added at the surface. This proportion should be similar to the ratio that was estimated to account for the difference in tritium between surface and subsurface waters. Taking a mixture of 70% meteoric water ($\delta^{18}O = -30$) and 30% meltwater ($\delta^{18}O = -3$) would give a $\delta^{18}O$ for the mixture of -22. If water of this type were allowed to mix with a saline end-member having a salinity of 34.5 ‰ (the value chosen is not critical, but is selected as a likely lower limit for freshwater penetration), the equation relating $\delta^{18}O$ and salinity can be predicted as

$$\delta^{18}O = -22 + 0.634S \text{ ‰}$$

The choice of $\delta^{18}O$ for the meteoric component has a critical effect on the value of the intercept at $S = 0$. The processes invoked to explain the distribution of geochemical parameters should yield a $\delta^{18}O$-salinity relationship between the two limits described by cases (1) and (2), with curvature due to some displacement of points toward higher salinity in those places where addition of brine is occurring.

The data (Figure 13) show some sign of displacement of points to higher salinity around 60 m and 130 m, otherwise they are indicative of dilution of the deeper waters with a mixture of meltwater and meteoric water in amounts similar to those used in the above calculation.

Although the $\delta^{18}O$ versus salinity plot in Figure 13 does not distinctly illustrate regions of brine addition, it does, by giving the proportion of meltwater present, indicate how much brine has been distributed through the water column. The way in which it becomes distributed is yet to be detailed. Here it is suggested that there is some localization of brine introduction immediately beneath the mixed layer and also at ca. 130–140 m. The question of whether any of the brine is transported to deep water is beyond the scope of this study, but it may be noted that a small enhancement of deep water salinities could much reduce the significance of brine addition in the relatively thin near-surface layers. *Aagaard* [1981] has discussed the question of salt addition to deep Arctic Ocean waters based on data from the LOREX site.

The difficulty here is trying to identify small variations in the $\delta^{18}O$-salinity gradient from a small number of data points having a precision that is low relative to the range of variability existing in the water column.

CONCLUSIONS

Measurements of silicate and tritium in the upper 200 m of the central Arctic Ocean make a valuable addition to temperature and salinity data; they exhibit a complex pattern but one that is consistent with the view that the halocline is supplied by horizontal advection with waters produced on the continental shelves from shallow waters by salinity enhancement with brine. A degree of complexity stems from the lateral inhomogeneity of the water column even at a great distance from the margins of the basin.

In addition to the well-characterized water mass having an origin in the Chukchi Sea region [*Kinney et al.*, 1970], another deeper contributor to the halocline can be recognized from these data; this water is characterized by low silicate concentrations and is sufficiently similar to the Atlantic layer to suggest that it is derived from those waters. A plausible mechanism for the transformation of the Atlantic water was put forward by *Coachman and Barnes* [1962].

This work demonstrates the value of chemical measurements in distinguishing between different water types particularly when they lie at the same density surface and have little temperature variation. It follows, too, that the chemical data should be able to give some indication of the rate at which horizontal mixing occurs. Silicate measurements are of particular value in the Arctic Ocean owing to both the range of concentrations in the upper waters and the precision of the measurements. On the other hand, stable oxygen isotope measurements appear not to have the dynamic range necessary to reveal in detail the effects of brine addition on the water column.

It is concluded that in view of the marked lateral inhomogeneity of the water column, it is important to collect samples simultaneously as far as is possible. Also, it is apparent that the greatest value can be derived from chemical measurements when they are made on the same water samples, so that direct comparison of parameters is possible rather than the less satisfactory comparison of profiles.

Future work on the chemistry of brines might result in sensitive tests for the extent of their influence on high-latitude water masses. Apart from their intrinsic chemistry, they may be further characterized by virtue of chemical modifications that occur while they lie in contact with the sediment surface, for example, losing oxygen and accumulating components that diffuse from the sediments: nutrients, radon-222, and radium-228.

Acknowledgments. The authors wish to thank for their assistance Hans Weber (Earth Physics Branch, Energy, Mines and Resources, Canada), George Hobson and Frank Hunt (Polar Continental Shelf Project), and H. Gote Östlund (University of Miami). Adrian Camfield and Malcolm Drury (Earth Physics Branch, Energy, Mines and Resources, Canada) and Sam Raymond (Benthos Inc.) are thanked for help in the field. We are grateful to the Bedford Institute of Oceanography and University of Washington for assistance and loan of equipment. The constructive criticism of reviewers is gratefully acknowledged. This work was supported by the Natural Science and Engineering Research Council, Canada. LOREX contribution 12.

REFERENCES

Aagaard, K., On the deep circulation in the Arctic Ocean, *Deep Sea Res., 28A*, 251–268, 1981.

Aagaard, K., L. K. Coachman, and E. Carmack, On the halocline of the Arctic Ocean, *Deep Sea Res., 28A*, 529–545, 1981.

Coachman, L. K., and C. A. Barnes, The contribution of Bering Sea water to the Arctic Ocean, *Arctic, 14*, 147–161, 1961.

Coachman, L. K., and C. A. Barnes, Surface water in the Eurasian Basin of the Arctic Ocean, *Arctic, 15*, 251–277, 1962.

Codispoti, L. A., and D. Lowman, A reactive silicate budget for the Arctic Ocean, *Limnol. Oceanogr., 18*, 448–456, 1973.

Kinney, P., M. E. Arhelger, and D. C. Burrell, Chemical characteristics of water masses in the Amerasian Basin of the Arctic Ocean, *J. Geophys. Res., 75*, 4097–4104, 1970.

Moore, R. M., Oceanographic distributions of zinc, cadmium, copper and aluminium in central Arctic waters, *Geochim. Cosmochim. Acta, 45*, 2475–2482, 1981.

Moore, R. M., The relationship between distributions of dissolved cadmium, iron, aluminium and hydrography in the central Arctic Ocean, in *NATO Symposium Volume: Trace Metals in Sea Water*, pp. 131–142, Plenum, New York, 1983.

Östlund, H. G., The residence time of the freshwater component in the Arctic Ocean, *J. Geophys. Res.*, *87*, 2035–2043, 1982.
SCOR Working Group 58, The Arctic Ocean heat budget, *Rep. 52*, 98 pp., Geophys. Inst., Univ. of Bergen, Bergen, Norway, 1979.
Strickland, J. D. M., and T. R. Parsons, A practical handbook of seawater analysis, *Bull. Fish. Res. Bd. Can.*, *167*, 310 pp., 1972.
Tan, F. C., and P. Strain, The distribution of sea ice meltwater in the Eastern Canadian Arctic, *J. Geophys. Res.*, *85*, 1925–1932, 1980.
Thorndike, A. S., D. A. Rothrock, G. A. Maykut, and R. Colony, The thickness distribution of sea ice, *J. Geophys. Res.*, *80*, 4501–4513, 1975.
Treshnikov, A. F., Ye. G. Nikiforov, and N. I. Blinov, Results of oceanological investigations by the 'North Pole' drifting stations, *Polar Geogr.*, *1*, 22–40, 1977.
van Donk, J., and G. Mathieu, Oxygen isotope compositions of foraminifera and water samples from the Arctic Ocean, *J. Geophys. Res.*, *74*, 3396–3407, 1969.
Vetshteyn, V. Ye., G. A. Malyuk, and V. P. Rusanov, Oxygen-18 distribution in the central Arctic Basin, *Oceanology*, *14*, 514, 1974.
Weston, R. E., Jr., Hydrogen isotope fractionation between ice and water, *Geochim. Cosmochim. Acta*, *8*, 281–284, 1955.

(Received May 10, 1982;
revised September 7, 1982;
accepted October 21, 1982.)

GEOPHYSICAL RESEARCH LETTERS, VOL. 10, NO. 12, PAGES 1168-1171, DECEMBER 1983

ANOMALOUS NEON-HELIUM RATIOS IN THE ARCTIC OCEAN

Zafer Top[1] and W.B. Clarke

Department of Physics, McMaster University, Hamilton, Ontario L8S 4K1 Canada

R.M. Moore

Department of Oceanography, Dalhousie University, Halifax, Nova Scotia B3H 4J1 Canada

Abstract. Measurements of dissolved helium and neon were made on seawater samples collected at the Lomonosov Ridge Experiment site (LOREX, 1979) and at the FRAM III drifting ice station (1981) in the Arctic Ocean. The most striking feature of the results is the high values of Ne/He in the shallow depths compared to previous results in other oceans. Ice formation and refreezing of meltwater appear to be the mechanisms which could explain the observed Ne/He anomaly.

Introduction

The atmosphere is the major source for oceanic helium and neon, both of which serve as conservative tracers. Both gases are often found in excess of solubility equilibrium in the upper layers due to the forced dissolution of air bubbles during wave action (air injection). Helium concentrations at some locations in the deep ocean are enhanced due to a radiogenic component from the solid earth. Neon concentrations, on the other hand, are believed to remain unaltered as there is no known process which produces significant quantities of neon. Because of this, the neon excess above solubility equilibrium can be used as an index to correct for the component of helium which is due to air injection, (Beg, 1971). In a study of Baffin Bay (Top et al., 1980) this procedure often resulted in helium concentrations which were less than equilibrium solubility values. Our conclusions were, then, that such a correction was probably an oversimplification, and that the ice formation and melting might have been influencing factors. The present work describes further results from the Arctic regions, and addresses probable causes of the observed He/Ne anomalies.

Experimental

Seawater samples subject to the present investigation were collected during the Lomonosov Ridge Experiment (LOREX) in 1979 and the FRAM III expedition in 1981. In the FRAM III expedition, the full profile was completed over a period of several days during which the ice camp had drifted approximately 30km. In the LOREX experiment the samples from the top 150m were collected over the Lomonosov Ridge in two days. The rest of the profile was completed ten days later over the Fram Basin side of the ridge. Water samples were collected in copper refrigeration tubings clamped at both ends. In the laboratory the neon-helium fraction of the dissolved gases was analyzed for the absolute concentrations of helium and neon using the isotope dilution technique on a 25 cm radius static mass-spectrometer. The precision of the measurements is 0.25% for helium and 0.10% for neon, including uncertainties in the "spikes" (^3He and ^{22}Ne) and standards (^3He, ^4He, ^{20}Ne and ^{22}Ne).

Results and Discussion

The results are presented in Tables 1-2* and Fig. 1. The temperature data were furnished by T.O. Manley for the FRAM III samples and are as yet preliminary. Salinities were measured at the University of Miami. The temperature and salinity measurements for the LOREX samples were made using reversing thermometers and a portable Bissett-Berman salinometer. Helium and neon concentration excesses above solubility equilibrium values were calculated using the solubility tables of Weiss (1971), and are expressed in Δ notation according to

$$\Delta C = \left(\frac{C_o}{C_{sol}} - 1 \right) \times 100\% \qquad (1)$$

where ΔC is the concentration excess, C_o is the observed concentration, and C_{sol} is the solubility equilibrium value. The uncertainties in ΔHe and ΔNe are ±1.5% and ±1%, respectively. At both stations, duplicate samples were taken from the same Niskin bottles. While the FRAM III 20m duplicates agree very well, the LOREX 200m duplicates are significantly different. No obvious explanation for the disagreement could be found for these samples. We tend to believe the results for the first 200m sample mainly because the duplicate 200m sample has the largest helium deficiency in the set, a result which could be due to slight underextraction of the dissolved gas. The four 5m (nominal depth) LOREX samples were not duplicates, but were collected in successive, individual casts. The observation that

[1]Present Address: Rosenstiel School of Marine and Atmospheric Science, University of Miami, Miami, FL 33149 USA

Paper number 3L1369.
0094-8276/83/003L-1369$03.00

*Supplement (tables 1, 2, and 3) is available with entire article on microfiche. Order from American Geophysical Union, 2000 Florida Ave., N.W., Washington, D.C. 20009. Document L83-005; $2.50. Payment must accompany order.

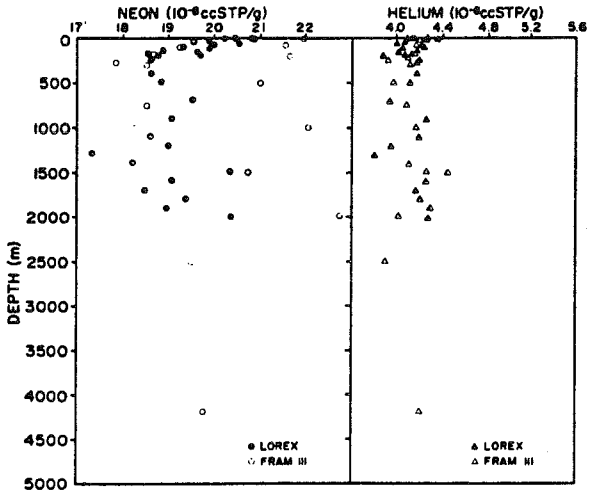

Fig. 1. Neon and helium concentrations at LOREX and FRAM III locations.

the helium and neon concentrations in the first three 5m samples vary within ±1% (1σ) gives confidence in the sampling and laboratory procedures. While this ±1% is significantly larger than the quoted analytical precision, the variability may well be real.

The main feature of the results is the unusually large scatter of the neon concentrations which are significantly greater than the mean oceanic values whereas the other properties exhibit reasonably smooth profiles. In all other oceans where we have measured neon concentrations, the profiles have almost always been smooth lines associated with little variation through the water column. A quirk in sampling peculiar to Arctic regions might be thought responsible for the observed pattern, such as freezing of water in the copper sampler. The most likely way to increase the neon concentration in a sample is to add some quantity of air to it. If we assume that some air did get in the samplers as a result of freezing, then an atmospheric component for helium should also be evident: the ΔHe values should be high (comparable to ΔNe); and the Ne/He ratios should be shifted toward 3.50, the atmospheric ratio. These are not observed. In addition, the helium isotope ratio (to be published elsewhere), although less sensitive to an atmospheric component, exhibits smooth profiles, and shows no signs of anomaly which may be attributed to mishandling of samples. A random contamination of the samples may also be excluded on the basis of the distribution of neon excess through the water column. There are no apparent correlations between neon, helium and other measured tracers: tritium (Ostlund et al., 1982; Ostlund, 1980), nutrients (Moore et al., 1983), trace metal concentrations (Moore, 1981). The present analysis is therefore concentrated on the variations of the excess neon and helium, and of the Ne/He ratio.

From here on we choose to work with the Ne/He ratio as it appears to be a more sensitive indicator of the neon anomaly. This is because, with the ratios, the effect of a possible atmospheric component is minimized, as such a component would lower the ratio below the anomalous values. Furthermore, the ratio may be compared, with more confidence, to the solubility equilibrium value, a quantity which is less prone to systematic error than the individual helium neon solubility concentrations. Solubility equilibrium values of neon and helium at a temperature of -1°C and a salinity of 30°/$_{oo}$ requires the Ne/He ratio to be 4.50 ± 0.05 in Arctic regions (Weiss, 1971). However, the observed ratios span a range between 4.26 and 5.66 with 65% of the measured values being higher than the solubility ratio. Fig. 2 shows the present Ne/He ratios as function of salinity with measurements from other oceans. Table 3* summarizes the ΔHe, ΔNe and Ne/He measurements from the present Arctic locations and from other oceans. Here, the Atlantic Core which is marked with higher temperature and salinity, and the layers above and below it are distinguished. Due to scatter and limited numbers of the data, a rigorous statistical analysis could not be attempted, however a few convincing points emerge from a comparison with the mean ocean values of ΔHe, ΔNe and Ne/He ratio:

1. At both locations the Ne/He ratio in the Atlantic Core is very close to the solubility equilibrium value, while it is 7.5% greater than the solubility equilibrium in the upper layers.
2. At both locations, the excess helium and excess neon are anticorrelated in the layer above the Atlantic Core.
3. At the LOREX location the observed helium excess in the upper layer is significantly lower than the world ocean average.
4. At the FRAM III location, the layer below the Atlantic Core is even more anomalous in the Ne/He ratio than the upper layer.

Without regard to the cause of the anomalous ratio, these observations lead us to suppose that the Ne/He ratio has the potential of being an independent mass tracer in the Arctic regions. As the source of the anomaly appears to be near the surface, the Ne/He ratio may be especially suitable to trace deep water formation. One immediate conclusion, on the basis of the Ne/He ratios, is that the deep water at the FRAM III location could not have been a local mixture of the surface and the Atlantic layers. The reason why the Atlantic Core is unaffected by the neon anomaly may be explained by the slowness of the vertical exchange process. ^{3}H-^{3}He age of the Atlantic Core is about 12 years (Ostlund et al. 1982) and its residence time in the Arctic Ocean is probably less than that. In terms of a diffusive vertical exchange, this is indeed a short time.

Cause of the Ne/He Anomaly

A number of mechanisms may be thought responsible for the observed anomaly. Among these are: a) differential diffusion of helium and neon in both ice and water, b) bubble formation during freezing, c) migration of air pockets through the ice, d) differential partition of helium and neon during ice formation, and e) the concentration enrichment by the meltwater. We examine these in order:

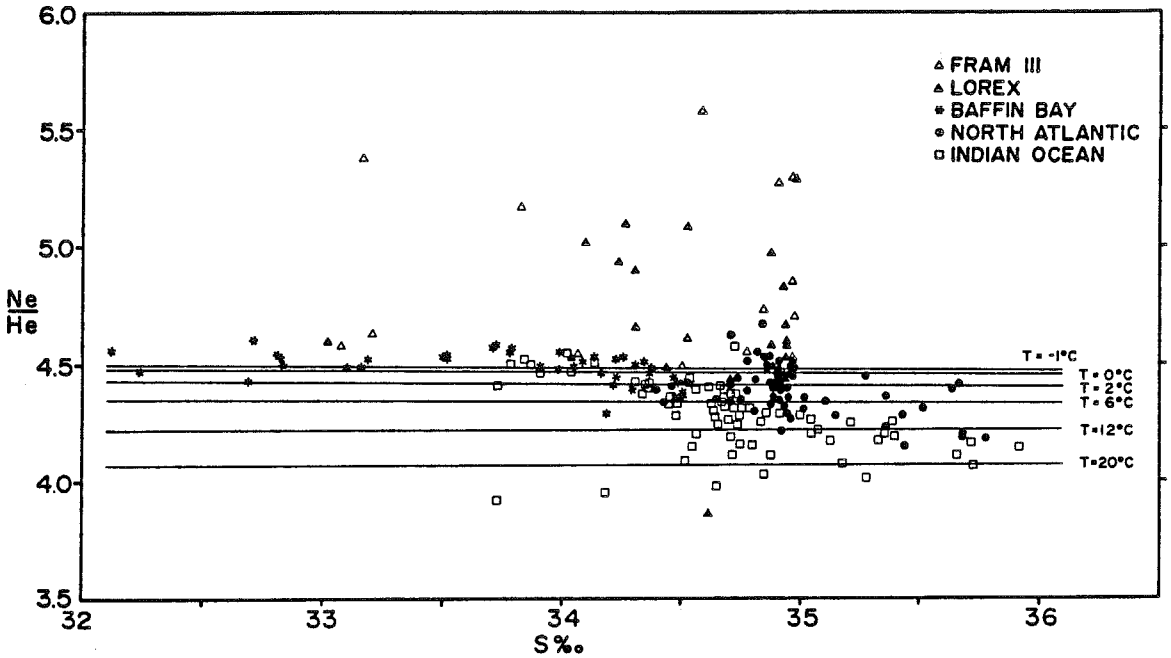

Fig. 2. Ne/He ratios as a function of salinity in various regions. Solid lines are the solubility equilibrium values of the ratio at indicated temperatures.

a) The differential diffusion of helium and neon in water ($D_{He}/D_{Ne} \simeq 2$, Wise and Houghton, 1966; 1968) and in ice ($D_{He}/D_{Ne} \simeq 10$-100, Davy and Miller, 1970) may produce the observed anomaly; however, in order to obtain the observed magnitude, the water-ice system must be isolated from the atmosphere for a period of time on the order of one hundred years or so. ^3H-^3He age of the surface waters is about 4.5 and 2.5 years at the FRAM III (Ostlund et al., 1982) and the LOREX locations, respectively. A steady state diffusion of dissolved helium into ice in such short periods might deplete the helium concentration by about 1% in the surface 5 m. This is a small effect to be identified outside the measurement uncertainties. However the faster diffusion of helium appears to be a likely mechanism to produce the observed ΔHe-ΔNe anticorrelation in the upper layers.

b) It has been shown, theoretically and experimentally, that dissolved gases form bubbles upon nucleation, during freezing (Matsuo and Mikaye, 1966; Bari and Hallett, 1974; and Tsurikov, 1979). This effect is expected to leave the liquid-phase deficient in both helium and neon, because the bubble formation does not fractionate dissolved gases significantly. This result is contrary to the present observations. The topic would, however, merit further investigation as to the extent of occurrence and its relative contribution to the anomaly.

c) Tsurikov (1979) has found that the migration of air pockets through ice was too slow a process to significantly alter the gas concentrations in the underlying water.

d) The solid phase to liquid phase ratios of the solubility of neon and helium are 0.9 and 2, respectively (Namiot and Bukhgalter, 1965). This implies that 10% of the dissolved neon in the liquid from which ice is being formed may be excluded from the solid phase while all the dissolved helium is retained in the solid phase. For the purpose of a simple calculation a conceptual model would have the surface 5m of water (the mixed layer) which is thus modified in neon concentrations and which subsequently mixes with the underlying waters mainly by convection. The calculation shows that by freezing 1m of the surface water (with neon at solubility equilibrium) the rejected 10% of the dissolved neon could increase the neon concentration in the underlying 5m water by 2%. All neon is assumed to remain in the liquid phase. Starting with a ΔNe of 5% due to an air injected component (a typical value for the North Atlantic water entering the Arctic Ocean) and repeating the process twice under static conditions, could result in a ΔNe of about 10%. Despite the simplicity of the assumptions, the freezing mechanism certainly points to the observed anomaly with comparable magnitude. The partial or complete exclusion of a gas from the solid phase is not, of course, particular to neon. Argon is reported to be insoluble in ice (Namiot and Bukhgalter, 1965) and removal of oxygen from liquid water by freezing has long been a standard degassing technique. Other heavier noble gases would also be excluded from the solid phase due to their relatively large atomic sizes. The only available measurements on these gases in the Arctic regions are of oxygen. Some of these measurements show supersaturation, some slight undersaturation. It appears that the complexity of oxygen production and utilization in this region (and others as well) will prevent the use of this gas in support of the present proposition until each and every component of the dissolved oxygen budget can be accounted for.

e) Seasonal melting of ice takes place both above and below the water surface. The following argument applies to the melting of ice above the water. The meltwater brings in helium and neon about 10% in excess of the surrounding water. This is because of two reasons. First, the solubility of these gases is a decreasing function of salinity at a given temperature. Second, the meltwater has a long enough time to equilibrate with the atmosphere as the ice floes generally develop raised edges and hold meltwater before it runs off to the surrounding water. The effect of the addition of meltwater (and/or freshwater runoff from the continents at shelf areas) is therefore to increase the concentration of neon as well as of helium. The present results, on the other hand, show an anti-correlation between helium and neon in the top few hundred meters at both Arctic locations. In order to explain the observed small helium excess, we must postulate that all or most of the meltwater refreezes before it is mixed in the surface mixed layer. This way, all of its helium content will be taken up by the ice while about 10% of its neon content will be excluded from the ice. A more detailed surface sampling both in winter and in the melting season is required to further evaluate the magnitude of these phenomena.

Approximately 50% of the yearly ice accumulation occurs in parts of the continental shelf areas (Koerner, 1973). These areas constitute only about 10% of the Arctic Ocean surface. We expect the Ne/He anomaly to have a larger magnitude in these areas because of the greater rate of ice formation and melting. It has been shown that the upper halocline of the Arctic Ocean is maintained by lateral advection from the shelf areas (Aagaard et al., 1981). The observation of the anomalous Ne/He in the upper halocline is therefore consistent with the source of halocline. Further, the observation of the anomalous Ne/He in the deep water at the FRAM III location is consistent with the idea that some shelf areas may also be a source for bottom water (e.g., Aagaard, 1981). From the magnitude of the anomaly we may guess that the FRAM III bottom water has been recently formed. This conclusion was also arrived at on the basis of radiocarbon and tritium measurements (Ostlund et al., 1982) at this location. The absence of a neon anomaly at the LOREX bottom layer, on the other hand, may be interpreted as indicating a lack of communication between the bottom layers of the two locations.

Conclusions

The anomalous Ne/He ratio in the Arctic regions is shown to have the potential of a water-mass tracer. Dissolved argon and other heavier noble gases promise to have the same quality as they are also excluded from the ice phase. Further work should be aimed at 1) utilizing Ne/He, Ar/He measurements where deep Arctic water formation is suspected, 2) seasonal variation studies of Ne/He and Ar/He concentration to quantify the magnitude of the anomaly generating mechanism, 3) laboratory and field work to obtain the physical parameters involved to model the mechanism.

Acknowledgements. This study was supported by Natural Sciences and Engineering Council of Canada, Grant No. A.2951 and the Office of Naval Research, of the U.S., Code 461, through contract No. N00014-79-C-0135. We are grateful to Drs. H.G. Ostlund, C. Rooth and P. Jones for helpful comments, to Valery Lee and M. Lowings for assistance during the field work, and to W.C. Eismont for assistance in the laboratory.

References

Aagaard, K., On the deep circulation in the Arctic Ocean, Deep-Sea Research, 28A, 251-268, 1981.

Aagaard, K., L.K. Coachman, and E. Carmack, On the halocline of the Arctic Ocean, Deep-Sea Research, 28A, 529-545, 1981.

Bari, S.A., and J. Hallett, Nucleation and growth of bubbles at an ice-water interface, J. Glaciology, 13, 489-520, 1974.

Beg, M.A., Helium isotope oceanography, Thesis, McMaster University, Hamilton, Ontario, Canada, 1971.

Davy, J.G., and K.W. Miller, The diffusion of helium through ice, Solid State Comm., 8, 1459-1461, 1970.

Koerner, R.M., The mass balance of the sea ice of the Arctic Ocean, J. Glaciology, 12, 173-185, 1973.

Matsuo, S., and Y. Miyake, Gas composition in ice samples from Antarctica, J. Geophys. Res., 71, 5235-5241, 1966.

Moore, R.M., Oceanic distributions of zinc, cadmium, copper and aluminum in waters of the Central Arctic, Geochim. Cosmochim. Acta, 45, 2475-2482, 1981.

Moore, R.M., M.G. Lowings, and F.C. Tan, Geochemical profiles in the central Arctic Ocean, J. Geophys. Res., 88, 2667-2674, 1983.

Namiot, A. Yu., and E.B. Bukhgalter, Clathrates formed by gases in ice, J. Structural Chem., 6, 873-874, 1965.

Ostlund, H.G., Data Release No. 80-25, University of Miami, 1980.

Ostlund, H.G., Z. Top, and V.E. Lee, Isotope dating of waters at FRAM III, Geophys. Res. Lett., 9, 1117-1119, 1982.

Top, Z., W.B. Clarke, W.C. Eismont, and E.P. Jones, Radiogenic helium in Baffin Bay bottom water, J. Mar. Res., 38, 435-452, 1980.

Tsurikov, V.L., The formation and composition of the gas content of sea ice, J. Glaciology, 22, 67-81, 1979.

Weiss, R., The solubility of helium and neon in water and seawater, J. Chem. Eng. Data, 16, 235-241, 1971.

Wise, D.L., and G. Houghton, The diffusion coefficients of ten slightly soluble gases in water at 10-60°C, Chem. Eng. Sci., 21, 999-1010, 1966.

Wise, D.L., and G. Houghton, Diffusion coefficients of neon, krypton, xenon, carbon monoxide and nitric oxide in water at 10-60°C, Chem. Eng. Sci., 23, 1211-1216, 1968.

(Received March 4, 1983;
accepted August 10, 1983.)

Deep-Sea Research, Vol. 30, No. 1, pp. 87 to 94, 1983.
Printed in Great Britain.

0198-0149/83/010087-08 $03.00/0

NOTE

Inputs and outputs of salt, fresh water, alkalinity, and silica in the Arctic Ocean

L. G. ANDERSON,* D. W. DYRSSEN,* E. P. JONES† and M. G. LOWINGS‡

(*Received* 30 *December* 1981; *in revised form* 28 *June* 1982; *accepted* 15 *September* 1982)

Abstract—On the basis of seawater volume flows, budgets for salt, fresh water, alkalinity, and silica are calculated for the Arctic Ocean. The inputs and outputs agree within estimated uncertainties.

INTRODUCTION

VARIOUS attempts to calculate budgets for heat, salt, and fresh water for the Arctic Ocean have been made by MOSBY (1963), AAGAARD and GREISMAN (1975), SCOR (1979), and STIGEBRANDT (1981a). Silica budgets have been proposed by CODISPOTI and OWENS (1975), CODISPOTI (1979), JONES and COOTE (1980), and ANDERSON and DYRSSEN (1981). In this paper we wish to use new data to calculate the budgets of salt, fresh water, alkalinity, and silica for the Arctic Ocean. The budget calculations should help to achieve an overall understanding of the Arctic Ocean with its impact on the climate of the northern hemisphere and its role in the transportation of Pacific water and river water with different constituents into the North Atlantic.

Alkalinities have been determined for the Bering Strait during expedition 022 with R.V. *Alpha Helix* (ANDERSON and LOWINGS, 1982), for the central Arctic Ocean during the LOREX project (LOWINGS, 1981), and for the southern Eurasian sector of the Arctic Ocean during the YMER-80 expedition (ANDERSON and DYRSSEN, 1981). The alkalinities in the Canadian Arctic outflows into Baffin Bay have been determined by JONES (unpublished data). Data on the discharge of river water and their content of carbonates and silica can be derived from the literature (see Table 1). Silica was also measured during the *Alpha Helix* expedition (ANDERSON and LOWINGS, 1982), the LOREX project (MOORE, LOWINGS and TAN, 1982), and the YMER-82 expedition (ANDERSON and DYRSSEN, 1981).

Crucial to the calculations is the water budget. For the Bering Strait we use an estimate by

* Department of Analytical and Marine Chemistry, Chalmers University of Technology and University of Gothenburg, S-412 96 Göteborg, Sweden.
† Division of Chemical Oceanography, Atlantic Oceanographic Laboratory, Bedford Institute of Oceanography, P.O. Box 1006, Dartmouth, Nova Scotia B2Y 4A2, Canada.
‡ Arctic Institute of North America, University of Calgary, 2500 University Drive N.W., Calgary, Alberta T2N 1N4, Canada.

Table 1. Discharges and alkalinities of the rivers entering the Arctic seas

River	Sea	Discharge ($m^3 s^{-1}$)	Alkalinity (mM)	Disch. alk. kmol s^{-1} (%)
Mackenzie	Beaufort	12000	1.74	20.9 (17.5)
Yukon	Bering–Chuckchi	5100	2.4 ± 0.4	12.2 (10.2)
Kolyma	E. Siberian	3800	0.37	1.41
Indigirka	E. Siberian	1800	0.72	1.30
Yana	Laptev	1000	0.39, 0.52	0.46
Lena	Laptev	15800	1.06, 1.09	16.99
Total		33500	0.97	32.5 (27.2)
Pyasina	Kara	2500	0.56	1.40
Yenisey	Kara	18600	0.67, 1.20	17.39
Ob	Kara	12500	0.97, 1.40	14.81
Total		42000	~1	42 (35.1)
Pechora	Barents	4100	0.59, 0.40	2.03
Mezen	Barents	800	0.68	0.54
N. Dvina	Barents	3500	2.18, 2.00	7.32
Total		13000	0.92	12.0 (10.0)
Total	Arctic Ocean	105600	1.13	119.6 (100)

Table 2. Inputs of salt, fresh water, alkalinity, and silica through Bering Strait

Volumes and concentrations

Depth (m)	Volume ($10^6 m^3 s^{-1}$)	Salinity	Alkalinity (mM_w)	Silica (μM)
0–15	0.45	29.7 ± 0.3	2.049 ± 0.020	23 ± 9
15–30	0.45	31.5 ± 0.3	2.173 ± 0.020	23 ± 9
30–45	0.45	32.5 ± 0.3	2.235 ± 0.020	23 ± 9
Total	1.35			

Inputs of salt, fresh water, alkalinity, and silica

Depth (m)	Salt (10^6 kg s^{-1})	Fresh water (10^6 kg s^{-1})	Alkalinity (10^6 mol s^{-1})	Silica (10^3 mol s^{-1})
0–15	13.70 ± 0.14	68 ± 4	0.945 ± 0.009	10.35 ± 4.05
15–30	14.51 ± 0.14	45 ± 4	1.002 ± 0.009	10.35 ± 4.05
30–45	14.94 ± 0.14	33 ± 4	1.031 ± 0.009	10.35 ± 4.05
Total	43.15 ± 0.42	146 ± 12	2.978 ± 0.027	31.05 ± 12.15

STIGEBRANDT (1981a) of $1.35 \times 10^6 m^3 s^{-1}$ (Table 2). For the Canadian sounds we select volumes previously used in silica budgets by CODISPOTI and OWENS (1975) and JONES and COOTE (1980) (Table 3). The volumes at different salinities in the East Greenland outflow and North Atlantic inflow have been provided by RUDELS and ANDERSSON (1982) (Tables 4 and 5). The water balance is used to calculate the input of deep Atlantic water in the West Spitsbergen Current (Table 4).

Table 3. Outputs of salt, fresh water, alkalinity, and silica through the Canadian Arctic Archipelago

Volumes and concentrations

Sound	Volume (10^6 m^3 s^{-1})	Salinity	Alkalinity (mM$_w$)	Silica (μM)
Lancaster	1.0	32.5 ± 0.3	2.210 ± 0.020	25 ± 1
Jones	0.5	33.3 ± 0.3	2.236 ± 0.020	22 ± 1
Smith	0.5	34.0 ± 0.3	2.263 ± 0.020	11 ± 1
Total	2.0			

Outputs of salt, fresh water, alkalinity, and silica

Sound	Salt (10^6 kg s^{-1})	Fresh water (10^6 kg s^{-1})	Alkalinity (10^6 mol s^{-1})	Silica (10^3 mol s^{-1})
Lancaster	33.31 ± 0.31	71 ± 9	2.265 ± 0.021	25.0 ± 1.0
Jones	17.07 ± 0.15	24 ± 4	1.146 ± 0.010	11.0 ± 0.5
Smith	17.43 ± 0.15	14 ± 4	1.160 ± 0.010	5.5 ± 0.5
Total	67.81 ± 0.61	109 ± 17	4.571 ± 0.041	41.5 ± 2.0

Table 4. Inputs of salt, fresh water, alkalinity, and silica through Fram Strait

Volumes and concentrations

Depth (m)	Volume (10^6 m^3 s^{-1})	Salinity	Alkalinity (mM$_w$)	Silica (μM)
0–50	0.13	33.86 ± 0.3	2.269 ± 0.020	5 ± 1
50–100	0.11	34.40 ± 0.3	2.300 ± 0.020	5 ± 1
100–150	0.14	34.77 ± 0.3	2.322 ± 0.020	5 ± 1
150–200	0.10	34.90 ± 0.3	2.329 ± 0.020	5 ± 1
200–2000	1.95	35.00 no	2.335 ± 0.020	5 ± 1
Total	2.43	error		

Inputs of salt, fresh water, alkalinity, and silica

Depth (m)	Salt (10^6 kg s^{-1})	Fresh water (10^6 kg s^{-1})	Alkalinity (10^6 mol s^{-1})	Silica (10^3 mol s^{-1})
0–50	4.51 ± 0.04	4.2 ± 1.1	0.302 ± 0.003	0.65 ± 0.13
50–100	3.88 ± 0.03	1.9 ± 0.9	0.259 ± 0.002	0.55 ± 0.11
100–150	4.99 ± 0.04	0.9 ± 1.2	0.333 ± 0.003	0.70 ± 0.14
150–200	3.58 ± 0.03	0.3 ± 0.9	0.239 ± 0.002	0.50 ± 0.10
200–2000	69.96 –	–	4.595 ± 0.040	9.60 ± 1.95
Total	86.92 ± 0.14	7.3 ± 4.1	5.728 ± 0.050	12.00 ± 2.43

SENSITIVITY TEST

To get some indication of the probable errors in the calculations of the inputs and outputs as well as the budgets we have assigned a ±1% error to the salinity and alkalinity data. The error assigned to the silica data is in general ±1 μM except for the silica-rich water in the Bering Strait inflow and the Fram Strait outflow, where larger variations may occur.

Table 5. Outputs of salt, fresh water, alkalinity, and silica through Fram Strait

Volumes and concentrations

Depth (m)	Volume (10^6 m^3 s^{-1})	Salinity	Alkalinity (mM$_w$)	Silica (μM)
0–50	0.4	32.06 ± 0.3	2.251 ± 0.020	6 ± 1
50–100	0.8	33.63 ± 0.3	2.295 ± 0.020	15 ± 2
100–150	0.2	34.23 ± 0.3	2.303 ± 0.020	8 ± 1
150–200	0.4	34.56 ± 0.3	2.307 ± 0.020	6 ± 1
Total	1.8			

Outputs of salt, fresh water, alkalinity, and silica

Depth (m)	Salt (10^6 kg s^{-1})	Fresh water (10^6 kg s^{-1})	Alkalinity (10^6 mol s^{-1})	Silica (10^3 mol s^{-1})
0–50	13.14 ± 0.12	34 ± 3	0.923 ± 0.008	2.40 ± 0.40
50–100	27.58 ± 0.25	31 ± 7	1.882 ± 0.016	12.00 ± 1.60
100–150	7.02 ± 0.06	4 ± 2	0.472 ± 0.004	1.60 ± 0.20
150–200	14.17 ± 0.12	5 ± 3	0.946 ± 0.008	2.40 ± 0.40
Total	61.91 ± 0.55	74 ± 15	4.223 ± 0.036	18.40 ± 2.50

A sensitivity test in the fresh water budget is based on volume deviations up to 10% in the individual contributions to the water balance (Table 11). The test shows a deviation in the fresh water budget of 94 × 10^6 kg s^{-1}, which is no less than 33% of the input or output. The good fresh water balance (Table 8) therefore indicates that volumes used in the calculations below are reasonably correct.

INPUTS AND OUTPUTS

The annual discharge, mean alkalinity, and average discharge alkalinity of major rivers that enter the Arctic Ocean are shown in Table 1. The estimates are based on reports by REEDER, HITCHOW and LEVINSON (1972), LIVINGSTONE (1963), DURAM, HEIDEL and TISON (1960), and KONOVALOV and IVANOVA (1968). The relatively high values for discharge alkalinity indicate that the Arctic Ocean receives significant 'excess' alkalinity from Arctic rivers. The annual river water discharge is roughly equal to the volume of sea ice exported southward through Fram Strait. The average discharge concentration of silica for each river is not known. The 125 μM$_w$ concentration used for the calculation in Table 10 is an estimate by CODISPOTI and OWENS (1975) for all Arctic rivers.

The inputs of salt, fresh water, alkalinity, and silica through Bering Strait are given in Table 2. The volumes of water transported in each 15-m layer are estimated from STIGEBRANDT (1981a). Salinity data are from COACHMAN, AAGAARD and TRIPP (1975), alkalinity and silica data from ANDERSON and LOWINGS (1982). The alkalinity data agree within 5 μM$_w$ with those reported by LOWINGS (1981) for Bering Winter Water in the central Arctic Ocean. The silica concentrations are lower than the 35 μM reported by CODISPOTI (1979). For that reason we have assigned a rather large error to the silica concentrations in Table 2. Fresh water input is calculated from (35-S)/35 times the volumes. The transports of salt and alkalinity are multiplied by 1.025 kg dm^{-3} to account for the density in the actual salinity range. The procedure is later used for all salt and alkalinity estimates.

Table 6. Export of multi-year sea ice, including estimates for the outputs of salt (10 kg m^{-3}), *alkalinity* (0.5 mM_w), *and silica* (1 μM). *The transport of sea ice in the East Greenland outflow is approximately* 100 000 m^3 s^{-1}

Salt	(1.03 ± 0.1) 10^6 kg s^{-1}
Fresh water	(71 ± 0.9) 10^6 kg s^{-1}
Alkalinity	(0.05 ± 0.002) 10^6 mol s^{-1}
Silica	(0.1 ± 0.1) 10^3 mol s^{-1}

Table 7. Salt budget for the Arctic Ocean (*in* 10^6 kg s^{-1})

Inputs:	Bering Strait	+ 43.1 ± 0.4
	Atlantic inflow above 200 m	+ 17.0 ± 0.14
	Atlantic inflow below 200 m	+ 70.0 –
	River water	Negl.
	Total	+ 130.1 ± 0.54
Outputs:	Canadian Archipelago	– 67.8 ± 0.6
	East Greenland and outflow	–61.9 ± 0.6
	Sea ice	– 1.0 ± 0.1
	Total	– 130.7 ± 1.3

Table 8. Fresh water budget for the Arctic Ocean (*in* 10^6 kg s^{-1})

Inputs:	Bering Strait	+ 146 ± 12
	Atlantic inflow above 200 m	+ 7 ± 4
	Atlantic inflow below 200 m	–
	River water	+ 110 ± 11
	Precipitation	+ 30 ± 1
	Total	+ 293 ± 22
Outputs:	Canadian Archipelago	– 109 ± 17
	East Greenland outflow	– 74 ± 15
	Sea ice	– 71 ± 1
	Evaporation	– 20 ± 1
	Total	– 274 ± 34

Table 9. Alkalinity budget for the Arctic Ocean (*in* 10^6 mol s^{-1})

Inputs:	Bering Strait	+ 2.98 ± 0.03
	Atlantic inflow above 200 m	+ 1.14 ± 0.01
	Atlantic inflow below 200 m	+ 4.60 ± 0.04
	River water	+ 0.12 ± 0.01
	Total	+ 8.84 ± 0.09
Outputs:	Canadian Archipelago	– 4.57 ± 0.04
	East Greenland and outflow	– 4.22 ± 0.04
	Sea ice	– 0.05 ± 0.002
	Total	– 8.85 ± 0.08

Table 10. *Silica budget for the Arctic Ocean (in* 10^3 mol s^{-1})

Inputs:	Bering Strait	+ 31.1 ± 12.2
	Atlantic inflow above 200 m	+ 2.4 ± 0.5
	Atlantic inflow below 200 m	+ 9.6 ± 2.0
	River water	+ 13.2 ± 2.0
	Total	+ 56.3 ± 16.7
Outputs:	Canadian Archipelago	− 41.5 ± 2.0
	East Greenland outflow	− 18.4 ± 2.6
	Sea ice	− 0.1 ± 0.1
	Total	− 60.0 ± 4.7

The outputs of salt, fresh water, alkalinity, and silica through the major straits and passages of the Canadian Arctic Archipelago are described in Table 3. Salinity and alkalinity values are unpublished data from recent work at the Bedford Institute of Oceanography. Mean concentrations are estimated from observations above the appropriate sill or threshold depths. The silica concentrations are taken from JONES and COOTE (1980), who observed progressively lower silica values from west to east in the archipelago. Fresh water output is again estimated from (35-S)/35 times the volumes.

Table 11. *Sensitivity test for the fresh water budget keeping the water balance. The volumes are changed by maximum* 10% *to give the largest deviations in the inputs and outputs of fresh water*

		Volume (10^6 m^3 s^{-1})	Mean salinity	Fresh water (10^6 kg s^{-1})
Inputs:	Bering Strait	1.35 − 0.14	31.147	133
	Atlantic inflow above 200 m	0.48 + 0.05	34.553	7
	Atlantic inflow below 200 m	1.95 + 0.20	35.000	0
	River water	0.11 − 0.011	0	99
	Precipitation	0.03 − 0.003	0	27
	Total	4.016		266
Outputs:	Lancaster Sound	1.0 + 0.1	32.50	79
	Jones and Smith Sound	1.0	33.65	38
	East Greenland outflow above 100 m	1.2 + 0.044	33.10	68
	East Greenland outflow below 100 m	0.6 − 0.06	34.44	9
	Sea ice	0.10 + 0.01	10	79
	Evaporation	0.02 + 0.002	0	22
	Total	4.016		295
Inputs:	Bering Strait	1.35 + 0.14	31.147	164
	Atlantic inflow above 200 m	0.48 − 0.05	34.553	5
	Atlantic inflow below 200 m	1.95 − 0.20	35.000	0
	River water	0.11 + 0.011	0	121
	Precipitation	0.03 + 0.003	0	33
	Total	3.824		323
Outputs:	Lancaster Sound	1.0 − 0.1	32.50	64
	Jones and Smith Sound	1.0	33.65	38
	East Greenland outflow above 100 m	1.2 − 0.044	33.10	63
	East Greenland outflow below 100 m	0.6 + 0.06	34.44	11
	Sea ice	0.10 + 0.01	10	64
	Evaporation	0.02 − 0.002	0	18
	Total	3.824		258

The inputs of salt, fresh water, alkalinity, and silica through Fram Strait are shown in Table 4. The value for northward flow below 200 m is required to balance the (total) water budget we use. The salinity and silica data are mean values reported by ANDERSON and DYRSSEN (1981) for the West Spitsbergen Current. Alkalinity data are calculated from the relation $A_t = 0.582\,S + 0.298$, a best-fit iteration of alkalinity data from ANDERSON and DYRSSEN (1981).

The outputs of salt, fresh water, alkalinity, and silica through Fram Strait are listed in Table 5. There are major discrepancies between the values and estimates by AAGAARD and GREISMAN (1975) and SCOR (1979). The salinity and silica values are average concentrations observed by ANDERSON and DYRSSEN (1981) in the East Greenland Current. Alkalinity values are estimated from the equations $A_t = 0.0488\,S + 0.686$ (above 50 m) and $A_t = 0.0122\,S + 1.885$ (below 50 m). The relations are based on the alkalinity distributions reported by ANDERSON and DYRSSEN (1981).

Estimates for salt, fresh water, alkalinity, and silica outputs from multi-year sea ice exported south through Fram Strait are listed in Table 6. Ice transport is taken from AAGAARD and GREISMAN (1975). An average ice with salinity of 10, alkalinity of 0.5 mM_w, and silica of 1 μM_w is used to calculate the relevant transports. Reliable field data for the salt, alkalinity, and silica of multi-year sea ice do not exist.

BUDGETS

Tables 7 to 10 are salt, fresh water, alkalinity, and silica budgets for the Arctic Ocean, based on the inputs and outputs shown in Tables 1 to 6. The balances are good for salt, fresh water, and alkalinity. The balance may be fortuitous because it is not known exactly how the surface water above 200 m (Table 4) flows around Svalbard. We have assumed little exchange of surface water between the Barents Sea and the Nansen Basin region. If, however, some of the surface water flows around Svalbard then the inputs above 200 m by way of the West Spitsbergen Current (Table 4) could be in error.

Otherwise the findings strongly support the transports through Fram Strait supplied by RUDELS and ANDERSSON (1982). It is not possible, for example, to increase the volume of the East Greenland outflow without upsetting the fresh water balance in Table 8. STIGEBRANDT (1981b) and MOSBY (1963) reported inflows and outflows through Fram Strait in the order of 1.5 to 2.0 $\times$ 10^6 $m^3\,s^{-1}$. The values are considerably lower than those determined by AAGAARD and GREISMAN (1975) and reviewed by SCOR (1979). Our budgets indicate the need for new assessments of the transports of salt and fresh water through Fram Strait.

The silica budget in Table 10 shows that more data are required for Bering Strait before one has an indication of the net deposition of silica in the Arctic Ocean as suggested by the work of CODISPOTI and OWENS (1975) and CODISPOTI (1979). In collecting more silica data seasonal variations should be considered. In spite of the uncertainties in the budget, silica is probably still the best or most effective chemical tracer for studying the advective pattern of Bering Strait water in the Arctic Ocean.

Acknowledgements—We acknowledge fruitful discussions with BERT RUDELS and ANDERS STIGEBRANDT at the Department of Oceanography, University of Göteborg. MGL acknowledges the support kindly provided by the Arctic Institute of North America, University of Calgary. DD acknowledges the support of the Swedish Natural Science Research Council.

REFERENCES

AAGAARD K. and P. GREISMAN (1975) Toward new mass and heat budgets for the Arctic Ocean. *Journal of Geophysical Research*, **80**, 3821–3827.

ANDERSON L. and D. DYRSSEN (1981) Chemical constituents of the Arctic Ocean in the Svalbard area. *Oceanologica Acta*, **4**, 305–312.

ANDERSON L. and M. LOWINGS (1982) Report on the chemistry of seawater XXX. Department of Analytical and Marine Chemistry, Chalmers University of Technology and University of Gothenburg, Göteborg, Sweden. (Unpublished document.)

COACHMAN L. K., K. AAGAARD and R. B. TRIPP (1975) *Bering Strait: the regional physical oceanography*. University of Washington Press, Seattle, 172 pp.

CODISPOTI L. A. (1979) Arctic Ocean processes in relation to the dissolved silicon content of the Atlantic. *Marine Science Communications*, **5**, 361–381.

CODISPOTI L. A. and T. G. OWENS (1975) Nutrient transports through Lancaster Sound in relation to the Arctic Ocean's reactive silicate budget and the outflow of Bering Strait waters. *Limnology and Oceanography*, **20**, 115–119.

DURAM W. H., S. G. HEIDEL and L. J. TISON (1960) Worldwide runoff of dissolved solids. *Intl. Assn. Sci. Hydrol. Pub.*, **51**, 618–628.

JONES E. P. and A. R. COOTE (1980) Nutrient distributions in the Canadian Archipelago: Indicators of summer water mass and flow characteristics. *Canadian Journal of Fisheries and Aquatic Sciences*, **37**, 589–599.

KONOVALOV G. S. and A. A. IVANOVA (1968) River discharge of trace elements into marine basins. *Oceanology*, **10**, 482–488. (English translation, 1970.)

LIVINGSTONE, D. A. (1963) Data of geochemistry, 6th Edition. Chemical composition of rivers and lakes, U.S. Geological Survey Professional Paper 440-G.

LOWINGS M. G. (1981) Carbonate chemistry in the central Arctic Ocean. M.Sc. Thesis, Dalhousie University, Halifax, Nova Scotia, Canada, 209 pp.

MOORE R. M., M. G. LOWINGS, and F. C. TAN (1982) Geochemical profiles in the central Arctic Ocean: their relation to freezing and shallow circulation. Submitted to *Journal of Geophysical Research*.

MOSBY H. (1963) Water, salt and heat balance in the North Polar Sea. In: *Proceedings of the Arctic Basin Symposium*, Arctic Institute of North America, pp. 69–83.

REEDER S. W., B. HITCHOW and A. A. LEVINSON (1972) Hydrogeochemistry of surface waters of the Mackenzie River drainage basin: I. Factors controlling inorganic composition. *Geochimica et Cosmochimica Acta*, **36**, 825–865.

RUDELS B. and L. ANDERSSON (1982) Observations of the mass, heat and salt exchange through Fram Strait. Department of Oceanography, University of Gothenburg, Sweden, Report No. 42, 17 pp.

SCIENTIFIC COMMITTEE ON OCEANIC RESEARCH (SCOR) (1979) *The Arctic Ocean heat budget*. Report 52, Working Group 58, Geophysical Institute, University of Bergen, Bergen, Norway, 98 pp.

STIGEBRANDT A. (1981a) Is the magnitude of the salinity difference between the North Atlantic and the North Pacific controlled by the topography of the Bering Strait? Department of Oceanography, University of Gothenburg, Sweden, Report No. 39, 9 pp.

STIGEBRANDT A. (1981b) A model for the thickness and salinity of the upper layer in the Arctic Ocean and the relationship between the ice thickness and some external parameters. *Journal of Physical Oceanography*, **11**, 1407–1422.

EPILOG

The LOREX 79 expedition was one of the largest multidisciplinary geoscience projects ever undertaken in the Arctic Ocean. Nearly a decade has passed since the field studies, and it is appropriate to reflect on the impact it had on Arctic geoscience and Arctic Ocean geoscience activities.

LOREX was the first concerted effort made, on such a large scale, to pool all available resources in order to solve a particular problem. AIDJEX, the Arctic Ice Dynamics Joint Experiment, conducted in the Beaufort Sea (Untersteiner, 1979), was of similar scale and operated over a much longer time period, but was essentially confined to oceanography.

LOREX provided a testing ground on a moving platform for methods, techniques and instruments never used before in high latitude arctic conditions. This included the use of a sophisticated computer-based satellite navigation system, of highly portable digital seismic recorders and of digital recording thermal gradiometers. The successful use of the LAPES method by the Armed Forces for parachuting supplies onto the pack ice of the polar region encouraged the military to build an airstrip on the ice, and to take on the task of deploying and evacuating the whole of the CESAR expedition, four years later.

The "Summary of LOREX Results" shows that the 59-day field operation contributed significantly to the understanding of the processes that formed the Arctic Ocean floor and crust and govern the movement of the Arctic Ocean water and ice cover.

The LOREX operation ran very smoothly, with excellent cooperation, not only between the different disciplines and the investigators and institutions they represented, but also administratively between Canadian and U.S. government agencies, including the Canadian Armed Forces and the U.S. Air Force and Office of Naval Research who largely supported the FRAM I operation that ran concurrently.

Factors that contributed to the success of LOREX, and later CESAR, include: the expertise of PCSP, the Armed Forces and the commercial aircraft operators in handling the logistic support; within the budget for logistics, PCSP and EPB management left the scientists a relatively free hand in the planning and execution of the operation and in the choice of investigators; PCSP and EPB were relatively small, autonomous organizations within EMR which facilitated planning and minimized obstructions of a bureaucratic nature; and last but not least, the enthusiasm that the expedition generated among the LOREX participants, the Armed Forces personnel and the commercial air crews.

The expertise and knowledge acquired on LOREX made the CESAR operation in 1983 possible and led, a year later, to the establishment of a semi-permanent, multidisciplinary ice island program. All subsequent major scientific expeditions into the Arctic Ocean region conducted since 1979 have been multidisciplinary in nature with international participation: Fram I to Fram IV, MIZEX, and the 1980 *Ymer* and 1987 *Polarstern* scientific cruises.

When we examine the 200 year history of scientific exploration of the Arctic Ocean region (Weber and Roots, 1989), it is already apparent that LOREX marks a change in direction that Arctic Ocean science is taking. It marks the beginning of a new era: one of unprecedented cooperation, both among institutions and nations, and between scientific disciplines. The cooperation is in part due to necessity - arctic logistics have become very expensive and are, therefore, only affordable through pooling of resources - but it also reflects an advance in understanding: that the interaction of physical, chemical and biological processes regulates the total Earth system. Increasingly, the Arctic Ocean region is being viewed in a global setting. Studies no longer focus on the Arctic Ocean alone, but include such global subjects as tectonics, upper atmosphere and magnetosphere research, dynamics of the water masses and their interaction with Atlantic and Pacific waters, oceanic and atmospheric transport of chemicals into and out of the polar regions, to mention just a few. The study of Arctic Ocean water and atmosphere play a key role in the global sense of the International Geosphere-Biosphere Program (IGBP). LOREX marks the latest of a number of milestones that shaped Arctic Ocean research.

REFERENCES

Heezen, B.C. and W.M. Ewing, 1961. The Mid-Oceanic Ridge and its extension through the Arctic Basin. In: G.O. Raasch (ed.), Geology of the Arctic, University of Toronto Press, Toronto, Ont., v. I, 622-642, 732 p..

Johnson, G.L., A. Grantz and J.R. Weber, 1989. Bathymetry and Physiography, Table 1. In: The Arctic Ocean Region. The Geology of North America, v. L, Geological Society of America, Boulder, Col., in press.

Perry, R.K., H.S. Fleming, J.R. Weber, Y. Kristoffersen, J.K. Hall, A. Grantz, G.L. Johnson, N.Z. Cherkis and B. Larsen, 1986. Bathymetry of the Arctic Ocean. Polar stereographic projection, scale 1:4 704 075 at latitude 78°N. Naval Research Laboratory, Washington, D.C.

Untersteiner, N., 1979. A review of the ADJEX Project, 1970-77. Polar Record, 19, 363-367.

Weber, J.R., 1989. Physiography and Bathymetry of the Arctic Ocean sea floor. In: Herman, Y. (ed.), Climatology, Oceanography and Geology of the Arctic Seas. Van Nostrand Reinhold Co. Inc., Stroudsburg, Penn. In press.

Weber, J.R., D.A. Forsyth and H.R. Jackson, 1986. Recommendations on future Arctic Ocean Science. Earth Physics Branch, Report No. 86-18, 13 p.

Weber, J.R. and E.F. Roots, 1989. Historical Background: Exploration, Concepts and Observations. In: Johnson, G.L., A. Grantz and J.F. Sweeney, eds., The Arctic Ocean Region, Decade of North American Geology, Vol. L, Chapter 2. Geological Society of America, Boulder, Colorado. In press.

Weber, J.R. and J.F. Sweeney, 1977. The Lomonosov Ridge Experiment: A proposal for the study of the Lomonosov Ridge. Earth Physics Branch, Internal Report, February, 1977, 46 p.

ACKNOWLEDGEMENTS

Permission to reproduce the selected LOREX contributions has been obtained from the authors and from the publishers, including the American Congress of Surveying and Mapping (#16), the American Geophysical Union (#1,4,12,15,18,21,27), the Arctic Institute of North America (#13), Crane, Russack & Co., Inc. (#14), Elsevier Science Publishers (#9,10), the Geological Association of Canada (#23), the Geological Society of America (#22), Pergamon Press (#3,6,11,28) and the Royal Canadian Geographical Society (#25,26).

Thanks to the LOREX principal investigators for summarizing their most significant results. I would also like to thank Dave Forsyth, Fred Roots, Jack Sweeney and Al Taylor for critical reading of this manuscript.

APPENDIX

List of LOREX Publications (by authors)

Published Articles

Aagard, K., 1981. On the deep sea circulation in the Arctic Ocean. Deep Sea Res. 28A, 3, 251-268. LOREX Contribution No. 3.

Anderson, L.G., Dryssen, D.W., Jones, E.P. and Lowings, M.G., 1983. Inputs and outputs of salt, fresh water, alkalinity and silica in the Arctic Ocean. Deep Sea Res., 30, 87-94. LOREX Contribution No. 28.

Blasco, S.M., Bornhold, B.D. and Lewis, C.F.M., 1979. Preliminary results of surficial geology and geomorphology studies of the Lomonosov Ridge, Central Arctic Basin, Current Res. GSC, 79-1C, 73-83. LOREX Contribution No. 2.

Forsyth, D.A. and Mair, J.A. 1984. Crustal structure of the Lomonosov Ridge and the Fram and Makarov basins near the North Pole. J. Geophys. Res. 89, 473-481. Contribution No. 948 of EPB. LOREX Contribution No. 15.

Johnson, G.W. 1984. Astronavigation for the Lomonosov Ridge Experiment. Surveying and Mapping 44, 237-245. LOREX Contribution No. 16.

Lewis, C.F.M. 1980. North Pole geology under the sea ice at LOREX 79. Geolog, 9, Part 1, 58-64. LOREX Contribution No. 23.

Livingston, H.D., Moore, R., Kupferman, S.L. and Bowen, V.T. 1983. Vertical profile of artificial radionuclide concentrations in the Central Arctic Ocean. Geochemica and Cosmochemica Acta, 48,2195-2203. LOREX Contribution No. 11.

Lowings, M. 1981. Carbonate chemistry in the Central Arctic Ocean. M.Sc. thesis, Dalhousie U., Dept. Oceanography, 209 p. LOREX Contribution No. 7.

MacInnes, J.B., 1980. Joe MacInnes explores the Arctic depths. #1 - LOREX Expedition. Can. Geographic, 100, 18-26. LOREX Contribution No. 25.

Mair, A. and Forsyth, D.A. 1982. Crustal structure of the Canada Basin near Alaska, the Lomonosov Ridge and adjoining basins near the North Pole. Tectonophysics 89, 239-253. Contribution No. 992 of EPB. LOREX Contribution No. 10.

Moore, R., 1981. Oceanic distributions of zink, cadmium, copper and aluminium in the Central Arctic Ocean. Geochemica and Cosmochemica Acta, 45, 2475-2482. LOREX Contribution No. 6.

Moore, R. 1983. The relationship between dissolved cadmium, iron and aluminium and hydrography in the Central Arctic Ocean. In: Wong, Boyle, Bruland and Goldberg (eds.), Trace Metals in Sea Water, p. 131 - 142. LOREX Contribution No. 8.

Moore, R., Lowings, M. and Tan, F.C. 1983. Geochemical profiles in the Central Arctic Ocean; their relation to freezing and shallow circulation. J. Geophys. Res. 88, 2667-2674, LOREX Contribution No. 12.

Morris, T.H. 1983. The stratigraphy and late Pleistocene sedimentological history of the Lomonosov Ridge-Makarov Basin, Central Arctic Ocean. M.Sc. thesis (geology), University of Wisconsin, Madison, 100 p. LOREX Contrib. No. 17.

Overton, A. 1980. Intermediate reflection profiles. AGU Spring Meeting, Toronto. Arctic Geophysics and Oceanography: LOREX and FRAM I. Abstract, EOS, 61, 276.

Overton, A. 1982. A seismic reflection profile across the Lomonosov Ridge, Central Arctic Ocean. Soc. Expl. Geophysicists, Technical Program Abstracts and Biographies. 52nd Annual Meeting, Dallas, pp. 87-89.

Pounder, E.R. 1980. Physical oceanography in the central Arctic. AGU Spring Meeting, Toronto. Arctic Geophysics and Oceanography: LOREX and FRAM I. Abstract, EOS, 61, 278.

Sweeney, J.F., Weber, J.R. and Halliday, D.W. 1980. Invited paper. AGU Spring Meeting, Toronto. Arctic Geophysics and Oceanography: LOREX and FRAM I. Abstract, EOS, 61, 277.

Weber, J.R. 1980. LOREX 79: Introduction. Invited paper. AGU Spring Meeting, Toronto. Arctic Geophysics and Oceanography: LOREX and FRAM I. Abstract, EOS, 61, 276.

Weber, J.R., Sweeney, J.F. and Halliday, D.W. 1980. Bathymetry and tectonic structure of the Lomonosov Ridge based on gravity and plumbline deflection observations. AGU Spring Meeting, Toronto. Arctic Geophysics and Oceanography: LOREX and FRAM I. Abstract, EOS, 61, 277.

Wells, D. and Popelar, J. 1980. LOREX satellite navigation. AGU Spring Meeting, Toronto. Arctic Geophysics and Oceanography: LOREX and FRAM I. Abstract, EOS, 61, 279.